frontiers | Research Topics

# Next generation sequencing (NGS) for rare diseases diagnosis, volume II

**Edited by**
Xiu-An Yang, Hu Hao and Can Liao

**Published in**
Frontiers in Genetics
Frontiers in Pediatrics

ISSN 1664-8714
ISBN 978-2-8325-3072-6
DOI 10.3389/978-2-8325-3072-6

## About Frontiers

Frontiers is more than just an open access publisher of scholarly articles: it is a pioneering approach to the world of academia, radically improving the way scholarly research is managed. The grand vision of Frontiers is a world where all people have an equal opportunity to seek, share and generate knowledge. Frontiers provides immediate and permanent online open access to all its publications, but this alone is not enough to realize our grand goals.

## Frontiers journal series

The Frontiers journal series is a multi-tier and interdisciplinary set of open-access, online journals, promising a paradigm shift from the current review, selection and dissemination processes in academic publishing. All Frontiers journals are driven by researchers for researchers; therefore, they constitute a service to the scholarly community. At the same time, the *Frontiers journal series* operates on a revolutionary invention, the tiered publishing system, initially addressing specific communities of scholars, and gradually climbing up to broader public understanding, thus serving the interests of the lay society, too.

## Dedication to quality

Each Frontiers article is a landmark of the highest quality, thanks to genuinely collaborative interactions between authors and review editors, who include some of the world's best academicians. Research must be certified by peers before entering a stream of knowledge that may eventually reach the public - and shape society; therefore, Frontiers only applies the most rigorous and unbiased reviews. Frontiers revolutionizes research publishing by freely delivering the most outstanding research, evaluated with no bias from both the academic and social point of view. By applying the most advanced information technologies, Frontiers is catapulting scholarly publishing into a new generation.

## What are Frontiers Research Topics?

Frontiers Research Topics are very popular trademarks of the *Frontiers journals series*: they are collections of at least ten articles, all centered on a particular subject. With their unique mix of varied contributions from Original Research to Review Articles, Frontiers Research Topics unify the most influential researchers, the latest key findings and historical advances in a hot research area.

Find out more on how to host your own Frontiers Research Topic or contribute to one as an author by contacting the Frontiers editorial office: frontiersin.org/about/contact

# Next generation sequencing (NGS) for rare diseases diagnosis - volume II

**Topic editors**

Xiu-An Yang — Chengde Medical University, China

Hu Hao — The Sixth Affiliated Hospital of Sun Yat-sen University, China

Can Liao — Prenatal Diagnostic Center, Guangzhou Women and Children's Medical Center, China

**Citation**

Yang, X.-A., Hao, H., Liao, C., eds. (2023). *Next generation sequencing (NGS) for rare diseases diagnosis - volume II*. Lausanne: Frontiers Media SA.

doi: 10.3389/978-2-8325-3072-6

# Table of contents

frontiers | Frontiers in Genetics

TYPE Editorial
PUBLISHED 10 July 2023
DOI 10.3389/fgene.2023.1249585



OPEN ACCESS

EDITED AND REVIEWED BY
Maxim B. Freidin,
Queen Mary University of London,
United Kingdom

*CORRESPONDENCE
Xiu-An Yang,
yangxiuan07@mails.ucas.edu.cn
Hu Hao,
haohu@mail.sysu.edu.cn
Can Liao,
canliao6008@163.com

RECEIVED 28 June 2023
ACCEPTED 04 July 2023
PUBLISHED 10 July 2023

CITATION
Yang X-A, Hao H and Liao C (2023), Editorial: Next generation sequencing (NGS) for rare diseases diagnosis - Volume II.
*Front. Genet.* 14:1249585.
doi: 10.3389/fgene.2023.1249585



# Editorial: Next generation sequencing (NGS) for rare diseases diagnosis - Volume II

Xiu-An Yang[1,2]*, Hu Hao[3,4]* and Can Liao[5]*

[1]Laboratory of Genetic Engineering and Genomics, School of Basic Medical Sciences, Chengde Medical University, Chengde, China, [2]Hebei Key Laboratory of Nerve Injury and Repair, Chengde Medical University, Chengde, China, [3]Department of Pediatrics, The Sixth Affiliated Hospital, Sun Yat-sen University, Guangzhou, China, [4]Inborn Errors of Metabolism Laboratory, The Sixth Affiliated Hospital, Sun Yat-sen University, Guangzhou, China, [5]Guangzhou Women and Children's Medical Center, Guangzhou, China

KEYWORDS

**next generation sequencing, rare diseases diagnosis, whole-exome sequencing, whole-genome sequencing, copy number variants (CNV) sequencing**

Editorial on the Research Topic
Next generation sequencing (NGS) for rare diseases diagnosis - Volume II

## Introduction

Next generation sequencing (NGS) has greatly facilitated the diagnosis of rare diseases. According to a 2013 statistic, 87% of Mendel's genetic disease-causing genes were discovered by NGS technology from 2007 to 2013 (McKusick, 2007). To emphasize the significance of NGS and present high-quality research on prevention, diagnostics, and treatment, we previously launched a Research Topic in Frontiers in Genetics. Due to popular demand, the Research Topics were extended as Volume II. A totally of 16 articles were published in this volume, comprising 16 articles covering various topics such as preimplantation and prenatal diagnosis, case reports of rare diseases, multiple case summaries, and hematological tumors.

## Preimplantation and prenatal diagnosis

Giving birth to a healthy baby (or babies) is an exceptional gift for families with genetic diseases. In the case of a male proband from unrelated healthy parents, several complications arose during the first pregnancy, including extensive neurogenic damage, developmental delay, and an enlarged heart (Shi and Ye). To determine the genetic pathogenic variant, karyotype analysis, Fluorescence *in situ* hybridization (FISH), whole exome sequencing (WES), and copy number variants (CNV) sequencing were conducted. WES revealed heterozygous variants in *DUOX2* (c.1588 A >T (p.K530X), c.2654G >T (p.R885 L)), respectively inherited from the mother and father. Although the karyotype analysis was normal, CNV sequencing showed a *de novo* Xq28-q28 duplication (5.59 Mb × 2) and 18q22.2-q23 deletion (9.85 Mb × 1) in the proband. FISH revealed that the mother was a carrier of a reciprocal translocation (RecT) between

ChrX and Chr18 [t (X; 18) (q28; q22.2)]. To identify embryos free of pathogenic variants, preimplantation genetic testing was conducted. This was followed by amniocentesis at gestational week 20, which confirmed the fetal genetic makeup. Ultimately, a healthy infant was delivered. This case report underscores the importance of using NGS in preimplantation prenatal diagnosis. Furthermore, the study highlights the need for a multi-technical approach that includes karyotype analysis, FISH, and linkage analysis in reproductive medicine.

Yu et al. reported a case of fetal tetrasomy 9p, which was initially identified by non-invasive prenatal testing (NIPT). The 37-year-old pregnant woman was healthy and had undergone NIPT due to advanced maternal age. At 12 weeks of gestation, an ultrasound screening revealed normal nuchal translucency (NT) and nasal bone. Unfortunately, at 15 weeks of gestation, the NIPT indicated a duplication at 9p24.3p11.2. The result was validated through amniocentesis, karyotyping, chromosome microarray (CMA), and FISH. Based on the opinions of the pregnant woman and her husband, the pregnancy was terminated. It is recommended that NIPT should be carried out in cases of advanced maternal age to rule out fetal genetic variations, even in the absence of fetal abnormalities revealed by ultrasound examination.

Norrie disease (ND) is an X-linked recessive disorder that can result in blindness in early postnatal stages due to retinal detachment (Meire et al., 1998). A 29-year-old pregnant woman gave birth to a son who was born with congenital bilateral blindness, but showed no signs of cognitive impairment or deafness (Li et al.). Prenatal diagnosis was conducted at 16 weeks of gestation, and WES identified a hemizygous variant, c.174 + 1G > A, in the *NDP* splicing site. *In vitro* splicing assays were performed on mRNA using HeLa and 293 T cells to study the effects of the *NDP* c.174 + 1G > A variant on splicing. The study highlighted the essentiality of NGS combined with relevant laboratory tests for diagnosing genetic diseases.

Short-rib thoracic dysplasia (SRTD), with or without polydactyly, is a group of autosomal recessive, genetically heterogeneous skeletal dysplasias. Mutations in the *DYNC2H1* gene have been identified as the genetic cause of short-rib thoracic dysplasia 3 with or without polydactyly (SRTD3; OMIM #613091) (Bonafe et al., 2015). The study conducted by Chen et al. included unrelated cases visiting for pregnancy check-up, both of whom had a history of pregnancy termination due to fetal dysplasia. WES identified two compound heterozygous variations in the *DYNC2H1* gene for one patient, namely c.2386C >T (p. Arg796Trp) and c.7289 T >C (p.Ile2430Thr), and exon (64–83) deletion and c.8190G >T (p.Leu2730Phe) for the other patient. Sanger sequencing validated the results, and RT-PCR analyses confirmed that the variants were inherited from the parents, who were carriers of the mutations. Chen et al. provided an extensive description of the pathogenic genes and *DYNC2H1* variants previously identified in SRTD.

The Ehlers-Danlos syndromes (EDS) are a group of connective tissue diseases that can be inherited. A specific subtype of EDS, known as Musculocontractural Ehlers-Danlos syndrome (mcEDS), can be caused by mutations in the carbohydrate sulfotransferase 14 (*CHST14*) or dermatan sulfate epimerase genes (Malfait et al., 2010). In this case, a 34-year-old woman who was 22 weeks pregnant had an ultrasound that showed her fetus had adduction flexion in the feet (Zhou et al.). She then underwent prenatal testing, which included WES, CNV sequencing, and amniotic fluid cell karyotype analysis. Two potential genetic causes for mcEDS were identified as variants in the *CHST14* gene (NM_130468.3 c.958C >T (p.Arg320*) and NM_130468.3 c.896A>G (p.Tyr299Cys)). This study has expanded our understanding of the genetic causes of mcEDS.

## Case reports of rare diseases

Before the advent of NGS, due to limitations in research methods, many pathogenic genes and sites of rare diseases were not fully studied. This resulted in a number of extremely rare diseases with only dozens or even fewer cases reported worldwide. In this volume, three extremely rare case reports were published. One case involved a healthy, non-consanguineous Chinese couple who gave birth to a full-term infant girl (Chen et al.). Unfortunately, the baby died at a few months of age due to severe respiratory infection and unknown respiratory failure. WES identified novel compound heterozygous splicing mutations in *RFX5*, namely c.353 + 6T >G and c.757 + 1 G >A. The results were confirmed through Sanger sequencing, and the pathogenicity of RFX5: c. 353 + 6T >G was further investigated using RT-PCR. RFX5 is a protein with two DNA-binding domains (DBDs), and the c.353 + 6T >G splicing mutation could lead to a truncated DBD. This could impair the ability of RFX5 to bind to the MHC II promoter and lead to reduced transcription of MHC II molecules. This study thus contributes to the extension of the genetic spectrum of MHC class II deficiency.

Biallelic variants in the *TENM3* gene can result in two distinct phenotypes: nonsyndromic microphthalmia with coloboma-9 (MCOPCB9) and microphthalmia and/or coloboma with developmental delay (MCOPS15) (Aldahmesh et al., 2012; Chassaing et al., 2016). To date, only eight cases have been documented. Lu et al. recently reported two cases of syndromic microphthalmia associated with *TENM3* variants . In one case, a 5-month-old girl was found to have compound heterozygous variants (p.Leu1283_Ser1285del; p. Thr1233Thrfs*20) in *TENM3* through trio-based WES. The p. Leu1283_Ser1285del variant was inherited from her mother, while TA cloning indicated that the other was a *de novo* mutation located on the Father-derived chromosome. The second patient was found to have compound heterozygous variants in the *TENM3* gene: c.6464T > C; p. Leu2155Pro and c.941C > T; p. Ala314Val, respectively inherited from each parent. The authors provided a clear description of the clinical presentation and summarized the features of all reported cases with *TENM3* variants to date.

The Cdc42 molecule is a small GTPase that belongs to the Rho GTPase family and plays multiple important physiological functions in regulating the cell cycle. The heterozygous c.191A >G (p.Tyr64Cys) variant is reported as the pathogenic molecular etiology of Takenouchi-Kosaki syndrome (TKS). TKS is a range of phenotypic syndromes characterized by psychomotor development, dysmorphic facial features, and hematologic or lymphatic defects (Martinelli et al., 2018). In a male infant, a genetic syndrome was suspected due to facial

dysmorphism, low-set ears, axial hypotonia with peripheral spasticity, camptodactyly, and cutaneous syndactyly of toes (Szczawińska-Popłonyk A et al.). WES revealed the c. 191A >G; p. Tyr64Cys (NM_001791.4) variant in the *CDC42* gene, which was later confirmed through Sanger sequencing. While this study did not identify novel genetic sites, it does expand the clinical spectrum of TKS.

## Multiple case summaries

With the wide application of NGS, an increasing number of relationships between pathogenic genes and the phenotypes of monogenic genetic diseases have been established. Additionally, the mutation sites of Mendelian disease-causing genes have been widely reported. It is well-documented that mutations in the *ATP7B* gene could lead to an autosomal recessive disease called Wilson's disease (WD). In this volume, 39 and 30 genetically diagnosed WD cases were respectively studied by Wang et al. and Zhou et al.The participants in Wang's study were from Yunnan province in China, including seven different ethnic groups. Homozygous mutation frequency is higher, whereas protein-truncating variant (PTV) is less frequent in ethnic minorities compared with the Han population found that the frequency of p. R778L and p. I1148T is relatively high. They suggested that elevated alanine transaminase (ALT), decreased ceruloplasmin level, and increased 24-h urinary copper level should be considered as three important indices for rapid diagnosis.

Autism spectrum disorder (ASD) is a cluster of common neurological developmental symptoms in the pediatric population. In this study, Zhang et al. recruited 354 ASD candidates and investigated the genetic etiology using WGS and RNA sequencing Pathogenic variants including single nucleotide variations (SNV), CNV, and structural variations (SV) were investigated. They found that ASD affected children had a relatively low frequency of rare CNV and SNV variants. The total positive rate (5.3%) was relatively lower than in other studies, and the authors attributed this to the mutation characteristics they focused on. It is worth noting that the authors used RNA sequencing and RT-PCR to validate the variants. Therefore, the false positive rate of mutations will be reduced.

Variants in the *LMNA* gene can give rise to a range of clinical manifestations called laminopathies. To explore the genetic basis of LMNA-related muscular dystrophies, Cesar et al. enrolled 26 patients from different parts of the world and sequenced 105 genes using a targeted approach. They identified that the most severe phenotypes resulted from the coexistence of a rare damaging variant in *LMNA* and another damaging variant in a gene involved in NMD. The authors highlighted the marked genetic heterogeneity of laminopathies and advocated for comprehensive genetic testing of both LMNA and other genes linked to muscle disorders to reveal potential causal mechanisms.

Fabry disease (FD) arises from variants in the X chromosome-located *GLA* gene, which encodes alpha-galactosidase A (α-Gal A). Abnormal expression or function in α-Gal A activity can cause the buildup of trihexosaccharide sphingolipid alcohol (GL-3) and its derivative, deacetyl GL-3 (Lyso-GL-3). The clinical manifestations of FD are highly heterogeneous. Li et al. retrospectively analyzed ten patients who visited their hospital and were diagnosed with FD. They provided a detailed description of the patients' clinical manifestations, laboratory and auxiliary examinations, FD-specific indexes and GLA genetic testing, pedigree screening, and treatment. The authors emphasized that it is critical for doctors to understand the clinical symptoms of FD and actively screen for early detection and diagnosis of the disease.

*CTNS* encodes a lysosomal cystine transporter cystinosin, and variants in this gene can cause the rare hereditary autosomal recessive disorder known as nephropathic cystinosis. Disruption of cystinosin function can lead to cystine accumulation in cells, particularly in the kidneys. Cystinosis can be classified into three subtypes based on symptom severity and age of onset. In a study conducted by Savostyanov et al. 40 children who were clinically diagnosed with nephropathic cystinosis and confirmed by molecular testing were examined. The methods employed included tandem mass spectrometry, Sanger sequencing, multiplex PCR, MLPA, and haplotype analysis. The researchers confirmed that the most common pathogenic variant was a 57 kb deletion, 22.5% of alleles were novel, and there was a founder effect for the c.1015G > A and c. 518A > G variants in the Karachay and Chechen ethnic groups, respectively.

Café-au-lait macules (CALMs) are common birthmarks that can increase in number and range over time. They are found in 2%–3% of healthy newborns, and the occurrence of six or more typical CALMs indicates neurofibromatosis type 1 (NF1), which is caused by variants in the *NF1* gene. In a study by Zhong et al. the variant characteristics in six Chinese Han populations diagnosed with CALMs were investigated. Sequencing revealed two novel variants in NF1—NC_ 000017.11(NM_ 001042492.2):c.7355G >A and NC_000017.11(NM_ 001042492.2):c.2739_2740del. The authors also used dermoscopy and reflectance confocal microscopy to demonstrate the features of CALMs. The skin imaging characteristics provided by the authors can assist clinicians in making decisions during CALMs diagnosis.

## Hematological tumor

The incidence of tumors in children is generally low. However, acute lymphoblastic leukemia (ALL) is often observed in this population, which is highly correlated with altered lymphoid precursor hyperplasia. Furthermore, *IKZF1* variants are frequently observed in children diagnosed with ALL. Zhang et al. conducted a study analyzing the clinical and genetic features of 200B-cell ALL pediatric patients by utilizing MLPA and targeted NGS methodologies. Their results indicate that *IKZF1* variants were identified in 22 patients and there was a significant association between *IKZF1* variants and higher WBC counts. Moreover, the study revealed that patients with *IKZF1* mutations had decreased sensitivity to glucocorticoid induction and higher levels of minimal residual disease compared with patients with *IKZF1* wildtype. This research sheds light on the association between genetic mutations and clinical features, providing new perspectives for targeted therapy in ALL.

## Author contributions

All authors listed have made a substantial, direct, and intellectual contribution to the work and approved it for publication.

## Funding

This study was supported by Natural Science Foundation of Hebei Province (No. H2020406049), Scientific and Technological Research Projects of Hebei Higher Education (No. ZD2019084), and Initial Scientific Research Fund for High-Level Talents of Chengde Medical University (No. 201901).

## Conflict of interest

The authors declare that the research was conducted in the absence of any commercial or financial relationships that could be construed as a potential conflict of interest.

## Publisher's note



## References

Aldahmesh, M. A., Mohammed, J. Y., Al-Hazzaa, S., and Alkuraya, F. S. (2012). Homozygous null mutation in ODZ3 causes microphthalmia in humans. *Genet. Med. official J. Am. Coll. Med. Genet.* 14, 900–904. doi:10.1038/gim.2012.71

Bonafe, L., Cormier-Daire, V., Hall, C., Lachman, R., Mortier, G., Mundlos, S., et al. (2015). Nosology and classification of genetic skeletal disorders: 2015 revision. *Am. J. Med. Genet. Part A.* 167A, 2869–2892. doi:10.1002/ajmg.a.37365

Chassaing, N., Ragge, N., Plaisancie, J., Patat, O., Genevieve, D., Rivier, F., et al. (2016). Confirmation of TENM3 involvement in autosomal recessive colobomatous microphthalmia. *Am. J. Med. Genet. Part A.* 170, 1895–1898. doi:10.1002/ajmg.a.37667

Malfait, F., Syx, D., Vlummens, P., Symoens, S., Nampoothiri, S., Hermanns-Le, T., et al. (2010). Musculocontractural Ehlers-Danlos Syndrome (former EDS type VIB) and adducted thumb clubfoot syndrome (ATCS) represent a single clinical entity caused by mutations in the dermatan-4-sulfotransferase 1 encoding CHST14 gene. *Hum. Mutat.* 31, 1233–1239. doi:10.1002/humu.21355

Martinelli, S., Krumbach, O. H. F., Pantaleoni, F., Coppola, S., Amin, E., Pannone, L., et al. (2018). Functional dysregulation of CDC42 causes diverse developmental phenotypes. *Am. J. Hum. Genet.* 102, 309–320. doi:10.1016/j.ajhg.2017.12.015

McKusick, V. A. (2007). Mendelian inheritance in man and its online version, OMIM. *Am. J. Hum. Genet.* 80, 588–604. doi:10.1086/514346

Meire, F. M., Lafaut, B. A., Speleman, F., and Hanssens, M. (1998). Isolated Norrie disease in a female caused by a balanced translocation t(X,6). *Ophthalmic Genet.* 19, 203–207. doi:10.1076/opge.19.4.203.2306

frontiers in Genetics

ORIGINAL RESEARCH
published: 10 February 2022
doi: 10.3389/fgene.2022.788658

# Early Diagnosis of Wilson's Disease in Children in Southern China by Using Common Parameters

*Jianli Zhou*[1], *Qiao Zhang*[1], *Yuzhen Zhao*[1], *Moxian Chen*[2], *Shaoming Zhou*[1,*] and *Yongwei Cheng*[1,*]

[1]Department of Gastroenterology, Shenzhen Children's Hospital, Shenzhen, China, [2]Co-Innovation Center for Sustainable Forestry in Southern China, Key Laboratory of National Forestry and Grassland Administration on Subtropical Forest Biodiversity Conservation, College of Biology and the Environment, Nanjing Forestry University, Nanjing, China

OPEN ACCESS

**Edited by:**
Louis Charles Penning,
Utrecht University, Netherlands

**Reviewed by:**
Julnar A. R. Usta,
American University of Beirut, Lebanon
Jinchen Li,
Central South University, China

***Correspondence:**
Shaoming Zhou
zhousm15d@aliyun.com
Yongwei Cheng
29060628@qq.com

**Specialty section:**
This article was submitted to Genetics of Common and Rare Diseases, a section of the journal Frontiers in Genetics

**Received:** 03 October 2021
**Accepted:** 14 January 2022
**Published:** 10 February 2022

**Citation:**
Zhou J, Zhang Q, Zhao Y, Chen M, Zhou S and Cheng Y (2022) Early Diagnosis of Wilson's Disease in Children in Southern China by Using Common Parameters. Front. Genet. 13:788658. doi: 10.3389/fgene.2022.788658

**Objective:** The aim of the study was to develop the early diagnostic criteria for Wilson's disease (WD) in young children in southern China by using alanine aminotransferase (ALT) elevation as the first manifestation.

**Methods:** A cross-sectional retrospective analysis of the clinical data and genetic test results of children with WD in southern China in the past 4 years and the follow-up of their short-term prognosis were performed in this study.

**Results:** A total of 30 children (5.08 ± 2.06 years old) with elevated ALT as the first manifestation of WD in southern China were enrolled in this study, including 14 females and 16 males. Specifically, in all of the 30 cases (100%), the serum ceruloplasmin (CP) level was decreased, whereas the 24-h urinary copper level was increased. The genetic mutation test of the *ATP7B* gene was used to confirm the diagnosis. In particular, the two mutation sites, including p.R778L and p.I1148T, had the highest mutation frequencies, approximately 23.0 and 10.7%, respectively. Through follow-up, most of the children had good recovery.

**Conclusion:** Early diagnosis and treatment of WD would substantially increase the survival rate and have a better prognosis. In addition, in 5-year-old children from southern China, early diagnosis could be performed quickly by referring to the following three parameters: elevated ALT, decreased ceruloplasmin level, and increased 24-h urinary copper level. It lays a foundation for further studies with a larger sample size.

**Keywords: children, southern China, hepatolenticular degeneration, clinical features, genetic mutation**

**Abbreviations:** ALT, alanine aminotransferase; ALP, alkaline phosphatase; AST, aspartic transaminase; BGI, Beijing Genomics Institute; CP, ceruloplasmin; EEG, electroencephalogram; EASL, European Association for the Study of the Liver; FIB, fibrinogen; GGT, gamma-glutamyl transpeptidase; HLD, hepatolenticular degeneration; INR, international normalized ratio; K–F, Kayser–Fleischer; MRI, magnetic resonance imaging; PT, prothrombin time; ULN, upper limit of normal; WES, whole-exome sequencing; WD, Wilson's disease.

# 1 INTRODUCTION

Hepatolenticular degeneration (HLD), also known as Wilson's disease (WD; OMIM 277900), is an autosomal recessive disorder of copper metabolism (Huster, 2010; Meranthi et al., 2020). The disease occurs all over the world, and the incidence rate in the human population is about 1:1,500–13,000 in East Asia and 1: 7,000 in the United Kingdom (Chen et al., 2019; Xiao et al., 2019; Meranthi et al., 2020). The clinical features of WD include liver function injury, nervous system damage, psychiatric abnormality, corneal Kayser–Fleischer (K–F) ring, and decreased serum ceruloplasmin (Xiao et al., 2019). The onset age of WD ranges from infancy to more than 70 years, with an average age of 15.9 years (Xiao et al., 2019). Late diagnosis and treatment or irregular medication of WD could lead to irreversible brain damage or even death. Therefore, early diagnosis and treatment are crucial to reduce the irreversible sequelae of WD (Xiao et al., 2019).

WD can result from the mutation of the *ATP7B* (OMIM 606882) gene that encodes the intracellular copper transporter on chromosome 13, leading to an impaired intracellular copper output (Meranthi et al., 2020). *ATP7B* is a P-type ATPase and is mainly expressed in the liver. It binds copper to its N-terminal domain and is responsible for the transport of copper across the membrane, using ATP as its energy source. Studies have demonstrated that mutations at different sites can affect ATPase activity. Until now, more than 1,000 different mutations of *ATP7B* have been found in patients with WD in the Human Gene Mutation Database (HGMD v2021.11) (Stenson et al., 2017). The mutation of the *ATP7B* gene in WD affects the interaction between copper ions and ceruloplasmin and subsequent copper excretion in bile, which is the major way of excreting liver copper. If the copper excretion from bile is reduced, copper is then deposited in places around the liver, causing damage to hepatocytes. In addition, it results in elevated ALT as the primary clinical manifestation. Gradually, copper accumulates in the brain, cornea, and kidneys, causing damage to the corresponding organs and accompanying clinical symptoms (European Association for Study of Liver, 2012). Over time, the liver becomes progressively damaged by copper deposits, and some patients end up with cirrhosis or liver failure, as well as severe nervous and blood system damage (European Association for Study of Liver, 2012). Therefore, early diagnosis with high accuracy is crucial for patients with WD and their prognosis. To this end, the clinical features and genetic characteristics of 30 children diagnosed with WD and treated at Shenzhen Children's Hospital in the past 4 years were analyzed in this study.

# 2 MATERIAL AND METHODS

## 2.1 Clinical Data Collection

This was a single-center cross-sectional retrospective study of 30 patients with WD with elevated ALT as their first manifestation in southern China, from May 2016 to May 2020. Medical history, physical examination, laboratory examination, and imaging findings were all collected as clinical data. Physical examination included jaundice, liver enlargement, K–F ring, and neurological symptoms. Laboratory tests included blood routine, hepatic, renal and immunological function tests, virology tests (hepatitis A, B, C, D, E, cytomegalovirus, and EB virus), ceruloplasmin, and 24-h urinary copper level. Imagological examinations included abdominal (liver) ultrasound, cardiac Doppler ultrasonography, and brain magnetic resonance imaging (MRI).

## 2.2 Genetic Data Collection

All of the cases were tested with *ATP7B* targeted gene panel sequencing (TGPS) or whole-exome sequencing (WES). The venous blood (2–5 ml) of the patient was drawn after the results of the serum ceruloplasmin (CP) level and 24-h urinary copper level were available, together with 5 ml of parental venous blood for comparison to verify the source of its pathogenic genes. All test protocols, including DNA extraction, construction of gene library, high-throughput sequencing, data analysis, Sanger sequencing verification, and bioinformatics analysis, were carried out by commercial companies such as BGI (The Beijing Genomics Institute, Shenzhen) and Mykino (Beijing).

## 2.3 Follow-Up Visit

All of the cases were carried out for follow-up studies using outpatient and telephone recordings, including examination, treatment, and outcome.

# 3 RESULTS

## 3.1 Clinical Features (Table 1)

### 3.3.1 Study Data

The subjects of the present study included 14 female and 16 male patients who were asymptomatic only with an elevated hepatase level. The minimum diagnosed age was 2 years, and the oldest patient was 11 years and 4 months old, with an average age of 5.08 ± 2.06 years. The average duration from the discovery of abnormal liver function to diagnosis was about 4 months, and the longest duration was 4 years and 5 months.

### 3.3.2 Blood Biochemical Test

The blood test suggested that ALT was elevated in all of the patients, ranging from 73 to 673 IU/L. In particular, ALT of 11 cases (36.6%) was found to be slightly elevated (increased <5 (upper limit of normal, ULN) times the reference value). In addition, the ALT levels of 14 cases (46.6%) were moderately elevated, that is, 5–10 ULN, whereas 5 cases (16.6%) were found to have severely elevated ALT levels (>10 ULN). Furthermore, the aspartic transaminase (AST) of patients ranged from 75 to 669 IU/L. Specifically, 27 cases (90%) were found to have an AST/ALT ratio of less than 1. In addition, only three cases (10.0%) showed an AST value higher than that of ALT, and the one with an AST/ALT of >2 had jaundice, coagulation dysfunction, liver failure, and eventually died.

**TABLE 1 |** Detailed clinical information of 30 children with WD.

| Case | Gender | Onset age (years) | Neurological symptoms | Corneal K–F ring | Hb (g/L) | ALT (IU/L) | AST (IU/L) | AST/ ALT | TB (umol/L) | CP (mg/dl) | 24-h urinary copper (μg/24 h) | Mutations of *ATP7B* | Zygotic type |
|---|---|---|---|---|---|---|---|---|---|---|---|---|---|
| Case 1 | Female | 4.5 | No | No | 118 | 212 | 113 | 0.53 | 3.3 | 2.8 | 82.3 | c.2975C > T (p.P992L) | Het |
| | | | | | | | | | | | | c.2333G > T (p.R778L) | Het |
| Case 2 | Female | 5.33 | No | No | 127 | 161 | 116 | 0.72 | 6.7 | 5.3 | 80.7 | c.2804C > T (p.T935M) | Het |
| | | | | | | | | | | | | c.2333G > T (p.R778L) | Het |
| | | | | | | | | | | | | c.2310C > G (p.L770L) | Het |
| Case 3 | Female | 4 | No | No | 121 | 358 | 222 | 0.62 | 13.4 | 4.5 | 85.2 | c.2662A > C (p.T888P) | Het |
| | | | | | | | | | | | | c.2333G > T (p.R778L) | Het |
| | | | | | | | | | | | | c.2310C > G (p.L770L) | Het |
| Case 4 | Male | 5 | No | No | 131 | 92 | 85 | 0.92 | 3.6 | 7.5 | 111.2 | c.314C > A (p.S105*) | Het |
| | | | | | | | | | | | | c.2975C > T (p.P992L) | Het |
| Case 5 | Male | 6.58 | No | No | 129 | 135 | 81 | 0.6 | 14.7 | 3.5 | 121.2 | c.2662A > C (p.T888P) | Het |
| | | | | | | | | | | | | c.2268G > A (p.A756A) | Het |
| Case 6 | Male | 3.5 | No | No | 130 | 233 | 150 | 0.64 | 10.7 | 4.8 | 105.3 | c.2804C > T (p.T935M) | Het |
| | | | | | | | | | | | | c.3809A > G (p.N1270S) | Het |
| Case 7 | Female | 2.91 | No | No | 128 | 289 | 212 | 0.73 | 8 | 2.2 | 51.1 | c.2662A > C (p.T888P) | Het |
| | | | | | | | | | | | | c.2333G > T (p.R778L) | Het |
| Case 8 | Male | 3 | No | No | 128 | 151 | 106 | 0.7 | 5.4 | 5.4 | 123.9 | c.2755C > G (p.R919G) | Het |
| | | | | | | | | | | | | c.2333G > T (p.R778L) | Het |
| Case 9 | Female | 5.83 | No | No | 127 | 320 | 167 | 0.52 | 9.6 | 4.4 | 189.1 | c.3316G > A (p.V1106I) | Het |
| | | | | | | | | | | | | c.525dupA | Het |
| Case 10 | Male | 3.75 | No | No | 124 | 673 | 371 | 0.55 | 4.9 | 4.1 | 187.3 | c.3426G > C (p.Q1142H) | Hom |
| | | | | | | | | | | | | c.3443T > C (p.I1148T) | Hom |
| Case 11 | Female | 3.66 | No | No | 148 | 348 | 222 | 0.64 | 13.7 | 9 | 83.4 | c.2662A > C (p.T888P) | Het |
| | | | | | | | | | | | | c.3587A > G (p.D1196G) | Het |
| Case 12 | Female | 2.91 | No | No | 125 | 348 | 135 | 0.39 | 4.3 | 2 | 92.3 | c.3244-2A > G | Het |
| | | | | | | | | | | | | c.3426G > C (p.Q1142H) | Het |
| | | | | | | | | | | | | c.3443T > C (p.I1148T) | Het |
| Case 13 | Male | 3.66 | No | No | 115 | 389 | 259 | 0.67 | 8.8 | 3.8 | 54.5 | c.2975C > T (p.P992L) | Het |
| | | | | | | | | | | | | c.2320_2321insTTGCCCAGGGCA | Het |
| Case 14 | Male | 3.33 | No | No | 139 | 440 | 243 | 0.55 | 7.5 | 4 | 191.4 | c.3443T > C (p.I1148T) | Het |
| | | | | | | | | | | | | c.4064G > A (p.G1355D) | Het |
| Case 15 | Female | 4.58 | No | No | 117 | 117 | 112 | 0.96 | 7.3 | 6.9 | 308.4 | c.2975C > T (p.P992L) | Het |
| | | | | | | | | | | | | c.3443T > C (p.I1148T) | Het |
| Case 16 | Female | 0.91 | No | No | 132 | 248 | 175 | 0.71 | 8.6 | 2.1 | 64.1 | c.1470C > A (p.C490*) | Het |
| | | | | | | | | | | | | c.3532A > G (p.T1178A) | Het |
| Case 17 | Female | 4.16 | No | No | 110 | 181 | 101 | 0.56 | 11.5 | 2.9 | 87.6 | c.3220G > A (p.A1074T) | Het |
| | | | | | | | | | | | | c.2333G > T (p.R778L) | Het |
| Case 18 | Male | 3 | No | No | 125 | 393 | 240 | 0.61 | 8.4 | 4.7 | 146.7 | c.3220G > A (p.A1074T) | Het |
| | | | | | | | | | | | | c.2333G > T (p.R778L) | Het |
| Case 19 | Female | 4.25 | No | No | 118 | 115 | 90 | 0.78 | 5.2 | 2.1 | 308.9 | c.2145C > A (p.Y715*) | Het |
| | | | | | | | | | | | | c.2333G > T (p.R778L) | Het |
| Case 20 | Female | 3 | No | No | 127 | 261 | 155 | 0.59 | 7.4 | 2.4 | 150.9 | c.2333G > T (p.R778L) | Het |
| | | | | | | | | | | | | c.525dupA | Het |
| | | | | | | | | | | | | c.2310C > G (p.L770L) | Het |
| Case 21 | Male | 5.25 | No | No | 137 | 519 | 360 | 0.69 | 17.6 | 6 | 134.7 | c.3532A > G (p.T1178A) | Het |
| | | | | | | | | | | | | c.3443T > C (p.I1148T) | Het |
| Case 22 | Male | 3.25 | No | No | 130 | 596 | 669 | 1.12 | 13.6 | 6.1 | 145.7 | c.3443T > C (p.I1148T) | Het |
| | | | | | | | | | | | | c.2333G > T (p.R778L) | Het |

(Continued on following page)

**TABLE 1 |** (*Continued*) Detailed clinical information of 30 children with WD.

| Case | Gender | Onset age (years) | Neurological symptoms | Corneal K–F ring | Hb (g/L) | ALT (IU/L) | AST (IU/L) | AST/ ALT | TB (umol/L) | CP (mg/dl) | 24-h urinary copper (μg/24 h) | Mutations of *ATP7B* | Zygotic type |
|---|---|---|---|---|---|---|---|---|---|---|---|---|---|
| Case 23 | Male | 1.91 | No | No | 121 | 73 | 75 | 1.03 | 5.7 | 3.8 | 68.3 | c.4059G > A (p.W1353*)<br>c.2621C > T (p.A874V) | Het<br>Het |
| Case 24 | Male | 7.41 | No | No | 131 | 330 | 170 | 0.52 | 6.3 | 1.9 | 256.1 | c.2621C > T (p.A874V)<br>c.2333G > T (p.R778L) | Het<br>Het |
| Case 25 | Male | 6 | No | No | 128 | 453 | 231 | 0.51 | 5.6 | 2.7 | 422 | c.2272A > G (p.R758G)<br>c.2333G > T (p.R778L) | Het<br>Het |
| Case 26 | Male | 3.75 | No | No | 125 | 219 | 135 | 0.62 | 13.3 | 6.3 | 94.8 | c.2139C > G (p.Y713*)<br>c.2755C > G (p.R919G) | Het<br>Het |
| Case 27 | Male | 11.33 | No | No | 144 | 143 | 121 | 0.85 | 5.5 | 3.9 | 298.7 | c.3443T > C (p.I1148T)<br>c.3809A > G (p.N1270S) | Het<br>Het |
| Case 28 | Female | 3 | No | No | 127 | 117 | 89 | 0.76 | 5.2 | 3.3 | 93.1 | c.2333G > T (p.R778L)<br>c.3452G > A (p.R1151H) | Het<br>Het |
| Case 29 | Male | 1.91 | No | No | 119 | 287 | 208 | 0.72 | 5.8 | 4.5 | 139.2 | c.2975C > T (p.P992L)<br>c.2333G > T (p.R778L) | Het<br>Het |
| Case 30 | Female | 7.33 | No | No | 98 | 106 | 350 | 3.3 | 43 | 5.6 | 840.7 | c.2333G > T (p.R778L)<br>c.4003G > C (p.G1335R)<br>c.525dupA | Het<br>Het |

*Note: Hb, hemoglobin; ALT, alanine aminotransferase; AST, aspartic transaminase; TB, total bilirubin; CP, ceruloplasmin; Het, heterozygous; Hom, homozygous.*

### 3.3.3 Corneal Kayser–Fleischer (K–F) Ring

The 30 children were examined by an ophthalmologist. No corneal K–F ring was found, indicating that there was no eye damage in this group.

### 3.3.4 Performance of the Nervous System

All of the 30 children had no neurological symptoms. In this group, 12 children underwent brain MRI, and none of them found abnormalities in the basal ganglia, thalamus, and brainstem.

### 3.3.5 Indicators of Copper Metabolism

The CP level was reduced in all of the 30 cases (100.00%), and the detection value was less than 10 mg/dl. Furthermore, the 24-h urinary copper level was increased in all 30 cases and was more than 40 μg/24 h. In particular, 4 cases (13.3%) reached 40–80 μg/24 h, and the remaining 26 cases (86.6%) were more than 80 μg/24 h.

## 3.2 Genetic Analysis (Table 2)

The mutation analysis of the *ATP7B* gene was performed for all of the 30 children, and a total of 65 allelic mutations were detected. This included 51 missense mutations (78.4%), 5 nonsense mutations (7.6%), 4 synonymous mutations (6.1%), 4 frameshift mutations (6.1%), and 1 splicing mutation (1.5%). In our study, there were a total of 28 mutation sites, including 23 reported mutation sites and 5 novel mutation sites. These 28 loci were distributed among different functional regions, including the metal binding units (MBUs), transmembrane domain (TM), actuator domain (A-domain), phosphorylation domain (P-domain), and nucleotide-binding domain (N-domain) (**Figure 1**). The mutation hot spot was identified as p.R778L, including 15 (23.0%) mutation sites at this spot. Furthermore, the second popular mutation site was p.I1148T, which occurred in 7 (10.7%) patients. The five novel mutations included c.2139C > G (p.Y713*), c.2268G > A (p.A756A), c.2272A > G (p.R758G), c.2320_2321insTTGCCCAGGGCA (p.L776Qfs*695), and c.3220G > A (p.A1074T). Variants p. Y713* and p. L776Qfs*695 can be interpreted as "likely pathogenic" according to the American College of Medical Genetics and Genomics (ACMG) standard (PVS1_strong + PM2+PP3), while the other three mutations can be classified as "variants with uncertain clinical significance" (PM2+PP3) (Richards et al., 2015).

## 3.3 Criteria of Disease Diagnosis

The diagnosis criteria for WD were according to EASL Clinical Practice Guidelines: Wilson's disease, from the European Association for Liver Research in 2012 (European Association for Study of Liver, 2012). The parameters used in this evaluation are listed as follows:

(1) Kayser–Fleischer ring (2 points);
(2) neuropsychiatric symptoms suggestive of WD (severe: 2 points and moderate: 1 point);
(3) serum ceruloplasmin content (normal value or >20 mg/dl) normal (0 point), 10–20 mg/dl (1 point), and <10 mg/dl (2 points);

**TABLE 2 |** Information of *ATP7B* gene mutations in 30 children with WD.

| Mutations in *ATP7B* gene | Location | Functional region | Mutation type | Number of mutations | Frequency of mutations (%) | Novelty |
|---|---|---|---|---|---|---|
| c.2333G > T (p.R778L) | Exon 8 | TM4 | Missense | 15 | 23.00 | |
| c.3443T > C (p.I1148T) | Exon 16 | ATP loop | Missense | 7 | 10.70 | |
| c.2975C > T (p.P992L) | Exon 13 | TM6 | Missense | 5 | 7.60 | |
| c.2662A > C (p.T888P) | Exon 11 | ATPase | Missense | 4 | 6.10 | |
| c.525dupA (p.V176Sfs*28) | Exon 2 | Cu2 | Fame-shift | 3 | 4.60 | |
| c.2310C > G (p.L770L) | Exon 8 | TM4 | Synonymous | 3 | 4.60 | |
| c.2621C > T (p.A874V) | Exon 11 | ATPase | Missense | 2 | 3.00 | |
| c.2755C > G (p.R919G) | Exon 12 | TM5 | Missense | 2 | 3.00 | |
| c.2804C > T (p.T935M) | Exon 12 | TM5 | Missense | 2 | 3.00 | |
| c.3426G > C (p.Q1142H) | Exon 16 | ATP loop | Missense | 2 | 3.00 | |
| c.3532A > G (p.T1178A) | Exon 16 | ATP loop | Missense | 2 | 3.00 | |
| c.3809A > G (p.N1270S) | Exon 18 | ATP hinge | Missense | 2 | 3.00 | |
| c.314C > A (p.S105*) | Exon 2 | Cu1 | Nonsense | 1 | 1.50 | |
| c.1470C > A (p.C490*) | Exon 3 | Cu5 | Nonsense | 1 | 1.50 | |
| c.2139C > G (p.Y713*) | Exon 8 | TM2/TM3 | Nonsense | 1 | 1.50 | Novel |
| c.2145C > A (p.Y715*) | Exon 8 | TM2/TM3 | Nonsense | 1 | 1.50 | |
| c.2268G > A (p.A756A) | Exon 8 | TM3/TM4 | Synonymous | 1 | 1.50 | Novel |
| c.2272A > G (p.R758G) | Exon 8 | TM3/TM4 | Missense | 1 | 1.50 | Novel |
| c.2320_2321insTTGCCCAGGGCA (p.L776Qfs*695) | Exon 8 | TM4 | Fame-shift | 1 | 1.50 | Novel |
| c.3220G > A (p.A1074T) | Exon 14 | ATP loop | Missense | 1 | 1.50 | Novel |
| c.3244-2A > G | Exon 15 | ATP loop | Splicing | 1 | 1.50 | |
| c.3316G > A (p.V1106I) | Exon 15 | ATP loop | Missense | 1 | 1.50 | |
| c.3446G > A (p.G1149E) | Exon 16 | ATP loop | Missense | 1 | 1.50 | |
| c.3452G > A (p.R1151H) | Exon 16 | ATP loop | Missense | 1 | 1.50 | |
| c.3587A > G (p.D1196G) | Exon 17 | ATP hinge | Missense | 1 | 1.50 | |
| c.4003G > C (p.G1335R) | Exon 19 | TM7 | Missense | 1 | 1.50 | |
| c.4059G > A (p.W1353*) | Exon 20 | TM8 | Nonsense | 1 | 1.50 | |
| c.4064G > A (p.G1355D) | Exon 20 | TM8 | Missense | 1 | 1.50 | |

*Note: WD, Wilson's disease; Cu, metal-binding domain; TM, transmembrane domain; ATPase, copper (or silver)-translocating P-type ATPase, domain.*

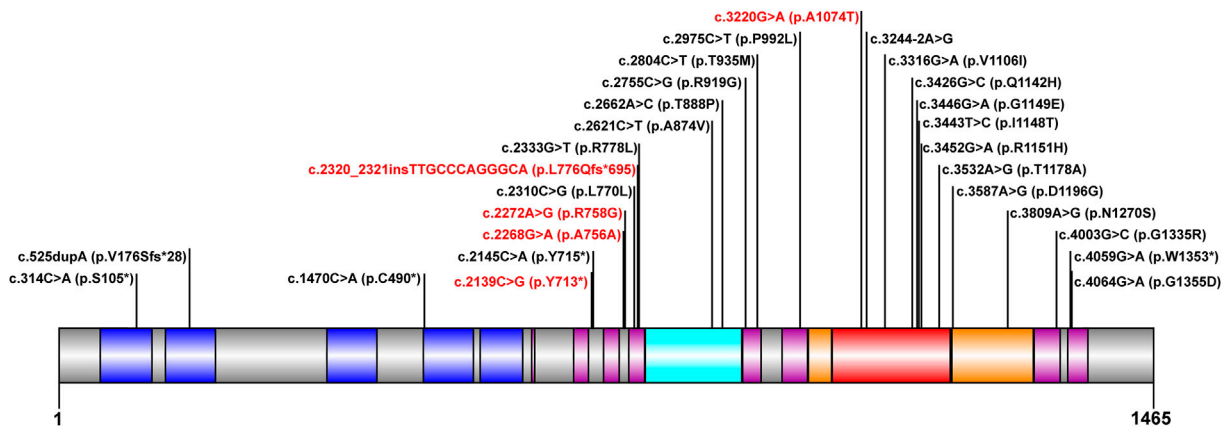


**FIGURE 1 |** Scheme of ATP7B with functional regions and mutations reported in our cohort. The metal binding unit, transmembrane domain, actuator domain, phosphorylation domain, and nucleotide-binding domain are colored in blue, purple, cyan, orange, and red, respectively. The novel mutations detected in this study are in red.

(4) Coombs negative hemolytic anemia with elevated serum copper (1 point);
(5) quantitative determination of liver copper: normal (−1 point), not more than 5 ULN (1 point), and greater than 5 ULN (2 points). Rhodanine staining of hepatocytes is positive (if the quantitative determination of liver copper cannot be obtained) (1 point);
(6) urine copper in the absence of acute hepatitis: normal (0 points), which is 1–2 ULN (1 point), more than 2 ULN (2 points), application of 2 doses of 0.5 g D-penicillamine, and the copper content is more than 5 ULN (2 points);
(7) analysis of gene mutation: pathogenic mutations on both chromosomes (4 points), pathogenic mutations on a single

**TABLE 3 |** Diagnosis score of the cases with WD.

| Case | Corneal K–F ring | Neurologic symptoms | CP | Coombs-negative hemolytic anemia | Liver copper | 24-h urinary copper | Mutation analysis | Total score |
|---|---|---|---|---|---|---|---|---|
| Case 1 | 0 | 0 | 2 | 0 | – | 2 | 4 | 8 |
| Case 2 | 0 | 0 | 2 | 0 | – | 2 | 4 | 8 |
| Case 3 | 0 | 0 | 2 | 0 | – | 2 | 4 | 8 |
| Case 4 | 0 | 0 | 2 | 0 | – | 2 | 4 | 8 |
| Case 5 | 0 | 0 | 2 | 0 | – | 2 | 4 | 8 |
| Case 6 | 0 | 0 | 2 | 0 | – | 2 | 4 | 8 |
| Case 7 | 0 | 0 | 2 | 0 | – | 1 | 4 | 7 |
| Case 8 | 0 | 0 | 2 | 0 | – | 2 | 4 | 8 |
| Case 9 | 0 | 0 | 2 | 0 | – | 2 | 4 | 8 |
| Case 10 | 0 | 0 | 2 | 0 | – | 2 | 4 | 8 |
| Case 11 | 0 | 0 | 2 | 0 | – | 2 | 4 | 8 |
| Case 12 | 0 | 0 | 2 | 0 | – | 2 | 4 | 8 |
| Case 13 | 0 | 0 | 2 | 0 | – | 1 | 4 | 7 |
| Case 14 | 0 | 0 | 2 | 0 | – | 2 | 4 | 8 |
| Case 15 | 0 | 0 | 2 | 0 | – | 2 | 4 | 8 |
| Case 16 | 0 | 0 | 2 | 0 | – | 1 | 4 | 7 |
| Case 17 | 0 | 0 | 2 | 0 | – | 2 | 4 | 8 |
| Case 18 | 0 | 0 | 2 | 0 | – | 2 | 4 | 8 |
| Case 19 | 0 | 0 | 2 | 0 | – | 2 | 4 | 8 |
| Case 20 | 0 | 0 | 2 | 0 | – | 2 | 4 | 8 |
| Case 21 | 0 | 0 | 2 | 0 | – | 2 | 4 | 8 |
| Case 22 | 0 | 0 | 2 | 0 | – | 2 | 4 | 8 |
| Case 23 | 0 | 0 | 2 | 0 | – | 1 | 4 | 7 |
| Case 24 | 0 | 0 | 2 | 0 | – | 2 | 4 | 8 |
| Case 25 | 0 | 0 | 2 | 0 | – | 2 | 4 | 8 |
| Case 26 | 0 | 0 | 2 | 0 | – | 2 | 4 | 8 |
| Case 27 | 0 | 0 | 2 | 0 | – | 2 | 4 | 8 |
| Case 28 | 0 | 0 | 2 | 0 | – | 2 | 4 | 8 |
| Case 29 | 0 | 0 | 2 | 0 | – | 2 | 4 | 8 |
| Case 30 | 0 | 0 | 2 | 1 | – | 2 | 4 | 9 |

*Note: WD, Wilson's disease; K–F ring, Kayser–Fleischer ring; CP, ceruloplasmin; -, no data.*

chromosome (1 point), and no pathogenic mutations (0 points).

If the total score is ≥4 points, the possibility of WD is high; if the score is 3 points, it is likely to be WD, but more tests are needed (liver biopsy is required); and if the score is ≤2 points, it is unlikely to be WD. According to the aforementioned criteria, all of the 30 cases were ≥4 points (without checking for liver copper level, the score was from 7 to 9) (**Table 3**). Since the liver biopsy was invasive, and their parents did not agree to do it, no liver biopsy was performed. Even if the liver biopsy is normal, we subtract one point, and it is still more than four points. Therefore, all of the 30 cases could be diagnosed as WD, and the genetic results confirmed our diagnosis.

## 3.4 Follow-Up Record and Prognosis Evaluation

The follow-up time was from 1 month to 4 years and 2 months after diagnosis. In detail, 28 of 30 cases (93.3%) were successfully recorded during the follow-up, and the other 2 cases were lost. In particular, 27 cases used basic treatment, including a low-copper diet, oral zinc preparations, and vitamins B, while 25 of them were treated with penicillamine. In total, 27 cases (90%) survived and had good recovery of liver function during the course of treatment, while 20 cases (20/25) were still treated with penicillamine and treatment for 5 cases was stopped. However, 1 child (3.3%) died of acute liver failure (**Figure 2**).

# 4 DISCUSSION

The clinical manifestations of children with WD may be diverse due to the starting time of treatment (Lorincz, 2010; Moores et al., 2012). In general, the copper excretion mechanism is not yet fully developed in newborn babies and becomes more effective within the first year after their birth. However, the key pathways of copper excretion in patients with WD fail to develop or have dysfunction, which leads to copper accumulation during the patient's life, gradually producing various clinical symptoms (Manolaki et al., 2009). Although WD is diagnosed in patients aged 5–35 years (mean, 13 years) (Lin et al., 2014), younger and older patients (>70) are also diagnosed (Stremmel et al., 1991; European Association for Study of Liver, 2012; Lin et al., 2014; Wiernicka et al., 2017). A study of 143 children with WD showed that 21 (15%) of them developed abnormal liver function before the age of 5 years (Wiernicka et al., 2017). At an average age of 9–13 years, the most common initial

presentation of children with WD is liver disease (Saito, 1987; Walshe, 1989). Moreover, about 8–10% of children with WD have chronic active hepatitis (Gitlin, 2003). As our cases were from 2 years old to 11 years and 4 months old (5.08 ± 2.06 years), all of them were asymptomatic and just showed up with elevated ALT. Previously, Japanese researchers have suggested that ALT could be the first parameter to screen children with WD between the ages 4 and 8 years (Hayashi et al., 2019), which was similar to our cases. In a previous study involving children and adults, liver presentation was more common in female patients, while neurological presentation was more common in male patients (Ferenci et al., 2019). However, our cases had hepatic presentations only, and the male/female relationship with WD needs to be further investigated in children.

Furthermore, in our group, no corneal K–F ring was detected, making it significantly different from the cases aged 20–30 years old reported in other studies (Bandmann et al., 2015). In addition, older patients (>15 years) are more likely to be diagnosed with neurological manifestations (Oder et al., 1991). The most common age at which WD develops neurological symptoms is 15–21 years (Saito, 1987; Oder et al., 1991; Lorincz, 2010; Žigrai et al., 2020). The discrepancy in the age of WD onset probably reflects variations in gene mutation and penetrance, extragenic factors, and other environmental factors (e.g., diet) (Ala and Schilsky, 2004). However, our cases were younger and were not accompanied by neurological manifestations, and 12 cases of the brain MRI were all negative. We believe that these young children with WD without neurological symptoms do not need to be routinely evaluated by brain MRI.

According to previous reports, the biochemical examination showed that 69.8% of patients with WD have low serum CP, and a serum CP of less than 20 mg/dL has very good accuracy in diagnosing WD (Kim et al., 2015). Furthermore, low CP had a sensitivity of 77–99% and a specificity of 55–88.2% (Ryan et al., 2019). In addition, research reported that 24-h urinary copper levels were increased in all patients (100%), and a level higher than 100 μg/24 h was useful for diagnosing WD (Vieira et al., 2012). In our study, all of the cases had high urinary copper levels (more than 40 μg/24 h) and low serum CP (less than 10 mg/dl). Meanwhile, a high urinary copper level and low serum CP had good diagnostic accuracy for WD (Aksu et al., 2018). Therefore, our results also support this argument.

WD is caused by homozygous or compound heterozygous mutations within *ATP7B*. At present, the human gene mutation database has more than 1,000 mutations of the *ATP7B* gene reported, including missense/nonsense mutations, splice site mutations, small deletion/insertion mutations, and frameshift mutations. Mutations can occur anywhere in the gene, including exons, introns, and even promoter regions (Coffey et al., 2013). Furthermore, the mutations of the *ATP7B* gene have genetic heterogeneity in different races and regions. For example, the most common type of mutation in the European population is p.H1069Q,

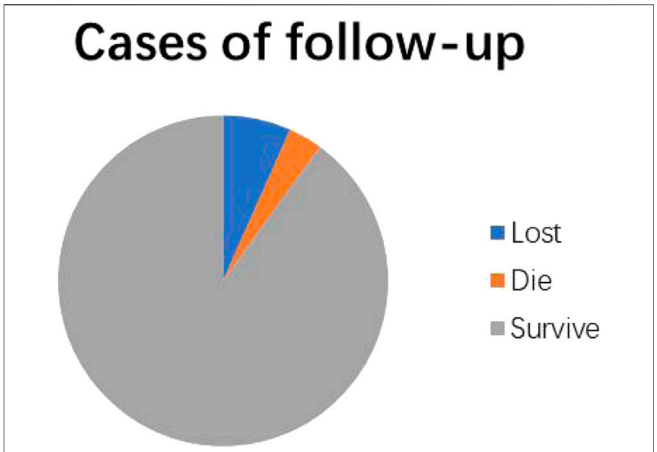


**FIGURE 2 |** Pie chart of statistics in follow-up record and prognosis evaluation.

which is more common in Italy, Sweden, and Romania, with an allele frequency ranging from 30 to 70% (Folhoffer et al., 2007). Contrastingly, the most common type of mutation in the Asian population is the missense mutation p.R778L, which is also the most common mutation in China, South Korea, and Japan, with an allele frequency ranging from 17.3 to 60% (Okada et al., 2000; Liu et al., 2004). Besides p.R778L, other high-frequency mutations include p.P992L and p.Q1399R. Similarly, our study also found that the most abundant mutation type was the missense mutation p.R778L, accounting for 23.0% of the total cases. In addition, the second abundant mutation type in our study was the missense mutation p.I1148T (10.7%). Whether this mutation type is representative of children in southern China remains to be investigated. However, the third abundant mutation type was the missense mutation p.P992L (7.6%), showing consistency with known Asian mutation frequencies. In our study, different gene mutations (affecting different functional domains) of the cases had almost identical clinical phenotypes, which were similar to the previous study (Ferenci et al., 2019). Only one patient died, whose *ATP7B* had three heterozygous mutations, including c.2333G > T (p.R778L), c.4003G > C (p.G1335R), and c.525dupA, and they included two missense mutations and one frameshift mutation, which affected the functional regions of MBU2, TM4, and TM7. Therefore, the more functional domains are affected, the worse the prognosis may be.

At present, the diagnosis of WD mainly relies on typical clinical manifestations, laboratory tests, and genetic testing (Huster, 2010). Early diagnosis and intervention are essential to delay the progression of the disease and prevent irreversible sequelae. In our study, 30 cases were diagnosed with an elevated ALT level as the first symptom, together with a decreased CP level, an increased 24-h urinary copper level, and *ATP7B* mutations, suggesting that these three parameters (namely, elevated ALT, decreased CP level, and increased 24-h urinary copper level) are closely related to the early

diagnosis of WD in about 5-year-old children in southern China. Thus, we propose that the combined detection of elevated ALT, decreased ceruloplasmin level, and increased 24-h urinary copper level can be useful for an early diagnosis of WD in about 5-year-old asymptomatic children in southern China. In recent years, some researchers thought that genetic screening following serum CP testing reduced costs and facilitated prioritization of non-invasive methods for definitive diagnosis, as well as in asymptomatic or family history cases (Barada et al., 2017; García-Villarreal et al., 2021). Furthermore, other researchers believed that the serum CP level, 24-h urinary copper excretion, and K–F rings could be used to identify patients with WD (Dong et al., 2021). Patients with serum CP levels below 12 mg/dl and children with urinary copper excretion above 40 μg/24 h should undergo genetic testing for WD. As WD needs to identify the diseases, namely, Menkes disease, occipital horn syndrome (OHS), Indian childhood cirrhosis (ICC), and some other diseases and in specific subgroups defined by age, ethnicity, or clinical subgroups, our three parameters (elevated ALT, decreased CP level, and increased 24-h urinary copper level) may not be suitable (Lorincz, 2018; Ryan et al., 2019). However, they can be useful for the early diagnosis of WD in about 5-year-old asymptomatic children in southern China.

Until now, WD was one of the few genetic diseases that could be controlled. The treatment principles are early diagnosis and treatment, lifetime care, and personalized protocol. Current treatment measures include drug therapy, surgical treatment, gene and cell therapy, and rehabilitation (Wiggelinkhuizen et al., 2009). Currently, penicillamine is one of the classic drugs for the treatment of hepatolenticular degeneration due to its effectiveness and cheap price. Studies have shown that certain molecular chaperone drugs (such as 4-phenylbutyric acid) and p38 and JNK inhibitors can correct the mislocalization of the mutant protein and restore the transport function of this protein (Mulligan and Bronstein, 2020). Furthermore, the small-molecule DPM-1001 can effectively reduce the copper deposition in the liver and the brain in the hepatolenticular degeneration mouse model (Krishnan et al., 2018). In particular, personalized cell and (or) gene therapy is the current research hot spot. Its fundamental purpose is to restore the function of *ATP7B*-mediated hepatic and bile duct excretion of copper (Murillo et al., 2016), and it may be the most promising treatment in the future. The incidence of acute liver failure in WD has previously been reported to be 15–47% (Das et al., 2021; Devarbhavi et al., 2014; Rukunuzzaman, 2015). Among the successful follow-up cases in this group, except for one case (3.3%) with liver failure, the liver function recovered well after the application of penicillamine, oral zinc preparations, B vitamins, and low-copper diet, etc. It showed that as long as early diagnosis and early treatment had been applied, there would be good clinical results in prognosis for children carrying genetic mutations of the *ATP7B* gene. Our low incidence of acute liver failure may be related to sample size and duration of follow-up.

## 5 CONCLUSION

WD is an autosomal recessive genetic disease with diverse clinical manifestations. The group of patients reported in this study came from cities in southern China. Early diagnosis and treatment of WD would substantially increase the survival rate and have a better prognosis. All of these cases had elevated ALT, decreased ceruloplasmin content, and an elevated 24-h urinary copper level, indicating solid first manifestation and potential large-scale screening methods to diagnose WD at an early stage in 5-year-old asymptomatic children in southern China. Although this initial diagnosis can be further confirmed by using genetic testing of the *ATP7B* gene, it should be confirmed by further research with larger sample sizes.

## DATA AVAILABILITY STATEMENT

The datasets for this article are not publicly available due to concerns regarding participant/patient anonymity. Requests to access the datasets should be directed to the corresponding authors.

## ETHICS STATEMENT

The studies involving human participants were reviewed and approved by the Ethics Committee of Shenzhen Children's Hospital. Written informed consent was obtained from the individual(s) and minor(s)' legal guardian/next of kin, for the publication of any potentially identifiable images or data included in this article.

## AUTHOR CONTRIBUTIONS

YC and SZ designed the experiments. JZ, QZ, YZ, and MC performed the experiments and analyzed data. JZ, YC, and SZ wrote the manuscript. YC critically commented and revised it.

## FUNDING

This work was supported by Shenzhen Fund for Guangdong Provincial High level Clinical Key Specialties (No. SZGSP012) and the Science Technology and Innovation Committee of Shenzhen (2021N062-JCYJ20210324115408023).

## ACKNOWLEDGMENTS

We gratefully thank Dr. Di Cui (Running Gene Inc.) for her assistance in genetic analysis.

## REFERENCES


Aksu, A. Ü., Sarı, S., Gürkan, Ö. E., and Dalgıç, B. (2018). Urinary 24-hour Copper Excretion at the Time of Diagnosis in Children with Wilson's Disease. *Acta Gastroenterol. Belg.* 81, 410–414.

Ala, A., and Schilsky, M. L. (2004). Wilson Disease: Pathophysiology, Diagnosis, Treatment, and Screening. *Clin. Liver Dis.* 8, 787–805. doi:10.1016/j.cld.2004.06.005

Bandmann, O., Weiss, K. H., and Kaler, S. G. (2015). Wilson's Disease and Other Neurological Copper Disorders. *Lancet Neurol.* 14, 103–113. doi:10.1016/s1474-4422(14)70190-5

Barada, K., El Haddad, A., Katerji, M., Jomaa, M., and Usta, J. (2017). Wilson's Disease in Lebanon and Regional Countries: Homozygosity and Hepatic Phenotype Predominance. *World J. Gastroenterol.* 23, 6715–6725. doi:10.3748/wjg.v23.i36.6715

Chen, Y.-C., Yu, H., Wang, R.-M., Xie, J.-J., Ni, W., Zhang, Y., et al. (2019). Contribution of Intragenic Deletions to Mutation Spectrum in Chinese Patients with Wilson's Disease and Possible Mechanism Underlying ATP7B Gross Deletions. *Parkinsonism Relat. Disord.* 62, 128–133. doi:10.1016/j.parkreldis.2019.01.001

Coffey, A. J., Durkie, M., Hague, S., McLay, K., Emmerson, J., Lo, C., et al. (2013). A Genetic Study of Wilson's Disease in the United Kingdom. *Brain* 136, 1476–1487. doi:10.1093/brain/awt035

Das, M. C., Sen Sarma, M., Srivastava, A., Yachha, S. K., and Poddar, U. (2021). Effect of Chelation Therapy in Pediatric Wilson's Disease: Liver and Endoscopic Outcome. *J. Hepatobiliary Pancreat. Sci.* 28, 336–345. doi:10.1002/jhbp.812

Devarbhavi, H., Singh, R., Adarsh, C. K., Sheth, K., Kiran, R., and Patil, M. (2014). Factors that Predict Mortality in Children with Wilson Disease Associated Acute Liver Failure and Comparison of Wilson Disease Specific Prognostic Indices. *J. Gastroenterol. Hepatol.* 29, 380–386. doi:10.1111/jgh.12356

Dong, Y., Wang, R.-M., Yang, G.-M., Yu, H., Xu, W.-Q., Xie, J.-J., et al. (2021). Role for Biochemical Assays and Kayser-Fleischer Rings in Diagnosis of Wilson's Disease. *Clin. Gastroenterol. Hepatol.* 19, 590–596. doi:10.1016/j.cgh.2020.05.044

European Association for Study of Liver (2012). EASL Clinical Practice Guidelines: Wilson's Disease. *J. Hepatol.* 56, 671–685. doi:10.1016/j.jhep.2011.11.007

Ferenci, P., Stremmel, W., Członkowska, A., Szalay, F., Viveiros, A., Stättermayer, A. F., et al. (2019). Age and Sex but Not ATP7B Genotype Effectively Influence the Clinical Phenotype of Wilson Disease. *Hepatology* 69, 1464–1476. doi:10.1002/hep.30280

Fernando, M., van Mourik, I., Wassmer, E., and Kelly, D. (2020). Wilson disease in children and adolescents. *Front. Med. (Lausanne)* 105, 499-–505. doi:10.1136/archdischild-2018-315705

Folhoffer, A., Ferenci, P., Csak, T., Horvath, A., Hegedus, D., Firneisz, G., et al. (2007). Novel Mutations of the ATP7B Gene Among 109 Hungarian Patients with Wilson's Disease. *Eur. J. Gastroenterol. Hepatol.* 19, 105–111. doi:10.1097/01.meg.0000223904.70492.0b

García-Villarreal, L., Hernández-Ortega, A., Sánchez-Monteagudo, A., Peña-Quintana, L., Ramírez-Lorenzo T, T., and Riaño, M. (2021). Wilson Disease: Revision of Diagnostic Criteria in a Clinical Series with Great Genetic Homogeneity. *J. Gastroenterol.* 56, 78–89. doi:10.1007/s00535-020-01745-0

Gitlin, J. D. (2003). Wilson Disease. *Gastroenterology* 125, 1868–1877. doi:10.1053/j.gastro.2003.05.010

Hayashi, H., Watanabe, K., Inui, A., Kato, A., Tatsumi, Y., Okumura, A., et al. (2019). Alanine Aminotransferase as the First Test Parameter for Wilson's Disease. *J. Clin. Transl Hepatol.* 7, 293–296. doi:10.14218/JCTH.2019.00042

Huster, D. (2010). Wilson Disease. *Best Pract. Res. Clin. Gastroenterol.* 24, 531–539. doi:10.1016/j.bpg.2010.07.014

Kim, J. A., Kim, H. J., Cho, J. M., Oh, S. H., Lee, B. H., Kim, G.-H., et al. (2015). Diagnostic Value of Ceruloplasmin in the Diagnosis of Pediatric Wilson's Disease. *Pediatr. Gastroenterol. Hepatol. Nutr.* 18, 187–192. doi:10.5223/pghn.2015.18.3.187

Krishnan, N., Felice, C., Rivera, K., Pappin, D. J., and Tonks, N. K. (2018). DPM-1001 Decreased Copper Levels and Ameliorated Deficits in a Mouse Model of Wilson's Disease. *Genes Dev.* 32, 944–952. doi:10.1101/gad.314658.118

Lin, L.-J., Wang, D.-X., Ding, N.-N., Lin, Y., Jin, Y., and Zheng, C.-Q. (2014). Comprehensive Analysis on Clinical Features of Wilson's Disease: an Experience over 28 Years with 133 Cases. *Neurol. Res.* 36, 157–163. doi:10.1179/1743132813y.0000000262

Liu, X.-Q., Zhang, Y. F., Liu, T. T., Hsiao, K. J., Zhang, J. M., Gu, X. F., et al. (2004). Correlation of ATP7B Genotype with Phenotype in Chinese Patients with Wilson Disease. *World J. Gastroenterol.* 10, 590–593. doi:10.3748/wjg.v10.i4.590

Lorincz, M. T. (2010). Neurologic Wilson's Disease. *Ann. N. Y Acad. Sci.* 1184, 173–187. doi:10.1111/j.1749-6632.2009.05109.x

Lorincz, M. T. (2018). Wilson Disease and Related Copper Disorders. *Handb Clin. Neurol.* 147, 279–292. doi:10.1016/b978-0-444-63233-3.00018-x

Manolaki, N., Nikolopoulou, G., Daikos, G. L., Panagiotakaki, E., Tzetis, M., Roma, E., et al. (2009). Wilson Disease in Children: Analysis of 57 Cases. *J. Pediatr. Gastroenterol. Nutr.* 48, 72–77. doi:10.1097/mpg.0b013e31817d80b8

Meranthi, F., Indra, V. M., Evangeline, W., et al. (2020). Wilson Disease in Children and Adolescents. *Arch. Dis. Child.* 105, 499–505.

Moores, A., Fox, S., Lang, A., and Hirschfield, G. (2012). Wilson Disease: Canadian Perspectives on Presentation and Outcomes from an Adult Ambulatory Setting. *Can. J. Gastroenterol.* 26, 333–339. doi:10.1155/2012/123431

Mulligan, C., and Bronstein, J. M. (2020). Wilson Disease. *Neurol. Clin.* 38, 417–432. doi:10.1016/j.ncl.2020.01.005

Murillo, O., Luqui, D. M., Gazquez, C., Martinez-Espartosa, D., Navarro-Blasco, I., Monreal, J. I., et al. (2016). Long-term Metabolic Correction of Wilson's Disease in a Murine Model by Gene Therapy. *J. Hepatol.* 64, 419–426. doi:10.1016/j.jhep.2015.09.014

Oder, W., Grimm, G., Kollegger, H., Ferenci, P., Schneider, B., and Deecke, L. (1991). Neurological and Neuropsychiatric Spectrum of Wilson's Disease: a Prospective Study of 45 Cases. *J. Neurol.* 238, 281–287. doi:10.1007/BF00319740

Okada, T., Shiono, Y., Hayashi, H., Satoh, H., Sawada, T., Suzuki, A., et al. (2000). Mutational Analysis ofATP7Band Genotype-Phenotype Correlation in Japanese with Wilson's Disease. *Hum. Mutat.* 15, 454–462. doi:10.1002/(sici)1098-1004(200005)15:5<454:aid-humu7>3.0.co;2-j

Richards, S., Aziz, N., Bale, S., Bick, D., Das, S., Gastier-Foster, J., et al. (2015). Standards and Guidelines for the Interpretation of Sequence Variants: a Joint Consensus Recommendation of the American College of Medical Genetics and Genomics and the Association for Molecular Pathology. *Genet. Med.* 17, 405–424. doi:10.1038/gim.2015.30

Rukunuzzaman, M. (2015). Wilson's Disease in Bangladeshi Children: Analysis of 100 Cases. *Pediatr. Gastroenterol. Hepatol. Nutr.* 18, 121–127. doi:10.5223/pghn.2015.18.2.121

Ryan, A., Nevitt, S. J., Tuohy, O., and Cook, P. (2019). Biomarkers for Diagnosis of Wilson's Disease. *Cochrane Database Syst. Rev.* 2019, CD012267. doi:10.1002/14651858.cd012267.pub2

Saito, T. (1987). Presenting Symptoms and Natural History of Wilson Disease. *Eur. J. Pediatr.* 146, 261–265. doi:10.1007/bf00716470

Stenson, P. D., Mort, M., Ball, E. V., Evans, K., Hayden, M., Heywood, S., et al. (2017). The Human Gene Mutation Database: towards a Comprehensive Repository of Inherited Mutation Data for Medical Research, Genetic Diagnosis and Next-Generation Sequencing Studies. *Hum. Genet.* 136, 665–677. doi:10.1007/s00439-017-1779-6

Stremmel, W., Meyerrose, K. W., Niederau, C., Hefter, H., Kreuzpaintner, G., Strohmeyer, G., et al. (1991). Wilson Disease: Clinical Presentation, Treatment, and Survival. *Ann. Intern. Med.* 115, 720–726. doi:10.7326/0003-4819-115-9-720

Vieira, J., Oliveira, P. V., Juliano, Y., Warde, K. R. J., Deguti, M. M., Barbosa, E. R., et al. (2012). Urinary Copper Excretion before and after Oral Intake of D-Penicillamine in Parents of Patients with Wilson's Disease. *Dig. Liver Dis.* 44, 323–327. doi:10.1016/j.dld.2011.11.001

Walshe, J. M. (1989). Wilson's Disease Presenting with Features of Hepatic Dysfunction: a Clinical Analysis of Eighty-Seven Patients. *Q. J. Med.* 70, 253–263.

Wiernicka, A., Dądalski, M., Jańczyk, W., Kamińska, D., Naorniakowska, M., Hüsing-Kabar, A., et al. (2017). Early Onset of Wilson Disease: Diagnostic Challenges. *J. Pediatr. Gastroenterol. Nutr.* 65, 555–560. doi:10.1097/mpg.0000000000001700

Wiggelinkhuizen, M., Tilanus, M. E. C., Bollen, C. W., and Houwen, R. H. J. (2009). Systematic Review: Clinical Efficacy of Chelator Agents and Zinc in the Initial Treatment of Wilson Disease. *Aliment. Pharmacol. Ther.* 29, 947–958. doi:10.1111/j.1365-2036.2009.03959.x

Xiao, H., Deng, S., Deng, X., Gu, S., Yang, Z., Yin, H., et al. (2019). Mutation Analysis of the ATP7B Gene in Seven Chinese Families with Wilson's Disease. *Digestion* 99, 319–326. doi:10.1159/000493314

Žigrai, M., Vyskočil, M., Tóthová, A., Vereš, P., Bluska, P., Valkovič, P., et al. (2020). Late-Onset Wilson's Disease. *Front. Med. (Lausanne)* 7, 26. doi:10.3389/fmed.2020.00026

**Conflict of Interest:** The authors declare that the research was conducted in the absence of any commercial or financial relationships that could be construed as a potential conflict of interest.

**Publisher's Note:** All claims expressed in this article are solely those of the authors and do not necessarily represent those of their affiliated organizations, or those of the publisher, the editors, and the reviewers. Any product that may be evaluated in this article, or claim that may be made by its manufacturer, is not guaranteed or endorsed by the publisher.

frontiers in Genetics

ORIGINAL RESEARCH
published: 28 March 2022
doi: 10.3389/fgene.2022.822832

# Clinical and Genetic Characteristics of *IKZF1* Mutation in Chinese Children With B-Cell Acute Lymphoblastic Leukemia

*Jingying Zhang*[1,2,3], *Xiao-Jun Xu*[1,2,3], *Lixia Liu*[4], *Hua Song*[1,2,3], *Heping Shen*[1,2,3], *Weiqun Xu*[1,2,3], *Fenying Zhao*[1,2,3], *Juan Liang*[1,2,3], *Chan Liao*[1,2,3], *Yan Wang*[1,2,3], *Tian Xia*[1,2,3], *Shanbo Cao*[4], *Yongmin Tang*[1,2,3]*, *Jiayue Qin*[4]* and *Diying Shen*[1,2,3]*

[1]Division/Center of Pediatric Hematology-Oncology, The Children's Hospital of Zhejiang University School of Medicine, Hangzhou, China, [2]The Pediatric Leukemia Diagnostic and Therapeutic Technology Research Center of Zhejiang Province, Hangzhou, China, [3]National Clinical Research Center for Child Health, Hangzhou, China, [4]Acornmed Biotechnology Co., Ltd., Tianjin, China

OPEN ACCESS

**Edited by:**
Sadeq Vallian,
University of Isfahan, Iran

**Reviewed by:**
Xujie Zhao,
St. Jude Children's Research Hospital, United States
Andrea Grioni,
Novartis Institutes for BioMedical Research, Switzerland

***Correspondence:**
Diying Shen
shendiying@zju.edu.cn
Jiayue Qin
jyqin@live.cn
Yongmin Tang
Y_M_Tang@zju.edu.cn

**Specialty section:**
This article was submitted to Human and Medical Genomics, a section of the journal Frontiers in Genetics

**Received:** 26 November 2021
**Accepted:** 22 February 2022
**Published:** 28 March 2022

**Citation:**
Zhang J, Xu X-J, Liu L, Song H, Shen H, Xu W, Zhao F, Liang J, Liao C, Wang Y, Xia T, Cao S, Tang Y, Qin J and Shen D (2022) Clinical and Genetic Characteristics of IKZF1 Mutation in Chinese Children With B-Cell Acute Lymphoblastic Leukemia. Front. Genet. 13:822832. doi: 10.3389/fgene.2022.822832

Acute lymphoblastic leukemia (ALL) is a malignancy associated with altered lymphoid precursor hyperplasia and accompanied with different genetic mutations. Few studies have been reported on the association between gene mutations and clinical features of *IKZF1* mutation in children with B-cell ALL (B-ALL). We investigated clinical and genetic characteristics in 200 newly diagnosed pediatric B-ALL through multiplex ligation-dependent probe amplification (MLPA) and targeted next-generation sequencing (NGS) method. We found that *IKZF1* mutations, including large segment deletions, small insertions or deletions (InDels) and single nucleotide variations (SNVs), were detected in 22 patients with a positive mutation rate of 11.0%. *IKZF1* mutation was significantly associated with higher WBC count ($19.38 \times 10^9$/L vs. $5.80 \times 10^9$/L, $p = 0.002$). Compared with *IKZF1* wild-type cases, a higher frequency of *IL7R* gene mutation was discovered in *IKZF1* mutant cases (9.1% vs. 0.0%, $p = 0.012$). Patients with *IKZF1* mutation were less sensitive to glucocorticoid induction than patients without *IKZF1* mutation (63.6% vs. 9.0%, $p < 0.001$). On the 15th day of induction, minimal residual disease (MRD) > $10^{-3}$ level were higher in *IKZF1* mutant patients than wild-type patients (45.5% vs. 22.3%, $p = 0.018$). In conclusion, our study reveals the association between genetic mutations and clinical features in Chinese children with B-ALL, which might contribute to molecular classification, risk stratification and prognosis evaluation, and provide new ideas for targeted therapy in ALL.

**Keywords: IKZF1 mutation, B-cell acute lymphoblastic leukemia, genetic characteristics, clinical features, targeted next-generation sequencing**

## INTRODUCTION

Acute lymphoblastic leukemia (ALL) is a malignancy associated with altered lymphoid precursor hyperplasia, and about 75% of children with ALL develop chromosomal changes, such as aneuploidy, translocation, copy number changes, or gene rearrangements (Holmfeldt et al., 2013). With the wide development of genome-wide analysis, some ALL children have *IKZF1* mutation, including large segment deletion, small insertions or deletions (InDels) and single nucleotide variations (SNVs), which is considered to be a marker of poor prognosis in pediatric ALL.

**TABLE 1 |** Clinical and genetic features in 200 B-ALL patients.

| Characteristics | Total cohort, *N* = 200 |
|---|---|
| Male, n (%) | 106 (53.0%) |
| Female, n (%) | 94 (47.0%) |
| Age, M (range) years | 3.71 (0.05–16.25) |
| WBC, M (range) $\times10^9$/L | 6.49 (0.35–544.34) |
| Lymphocyte, M (range) $\times10^9$/L | 64.80 (0.06–97.10) |
| Neutrophil, M (range) $\times10^9$/L | 10.00 (0.00–80.20) |
| Hemoglobin, M (range) ×g/L | 81.00 (27.00–129.00) |
| Platelet, M (range) $\times10^9$/L | 60.00 (3.00–483.00) |
| Insensitive to glucocorticoid, n (%) | 30 (15.0%) |
| MRD $>10^{-3}$ (the 15th day after treatment) n (%) | 49 (24.9%) |
| MRD $>10^{-4}$ (the 33rd day after treatment) n (%) | 12 (6.0%) |
| Low risk, n (%) | 80 (40.0%) |
| Intermediate risk, n (%) | 70 (35.0%) |
| High risk, n (%) | 50 (25.0%) |

*IKZF1* gene is located on chromosome 7p12.2 band and consists of 8 exons, encoding transcription factor IKAROS, which plays a key regulatory role in lymphocyte production (Rebollo & Schmitt, 2003). IKAROS contains six zinc finger structures, four of which are located in DNA binding domains encoded by exons 4 to 6 and are essential for maintaining IKAROS tumor suppressor function. The remaining 2 zinc fingers are encoded by exon 8 and mediate IKAROS as homologous dimerization or heterodimerization with other transcription factors of the family, such as AIOLOS and spirochetes (Stanulla et al., 2020). The presence of *IKZF1* deletion was associated with older age at diagnosis, higher white blood cell count, and higher minimal residual disease (MRD) levels after induction and consolidation (Mullighan et al., 2009; Waanders et al., 2011; Asai et al., 2013; Dorge et al., 2013; Palmi et al., 2013; Volejnikova et al., 2013; Yamashita et al., 2013; Vrooman et al., 2018; Yeoh et al., 2018). However, the distribution of *IKZF1* mutation in Chinese children with B-cell ALL (B-ALL) has been relatively poorly studied.

Here, we systematically analyzed the clinical and genetic characteristics of Chinese B-ALL children with *IKZF1* mutation in our single center. These data may provide evidence for risk stratification and individualized treatment for B-ALL.

# METHODS

## Patients

A retrospective analysis was performed on 200 newly diagnosed patients with B-ALL aged 0–16 years who were admitted to the Children Hospital of Zhejiang University School of Medicine from 1 October 2017 to 31 August 2020. The diagnosis of B-ALL was based on the 2016 World Health Organization (WHO) classification criteria for hematopoietic and lymphoid tissue tumors (Arber et al., 2016). All patients were confirmed by comprehensive diagnosis of cytomorphology, immunology, cytogenetics and molecular biology, and complete medical history could be traced. Exclusion criteria: untraceable biological samples; unable to obtain necessary biological information; acute promyelocytic leukemia; other hematologic or non-hematologic tumors. The study was approved by the institutional review board of the Children's Hospital of Zhejiang University Medical College and informed consents were obtained from patients and/or their legal guardians in accordance with the Declaration of Helsinki.

## Chromosome, Leukemia Fusion Gene and Flow Minimal Residual Disease Detection

Chromosomes were tested by Adicon Clinical Laboratory (Hangzhou, China). Leukemia fusion genes were sequenced by Kindstar Globalgene Technology (Wuhan, China). Flow cytometry (FCM) MRD were detected by the Children's Hospital Leukemia Laboratory affiliated to the Children Hospital of Zhejiang University School of Medicine (Hangzhou, China). Hazard groups refer to CCLG-ALL-2008 scheme criteria (Brown et al., 2019; Brown et al., 2020). MRD detection for children examined by FCM: residual status of bone marrow tumor cells after induction ($D_{15}$) and before consolidation ($D_{33}$) treatment.

## Determination of *IKZF1* Large Segment Deletion by Multiplex Ligation-dependent Probe Amplification

Targeted copy number screening of the *IKZF1* gene was performed by multiplex ligation-dependent probe amplification (MLPA). The children's mono-nuclear cells were retained at the initial diagnosis. DNA was extracted and analyzed using the SALSA MLPA KIT P335-B1 ALL-*IKZF1* probemix according to the manufacturer's instructions. This SALSA contained a probe for each *IKZF1* exon. All MLPA reactions, including DNA denaturation, hybridization, ligation, and PCR, were carried out in a 96-well PCR thermocycler. The amplification products were quantified and identified by capillary electrophoresis. Normalization of the data was carried out by dividing the peak area of each probe by the average peak area of the control probes. This normalized peak pattern was divided by the average peak pattern of all the samples in the same experiment. The resulting values were 0–1 for every wild-type peak, 0.5 for heterozygous deletions and 1.5 for heterozygous duplications.

## Targeted Next-Generation Sequencing

DNA was extracted from whole bone marrow collected at diagnosis. Based on next-generation sequencing (NGS) of targeted capture, the mutation hotspots or entire coding region of 185 genes known to mutate frequently in hematological malignancies were sequenced (**Supplementary Table S1**). The following criteria were used to filter raw variant results: average effective sequencing depth on target per sample ≥1,000×; mapping quality ≥30; and base quality ≥30; variant allele frequency (VAF) ≥1% for SNVs and small InDels. Burrows-Wheeler alignment (BWA, version 0.7.12) was

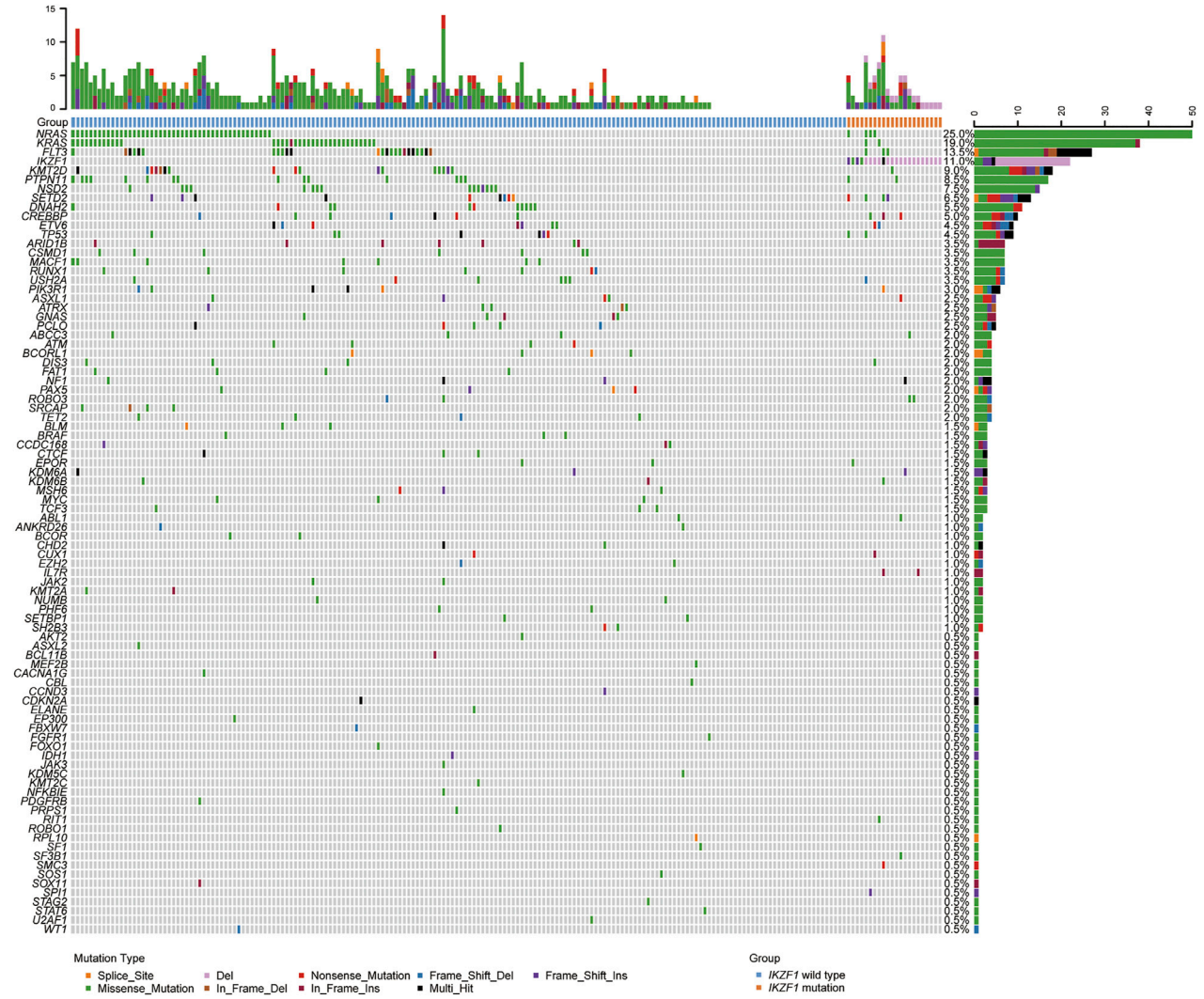


**FIGURE 1 |** Overview of the gene mutations identified by targeted next-generation sequencing and multiplex ligation-dependent probe amplification in 200 B-ALL patients. Heatmap shows the specific mutations in each patient based on different gene mutation types, including large segment deletions, small insertions or deletions, and single nucleotide variations.

performed to align the trimmed reads. MarkDuplicates tool from Picard was used to mark the PCR duplicates. IndelRealigner and BaseRecalibrator from Genome Analysis Toolkit (GATK, version 3.8) were applied for realignment and recalibration of the BWA data, respectively. Variant calling, including SNVs and small InDels, was performed in Mutect2. ANNOVAR software was used to annotate all the variants including 1000G projects, COSMIC, SIFT, and PolyPhen.

## Statistics

Statistical analyses were carried out using R (version 3.5.2) or SPSS software (version 22.0). Mann-Whiney U test was used to compare the continuous variables. Chi-square test or Fisher's exact test was used to compare the categorical variables. $p < 0.05$ was considered to indicate a statistically significant difference.

# RESULTS

## Patient Characteristics

A total of 200 B-ALL patients were enrolled in our study, including 106 males and 94 females, with a median age of 3.71 years (range, 0.05–16.25), as shown in **Table 1**. The median white blood cell (WBC) count, hemoglobin (Hb) concentration, and platelet (PLT) count was $6.49 \times 10^9$/L, 81.00 g/L and $60.00 \times 10^9$/L, respectively. Sixty-eight patients with a hyperdiploid chromosome karyotype (34.0%) were discovered in our cohort. On the 15th day of induction, 49 cases were with MRD $>10^{-3}$ (24.9%). On the 33rd day of induction, 12 cases were with MRD $>10^{-4}$ (6.0%). According to hazard groups from CCLG-ALL-2008 scheme criteria, 80 patents were assigned to the low-risk group (40%), 70 cases were in the intermediate risk group (35.0%) and 50 cases in the high risk group (25.0%). In 200 B-ALL patients, the

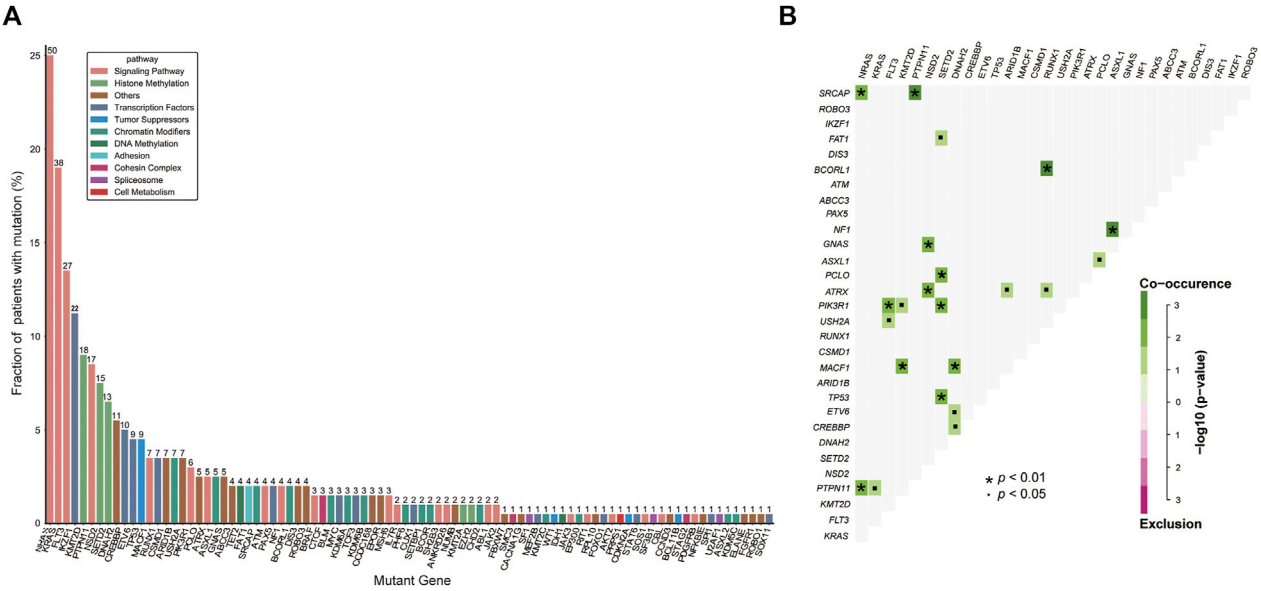


**FIGURE 2 |** Genetic analyses in the whole cohort. **(A)** Histogram shows the frequency of gene mutations detected in the whole cohort according to the different functional groups assigned to each gene. **(B)** Diagram shows pairwise gene mutation correlations on the basis of the mutated genes detected in ≥2% patients. The odds ratio of the correlation is coded by different colors, and the significance level is marked by the symbol in each field.

**TABLE 2 |** Comparison of clinical and genetic features between *IKZF1* mutant and wild-type patients.

| Characteristics | *IKZF1* mutant (*n* = 22) | *IKZF1* wild-type (*n* = 178) | *p-value* |
|---|---|---|---|
| Male, n (%) | 14 (63.6%) | 92 (51.7%) | 0.280 |
| Female, n (%) | 8 (36.4%) | 86 (48.3%) | |
| Age, M (range) years | 5.90 (0.90–13.40) | 3.50 (0.05–16.25) | 0.700 |
| WBC, M (range) $\times 10^9$/L | 19.38 (3.08–544.34) | 5.80 (0.35–515.00) | 0.002 |
| Lymphocyte, M (range) $\times 10^9$/L | 58.50 (8.00–83.90) | 65.70 (0.06–97.10) | 0.190 |
| Neutrophil, M (range) $\times 10^9$/L | 6.00 (2.00–26.00) | 10 (0.00–80.20) | 0.170 |
| Hemoglobin, M (range) ×g/L | 84.00 (32.00–113.00) | 81 (27.00–129.00) | 0.940 |
| Platelet, M (range) $\times 10^9$/L | 43.50 (3.00–167.00) | 62.00 (3.00–483.00) | 0.065 |
| Insensitive to glucocorticoid, n (%) | 14 (63.6%) | 16 (9.0%) | <0.001 |
| MRD $>10^{-3}$, n (%) (the 15th day after treatment) | 10 (45.5%) | 39 (22.3%) | 0.018 |
| MRD $>10^{-4}$, n (%) (the 33rd day after treatment) | 2 (9.1%) | 10 (5.6%) | 0.830 |

overall rate of mutation prevalence was 82.0% (164/200) (**Figure 1**). A total of 88 mutated genes were detected, and the most common mutated gene was *NRAS* (25.0%), followed by *KRAS* (19.0%) and *FLT3* (13.5%) (**Figure 2A**). In total, 553 mutation sites were detected, and nonsynonymous SNV (65.0%) was the most common mutation type (**Figure 1**). Significant associations were discovered between mutated *SETD2* and mutations in *TP53*, *PCLO*, *PIK3R1* and *FAT1*, and between mutated *ASXL1* and *CHD2* and *NF1* mutations (**Figure 2B**).

## Comparison of Clinical and Genetic Characteristics Between *IKZF1* Mutant and Wild-Type Patients

*IKZF1* mutations, including large segment deletions, small InDels and SNVs, were detected in 22 of 200 B-ALL children, with a positive mutation rate of 11.0%. The median WBC count in *IKZF1* mutant children was $19.38 \times 10^9$/L, and was about 4 times higher than that in *IKZF1* wild-type children ($p = 0.002$). Both the median hemoglobin levels and platelet counts were not significantly different between *IKZF1* mutant and wild-type patients. More than half of cases with *IKZF1* mutation were not sensitive to glucocorticoid induction, and the proportion was more than 5 times higher than that of wild-type cases (63.6% vs. 9.0%, $p < 0.001$). On the 15th day of induction, 10 *IKZF1* mutant cases were MRD $>10^{-3}$ by FCM, while 39 *IKZF1* wild-type cases were MRD $>10^{-3}$ (45.5% vs. 22.3%, $p = 0.018$) (**Table 2**).

The incidence of *IKZF1* mutation was shown in **Figure 3A**. 36.0% of *IKZF1* wild-type cases carried a hyperdiploid chromosome karyotype, while only 18.2% of *IKZF1* mutant cases were with hyperdiploid ($p = 0.097$). 97.9% of *TEL-AML1* positive B-ALL children had the wild-type *IKZF1*, and only one case had

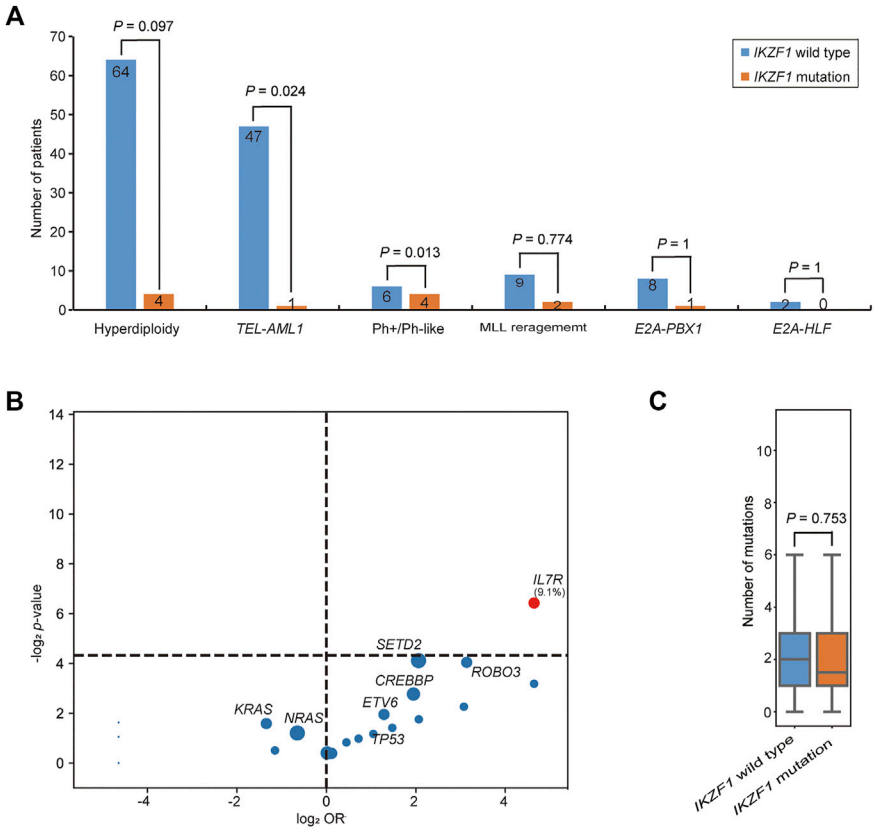


**FIGURE 3 |** Comparison of genetic characteristics between *IKZF1* mutant and wild-type patients. **(A)** Bar chart shows the associations between *IKZF1* mutations and different cytogenetics or genetic aberrations. **(B)** Volcano plot shows the distribution of genetic characteristics according to *IKZF1* mutant and wild-type patients. The x axis indicates the magnitude of association ($log_2$ odds ratio), and the y axis represents the $-log_2$ *p* value. Each circle shows a mutated gene and the size of each circle represents the frequency of the mutated gene. **(C)** Box plot shows the comparison of the number of mutations between *IKZF1* mutant and wild-type patients.

abnormal *IKZF1* (2.1%). For 11 MLL rearrangement positive B-ALL cases, *IKZF1* mutations were detected in 2 cases, and wild-type *IKZF1* was in 9 cases (18.2% vs. 81.8%). *IKZF1* mutation was not detected in the *E2A-HLF* subgroup (0%). Of the 9 *E2A-PBX1* positive cases, only one case had abnormal *IKZF1*, while of the 10 Ph+/Ph-like cases, 4 (40.0%) had *IKZF1* mutations. Compared with *IKZF1* wild-type cases, the interleukin (IL)-7 receptor (IL7R) gene mutation only occurred in *IKZF1* mutant cases, and the difference was statistically significant (9.1% vs. 0.0%, $p = 0.012$) (**Figure 3B**). *SETD2* and *ROBO3* mutations were found in 18.2% and 9.1% of *IKZF1* mutant cases, respectively, which seemed higher than that in wild-type cases (18.2% vs. 5.1%; 9.1% vs. 1.1%, respectively), but no statistical difference was discovered. Furthermore, based on the analysis of the number of mutated genes, there was no significant difference between *IKZF1* mutant and wild-type patients ($p = 0.753$) (**Figure 3C**).

## Association Analysis of Genetic Mutations in Patients With *IKZF1* Mutation

Among 22 *IKZF1* mutant cases, 17 cases carried only *IKZF1* large segment deletion, 4 cases had SNV or small InDel mutations in the *IKZF1* gene, and 1 case had both *IKZF1* large segment deletion and SNV mutation**.** For large segment deletion, 4 (18.2%) cases involved exon 1–8 deletion of the entire gene, while 14 (63.6%) cases involved focal gene deletion, including exon 4–7 deletion in 8 cases (36.4%), exon 2–7 deletion in 3 cases (13.6%), exon 4–8 deletion in 2 cases (9.1%), and exon 2–8 deletion in one case (4.5%) (**Figure 4A**). For *IKZF1* SNV and small InDel mutations, the main types were frameshift and missense mutations, two of which were located in the zinc finger structure of exon 4–7, including *IKZF1* G158S and L161fs (**Figure 4B**). Based on the analysis of two different *IKZF1* mutation types, including large segment deletion, and SNV or small InDel, the correlations between paired genes were revealed (**Figure 4C**).

According to the distribution of mutations in 22 *IKZF1* mutant patients, 26 mutant genes were discovered, and *NRAS*, *SETD2*, *FLT3*, *CREBBP* were common detected genes (**Supplementary Figure S1A**). The cluster analysis based on gene function pathways showed that the mutant genes were mainly related to signaling pathway (40.5%) and transcription factor (16.7%) (**Supplementary Figure S1B**). The *IL7R* mutation accounted for 50.0% of B-ALL cases with Ph+/Ph-like combined with *IKZF1* abnormalities (50.0% vs. 0%, $p = 0.03$) (**Figure 4D**).

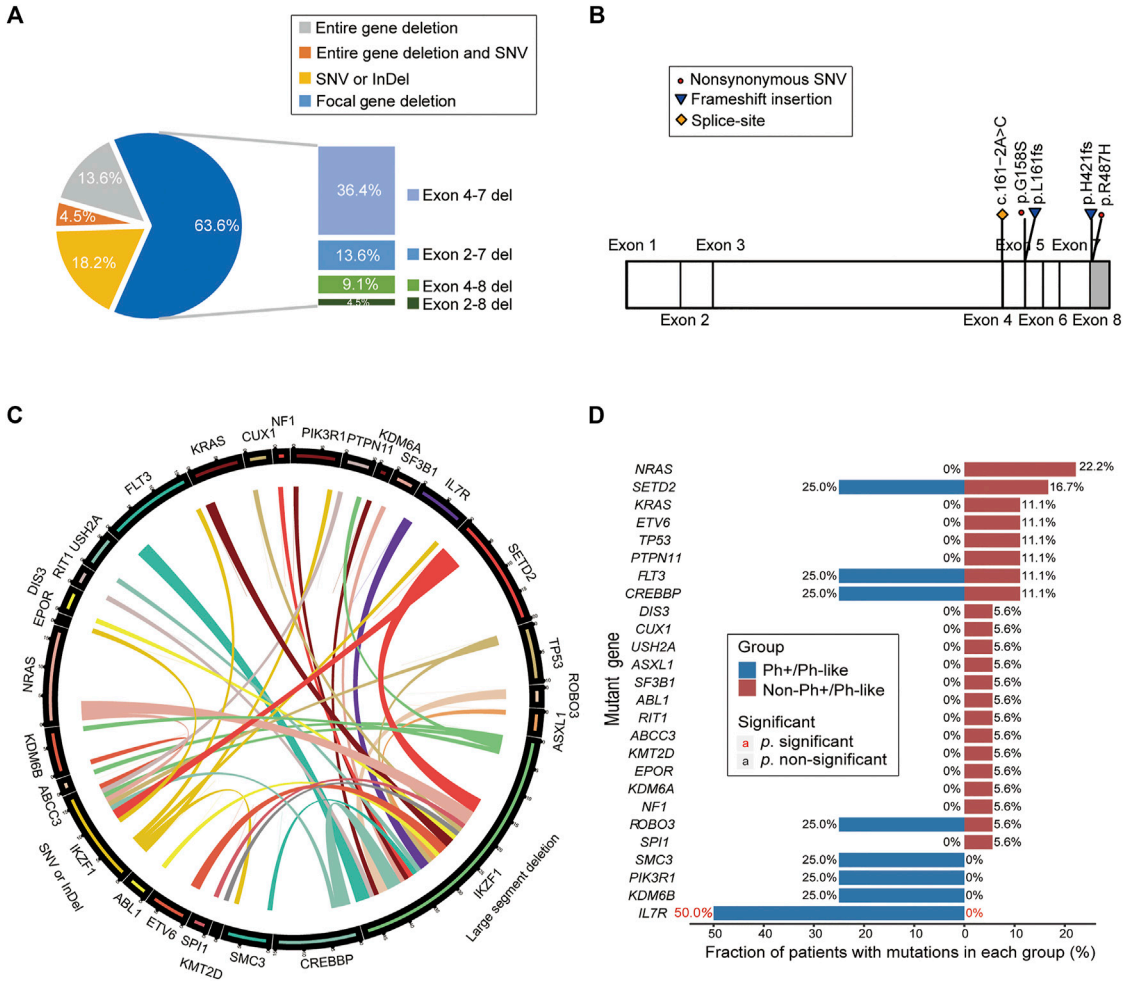


**FIGURE 4 |** Analysis of gene mutation characteristics in patients with *IKZF1* mutation. **(A)** Pie chart shows specific types of *IKZF1* mutations, including the entire gene deletions, focal gene deletions, single nucleotide variations, and small insertions or deletions. **(B)** Schematic representation of the mutations detected in the *IKZF1* gene, only for single nucleotide variations, and small insertions or deletions. **(C)** Circos plot shows all the genetic mutations in the *IKZF1* mutation cohort, corresponding to the relative frequency and pairwise co-occurrence of gene mutations. The length of the arc indicates the frequency of mutations in the first gene, and the width of the ribbon represents the percentage of patients carrying the second gene mutation. **(D)** Comparison of the mutational genotypes of Ph+/Ph-like positive and Ph+/Ph-like negative B-ALL with *IKZF1* mutation. Percentage frequencies in each group are depicted.

## DISCUSSION

In this study, we systematically identified clinical and genetic characteristics of Chinese B-ALL children with *IKZF1* mutation. *IKZF1* mutation has been a hot topic in the field of leukemia since Mullighan *et al.* firstly reported in ALL patients in 2008 that single allele focal deletion affects its coding region (Mullighan et al., 2008). *IKZF1* mutation will lead to the obstruction of lymphocyte differentiation and development, resulting in leukemia. Based on MLPA to determine the partial or complete *IKZF1* large segment deletions, our study found *IKZF1* large segment deletion frequency was 9.0%, which was consistent with the result that Asai *et al.* reported 19 of 202 (9.4%) patients were carrying *IKZF1* large segment deletions (Asai et al., 2013). However, other studies observed differences in *IKZF1* large segment deletion frequency: 12% in German patients, 20.6% in Mexico patients, 16% in Swedish patients, and 28.6% in American patients. *IKZF1* SNV and small InDel mutation in our study was 2.5%, almost close to the proportion reported in the literature (<1%) (Mullighan et al., 2008; Dorge et al., 2013; Ofverholm et al., 2013; Ayon-Perez et al., 2019; Stanulla et al., 2020).

Previous studies showed that the different type of *IKZF1* mutations, including large segment deletion, small InDel and SNV, produced different molecular results. Deficiencies from these sites, such as the entire gene (including exons 1–8), or focal gene (including exons 2 and/or 8), or untranscriptional regulatory regions (including exon 1), can lead to *IKZF1* hypofunction (Iacobucci & Mullighan, 2017). The deletion of exons 4–7, lacking the ability to bind DNA, was a negative domain and thus led to leukemia (Mullighan et al., 2008; Iacobucci et al., 2009; Chiaretti et al., 2016), which was the most common deletion pattern of *IKZF1* in our cohort (36%),

consistent with results in Germany, Japan, Sweden and the US and different from results in Mexico, where the deletion of exon 1 (85%) occurred most frequently (Ayon-Perez et al., 2019). Although SNV or small InDel mutations of *IKZF1* were infrequent and present, their molecular consequences could be either haploid insufficiency or dominant negative effects, as with deletions. Given this, the molecular effects of these types of mutations can be further judged by gene expression. Recent research discovered that *IKZF1* missense mutation (p.N159Y) affect the DNA binding domain and validated by gene expression profile (Li et al., 2018; Gu et al., 2019). Five *IKZF1* mutations, including SNV or small InDel mutations, were also detected in our study, whose final molecular effects need to be further clarified by transcriptome sequencing.

However, *IKZF1* is controversial as an independent risk factor for patient prognostic stratification. Some studies suggested *IKZF1* large segment deletion was closely related to the high recurrence and low survival of pediatric B-ALL (Kuiper et al., 2010; Yang et al., 2011; Buitenkamp et al., 2012). Boer *et al.* showed that any kind of *IKZF1* large segment deletion increased risk compared to patients with wild-type *IKZF1*, based on their high WBC count >50,000/μl (Boer et al., 2016). Indeed, we observed this phenomenon for 22 patients with *IKZF1* mutations in this study, who had higher levels of leukocytes at the time of initial diagnosis, insensitivity to glucocorticoid, and higher levels of MRD on day 15th of induction remission.

We also found that the partner mutant genes associated with the *IKZF1* mutations are closely related to the signaling pathway and transcription factor function (*NRAS*, *SETD2*, *FLT3* and *CREBBP*). In particular, the mutation in *IL7R* was only found in *IKZF1* mutation cases, suggesting the *IL7R* mutation may be synergistic with the *IKZF1* mutation and participate in the occurrence of the B-ALL. In our study, these two patients with *IL7R* mutation were insensitive to glucocorticoid therapy. Several research suggested that *IL7R* functional acquired mutations made *IL7R* highly expressed, and *IKZF1* deletion deprived the IKAROS of its inhibitory effect on the promoter region. *IKZF1* and *IL7R* synergistically activated downstream JAK/STAT5 and PI3K/Akt/mTOR signaling pathways to promote leukemia (Ge et al., 2016). Thomas et al. (2021) showed that *IL7R* mutation led to B-ALL alone in a mouse model and *IKZF1* mutation contributed to the process of leukemogenesis.

Our study has several limitations. First of all, due to the lack of follow-up data, the long-term prognostic value of *IKZF1* mutation remains to be explored. Secondly, this study is a single-center result, which may not fully reflect the distribution of clinical and genetic characteristics in the Chinese population. Therefore, large-scale multi-center studies and long-term follow-up should be included in the future.

Inconclusion, our research showed clinical and genetic characteristics of *IKZF1* mutation in Chinese Children with B-ALL. This study reveals the association between genetic mutations and clinical features. These investigations might contribute to molecular classification, risk stratification and prognosis evaluation, and provide new ideas for targeted therapy.

## DATA AVAILABILITY STATEMENT

The data that support the findings of this study have been deposited into CNGB Sequence Archive (CNSA) of China National GeneBank DataBase (CNGBdb) with accession number CNP0002707 https://db.cngb.org/search/project/CNP0002707.

## ETHICS STATEMENT

The studies involving human participants were reviewed and approved by the Children's Hospital of Zhejiang University Medical College. Written informed consent to participate in this study was provided by the participants' legal guardian/next of kin.

## AUTHOR CONTRIBUTIONS

DS, JQ and YT designed the study and approved the final manuscript. JZ, XX, HS, HS, WX, FZ, JL, CL, YW and TX collected the clinical sample and data. LL and SC performed the NGS platform and statistical analysis. JZ, YT, JQ, and DS wrote and edited the manuscript. All authors contributed to the article and approved the submitted version.

## FUNDING

This work was supported by National Natural Science Foundation (No. 81770202), Zhejiang Provincial Science and Technology Department Fund (No. 2019C03032) and Pediatric Leukemia Diagnostic and Therapeutic Technology Research Center of Zhejiang Province (No. JBZX-201904).

## ACKNOWLEDGMENTS

We thank all the patients who participated in this study.

## SUPPLEMENTARY MATERIAL

The Supplementary Material for this article can be found online at: https://www.frontiersin.org/articles/10.3389/fgene.2022.822832/full#supplementary-material

## REFERENCES


Arber, D. A., Orazi, A., Hasserjian, R., Thiele, J., Borowitz, M. J., Le Beau, M. M., et al. (2016). The 2016 Revision to the World Health Organization Classification of Myeloid Neoplasms and Acute Leukemia. *Blood* 127 (20), 2391–2405. doi:10.1182/blood-2016-03-643544

Asai, D., Imamura, T., Suenobu, S. i., Saito, A., Hasegawa, D., Deguchi, T., et al. (2013). IKZF1 Deletion Is Associated with a Poor Outcome in Pediatric B-Cell Precursor Acute Lymphoblastic Leukemia in Japan. *Cancer Med.* 2 (3), 412–419. doi:10.1002/cam4.87

Ayón-Pérez, M. F., Pimentel-Gutiérrez, H. J., Durán-Avelar, M. d. J., Vibanco-Pérez, N., Pérez-Peraza, V. M., Pérez-González, Ó. A., et al. (2019). IKZF1 Gene Deletion in Pediatric Patients Diagnosed with Acute Lymphoblastic Leukemia in Mexico. *Cytogenet. Genome Res.* 158 (1), 10–16. doi:10.1159/000499641

Boer, J. M., van der Veer, A., Rizopoulos, D., Fiocco, M., Sonneveld, E., de Groot-Kruseman, H. A., et al. (2016). Prognostic Value of Rare IKZF1 Deletion in Childhood B-Cell Precursor Acute Lymphoblastic Leukemia: an International Collaborative Study. *Leukemia* 30 (1), 32–38. doi:10.1038/leu.2015.199

Brown, P. A., Wieduwilt, M., Logan, A., DeAngelo, D. J., Wang, E. S., Fathi, A., et al. (2019). Guidelines Insights: Acute Lymphoblastic Leukemia, Version 1.2019. *J. Natl. Compr. Canc Netw.* 17 (5), 414–423. doi:10.6004/jnccn.2019.0024

Brown, P., Inaba, H., Annesley, C., Beck, J., Colace, S., Dallas, M., et al. (2020). Pediatric Acute Lymphoblastic Leukemia, Version 2.2020, NCCN Clinical Practice Guidelines in Oncology. *J. Natl. Compr. Canc Netw.* 18 (1), 81–112. doi:10.6004/jnccn.2020.0001

Buitenkamp, T. D., Pieters, R., Gallimore, N. E., van der Veer, A., Meijerink, J. P. P., Beverloo, H. B., et al. (2012). Outcome in Children with Down's Syndrome and Acute Lymphoblastic Leukemia: Role of IKZF1 Deletions and CRLF2 Aberrations. *Leukemia* 26 (10), 2204–2211. doi:10.1038/leu.2012.84

Chiaretti, S., Gianfelici, V., O'Brien, S. M., and Mullighan, C. G. (2016). Advances in the Genetics and Therapy of Acute Lymphoblastic Leukemia. *Am. Soc. Clin. Oncol. Educ. Book* 35, e314–e322. doi:10.1200/edbk_156628

Dorge, P., Meissner, B., Zimmermann, M., Moricke, A., Schrauder, A., Bouquin, J.-P., et al. (2013). IKZF1 Deletion Is an Independent Predictor of Outcome in Pediatric Acute Lymphoblastic Leukemia Treated According to the ALL-BFM 2000 Protocol. *Haematologica* 98 (3), 428–432. doi:10.3324/haematol.2011.056135

Ge, Z., Gu, Y., Xiao, L., Han, Q., Li, J., Chen, B., et al. (2016). Co-existence of IL7R High and SH2B3 Low Expression Distinguishes a Novel High-Risk Acute Lymphoblastic Leukemia with Ikaros Dysfunction. *Oncotarget* 7 (29), 46014–46027. doi:10.18632/oncotarget.10014

Gu, Z., Churchman, M. L., Roberts, K. G., Moore, I., Zhou, X., Nakitandwe, J., et al. (2019). PAX5-driven Subtypes of B-Progenitor Acute Lymphoblastic Leukemia. *Nat. Genet.* 51 (2), 296–307. doi:10.1038/s41588-018-0315-5

Holmfeldt, L., Wei, L., Diaz-Flores, E., Walsh, M., Zhang, J., Ding, L., et al. (2013). The Genomic Landscape of Hypodiploid Acute Lymphoblastic Leukemia. *Nat. Genet.* 45 (3), 242–252. doi:10.1038/ng.2532

Iacobucci, I., and Mullighan, C. G. (2017). Genetic Basis of Acute Lymphoblastic Leukemia. *J. Clin. Oncol.* 35 (9), 975–983. doi:10.1200/JCO.2016.70.7836

Iacobucci, I., Storlazzi, C. T., Cilloni, D., Lonetti, A., Ottaviani, E., Soverini, S., et al. (2009). Identification and Molecular Characterization of Recurrent Genomic Deletions on 7p12 in the IKZF1 Gene in a Large Cohort of BCR-ABL1-Positive Acute Lymphoblastic Leukemia Patients: on Behalf of Gruppo Italiano Malattie Ematologiche dell'Adulto Acute Leukemia Working Party (GIMEMA AL WP). *Blood* 114 (10), 2159–2167. doi:10.1182/blood-2008-08-173963

Kuiper, R. P., Waanders, E., van der Velden, V. H. J., van Reijmersdal, S. V., Venkatachalam, R., Scheijen, B., et al. (2010). IKZF1 Deletions Predict Relapse in Uniformly Treated Pediatric Precursor B-ALL. *Leukemia* 24 (7), 1258–1264. doi:10.1038/leu.2010.87

Li, J.-F., Dai, Y.-T., Lilljebjörn, H., Shen, S.-H., Cui, B.-W., Bai, L., et al. (2018). Transcriptional Landscape of B Cell Precursor Acute Lymphoblastic Leukemia Based on an International Study of 1,223 Cases. *Proc. Natl. Acad. Sci. USA* 115 (50), E11711–E11720. doi:10.1073/pnas.1814397115

Mullighan, C. G., Miller, C. B., Radtke, I., Phillips, L. A., Dalton, J., Ma, J., et al. (2008). BCR-ABL1 Lymphoblastic Leukaemia Is Characterized by the Deletion of Ikaros. *Nature* 453 (7191), 110–114. doi:10.1038/nature06866

Mullighan, C. G., Su, X., Zhang, J., Radtke, I., Phillips, L. A. A., Miller, C. B., et al. (2009). Deletion ofIKZF1and Prognosis in Acute Lymphoblastic Leukemia. *N. Engl. J. Med.* 360 (5), 470–480. doi:10.1056/NEJMoa0808253

Öfverholm, I., Tran, A. N., Heyman, M., Zachariadis, V., Nordenskjöld, M., Nordgren, A., et al. (2013). Impact of IKZF1 Deletions and PAX5 Amplifications in Pediatric B-Cell Precursor ALL Treated According to NOPHO Protocols. *Leukemia* 27 (9), 1936–1939. doi:10.1038/leu.2013.92

Palmi, C., Valsecchi, M. G., Longinotti, G., Silvestri, D., Carrino, V., Conter, V., et al. (2013). What Is the Relevance of Ikaros Gene Deletions as a Prognostic Marker in Pediatric Philadelphia-negative B-Cell Precursor Acute Lymphoblastic Leukemia? *Haematologica* 98 (8), 1226–1231. doi:10.3324/haematol.2012.075432

Rebollo, A., and Schmitt, C. (2003). Ikaros, Aiolos and Helios: Transcription Regulators and Lymphoid Malignancies. *Immunol. Cel Biol* 81 (3), 171–175. doi:10.1046/j.1440-1711.2003.01159.x

Stanulla, M., Cavé, H., and Moorman, A. V. (2020). IKZF1 Deletions in Pediatric Acute Lymphoblastic Leukemia: Still a Poor Prognostic Marker. *Blood* 135 (4), 252–260. doi:10.1182/blood.2019000813

Thomas, K. R., Allenspach, E. J., Camp, N. D., Wray-Dutra, M. N., Khim, S., Zielinska-Kwiatkowska, A., et al. (2021). Activated Interleukin-7 Receptor Signaling Drives B-Cell Acute Lymphoblastic Leukemia in Mice. *Leukemia* 36, 42–57. doi:10.1038/s41375-021-01326-x

Volejnikova, J., Mejstrikova, E., Dörge, P., Meissner, B., Zimmermannova, O., Svojgr, K., et al. (2013). Ikaros (IKZF1 ) Alterations and Minimal Residual Disease at Day 15 Assessed by Flow Cytometry Predict Prognosis of Childhood BCR/ABL -negative Acute Lymphoblastic Leukemia. *Pediatr. Blood Cancer* 60 (3), 420–427. doi:10.1002/pbc.24299

Vrooman, L. M., Blonquist, T. M., Harris, M. H., Stevenson, K. E., Place, A. E., Hunt, S. K., et al. (2018). Refining Risk Classification in Childhood B Acute Lymphoblastic Leukemia: Results of DFCI ALL Consortium Protocol 05-001. *Blood Adv.* 2 (12), 1449–1458. doi:10.1182/bloodadvances.2018016584

Waanders, E., van der Velden, V. H., van der Schoot, C. E., van Leeuwen, F. N., van Reijmersdal, S. V., de Haas, V., et al. (2011). Integrated Use of Minimal Residual Disease Classification and IKZF1 Alteration Status Accurately Predicts 79% of Relapses in Pediatric Acute Lymphoblastic Leukemia. *Leukemia* 25 (2), 254–258. doi:10.1038/leu.2010.275

Yamashita, Y., Shimada, A., Yamada, T., Yamaji, K., Hori, T., Tsurusawa, M., et al. (2013). IKZF 1 and CRLF 2 Gene Alterations Correlate with Poor Prognosis in Japanese BCR - ABL 1 -negative High-Risk B-Cell Precursor Acute Lymphoblastic Leukemia. *Pediatr. Blood Cancer* 60 (10), 1587–1592. doi:10.1002/pbc.24571

Yang, Y.-L., Hung, C.-C., Chen, J.-S., Lin, K.-H., Jou, S.-T., Hsiao, C.-C., et al. (2011). IKZF1 Deletions Predict a Poor Prognosis in Children with B-Cell Progenitor Acute Lymphoblastic Leukemia: a Multicenter Analysis in Taiwan. *Cancer Sci.* 102 (10), 1874–1881. doi:10.1111/j.1349-7006.2011.02031.x

Yeoh, A. E. J., Lu, Y., Chin, W. H. N., Chiew, E. K. H., Lim, E. H., Li, Z., et al. (2018). Intensifying Treatment of Childhood B-Lymphoblastic Leukemia with IKZF1 Deletion Reduces Relapse and Improves Overall Survival: Results of Malaysia-Singapore ALL 2010 Study. *J. Clin. Oncol.* 36 (26), 2726–2735. doi:10.1200/JCO.2018.78.3050


**Conflict of Interest:** Authors LL, SC, and JQ were employed by the company Acornmed Biotechnology Co., Ltd.

The remaining authors declare that the research was conducted in the absence of any commercial or financial relationships that could be construed as a potential conflict of interest.

frontiers | Frontiers in Genetics

CASE REPORT
published: 08 April 2022
doi: 10.3389/fgene.2022.853907

# Case Report: A Novel Mutation Identified in *CHST14* Gene in a Fetus With Structural Abnormalities

*Yuan-Yuan Zhou*†, Yu-Fang Du†, Qing Lu, Xiu-Zhang Zhai, Ming-Fang Shi, Dan-Yun Chen, Sun-Rong Liu and Ying Zhong*

*Department of Clinical Laboratory, The Third Affiliated Hospital of Guangxi Medical University, Nanning, China*

**Background:** Musculocontractural Ehlers–Danlos syndrome (mcEDS) is a rare heritable connective tissue disease with various symptoms. The diagnosis of mcEDS is difficult because of the large overlap of clinical symptoms between different EDS subtypes.

**Methods:** We performed karyotype analysis, gene copy number variation detection, whole-exome sequencing, and Sanger sequencing to reveal the underlying genetic etiology of a fetus with structural abnormalities in feet and kidneys.

**Results:** A likely pathogenic mutation [NM_130468.3 c.958C>T (p.Arg320*)] and an uncertain significance mutation [NM_130468.3 c.896A>G (p.Tyr299Cys)] were identified in the carbohydrate sulfotransferase 14 (*CHST14*) gene by whole-exome sequencing and validated by Sanger sequencing.

**Conclusion:** The two identified mutations appear highly likely to be the genetic causes of the fetal structural abnormalities.

**Keywords: whole-exome sequencing, prenatal diagnosis, *CHST14*, Ehlers–Danlos syndrome, structural abnormalities**

OPEN ACCESS

***Edited by:***
*Douglas Mark Ruden, Wayne State University, United States*

***Reviewed by:***
*Shuji Mizumoto, Meijo University, Japan*
*Yiqun Wu, Shanghai Jiao Tong University, China*
*Alina Hilger, University of Bonn, Germany*

****Correspondence:***
*Yuan-Yuan Zhou*
*yuanyuanzhou2003@163.com*

*†These authors have contributed equally to this work*

***Specialty section:***
*This article was submitted to Genetics of Common and Rare Diseases, a section of the journal Frontiers in Genetics*

***Received:*** *13 January 2022*
***Accepted:*** *03 March 2022*
***Published:*** *08 April 2022*

***Citation:***
*Zhou Y-Y, Du Y-F, Lu Q, Zhai X-Z, Shi M-F, Chen D-Y, Liu S-R and Zhong Y (2022) Case Report: A Novel Mutation Identified in CHST14 Gene in a Fetus With Structural Abnormalities. Front. Genet. 13:853907. doi: 10.3389/fgene.2022.853907*

## 1 INTRODUCTION

Fetal structural abnormalities emerge in approximately 3.0% of pregnancies, which can be related to all types of genetic variants (Persson et al., 2017; Lord et al., 2019). Karyotyping and chromosomal microarray analysis are recommended as the preferred diagnostic methods for fetal structural abnormalities (International Society for Prenatal Diagnosis, 2018). However, more than 60% of fetal structural abnormalities cannot be explained by chromosomal karyotyping and microarray analysis (Wapner et al., 2012). Recently, whole-exome sequencing (WES) has been confirmed to be a valuable diagnostic approach for explicating the underlying genetic etiology for many likely Mendelian disorders (Petrovski et al., 2019).

The Ehlers–Danlos syndromes (EDS) are a group of heritable connective tissue diseases involving at least 17 genes and 13 subtypes, with various symptoms, characteristically joint hypermobility, skin hyperextensibility, and tissue fragility (Malfait et al., 2017). Musculocontractural Ehlers–Danlos syndrome (mcEDS) is a subtype of EDS caused by homozygous or compound heterozygous mutations of the carbohydrate sulfotransferase 14 (*CHST14*) or dermatan sulfate epimerase gene (Malfait et al., 2010). Three major clinical criteria are defined for the diagnosis of mcEDS, including 1) congenital multiple contractures, typically adduction-flexion contractures, and/or talipes equinovarus (clubfoot); 2) characteristic craniofacial features; and 3) characteristic cutaneous features, for example, skin hyperextensibility, easy bruisability, and skin fragility (Malfait et al., 2017).

The diagnosis of EDS once mainly relied on clinical features (Beighton et al., 1988). Then, in 1997, the biochemical and molecular bases were required to classify EDS (Beighton et al., 1998). A molecular confirmation is very important for the diagnosis and counseling in view of the overlap of clinical symptoms between different EDS subtypes. Recently, it has been recommended that molecular detection should base on next-generation sequencing technologies, such as copy number variation (CNV) detection, WES, and whole-genome sequencing (WGS) (Malfait et al., 2017). Prenatal diagnosis of mcEDS is more difficult than postnatal diagnosis, as the craniofacial and cutaneous features have not been represented completely. Up till now, prenatal mcEDS has not yet been reported. We herein introduce an mcEDS case diagnosed by prenatal WES and Sanger sequencing.

# 2 MATERIALS AND METHODS

## 2.1 Case Information

A 34-year-old woman with 22-week gestation visited the Department of Genetic Counseling of the Third Affiliated Hospital of Guangxi Medical University (Nanning, China) for genetic counseling on the fetal abnormalities revealed by ultrasound examination. The ultrasound report showed adduction flexion (**Supplementary Figure S1**) in the fetal feet. The renal pelvis in both kidneys was separated, the left test was as large as 5.5 mm, and the right test was 5.2 mm. The estimated weight of the fetus was about 539 g. The fetal biparietal diameter, head circumference, abdominal circumference, transverse diameter of cerebellum, length of the humerus, and length of the femur were 53, 198, 182, 24, 39, and 40 mm, respectively. The woman and her husband were both in good health conditions. Family history of genetic diseases and consanguineous marriage were denied by the couple.

## 2.2 Amniotic Fluid Cell Karyotype Analysis

A total of 20 ml amniotic fluid was obtained under the guidance of ultrasound by an experienced obstetrician. After that, 15 ml of amniotic fluid was transferred into two cell culture bottles and then placed in an incubator with 37°C and 5% $CO_2$ for a week. Chromosomes are prepared according to a routine chromosomal collection process, and at least 40 meta-phase cells were analyzed by two experienced technicians using the ZEISS meta-system (CARL ZEISS AG, Jena, Germany).

## 2.3 DNA Extraction

Fetal DNA was extracted from 5 ml amniotic fluid, and biological parental DNA was extracted from corresponding venous blood using the introduction of the QIAmp DNA extraction Kit (QIAGEN, Dusseldorf, Germany). All DNA was stored at −80°C after extraction.

## 2.4 Copy Number Variation Sequencing

Library construction was performed through a series of experiments, including DNA fragmentation, label ligation, pre-PCR purification, PCR, and post-PCR purification, according to the standard operation procedures (CapitalBio, Beijing, China). CNV-seq was performed using the bio-electronseq 400 (CapitalBio, Beijing, China) and the life ion torrent platform (CapitalBio, Beijing, China). The lower detective limits of CNV-seq are 100 kb for micro-deletion and micro-duplication and 10% for mosaicism.

## 2.5 Whole-Exome Sequencing and Sanger Sequencing

Library preparation was carried out according to the standard procedure (Basic Graphics Interface (BGI), Shenzhen, China). BGI V4 chip was used to capture and enrich the exome of target genes. Mgiseq-2000 sequencing platform (BGI) was employed to detect gene variations. The sequencing reads were compared with the genome UCSC hg19 by the Burrows–Wheeler Aligner. The Genome Analysis Toolkit (Broad Institute, Cambridge, MA, United States) was used to detect single nucleotide variations, basal insertion, and genotype. EXOME DEPTH was used to test copy number variation at the exome level. Sanger sequencing was performed to validate any identified mutation. The pathogenicity was evaluated according to the guidelines of the American College of Medical Genetics and Genomics (ACMG) (Richards et al., 2015) and analyzed in three databases: SIFT, PolyPhen, and MutationTaster.

# 3 RESULTS

## 3.1 Results of Chromosomal Karyotyping and CNV Sequencing

The fetal chromosomal karyotype was normal, and no known pathogenic micro-deletion (>100 kb), pathogenic micro-duplication (>100 kb), mosaicism (>10%), or aneuploidy was detected in the fetus.

## 3.2 Whole-Exome Sequencing Analysis

A total of 405 variants (**Supplementary Table S1**) were filtered out by a filtering process (**Supplementary Figure S2**). Two mutations identified in the *CHST14* gene of the fetus were considered of clinical significance. According to the ACMG guidelines [NM_130468.3 c.958C>T (p.Arg320*)] was classified as a likely pathogenic variant and [NM_130468.3 c.896A>G (p.Tyr299Cys)] was uncertain significance. Meanwhile, the likely pathogenic variant was also identified in the mother, and the uncertain significance variant was also identified in the father. Predicted pathogenicity is shown in **Table 1**.

## 3.3 Sanger Sequencing Validation

Sanger sequencing detected two mutations [NM_130468.3 c.958C>T (p.Arg320 *)] and [NM_130468.3 c. 896A>G (p.Tyr299Cys)], and these results were consistent with those of WES (**Figures 1A,B**).

# 4 DISCUSSION

Next-generation sequencing such as CNV-seq, WES, and WGS has been widely used in clinical practice in the last decade. It has been reported that WES-trio achieved a diagnostic rate of 40% in

**TABLE 1 |** Two mutations identified in the *CHST14* gene.

| Cytogenetic location/gene subregion | Variants (protein) [RefSeq ID] | Inheritance/ zygosity | Detection of family members | Disease association(s) [MIM #] | Pathogenicity (ACMG guidelines/SIFT/PolyPhen/MutationTaster) |
|---|---|---|---|---|---|
| chr15:4076-4370/ EX1E | c.958C>T (p.Arg320*) [NM_130468.3] | AR/het | Mother (het) | mcEDS [601776] | Likely pathogenic/—/—/disease-causing |
| chr15:4076-4308/ EX1E | c.896A>G (p.Tyr299Cys) [NM_130468.3] | AR/het | Father (het) | mcEDS [601776] | Uncertain significance/damaging/probably damaging/disease-causing |

*AR, autosomal recessive; EX1E, exome 1E region; het, heterozygous; mcEDS, musculocontractural Ehlers–Danlos syndrome.*

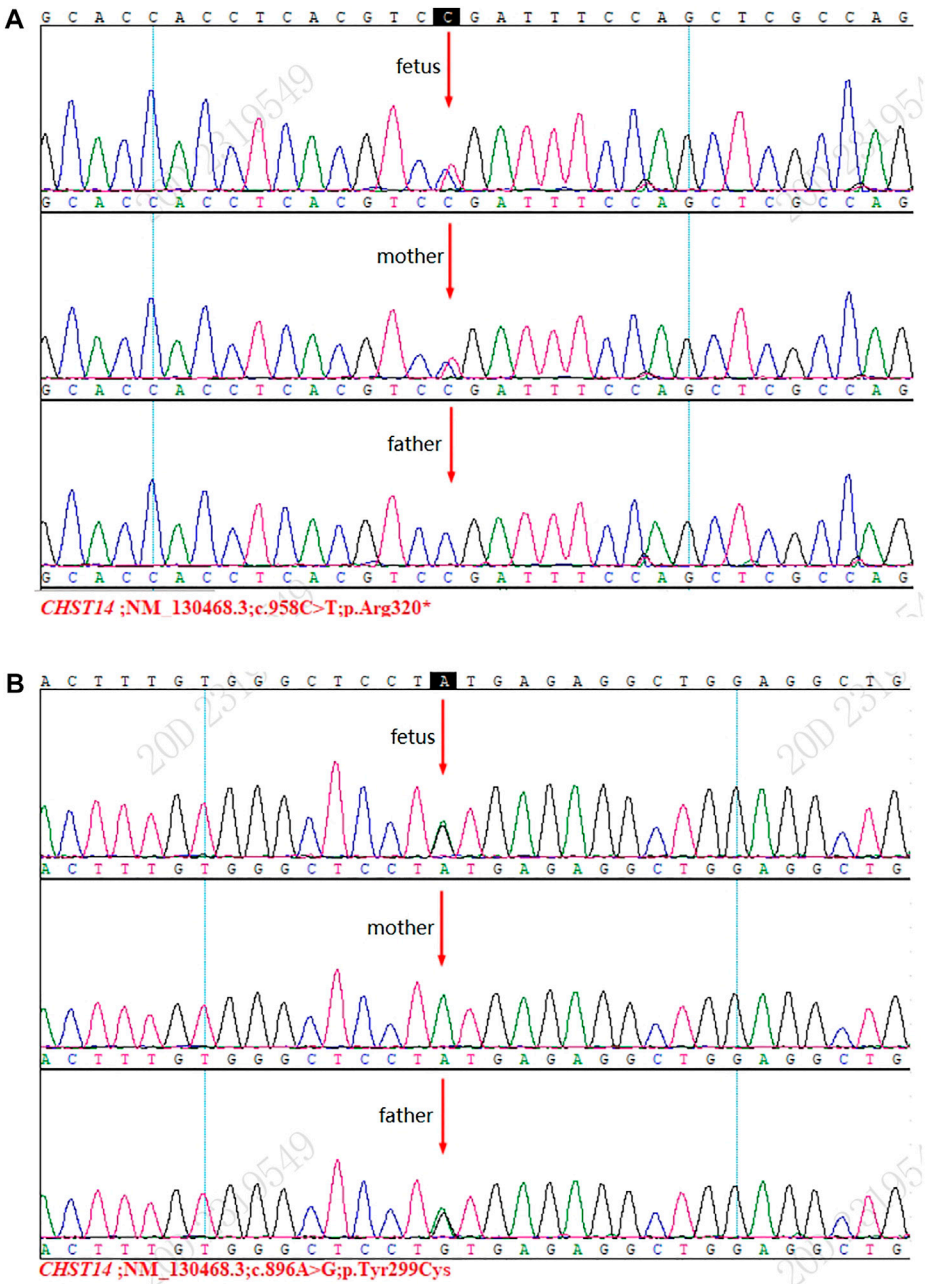


**FIGURE 1 |** Results of Sanger sequencing. **(A)** Mutation [NM_130468.3 c.958C>T (p.Arg320*)] was detected in the fetus and the mother. **(B)** Mutation [NM_130468.3 c.896A>G (p.Tyr299Cys)] was detected in the fetus and the father.

diagnosing genetic disorders, which was almost as high as that of WGS-trio (42%) (Lord et al., 2019). Seven genes implicating stillbirth were identified by WES, with a detection rate of 6.1% (Stanley et al., 2020). Therefore, WES has recently been recommended to be used in prenatal clinical practice to uncover the underlying genetic causes of fetal structural anomalies while abnormal karyotype and pathogenic CNV had been excluded (Petrovski et al., 2019).

*CHST14* gene is located in number 15 chromosome (15q15.1), involving only one exon and encoding N-acetylgalactosamine 4-O-sulfotransferase 1 (D4ST1), which plays an essential role in the biosynthesis of proteoglycans (CHST14 carbohydrate sulfotransferase 14 [Homo sapiens (human)] - Gene - NCBI (nih.gov)). Proteoglycans are abundant in the extracellular matrix and important in a wide range of physiological functions, such as interacting with collagen (Malfait et al., 2020). Pathogenetic mutations in the *CHST14* gene result in deficiency of D4ST1, which consequently leads to the decrease of proteoglycans and further abnormal regulation of collagen fibrils assembly and finally gives rise to the mcEDS (Dundar et al., 2009; Malfait et al., 2020).

To our best knowledge, at least 26 variants of the *CHST14* gene have been reported. However, no apparent relationship between genotype and phenotype is noted (Minatogawa et al., 2021). Dundar et al. (2009) discovered a 1 bp deletion (c.145_146 delG), a missense mutation (c.638G>C), and a complex allele (c.404C>G; 410T>A) in *CHST14* in Australian Turks with thumb-clubfoot Syndrome. Miyake et al. (2010) reported four mutations (c.842C>T p.P281L, c.866G>C p.C289S, c.878A>G p.Y293C, c.205A>T p.K69*) of the *CHST14* gene in six Japanese patients with Kosho type EDS. In fact, thumb-clubfoot syndrome and Kosho type EDS have a common clinical condition, so they are termed mcEDS (Malfait et al., 2010).

In this study, novel and reported mutations in *CHST14* were detected in a fetus with adduction flexion in the feet and renal pelvis in the kidneys. A likely pathogenic mutation [NM_130468.3 c.958C>T (p.Arg320*)], which was also found in the mother, had been reported previously by Minatogawa et al. (2021) in a study involving 66 mcEDS patients. A novel variation [NM_130468.3 c.896A>G (p.Tyr299Cys)], which was also found in the father, was evaluated as an uncertain significance mutation according to the ACMG guidelines. However, it was predicted to be a disease-causing or probably damaging mutation in *in silico* analyses. The two detected variants are located in the middle of the sulfotransferase domain and presumably result in partial or complete loss of function of D4ST1 (Minatogawa et al., 2021).

The couple decided to terminate this pregnancy after genetic counseling. Clubfeet (**Supplementary Figure S3**) were confirmed by autopsy, and this was consistent with the ultrasound results. The autopsy record about kidneys was unknown. Clubfoot was one of the three major criteria for diagnosing mcEDS and 95% (59/62) mcEDS patients developed clubfoot, while renal structural abnormalities were not observed (Minatogawa et al., 2021). By considering the clinical symptom (clubfeet) and the molecular detective results, an alternative diagnosis of mcEDS was made to the fetus. It was clear that the fetus inherited the two mutations from both parents and became a carrier of compound heterozygous mutations of the *CHST14* gene. It appears highly likely that the structural abnormalities, especially clubfeet, are caused by the two mutations. However, further functional studies, such as cell experiments, are needed to support the assumption.

In conclusion, we identified a novel mutation [NM_130468.3 c.896A>G (p.Tyr299Cys)] and a reported likely pathogenic mutation [NM_130468.3 c.958C>T (p.Arg320*)] in the *CHST14* gene of by WES prenatally, which can perhaps be claimed as the potential genetic etiology of the fetal structural abnormalities.

## DATA AVAILABILITY STATEMENT

The datasets for this article are not publicly available due to concerns regarding participant/patient anonymity. Requests to access the datasets should be directed to the corresponding author.

## ETHICS STATEMENT

The studies involving human participants were reviewed and approved by the Institutional review board of Third Affiliated Hospital of Guangxi Medical University. The patients/participants provided their written informed consent to participate in this study.

## AUTHOR CONTRIBUTIONS

YYZ and YD drafted the overall design of this study. YD wrote the article. QL collected the amniotic fluid and the details about the patients. XZ, DC, and SL analyzed the chromosome karyotype. YYZ, YD, MS, and YZ performed the CNV-seq and WES tests. YYZ reviewed and revised the manuscript.

## ACKNOWLEDGMENTS

We thank the all the participants for their generous help provided to this work.

## SUPPLEMENTARY MATERIAL

The Supplementary Material for this article can be found online at: https://www.frontiersin.org/articles/10.3389/fgene.2022.853907/full#supplementary-material

**Supplementary Figure S1 |** Adduction-flexion revealed by ultrasound.

**Supplementary Figure S2 |** Filtering process of WES data.

**Supplementary Figure S3 |** Clubfeet in the fetus.

## REFERENCES


Beighton, P., de Paepe, A., Danks, D., Finidori, G., Gedde-Dahl, T., Goodman, R., et al. (1988). International Nosology of Heritable Disorders of Connective Tissue, Berlin, 1986. *Am. J. Med. Genet.* 29 (3), 581–594. doi:10.1002/ajmg.1320290316

Beighton, P., De Paepe, A., Steinmann, B., Tsipouras, P., and Wenstrup, R. J. (1998). Ehlers-Danlos Syndromes: Revised Nosology, Villefranche, 1997. Ehlers-Danlos National Foundation (USA) and Ehlers-Danlos Support Group (UK). *Am. J. Med. Genet.* 77 (1), 31–37. doi:10.1002/(sici)1096-8628(19980428)77:1<31::aid-ajmg8>3.0.co;2-o

Dündar, M., Müller, T., Zhang, Q., Pan, J., Steinmann, B., Vodopiutz, J., et al. (2009). Loss of Dermatan-4-Sulfotransferase 1 Function Results in Adducted Thumb-Clubfoot Syndrome. *Am. J. Hum. Genet.* 85 (6), 873–882. doi:10.1016/j.ajhg.2009.11.010

International Society for Prenatal Diagnosis (2018). Joint Position Statement from the International Society for Prenatal Diagnosis (ISPD), the Society for Maternal Fetal Medicine (SMFM), and the Perinatal Quality Foundation (PQF) on the Use of Genome-wide Sequencing for Fetal Diagnosis. *Prenat Diagn.* 38 (1), 6–9. doi:10.1002/pd.5195

Lord, J., McMullan, D. J., Eberhardt, R. Y., Rinck, G., Hamilton, S. J., Quinlan-Jones, E., et al. (2019). Prenatal Exome Sequencing Analysis in Fetal Structural Anomalies Detected by Ultrasonography (PAGE): a Cohort Study. *Lancet* 393 (10173), 747–757. doi:10.1016/S0140-6736(18)31940-8

Malfait, F., Syx, D., Vlummens, P., Symoens, S., Nampoothiri, S., Hermanns-Lê, T., et al. (2010). Musculocontractural Ehlers-Danlos Syndrome (Former EDS Type VIB) and Adducted Thumb Clubfoot Syndrome (ATCS) Represent a Single Clinical Entity Caused by Mutations in the Dermatan-4-Sulfotransferase 1 Encoding CHST14 Gene. *Hum. Mutat.* 31 (11), 1233–1239. doi:10.1002/humu.21355

Malfait, F., Francomano, C., Byers, P., Belmont, J., Berglund, B., Black, J., et al. (2017). The 2017 International Classification of the Ehlers-Danlos Syndromes. *Am. J. Med. Genet. C Semin. Med. Genet.* 175 (1), 8–26. doi:10.1002/ajmg.c.31552

Malfait, F., Castori, M., Francomano, C. A., Giunta, C., Kosho, T., and Byers, P. H. (2020). The Ehlers-Danlos Syndromes. *Nat. Rev. Dis. Primers* 6 (1), 64. doi:10.1038/s41572-020-0194-9

Minatogawa, M., Unzaki, A., Morisaki, H., Syx, D., Sonoda, T., Janecke, A. R., et al. (2021). Clinical and Molecular Features of 66 Patients with Musculocontractural Ehlers–Danlos Syndrome Caused by Pathogenic Variants in CHST14 (mcEDS-CHST14). *J. Med. Genet.* 0, 1–13. doi:10.1136/jmedgenet-2020-107623

Miyake, N., Kosho, T., Mizumoto, S., Furuichi, T., Hatamochi, A., Nagashima, Y., et al. (2010). Loss-of-function Mutations of CHST14 in a New Type of Ehlers-Danlos Syndrome. *Hum. Mutat.* 31 (8), 966–974. doi:10.1002/humu.21300

Persson, M., Cnattingius, S., Villamor, E., Söderling, J., Pasternak, B., Stephansson, O., et al. (2017). Risk of Major Congenital Malformations in Relation to Maternal Overweight and Obesity Severity: Cohort Study of 1.2 Million Singletons. *BMJ* 357, j2563. doi:10.1136/bmj.j2563

Petrovski, S., Aggarwal, V., Giordano, J. L., Stosic, M., Wou, K., Bier, L., et al. (2019). Whole-exome Sequencing in the Evaluation of Fetal Structural Anomalies: a Prospective Cohort Study. *Lancet* 393 (10173), 758–767. doi:10.1016/S0140-6736(18)32042-7

Richards, S., Aziz, N., Bale, S., Bick, D., Das, S., Gastier-Foster, J., et al. (2015). Standards and Guidelines for the Interpretation of Sequence Variants: a Joint Consensus Recommendation of the American College of Medical Genetics and Genomics and the Association for Molecular Pathology. *Genet. Med.* 17 (5), 405–424. doi:10.1038/gim.2015.30

Stanley, K. E., Giordano, J., Thorsten, V., Buchovecky, C., Thomas, A., Ganapathi, M., et al. (2020). Causal Genetic Variants in Stillbirth. *N. Engl. J. Med.* 383 (12), 1107–1116. doi:10.1056/NEJMoa1908753

Wapner, R. J., Martin, C. L., Levy, B., Ballif, B. C., Eng, C. M., Zachary, J. M., et al. (2012). Chromosomal Microarray versus Karyotyping for Prenatal Diagnosis. *N. Engl. J. Med.* 367 (23), 2175–2184. doi:10.1056/NEJMoa1203382


**Conflict of Interest:** The authors declare that the research was conducted in the absence of any commercial or financial relationships that could be construed as a potential conflict of interest.

**Publisher's Note:** All claims expressed in this article are solely those of the authors and do not necessarily represent those of their affiliated organizations or those of the publisher, the editors and the reviewers. Any product that may be evaluated in this article, or claim that may be made by its manufacturer, is not guaranteed or endorsed by the publisher.

frontiers | Frontiers in Genetics

ORIGINAL RESEARCH
published: 28 April 2022
doi: 10.3389/fgene.2022.863157

# Genetic Landscape of Nephropathic Cystinosis in Russian Children

*K. V. Savostyanov[1]*, A. A. Pushkov[1], O. A. Shchagina[2], V. V. Maltseva[1], E. A. Suleymanov[3], I. S. Zhanin[1], N. N. Mazanova[1], A. P. Fisenko[1], P. S. Mishakova[2], A. V. Polyakov[2], E. V. Balanovska[2], R. A. Zinchenko[2] and A. N. Tsygin[1]*

[1]National Medical Research Center for Children's Health Federal State Autonomous Institution of the Ministry of Health of the Russian Federation, Moscow, Russia, [2]Research Centre for Medical Genetics, Moscow, Russia, [3]Ministry of Public Health, Republic of Chechnya, Grozny, Russia

Nephropathic cystinosis is a rare autosomal recessive disorder characterized by amino acid cystine accumulation and caused by biallelic mutations in the *CTNS* gene. The analysis methods are as follows: tandem mass spectrometry to determine the cystine concentration in polymorphonuclear blood leukocytes, Sanger sequencing for the entire coding sequence and flanking intron regions of the *CTNS* gene, multiplex PCR to detect a common mutation—a 57 kb deletion, and multiplex ligation-dependent probe amplification to analyze the number of exon copies in the *CTNS* gene. Haplotype analysis of chromosomes with major mutations was carried out using microsatellite markers D17S831, D17S1798, D17S829, D17S1828, and D17S1876. In this study, we provide clinical, biochemical, and molecular genetic characteristics of 40 Russian patients with mutations in the *CTNS* gene, among whom 30 patients were selected from a high-risk group of 85 people as a result of selective screening, which was carried out through cystine concentration measurement in polymorphonuclear blood leukocytes. The most common pathogenic variant, as in most described studies to date, was the 57 kb deletion, which represented 25% of all affected alleles. Previously non-described variants represented 22.5% of alleles. The founder effect in the Karachay and Chechen ethnic groups was shown for the following major variants: c.1015G > A and c.518A > G.

**Keywords: cystinosis, cystine, children, lysosomal storage diseases, selective screening, therapy monitoring, novel mutations in the CTNS gene**

OPEN ACCESS

***Edited by:***
*Desheng Liang,*
*Central South University, China*

***Reviewed by:***
*Xianjun Zhu,*
*Sichuan provincial people's hospital, China*
*Mohamed A. Elmonem,*
*Cairo University, Egypt*

****Correspondence:***
*K. V. Savostyanov*
*7443333@gmail.com*

***Specialty section:***
*This article was submitted to Genetics of Common and Rare Diseases, a section of the journal Frontiers in Genetics*

***Received:*** *26 January 2022*
***Accepted:*** *18 March 2022*
***Published:*** *28 April 2022*

***Citation:***
*Savostyanov KV, Pushkov AA, Shchagina OA, Maltseva VV, Suleymanov EA, Zhanin IS, Mazanova NN, Fisenko AP, Mishakova PS, Polyakov AV, Balanovska EV, Zinchenko RA and Tsygin AN (2022) Genetic Landscape of Nephropathic Cystinosis in Russian Children. Front. Genet. 13:863157. doi: 10.3389/fgene.2022.863157*

## INTRODUCTION

Nephropathic cystinosis is a rare hereditary disorder caused by the mutations in the *CTNS* gene, which encodes cystinosin, a lysosomal cystine transporter. It contains 367 amino acid residues and transports cystine via lysosomal proton gradient (Ruivo et al., 2012). Biallelic mutations in this gene lead to protein function disruption and intralysosomal cystine crystal accumulation in cells of various organs and tissues, predominantly the kidneys. The pathogenic variants in the *CTNS* gene, which are located at 17p13.2, lead to cystinosin defects, causing disruptions in cystine transportation into the cytoplasm, which leads to gradual intralysosomal cystine accumulation with subsequent crystallization due to its low solubility in water.

The genetic landscape of cystinosis varies greatly depending on the ethnicity (David et al., 2019) and geographic location (Ebbesen et al., 1976; Anikster et al., 1999; Hult et al., 2014; Angileri et al., 2015). The highest incidence (1:3600) was found in Pakistani people in the West Midlands, United Kingdom (Hutchesson et al., 1998). The number of affected people is constantly

growing, and 15–20 new cases per year are registered only in the United States (Nesterova and Gahl, 2008).

There are three types of cystinosis based on the symptom severity and age of manifestation: classic infantile nephropathic (OMIM 219800), juvenile nephropathic (OMIM 219900), and adult non-nephropathic (OMIM 219750).

As of date, 161 pathogenic *CTNS* variants are described in the HGMD Professional 2021.2 international database (https://portal.biobase-international.com/hgmd/pro/gene.php?gene=CTNS). The most common variant, according to the literature, is the 57 kb deletion, which partially affects the following genes: *CTNS*, *TRPV1*, and *CARKL*. This deletion is detected in patients with cystinosis in approximately 75% of all the described European cases (Touchman et al., 2000; Kalatzis, 2002). Patients with this deletion are characterized by a distinct extrarenal cystinosis phenotype and early mortality (Gahl et al., 2007).

As of date, the golden standard of laboratory diagnostics for cystinosis is tandem mass spectrometry with high-performance liquid chromatography (HPLC), which is widely used for treatment monitoring due to its high sensitivity and specificity, allowing it to detect the cystine concentrations as low as 0.02 μmol/L (Chabli et al., 2007). The confirmatory diagnostic method is molecular genetic diagnostics directed at pathogenic variants in the *CTNS* gene. The introduction of tandem mass spectrometry and genetic diagnostics in modern clinical practice in recent years allows to successfully detect patients with cystinosis in high-risk groups at an early age and to monitor the pathogenetic therapy (Savostyanov et al., 2018).

We provide clinical, genographic, and molecular genetic data of Russian patients with nephropathic cystinosis in this study.

# MATERIALS AND METHODS

## Subjects

The examined cohort included 40 children with a clinical diagnosis of "nephropathic cystinosis," confirmed by molecular genetic methods: 23 (57.5%) boys and 17 (42.5%) girls. The patients lived in different federal districts of the Russian Federation and neighboring countries: 13 patients from the North Caucasian FD (the Republic of Chechnya, Dagestan, Ingushetia, Karachay-Cherkessia, Kabardino-Balkaria, and Stavropol Krai), 7 from the Povolzhskiy FD (the Republic of Mordovia, Tatarstan, Bashkortostan, and Orenburg Oblast), 5 from the Central FD (Moscow, Kostroma, and Smolensk Oblast), 4 from the Siberian FD (Novosibirsk, Omsk Oblast, and the Republic of Altai), 3 from the Northwest FD (St. Petersburg and the Republic of Komi), 3 from Ukraine, 2 from the Southern FD (the Republic of Crimea and Krasnodar Krai), 1 from Belarus, and 1 with an undetermined place of residence. The average age of the examined patients was 6 years and 6 months, with a median of 6 years and 10 months (from 11 months to 16 years) at the time of the examination.

A total of 30 patients were selected for the examined group based on the selective screening carried out in the molecular genetics and medical genomics laboratory of the Federal State Budget Healthcare Institution, Central Children Clinical Hospital, from January 2016 to April 2021. The screening was carried out for 85 Russian patients aged 5 months to 8 years, with a male-to-female ratio of 2:1. The selection criteria were as follows: physical development delay, skeleton deformations, vomiting, dehydration, polyuria, metabolic acidosis, Fanconi syndrome, and photophobia. Additionally, we included ten patients with a diagnosis confirmed by using molecular genetic methods in the molecular genetics and medical genomics laboratory of the Federal State Budget Healthcare Institution, Central Children Clinical Hospital, and the DNA diagnostics laboratory of the Federal State Budgetary Institution, Research Centre for Medical Genetics.

The DNA samples of 197 healthy ethnic Karachay people from various regions of Karachay-Cherkessia and 178 ethnic Chechen people were used as a control group.

## Biochemical Testing

The cystine concentration was measured on an maXis Impact tandem mass spectrometer (Bruker, Germany). Whole blood was used as the biological material; leukocytes were extracted using the gradient method using Ficoll-Paque (Amresco, United States). Chromatographic separation was carried out on an Agilent 1260 chromatography machine (United States) using a SIELC Primesep 200 column (United States). Mass spectrometry detection was carried out in the positive ion registration mode using electrospray ionization (a thorough description of the methods is provided in **Supplementary Material S1**).

To determine the reference values, the cystine concentration in blood leukocytes was measured in a control group of 100 healthy donors. The male group consisted of 50 people (50%) aged 3 months to 15 years, with an average age of 8.5 years. The female group consisted of 50 people (50%) aged 2 months to 14 years, with an average age of 7 years. As an internal control, the cystine concentration was measured in seven patients (3 girls and four boys) with mutations in the *CTNS* gene. At the time of biochemical diagnostics, the patients were diagnosed based on distinct clinical features and molecular genetic analysis. The patients did not receive substrate reduction therapy.

In the healthy donor group, the cystine concentration levels varied from 0.11 to 0.45 nmol of ½cystine per milligram of protein, with a median of 0.30 nmol of ½cystine per milligram of protein, while in the group of patients with cystinosis, the cystine levels were 2.60–6.90 nmol of ½cystine per milligram of protein, with a median of 4.31 nmol of ½cystine per milligram of protein. The cutoff point was 1.0 nmol of ½cystine per milligram of protein based on the cutoff point values in international studies (Gertsman et al., 2016), the obtained reference cystine levels, and the levels in patients with cystinosis.

Two of these seven children had cystine levels of 0.15 nmol of ½cystine per milligram of protein and 0.28 nmol of ½cystine per milligram of protein, while in their genomes, we detected nucleotide variants described as pathogenic in the HGMD database, which allowed us to count these levels as false negative. An experiment showed that the cause of false-positive values was the decrease in the cystine concentration

in the analyzed fraction, which could be caused by the molecule breakdown without a stabilizer. The measurement of cystine concentration in leukocytes was carried out during cell lysis via sonication with different incubation time intervals at room temperature, which showed that in 20 min of incubation, the concentration decreases by more than 50%, and in 60 min, the concentration is close to zero.

The diagnostic method was optimized as follows:

The cystine concentration was measured in polymorphonuclear leukocytes, which were obtained using a double-gradient method using HISTOPAQUE-1077 and HISTOPAQUE-1119 manufactured by SIGMA (Germany). To avoid cystine breakdown, the cellular sediment was stabilized with a solution of N-ethylmaleimide manufactured by SIGMA (Germany) following the manufacturer's protocol described previously (Giustarini et al., 2006). The cystine concentration was measured again using the modified method in all seven internal control samples in three repetitions, with the lysis time of the analyzed fraction increased from 20 to 60 min at room temperature. All the seven samples, including the two previously noted false-positive samples, showed cystine levels above the cutoff point, even with 60 min of incubation.

## DNA Isolation and Genetic Testing

Genomic DNA was extracted using a DNA Blood Mini Kit (QIAGEN, Germany) on a QIAcube automated station (QIAGEN, Germany) following the manufacturer's protocol. Whole blood was used as the biological material. DNA was eluted in 100 μL of DNAase-free water. The DNA quality and quantity were evaluated spectrophotometrically on a NanoPhotometer N60 spectrophotometer (Implen, Germany) and using a Qubit dsDNA HS Assay Kit for a Qubit 3.0 Fluorometer (Invitrogen, United States). The oligonucleotides for PCR were synthesized by JSC Evrogen (Russia).

Sanger sequencing was carried out using a BigDye® Terminator v3.1 Cycle Sequencing Kit (Thermo Fisher Scientific, United States) following the manufacturer's protocol. The amplification was performed on Bio-Rad T100 (Bio-Rad, United States) and ProFlex (Thermo Fisher Scientific, United States) thermocyclers. Capillary electrophoresis was carried out on ABI 3500XL and ABI 3500 (Thermo Fisher Scientific, United States) genetic analyzers. The obtained sequences were compared to the RefSeqGene references from the National Center for Biotechnology Information (NCBI) database.

To detect the 57 kb deletion, we used the multiplex PCR method suggested by Forestier et al. (1999).

To detect other gross deletions and duplications in the *CTNS* gene, we used multiplex ligase-dependent probe amplification (MLPA). The analysis was carried out using the P473 kits by MRC Holland (Netherlands).

The detection of c.1015G > A (p.G339R) and c.518A > G (p.Y173C) mutations in the *CTNS* gene was carried out during the haplotype analysis using a custom system based on allele-specific ligase reaction (probe sequences are provided in **Supplementary Material S2**). The results were registered via electrophoresis in polyacrylamide gel with subsequent ethidium bromide staining and UV visualization.

## Population Genetic Analysis

We examined the following four microsatellite markers from 17p13.2 (2.44-kb region around the *CTNS* gene): D17S831, D17S1798, D17S1828, D17S1876, and one intragenic marker D17S829. All the markers were chosen using the Marshfield NCBI genetic map (primer sequences are provided in **Supplementary Material S3**). The microsatellite markers were examined by AFLP analysis. The DNA fragments were amplified using PCR. The results were registered via electrophoresis in polyacrylamide gel with subsequent ethidium bromide staining and UV visualization.

Massive parallel sequencing (NGS) of 298 genes for four patients with a c.518A > G mutation in a homozygous state and nine non-related control samples of the Russian Federation residents of Chechen origin was used for phylogenetic analysis. The libraries for NGS were prepared using a KAPA HyperPlus Kit (Roche, United States) following the manufacturer's protocol. The DNA fragmentation time to achieve the average fragment length of 350 bp was 15 min. Target enrichment was carried out using KAPA HyperCap hybridization probes (Roche, United States). Massive parallel sequencing was performed on the MiSeq platform (Illumina, United States) with V2 chemistry (500 cycles, paired-end reads). On average, in every run, 31.5 million reads were obtained, 88% with a Phred score higher than Q30. Bioinformatics analysis was carried out in accordance with GATK Best Practices recommendations (https://gatk.broadinstitute.org/). Genetic variants of all samples were loaded into the VCF2PopTree program (Subramanian et al., 2019) for pairwise genetic distance calculation. Based on these data, we built a phylogenetic tree.

The statistical analysis of the allele frequencies on mutant chromosomes and control group chromosomes was based on the $\chi 2$ test for a 2*2 contingency table comparing two groups: associated allele and all the other alleles. To evaluate linkage disequilibrium (LD), we used the following formula: $\delta$=(PD–PN)/(1–PN), where PD is the frequency of the associated allele among mutant chromosomes and PN is the frequency of the same allele among the normal chromosomes (Bengtsson and Thomson, 1981). The confidence interval (CI) for $\delta$ was calculated as described by Diaz et al. (2000).

## Statistical Analysis

To find the association between cystine levels and *CTNS* mutation types, we used nonparametric statistical analysis methods (Mann–Whitney *U* test). The confidence calculation of differences in cystine concentration values prior to substrate reduction therapy and 6 months after the initial cystagon administration was carried out using the Wilcoxon criterion. A qualitative comparison was performed using an exact F-test.

# RESULTS

## Clinical Results

Selective biochemical screening was carried out for 85 patients with a presumptive diagnosis of cystinosis. As a result, 30 (35.4%) examined children had cystine concentrations higher than the

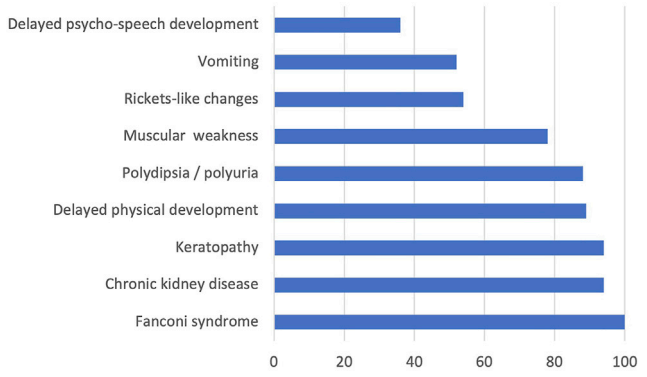


**FIGURE 1 |** Calibration characteristics of the analytics system. The square of the calibration characteristic correlation quotient was 0.997. The lower threshold of quantitative cystine detection was 0.11 μmol/L. The cystine detection threshold was 0.01 μmol/L (**Figure 2**). The time of analysis for one probe was 15 min. The obtained data were processed using a built-in Bruker Data Analysis 4.1 program package.

cutoff point: 2.6–8.9 nmol of ½cystine per milligram of protein, which is very close to the values obtained in corresponding international studies (Wilmer et al., 2011).

All the examined children with available descriptions of clinical symptoms had Fanconi syndrome; 94% of them had chronic kidney disease, 94% had keratopathy, 89% had delayed physical development, 88% had polydipsia/polyuria, 78% had muscular weakness, 54% of the examined children had rickets-like changes, 52% had vomiting, and 36% had delayed psycho-speech development. The data on detected clinical features mostly corresponded to the results of international studies (Nesterova and Gahl, 2008). Only two patients (patients 11 and 16, see **Supplementary Material S5**) had juvenile cystinosis, while the rest had nephropathic cystinosis. The frequencies of different clinical cystinosis symptoms at the time of hospitalization after the confirmed laboratory diagnosis and before the substrate reduction therapy are presented in **Figure 1**.

We detected 23 different pathogenic *CTNS* variants in 40 non-related patients using various molecular genetic analysis methods. The spectra and frequencies of detected variants are presented in **Table 1**. The patients' genotypes are provided in **Supplementary Material S4**.

It is worth noting that 13 mutations detected on 62 chromosomes (77.5%) were previously described, while 10 variants detected on 18 chromosomes (22.5%) were novel. Among the described *CTNS* variants, the 57 kb deletion was the most frequent; it was detected on 20 alleles (25.0%) in 15 (37.5%) children with infantile nephropathic cystinosis. This pathogenic variant was described in 50–60% of patients with cystinosis among European and North American residents (Anikster et al., 1999; Heil et al., 2001; Kleta et al., 2001; Kiehntopf et al., 2002). The differences in allelic frequencies of this major variant in European and Russian patients can be explained by population diversity.

The missense c.518A > G mutation leading to the p.Y173C amino acid residue replacement was previously described once (Topaloglu et al., 2012). It was detected on 11 (13.8%) alleles in children from six non-related families, five out of which are ethnically Chechen and live in the Republic of Chechnya and Ingushetia. The pathogenic c.1015G > A variant, which leads to the p.G339R amino acid residue replacement and was previously described in American, Turkish, and Iranian patients with infantile cystinosis (Topaloglu et al., 2012; Zykovich et al., 2015; Ghazi et al., 2017), was detected on 10 alleles

**TABLE 1 |** Allelic frequencies of *CTNS* (*NM_001031681.2*) GRch37 variants.

| Variant | Number of chromosomes with the variant | Allelic frequency (%) (80 chromosomes) |
|---|---|---|
| *57 kb del* | 20 | 25.00 |
| c.518A>G, p.Y173C | 11 | 13.75 |
| c.1015G>A, p.G339R | 10 | 12.50 |
| c.433C>T, p.Q145* | 6 | 7.50 |
| c.785G>A, p.W262* | 5 | 6.25 |
| c.18_21del, p.Thr7Phefs*7 | 3 | 3.75 |
| g.(?_3558266)_(3565849_?)del (ex.6-13del) | 2 | 2.50 |
| g.(?_3550706)_(3552123_?)del *(ex4-5del)* | 2 | 2.50 |
| c.699_700del, p.S234Lfs*61 | 2 | 2.50 |
| c.451A>G, p.R151G | 2 | 2.50 |
| c.283G>T, p.G95* | 2 | 2.50 |
| g.(?_ 3558266)_( 3558736_?)del (*ex6-7del)* | 2 | 2.50 |
| c.140+2dup | 2 | 2.50 |
| c.627C>A, p.S209R | 2 | 2.50 |
| c.681G>A, p.E227E | 1 | 1.25 |
| *c.681+1G>A* | 1 | 1.25 |
| c.323del, p.Q108Rfs*10 | 1 | 1.25 |
| c.613G>A, p.D205K | 1 | 1.25 |
| c.198_218del p.(Ile67_Pro73del) | 1 | 1.25 |
| c.1000del, p.T334Pfs*65 | 1 | 1.25 |
| c.505G>T, p.G169C | 1 | 1.25 |
| c.413G>A, p.W138* | 1 | 1.25 |
| c.450G>A, p.W150* | 1 | 1.25 |

(12.5%) in children from six non-related families of Karachay ethnicity from the Republic of Karachay-Cherkessia, Kabardino-Balkaria, and Stavropol Krai. The nucleotide variant c.433C > T, which leads to p.Q145* premature translation termination and was described in an Iranian patient (Najafi et al., 2019), was detected on five alleles in four (10.0%) patients from various regions of Russia. A previously non-described c.785G > A nucleotide variant, which leads to a p.W262* premature translation termination, was detected in four patients from three families from Tatarstan, Bashkortostan, and Moscow Oblast.

The ex.6-13del gross deletion was detected on two alleles in two non-related patients from Omsk and Smolensk Oblast. A previously non-described pathogenic c.450G > A, p.W150* variant, was detected in a homozygous state in a boy from Khabarovsk Krai. The c.413G > A, p.W138* variant was detected in a compound heterozygous state with the c.433C > T variant in a boy from the Republic of Mordovia. Both suffered from infantile nephropathic cystinosis with manifestation at the age of 7 months.

A boy with severe infantile nephropathic cystinosis had a previously non-described single-nucleotide deletion c.1000del leading to a p.T334Pfs*65 frameshift in a compound heterozygous state with 57 kb deletion. A missense c.627C > A, p.S209R variant was detected in a homozygous state in a boy with juvenile nephropathic cystinosis from the Republic of Bashkortostan. This variant has not been described in the gnomAD database (version 2.1.1) and was not present in exomes of 1337 Russian patients with various referral diagnoses. Overall, 10 programs (BayesDel_addAF, DANN, DEOGEN2, FATHMM-MKL, LIST-S2, M-CAP, MVP, MutationAssessor, MutationTaster, and SIFT) predict the pathogenicity of this variant. The patient had distinct clinical and biochemical data in favor of the "nephropathic cystinosis" diagnosis; thus, the variant was interpreted as likely pathogenic. Another previously non-described variant—a gross deletion including exons 6 and 7 of the *CTNS* gene—was detected in a homozygous state in a patient from Ukraine.

A female patient from Belarus also suffering from juvenile nephropathic cystinosis had a previously non-described c.140+2dup duplication in a homozygous state. This variant was present on one chromosome out of 251,172 in the gnomAD database (version 2.1.1) and not present in the 1337 Russian exomes. The variant, according to prediction programs (NETGENE2 and HSF), is very likely to affect the donor splice site of exon 4 (NM_001031681.2). However, despite the typical clinical and biochemical phenotypes of the patient, this variant was interpreted as VUS.

Two Ukrainian patients had three previously described (Shotelersuk et al., 1998; Town et al., 1998; Mason et al., 2003) pathogenic variants: c.699_700del, p.S234Lfs*61 in a homozygous state and c.18_21del, p.T7Ffs*7 in compound heterozygous state with c.613G > A, p.D205K.

A high percentage of homozygous *CTNS* variants allowed us to describe the correlations of certain mutation types with blood cystine levels prior to the substrate reduction therapy. The lowest concentration was detected in a patient with a missense variant c.627C > A, p.S209R in a homozygous state, while the patient with a nonsense c.283G > T, p.G95* variant in a homozygous state showed the highest cystine concentration (**Figure 2**).

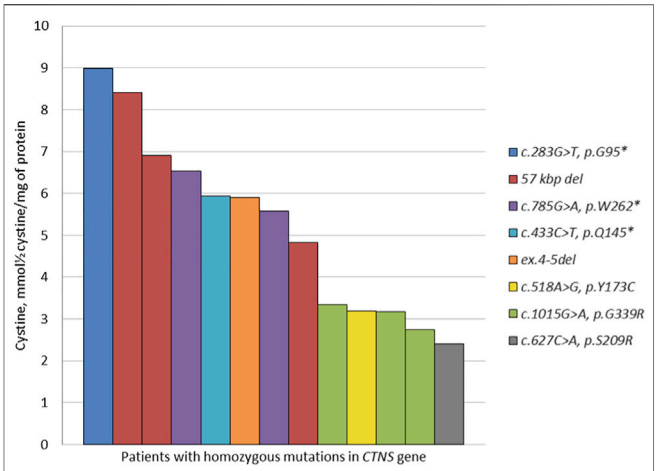


**FIGURE 2 |** Chromatogram of the standard cystine solution with a concentration of 0.11 μmol/L corresponding to the lower threshold of the quantitative detection method.

Based on the analysis of the obtained data, we detected statistically valid differences ($p$ = 0.003) between high cystine concentrations in a group of patients with homozygous LoF variants (the 57 kb deletion, nonsense c.283G > T, c.433C > T, c.785G > A mutations) compared to the group of patients with homozygous missense c.518A > G, c.627C > A, c.1015G > A mutations in the *CTNS* gene (**Table 2**).

The patients responded adequately to pathogenetic therapy with cysteamine bitartrate in most cases, which is confirmed by normal—0.78 (0.2–1.1)—levels of cystine measured 6 months after the start of the therapy. The excess cystine level detected in two cases was caused by a break from taking the medication in one child and the necessity of dose correction in another. Considering those factors, the treatment was corrected, and both patients showed normal cystine levels at the time of the next hospitalization.

Considering that nephropathic cystinosis has autosomal recessive inheritance, this condition might prevail in some ethnic and geographic isolates because of local founder effects or the high number of inbred marriages. In the examined patient groups, we detected a high frequency of the c.1015G > A pathogenic variant in Karachay residents and the c.518A > G variant in Chechen residents.

Kinship of probands with the same mutations was excluded via questioning relatives in at least three generations.

The c.1015G > A variant was the main cause of nephrotic cystinosis in ethnic Karachay patients: four out of six patients with this variant were Karachay-Cherkessia residents and the other two were from neighboring regions: Stavropol Krai and the Republic of Kabardino-Balkaria. All families of patients with this variant were ethnically Karachay.

## Population Genetic Analysis Results

We analyzed the five following microsatellite markers from the *CTNS* gene region: D17S831, D17S1798, D17S1828, D17S1876, and D17S829; haplotype analysis was carried out

**TABLE 2 |** Cystine levels in groups of patients with different *CTNS* mutation types.

| Parameter | Patients with homozygous missense mutations | Patients with homozygous Lof mutations | p-value (Mann–Whitney U test) |
|---|---|---|---|
| Cystine concentration, ½cystine per milligram of protein | 3.2 (2.9–3.2) | 6.3 (5.9–7.3) | 0.003 |

Note: *Cystine concentrations are presented as median values and quartiles (25%–75%).*

**TABLE 3 |** Haplotypes of chromosomes with the c.1015G>A mutation for markers D17S831-D17S1798-D17S829-D17S1828-D17S1876.

| Patient | Marker | D17S831 | D17S1798 | CTNS | D17S829 | D17S1828 | D17S1876 |
|---|---|---|---|---|---|---|---|
| | Coordinate (kB) | 1.910 | 2.706 | 3.540-3.566 | 3.550 | 3.810 | 4.345 |
| | Place of residence | | | | | | |
| BM | Republic of Karachay-Cherkessia | 1 | 1 | c.1015G>A | 3 | 3 | 9 |
| | | 1 | 1 | c.1015G>A | 3 | 3 | 9 |
| SF | Republic of Karachay-Cherkessia | 1 | 1 | c.1015G>A | 3 | 3 | 9 |
| | | 8 | 3 | c.1015G>A | 3 | 3 | 10 |
| TSR | Republic of Karachay-Cherkessia | 1 | 1 | c.1015G>A | 3 | 3 | 9 |
| | | 1 | 1 | c.1015G>A | 3 | 3 | 9 |
| KI | Republic of Karachay-Cherkessia | 3 | 1 | c.1015G>A | 3 | 3 | 9 |
| | | 3 | 7 | c.18_21del | 7 | 3 | 8 |
| BRA | Republic of Kabardino-Balkaria | 3 | 1 | c.1015G>A | 3 | 3 | 7 |
| | | 7 | 2 | c.681G>A | 7 | 4 | 6 |
| ESA | Republic of Karachay-Cherkessia | 1 | 2 | c.1015G>A | 3 | 3 | 9 |
| | | 1 | 2 | c.1015G>A | 3 | 3 | 9 |

**TABLE 4 |** Linkage disequilibrium analysis between *CTNS* c.1015G>A mutation and microsatellites closest to the *CTNS* gene.

| Marker | Coordinate cM | Allele | p-value | δ±95 CI |
|---|---|---|---|---|
| D17S831 | 6.60 | 1 | p<0.05 | 0.864±0.256 |
| D17S1798 | 6.60 | 1 | p>0.05 | 0.289±0.694 |
| D17S829 (CTNS) | 10.02 | 3 | — | — |
| D17S1828 | 10.02 | 3 | — | — |
| D17S1876 | 10.72 | 9 | p<0.05 | 0.868±0.248 |

on the material of four non-related patients homozygous on the c.1015G > A variant and two compound heterozygous: c [1015G > A]; [18_21del] and c[1015G > A]; [681G > A]. The genotyping results are presented in **Table 3**. The presumed founder haplotype is highlighted with gray.

As a control group, we typed DNA samples of 18 non-related Karachay people without the c.1015G > A mutation on the same microsatellite markers. The allelic frequencies in eight mutant (D) chromosomes of homozygous patients and 38 control chromosomes (N) for five microsatellite loci above (D17S831, D17S1798), below (D17S1828, D17S1876), and in the intron (D17S829) of the *CTNS* gene on a Marshfield genetic map are provided in **Supplementary Material S6**. F-test results for alleles of markers with the highest linkage disequilibrium parameter δ are presented in **Table 4**.

Thus, the 1-1-3-3-9 haplotype on markers D17S831-D17S1798-D17S829-D17S1828-D17S1876 is highly likely to be the founder haplotype subjected to gradual decay, and the accumulation of the c.1015G > A mutation in the *CTNS* gene in the Republic of Karachay-Cherkessia is caused by the founder effect.

We scanned DNA samples of 197 healthy Karachay residents from various regions of the Republic of Karachay-Cherkessia for the c.1015G > A mutation and did not detect any carriers of this variant. Thus, despite the undoubted presence of the founder effect for this mutation, its carrier frequency is not very high on the territory of the Republic of Karachay-Cherkessia, and the accumulation of patients with this mutation is most likely caused by inbred marriages, although the parents of the probands with the *CTNS* variant in a homozygous state deny kinship.

The c.518A > G variant was the most common among patients from the Republic of Chechnya: four patients from this republic had the mutation in a homozygous state, and an additional patient from Ingushetia, which borders Chechnya. Outside of the Republic of North Caucasus, the c.518A > G mutation was detected in a compound heterozygous state with the common 57 kb deletion in one Russian patient from the Moscow Oblast. Four homozygous samples were genotyped using the following microsatellite markers: D17S831-D17S1798-D17S829-D17S1828-D17S1876 (**Table 5**).

The control group consisted of 17 non-related Chechnya residents without the c.518A > G mutation. The genotyping results are presented in **Table 5**. The presumed founder haplotype is highlighted with gray. The frequencies of alleles carrying the mutation on homozygous patients' chromosomes and control chromosomes for five microsatellite loci above (D17S831, D17S1798), below (D17S1828, D17S1876), and in the intron (D17S829) of the *CTNS* gene on the Marshfield genetic map are provided in **Supplementary Material S7**.

**TABLE 5 |** Haplotypes of chromosomes with the c.518A > G mutation for markers D17S831-D17S1798-D17S829-D17S1828-D17S1876.

| Patient | Marker | D17S831 | D17S1798 | CTNS | D17S829 | D17S1828 | D17S1876 |
|---|---|---|---|---|---|---|---|
| — | Coordinate (kB) | 1.910 | 2.706 | 3.540–3.566 | 3.550 | 3.810 | 4.345 |
| | Place of residence | | | | | | |
| MM | Chechnya | 4 | 1 | c.518A > G | 1 | 5 | 7 |
| | | 4 | 1 | c.518A > G | 1 | 5 | 7 |
| MSU | Chechnya | 6 | 1 | c.518A > G | 1 | 5 | 7 |
| | | 6 | 2 | c.518A > G | 1 | 2 | 1 |
| IAM | Chechnya | 9 | 2 | c.518A > G | 1 | 8 | 7 |
| | | 1 | 1 | c.518A > G | 1 | 5 | 7 |
| EIS | Ingushetia | 3 | 2 | c.518A > G | 1 | 8 | 7 |
| | | 3 | 3 | c.518A > G | 1 | 5 | 7 |

**TABLE 6 |** Linkage disequilibrium analysis between *CTNS* c.518A > G mutation and microsatellites closest to the *CTNS* mgene.

| Marker | Coordinate cM | Allele | *p*-value | δ±95 CI |
|---|---|---|---|---|
| D17S831 | 6.60 | 6 | $p > 0.05$ | 0.177 ± 0.348 |
| D17S1798 | 6.60 | — | — | — |
| D17S829 (CTNS) | 10.02 | 1 | — | — |
| D17S1828 | 10.02 | 5 | $p > 0.05$ | 0.469 ± 0.502 |
| D17S1876 | 10.72 | 9 | $p < 0.05$ | 0.863 ± 0.257 |

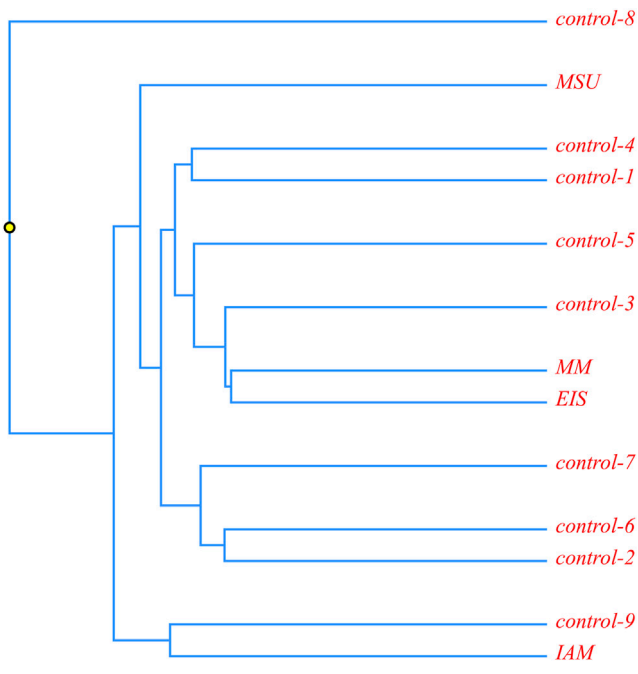


**FIGURE 3 |** Phylogenetic analysis of ethnic Chechen children with the c.518A>G pathogenic variant; and control samples without it.

The F-test results for alleles of markers with the highest linkage disequilibrium values ($\delta$) are presented in **Table 6**.

Even though the founder effect is traceable for this mutation, the decay of this genotype is very strong, starting in the genetic coordinates of the *CTNS* gene at marker D17S1828. It is possible that later two more local founder effects caused the two genotype groups on markers D17S1798-D17S829-D17S1828-D17S1876: 1-1-5-7 and 2-1-8-7.

During the analysis of 178 DNA samples of ethnic Chechen people, we detected one carrier of the c.518A > G mutation in a heterozygous state.

A phylogenetic analysis was carried out for four patients with the c.518A > G mutation in a homozygous state. It was suggested that in case of a founder effect, the genetic distance between the samples would be minimal, and on phylogenetic trees, these samples will form a separate cluster. The tree diagram illustrating the genetic distance between the samples is presented in **Figure 3**.

It is obvious that the samples with the homozygous c.518A > G mutation are located in different clusters and are not isolated from the control samples. This allows us to suggest that this mutation could appear in several isolates during an insignificant time frame or that its accumulation is a result of inbred marriages.

## DISCUSSION

More than 90% of detected cystinosis cases are caused by a 57 kb deletion and mutations located in exons 7–10 and 12a of the *CTNS* gene, which mostly corresponds with international studies (Anikster et al., 1999; Forestier et al., 1999). Among the previously described *CTNS* variants, the most frequent was the 57257-bp deletion, which was found on 20 alleles (25.0%) in 15 (37.5%) children with infantile cystinosis. The differences in frequencies of this major variant among European and Russian patients can be explained by the prevalence of patients from the Republic of Chechnya (4/11.4%) and the Republic of Karachay-Cherkessia (4/11.4%) in the examined group. In the North Caucasian Republic, the c.518A > G mutation in the Chechen ethnos and the c.1015G > A in the Karachay ethnos are accumulated as a result of local founder effects and inbred marriages.

In this study, we detected ten novel variants of the *CTNS* gene, eight of which are classified as pathogenic, one as likely pathogenic, and one as VUS in accordance with the Russian guide for the interpretation of the human DNA sequence data (Рыжкова et al., 2019). A previously non-described c.785G > A (p.W262*) nucleotide variant was detected in patients from three families; it also shows the tendency to accumulate in patients

from Povolzhye. A previously non-described ex.6-13del gross deletion was detected in two non-related patients. Each of the remaining novel mutation was detected once.

In total, among 23 detected variants in the *CTNS* gene, LoF variants prevailed: nine (39.1%) deletions, including four gross deletions (18%), five (21.7%) nonsense mutations, and one (4.4%) canonic splice site mutation. Aside from that, we detected seven (30.4) pathogenic and likely pathogenic missense mutations and one VUS variant affecting the canonic splice site. According to the information presented in the HGMD professional database on the types of detected mutations in the *CTNS* gene, missense and nonsense mutations had the highest percentage (41%). However, there were differences as well. Thus, a significant percentage (18%) of gross deletions detected in this study is slightly higher than that in the HGMD database, where this value is 12%. On the other side, the percent of canonic splice site mutations described in the literature is slightly higher (14%). These differences are likely to be caused by the small number of patients in our cohort compared to the worldwide data in the HGMD professional database.

The patients presented in this study mostly had infantile nephropathic cystinosis and responded to cysteamine bitartrate pathogenetic therapy, which is confirmed by multiple measurements of cystine levels during the therapy monitoring. We showed the difference between the mutation type (LoF or missense) and blood cystine levels prior to the pathogenetic therapy. Studies of international scientists describing various population groups demonstrate the association of mutations that prematurely interrupt the protein synthesis with early manifestation and severe clinical picture of cystinosis (Taranta et al., 2010; Al-Haggar, 2013; Alcántara-Ortigoza et al., 2013; Ferreira et al., 2018). According to these data, we can assume that high cystine levels may correlate directly with the severity of cystinosis and may be an unfavorable prognostic factor for patients with LoF mutations in the *CTNS* gene.

## CONCLUSION

The genetic landscape of nephropathic cystinosis in Russian patients shows the major variants c.1015G > A and c.518A > G to be characteristic for Karachay and Chechen ethnic groups.

Nephropathic cystinosis is an orphan disease of metabolic nature, which requires a complex approach for its diagnosis. The practice of screening the population for cystinosis by biochemical testing is currently technically complicated due to high blood volume and short lifetime of polymorphonuclear leukocytes; therefore, the effort aimed at the reduction of the number of disease cases should be primarily focused on selecting patients into the risk group at the youngest age, as well as on cascade analysis of relatives in affected families.

An early diagnostics using the methods presented in this study and the early start of complex therapy combining symptomatic and pathogenetic substrate reduction therapy, continuing the latter during the patient's life, have significant importance in establishing the best control over the disease, preventing the growth deceleration, and delaying chronic kidney disease and other renal and extrarenal complications.

## DATA AVAILABILITY STATEMENT

The datasets presented in this study can be found in online repositories. The names of the repository/repositories and accession number(s) can be found at: https://www.ncbi.nlm.nih.gov/, PRJNA804010.

## ETHICS STATEMENT

The studies involving human participants were reviewed and approved by the Local Ethics Committee of National Medical Research Center for Children's Health, Moscow, Russian Federation. Written informed consent to participate in this study was provided by the participants' legal guardian/next of kin.

## AUTHOR CONTRIBUTIONS

KS: methodology, conceptualization, writing the original draft, and review and editing; AP: data curation and review and editing; OS: formal analysis, investigation, writing—original draft, and methodology; VM: collection of biological material and patient management; ES: collection of biological material and patient management; IZ: conducting MLPA, NGS and partly bioinformatics analysis; NM: measure the cystine concentration; AF: project administration and final editing; PM: formal analysis and investigation; AP: conceptualization, writing—original draft, and supervision; EB: data curation; RZ: data curation; and AT: development of criteria for selective screening.

## SUPPLEMENTARY MATERIAL

The Supplementary Material for this article can be found online at: https://www.frontiersin.org/articles/10.3389/fgene.2022.863157/full#supplementary-material

## REFERENCES

Al-Haggar, M. (2013). Cystinosis as a Lysosomal Storage Disease with Multiple Mutant Alleles: Phenotypic-Genotypic Correlations. *World J. Nephrol.* 2, 94–102. doi:10.5527/wjn.v2.i4.94

Alcántara-Ortigoza, M. A., Martínez-Bernal, A. B., Belmont-Martínez, L., Vela-Amieva, M., and González-del Angel, A. (2013). CTNS Gene Analysis Emphasizes Diagnostic Value of Eye Examination in Patients with Cystinosis. *J. Pediatr. Genet.* 2, 129–132. doi:10.3233/PGE-13060

Angileri, F., Bergeron, A., Morrow, G., Lettre, F., Gray, G., Hutchin, T., et al. (2015). Geographical and Ethnic Distribution of Mutations of the Fumarylacetoacetate

Hydrolase Gene in Hereditary Tyrosinemia Type 1. *JIMD Rep.* 19, 43–58. doi:10.1007/8904_2014_363

Anikster, Y., Shotelersuk, V., and Gahl, W. A. (1999). CTNS Mutations in Patients with Cystinosis. *Hum. Mutat.* 14, 454–458. doi:10.1002/(sici)1098-1004(199912)14:6<454::aid-humu2>3.0.co;2-h

Bengtsson, B. O., and Thomson, G. (1981). Measuring the Strength of Associations between HLA Antigens and Diseases. *Tissue antigens* 18, 356–363. doi:10.1111/j.1399-0039.1981.tb01404.x

Chabli, A., Aupetit, J., Raehm, M., Ricquier, D., and Chadefaux-Vekemans, B. (2007). Measurement of Cystine in Granulocytes Using Liquid Chromatography-Tandem Mass Spectrometry. *Clin. Biochem.* 40, 692–698. doi:10.1016/j.clinbiochem.2007.02.005

David, D., Princiero Berlingerio, S., Elmonem, M. A., Oliveira Arcolino, F., Soliman, N., van den Heuvel, B., et al. (2019). Molecular Basis of Cystinosis: Geographic Distribution, Functional Consequences of Mutations in the CTNS Gene, and Potential for Repair. *Nephron* 141, 133–146. doi:10.1159/000495270

Diaz, G. A., Gelb, B. D., Risch, N., Nygaard, T. G., Frisch, A., Cohen, I. J., et al. (2000). Gaucher Disease: The Origins of the Ashkenazi Jewish N370S and 84GG Acid β-Glucosidase Mutations. *Am. J. Hum. Genet.* 66, 1821–1832. doi:10.1086/302946

Ebbesen, F., Mygind, K. I., and Holck, F. (1976). Infantile Nephropatic Cystinosis in Denmark. *Dan Med. Bull.* 23, 216–222. Available at: http://www.ncbi.nlm.nih.gov/pubmed/975942.

Ferreira, F., Leal, I., Sousa, D., Costa, T., Mota, C., Gomes, A. M., et al. (2018). CTNS Molecular Genetics Profile in a Portuguese Cystinosis Population. *OJGen* 08, 91–100. doi:10.4236/ojgen.2018.84008

Forestier, L., Jean, G., Attard, M., Cherqui, S., Lewis, C., van't Hoff, W., et al. (1999). Molecular Characterization of CTNS Deletions in Nephropathic Cystinosis: Development of a PCR-Based Detection Assay. *Am. J. Hum. Genet.* 65, 353–359. doi:10.1086/302509

Gahl, W. A., Balog, J. Z., and Kleta, R. (2007). Nephropathic Cystinosis in Adults: Natural History and Effects of Oral Cysteamine Therapy. *Ann. Intern. Med.* 147, 242. doi:10.7326/0003-4819-147-4-200708210-00006

Gertsman, I., Johnson, W. S., Nishikawa, C., Gangoiti, J. A., Holmes, B., and Barshop, B. A. (2016). Diagnosis and Monitoring of Cystinosis Using Immunomagnetically Purified Granulocytes. *Clin. Chem.* 62, 766–772. doi:10.1373/clinchem.2015.252494

Ghazi, F., Hosseini, R., Akouchekian, M., Teimourian, S., Ataei Kachoei, Z., Otukesh, H., et al. (2017). CTNS Molecular Genetics Profile in a Persian Nephropathic Cystinosis Population. *Nefrología* 37, 301–310. doi:10.1016/j.nefro.2016.11.024

Giustarini, D., Dalle-Donne, I., Lorenzini, S., Milzani, A., and Rossi, R. (2006). Age-Related Influence on Thiol, Disulfide, and Protein-Mixed Disulfide Levels in Human Plasma. *Journals Gerontol. Ser. A: Biol. Sci. Med. Sci.* 61, 1030–1038. doi:10.1093/gerona/61.10.1030

Heil, S. G., Levtchenko, E., Monnens, L. A. H., Trijbels, F. J. M., van der Put, N. M. J., and Blom, H. J. (2001). The Molecular Basis of Dutch Infantile Nephropathic Cystinosis. *Nephron* 89, 50–55. doi:10.1159/000046043

Hult, M., Darin, N., von Döbeln, U., and Månsson, J.-E. (2014). Epidemiology of Lysosomal Storage Diseases in Sweden. *Acta Paediatr.* 103, 1258–1263. doi:10.1111/apa.12807

Hutchesson, A. C., Bundey, S., Preece, M. A., Hall, S. K., and Green, A. (1998). A Comparison of Disease and Gene Frequencies of Inborn Errors of Metabolism Among Different Ethnic Groups in the West Midlands, UK. *J. Med. Genet.* 35, 366–370. doi:10.1136/jmg.35.5.366

Kalatzis, V. (2002). Cystinosis: from Gene to Disease. *Nephrol. Dial. Transplant.* 17, 1883–1886. doi:10.1093/ndt/17.11.1883

Kiehntopf, M., Schickel, J., Gönne, B. v. d., Koch, H. G., Superti-Furga, A., Steinmann, B., et al. (2002). Analysis of the CTNS Gene in Patients of German and Swiss Origin with Nephropathic Cystinosis. *Hum. Mutat.* 20, 237. doi:10.1002/humu.9063

Kleta, R., Anikster, Y., Lucero, C., Shotelersuk, V., Huizing, M., Bernardini, I., et al. (2001). CTNS Mutations in African American Patients with Cystinosis. *Mol. Genet. Metab.* 74, 332–337. doi:10.1006/mgme.2001.3218

Mason, S., Pepe, G., Dall'Amico, R., Tartaglia, S., Casciani, S., Greco, M., et al. (2003). Mutational Spectrum of the CTNS Gene in Italy. *Eur. J. Hum. Genet.* 11, 503–508. doi:10.1038/sj.ejhg.5200993

Najafi, M., Tamandani, D. M. K., Azarfar, A., Bakey, Z., Behjati, F., Antony, D., et al. (2019). A 57 kB Genomic Deletion Causing CTNS Loss of Function Contributes to the CTNS Mutational Spectrum in the Middle East. *Front. Pediatr.* 7. doi:10.3389/fped.2019.00089

Nesterova, G., and Gahl, W. (2008). Nephropathic Cystinosis: Late Complications of a Multisystemic Disease. *Pediatr. Nephrol.* 23, 863–878. doi:10.1007/s00467-007-0650-8

Ruivo, R., Bellenchi, G. C., Chen, X., Zifarelli, G., Sagné, C., Debacker, C., et al. (2012). Mechanism of Proton/substrate Coupling in the Heptahelical Lysosomal Transporter Cystinosin. *Proc. Natl. Acad. Sci. U.S.A.* 109, E210–E217. doi:10.1073/pnas.1115581109

Savostyanov, K. W., Mazanova, N. N., Mazanova, N. N., Pushkov, A. A., Ananyin, P. V., Sukhozhenko, A. V., et al. (2018). Chromatography- Mass Spectrometry and Molecular Genetic Diagnosis of Cystinosis in Russian Children. *Pediatria* 97, 71–78. doi:10.24110/0031-403X-2018-97-5-71-78

Shotelersuk, V., Larson, D., Anikster, Y., Mcdowell, G., Lemons, R., Bernardini, I., et al. (1998). CTNS Mutations in an American-Based Population of Cystinosis Patients. *Am. J. Hum. Genet.* 63, 1352–1362. doi:10.1086/302118

Subramanian, S., Ramasamy, U., and Chen, D. (2019). VCF2PopTree: a Client-Side Software to Construct Population Phylogeny from Genome-wide SNPs. *PeerJ* 7, e8213. doi:10.7717/peerj.8213

Taranta, A., Wilmer, M. J., van den Heuvel, L. P., Bencivenga, P., Bellomo, F., Levtchenko, E. N., et al. (2010). Analysis of CTNS Gene Transcripts in Nephropathic Cystinosis. *Pediatr. Nephrol.* 25, 1263–1267. doi:10.1007/s00467-010-1502-5

Topaloglu, R., Vilboux, T., Coskun, T., Ozaltin, F., Tinloy, B., Gunay-Aygun, M., et al. (2012). Genetic Basis of Cystinosis in Turkish Patients: a Single-center Experience. *Pediatr. Nephrol.* 27, 115–121. doi:10.1007/s00467-011-1942-6

Touchman, J. W., Anikster, Y., Dietrich, N. L., Maduro, V. V. B., McDowell, G., Shotelersuk, V., et al. (2000). The Genomic Region Encompassing the Nephropathic Cystinosis Gene (CTNS): Complete Sequencing of a 200-kb Segment and Discovery of a Novel Gene within the Common Cystinosis-Causing Deletion. *Genome Res.* 10, 165–173. doi:10.1101/gr.10.2.165

Town, M., Jean, G., Cherqui, S., Attard, M., Forestier, L., Whitmore, S. A., et al. (1998). A Novel Gene Encoding an Integral Membrane Protein Is Mutated in Nephropathic Cystinosis. *Nat. Genet.* 18, 319–324. doi:10.1038/ng0498-319

Wilmer, M. J., Schoeber, J. P., van den Heuvel, L. P., and Levtchenko, E. N. (2011). Cystinosis: Practical Tools for Diagnosis and Treatment. *Pediatr. Nephrol.* 26, 205–215. doi:10.1007/s00467-010-1627-6

Zykovich, A., Kinkade, R., Royal, G., and Zankel, T. (2015). CTNS Mutations in Publicly-Available Human Cystinosis Cell Lines. *Mol. Genet. Metab. Rep.* 5, 63–66. doi:10.1016/j.ymgmr.2015.10.007

Рыжкова, О. П., Кардымон, О. Л., Прочорчук, Е. Б., Коновалов, Ф. А., Масленников, А. Б., СтеПанов, В. А., et al. (2019). Руководство По интерПретации данныч Последовательности ДНК человека, Полученныч методами массовоГо ПараллельноГо секвенирования (MPS) (редакция 2018, версия 2). *Nauchno-prakticheskii zhurnal «Medicinskaia genetika»*, 3–23. doi:10.25557/2073-7998.2019.02.3-23

**Conflict of Interest:** The authors declare that the research was conducted in the absence of any commercial or financial relationships that could be construed as a potential conflict of interest.

**Publisher's Note:** All claims expressed in this article are solely those of the authors and do not necessarily represent those of their affiliated organizations, or those of the publisher, the editors, and the reviewers. Any product that may be evaluated in this article, or claim that may be made by its manufacturer, is not guaranteed or endorsed by the publisher.

frontiers | Frontiers in Genetics

TYPE Original Research
PUBLISHED 12 August 2022
DOI 10.3389/fgene.2022.870232



OPEN ACCESS

EDITED BY
Babak Behnam,
National Sanitation Foundation International, United States

REVIEWED BY
Aldesia Provenzano,
University of Florence, Italy
Robert Henderson,
Great Ormond Street Hospital for Children NHS Foundation Trust, United Kingdom
Subbulakshmi Chidambaram,
University of Toronto, Canada

*CORRESPONDENCE
Xingsheng Dong,
xingsheng85@163.com

SPECIALTY SECTION
This article was submitted to Genetics of Common and Rare Diseases, a section of the journal *Frontiers in Genetics*.

RECEIVED 06 February 2022
ACCEPTED 27 June 2022
PUBLISHED 12 August 2022

CITATION
Li H, Li Z, Wang D, Chen C, Chen Z, Wang J, Xu C and Dong X (2022), Next-generation sequencing reveals a case of Norrie disease in a child with bilateral ocular malformation.
*Front. Genet.* 13:870232.
doi: 10.3389/fgene.2022.870232



# Next-generation sequencing reveals a case of Norrie disease in a child with bilateral ocular malformation

Haijun Li[1], Zhiming Li[1], Degang Wang[1], Chuanming Chen[2], Zhiqiang Chen[3], Jinhua Wang[4], Chenxia Xu[1] and Xingsheng Dong[1]*

[1]Prenatal Diagnosis Center, Boai Hospital of Zhongshan, Zhongshan, GD, China, [2]Radiological Department, Boai Hospital of Zhongshan, Zhongshan, GD, China, [3]Pathology Department, Boai Hospital of Zhongshan, Zhongshan, GD, China, [4]Gynaecology Department, Boai Hospital of Zhongshan, Zhongshan, GD, China

A Norrie disease protein gene (*NDP*) variant, c.174 + 1G > A, was found in a Chinese family through next-generation sequencing and verified with Sanger sequencing. A case of Norrie disease was reported in the first child, and the symptoms were consistent with the results of gene sequencing. The child's mother, who was pregnant at the time, was found to be a carrier of the identified pathogenic variant. To determine if the fetus carried the same disease-causing variant, prenatal examination and prenatal diagnosis were conducted. The fetus had biocular vitreous abnormalities and complete retinal abnormalities. Genetic testing showed that the fetus had maternally inherited the *NDP* gene variant found in the proband. It was concurrently confirmed that the *NDP* gene variant led to the deletion of 246 bp at the 3′ end of exon 2, resulting in the deletion of the initiation codon and the occurrence of disease. Our study suggests that the diagnosis of rare diseases through next-generation sequencing, combined with prenatal ultrasound and prenatal diagnosis, can help families with known familial genetic diseases. Furthermore, the findings of this study broaden the known genetic spectrum of Norrie disease.

KEYWORDS

**Norrie disease, next-generation sequencing, variant, genetic, NDP**

## Introduction

Norrie disease (ND) (OMIM #310600), first reported in 1927 (Norrie, 1927), is an extremely rare X-linked recessive disorder characterized by exudative hyperplasia (Meire et al., 1998) in which blindness can occur in the early postnatal period due to retinal detachment caused by vitreoretinal dysplasia (Andersen and Warburg, 1961; Warburg, 1966). Moreover, 25–50% of patients have extraocular symptoms such as sensorineural deafness and intellectual disability (Fangting et al., 2016; Wu et al., 2017). The pathogenic ND gene is located on chromosome Xp11.3 (ChrX: 4,36,92,969–4,37,17,694) (GRCh37).

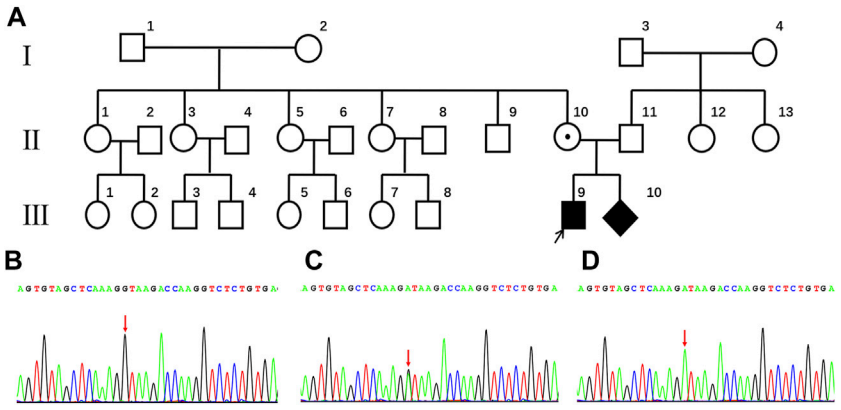


FIGURE 1
**(A)** Pedigree of the family with Norrie disease. **(B)** partial wild-type *NDP* sequences from the family (I-1, I-2, II-1, II-5, II-9, II-11, III-5, and III-6). The arrow indicates the proband in this study. **(C)** partial sequences of the family member heterozygous for the c.174 + 1G > A genotype (II-10). **(D)** partial sequences of family members hemizygous for the c.174 + 1G > A genotype (III-9 and III-10).

The *NDP* gene is composed of three exons that encode the 133 amino acids that comprise the Norrin protein (Chen et al., 1993). Norrin is a secreted protein with a cystine-knot motif that activates the Wnt/beta-catenin pathway.

The diagnosis of ND is based on a combination of clinical ocular manifestations and molecular genetic testing. There are no biochemical or functional tests currently used as disease markers. Therefore, identifying novel mutations is essential for clinical and genetic diagnosis.

The purpose of this study was to identify genetic defects in a Chinese ND family and provide clinical guidance for the prevention of birth defects. Next-generation sequencing allowed us to identify a novel *NDP* gene variant (c.174 + 1G > A) in the affected patient in this family, and we established that the variant was inherited from the mother. The pathogenic mechanism of the *NDP* variant c.174 + 1G > A was confirmed to involve the deletion of exon 2, which leads to the deletion of the original start codon and abnormal mRNA expression. In the next pregnancy, the *NDP* gene was sequenced using fetal umbilical vein blood at 27 weeks of gestation for prenatal diagnosis. The fetus in this subsequent pregnancy inherited the same variant, with imaging studies matching the finding. The parents opted to terminate the pregnancy, considering the poor prognosis of their first son.

# Materials and methods

## Patients, editorial policies, and ethical considerations

A three-generation Chinese family was recruited. The family pedigrees are shown in Figure 1A. The woman (II-10) had been pregnant for 16 weeks and came to the hospital with her blind son. Because of the blindness of III-9, a series of clinical examinations and related genetic testing were carried out. The pregnant women underwent a level III ultrasound screening at 25 weeks of gestation. However, no obvious fetal structural abnormalities were found, and fetal eyeball ultrasound monitoring was not performed at that time. Umbilical vein puncture (Daffos et al., 1985) was performed at 27 weeks of gestation. Some other family members of the pregnant women also participated in the study (Figure 1). All participants provided written informed consent. All protocols involving human subjects used in this study were approved by the Ethical Review Committee of the Boai Hospital of Zhongshan. In addition, the research complies with the ethical principles of medical research involving human subjects described in the Declaration of Helsinki.

## Library preparation and next-generation sequencing

Library preparation and next-generation sequencing was performed at the Beijing Genomics Institute (BGI), China. Genomic DNA was extracted according to the manufacturer's instructions from 300 μl of venous blood collected from the proband (III-9) using the MagPure Buffy Coat DNA Midi KF Kit (Magen, China). To generate short DNA fragments (100–500 bp), the extracted genomic DNA was fragmented using segmentase (BGI, China) and screened with magnetic beads to enrich the fragments with sizes ranging from 280 to 320 bp. Then, the ends were filled, an "adenine" base was added to the 3′ end to facilitate ligation of the DNA fragment to the adapter, and a "thymine" base was added at the 5′ end. A library

TABLE 1 The primer for sanger sequencing.

| | |
|---|---|
| Forward primer | 5′-CAGAAAGCTTCAGCCCGAT-3′ |
| Reverse primer | 5′-TTGGAAAAGCACACTACCACT-3′ |

was constructed using the purified DNA fragments amplified *via* a ligation-mediated polymerase chain reaction (PCR). The library was enriched by array hybridization, according to the manufacturer's instructions (Roche NimbleGen, United States), eluted, and amplified post capture. The magnitude of product enrichment was estimated using an Agilent 2100 Bioanalyzer. All amplified libraries were subsequently sent to BGI for circularization and sequencing on the MGIseq-2000 platform using a paired-end 100 bp sequencing strategy. The sequencing reads were automatically demultiplexed using the index.

## Bioinformatic analysis

"Clean reads" were generated using the previously published filtering criteria (Wei et al., 2011). These reads were mapped to the human reference genome (hg19) using the Burrows-Wheeler Aligner software (Li & Durbin, 2009). The alignment output files were further subjected to sequencing coverage and depth analyses of the target region, single-nucleotide variants (SNVs), and insertions and deletions (InDels) calling. SNVs and indels were detected using the Genome Analyses Tool Kit (version 3.3), filtered, and assessed using multiple databases, which included the dbSNP (147), 1000 Genome database (phase 3), as well as a database of 100 healthy Chinese adults. The effects of the variants were predicted using scale-invariant feature transform and PolyPhen2. Variants were evaluated according to the American College of Medical Genetics (ACMG) protocol (Richards et al., 2015). Mutations reported in the published studies were screened using the Human Gene Mutation Database (HGMD).

## Sanger sequencing

To validate and detect the novel variant in both the proband (III-9) and the family members (I-1, I-2, II-1, II-2, II-3, and III-2), conventional Sanger sequencing was performed at BGI, China. The primer is shown in Table 1.

## Cell lines, culture media, and culture conditions

The HEK293T and HeLa cell lines were purchased from the China Center for Type Culture Collection (China). The cells were cultured with high-glucose Dulbecco's modified Eagle's medium (Gibco, United States) containing 10% fetal bovine serum (Gibco, United States) and 1% penicillin–streptomycin (Gibco, United States). Cells were cultured in a constant temperature incubator at 37°C and 5% $CO_2$ with saturated humidity.

TABLE 2 The amplified plasmid-specific primers.

| Primer name | Primer sequence |
|---|---|
| 13702-NDP-F | ctggagagatctctggaccc |
| 13953-NDP-F | agtttgtcatcagtgctggg |
| 15833-NDP-R | atggagagtggagggattgg |
| 16196-NDP-R | agtcaaccttacatgggccc |
| pcMINI-NDP-KpnI-F | ggtaGGTACCcgttgttgccagaacaacat |
| pcMINI-NDP-EcoRI-R | TGCAGAATTCagaaaggctcagaccacaaa |
| pcMINI-N-NDP-KpnI-F | GCTTGGTACCCTGTGCAGCAGATACTGTGA |
| pcMINI-N-NDP-EcoRI-R | TGCAGAATTCtggtggccttttaagcatga |

## Plasmid construction and transfection

To construct a minigene, wild-type and mutant minigenes were inserted into pcMINI and pcMINI-N vectors, respectively. For the pcMINI–*NDP*–wt/mut construct, part of intro 1 (316 bp), exon 2 (381 bp), and part of intro 2 (441 bp) were inserted into the pcMINI vector. The latter contains the universal ExonA-intronA-MCS-introB-ExonB sequence. Cells were then transfected to observe whether the ExonA-Exon2-ExonB shear mode was abnormal.

The minigene construction strategy for pcMINI–N–*NDP*–wt/mut included inserting Exon 2 (381 bp) and part of intro 2 (617 bp) into the pcMINI-N vector. This vector contains the universal MCS-introB-ExonB sequence. After transfection, cells were observed to determine if there was abnormal cutting due to disruptions in Exon B. According to the manufacturer's instructions (Yeasen Biotech, China), wild-type and mutant vectors were transfected into HEK293T cells using Lipofectamine 2000.

## Minigene splicing assay

Total RNA was extracted from HEK293T and HeLa cells at 48 h post-transfection using TRIzol reagent (Takara, Japan). The extracted RNA was treated with DNase I (Thermo Scientific, United States) and reverse transcribed using the ImProm-II™ Reverse Transcription System according to the manufacturer's instructions (Promega, United States). To detect alterations in splicing, minigene-specific cDNA was amplified using plasmid-specific primers (Table 2). The PCR products were separated by 12% agarose gel electrophoresis. To characterize the splicing patterns, the PCR products were subjected to Sanger sequencing.

## Alternative splicing analysis

RNA (500 ng) was extracted using TRIzol and then reverse transcribed to cDNA using the Illumina TruSeq™ RNA sample preparation kit. RNA-Seq libraries were prepared using the Illumina TruSeq™ RNA sample preparation kit (Illumina, San Diego, CA) and sequenced using the paired-end (150 base paired-end reads) method on an Illumina NovaSeq 6000 platform. Raw data were then quality filtered to generate "clean reads" for further analysis. Clean reads were aligned to the human genome reference (hg19) using the STAR software (Dobin. et al., 2013), with a reference-based assembly of transcripts being performed using HISAT2. Picard was used to compare the results to remove redundancy, with the resultant outputs being screened using Sentieon software to detect SNVs and indels. All previously identified SNVs and indels were determined by using the dbSNP (147) database. The gene expression values were expressed as reads per kilobase of exon per million fragments mapped using Kallisto software. To identify true differentially expressed genes (DEGs), the false discovery rate was used for the rectification of the *p*-values. The significant DEGs ($p \leq 0.05$, $|\text{Log2FC}| \geq 1$) were subjected to GO enrichment and KEGG pathway analyses. Protein-to-protein interaction network analyses of DEGs were performed using the STRING database, while the protein–protein interaction network relationship was visualized using Cytoscape software.

# Results

## Clinical characteristics

Having a gravidity of 5 and parity of 1, a 29-year-old woman was referred to the Boai Hospital of Zhongshan at 16 weeks of gestation because her first son suffered from congenital bilateral blindness, without cognitive impairment and deafness. Ultrasonic examination of the affected boy's eyes showed that the corneas had degenerated, the internal structure of the eyeballs was disordered, and the eyeballs were atrophic. Computed tomography (CT) and magnetic resonance imaging (MRI) scans showed that the brain was normal. However, while the underlying causes of these symptoms and signs have not been identified, in the mother's family, only the son has this eye disease (Figure 1A).

## Novel likely pathogenic variant identified using whole exome sequencing

The genetic cause of eye disease in the family was determined by performing whole-exome sequencing (WES) on the sample obtained from the proband (III-9). WES generated and aligned 21.47 billion sequenced bases to those found sequences included in hg19. With an average depth of 147.15× and a coverage rate of 99.76%, the bases were mapped to the targeted regions. A total of 23,067 SNVs and indels were detected in 5,700 candidate genes. A hemizygous variant, c.174 + 1G > A, was detected at the *NDP* splicing site. This finding was verified by Sanger sequencing (Figure 1D).

## Sanger sequencing verified the carrier status among family members

Further validation using Sanger sequencing confirmed the heterozygous presence of the variant in the proband's mother (Figure 1C). In addition, no *NDP* variants were detected in the proband's maternal grandparents, siblings, or father (I-1, I-2, II-1, II-5, II-9, II-10, II-11, III-5, and III-6; Figure 1B).

## Identified *NDP* variant appears in the fetus

Because ND is an X-linked recessive disease and the expectant mother was a carrier of the *NDP* gene variant, prenatal diagnosis of the fetus was considered. Before conducting the cordocentesis, a level III ultrasound examination was reperformed and a significant exudate was found in the fetal eyeball (Figure 2A). This was accompanied by an MRI examination (Figure 2B); in addition, retinal detachment was found in the fetus by MRI (Figure 2C) and CT (Figure 2D). After cordocentesis, maternal blood contamination was excluded from the cord blood sample. Chromosome karyotype analysis, chromosome microarray analysis (CMA), and *NDP* gene sequencing were subsequently conducted. The chromosome results were 46, XY, and the CMA was normal. The sequencing result indicated the presence of the c.174 + 1G > A variant in the NDP gene.

## Pathology was consistent with Norrie disease

The parents opted for termination of the pregnancy, considering the poor prognosis of their first son. At 30 + weeks, the stillborn male infant was delivered. With the consent of the hospital medical ethics committee and the parents, an autopsy was performed on the fetus. The autopsy showed that the external appearance of both eyes of the fetus was normal and that the eyeballs were bilaterally symmetrical. However, the corneas of both eyes were transparent, with reduced transparency of both lenses also being noted. Grayish white opacity was observed behind the lenses of both eyes. The histopathological examination of the eyeball showed the degeneration of the uvea and retina,

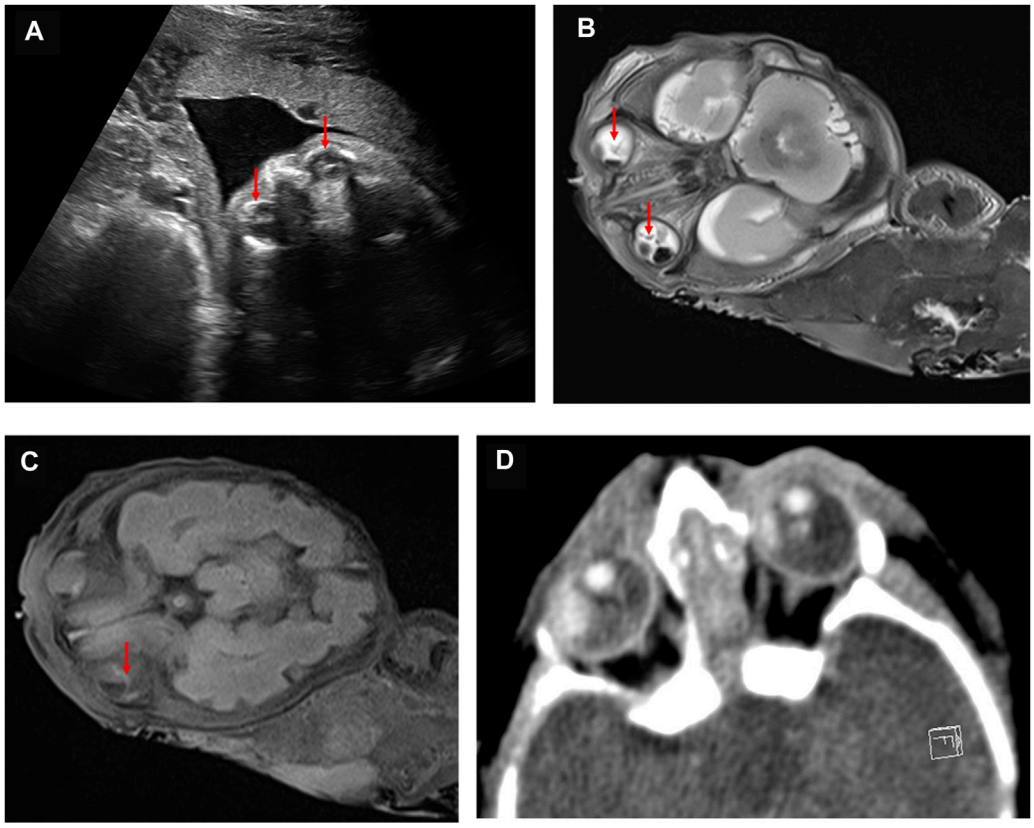


FIGURE 2
Abnormal fetal imaging results. **(A)** ultrasound showed a hyperechoic mass in both eyes of the fetus at 25 weeks. **(B)** MRI showed abnormally enhanced signals in the bilateral vitreous body of the fetus at 27 weeks. **(C)** as indicated by the arrow, MRI suggests that the fetus at 27 weeks may have a bilateral retinal detachment. **(D)** CT scan showed abnormal bilateral enhancement of the eyeballs in the stillborn infant.

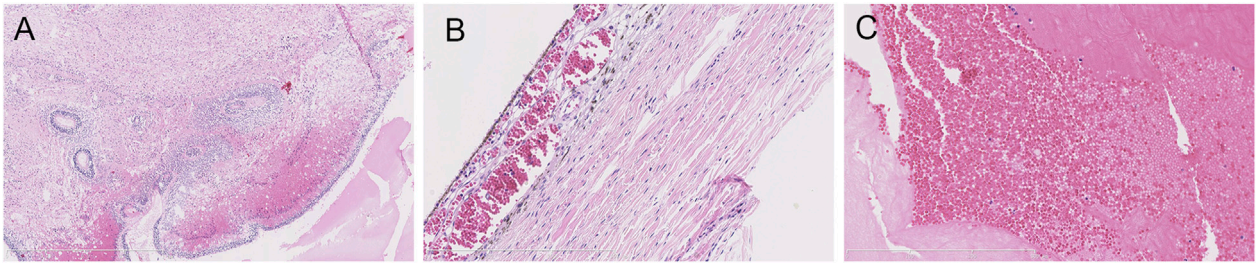


FIGURE 3
Histopathological examination of the eyeball by HE staining. **(A)** uveal and retinal degeneration and complete retinal detachment (lens, ×4). **(B)** massive bleeding and exudation can be seen under the retina (lens, ×120). **(C)** intraocular fibrous tissue hyperplasia and degeneration and crystal fiber degeneration (lens, ×120).

complete detachment of the retina, massive bleeding and exudation under the retina, proliferation and degeneration of intraocular fibrous tissue, and degeneration of crystalline fibers (Figure 3). These features are characteristic of ND. No pathological changes were found in other fetal organs during the autopsy.

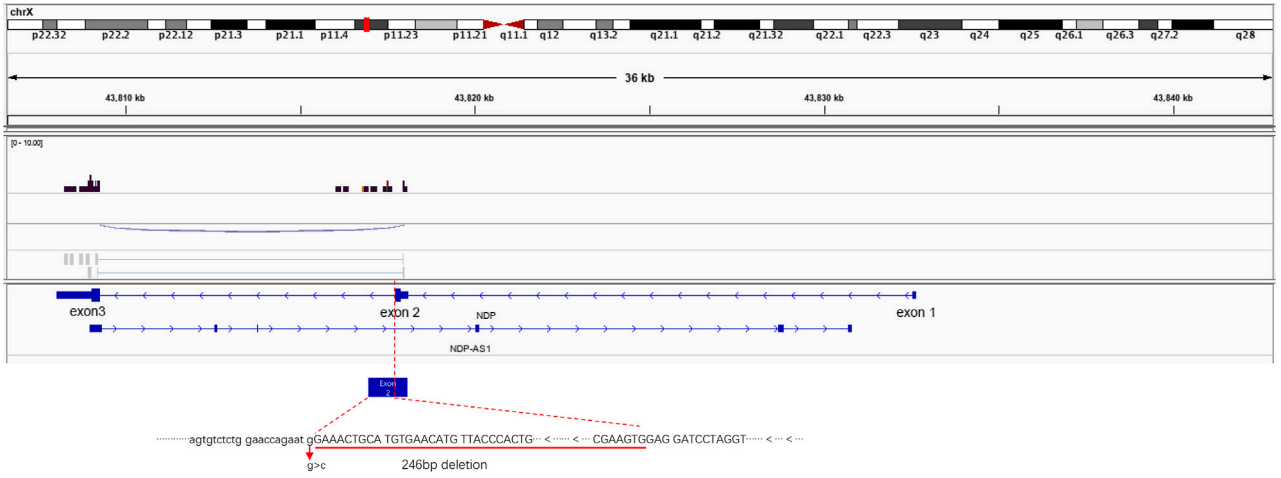


FIGURE 4
Illustrative examples of variant splicing analysis. RNA-seq was performed to a ×2 sequencing depth to detect the *NDP*-associated RNA. The results were compared to the wild-type transcript sequences. It was found that there was a 246 bp deletion at the 3′ end of *NDP* exon 2.

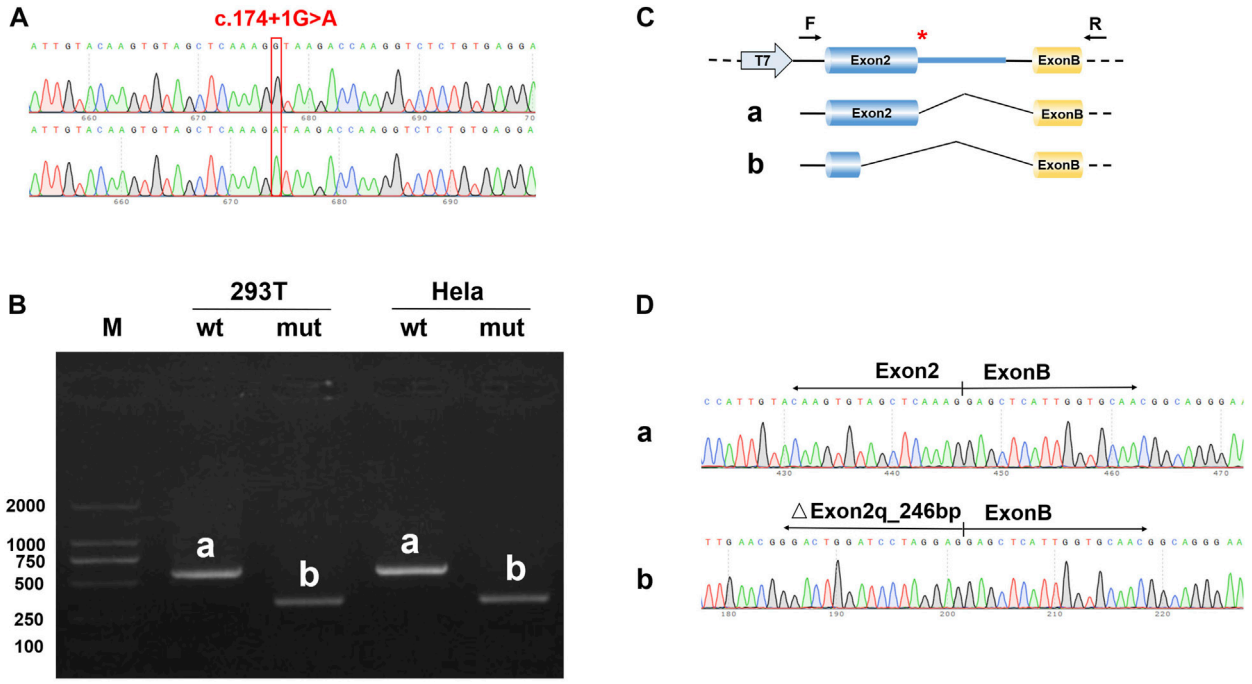


FIGURE 5
Results of the minigene splicing assay for *NDP* c.174 + 1G > A in HeLa and 293 T cells. **(A)** sequencing map of the minigene constructs, with the WT sequence at the top and the mutant sequence at the bottom. **(B)** electrophoretic map of RT-PCR transcription analysis. The pcMINI–N–*NDP*–wt/mut constructs were transfected into HeLa and 293 T cells, respectively. The RT-PCR results showed that there was a band (band a) associated with wild-type sequences in HeLa and 293 T cells, which was consistent with the expected size (581 bp). The variant resulted in a band (band b) that was smaller than that of the wild-type. **(C)** in the minigene splicing assay, exon 2 (381 bp) and a partial intro 2 sequence (617 bp) were inserted into the pcMINI-N vector. This vector contained the universal MCS-introB-ExonB. The c.174 + 1G > A *NDP* variant was at the 3′ end of exon 2. The wild-type band (band a) shows normal shearing, and the shear mode is Exon 2 (381 bp)-Exon B (57 bp). The variant band (band b) is missing 246 bp at the 3′ end of Exon 2, and the shear mode is Exon 2 (135 bp)-Exon B (57 bp). **(D)** the sequencing results of bands a and b showed that there was a 246 bp deletion at the 3′ end of exon 2.

## RNA-seq suggested that *NDP* exon 2 was deleted

To observe the *NDP* gene mRNA splicing in the presence of the c.174 + 1G > A variant, RNA-seq was used to detect the splicing of the *NDP* gene. When the c.174 + 1G > A variant was present, exon 1 of *NDP* was not expressed, and the expression of exon 2 was prematurely terminated. The expression of exon 3 was not affected (Figure 4).

## *NDP* c.174 + 1G > A variant leads to a 246-bp deletion in exon 2

To detect the splicing effect of the *NDP* c.174 + 1G > A variant on mRNA *in vitro*, two plasmids were constructed. In the first construct, part of intro 1 (316 bp), exon 2 (381 bp), and part of intro 2 (441 bp) were inserted into the pcMINI vector. In the second construct, exon 2 (381 bp) and part of intro 2 (617 bp) were inserted into the pcMINI-N vector. The wild-type and mutant forms of the two plasmids were respectively transfected into HeLa and 293 T cells to observe whether the splicing was abnormal. As shown in Figure 5 and the Supplementary Image, the RT-PCR results showed that two different bands appeared in wild-type and mutant plasmids. After sequencing the two PCR products, it was found that the mutant PCR products had a 246-bp deletion at the 3′ end of exon 2. Given the consistency in results across the two sets of vectors, it was concluded that the c.174 + 1G > A variant disrupts the normal mRNA splicing profile. Following the mutation, a new donor site is generated in the middle of exon 2, which results in a 246-bp deletion at the 3′ end of exon 2. This leads to the deletion of the initiation codon.

# Discussion

ND is caused by variations in the *NDP* gene (Berger et al., 1992). More than 140 point mutations (Zhang et al., 2013), chromosomal rearrangements, frame-shift variants (Wang et al., 2022), nucleotide insertions (Andarva et al., 2018), deletions in the coding region (Zhou et al., 2021) splice site variations, and 5′UTR mutations (Jia and Ma, 2021) have been identified in the *NDP* gene. However, *NDP* gene variants are associated with many retinopathy-related diseases (Dickinson et al., 2006). These diseases, including X-linked familial exudative vitreoretinopathy (FEVR; OMIM #305390), Coat's disease (OMIM #300216), and retinopathy of prematurity, have similar ocular features to ND. In this study, the proband gradually lost his sight 2 months after birth, while the fetus showed bilateral eyeball deformity by ultrasound examination in the third trimester of pregnancy. Indicating the pathological changes associated with ND, the histopathological examination of the eyes showed bilateral retinal detachment and a lack of retinal nerve cells. Furthermore, the typical family history of congenital blindness in the affected fetus' biological brother provided an important basis for the diagnosis of the hereditary ophthalmic disease. In the differential diagnosis based on the abnormal ultrasonic images and MRI results, X-linked familial exudative vitreoretinopathy (XL-FEVR) and persistent fetal vasculature (PFV) were the other potential conditions to be considered alongside ND. However, the pathogenic gene *ATOH7* associated with the autosomally inherited condition known as PFV is located on chromosome 10q21.3. Therefore, this disease was not considered further. The pathogenic gene associated with XL-FEVR is located on chromosome Xp11.3; however, disease progression in XL-FEVR is slower than that in ND, with blindness usually manifesting in adolescence (Sızmaz et al., 2015). XL-FEVR is a rare retinal vascular development disorder, which mainly affects retinal angiogenesis. This leads to incomplete vascularization of the peripheral retina and poor vascular differentiation (Gilmour, 2015). While it is often difficult to distinguish ND from PFV and FEVR, genetic analysis may help clinicians accurately diagnose the disease. In this family, the diagnosis of ND was ultimately confirmed by DNA sequencing and ocular histopathological examination.

ND is a complex entity involving severe congenital blindness and progressive deafness in males. According to statistics, more than 60% of ND patients have point variations, while about 20% of patients have *NDP* gene deletions (Huang et al., 2017). However, most *NDP* variations include missense (Meindl et al., 1995), deletion (Schuback et al., 1995), and nonsense variants. Because of the base changes, changes in amino acid structures are often found. This leads to the occurrence of diseases. In this study, a splice site variation was identified in the *NDP* gene. This changed the splicing mode of the mRNA precursor to produce a mature mRNA void of the exon 2 sequence (Figures 4 and 5). This variant, which was inherited from the mother, was novel in the family. All boys who inherited the variant presented pathogenic states.

The *NDP* variant found in this study is a classic splice site variation. According to the ACMG classification standard, the ectopic site of the variant was evaluated as being likely pathogenic. The variant was not found in the HGMD database, suggesting that it is a novel variant. Databases such as dbSNP, OMIM, ESP, Clinvar, 1000 Genomes, and others showed that the pathogenicity of this locus was very high and that the c.174 + 1G > A variant was consistent with being the cause of the common separation disease phenotype in this family. In this study, RNA-seq and minigene results confirmed that c.174 + 1G > A could lead to *NDP* splicing errors resulting in the occurrence of the disease. Splicing variations often occur at the donor (5′) and receptor (3′) ends. These will lead to "exon skipping" and result in mRNA translation errors (Patel and Steitz. 2003). However, in our study, it was found that c.174 + 1G > A affected the

normal mRNA splicing structure and resulted in a 246 bp deletion at the 3′ end of *NDP* exon 2. This deletion leads to the absence of the initiation codon. However, the 246 bp deletion did not change the reading frame of exon 3, so the transcription of exon 3 remained unaffected (Figure 4). However, we speculated that c.174 + 1g > A would lead to the loss of the donor site at the 5′ end of intron 2 of *NDP*, and a new donor site would be generated in the middle of exon 2, resulting in the deletion of 246 bp at the 3′ end of exon 2. This deletion would lead to the deletion of the initiation codon of *NDP*, and the translation may start from the downstream AUG, or the protein translation may not initiate. In *NDP*, the next downstream AUG is located at codon 59. Translation may start from this codon, but the translated protein would lack 58 amino acids at the N′-end compared to the wild-type Norrie protein. However, it is unclear how the deletion of exon 2 affects the expression of the Norrie protein and the resultant occurrence of the disease. Maybe it affects changes in the Norrie protein domain or leads to the degradation of the Norrie protein.

In 1996, Fuchs et al. (1996) reported the same variant site as that observed in this study, but identified a G > C transversion variant instead of a G > A transition variant. Their patient presented with bilateral leukocoria and iris dysplasia, as well as posterior synechia and a small cornea in the left eye. The patient showed no signs of deafness or intellectual disability. In this study, the main symptoms of the patients included ocular lesions, such as bilateral leukocoria and atrophy of both eyeballs, but no hearing loss and intellectual disability.

In this study, the function of the c.174 + 1G > A variant was verified through both alternative splicing analysis and a minigene splicing assay. The results suggested that c.174 + 1G > A would lead to a truncated *NDP* exon 2. With a truncated size of 246 bp, this resulted in the expression of a truncated *NDP* gene and the occurrence of ND. However, in this study, it was not verified whether c.174 + 1G > C could also lead to the truncation variation of *NDP* exon 2 or whether the variation size was the same. Therefore, it can be speculated that *NDP* variations at site c.174 + 1 may lead to more serious eye symptoms, but not serious cognitive development and hearing impairment.

As seen in this case, the onset of ND is likely to be a gradual process; we observed abnormalities in the eyeballs of the 27-week fetus, while the brother gradually became blind after birth as described by Wu et al. (2017). However, the occurrence of ND may also be observed in earlier gestational age fetuses. ND is suspected to be responsible for the blindness seen in the child in this family. As a result, in the next pregnancy of the proband's mother, the doctor should pay attention to the changes in the fetal eyeball by ultrasound in the second trimester of pregnancy. This will assist in finding abnormal fetuses as soon as possible to make a prenatal diagnosis.

## Conclusion

We found a novel ND-associated variant, c.174 + 1G > A, in the *NDP* gene that results in a splicing variation. A new donor site will be generated by this variant in the middle of exon 2, resulting in a 246-bp deletion at the 3′ end of exon 2. This leads to the deletion of the initiation codon. When the diagnosis cannot be made based on clinical characteristics, WES may be a good way to find the root cause of the disease.

## Data availability statement

The datasets for this article are not publicly available due to concerns regarding participant/patient anonymity. Requests to access the datasets should be directed to the corresponding author.

## Ethics statement

The studies involving human participants were reviewed and approved by the Ethical Review Committee of the Boai Hospital of Zhongshan, Guangdong, China. Written informed consent to participate in this study was provided by the participants' legal guardian/next of kin. Written informed consent was obtained from the individual(s) for the publication of any potentially identifiable images or data included in this article.

## Author contributions

HL, DW, and XD designed the study. ZL, HL, ZC, and CC performed the experiments. HL and XD processed the clinical data, XD performed the bioinformatics analysis, and HL wrote the manuscript draft and prepared the figures and tables. CX, JW, and XD reviewed the draft. All authors read and approved the final manuscript.

## Funding

The clinical study and genetic experiments that form the basis of these analyses were supported by a research grant from the Zhongshan Science and Technology Bureau (Nos 2020B1057, 2021B1084, and 2022B1022).

## Conflict of interest

The authors declare that the research was conducted in the absence of any commercial or financial relationships that could be construed as a potential conflict of interest.

## Publisher's Note



## Supplementary material

The Supplementary Material for this article can be found online at: https://www.frontiersin.org/articles/10.3389/fgene.2022.870232/full#supplementary-material

**SUPPLEMENTARY IMAGE S1**
Results of the minigene splicing assay for NDP c.174 + 1 G > A in HeLa and 293 T cells. **(A)** sequencing map of the minigene constructs, with WT at the top and mut constructs at the bottom. **(B)** electrophoretic map of RT-PCR transcription analysis. The pcMINI−NDP−wt/mut constructs were transfected into HeLa and 293 T cells, respectively. The RT-PCR results showed that there was a band (band a) associated with wild-type sequences with the expected size (770 bp) in HeLa and 293 T cells. The variant had a band smaller than that of the wild-type, named band b. **(C)** in the minigene splicing assay, partial intro 1 (316 bp), exon 2 (381 bp), and partial intro 2 (441 bp) sequences were inserted into the pcMINI vector which contained universal Exon A-intro A-MCS-intro B-Exon B. The NDP c.174 + 1G > A variant was at the 3′ end of exon 2. The wild-type band (band a) indicates normal shearing, and the shear mode is Exon A (192 bp)-Exon 2 (381 bp)-Exon B (57 bp); the variant band (band b) is missing 246 bp at the3′ end of Exon 2, and the shear mode is Exon A (192 bp)-△ Exon 2 (135 bp)-Exon B (57 bp). **(D)** the sequencing results of bands a and b showed that there was a 246 bp deletion on the right side of Exon 2.

## References

Andarva, M., Jamshidi, J., Ghaedi, H., Daftarian, N., Emamalizadeh, B., Alehabib, E., et al. (2018). A novel c.240_241insGG mutation in NDP gene in a family with Norrie disease. *Clin. Exp. Optom.* 101 (2), 255–259. doi:10.1111/cxo.12599

Andersen, S. R., and Warburg, M. (19611960). Norrie's disease: Congenital bilateral pseudotumor of the retina with recessive X-chromosomal inheritance; preliminary report. *Arch. Ophthalmol.* 66, 614–618. doi:10.1001/archopht.1961.00960010616003

Berger, W., Meindl, A., van de Pol, T. J., Cremers, F. P., Ropers, H. H., Döerner, C., et al. (1992). Isolation of a candidate gene for Norrie disease by positional cloning. *Nat. Genet.* 1 (3), 199–203. doi:10.1038/ng0692-199

Chen, Z. Y., Battinelli, E. M., Fielder, A., Bundey, S., Sims, K., Breakefield, X. O., et al. (1993). A mutation in the Norrie disease gene (NDP) associated with X-linked familial exudative vitreoretinopathy. *Nat. Genet.* 5 (2), 180–183. doi:10.1038/ng1093-180

Daffos, F., Capella-Pavlovsky, M., and Forestier, F. (1985). Fetal blood sampling during pregnancy with use of a needle guided by ultrasound: A study of 606 consecutive cases. *Am. J. Obstet. Gynecol.* 153 (6), 655–660. doi:10.1016/s0002-9378(85)80254-4

Dobin, A., Davis, C. A., Schlesinger, F., Drenkow, J., Zaleski, C., Jha, S., et al. (2013). Star: Ultrafast universal RNA-seq aligner. *Bioinforma. Oxf. Engl.* 29 (1), 15–21. doi:10.1093/bioinformatics/bts635

Fangting, L., Lvzhen, H., and Xiaoxin, L. (2016). A novel c.2T>A NDP missense mutation in a Chinese family with Norrie disease. *Acta Ophthalmol.* 94 (6), e516–e517. doi:10.1111/aos.12904

Fuchs, S., van de Pol, D., Beudt, U., Kellner, U., Meire, F., Berger, W., et al. (1996). Three novel and two recurrent mutations of the Norrie disease gene in patients with Norrie syndrome. *Hum. Mutat.* 8 (1), 85–88. doi:10.1002/(SICI)1098-1004(1996)8:1<85::AID-HUMU15>3.0.CO;2-N

Gilmour, D. F. (2015). Familial exudative vitreoretinopathy and related retinopathies. *Eye Lond. Engl.* 29 (1), 1–14. doi:10.1038/eye.2014.70

Huang, X., Tian, M., Li, J., Cui, L., Li, M., Zhang, J., et al. (2017). Next-generation sequencing reveals a novel NDP gene mutation in a Chinese family with Norrie disease. *Indian J. Ophthalmol.* 65 (11), 1161–1165. doi:10.4103/ijo.IJO_442_17

Jia, L. Y., and Ma, K. (2021). Novel Norrie disease gene mutations in Chinese patients with familial exudative vitreoretinopathy. *BMC Ophthalmol.* 21 (1), 84. doi:10.1186/s12886-021-01852-3

Li, H., and Durbin, R. (2009). Fast and accurate short read alignment with Burrows-Wheeler transform. *Bioinforma. Oxf. Engl.* 25 (14), 1754–1760. doi:10.1093/bioinformatics/btp324

Meindl, A., Lorenz, B., Achatz, H., Hellebrand, H., Schmitz-Valckenberg, P., and Meitinger, T. (1995). Missense mutations in the NDP gene in patients with a less severe course of Norrie disease. *Hum. Mol. Genet.* 4 (3), 489–490. doi:10.1093/hmg/4.3.489

Meire, F. M., Lafaut, B. A., Speleman, F., and Hanssens, M. (1998). Isolated Norrie disease in a female caused by a balanced translocation t(X, 6). *Ophthalmic Genet.* 19 (4), 203–207. doi:10.1076/opge.19.4.203.2306

Norrie, G. (1927). Cause of blindness in children. *Acta Ophthalmol.* 5, 357–386. doi:10.1111/j.1755-3768.1927.tb01019.x

Patel, A. A., and Steitz, J. A. (2003). Splicing double: Insights from the second spliceosome. *Nat. Rev. Mol. Cell Biol.* 4 (12), 960–970. doi:10.1038/nrm1259

Richards, S., Aziz, N., Bale, S., Bick, D., Das, S., Gastier-Foster, J., et al. (2015). Standards and guidelines for the interpretation of sequence variants: A joint consensus recommendation of the American College of medical genetics and genomics and the association for molecular pathology. *Genet. Med.* 17 (5), 405–424. doi:10.1038/gim.2015.30

Schuback, D. E., Chen, Z. Y., Craig, I. W., Breakefield, X. O., and Sims, K. B. (1995). Mutations in the Norrie disease gene. *Hum. Mutat.* 5 (4), 285–292. doi:10.1002/humu.1380050403

Sızmaz, S., Yonekawa, Y., and T Trese, M. (2015). Familial exudative vitreoretinopathy. *Turk. J. Ophthalmol.* 45 (4), 164–168. doi:10.4274/tjo.67699

Wang, H., Liu, Z., Zhou, Y., Ma, Y., and Tao, D. (2022). A novel frameshift c.22_25dupGCAT mutation of the NDP gene in a Chinese infant with Norrie disease: A case report. *Medicine* 101 (1), e28523. doi:10.1097/MD.0000000000028523

Warburg, M. (1966). Norrie's disease. A congenital progressive oculo-acousticocerebral degeneration. *Acta Ophthalmol.*, Suppl 89:1-47.

Wei, X., Ju, X., Yi, X., Zhu, Q., Qu, N., Liu, T., et al. (2011). Identification of sequence variants in genetic disease-causing genes using targeted next-generation sequencing. *PloS one* 6 (12), e29500. doi:10.1371/journal.pone.0029500

Wu, L. H., Chen, L. H., Xie, H., and Xie, Y. J. (2017). Prenatal diagnosis of a case of Norrie disease with late development of bilateral ocular malformation. *Fetal Pediatr. Pathol.* 36 (3), 240–245. doi:10.1080/15513815.2017.1307474

Zhang, X. Y., Jiang, W. Y., Chen, L. M., and Chen, S. Q. (2013). A novel Norrie disease pseudoglioma gene mutation, c.-1_2delAAT, responsible for Norrie disease in a Chinese family. *Int. J. Ophthalmol.* 6 (6), 739–743. doi:10.3980/j.issn.2222-3959.2013.06.01

Zhou, Y., Shapiro, M. J., Burton, B. K., Mets, M. B., and Kurup, S. P. (2021). Case report: A case of Norrie disease due to deletion of the entire coding region of NDP gene. *Am. J. Ophthalmol. Case Rep.* 23, 101151. doi:10.1016/j.ajoc.2021.101151

frontiers | Frontiers in Genetics

TYPE Case Report
PUBLISHED 07 October 2022
DOI 10.3389/fgene.2022.978688



OPEN ACCESS

EDITED BY
Fatma Savran Oguz,
Istanbul University, Turkey

REVIEWED BY
Afagh Alavi,
University of Social Welfare and Rehabilitation Sciences, Iran
Klara Dalva,
Tissue Typing Laboratory, Turkey

*CORRESPONDENCE
Minyue Dong,
dongmy@zju.edu.cn
Zhaohui Li,
li6336@163.com

†These authors have contributed equally to this work

SPECIALTY SECTION
This article was submitted to Genetics of Common and Rare Diseases, a section of the journal Frontiers in Genetics

RECEIVED 26 June 2022
ACCEPTED 08 September 2022
PUBLISHED 07 October 2022

CITATION
Chen S, Xu Y, Qian Y, Li Z and Dong M (2022), Case Report: Novel splicing mutations in RFX5 causing MHC class II deficiency.
*Front. Genet.* 13:978688.
doi: 10.3389/fgene.2022.978688



# Case Report: Novel splicing mutations in *RFX5* causing MHC class II deficiency

Shan Chen[1], Yuqing Xu[2,3], Yeqing Qian[2,3], Zhaohui Li[1*†] and Minyue Dong[2,3*†]

[1]Laboratory of Prenatal Diagnosis, Mindong Hospital Affiliated to Fujian Medical University, Ningde, Fujian, China, [2]Women's Hospital, School of Medicine, Zhejiang University, Hangzhou, China, [3]Key Laboratory of Reproductive Genetics, Ministry of Education (Zhejiang University), Hangzhou, China

Mutations of the Regulatory Factor X5 (*RFX5*) have been associated with the autosomal recessive major histocompatibility class II (MHC-II) deficiency, which is a severe immunodeficiency characterized by constitutive and interferon-gamma induced MHC II expression disorder and leads to the absence of cellular and humoral T-cell response to antigen challenge. The compound heterozygous splicing mutations of *RFX5*: c.353 + 6T>G (maternally inherited) and c.757 + 1G>A (paternally inherited) were identified in an infant diagnosed severe immunodeficiency. The mutation c.757 + 1G>A was classified as likely pathogenic while c.353 + 6T>G was classified as the variant of uncertain significance according to American College of Medical Genetics and Genomics (ACMG). To investigate the pathogenicity of *RFX5*: c.353 + 6T>G, reverse transcription PCR (RT-PCR) was conducted with the mother's peripheral blood. An insertion of 191-bp intronic sequence (intron 6) was found in the transcripts, and this resulted in a frameshift and premature truncation of the protein, especially reduced the DNA-binding domain (DBD) of the RFX5 protein. Our data expanded the spectrum of pathogenic mutations in MHC-II deficiency and put new insights into the genetic counseling, prenatal diagnosis and preimplantation genetic testing (PGT) for the disease.

KEYWORDS

**RFX5, MHC-II deficiency, splicing mutation, DNA-binding domain, whole exome sequencing**

## Introduction

Regulatory factor X-5 (*RFX5*) is essential for the regulation of major histocompatibility class II (MHC II) gene expression (Villard et al., 1997; Djidjik et al., 2012). RFX5 contains highly conserved DNA-binding domains (*DBDs*), located in the 90–166 residues and 407–614 residues, which bind the X box of MHC II before transcription (Clarridge et al., 2016; Farrokhi et al., 2018).

Mutations in *RFX5* have been associated with the MHC-II deficiency, also named as the Bare Lymphocyte Syndrome (BLS) (OMIM:209,920) (Reith and Mach, 2001; Nekrep et al., 2002). MHC-II deficiency, a rare autosomal recessive disease, is characterized by constitutive and interferon-gamma induced MHC II expression disorder, and results in

TABLE 1 Abnormal immunological findings of the infant with the associated normal range.

| | Patient data | Normal range | Unit |
|---|---|---|---|
| Cell count | | | |
| White Blood Cell | 17.81 | 4–10 | $10^9$/L |
| Lymphocyte | 2.91 | 0.8–4 | $10^9$/L |
| Monocyte | 0.74 | 0.12–1.2 | $10^9$/L |
| Platelet | 351 | 100–300 | $10^9$/L |
| Immunophenotyping | | | |
| CD3 | 38 | 55–84 | % |
| CD4 | 11 | 31–60 | % |
| CD8 | 26 | 13–41 | % |
| CD4/CD8 ratio | 0.44 | 0.8–2.8 | |
| Ig concentration | | | |
| IgG | 0.41 | 5.2–16 | g/L |
| IgA | 0.02 | 0.24–3.3 | g/L |
| IgM | 0.22 | 0.5–2.2 | g/L |

the absence of cellular and humoral T-cell response to antigen challenge, hypogammaglobulinemia and impaired antibody production (Garvie et al., 2007; Hanna and Etzioni, 2014). Over 200 cases have been reported and the prevalence varies significantly in different regions based on previous published data. Around two-thirds of the patients come from North Africa while less than 10 cases have been reported in East Asia (Djidjik et al., 2012; El Hawary et al., 2019). Children with MHC-II deficiency are extremely susceptible to a broad range of viral, bacterial and fungal, among which *Pneumocystis jirovecii, Salmonella*, cytomegalovirus *(CMV), Cryptosporidium* species and *herpes simplex virus* (HPV) are the most common pathogens (Hanna and Etzioni, 2014). Therefore, these patients are mainly characterized by severe and recurrent infections within the first year of life, especially involving the respiratory and gastrointestinal tract. What's worse, the infection may be lethal (Reith and Mach, 2001; Farrokhi et al., 2018).

In the current investigation, we described a Chinese infant with MHC II deficiency caused by two novel splicing mutations, c.353 + 6T>G (maternally inherited) and c.757 + 1G>A (paternally inherited) in the *RFX5* gene.

# Methods

## Subject

A 30-year-old healthy woman who delivered an infant (the proband) diagnosed severe immunodeficiency was referred to the Department of Reproductive Genetics, Women's Hospital, School of Medicine Zhejiang University. Her infant presented recurrent pneumonia, reduced CD3 and CD4 positive leucocyte cell ratio, inverted CD4/CD8 ratio and reduced serum immunoglobulins levels (concentrations of IgG, IgA, and IgM) at 6 months of her age (Table 1). The infant died at 22 months of her age due to severe respiratory infection and respiratory failure. Severe immunodeficiency was diagnosed with unknown cause. The infant was born at full term to healthy un-consanguineous Chinese parents without family history of any genetic disorders.

The use of medical records of this family is was approved by the Institutional Review Board of the Women's Hospital, School of Medicine, Zhejiang University and the participants provided their written informed consents.

## WES and bioinformatic analysis

To determine the cause for severe immunodeficiency, the whole exome sequencing (WES) was provided. Genomic DNA from all the family members was extracted by a QIAamp DNA blood midi kit (Qiagen, Hilden, Germany) according to the manufacturer's protocol and then was fragmented by Covaris LE220 (Massachusetts, United States) to generate a paired-end library (200–250 bp). All amplified libraries were performed on the BGISEQ-500 platform (BGI, Shenzhen, China), the single-strand DNA was mixed with MGIEasy™ DNA Library Prep Kit V1 (BGI, Shenzhen, China) and then sequenced using 100SR chemistry with BGISEQ-500RS high-throughput sequencing Kit (BGI, Shenzhen, China).

Splice AI (https://spliceailookup.broadinstitute.org/) was used to predict the effect of variants. Pathogenic variants are assessed according to the protocol issued by the American College of Medical Genetics and Genomics (ACMG) (Richards et al., 2015). DECIPHER (http://decipher.sanger.ac.uk), OMIM (http://omim.org/), PubMed (http://www.ncbi.nlm.nih.gov/pubmed), ClinVar (https://www.ncbi.nlm.nih.gov/clinvar/), and HGMD (http://www. hgmd. cf.ac.uk/ac/index. php) databases were used to investigate the clinical relevance of the mutations.

## Sanger sequencing validation

Sanger sequencing was carried out to confirm the variants in *RFX5* gene. The primers used for c.757 + 1G>A were as follows: *RFX5*-E9F, TAGCTGAGGCAGAGGATGAAGA; and *RFX5*-E9R, GGTGAGGAGGAAACTGAGGAAT. The primers used for c.353 + 6T>G were as follows: *RFX5*-E5F, GTTAGGGTCTTAGTAATGCTTGTTCC; and *RFX5*-E5R, CCTTCGAGCTTTGATGTCAGG. The primers were designed using Oligo Primer Designer (Rychlik 2007). The DNA was amplified using the following procedure: 94°C for 10 min; 35 cycles at 94°C for 30 s, 60°C for 30 s, 72°C for 30 s; 72°C for 10 min. Sequencing was performed by an ABI 3130 DNA analyzer.

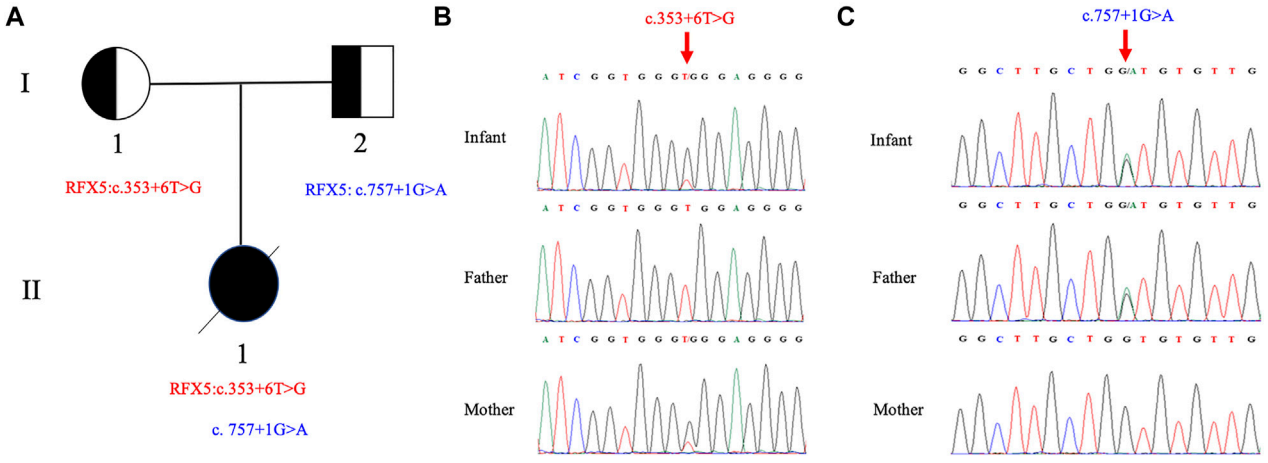


FIGURE 1
Pedigree of the family and Sanger sequence analysis. **(A)** $II_1$(proband) have two compound splicing variants in *RFX5* gene. One variant (c.353+6T > G) is from $I_1$ (mother) and the other (c.757+1G > A) is from $I_2$ (father). Chromatograms of **(B)** c.353+6T > G and **(C)** c.757+1G > A are identified by Sanger sequencing, respectively. The top chromatograms are from the infant, the middle two are from the father, and the bottom two are from the mother (red arrows indicate the mutation).

## RNA extraction, real time-PCR, and sequencing

Total RNAs of the mother's peripheral blood cells was extracted using TRIzol (Takara, Japan). Extracted total RNAs was reverse-transcribed using RT Kit (Takara, Japan) following the manufacturer's instructions. RT-PCR was performed using GoldStar Best Master Mix (CWBIO, Beijing). Sequences of primers used were as follows: RFX5-spF, GAAGATGAGCCT GATGCTAAGAG; and RFX5-spR, GGCGACCTCAACGATGGA AC. The procedure of the PCR was as follows: 94°C for 10 min followed by 35 cycles at 94°C for 30 s, 60°C for 30 s, 72°C for 30 s, and a final extension step at 72°C for 10 min. Sequencing was performed by an ABI 3130 DNA analyzer.

# Results

## Identification of the compound heterozygous mutations in *RFX5*

Compound heterozygous splicing mutations in *RFX5*: c.353 + 6 T>G and c.757 + 1 G>A were identified by WES and confirmed by Sanger sequencing (Figure 1). These mutations have never been reported in any database (gnomAD, ClinVar or HGMD) or literature. Splice AI was used to predict the effects of the *RFX5*: c.353 + 6T>G and c.757 + 1G>A on splicing. The delta score of donor loss were 0.79 and 0.85, respectively. The result indicates that both of the mutations affect the splicing. The mutation *RFX5*: c.757 + 1G>A was inherited from her father and classified as likely pathogenic, while the mutation *RFX5*: c.353 + 6T>G was maternally inherited and classified as variant of uncertain significance (VUS) according to ACMG recommendations.

## Pathogenicity of *RFX5*: c.353 + 6T>G

Based on the genotype–phenotype correlation, we hypothesized that *RFX5*: c.353 + 6T>G may affect the splicing. To confirm this hypothesis, mRNA was extracted from the women's peripheral blood cells. RT-PCR was performed with the primers (RFX5-spF/RFX5-spR) designed to amplify exons three to nine of *RFX5*. It was found that the woman ($I_1$) and the controls (C1 and C2) shared the band of PCR products at 675 bp, while $I_1$ had another bigger band of 866 bp (Figure 2A). The Sanger sequencing of the bigger band (866 bp) showed that 191-bp intron six sequences were retained from the transcripts of the mother, compared with the 675 bp band (Figures 2B,C). The mutation (c.353 + 6T>G) introduced an insertion of 191-bp intron six sequences, which may cause a truncated RFX5 protein by a frameshift and creation of a premature stop codon. As is showed in Figure 2D, wild-type deduced RFX5 protein has three domains, among which two domains are DNA-binding domains (DBDs). However, the deduced RFX5 protein of c.353 + 6T>G splicing mutation only has one truncated DBD. The truncated DBD may damage the ability of RFX5 to bind X box of the MHC II promoter and then reduce the expression of MHC II molecular at the transcriptional level.

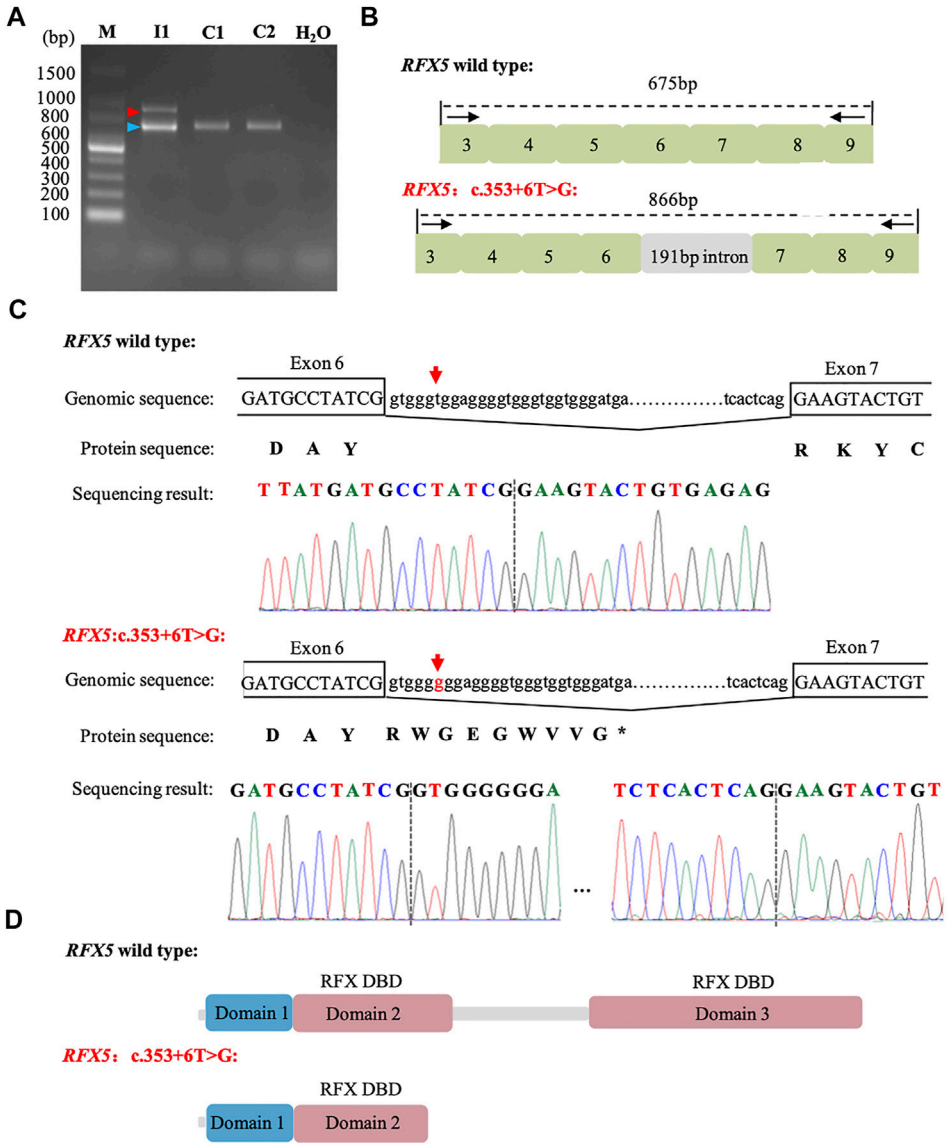


FIGURE 2
Analysis of c. 353 + 6T>G splicing mutation in *RFX5*. **(A)**: RT-PCR analysis of *RFX5* cDNA from peripheral blood samples. Agarose gel (1.5%) electrophoresis of RT-PCR products generated from $I_1$ (mother), C1 and C2 (normal controls). Amplicons resulting from aberrantly spliced mRNA and normal spliced mRNA are marked by red and blue arrowheads, respectively. **(B)**: Schematic representation of exon three to nine and intron six organization in RFX5. **(C)**: Sequence analysis of the RT-PCR products from the mother. The arrows indicate the position of the c. 353 + 6T>G mutation. **(D)**: The structure with domains of wild-type and c. 353 + 6T>G splicing mutation RFX5 protein. Wild-type RFX5 protein consists of three domains, among which domain two and domain three are the important DBDs while the splicing mutation leads to the premature of the protein and significantly damages the protein structure.

## Discussion

In the current investigation, we described a Chinese infant with MHC class II deficiency due to the compound heterozygous splicing mutations of the *RFX5* gene for the first time. The paternally inherited mutation c.757 + 1G>A of *RFX5* was likely pathogenic and the maternally inherited mutation c.353 + 6T>G was proved to affect splicing, which may result in frameshift and truncation of the protein. Both of the mutations have never been reported in any database or literature, indicating our findings expand the spectrum of the diagnose for the MHC II deficiency and provide insight and information for genetic counseling.

Major histocompatibility complex (MHC) II deficiency is a primary immunodeficiency with an autosomal recessive inheritance pattern and is characterized by the early onset of

severe and recurrent respiratory and gastrointestinal infections, developmental delay, and death in early life (Plaeger-Marshall et al., 1988; Lum et al., 2020). Almost all of the patients suffer from recurrent pneumonia and prolonged diarrhea (Clement, 1990; Ben-Mustapha et al., 2013). In the present study, the infant presented typically clinical and immunological features, like severe pneumonia, reduced CD3 and CD4 positive leucocyte cell ratio, inverse CD4/CD8 ratio and reduced serum immunoglobulin levels (concentrations of IgG, IgA, and IgM). The infant eventually died at 22 months of age due to acute respiratory infection and respiratory failure.

The underlying cause of MHC class II deficiency lies in the absence or reduced expression of MHC class II molecules which are regulated by MHC II enhanceosome (a cell-specific multiprotein complex) (Masternak et al., 2000; Hanna and Etzioni, 2014). The MHC class II molecules, also referred to as human leukocyte antigens (HLAs), are multigenic and highly polymorphic glycoproteins that aggregate to form heterodimers of *a* and β chains (Hanna and Etzioni, 2014). Moreover, HLAs are usually divided into three molecules, HLA-DR, -DP, and -DQ, which are located on the surface of antigen-presenting cells (APCs) such as dendritic cells and macrophages (Waldburger et al., 2000). HLAs present antigens endocytosed by APCs to the receptor of $CD4^+$ helper T cells, directing the T cell activation, differentiation, and proliferation (Villard et al., 2000). It is reported that MHC class II gene mutations might damage cellular and humoral immunity by affecting CD4 T-cell development and reducing the Th-cell-dependent antibody production (Nonoyama et al., 1998; Sage et al., 2014; Aluri et al., 2018). Class II transactivator (*CIITA*), RFX-associated protein (*RFXAP*), regulatory factor X-5 (*RFX5*), and RFXAP-containing ankyrin repeat (*RFXANK*) are widely recognized key enhanceosome of MHC class II molecules so far. Accordingly, based on the four different transcript factors, MHC II deficiency is divided into four groups from group A to D, which are summarized by the deficiency of *CIITA, RFXANK, RFX5*, and *RFXAP*, respectively (Steimle et al., 1995; Scholl et al., 1997). In our study, two splicing mutations (c. 757 + 1G>A and c. 353 + 6T>G) in *RFX5* gene were found in the proband, who belongs to group C. The former mutation was located at the classical splicing site, and the latter mutation was proven to lead to a stop codon after amino acid 126, leading to a loss of more than 50% of the protein including the highly conserved DBD. Therefore, the ability of *RFX5* to bind X box could be affected and the expression of MHC II molecular reduced. Taken together, the compound heterozygous mutations in proband might explain the cause for immune deficiency.

Up to now, 19 pathogenic/uncertain significance mutations have been reported in RFX5(HGMD Professional 2022.2). Among them, are five missense mutations (two pathogenic mutations and three uncertain significance mutations), four nonsense mutations (all pathogenic mutations), five splicing mutations (all pathogenic mutations), four small deletions mutations (three pathogenic mutations and one uncertain significance mutation) and one small insertions mutation (pathogenic mutation). The five splicing mutations are c.116 + 1G>A, c.151-1G>A, c.234-1G>A, c.556–2A>G and c.116 + 5G>A, respectively. Four of them are of the classical splice site variants, the last one (c.116 + 5 G>A) is a point mutation in a splice donor site, which results in 10 nucleotide upstream in exon two deletion in *RFX5* mRNA (Villard et al., 1997). The splicing mutations reported in this study are novel.

Hematopoietic stem cell transplantation (HSCT) is currently the only available curative treatment for MHC-II deficiency. However, the success rate is reported to be poor in MHC class II-deficient patients (Small et al., 2013; Posovszky et al., 2019). On the basis of a previous study, two patients did not survive although they underwent HSCT after diagnosis. One patient died of diarrhea and Gram-negative sepsis within 8 days of transplant procedure and the other died post-HSCT due to lung damage and systemic candidiasis (Aluri et al., 2018). Even though the patients with MHC II deficiency do not express MHC II required for the rejection process, the residual host immunity is sufficient to cause rejection even with immunosuppression. In a recent study, it was suggested that the low survival rate in these patients may lie in the presentation of donor antigens by donor antigen-presenting cells to recipient Th cells leading to graft rejection. (Kallen and Pullarkat, 2015). Apart from poor engraftment, a high rate of post-HSCT death can be caused by diagnosis and/or treatment delays, multiorgan failure and persistent viral infections. More importantly, pregnant women with immunodeficiency fetuses mostly experience normal prenatal examination in imaging (ultrasound or MRI) and laboratory tests, like the mother in our study. Therefore, it is of great value to carry out prenatal diagnosis or PGD in such families.

In summary, we reported two novel splicing mutations (c.353 + 6T>G and c.757 + 1G>A) in *RFX5* which are associated with MHC class II deficiency. The mutations were predicted to affect the RFX5 protein translation and even result in the premature of the protein. In addition, our study validates that the RT-PCR is necessary if the genotype–phenotype correlation was very consistent while only one classical splicing site gene mutation of autosomal recessive disease was detected. It contributed to a new genetic foundation for prenatal diagnosis and prenatal diagnosis of MHC class II deficiency.

## Data availability statement

The datasets for this article are not publicly available due to concerns regarding participant/patient anonymity. Requests to access the datasets should be directed to the corresponding authors.

## Ethics statement

The studies involving human participants were reviewed and approved by the Ethics Committee of Women's Hospital, School of Medicine Zhejiang University. Written informed consent to

participate in this study was provided by the participants' legal guardian/next of kin. Written informed consent was obtained from the individual(s), and minor(s)' legal guardian/next of kin, for the publication of any potentially identifiable images or data included in this article.

## Author contributions

MD conceived of the study, participated in its design and revised the manuscript; ZL analyzed the clinical data; SC collected clinical data and drafted the manuscript; YX carried out the RT-PCR and revised the manuscript; YQ extracted the genomic DNA and designed primers; All authors have read and approved the final manuscript.

## Funding

This work was supported by the Key Research and Development Program of Zhejiang Province (grant numbers 2019C03025), Zhejiang Provincial Natural Science Foundation of China (grant numbers LY22H110004) and the National Natural Science Foundation of China (grant numbers 81901382).

## Conflict of interest

The authors declare that the research was conducted in the absence of any commercial or financial relationships that could be construed as a potential conflict of interest.

## Publisher's note



## References

Aluri, J., Gupta, M., Dalvi, A., Mhatre, S., Kulkarni, M., Hule, G., et al. (2018). Clinical, immunological, and molecular findings in five patients with major histocompatibility complex class II deficiency from India. *Front. Immunol.* 9, 188. doi:10.3389/fimmu.2018.00188

Ben-Mustapha, I., Ben-Farhat, K., Guirat-Dhouib, N., Dhemaied, E., Larguèche, B., Ben-Ali, M., et al. (2013). Clinical, immunological and genetic findings of a large tunisian series of major histocompatibility complex class II deficiency patients. *J. Clin. Immunol.* 33, 865–870. doi:10.1007/s10875-013-9863-8

Clarridge, K., Leitenberg, D., Loechelt, B., Picard, C., and Keller, M. (2016). Major histocompatibility complex class II deficiency due to a novel mutation in RFXANK in a child of Mexican descent. *J. Clin. Immunol.* 36, 4–5. doi:10.1007/s10875-015-0219-4

Clement, L. T. (1990). The class II major histocompatibility complex antigen deficiency syndrome: Consequences of absent class II major histocompatibility antigens for lymphocyte differentiation and function. *J. Invest. Dermatol.* 94, 118S–121s. doi:10.1111/1523-1747.ep12876078

Djidjik, R., Messaoudani, N., Tahiat, A., Meddour, Y., Chaib, S., Atek, A., et al. (2012). Clinical, immunological and genetic features in eleven Algerian patients with major histocompatibility complex class II expression deficiency. *Allergy Asthma Clin. Immunol.* 8, 14. doi:10.1186/1710-1492-8-14

El Hawary, R. E., Mauracher, A. A., Meshaal, S. S., Eldash, A., Abd Elaziz, D. S., Alkady, R., et al. (2019). MHC-II deficiency among Egyptians: Novel mutations and unique phenotypes. *J. Allergy Clin. Immunol. Pract.* 7, 856–863. doi:10.1016/j.jaip.2018.07.046

Farrokhi, S., Shabani, M., Aryan, Z., Zoghi, S., Krolo, A., Boztug, K., et al. (2018). MHC class II deficiency: Report of a novel mutation and special review. *Allergol. Immunopathol.* 46, 263–275. doi:10.1016/j.aller.2017.04.006

Garvie, C. W., Stagno, J. R., Reid, S., Singh, A., Harrington, E., and Boss, J. M. (2007). Characterization of the RFX complex and the RFX5(l66a) mutant: Implications for the regulation of MHC class II gene expression. *Biochemistry* 46, 1597–1611. doi:10.1021/bi6023868

Hanna, S., and Etzioni, A. (2014). MHC class I and II deficiencies. *J. Allergy Clin. Immunol.* 134, 269–275. doi:10.1016/j.jaci.2014.06.001

Kallen, M. E., and Pullarkat, S. T. (2015). Type II bare lymphocyte syndrome: Role of peripheral blood flow cytometry and utility of stem cell transplant in treatment. *J. Pediatr. Hematol. Oncol.* 37, e245–e249. doi:10.1097/MPH.0000000000000278

Lum, S. H., Anderson, C., Mcnaughton, P., Engelhardt, K. R., Mackenzie, B., Watson, H., et al. (2020). Improved transplant survival and long-term disease outcome in children with MHC class II deficiency. *Blood* 135, 954–973. doi:10.1182/blood.2019002690

Masternak, K., Muhlethaler-Mottet, A., Villard, J., Zufferey, M., Steimle, V., and Reith, W. (2000). CIITA is a transcriptional coactivator that is recruited to MHC class II promoters by multiple synergistic interactions with an enhanceosome complex. *Genes Dev.* 14, 1156–1166. doi:10.1101/gad.14.9.1156

Nekrep, N., Jabrane-Ferrat, N., Wolf, H. M., Eibl, M. M., Geyer, M., and Peterlin, B. M. (2002). Mutation in a winged-helix DNA-binding motif causes atypical bare lymphocyte syndrome. *Nat. Immunol.* 3, 1075–1081. doi:10.1038/ni840

Nonoyama, S., Etzioni, A., Toru, H., Ruggerie, D. P., Lewis, D., Pollack, S., et al. (1998). Diminished expression of CD40 ligand may contribute to the defective humoral immunity in patients with MHC class II deficiency. *Eur. J. Immunol.* 28, 589–598. doi:10.1002/(SICI)1521-4141(199802)28:02<589::AID-IMMU589>3.0.CO;2-J

Plaeger-Marshall, S., Haas, A., Clement, L. T., Giorgi, J. V., Chen, I. S., Quan, S. G., et al. (1988). Interferon-induced expression of class II major histocompatibility antigens in the major histocompatibility complex (MHC) class II deficiency syndrome. *J. Clin. Immunol.* 8, 285–295. doi:10.1007/BF00916557

Posovszky, C., Sirin, M., Jacobsen, E., Lorenz, M., Schwarz, K., Schmidt-Choudhury, A., et al. (2019). Persisting enteropathy and disturbed adaptive mucosal immunity due to MHC class II deficiency. *Clin. Immunol.* 203, 125–133. doi:10.1016/j.clim.2019.04.012

Reith, W., and Mach, B. (2001). The bare lymphocyte syndrome and the regulation of MHC expression. *Annu. Rev. Immunol.* 19, 331–373. doi:10.1146/annurev.immunol.19.1.331

Sage, A. P., Murphy, D., Maffia, P., Masters, L. M., Sabir, S. R., Baker, L. L., et al. (2014). MHC Class II-restricted antigen presentation by plasmacytoid dendritic cells drives proatherogenic T cell immunity. *Circulation* 130, 1363–1373. doi:10.1161/CIRCULATIONAHA.114.011090

Scholl, T., Mahanta, S. K., and Strominger, J. L. (1997). Specific complex formation between the type II bare lymphocyte syndrome-associated transactivators CIITA and RFX5. *Proc. Natl. Acad. Sci. U. S. A.* 94, 6330–6334. doi:10.1073/pnas.94.12.6330

Small, T. N., Qasim, W., Friedrich, W., Chiesa, R., Bleesing, J. J., Scurlock, A., et al. (2013). Alternative donor SCT for the treatment of MHC class II deficiency. *Bone Marrow Transpl.* 48, 226–232. doi:10.1038/bmt.2012.140

Steimle, V., Durand, B., Barras, E., Zufferey, M., Hadam, M. R., Mach, B., et al. (1995). A novel DNA-binding regulatory factor is mutated in primary MHC class II deficiency (bare lymphocyte syndrome). *Genes Dev.* 9, 1021–1032. doi:10.1101/gad.9.9.1021

Villard, J., Peretti, M., Masternak, K., Barras, E., Caretti, G., Mantovani, R., et al. (2000). A functionally essential domain of RFX5 mediates activation of major histocompatibility complex class II promoters by promoting cooperative binding between RFX and NF-Y. *Mol. Cell. Biol.* 20, 3364–3376. doi:10.1128/mcb.20.10.3364-3376.2000

Villard, J., Reith, W., Barras, E., Gos, A., Morris, M. A., Antonarakis, S. E., et al. (1997). Analysis of mutations and chromosomal localisation of the gene encoding RFX5, a novel transcription factor affected in major histocompatibility complex class II deficiency. *Hum. Mutat.* 10, 430–435. doi:10.1002/(SICI)1098-1004(1997)10:6<430::AID-HUMU3>3.0.CO;2-H

Waldburger, J. M., Masternak, K., Muhlethaler-Mottet, A., Villard, J., Peretti, M., Landmann, S., et al. (2000). Lessons from the bare lymphocyte syndrome: Molecular mechanisms regulating MHC class II expression. *Immunol. Rev.* 178, 148–165. doi:10.1034/j.1600-065x.2000.17813.x

frontiers | Frontiers in Genetics

TYPE Case Report
PUBLISHED 31 October 2022
DOI 10.3389/fgene.2022.1020525



OPEN ACCESS

EDITED BY
Can Liao,
Guangzhou Women and Children's Medical Center, China

REVIEWED BY
Horacio Rivera,
University of Guadalajara, Mexico
Haydee Rosas-Vargas,
Unidad de Investigación Médica en Genética Humana, IMSS, Mexico

*CORRESPONDENCE
Minyue Dong,
dongmy@zju.edu.cn

SPECIALTY SECTION
This article was submitted to Human and Medical Genomics, a section of the journal Frontiers in Genetics

RECEIVED 16 August 2022
ACCEPTED 10 October 2022
PUBLISHED 31 October 2022

CITATION
Yu J, Chen N, Chen M, Shen M, Qian Y and Dong M (2022), Case Report: Prenatal diagnosis of fetal tetrasomy 9p initially identified by non-invasive prenatal testing.
*Front. Genet.* 13:1020525.
doi: 10.3389/fgene.2022.1020525



# Case Report: Prenatal diagnosis of fetal tetrasomy 9p initially identified by non-invasive prenatal testing

Jialing Yu[1], Na Chen[1], Min Chen[1], Min Shen[1], Yeqing Qian[1] and Minyue Dong[1,2,3]*

[1]Women's Hospital, School of Medicine, Zhejiang University, Hangzhou, Zhejiang, China, [2]Key Laboratory of Reproductive Genetics Zhejiang University, Ministry of Education, Hangzhou, Zhejiang, China, [3]Key Laboratory of Women's Reproductive Health of Zhejiang Province, Women's Hospital, School of Medicine, Zhejiang University, Hangzhou, China

Tetrasomy 9p is a rare syndrome characterized by fetal growth restriction, Dandy-Walker malformation, cardiac anomalies, and facial abnormalities and is discovered by ultrasound during the prenatal examination. Herein, we report a fetus of tetrasomy 9p without obvious phenotypic manifestations during the first trimester that was identified by non-invasive prenatal testing (NIPT). NIPT revealed that the gain of 9p24.3–9p11 that was approximately 46.36 Mb in size. Karyotyping of amniocytes indicated an additional marker in all metaphase. Chromosome microarray and fluorescence *in situ* hybridization on uncultured amniocytes revealed tetrasomic of 9p24.3q13, and that the supernumerary chromosome is a dicentric isochromosome consisted of two copies of the 9p arm. Taken together, it was indicated that the fetal karyotype was 47,XY,+idic (9) (q13), and that multiple techniques are crucial to the prenatal diagnosis.

KEYWORDS

**tetrasomy 9p syndrome, NIPT, prenatal diagnosis, CMA, karyotyping**

## Introduction

Tetrasomy 9p (T9p), which was first defined in 1973 (Ghymers et al., 1973), is a rare abnormality typically resulting from a supernumerary isochromosome and mostly documented after birth. The phenotype of T9p varies from fetuses with multiple abnormalities to phenotypically normal adults (Bellil et al., 2020; Shu et al., 2021). Fetuses with T9p usually exhibit abnormal ultrasound findings including facial clefts, fetal growth retardation (FGR), and Dandy-Walker variant (Chen et al., 2007). So far, few cases have been diagnosed prenatally.

Non-invasive prenatal testing (NIPT) is emerging as a robust technique to screen for trisomies in 13, 18, 21, and sex chromosome (Lo et al., 1997; Lo et al., 1998; Song et al., 2013; Yin et al., 2015; Gross et al., 2016). Furthermore, its ability in screening for subchromosomal abnormalities such as Cri-du-chat deletions, 1p36 deletion syndrome,

Wolf-Hirschhorn syndrome, Prader-Willi deletions, or Angelman deletions, has been proven as shown by high predictive positive value (Liu et al., 2016; Liang et al., 2019).

In the current investigation, we present a case of non-mosaic T9p that was identified through NIPT and validated by the combination of karyotyping, chromosome microarray (CMA), and fluorescence *in situ* hybridization (FISH).

# Patients and methods

## Case presentation

A healthy 37-years-old pregnant woman, who claimed no family history of genetic abnormalities and previously delivered two healthy boys, was referred to Women's Hospital, School of medicine, Zhejiang University. She had unremarkable ultrasound screening at 12$^{th}$ week of gestation that revealed a normal nuchal translucency (NT) and the presence of nasal bone, while she received NIPT at the 15$^{th}$ week of gestation because of advanced maternal age. NIPT showed a duplication at 9p24.3p11.2. Amniocentesis was performed at the 18th week of gestation, and the fetal sample was analyzed by karyotyping, CMA, and FISH.

After genetic counseling, the woman and her husband decided to terminate the pregnancy; however, they declined to undergo a fetal MRI and fetal autopsy.

## Non-invasive prenatal testing screening

NIPT procedures, including cell-free DNA extraction, library construction, and next-generation sequencing (NGS) were performed as described previously (Chen et al., 2019). Bioinformatic methods combined with a locally weighted polynomial regression were used to eliminate GC-bias, and a binary hypothesis was performed to obtain a higher accuracy for NIPT detection. Low coverage whole genome sequencing of plasma DNA was carried out on each sample, resulting in 10.19 million unique reads that corresponds to 0.1 × human genome depth. A fetal copy-number analysis (CNV) was performed to detect subchromosomal deletion and duplication, as previously described (Chen et al., 2019).

## DNA extraction

DNA extraction was performed as described previously (Qian et al., 2019). Briefly, 10 ml maternal blood sample was centrifuged at 1,600 g for 10 min. The supernatant was re-centrifuged at 14,000 g for another 10 min. The plasma fraction was aliquoted and stored at −80°C for subsequent NIPT. The amniotic fluid was centrifuged at 1,600 g for 10 min. Fetal DNA from the centrifuged amniotic fluid cells were then extracted with QIAamp DNA Blood Mini Kit (Qiagen, Hilden, Germany).

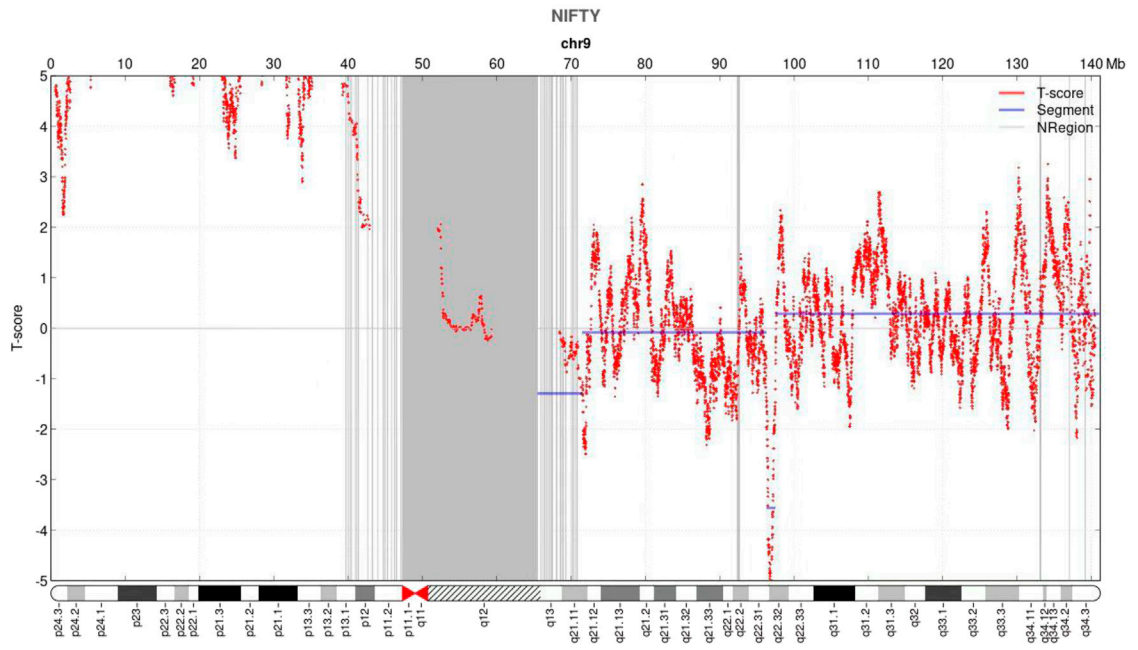


FIGURE 1
Non-invasive prenatal testing (NIPT) results of fetal chromosome 9. The horizontal axis represents genomic location (Mb), and the vertical axis represents t-score. NIPT revealed an increase in the signal of the p arm of chromosome 9.

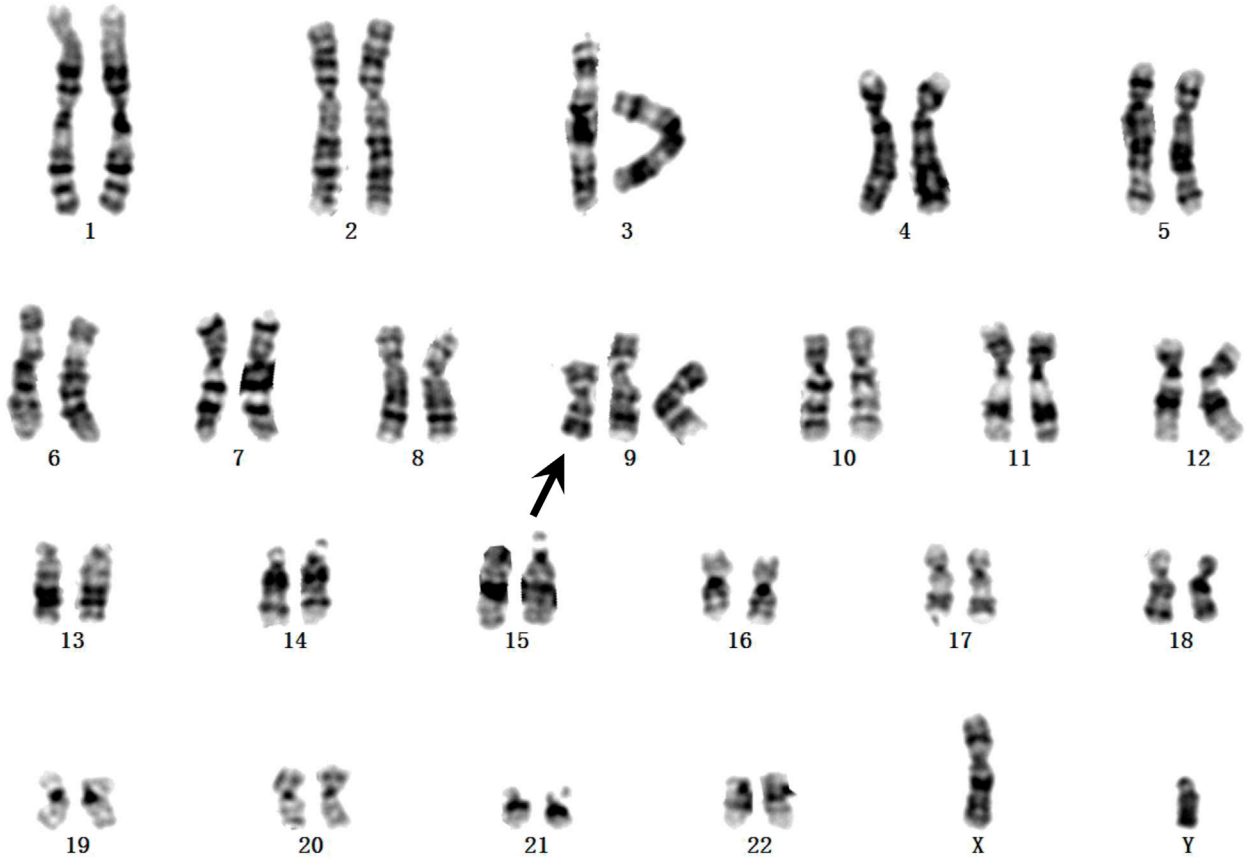


FIGURE 2
GTG-banding from the amniotic fluid sample. The supernumerary chromosome is shown by black arrow.

## Amniocentesis and cytogenetic analysis

Transabdominal amniocentesis was performed under the real-time sonographic guidance. A total of 20 ml of amniotic fluid was withdrawn after discarding the first 2 ml of amniotic fluid (Jindal et al., 2022). Fetal amniocytes were cultured, and GTG-banding was performed according to standard cytogenetic procedures, yielding a 320–400 band level with a resolution of around 10 Mb. Generally, 30 metaphases were counted, and 5 metaphases were analyzed (Jin et al., 2021).

## Chromosome microarray

Genomic DNA was extracted with the GentraPuregene Kit (Qiagen, Germany) from fetal amniotic cells. CytoScan™ HD array (Affymetrix, United States) was used in copy number analysis according to the manufacture's instructions. The array is characterized by > 2,600,000 CNV markers, including 750,000 SNP probes and >1,900,000 non–polymorphism probes for comprehensive whole genome coverage. Chromosome Analysis Suite (ChAS) software (Affymetrix, United States) was used to visualize and analyze the results. The reporting threshold of the copy number result was set at 500 kb with marker count ≥50 for gains and 200 kb with a marker count of ≥50 for losses. The analysis was based on the GRCh37/hg19 assembly.

## Fluorescence *in situ* hybridization analysis

Amniocytes were quadruple stained with the chromosome 9 subtelomeric p, q, and centromeric probe (Vysis, Downers Grove, IL) and DAPI (Vysis, Downers Grove, IL). The slides were hybridized according to the manufacture's instruction and counterstained with DAPI, then analyzed by Zeiss Imager A2 microscope (Zeiss, France). Image acquisition was subsequently performed using a CCD camera with Isis (FISH Imaging System, MetaSystems, Germany).


FIGURE 3
Chromosome microarray on DNA prepared from uncultured amniocytes. Results for chromosome 9 showing gain of the entire p arm and a portion of the q arm.

# Results

## Non-invasive prenatal testing results

NIPT showed negative for other chromosomes expect for the chromosome 9 with a fetal fraction DNA concentration of 10.72%. Additionally, an elevated amount of DNA from the p-arm of chromosome 9 was observed with a mean t-score of 11.528, suggesting a gain of approximately 46.36 Mb that encompassed chromosome bands 9p24.3–9p11 (Figure 1).

## Karyotyping, chromosome microarray, and fluorescence *in situ* hybridization results

Fetal karyotyping of the cultured aminocytes showed a male karyotype with the presence of supernumerary marker chromosome (SMC) (30/30) (Figure 2). CMA of the fetal DNA extracted from the uncultured aminocytes revealed a gain of approximately 68.126 Mb spanning from 9pter to 9q13 with a four-fold dose as indicated by five lines in both allele difference and BAF graphics (Figure 3). The array karyotype was: arr [GRCh37] 9p24.3q13 (203862_68330127)x4 (Figure 3).

These findings suggest that the SMC was a tetrasomy of 9p. The gain of the short arm of chromosome 9 was confirmed by FISH, which was carried out using the chromosome 9 specific subtelomeric p, q, and centromeric probe (Figure 4). FISH showed that the SMC was an isochromosome consisting of two copies of the entire short arm and the heterochromatic region of the long arm of a chromosome 9 with two centromeres. Based on karyotyping, CMA and FISH, the fetal karyotype was 47,XY,+idic (9) (q13).ish idic (9) (q13) (305J7-T7+,D9Z1+,D9Z1+,305J7-T7+).arr [GRCh37] 9p24.3q13 (203862_68330127)x4.

# Discussion

Herein, we reported a prenatal case of tetrasomy 9p that presented without obvious ultrasound anomalies during the first trimester. To the best of our knowledge, our case is the first prenatal case of non-mosaic tetrasomy 9p identified through NIPT.

NIPT may detect CNVs with a size greater 10 Mb with high sensitivity and specificity (Lo et al., 1997; Lo et al., 1998; Song et al., 2013; Yin et al., 2015; Gross et al., 2016). Additionally, it has good performance in detecting known microduplication/microdeletion syndromes (MMS), which are smaller than

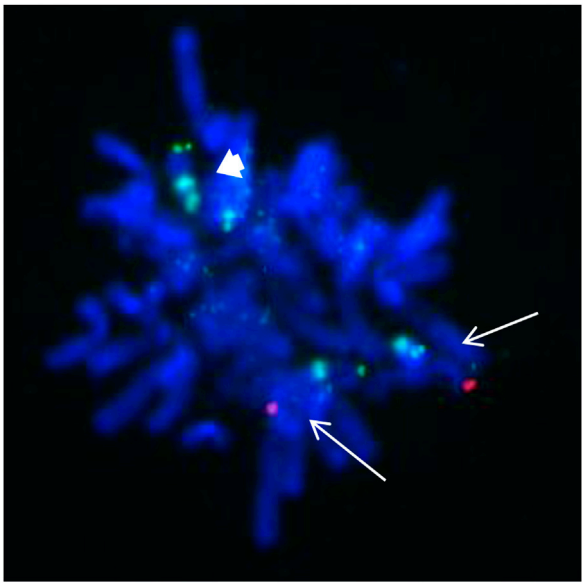

FIGURE 4
FISH from the uncultured amniocytes. Green signals indicate the subtelomeric part of chromosome 9p; red signals indicate the subtelomeric part of chromosome 9q; aqua signals indicate the centromeic of chromosome 9. Two normal chromosome 9 contain both green and red signals as showed with white arrow. The isodicentric chromosome 9p (bold white arrow) with two green signals and two aqua signals.

10 Mb, such as DiGeorge (93%) and 22q11.22 microduplication (68%) (Liang et al., 2019). Our data showed that NIPT provided quite precise duplication localization which was validated by amniocyte CMA results, suggesting the reliability of NIPT in detecting rare chromosome anomalies such as tetrasomy 9p.

Besides, NIPT can screen MMS before visible abnormalities are revealed on routine prenatal ultrasound examination. Most T9p fetuses were identified through ultrasound findings. Among the 60% of cases reviewed by Vinksel et al. (2019) fetuses with T9p were identified through ultrasound performed during the second and third trimesters. Among the cases reported in the first trimester, increased NT was the most common features, which can be present as an isolated phenotype or accompanied by other anomalies (cleft lip and/or palate, facial dysmorphism and skeletal abnormalities) (Vinksel et al., 2019; Kok Kilic et al., 2022). In our case, only the first trimester ultrasound scan was performed; therefore, other common abnormalities associated with T9p might not have displayed. In another case of mosaic T9p identified through NIPT, the pregnant women presented with a normal NT and nasal bone in the first trimester, while showed isolated persistent left superior vena cava until 25$^{th}$ week gestation ultrasound examination (Wang et al., 2015). Both this case and our case indicate that NIPT is superior to echography in screening for early prenatal abnormalities.

It was suggested that the degree of the mosaicism is associated with the severity of the phenotype of T9p. However, the severity of the phenotype of T9p is not linearly correlated with the mosaic level of the supernumerary chromosome in lymphocyte samples. A case with full tetrasomy 9p in the blood, 65% mosaic in the buccal mucosa, was a health woman who was accidentally identified due to her previous pregnancy with an inv (7) baby (Papoulidis et al., 2012). Among the 8 cases reported with a clinically normal phenotype, the tetrasomic clone ranged from 6% to 100% in peripheral blood lymphocytes, except in five cases that had fertility related issues (5/8) (Papoulidis et al., 2012; Bellil et al., 2020; Shu et al., 2021).

One might speculate that the tissue-limited mosaicism is related to severity of the phenotype of T9p. Supporting this, patients with i (9p) in fibroblasts tend to have more severe manifestations than those whose i (9p) is limited to lymphocytes, especially in terms of cardiac defects and viability (El Khattabi et al., 2015). Numerous data suggest that isochromosome 9p is predominantly present in peripheral blood but with a lower frequency in cell lines derived from the skin, amniotic fluid, or chorionic villus sampling. Hence, even a normal karyotype from amniocytes does not necessarily rule out the possibility of tetrasomy 9p (Cuoco et al., 1982; Papenhausen et al., 1990; Schaefer et al., 1991; Grass et al., 1993; Lloveras et al., 2004; McAuliffe et al., 2005). Additionally, the tissue-limited mosaicism mechanism at some extent unveiled that the prenatal cases of T9p showed numerous ultrasound abnormalities even with low-level mosaic status as the amniocytes are a mixture of cells derived from different germ layers (Chen et al., 2007). Based on published reports, non-mosaic fetuses have poorer prognosis, which explains the higher incidence of early death, FGR, Dandy-Walker malformation, and other congenital anomalies (Tang et al., 2004; Tan et al., 2007; El Khattabi et al., 2015). As such, the patient in the present study decided to terminate the pregnancy after genetic consultation.

Another factor that may affect the severity of the phenotype is breakpoint position; however, this remains controversial (Grass et al., 1993; Stumm et al., 1999; El Khattabi et al., 2015; Pinto et al., 2018; Vinksel et al., 2019). Some suggested that the phenotype will be more severe in patients that harbor the large portion of 9q extending to 9q21, which encompasses a large duplicated region with several OMIM morbid genes compared with those containing exclusively the entire 9p (El Khattabi et al., 2015; Pinto et al., 2018; Vinksel et al., 2019). A total of 21 prenatal cases with ultrasound anomalies have been reviewed and showed that involvement of the 9q region appears to have similar phenotypes to the p10 region in terms of facial anomalies, FGR, central nervous system dysfunction and cardiac anomalies (Table 1). Surprisingly, cardiac malformation seems to be much frequent when the region q12-q13 is involved.

TABLE 1 Malformations in relation to breakpoints among prenatal cases associated with T9p.

| Breakpoints | Facial | FGR | CNS | Cardiac |
|---|---|---|---|---|
| p10 or p11 ($n$ = 8) | 4 (50%) | 4 (50%) | 4 (50%) | 1 (12.5%) |
| McDowall et al. (1989); Schaefer et al. (1991); Dutly et al. (1998); Tang et al. (2004); Nakamura-Pereira et al. (2009); El Khattabi et al. (2015) | | | | |
| q12 or q13 ($n$ = 11) | 6 (54.54%) | 4 (36.36%) | 6 (54.54%) | 6 (54.54%) |
| Dhandha et al. (2002); Cazorla Calleja et al. (2003); Deurloo et al. (2004); Hengstschläger et al. (2004); Chen et al. (2007); di Vera et al. (2008); Lazebnik and Cohen, (2015); Wang et al. (2015); Vinkšel et al. (2019); Kok Kilic et al. (2022) | | | | |
| q21 ($n$ = 2) | 1 (50%) | 2 (100%) | 0 | 0 |
| Tan et al. (2007); Chen et al. (2014) | | | | |

Facial, facial dysmorphism including cleft/palate; FGR, fetal growth retardation; CNS, central nervous system dysfunction; Cardiac, cardiac anomalies.

Due to the poor resolution of conventional cytogenetic techniques, CMA with high throughput has been widely complemented into prenatal examinations for fetuses with ultrasound anomalies as it offers several advantages, such as fast reporting (without further cell culture) and high resolution in detecting copy number changes. Furthermore, it can provide a more precise location of the breakpoint of the tetrasomy 9p, thus improving the understanding of the genotype-phenotype correlation. However, the breakpoints of 9p10, q12, and q13 are located in the heterochromatin region, wherein a few markers have been set in CMA, making it hazardous to define the precise localization. With the release of the T2T-CHM13 reference genome, long-reads based whole genome sequencing may overcome the remaining gaps and provide convincing breakpoints for the complex chromosome rearrangement, including in T9p (Aganezov et al., 2022; Nurk et al., 2022).

T9p usually occurs *de novo*, and recurrence has been observed in only one report, indicating gonadal mosaicism (El Khattabi et al., 2015). Most supernumerary chromosomes are of maternal origin, including T9p (Kotzot et al., 1996; Dutly et al., 1998). The supernumerary chromosome can be separated into two forms according to the number of centromeres: i (9) with a single centromeric region or two centromeres forming idic (9). Several models have been proposed to explain the formation of an isochromosome. One mechanism relies on homologous recombination (HR) when intra-chromosomal U-type recombination occurs during meiosis I followed by non-disjunction in meiosis II (Floridia et al., 1996; Kotzot et al., 1996; Dutly et al., 1998; Knijnenburg et al., 2007). This U-type exchange is more likely to result in a dicentric than in a monocentric isochromosome. Another mechanism refers to the formation of monocentric isochromosomes and relies on centromere misdivision during the premeiotic stage followed by non-disjuntion at meiosis I (Rivera et al., 1986); alternatively, a non-disjuntion at meiosis II is followed by post-zygotic centromere misdivision (de Ravel et al., 2004). However, Kotzot et al. (1996) oppose to the former hypothesis in the formation of isochromosome 18p as this would require two abnormal cell divisions.

In conclusion, tetrasomy 9p is a rare chromosome rearrangement that often occurs *de novo*. A prenatal case of tetrasomy 9p without any ultrasound abnormality during the first trimester was revealed by NIPT and confirmed by invasive diagnosis. NIPT can screen not only for canonical trisomy 13, 18, and 21 but also large fragment copy number changes, such as tetrasomy 9p before it manifests with a significant phenotype. Furthermore, multiple techniques, such as karyotyping, FISH and CMA, are critical for a precise prenatal diagnostic.

## Data availability statement

The datasets presented in this study can be found in online repositories. The names of the repository/repositories and accession number(s) can be found below: NCBI repository with the Accession number PRJNA880763, with the URL: https://dataview.ncbi.nlm.nih.gov/object/PRJNA880763.

## Ethics statement

The studies involving human participants were reviewed and approved by Ethics Committee of Women's Hospital, School of Medicine Zhejiang University (IRB-20220260-R). The patients/participants provided their written informed consent to participate in this study.

## Author contributions

Patient workups were contributed by MS and YQ Genetic analysis was contributed by JY and NC Pathological analysis was contributed by JY. Manuscript drafting was contributed by JY, MC, YQ, and MD. Final approval of the version to be submitted

for publishing consideration was contributed by JY, NC, MC, MS, YQ, and MD.

## Funding

This work was supported by the National Natural Science Foundation of China (grant numbers 81900904, 82001625, and 81901382).

## Acknowledgments

We thank the patients and volunteers for their supports during this study.

## Conflict of interest

The authors declare that the research was conducted in the absence of any commercial or financial relationships that could be construed as a potential conflict of interest.

## Publisher's note

All claims expressed in this article are solely those of the authors and do not necessarily represent those of their affiliated organizations, or those of the publisher, the editors and the reviewers. Any product that may be evaluated in this article, or claim that may be made by its manufacturer, is not guaranteed or endorsed by the publisher.

## References

Aganezov, S., Yan, S. M., Soto, D. C., Kirsche, M., Zarate, S., Avdeyev, P., et al. (2022). A complete reference genome improves analysis of human genetic variation. *Science* 376 (6588), eabl3533. doi:10.1126/science.abl3533

Bellil, H., Herve, B., Herzog, E., Ayoubi, J. M., Vialard, F., and Poulain, M. (2020). A high level of tetrasomy 9p mosaicism but no clinical manifestations other than moderate oligozoospermia with chromosomally balanced sperm: A case report. *J. Assist. Reprod. Genet.* 37 (3), 573–577. doi:10.1007/s10815-020-01690-0

Cazorla Calleja, M. R., Verdú, A., and Félix, V. (2003). Dandy-Walker malformation in an infant with tetrasomy 9p. *Brain Dev.* 25 (3), 220–223. doi:10.1016/s0387-7604(02)00211-5

Chen, C. P., Chang, T. Y., Chern, S. R., Lee, C. C., Town, D. D., Lee, M. S., et al. (2007). Prenatal diagnosis of low-level mosaic tetrasomy 9p by amniocentesis. *Prenat. Diagn.* 27 (4), 383–385. doi:10.1002/pd.1678

Chen, C. P., Wang, L. K., Chern, S. R., Wu, P. S., Chen, Y. T., Kuo, Y. L., et al. (2014). Mosaic tetrasomy 9p at amniocentesis: Prenatal diagnosis, molecular cytogenetic characterization, and literature review. *Taiwan. J. Obstet. Gynecol.* 53 (1), 79–85. doi:10.1016/j.tjog.2013.12.002

Chen, M., Fu, X. Y., Luo, Y. Q., Qian, Y. Q., Pan, L., Wang, L. Y., et al. (2019). Detection of fetal duplication 16p11.2q12.1 by next-generation sequencing of maternal plasma and invasive diagnosis. *J. Matern. Fetal. Neonatal Med.* 32 (1), 38–45. doi:10.1080/14767058.2017.1369947

Cuoco, C., Gimelli, G., Pasquali, F., Poloni, L., Zuffardi, O., Alicata, P., et al. (1982). Duplication of the short arm of chromosome 9. Analysis of five cases. *Hum. Genet.* 61 (1), 3–7. doi:10.1007/bf00291321

de Ravel, T. J., Keymolen, K., van Assche, E., Wittevronghel, I., Moerman, P., Salden, I., et al. (2004). Post-zygotic origin of isochromosome 12p. *Prenat. Diagn.* 24 (12), 984–988. doi:10.1002/pd.956

Deurloo, K. L., Cobben, J. M., Heins, Y. M., de Ru, M., Wijnaendts, L. C., and van Vugt, J. M. (2004). Prenatal diagnosis of tetrasomy 9p in a 19-week-old fetus with dandy-walker malformation: A case report. *Prenat. Diagn.* 24 (10), 796–798. doi:10.1002/pd.850

Dhandha, S., Hogge, W. A., Surti, U., and McPherson, E. (2002). Three cases of tetrasomy 9p. *Am. J. Med. Genet.* 113 (4), 375–380. doi:10.1002/ajmg.b.10826

Di Vera, E., Liberati, M., Celentano, C., Calabrese, G., Guanciali-Franchi, P. E., Morizio, E., et al. (2008). Rhombencephalosynapsis in a severely polymalformed fetus with non-mosaic tetrasomy 9p, in intracytoplasmic-sperm-injection pregnancy. *J. Assist. Reprod. Genet.* 25 (11-12), 577–580. doi:10.1007/s10815-008-9257-7

Dutly, F., Balmer, D., Baumer, A., Binkert, F., Schinzel, A., and Schinzel, A. (1998). Isochromosomes 12p and 9p: Parental origin and possible mechanisms of formation. *Eur. J. Hum. Genet.* 6 (2), 140–144. doi:10.1038/sj.ejhg.5200168

El Khattabi, L., Jaillard, S., Andrieux, J., Pasquier, L., Perrin, L., Capri, Y., et al. (2015). Clinical and molecular delineation of tetrasomy 9p syndrome: Report of 12 new cases and literature review. *Am. J. Med. Genet. A* 167 (6), 1252–1261. doi:10.1002/ajmg.a.36932

Floridia, G., Piantanida, M., Minelli, A., Dellavecchia, C., Bonaglia, C., Rossi, E., et al. (1996). The same molecular mechanism at the maternal meiosis I produces mono- and dicentric 8p duplications. *Am. J. Hum. Genet.* 58 (4), 785–796.

Grass, F. S., Parke, J. C., Jr., Kirkman, H. N., Christensen, V., Roddey, O. F., Wade, R. V., et al. (1993). Tetrasomy 9p: Tissue-limited idic(9p) in a child with mild manifestations and a normal CVS result. Report and review. *Am. J. Med. Genet.* 47 (6), 812–816. doi:10.1002/ajmg.1320470603

Gross, S. J., Stosic, M., McDonald-McGinn, D. M., Bassett, A. S., Norvez, A., Dhamankar, R., et al. (2016). Clinical experience with single-nucleotide polymorphism-based non-invasive prenatal screening for 22q11.2 deletion syndrome. *Ultrasound Obstet. Gynecol.* 47 (2), 177–183. doi:10.1002/uog.15754

Hengstschläger, M., Bettelheim, D., Drahonsky, R., Repa, C., Deutinger, J., and Bernaschek, G. (2004). Prenatal diagnosis of tetrasomy 9p with Dandy-Walker malformation. *Prenat. Diagn.* 24 (8), 623–626. doi:10.1002/pd.933

Jin, P., Gao, X., Wang, M., Qian, Y., Yang, J., Yang, Y., et al. (2021). Case Report: Identification of maternal low-level mosaicism in the dystrophin gene by droplet digital polymerase chain reaction. *Front. Genet.* 12, 686993. doi:10.3389/fgene.2021.686993

Jindal, A., Sharma, M., and Chaudhary, C. (2022). "Amniocentesis," in StatPearls. *(Treasure island (FL)* (Florida,United States: StatPearls Publishing LLC.).

Knijnenburg, J., van Haeringen, A., Hansson, K. B., Lankester, A., Smit, M. J., Belfroid, R. D., et al. (2007). Ring chromosome formation as a novel escape mechanism in patients with inverted duplication and terminal deletion. *Eur. J. Hum. Genet.* 15 (5), 548–555. doi:10.1038/sj.ejhg.5201807

Kok Kilic, G., Pariltay, E., Karaca, E., Durmaz, B., Ekici, H., Imamoglu, M., et al. (2022). Prenatal diagnosis of a case with tetrasomy 9p confirmed by cytogenetics, FISH, microarray analysis and review. *Taiwan. J. Obstet. Gynecol.* 61 (1), 122–126. doi:10.1016/j.tjog.2021.10.003

Kotzot, D., Bundscherer, G., Bernasconi, F., Brecevic, L., Lurie, I. W., Basaran, S., et al. (1996). Isochromosome 18p results from maternal meiosis II nondisjunction. *Eur. J. Hum. Genet.* 4 (3), 168–174. doi:10.1159/000472191

Lazebnik, N., and Cohen, L. (2015). Prenatal diagnosis and findings of tetrasomy 9p. *J. Obstet. Gynaecol. Res.* 41 (7), 997–1002. doi:10.1111/jog.12706

Liang, D., Cram, D. S., Tan, H., Linpeng, S., Liu, Y., Sun, H., et al. (2019). Clinical utility of noninvasive prenatal screening for expanded chromosome disease syndromes. *Genet. Med.* 21 (9), 1998–2006. doi:10.1038/s41436-019-0467-4

Liu, H., Gao, Y., Hu, Z., Lin, L., Yin, X., Wang, J., et al. (2016). Performance evaluation of NIPT in detection of chromosomal copy number variants using low-coverage whole-genome sequencing of plasma DNA. *PLoS One* 11 (7), e0159233. doi:10.1371/journal.pone.0159233

Lloveras, E., Pérez, C., Solé, F., Zamora, L., Lladonosa, A., Espinet, B., et al. (2004). Two cases of tetrasomy 9p syndrome with tissue limited mosaicism. *Am. J. Med. Genet. A* 124a (4), 402–406. doi:10.1002/ajmg.a.20447

Lo, Y. M., Corbetta, N., Chamberlain, P. F., Rai, V., Sargent, I. L., Redman, C. W., et al. (1997). Presence of fetal DNA in maternal plasma and serum. *Lancet* 350 (9076), 485–487. doi:10.1016/s0140-6736(97)02174-0

Lo, Y. M., Tein, M. S., Lau, T. K., Haines, C. J., Leung, T. N., Poon, P. M., et al. (1998). Quantitative analysis of fetal DNA in maternal plasma and serum: Implications for noninvasive prenatal diagnosis. *Am. J. Hum. Genet.* 62 (4), 768–775. doi:10.1086/301800

McAuliffe, F., Winsor, E. J., and Chitayat, D. (2005). Tetrasomy 9p mosaicism associated with a normal phenotype. *Fetal diagn. Ther.* 20 (3), 219–222. doi:10.1159/000083909

McDowall, A. A., Blunt, S., Berry, A. C., and Fensom, A. H. (1989). Prenatal diagnosis of a case of tetrasomy 9p. *Prenat. Diagn.* 9 (11), 809–811. doi:10.1002/pd.1970091110

Nakamura-Pereira, M., Cima, L. C., Llerena, J. C., Jr., Guerra, F. A., and Peixoto-Filho, F. M. (2009). Sonographic findings in a case of tetrasomy 9p associated with increased nuchal translucency and Dandy-Walker malformation. *J. Clin. Ultrasound* 37 (8), 471–474. doi:10.1002/jcu.20612

Nurk, S., Koren, S., Rhie, A., Rautiainen, M., Bzikadze, A. V., Mikheenko, A., et al. (2022). The complete sequence of a human genome. *Science* 376 (6588), 44–53. doi:10.1126/science.abj6987

Papenhausen, P., Riscile, G., Miller, K., Kousseff, B., and Tedesco, T. (1990). Tissue limited mosaicism in a patient with tetrasomy 9p. *Am. J. Med. Genet.* 37 (3), 388–391. doi:10.1002/ajmg.1320370319

Papoulidis, I., Kontodiou, M., Tzimina, M., Saitis, I., Hamid, A. B., Klein, E., et al. (2012). Tetrasomy 9p mosaicism associated with a normal phenotype in two cases. *Cytogenet. Genome Res.* 136 (4), 237–241. doi:10.1159/000337520

Pinto, I. P., Minasi, L. B., Steckelberg, R., da Silva, C. C., and da Cruz, A. D. (2018). Mosaic tetrasomy of 9p24.3q21.11 postnatally identified in an infant born with multiple congenital malformations: A case report. *BMC Pediatr.* 18 (1), 298. doi:10.1186/s12887-018-1275-8

Qian, Y. Q., Wang, X. Q., Chen, M., Luo, Y. Q., Yan, K., Yang, Y. M., et al. (2019). Detection of fetal subchromosomal aberration with cell-free DNA screening led to diagnosis of parental translocation: Review of 11344 consecutive cases in a University hospital. *Eur. J. Med. Genet.* 62 (2), 115–123. doi:10.1016/j.ejmg.2018.06.012

Rivera, H., Rivas, F., and Cantú, J. M. (1986). On the origin of extra isochromosomes. *Clin. Genet.* 29 (6), 540–541. doi:10.1111/j.1399-0004.1986.tb00557.x

Schaefer, G. B., Domek, D. B., Morgan, M. A., Muneer, R. S., and Johnson, S. F. (1991). Tetrasomy of the short arm of chromosome 9: Prenatal diagnosis and further delineation of the phenotype. *Am. J. Med. Genet.* 38 (4), 612–615. doi:10.1002/ajmg.1320380422

Shu, W., Cheng, S. S. W., Xue, S., Chan, L. W., Soong, S. I., Kan, A. S. Y., et al. (2021). First case report of maternal mosaic tetrasomy 9p incidentally detected on non-invasive prenatal testing. *Genes (Basel)* 12 (3), 370. doi:10.3390/genes12030370

Song, Y., Liu, C., Qi, H., Zhang, Y., Bian, X., and Liu, J. (2013). Noninvasive prenatal testing of fetal aneuploidies by massively parallel sequencing in a prospective Chinese population. *Prenat. Diagn.* 33 (7), 700–706. doi:10.1002/pd.4160

Stumm, M., Tönnies, H., Mandon, U., Götze, A., Krebs, P., Wieacker, P. F., et al. (1999). Mosaic tetrasomy 9p in a girl with multiple congenital anomalies: Cytogenetic and molecular-cytogenetic studies. *Eur. J. Pediatr.* 158 (7), 571–575. doi:10.1007/s004310051149

Tan, Y. Q., Chen, X. M., Hu, L., Guan, X. Y., and Lu, G. X. (2007). Prenatal diagnosis of nonmosaic tetrasomy 9p by microdissection and FISH: Case report. *Chin. Med. J.* 120 (14), 1281–1283. doi:10.1097/00029330-200707020-00016

Tang, W., Boyd, B. K., Hummel, M., and Wenger, S. L. (2004). Prenatal diagnosis of tetrasomy 9p. *Am. J. Med. Genet. A* 126a (3), 328. doi:10.1002/ajmg.a.20511

Vinkšel, M., Volk, M., Peterlin, B., and Lovrecic, L. (2019). A systematic clinical review of prenatally diagnosed tetrasomy 9p. *Balk. J. Med. Genet.* 22 (1), 11–20. doi:10.2478/bjmg-2019-0012

Wang, H., Xie, L. S., Wang, Y., and Mei, J. (2015). Prenatal diagnosis of mosaic tetrasomy 9p in a fetus with isolated persistent left superior vena cava. *Taiwan. J. Obstet. Gynecol.* 54 (2), 204–205. doi:10.1016/j.tjog.2014.12.005

Yin, A. H., Peng, C. F., Zhao, X., Caughey, B. A., Yang, J. X., Liu, J., et al. (2015). Noninvasive detection of fetal subchromosomal abnormalities by semiconductor sequencing of maternal plasma DNA. *Proc. Natl. Acad. Sci. U. S. A.* 112 (47), 14670–14675. doi:10.1073/pnas.1518151112

frontiers | Frontiers in Pediatrics

TYPE Original Research
PUBLISHED 03 February 2023
DOI 10.3389/fped.2023.1084336



OPEN ACCESS

EDITED BY
Can Liao,
Guangzhou Women and Children's Medical Center, China

REVIEWED BY
Hui Xu,
First Hospital of Lanzhou University, China
Xu Haixia,
Maternal and Child Health Care Hospital of Guiyang City, China
Cuirong Duan,
Hunan Children's Hospital, China

*CORRESPONDENCE
Shuzhen Sun
shuzhens01@126.com

†These authors have contributed equally to this work

SPECIALTY SECTION
This article was submitted to Genetics of Common and Rare Diseases, a section of the journal Frontiers in Pediatrics

RECEIVED 21 November 2022
ACCEPTED 12 January 2023
PUBLISHED 03 February 2023

CITATION
Li Q, Wang J, Tian M, Yang Z, Yu L, Liu S, Wang C, Wang X and Sun S (2023) Clinical features and enzyme replacement therapy in 10 children with Fabry disease.
Front. Pediatr. 11:1084336.
doi: 10.3389/fped.2023.1084336



# Clinical features and enzyme replacement therapy in 10 children with Fabry disease

Qian Li[1,2†], Jing Wang[1,2†], Minle Tian[3], Zhenle Yang[1,2], Lichun Yu[1,2], Suwen Liu[1,2], Cong Wang[1,2], Xiaoyuan Wang[1,2] and Shuzhen Sun[1,2*]

[1]Department of Pediatric Nephrology and Rheumatism and Immunology, Shandong Provincial Hospital, Cheeloo College of Medicine, Shandong University, Jinan, China, [2]Department of Pediatric Nephrology and Rheumatism and Immunology, Shandong Provincial Hospital Affiliated to Shandong First Medical University, Jinan, China, [3]School of Basic Medical Sciences, Shandong First Medical University, Taian, China

**Objective:** To summarize the clinical features, diagnosis and enzyme replacement therapy(ERT) of Fabry disease (FD) in children.
**Methods:** The clinical data, laboratory tests, genetic variations and treatment of 10 FD children diagnosed in Shandong Provincial Hospital from September 2020 to June 2022 were retrospectively analyzed.
**Results:** Among the 10 cases from 6 families, 7 patients were boys of 4 to 13 years of age, and 3 were girls of 12 to 15 years of age. There were 7 symptomatic patients, including 6 boys and 1 girl. All 7 patients presented with acral neuralgia. Five patients had little or no sweating. Five patients presented with cutaneous angiokeratoma. Two patients had abdominal pain. One patient developed joint symptoms. Four patients had corneal opacity. One patient had hearing loss; one patient had short stature. One patient had mild proteinuria and 1 patient had dysplasia of the right kidney with decreased eGFR (55.28 ml/min.1.73 $m^2$). The left ventricular mass index was slightly elevated in 1 patient. Three patients had mild obstructive ventilatory dysfunction; a small amount of effusion in the intestinal space of the lower abdomen or mild fatty liver was found in 2 patients. Partial empty sella turcica in 1 patient. A total of 6 GLA gene variants were detected in 10 children, among which C.1059_1061delGAT (p.met353del) was a newly discovered mutation. Five children received ERT, of which 4 were treated with agalsidase beta and 1 was treated with agalsidase alpha. Only 1 patient had anaphylaxis. Lyso-GL-3 levels decreased significantly in the first 3 months of ERT initiation and remained relatively stable thereafter in 3 patients. The Lyso-GL-3 level was decreased, but renal impairment continued to progress in 1 patient treated with agalsidase alpha.
**Conclusion:** The clinical manifestations of FD in childhood are diverse, and it is necessary to make a definite diagnosis by combining family history, enzyme activity, biomarkers, gene testing and other indicators. Pedigree screening and high-risk population screening are helpful for early identification, early diagnosis and early treatment. No serious adverse reactions were found during the short-term treatment with agalsidase alpha and beta.

KEYWORDS

Fabry disease, children, clinical analysis, screening, enzyme replacement therapy

## Introduction

Fabry disease (FD) is an X-linked inherited lysosomal storage disorder. The GLA gene is located on the long arm of the X chromosome (Q22.1) and encodes alpha-galactosidase A ($\alpha$-Gal A). Mutations in this gene decrease or delete $\alpha$-Gal A activity due to misfolding and modifications. This results in the progressive accumulation of trihexosaccharide sphingolipid

alcohol (GL-3) and its derivative deacetyl GL-3 (Lyso-GL-3) in tissues, eventually leading to irreversible damage to multiple organ systems (1). FD was included in China's first list of 121 rare diseases issued in May 2018. The exact prevalence is not known, but the estimated prevalence in the general population is 1 in 100,000. The incidence in neonates is approximately 1/8 882 to 1/1 250, while in male neonates, it is 1/117,000–1/40,000 (2, 3). Due to the insidious onset of the disease in children, diverse clinical manifestations, uncertainty between clinical phenotypes and genotypes, easy misdiagnosis, continuous progression of the disease, and poor prognosis, early diagnosis and treatment in childhood are extremely important. In this study, the clinical characteristics and diagnosis and treatment of 10 children with FD were retrospectively analyzed and summarized to improve clinicians' understanding of FD in children.

# Objects and methods

## Objects

The clinical data of 10 children with FD who were admitted to the Department of Pediatric Nephrology and Rheumatology of Shandong Provincial Hospital from September 2020 to June 2022 were retrospectively analyzed. This study was approved by the Medical Ethics Committee of Shandong Provincial Hospital.

# Methods

## Collection of clinical data

We consulted the medical records of children through the electronic medical record system of the hospital and collected clinical data. The collected information included sex, age, age at diagnosis, time from symptom onset to diagnosis, clinical manifestations, such as acral neuralgia, sweating disorder, cutaneous angiokeratoma, gastrointestinal dysfunction, joint symptoms, eye abnormalities, and hearing abnormalities, routine blood tests, liver and kidney function tests, urine tests, other laboratory tests, electrocardiogram, cardiac color ultrasound, pulmonary function, chest CT, abdominal ultrasound, head magnetic resonance imaging and other auxiliary examinations, enzyme activity levels, Lyso-GL-3 levels, GLA gene variations and treatment options.

## Diagnosis of FD

The clinical manifestations of FD in children lack specificity and are often characterized by acral neuralgia, oligohidrosis, angiokeratoma, gastrointestinal symptoms and corneal opacity. A comprehensive analysis of family history, enzyme activity, biomarkers, pathology and genetic testing is needed to confirm the diagnosis (4).

## Treatment protocol

The current treatment approach for FD includes specific treatment and nonspecific treatment. The former includes enzyme replacement therapy (ERT) and molecular chaperone therapy, and the latter includes symptomatic treatment and psychological support for different organs. There are two kinds of ERT drugs that are available: agalsidase beta (Fabrazyme, 1.0 mg/kg, intravenous infusion every 2 weeks, recommended treatment dose for age ≥8 years) and agalsidase alpha (Replagal, 0.2 mg/kg, intravenous infusion every 2 weeks, recommended treatment dose for age ≥7 years).

## Statistical analysis

Descriptive analysis. Enumeration data are presented as examples, and measurement data are presented as M(range).

# Results

## Clinical manifestations

There were 7 boys and 3 girls from 6 families. The seven boys were diagnosed between the ages of 4 and 13 years. There was one 4-year-old boy who was identified by pedigree screening (case 8). The remaining six boys were between the ages of 11 and 13 years, with a time interval from the first symptom onset to diagnosis ranging from 2 to 9 years. The age range of the three girls was 12–15 years old, and all three of these patients were found by pedigree screening. Seven patients had clinical symptoms, including 6 boys and 1 girl. All 7 patients had acral neuralgia (100%). Five patients (71%) presented with little or no sweating. Five patients (71%) presented with cutaneous angiokeratoma, which was distributed in the fingers, palms, thighs, lower back, buttocks and perineum. Abdominal pain was present in 2 patients (28%). One patient had joint symptoms (14%), involving the bilateral finger joints and knee joints. Corneal opacity was found in 4 patients (57%). Hearing loss was found in 1 patient (14%). One patient had short stature and had been treated with growth hormone (**Table 1**).

## Laboratory examination and auxiliary examination

Of the 7 symptomatic children, 2 were not systematically evaluated in our hospital for personal reasons. Among the other 5 patients, 2 patients had renal involvement. Case 2 showed only mild proteinuria, and the 24-hour urine protein quantification was 0.17 g. After repeated examination, routine urine and microalbumin were normal. Case 4 had dysplasia of the right kidney and right renal artery, mild proteinuria (mainly tubular proteinuria), and decreased eGFR (55.28 ml/min.1.73 $m^2$) and was diagnosed as chronic kidney disease stage 3b. One patient had a slightly elevated left ventricular mass index and mild left ventricular hypertrophy (Case 3). Three children had mild

10.3389/fped.2023.1084336

TABLE 1 Clinical manifestations of children with Fabry disease.

| Cases | Sex | Age at diagnosis (years) | Interval time (year) | Acral neuralgia | Perspiration disorder | Cutaneous angiokeratoma | Gastrointestinal dysfunction | Arthralgia | Corneal opacity | Hearing loss | Short stature |
|---|---|---|---|---|---|---|---|---|---|---|---|
| 1 | Male | 11 | 7 | Yes | No sweat | Yes | No | No | Yes | Yes | No |
| 2 | Male | 13 | 8 | Yes | Little sweat | No | No | No | No | No | No |
| 3 | Male | 10 | 2 | Yes | No | Yes | No | No | No | No | No |
| 4 | Male | 11 | 2 | Yes | Little sweat | No | Abdominal pain | No | Yes | No | No |
| 5 | Male | 13 | 9 | Yes | Little sweat | Yes | Abdominal pain, diarrhea | Yes | Yes | No | No |
| 6 | Male | 12 | 9 | Yes | No sweat | Yes | No | No | Yes | ND | No |
| 7 | Female | 12 | 2 | Yes | No | Yes | No | No | ND | ND | Yes |
| 8 | Male | 4 | | No | No | No | No | No | ND | ND | No |
| 9 | Female | 15 | | No | No | No | No | No | ND | ND | No |
| 10 | Female | 15 | | No | No | No | No | No | ND | ND | No |

ND: no data.

obstructive ventilatory dysfunction (Cases 1, 2, and 3). Two cases had mild abdominal ultrasound abnormalities, including a small amount of effusion in the intestinal space of the lower abdomen and mild fatty liver (Cases 1 and 4). Brain magnetic resonance imaging showed partially empty sella turcica in 1 patient (Case 5). The Mainz Severity Score Index (MSSI) was used to score 5 children, with scores ranging from 9 to 21 (Table 2).

## FD-specific indexes and GLA genetic testing

Among the 10 children, serum $\alpha$-gal A enzyme activity was significantly decreased, and serum Lyso-GL-3 levels were significantly increased in 7 boys. Three girls showed normal or mildly decreased enzyme activity with moderately elevated blood Lyso-GL-3 levels. A total of 6 mutations in the GLA gene were found in 10 patients, including 1 nonsense mutation (c.140G > A), 2 deletion mutations (c.1080_1082delTGG and c.1059_1061delGAT), and 3 missense mutations (c.671A > G, c.124A > G, and c.95T > C) (Table 3). Only one mutation was derived from the father, and the rest were derived from the mother. The in-frame deletion variant c.1059_1061delGAT (p.Met353del) is a newly discovered mutation (Case 5) that has not been reported in the literature. This variant is an in-frame deletion mutation that may result in the deletion of the encoded amino acid methionine (Met) at position 353 and was rated as potentially pathogenic according to the ACMG guidelines.

## Pedigree screening

Case 1 was the first FD case admitted to our department. The age at onset of the disease for this patient was 4 years old. In his family, both the mother and the aunt had a history of acroparesthesia at the age of 13–14 years. A maternal GLA gene heterozygous variation was identified, and blood Lyso-GL-3 levels of his mother slightly increased (6.17 ng/ml). His aunt was not screened.

The patients in Case 2 and Case 3 were from the same family. Both of these patients had acroparesthesia. Additionally, one patient had hypohidrosis, and one patient had angiokeratoma. Their maternal grandmothers were siblings, and both had a history of heart disease. The maternal grandmother of Case 3 also had renal dysfunction. Her two brothers died of liver cancer and myocardial infarction at the ages of 42 and 50, respectively. In this family, the mother and sister of Case 2 and the mother and brother of Case 3 were found to carry heterozygous GLA variants, and all were asymptomatic. Serum $\alpha$-Gal A levels decreased slightly and Lyso-GL-3 levels increased slightly in 3 female patients. The younger brother was only 4 years old. His serum $\alpha$-gal A enzyme activity was significantly decreased (0.32 μmol/L·h), and his serum Lyso-GL-3 level was significantly increased (88.73 ng/ml).

The patient in Case 4 presented with intermittent fever with limb pain, little sweating and unexplained abdominal pain at the age of 9. When he was 11 years old, multiple tests were performed. CT examination revealed right kidney atrophy. Additionally, his urine protein was 1+, and serum creatinine was increased (103 μmol/L). All exon parallel genetic testing screening revealed a hemizygous GLA gene mutation; therefore, he was diagnosed with FD.

Heterozygous variants of the GLA gene were found in his maternal grandmother, mother, aunt and sister, and they were all asymptomatic, with normal or slightly decreased blood $\alpha$-Gal A levels and slightly increased Lyso-GL-3 levels.

The patient in Case 5 presented with foot pain and arthralgia involving the bilateral finger joints and knee joints since 4 years of age. The patient was misdiagnosed with a cold, growing pains, and juvenile idiopathic arthritis and treated with calcium tablets, nonsteroidal anti-inflammatory drugs, anti-rheumatism medicine, a variety of biological agents, and glucocorticoid treatment without obvious improvement. He was found to have cutaneous angiokeratoma, hypohidrosis symptoms, unexplained abdominal pain and diarrhea since childhood when he came to our department. The patient was diagnosed by screening for FD. His maternal grandmother died of unknown causes in her forties. His mother, maternal uncle and aunt were found to carry the same GLA mutations. His mother had cold finger discomfort when she was approximately 20 years old, and she had a slight decrease in $\alpha$-Gal A levels (1.64 μmol/L·h) and a slight increase in Lyso-GL-3 levels (4.51 ng/ml). His maternal uncle showed acroparesthesia, cutaneous angioglioma, a significant decrease in $\alpha$-Gal A levels (0.24 μmol/L·h), and a significant increase in Lyso-GL-3 levels (58.83 ng/ml). The aunt was asymptomatic, and she had a slight decrease in $\alpha$-Gal A levels (0.58 μmol/L·h) and a slight increase in Lyso-GL-3 levels (8.86 ng/ml).

The patient in Case 6 was diagnosed by screening for FD and presented with hypohidrosis, cutaneous angioglioma, and acroparesthesia at the age of 3 years. Her grandmother had foot pain when she was young, which disappeared after marriage. This family was not screened by experts due to personal factors.

The patient in Case 7 was a girl whose father was diagnosed with FD due to chronic kidney disease, hypertrophic cardiomyopathy, and paroxysmal acroparesthesia. The patient presented with acroparesthesia and was diagnosed with a GLA mutation by screening.

## Treatment

Of the 7 symptomatic patients, two children refused treatment in our hospital for personal reasons and five children were treated with ERT, including 4 with agalsidase beta and 1 with agalsidase alpha. Case 1 was treated with agalsidase beta once every 2 weeks after diagnosis. To date, 35 infusions of agalsidase beta have been used, and no adverse reactions, such as rash, angioedema or blood pressure reduction, have occurred. The patient had a transient exacerbation of acroparesthesia after the fourth infusion of agalsidase beta, which was relieved by oral administration of oxcarbazepine. Up to the follow-up time, the child had been treated with ERT for 1.5 years. During this period, the duration of pain episodes was shorter, and the interval between episodes was longer than it was previously. The child's anhidrosis symptoms were improved, and he reported a sense of dampness in the neck skin. There were no significant changes in cutaneous angiokeratoma or hearing loss. The corneal vortex opacity disappeared after ophthalmic review. The level of Lyso-GL-3 decreased significantly in the first 3 months of ERT initiation and remained between 14.11 and 20.51 ng/ml thereafter.

In Case 2 and Case 3, agalsidase beta therapy was initiated at the time of diagnosis, and in both cases, it had been applied 22 times. Case 2 exhibited anaphylaxis when he was given the third infusion of agalsidase beta. This patient presented with a facial itchy rash, urticaria and hypotension (87/56 mmHg). The symptoms disappeared after adopting dexamethasone and loratadine treatment. Anaphylaxis did not occur when the patient received the following repeated ERT. During the follow-up 12 months after the initiation of ERT, there was no significant relief of acroparesthesia, hypohidrosis, or angiokeratoma in these two patients who were treated with intermittent oral carbamazepine. Case 2 had transient mild proteinuria at the time of diagnosis. However, mild proteinuria (uMALB, U$\beta$2-ml, U$\alpha$1-M1, uNAG) reoccurred after 12 months, and benazepril and Beling capsules were added for treatment. In Case 3, transient mild proteinuria (urinary protein±, microalbumin 30.27 mg/L) occurred at 6 months after the initiation of ERT. After the addition of benazepril and Beling capsules, the urinary protein and microalbumin levels returned to normal. The levels of Lyso-GL-3 in Cases 2 and 3 also decreased significantly after 3 months of ERT and remained relatively stable thereafter.

Case 4 was treated with agalsidase alpha once every 2 weeks. To date, 7 courses of ERT have been used without adverse drug reactions. This patient had decreased renal function accompanied by proteinuria and was treated with drugs such as ACEI, coenzyme Q10 and polysaccharide iron complex. After 2 courses of treatment, the degree of acroparesthesia was significantly reduced, and abdominal pain did not occur again. However, his serum creatinine level continued to rise to 134 μmol/L, and the serum Lyso-GL-3 level decreased to 11.55 ng/ml.

Case 5 recently started agalsidase beta treatment. To date, 2 courses of ERT have been given, and no adverse reactions have occurred. Antirheumatic drugs and biological agents, oral oxcarbazepine, probiotics and other treatments were stopped. The specific efficacy needs to be further evaluated.

# Discussion

FD can be divided into classic and late-onset types, according to clinical manifestations. Classic FD presents with decreased or absent $\alpha$-Gal A activity and multisystem involvement (brain, kidney, heart, etc.), and the onset of classic FD mostly occurs during childhood (males: 6–10 years old, females: 9–15 years old). Late-onset FD is characterized by a partial decrease in enzymatic activity, and the onset of this type mainly occurs in adulthood. Additionally, the damage is confined to the kidney or heart. Childhood FD is often characterized by acral nerve burning pain, little or no sweat, cutaneous angiokeratoma, proteinuria or microalbuminuria, corneal vorticity, etc (5, 6). Tinnitus, chronic fatigue, and difficulty gaining weight can also occur. Early signs of cardiac involvement (e.g., shortened PR interval, arrhythmias, impaired heart rate variability, valvular sinus aortic dilatation, and mild valvular stenosis) (7) and cerebrovascular abnormalities (involvement of small cerebral vessels) (8) can also occur during adolescence. Although not accompanied by major organ dysfunction, this involvement can lead to physical discomfort and poor school and social

TABLE 2 Laboratory examination and MSSI scores of 5 children with Fabry disease.

| Case | Blood urea nitrogen (mmol/l) | Serum creatinine (umol/l) | Glomerular filtration rate (ml/min.1.73 $m^2$) | Urine protein | Urine microalbumin | Urine red blood cells (cells/HP) | Urine protein creatinine ratio (mg/mg) | 24-hour urine protein quantification (g) | Left ventricular mass index (g/m2.7) | Pulmonary function | Abdominal ultrasound | Brain MR | MSSI score |
|---|---|---|---|---|---|---|---|---|---|---|---|---|---|
| 1 | 3.1 | 25.1 | 210.86 | Negative | Normal | Normal | 0.11 | 0.09 | 29.3 | Mild obstructive ventilation dysfunction | Small effusion in the lower abdominal intestinal space | Normal | 11 |
| 2 | 3.8 | 36.3 | 156.86 | Negative | Normal | Normal | 0.16 | 0.17 | 31 | Mild obstructive ventilation dysfunction | Normal | Normal | 10 |
| 3 | 4.2 | 31.5 | 168.02 | Negative | Normal | Normal | 0.1 | 0.06 | 38.4 | Mild obstructive ventilation dysfunction | Normal | Normal | 9 |
| 4 | 8.2 | 103 | 55.28 | ±~1+(mixed proteinuria, mainly tubular) | Increased | Normal | 0.51 | 0.31 | 23.9 | Normal | Mild fatty liver, small right kidney and dysplasia of the right renal artery | Normal | 21 |
| 5 | 3.9 | 44.2 | 125.52 | Negative | Normal | Normal | 0.07 | 0.05 | 22.4 | Normal | Normal | Partially empty butterfly saddle | 13 |





10.3389/fped.2023.1084336

TABLE 3 FD-specific indexes and GLA gene in children with Fabry disease.

| Cases | Sex | Blood α-Gal A (2.40–17.65 umol/L·h) | Lyso-GL-3 (<1.11 ng/mL) | Exon | GLA gene mutation site | Change in protein sequence | Type of variation | Source of variation |
|---|---|---|---|---|---|---|---|---|
| 1 | Male | 0.41 | 92.98 | 7 | c.140G > A | p.W47X | Nonsense mutation | Mother |
| 2 | Male | 0.31 | 96.4 | 7 | c.1080_1082delTGG | p.Gly361del | Deletion mutation | Mother |
| 3 | Male | 0.31 | 89.9 | 7 | c.1080_1082delTGG | p.Gly361del | Deletion mutation | Mother |
| 4 | Male | 0.4 | 42.58 | 5 | C.671A > G | p.Asn224Ser | Missense mutation | Mother |
| 5 | Male | 0.29 | 88.47 | 7 | c.1059_1061delGAT | p.Met353del | In-frame deletion mutations | Mother |
| 6 | Male | 1.14 | 69.54 | 1 | c.124A > G | p.Met42Val | Missense mutation | Mother |
| 7 | Female | 2.03 | 8.35 | 1 | c.95T > C | p.Leu32Pro | Missense mutation | Father |
| 8 | Male | 0.32 | 88.73 | 7 | c.1080_1082delTGG | p.Gly361del | Deletion mutation | Mother |
| 9 | Female | 2.39 | 6.18 | 7 | c.1080_1082delTGG | p.Gly361del | Deletion mutation | Mother |
| 10 | Female | 2.61 | 1.53 | 5 | C.671A > G | p.Asn224Ser | Missense mutation | Mother |

performance in children (9). In this study, 7 symptomatic children were diagnosed as classic FD and presented with acral neuralgia. Among these 7 patients, 5 presented with little or no sweat, 5 presented with cutaneous angiokeratoma, 2 presented with abdominal pain, 1 presented with arthralgia, 4 presented with corneal opacity, and 1 presented with hearing loss. Renal involvement occurred in 2 cases. Of these cases, 1 case presented with mild proteinuria, and 1 case presented with right kidney and right renal artery dysplasia, mild proteinuria (mainly tubular proteinuria) and decreased eGFR (55.28 ml/min.1.73 $m^2$), which was diagnosed as chronic kidney disease stage 3b. The left ventricular mass index was slightly elevated in 1 case. Three cases had mild obstructive ventilatory dysfunction; a small amount of effusion in the intestinal space of the lower abdomen or mild fatty liver was found in 2 cases by abdominal ultrasound. Magnetic resonance imaging showed partial empty sella turcica in 1 patient. The Mainz Severity Score Index (MSSI) was used to score 5 children with scores ranging from 9 to 21.

Because the clinical manifestations of FD are diverse and nonspecific, most children cannot be diagnosed early after birth or diagnosed immediately after the onset of symptoms. On average, patients with FD see an average of 10 specialists before they are properly diagnosed, and they are often not diagnosed until adulthood. The mean age at diagnosis is 29 years old (10, 11). Reisin R et al. studied 586 FD patients from Europe and other parts of the world and found that the age of diagnosis in children with FD from 2001 to 2006 and from 2007 to 2013 was 7.0 (5.0 to 11.0) years old and 9.0 (6.0 to 11.0) years old, respectively (12). In this study, all 7 symptomatic children had visited other hospitals numerous times. However, due to the atypical clinical symptoms and the lack of understanding of this disease by clinicians, the average age of diagnosis was 11.7 years old (10.0–13.0 years old), and the average delay in diagnosis was 5.57 years (2.0–9.0 years). These findings are close to those of previous reports. Lu ZH et al. reported that two boys with FD were diagnosed at 13.9 years old and 10.9 years old, and the delay of diagnosis was 3 years and 6 years, respectively (13). Zhu XM et al. reported that two boys in two families with FD presented with acroparesthesia at 10 and 14 years old, and the diagnosis was delayed by 6 and 1 years, respectively (14). Therefore, it is very important to improve clinicians' understanding of FD in children for early identification and correct diagnosis of the disease.

Peripheral neuralgia is an early onset, common and suggestive clinical symptom of FD. The main manifestation is acral paroxysmal burning pain, which lasts for several minutes to several weeks. It is often induced by exercise, increased temperature and other factors and is often accompanied by fever and less sweating. Some patients may present with cold or heat hyposensation. FD patients have a marked reduction in myelinated A$\delta$ fibers (which regulate sharp pain and sense cold), nonmyelinated class C fibers (pain, warm sensation), and nonmyelinated autonomic fibers. The cause of temperature paresthesia is related to small nerve C fibers, which are particularly associated with A$\delta$ fiber dysfunction (15). Neuralgia in FD can also present as arthralgia. However, due to the heterogeneity of clinical manifestations and insufficient understanding of clinicians, this disease is easily misdiagnosed as growth pains, arthritis, rheumatic fever, dermatomyositis and other diseases. In this study, Case 5 presented with foot pain and arthralgia involving the bilateral finger joints and knee joints since 4 years of age. However, he was misdiagnosed with a cold, growing pains, and juvenile idiopathic arthritis and treated with calcium tablets, nonsteroidal anti-inflammatory drugs, anti-rheumatism medicine, a variety of biological agents, and glucocorticoid treatment without obvious improvement. FD was diagnosed in our center because the patient presented with cutaneous angiokeratoma, acral burning pain, and hypohidrosis, with positive results for enzyme activity, substrates and genes of FD. The deletion variant C.1059_1061delGAT (p.mET353del) in the GLA gene found in this patient's family is a new mutation that has not been reported in the literature. This variant is an in-frame deletion mutation that may result in the deletion of the encoded amino acid methionine (Met) at position 353 and was rated as potentially pathogenic according to the ACMG guidelines. Although the incidence is very low, joint pain needs to be considered a special

type of neuralgia in FD by clinicians to avoid misdiagnosis and missed diagnosis to the greatest extent.

As the kidney is the main deposition site and one of the main target organs of GL-3 and the progression to end-stage renal disease (ESRD) is the main cause of death in patients with FD, renal damage has attracted much attention as an important clinical manifestation of FD. GL-3 deposition occurs in almost all cell types of the kidney, including vascular endothelial cells, vascular smooth muscle cells, mesangial cells, mesenchymal cells, podocytes, and distal tubular epithelial cells, and GL-3 deposition begins as early as fetal development (16). Microalbuminuria and increased albuminuria are the first signs of renal impairment, as these conditions occur before the age of 10 years. In typical patients, the glomerular filtration rate (GFR) decreases beginning in puberty (17). With the progression of chronic kidney disease (CKD), albuminuria and massive albuminuria will occur in patients at 20 years of age. Additionally, the severity of renal pathology will increase, and chronic renal impairment will gradually occur and finally develop into ESRD from 30 to 50 years old (18). In this study, 2 cases had renal involvement. Case 2 showed mild proteinuria. Case 4 had dysplasia of the right kidney and right renal artery, mild proteinuria (mainly tubular proteinuria), and decreased eGFR (55.28 ml/min.1.73 $m^2$) and was diagnosed with chronic kidney disease stage 3b. The maternal grandmother, mother, aunt and sister of Case 4 harbored the the heterozygous GLA missense mutation C.671A > G (p.Asn224Ser) but were asymptomatic. This locus has been previously reported (19) in a 44-year-old female patient with FD who presented with hypertrophic cardiomyopathy, shortened PR interval, and unexplained syncope. However, her renal function was normal, which was different from the phenotype of this patient. Discordant clinical phenotypes of the same genotype may be associated with the compensatory effects of some related genes, environmental factors, and other factors affecting lysosomal function, which are involved in the occurrence of disease phenotypes (20). Clinicians should carefully consider genetic counseling and prognosis judgment according to family history and genetic testing results, especially in young patients.

FD is an X-linked inherited lysosomal disease; therefore, sex differences have been a concern. The enzyme activity was lower in male patients, mainly in those with the classic type, but the enzyme activity was relatively preserved in female patients, mainly in those with the late type. In this study, we found 13 children and family members with acroneuralgia, including 6 boys, 2 adult males, 1 girl, and 4 adult females. The onset age of pain in boys was between 3 and 9 years old. Most of the female patients were asymptomatic, and a minority of women had acroparesthesia, which began in adolescence and gradually eased with increasing age. Correspondingly, boys and adult males showed significantly reduced enzyme activity and significantly increased substrate levels. Girls and female adults with GLA heterozygous mutations showed normal or slightly decreased enzyme activity and slightly increased substrate levels. Miao YF reported neuralgia in patients with an average starting age of 9 years of age, with an average alleviation at age 20, and a remission rate of 22.8%. Male patients showed more intense pain, and the condition had a greater influence on life in males than in females (21). Male patients with FD tend to progress to ESRD and need dialysis between the ages of 40 to 50 years. However, female heterozygous patients have less renal insufficiency, and the severity is lower than that of male FD. Only a few cases of ESRD in heterozygous women have been reported (22). The severity of disease in female patients varies from asymptomatic to severely involved phenotypes. The occurrence of these conditions is related to the random inactivation of the X chromosome and the severity of pathogenic variants. Echevaria found that an X-chromosome inactivation bias occurred in 29% of 56 female patients with FD, and significant differences in residual enzyme activity, disease severity score, progression in cardiomyopathy, and renal function were associated with different X-chromosome inactivation modes. Therefore, the pattern of X-chromosome inactivation was suggested to significantly affect the phenotype of female patients with FD (23). In addition to these factors, a recent Turkish study showed that coexisting factors might significantly influence the phenotypes of women and men with FD. These factors include elevated levels of lipoprotein (A), homocysteine, total and low-density cholesterol, and antithrombin 3, the prothrombin p.G20210a and factor V Leiden pathogenic variants, and diseases (such as rheumatism or celiac disease) (24). These coexisting factors should be considered in the assessment of patients with FD.

FD usually develops in adolescence and worsens with the progression of the disease. It causes great suffering to patients and their families and imposes a heavy burden on society. As a rare disease, the screening of a high-risk population and family screening can aid in the diagnosis of patients with FD and could result in earlier treatments. If children present with fever accompanied by burning pain of hands and feet, whirlpool cloudy eyes, cutaneous angiokeratoma, and/or the involvement of heart, brain or kidney, and/or a positive family history of disease, they should be screened for enzyme activity and should undergo metabolic substrate screening and genetic screening for FD. Pedigree screening for confirmed patients with FD can help identify potential patients who should receive ERT and other treatments early and improve the prognosis of these patients. According to previous reports, proband-based family screening may detect 3–5 new patients on average. At present, the dry blood disk method (DBS) is often used to screen for FD. Additionally, the activity of $\alpha$-Gal A and Lyso-GL-3 levels in blood can be detected, and GLA gene analysis can be performed simultaneously. In this study, one asymptomatic boy of 4 years of age was identified by pedigree screening, and the remaining 6 cases were identified by the DBS method and/or genetic testing. All 3 girls were identified by pedigree screening. Therefore, it is necessary to improve the understanding of FD and actively carry out high-risk population screening and family screening for the early detection, early diagnosis and treatment of childhood FD.

Enzyme replacement therapy (ERT) has been used in clinical practice since 2001. ERT should be considered for symptomatic boys and girls with neuropathic pain, pathological albuminuria, severe GI involvement and abdominal pain or cardiac involvement. ERT also should be considered for asymptomatic boys with classical (severe) mutations. Timing of ERT depends on individual case for asymptomatic female patients and asymptomatic male patients with late-onset mutations. Organ involvement should be treated as

needed (2, 4). Many clinical studies have demonstrated that ERT has positive effects on school attendance, exercise performance, energy level and pain and significantly improves the quality of life of children. The improvement of neuropathic pain with early ERT treatment is more significant and can be maintained in the long term (25). Borgwardt L reported that 10 children between 9 and 16 years of age with FD were treated with agalsidase beta for 1–8 years. During the follow-up period, the symptoms of most patients, such as headache, limb pain and gastrointestinal involvement, were improved (26). However, Mehta A reported (27) that 64 boys and 34 girls with FD were treated with agalsidase alpha for 12 and 24 months. Their renal function and left ventricular mass index remained stable, but there was no significant reduction in the incidence of gastrointestinal symptoms, neuropathic pain, or pain crisis. This study also reported 58 treatment-related adverse events in 23 patients, of which 55 were infusion reactions. In our study, 5 patients were treated with ERT. Of these, 4 patients were treated with agalsidase beta, and 1 was treated with agalsidase alpha. The longest duration of application was 1.5 years, and the shortest duration was 4 weeks. Anaphylaxis occurred in only one case. It presented as a urticaria and hypotension, which quickly subsided after anti-anaphylaxis treatment. Mild proteinuria occurred in case 2 and case 3 at 12 months and 6 months after the initiation of agarsylase $\beta$ respectively. Case 3 received oral benazepril and Beling capsules treatment and proteinuria returned to normal later. Lu ZH et al. reported that one child also experienced transient aggravation of proteinuria after 3 course treated with agarsylase $\beta$ (13). Therefore the changes of proteinuria might be one of the adverse reactions of agarsylase $\beta$, but the mechanism needs further study. After ERT treatment, acroparesthesia was relieved in 2 children, hypohidrosis was slightly improved in 1 child. Lyso-GL-3 levels decreased significantly in the first 3 months of ERT initiation and remained relatively stable thereafter. This is consistent with previous literature reports (28). However, one child received agalsidase alpha treatment. Although the level of Lyso-GL-3 in blood decreased, the renal function damage continued to progress. Thus, its efficacy needs to be further investigated. Arends M reported a study that enrolled 387 patients. Of these patients, 248 were treated with agalsidase alpha, and 139 were treated with agalsidase beta. After initiation of ERT, plasma Lyso-GL-3 concentrations decreased rapidly and subsequently stabilized in all subgroups. After adjusting for baseline Lyso-GL-3 concentration, sex, and phenotype, the decrease in Lyso-GL-3 levels in patients with classic FD was more pronounced than that in patients treated with $\beta$-galactosidase (29). However, due to the short duration of ERT treatment in our study, longer follow-up and observation are needed to compare the efficacy and safety of agalsidase $\alpha$ and $\beta$.

In conclusion, FD is a rare X-linked inherited lysosomal storage disease that is prone to misdiagnosis due to its insidious onset and diverse clinical manifestations. For patients with clinical symptoms such as acroparesthesia, little or no sweat, skin angiokeratoma, and corneal opacity, this disease should be highly considered, and the diagnosis should be made based on family history, enzyme activity, biomarkers, gene testing and other indicators. Clinicians should enhance their knowledge and understanding of FD and actively carry out family screening and high-risk population screening, which are helpful for the early identification, early diagnosis and early treatment. No serious adverse reactions were found during the short-term treatment with agalsidase alpha and beta. The comparison of efficacy and safety of agalsidase alpha and beta requires longer periods of follow-up and observation.

## Data availability statement

The original contributions presented in the study are included in the article/Supplementary material, further inquiries can be directed to the corresponding author.

## Ethics statement

The studies involving human participants were reviewed and approved by Biomedical Research Ethic Committee of Shandong Provincial Hospital. Written informed consent to participate in this study was provided by the participants' legal guardian/next of kin.

## Author contributions

QL and JW conceptualized and designed the study, drafted the initial manuscript, and reviewed and revised the manuscript. MT, ZY, LY designed the data collection instruments, collected data and carried out the initial analyses. SL, CW and XW reviewed and revised the manuscript. SS coordinated and supervised data collection, and critically reviewed the manuscript for important intellectual content. All authors approved the final manuscript as submitted and agree to be accountable for all aspects of the work. All authors contributed to the article and approved the submitted version.

## Funding

This work was supported by the Youth Foundation Project of National Natural Foundation in China (82100771) and the Youth Foundation Project of Shandong Provincial Natural Foundation (ZR202102230580, ZR202102220321).

## Conflict of interest

The authors declare that the research was conducted in the absence of any commercial or financial relationships that could be construed as a potential conflict of interest.

## Publisher's note

# References

1. Michaud M, Mauhin W, Belmatoug N, Garnotel R, Bedreddine N, Catros F, et al. When and how to diagnose fabry disease in clinical pratice. *Am J Med Sci*. (2020) 360 (6):641–9. doi: 10.1016/j.amjms.2020.07.011

2. Chinese Fabry Disease Expert Panel. Expert consensus for diagnosis and treatment of fabry disease in China (2021). *Chin J Intern Med*. (2021) 60(4):321–30. doi: 10.3760/cma.j.cn112138-20201218-01028

3. Turkmen K, Baloglu I. Fabry disease: where are we now? *Int Urol Nephrol*. (2020) 52 (11):2113–22. doi: 10.1007/s11255-020-02546-3

4. Germain DP, Fouilhoux A, Decramer S, Tardieu M, Pillet P, Fila M, et al. Consensus recommendations for diagnosis, management and treatment of fabry disease in paediatric patients. *Clin Genet*. (2019) 96(2):107–17. doi: 10.1111/cge.13546

5. Ortiz A, Germain DP, Desnick RJ, Politei J, Mauer M, Burlina A, et al. Fabry disease revisited: management and treatment recommendations for adult patients. *Mol Genet Metab*. (2018) 123:416–27. doi: 10.1016/j.ymgme.2018.02.014

6. Miller JJ, Kanack AJ, Dahms NM. Progress in the understanding and treatment of fabry disease. *Biochim Biophys Acta Gen Subj*. (2020) 1864:129437. doi: 10.1016/j.bbagen.2019.129437

7. Kampmann C, Wiethof CM, Whybra C, Baehner FA, Mengel E, Beck M. Cardiac manifestations of anderson–fabry disease in children and adolescents. *Acta Paediatr*. (2008) 97:463–9. doi: 10.1111/j.1651-2227.2008.00700.x

8. Cabrera-Salazar MA, O'Rourke E, Charria-Ortiz G, Barranger JA. Radiological evidence of early cerebral microvascular disease in young children with fabry disease. *J Pediatr*. (2005) 147:102–5. doi: 10.1016/j.jpeds.2005.03.004

9. Ries M, Gupta S, Moore DF, Sachdev V, Quirk JM, Murray GJ, et al. Pediatric fabry disease. *Pediatrics*. (2005) 115:e344–55. doi: 10.1542/peds.2004-1678

10. Curiati MA, Aranda CS, Kyosen SO, Varela P. The challenge of diagnosis and indication for treatment in fabry disease. *J Inborn Errors Metab Screen*. (2017) 5:1–7. doi: 10.1177/2326409816685735

11. Martins AM, D'Almeida V, Kyosen SO, Takata ET, Delgado AG, Gonçalves AM, et al. Guidelines to diagnosis and monitoring of fabry disease and review of treatment experiences. *J Pediatr*. (2009) 155(4 Suppl):S19–31. doi: 10.1016/j.jpeds.2009.07.003

12. Reisin R, Perrin A, Garcia-Pavia P. Time delays in the diagnosis and treatment of fabry disease. *Int J Clin Pract*. (2017) 71(1):e12914. doi: 10.1111/ijcp.12914

13. Lu ZH, Wang JJ, Yu L, Mao JH. Clinical features and enzyme replacement therapy in 4 children with fabry disease. *Chin J Pediatr*. (2021) 59(04):322–6. doi: 10.3760/cma.j.cn112140-20200902-00842

14. Zhu XM, Cheng SC, Gong YH, Lu S, Zhao HL. Clinical features and genetic analysis of two cases with anderson- fabry syndrome. *J Clin Pediatr*. (2019) 37 (5):385–7. doi: 10.3969/j.issn.1000-3606.2019.05.015

15. Franques J, Sahuc P, Dussol B, Penaranda G, Swiader L, Froissart R, et al. Peripheral nerve involvement in Fabry's disease: Which investigations? A case series and review of the literature. *Rev Neurol (Paris)*. (2017) 173(10):650–7. doi: 10.1016/j.neurol.2017.05.007

16. Hsu TR, Niu DM. Fabry disease: review and experience during newborn screening. *Trends Cardiovasc Med*. (2018) 28:274–81. doi: 10.1016/j.tcm.2017.10.001

17. Ramaswami U, Najafan B, Schieppati A, Mauer M, Bichet DG. Assessment of renal pathology and dysfunction in children with fabry disease. *Clin J Am Soc Nephrol*. (2010) 5:365–70. doi: 10.2215/CJN.08091109

18. Ezgu F, Alpsoy E, Bicik Bahcebasi Z, Kasapcopur O, Palamar M, Onay H, et al. Expert opinion on the recognition, diagnosis and management of children and adults with fabry disease: a multidisciplinary Turkey perspective. *Orphanet J Rare Dis*. (2022) 17(1):90. doi: 10.1186/s13023-022-02215-x

19. Seo J, Kim M, Hong GR, Kim DS, Son JW, Cho IJ, et al. Fabry disease in patients with hypertrophic cardiomyopathy: a practical approach to diagnosis. *J Hum Genet*. (2016) 61(9):775–80. doi: 10.1038/jhg.2016.52

20. Rigoldi M, Concolino D, Morrone A, Pieruzzi F, Ravaglia R, Furlan F, et al. Intrafamilial phenotypic variability in four families with anderson-fabry disease. *Clin Genet*. (2014) 86(3):258–63. doi: 10.1111/cge.12261

21. Miao YF, Zhao YW, Liu J, Li F, Wang ZX, Yuan Y, et al. Characteristics of neuralgia in patients with fabry disease in China. *Chin J Neuro*. (2022) 55(01):15–20. doi: 10.3760/cma.j.cn113694-20210430-00311

22. MacDermot J, MacDermot KD. Neuropathic pain in AndersonFabry disease: pathology and therapeutic options. *Eur J Pharmacol*. (2001) 429:121–5. doi: 10.1016/S0014-2999(01)01312-7

23. Echevarria L, Benistan K, Toussaint A, Dubourg O, Hagege AA, Eladari D, et al. X-chromosome inactivation in female patients with fabry disease. *Clin Genet*. (2016) 89 (1):44–54. doi: 10.1111/cge.12613

24. Koca S, Tumer L, Okur I, Erten Y, Bakkaloglu S, Biberoglu G, et al. High incidence of co-existing factors signifcantly modifying the phenotype in patients with fabry disease. *Gene*. (2019) 687:280–8. doi: 10.1016/j.gene.2018.11.054

25. Hopkin RJ, Jefferies JL, Laney DA, Lawson VH, Mauer M, Taylor MR, et al. The management and treatment of children with fabry disease: a United States-based perspective. *Mol Genet Metab*. (2016) 117(2):104–13. doi: 10.1016/j.ymgme.2015.10.007

26. Borgwardt L, Feldt-Rasmussen U, Rasmussen AK, Ballegaard M, Meldgaard Lund A. Fabry disease in children: agalsidase-beta enzyme replacement therapy. *Clin Genet*. (2013) 83(5):432–8. doi: 10.1111/j.1399-0004.2012.01947.x

27. Mehta A, Ricci R, Widmer U, Dehout F, Garcia de Lorenzo A, Kampmann C, et al. Fabry disease defined: baseline clinical manifestations of 366 patients in the fabry outcome survey. *Eur J Clin Invest*. (2004) 34(3):236–42. doi: 10.1111/j.1365-2362.2004.01309.x

28. van Breemen MJ, Rombach SM, Dekker N, Poorthuis BJ, Linthorst GE, Zwinderman AH, et al. Reduction of elevated plasma globotriaosylsphingosine in patients with classic fabry disease following enzyme replacement therapy. *Biochim Biophys Acta*. (2011) 1812(1):70–6. doi: 10.1016/j.bbadis.2010.09.007

29. Arends M, Biegstraaten M, Wanner C, Sirrs S, Mehta A, Elliott PM, et al. Agalsidase alfa versus agalsidase beta for the treatment of fabry disease: an international cohort study. *J Med Genet*. (2018) 55(5):351–8. doi: 10.1136/jmedgenet-2017-104863

frontiers | Frontiers in Genetics

TYPE Case Report
PUBLISHED 17 February 2023
DOI 10.3389/fgene.2023.1066199



OPEN ACCESS

EDITED BY
Xiu-An Yang,
Chengde Medical College, China

REVIEWED BY
Rincic Martina,
University of Zagreb, Croatia
Liang Hu,
Central South University, China
Yihong Guo,
First Affiliated Hospital of Zhengzhou University, China

*CORRESPONDENCE
Yinghui Ye,
yeyh1999@zju.edu.cn

SPECIALTY SECTION
This article was submitted to Genetics of Common and Rare Diseases, a section of the journal Frontiers in Genetics

RECEIVED 10 October 2022
ACCEPTED 06 February 2023
PUBLISHED 17 February 2023

CITATION
Shi B and Ye Y (2023), Case report: A reciprocal translocation-free and pathogenic *DUOX2* mutation-free embryo selected by complicated preimplantation genetic testing resulted in a healthy live birth.
*Front. Genet.* 14:1066199.
doi: 10.3389/fgene.2023.1066199



# Case report: A reciprocal translocation-free and pathogenic *DUOX2* mutation-free embryo selected by complicated preimplantation genetic testing resulted in a healthy live birth

Biwei Shi and Yinghui Ye*

Department of Reproductive Endocrinology, Women's Hospital, Zhejiang University School of Medicine, Hangzhou, China

Preimplantation genetic testing (PGT) is an effective approach to improve clinical outcomes and prevent transmission of genetic imbalances by selecting embryos free of disease-causing genes and chromosome abnormalities. In this study, PGT was performed for a challenging case in which a couple simultaneously carried a maternal subchromosomal reciprocal translocation (RecT) revealed by fluorescence *in situ* hybridization involving the chromosome X (ChrX) and heterozygous mutations in dual oxidase 2 (*DUOX2*). Carriers of RecT are at increased risk for infertility, recurrent miscarriages, or having affected children due to the unbalanced gametes produced. *DUOX2* mutation results in congenital hypothyroidism. Pedigree haplotypes for *DUOX2* was constructed after the mutations were verified by Sanger sequencing. Since male carriers of X-autosome translocations may exhibit infertility or other abnormalities, pedigree haplotype for chromosomal translocation was also constructed to identify embryo with RecT. Three blastocysts were obtained by *in vitro* fertilization and underwent trophectoderm biopsy, whole genomic amplification, and next-generation sequencing (NGS). A blastocyst lacking copy number variants and RecT but carrying the paternal gene mutation in *DUOX2*, c.2654G>T (p.R885L) was used for embryo transfer, resulting in a healthy female infant whose genetic properties were confirmed by amniocentesis. Cases containing RecT and single gene disorder are rare. And the situation is more complicated when the subchromosomal RecT involving ChrX cannot be identified with routine karyotype analysis. This case report contributes significantly to the literature and the results have shown that the NGS-based PGT strategy may be broadly useful for complex pedigrees.

KEYWORDS

**reciprocal translocation, next-generation sequencing, preimplantation genetic testing, SNP-based linkage analysis, live birth, *DUOX2***

# Introduction

Hydrogen peroxide ($H_2O_2$) oxidizes iodide by thyroid peroxidase during thyroid hormonogenesis (De Deken and Miot, 2019). Genetic alterations in the $H_2O_2$-generating system have been implicated in the pathogenesis of congenital hypothyroidism (CH), one of the most frequent congenital endocrine disorders in childhood (Weber et al., 2013). Dual oxidase 2 (DUOX2) is one of the main enzymes in the $H_2O_2$-generating system. DUOX2 defects are one of the leading causes of dyshormonogenesis (Muzza and Fugazzola, 2017). Human *DUOX2* is located on chromosome 15 (15q15.3) and spans 21.5 kb containing 34 exons, of which 33 are coding exons and encode a protein with 1548 amino acid residues (De Deken and Miot, 2019). Mutations in *DUOX2* have highly variable phenotypic effects, ranging from transient to permanent forms of CH (Weber et al., 2013). Reciprocal translocation (RecT) is a category of chromosomal abnormality in which reciprocal exchange occurs between partial arms of any two chromosomes. It is the most common chromosomal rearrangement affecting humans, with an estimated incidence of 0.16%–0.20% of live births (Morin et al., 2017). Most cases with RecT exhibit a normal phenotype, as key genes are not lost (Zhang et al., 2016). However, due to high rates of unbalanced gametes, patients have high risks of infertility as well as chromosomal abnormalities in pregnancy, leading to recurrent spontaneous abortion or affected offspring (Scriven et al., 1998; Fiorentino et al., 2011).

Preimplantation genetic testing (PGT), a branch of *in vitro* fertilization technology, includes testing for monogenic disorders (PGT-M), structural rearrangements (PGT-SR), and aneuploidy (PGT-A) (Zegers-Hochschild et al., 2017). In the present study, we studied the pedigree of a family in which the proband harbored compound heterozygous mutations in *DUOX2* and chromosomal aneuploidies in partial chromosomes X and 18. To simultaneously address the monogenetic disorders and chromosomal abnormalities in the family, a PGT strategy based on whole-genome amplification (WGA), next-generation sequencing (NGS), and a single-nucleotide polymorphism (SNP)-based linkage analysis was applied to select embryos free of pathogenic *DUOX2* mutations, screen chromosomal aneuploidies, and distinguish between translocation carrier embryos and normal embryos. A healthy baby was born at term.

# Material and methods

## Case description

The proband was a male child hospitalized for cleft palate and neonatal septicemia. Clinical examination identified multiple problems: a large heart, CH, developmental delay, extensive neurogenic damage involving the limbs, hearing impairment, and photophobia. Initially, thyroid-stimulating hormone (TSH) levels of the proband was 48.83 mIU/L (27 December 2016). After thyroxine treatment, his TSH levels decreased to 2.22 mIU/L (11 April 2017) (Supplementary Figure S1). But the proband still presents intellectual disabilities, hearing impairment, etc. The proband was the first pregnancy of unrelated healthy parents.

Karyotype analysis of the proband and his parents revealed normal results (Supplementary Figure S2). Whole exome sequencing (WES) and copy number variants (CNV) sequencing were performed simultaneously for the family. The average coverage of WES was more than 99%. WES results revealed that mother (29 years) of the proband was a carrier of a heterozygous mutation in *DUOX2*, c.1588A>T (p.K530X), his father (30 years) carried a heterozygous mutation in *DUOX2*, c.2654G>T (p.R885L), and the proband harbored both heterozygous mutations in *DUOX2*, which is associated with CH. *DUOX2*, c.1588A>T (p.K530X) was classified as pathogenic (PVS + PM + PP), and *DUOX2*, c.2654G>T (p.R885L) was classified as likely pathogenic (2PM+2PP) in accordance with the ACMG guidelines. The gene variant pedigree of the family was constructed (Supplementary Figure S3). The results of CNV sequencing (0.6× sequencing depth) revealed that the proband exhibited an Xq28-q28 duplication (5.59 Mb × 2) and 18q22.2-q23 deletion (9.85 Mb × 1) and the CNVs of the parents were normal (Supplementary Figure S4). According to CNV results, fluorescence *in situ* hybridization (FISH) was performed for the parents and the results showed that the mother was a carrier of a RecT between ChrX and Chr18 [t (X; 18) (q28; q22.2)] (Supplementary Figure S5). With the help of PGT technology, the couple hoped to give birth to a healthy baby (babies) free of pathogenic *DUOX2* mutations and RecT.

## Pedigree haplotype construction for *DUOX2* and chromosomal translocation

Genomic DNAs from the proband and his parents were extracted from blood samples. NGS was performed on the Illumina NextSeq 550 platform (San Diego, CA, United States). The *DUOX2* mutations in the family were verified by Sanger sequencing. Haplotype information for alleles in linkage with wild-type/mutant and translocation/no translocation alleles was established based on informative SNPs.

## Stimulation protocol

The cycles were subjected to controlled ovarian hyperstimulation protocols. Ovarian stimulation was performed using a GnRH antagonist protocol. Transvaginal sonography and serial E2 levels were used to monitor ovarian follicular development. Once a dominant follicle reached 19–20 mm, 10,000 IU of human chorionic gonadotropin (hCG) was administered. Thirty-6 hours later, transvaginal ultrasound-guided oocyte retrieval was performed (Ye et al., 2021).

## Embryo biopsy, cryopreservation, and thawing

Embryo biopsies were performed after intracytoplasmic sperm injection (ICSI) and embryo culture. According to the Gardner scoring system (Gardner et al., 2000), trophectoderm (TE) cell biopsy of high-grade blastocysts (greater than 4CB or 4BC) was

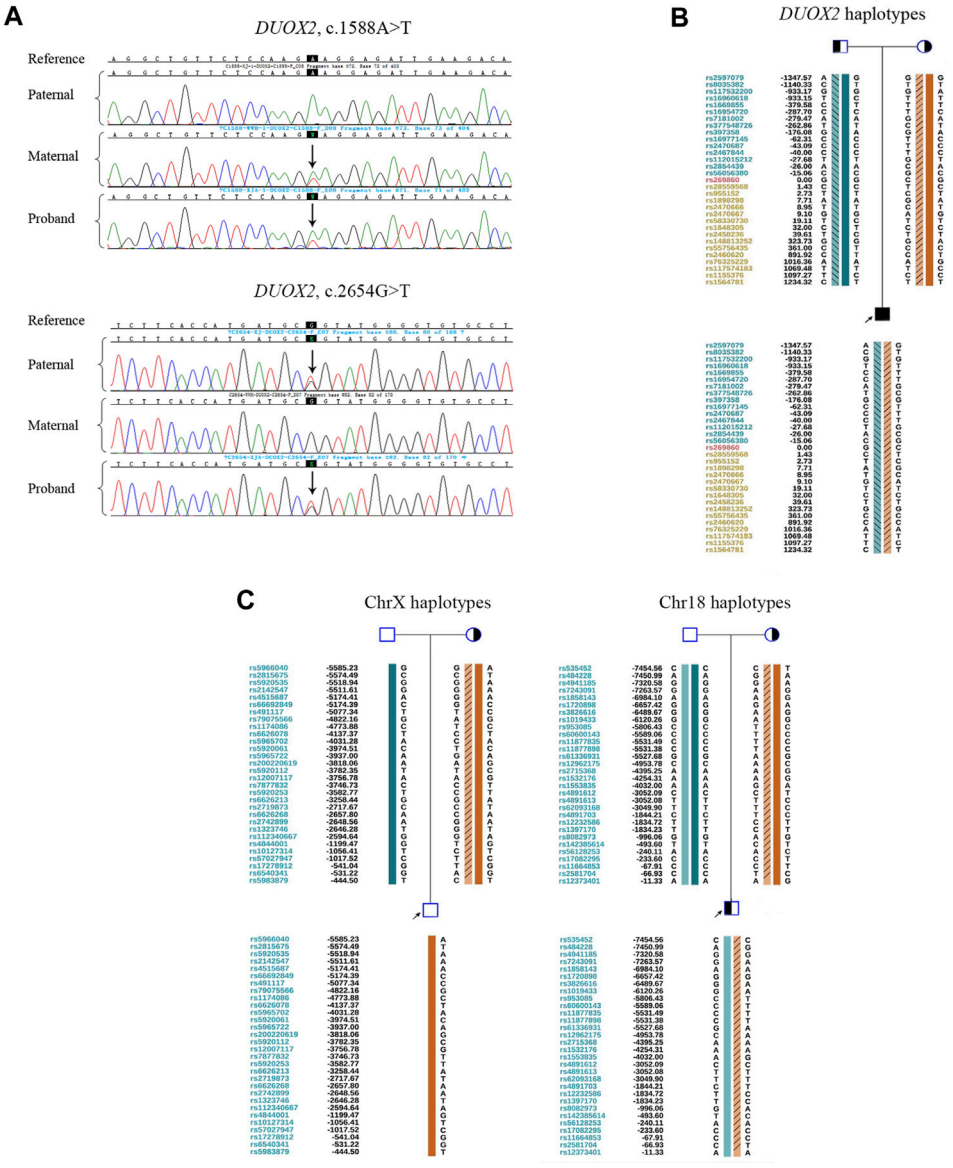


FIGURE 1
Preliminary experiments. **(A)** Sanger sequencing results for validation of the *DUOX2* mutations in c.1588A>T (p.K530X) and c.2654G>T (p.R885L) in family members. The black background indicates the targeted mutation sites. Arrows denote mutations. **(B)** Pedigree haplotyping analysis based on informative SNPs flanking *DUOX2*. The arrow indicates the proband. Circles and squares indicate females and males, respectively. The filled symbol represents the affected patient. Half-filled symbols represent *DUOX2* mutation carriers. Haplotypes are represented by colorful bars combined or not combined with diagonal lines. The dark green bar indicates a paternal wild-type haplotype. The light green bar combined with diagonal lines denotes a paternal mutation: *DUOX2*, c.2654G>T (p.R885L). The dark orange bar denotes a maternal wild-type haplotype. The light orange bar combined with diagonal lines indicates a maternal mutation: *DUOX2*, c.1588A>T (p.K530X). **(C)** Pedigree haplotypes around chromosomal breakpoint regions. The arrow indicates the proband. Circles and squares indicate females and males, respectively. Half-filled symbols represent derivative chromosome carriers. In ChrX, the dark green bar indicates the normal paternal ChrX haplotype. The dark orange bar denotes the normal maternal ChrX haplotype. Light orange bars with diagonal lines represent the derivative ChrX haplotype. In Chr18, the dark and light green bars indicate a pair of paternal normal Chr18 haplotypes in two homologous chromosomes. The dark orange bar represents the normal maternal Chr18 haplotype. The light orange bar combined with diagonal lines denotes the derivative Chr18 haplotype.

performed on day 5 or 6 of the culture. The biopsied TE cells were immediately washed in 1% polyvinylpyrrolidone and transferred into sample collection tubes (Yikon Genomics, Shanghai, China) (Ye et al., 2021). After the biopsy, blastocysts were cryopreserved by vitrification using the Oocyte/Embryo Vitrification Kit VT101 (Kitazato, Tokyo, Japan). According to the PGT results, normal blastocysts were thawed using the Oocyte/Embryo Thaw Kit VT102 (Kitazato). After thawing, the blastocytes were cultured in a G-2 medium (Vitrolife, Gothenburg, Sweden) for 2 h before embryo transfer.

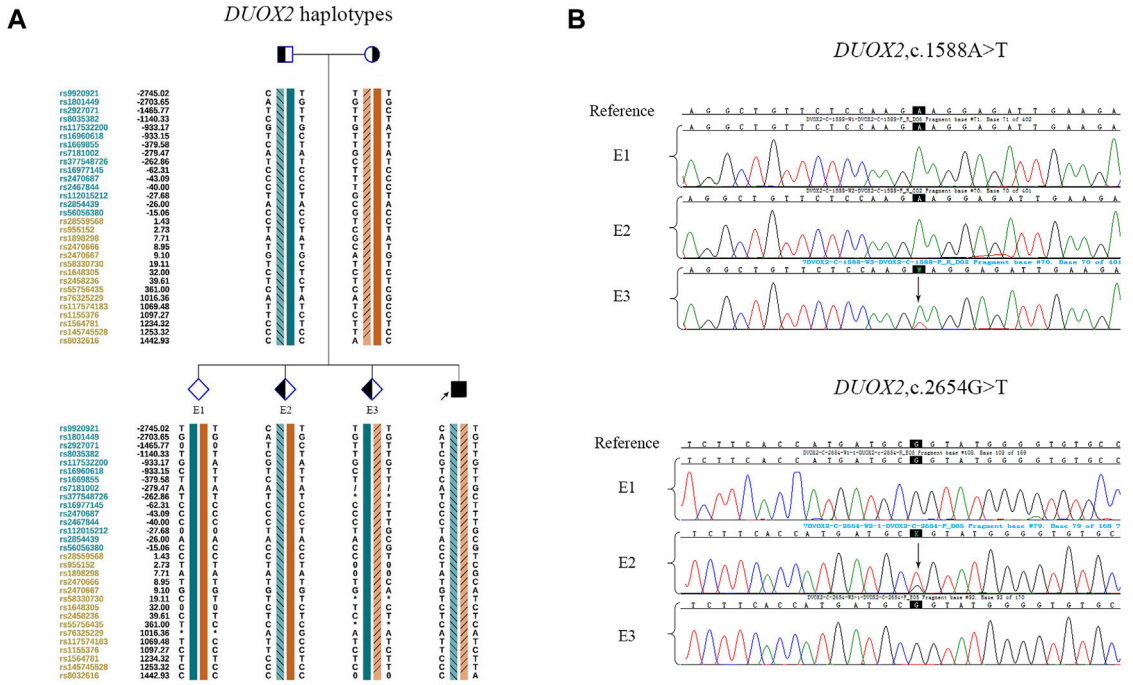


FIGURE 2
Linkage analysis and mutation detection in embryos. **(A)** Haplotypes around *DUOX2* of the family members and embryos. Diamonds indicate embryos, and the interpretation of other symbols and bars is explained in the legend of Figure 1B. E1 inherited both wild-type haplotypes from parents. E2 inherited the paternal mutation and maternal wild-type haplotype. E3 inherited the paternal wild-type haplotype and maternal mutation. **(B)** The mutations in embryos were identified by Sanger sequencing. The results were consistent with those of the SNP-based linkage analysis.

## WGA, specific PCR, and NGS

An improved MALBAC (multiple annealing and looping-based amplification cycles) WGA strategy was used to amplify the genomes of biopsied TE cells. The specific steps of WGA with MALBAC are described previously (Ye et al., 2021). Two mutation sites in *DUOX2*, c.1588 A>T (p.K530X) and c. 2654 G>T (p.R885L) were targeted from the WGA product. The specific polymerase chain reaction (PCR) products were mixed with the corresponding WGA product to construct a library using the NGS Library Preparation Kit (Yikon Genomics). The mixture was sequenced by NGS with a 2 × sequencing depth. The sequencing data was used to separate the mutant and wild-type haplotypes, to detect CNVs and to identify the translocation-carrying allele.

## SNP-based linkage analysis

For *DUOX2* mutations, using the pedigree haplotyping results as a reference, the SNP readouts at the positions adjacent to the mutant loci allowed the identification of the mutation-carrying allele in embryos. Mutations were also validated by Sanger sequencing. After the translocation-carrying allele was identified in the proband, the same SNP markers were used to corroborate whether the embryo carried chromosomally balanced RecT. The bioinformatics analysis was performed using ChromGo (Yikon Genomics).

## Confirmation of pregnancy and prenatal diagnosis

Pregnancy was confirmed by the level of serum β-hCG 14 days after frozen-thawed embryo transfer (FET) and by the presence of a gestational sac on ultrasound 35 days after FET. Amniotic fluid was collected for karyotyping, chromosomal aneuploidy detection, and *DUOX2* mutation analysis. G-band karyotyping, an SNP array analysis, and Sanger sequencing were performed for the above three examinations.

# Results

*DUOX2* variants in the family were validated by Sanger sequencing. The proband was a carrier of compound heterozygous mutations c.1588 A>T (p.K530X) and c. 2654 G>T (p.R885L). His mother carried the heterozygous mutation c.1588 A>T (p.K530X), and his father carried the heterozygous mutation c. 2654 G>T (p.R885L) (Figure 1A). In total, 187 SNPs within 2 Mb of the mutation site were evaluated by NGS. Pedigree haplotypes with linkage to the wild-type allele and mutation alleles c. 2654 G>T (p.R885L) or c.1588 A>T (p.K530X) were separated (Figure 1B). Translocation breakpoints in the proband were identified based on the copy number. The positions of breakpoints were ChrX: 149,327,063 and Chr18: 68,144,137. Subsequently, 60 SNP markers flanking the chromosomal breakpoints (within 1 Mb) were used to identify the

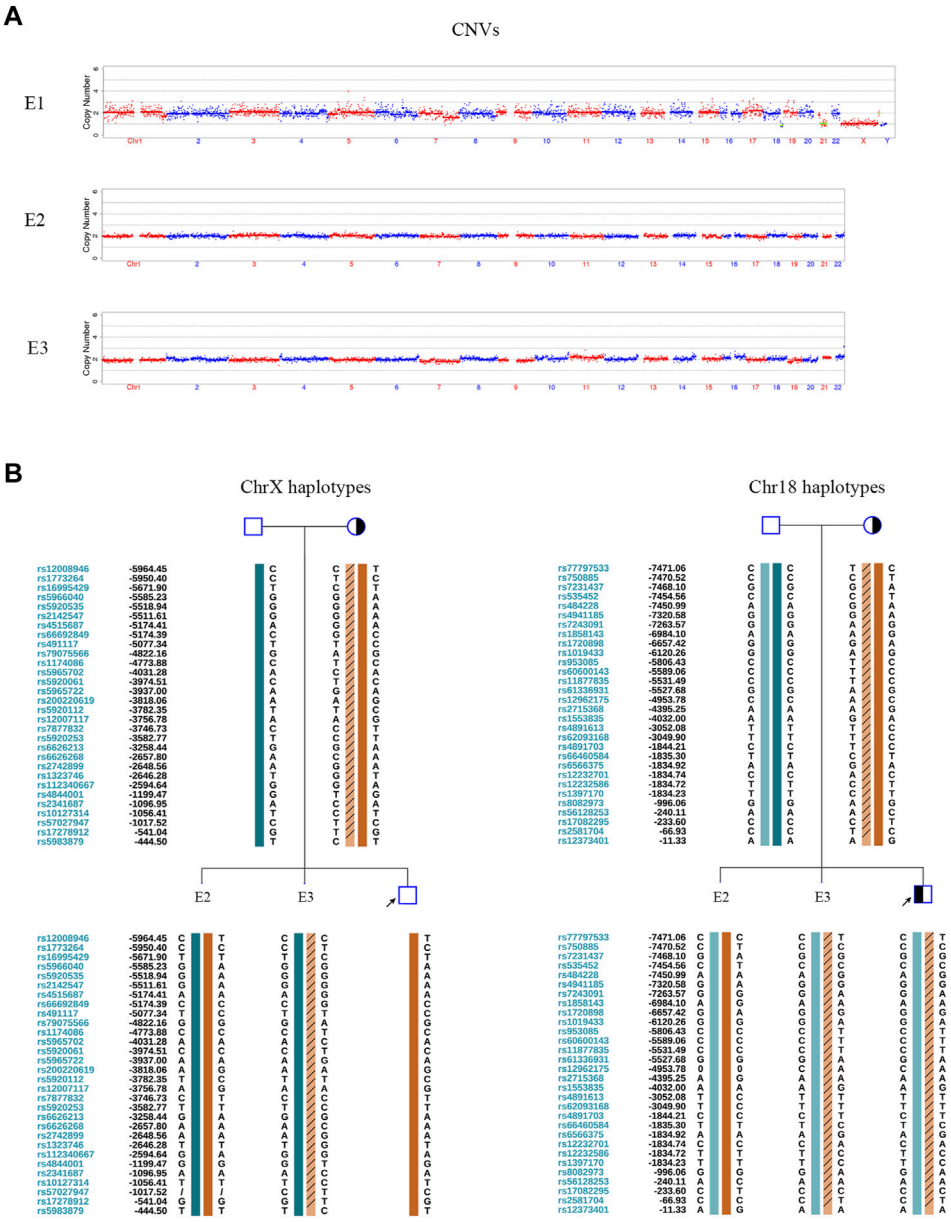


FIGURE 3
CNV tests and SNP-based linkage analysis for RecT detection in embryos. **(A)** Embryonic CNV results. E1 was unbalanced. E2 and E3 were chromosomally balanced. **(B)** Pedigree haplotyping around chromosomal breakpoints. The interpretation of symbols and bars is explained in the legend of Figure 1C. E2 inherited its two wild-type X chromosomes and two wild-type 18 chromosomes from their parents. It was female and free of RecT. E3 inherited a derivative ChrX and derivative Chr18 from the mother. It carried RecT between ChrX and Chr18.

translocation-carrying alleles in the proband and his mother (Figure 1C).

In the PGT cycle, 12 oocytes were retrieved. Seven oocytes were mature, and all were fertilized. Three fertilized eggs developed into blastocysts with Gardner scores of 3BB, 4BB, and 4BB. The haplotyping results revealed that E1 carried paternal and maternal wild-type haplotypes and was free of *DUOX2* mutations c. 2654 G>T (p.R885L) and c.1588 A>T (p.K530X). E2 carried the paternal *DUOX2* mutation c. 2654 G>T (p.R885L), and E3 was identified as a carrier of the maternal *DUOX2* gene variant c.1588 A>T (p.K530X) (Figures 2A,B). A CNV analysis of these three embryos showed that E1 was chromosomally unbalanced, whereas E2 and E3 were balanced (Figure 3A). An analysis of targeted SNP sites flanking the breakpoint confirmed that E2 inherited wild-type Chr18 and ChrX haplotypes from parents and was free of RecT. E3 inherited translocation-carrying haplotypes of Chr18 and ChrX from the mother. Accordingly, E3 was a carrier of RecT between Chr18 and ChrX (Figure 3B). Based on these findings (i.e., E1 lacked

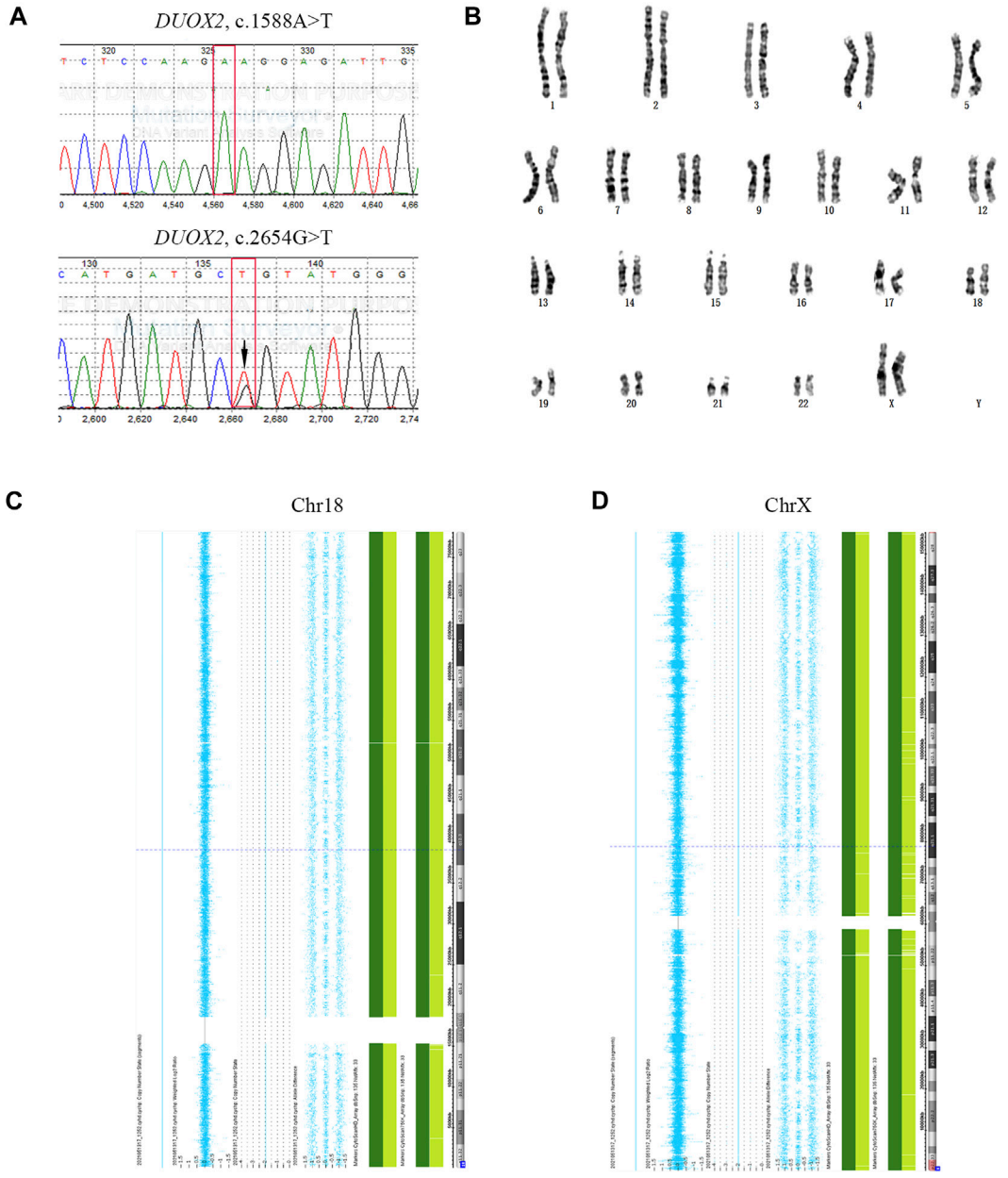


FIGURE 4
Prenatal diagnostic results. **(A)** Sanger sequencing results for fetal *DUOX2* mutations. Red boxes represent targeted mutation sites. The arrow indicates the *DUOX2*, c.2654G>T (p.R885L) mutation. **(B)** Amniotic fluid karyotyping of the fetus, revealing a normal karyotype. **(C, D)** Results of SNP array-based comprehensive chromosome screening.

mutations but was chromosomally unbalanced, E2 lacked RecT but was a carrier of the paternal gene mutation, and E3 inherited RecT and the heterozygous mutation from the mother), E2 was chosen for embryo transfer.

The serum β-hCG level of the mother was 1607 IU/L 14 days after FET. A gestational sac was detected by ultrasound 35 days after FET. Amniocentesis was performed at gestational week 20 to confirm the genetic properties of the fetus. The results were consistent with the PGT results for E2 (Figure 4). A healthy female infant weighing 3.25 kg was delivered by caesarean section at gestational week 38.5.

## Discussion

We diagnosed a complex, rare case in which a family simultaneously exhibited pathogenic compound heterozygous gene mutations and a chromosomal abnormality involving ChrXq. We utilized PGT based on NGS and an SNP linkage analysis to exclude monogenic disorders and RecT. Two sets of informative SNPs obtained by NGS were utilized to detect gene mutations and RecT in embryos. The selection of a RecT-free but monoallelic *DUOX2* mutation-carrying embryo resulted in a healthy live birth.

Although the Xq28-q28 duplication and 18q22.2-q23 deletion were detected in the proband by a CNV sequencing, the parents presented normal G-band karyotyping. A subchromosomal RecT (<10 Mb) in the mother was confirmed by FISH. G-band karyotyping is a routine laboratory test used for genetic diagnosis with a resolution of 5–10 Mb. However, given the variation in banding resolution among prenatal preparations, 10–20 Mb or greater is a more realistic threshold for detection in conventional karyotype analyses (Levy and Wapner, 2018; Kamath et al., 2022). CNV analyses offer additional diagnostic benefits by revealing sub-microscopic imbalances or CNVs that are substantially small to be detected on a standard G-banded chromosome preparation (Levy and Wapner, 2018). Several studies have demonstrated that, for the cases with normal parental karyotypes, the inspection of products of conception by CNV analyses is required to identify sub-microscopic chromosomal abnormalities in parents (Qian et al., 2018; Chen et al., 2021).

RecT carriers usually present a normal phenotype; however, they have elevated risks of reproductive abnormalities, including infertility, spontaneous abortion, and congenital disabilities. The PGT strategy based on NGS and an SNP linkage analysis to exclude RecT is expected to be an effective approach. In this case, RecT-carrying male offspring are at risk of disorders related to X-autosome translocation. X-autosomal translocations are rare and generally of the maternal origin or arise *de novo* (Kalz-Fuller et al., 1999). Both female and male carriers of X-autosomal translocations may present disorders. In female carriers, normal X chromosome inactivation leads to multiple anomalies and/or intellectual disabilities due to the derivative X chromosome in the active state (Ma et al., 2003). Breakpoints in the Xq13-q26 region are associated with infertility, ranging from gonadal dysgenesis to premature ovarian failure (Madan, 1983; Choi et al., 2020). Male carriers of X-autosome translocations may exhibit a disturbance in spermatogenesis, leading to severe subfertility or infertility (Madan, 1983). This is explained by the fact that the derivative X chromosome may interfere with sex vesicle formation, leading to meiotic disturbance and, consequently, to spermatogenetic arrest (Perrin et al., 2008). Although the RecT-carrying female in our case had a normal phenotype, the risk of disorders related to an X-autosome translocation in male offspring cannot be ruled out.

A 2002 study demonstrated that biallelic inactivating mutations in *DUOX2* resulted in the complete disruption of thyroid hormone synthesis and were associated with severe and permanent CH. Monoallelic mutations are associated with mild, transient hypothyroidism caused by insufficient thyroidal hydrogen peroxide production (Moreno et al., 2002). Several later studies have provided evidence that the transient or persistent nature of the hypothyroid phenotype is not directly related to the number of inactivated *DUOX2* alleles (Maruo et al., 2008; Ohye et al., 2008; Hoste et al., 2010). In 2018, a study in China revealed that *DUOX2* is the causative gene in patients with biallelic *DUOX2* mutations (containing compound heterozygous and homozygous mutations); however, *DUOX2* may not be the causative gene for patients carrying a monoallelic *DUOX2* mutation (Sun et al., 2018). Referring to the relevant literature and considering the normal phenotypes of the parents who carried monoallelic *DUOX2* mutations, we decided to transfer E2.

Genome-wide technologies have replaced FISH and PCR over the last decade (ESHRE PGT-SR/PGT-A Working Group et al., 2020). Genome-wide testing is typically applied to TE biopsy and used with a freeze-all strategy. TE biopsy can be applied to multiple cells and enables subsequent improvements in the accuracy of results with decreased amplification errors (Veiga et al., 1997; Sullivan-Pyke and Dokras, 2018). NGS-based SNP haplotyping avoids pitfalls associated with allele dropout and improves the accuracy of PGT-M (Chen et al., 2019). As the cost of NGS continues to decline, PGT is moving towards a sequencing-based all-in-one solution for PGT-M, PGT-SR, and PGT-A (De Rycke and Berckmoes, 2020; Wang et al., 2020), which would significantly simplify the procedure of PGT and broaden the applicable situations of the PGT technique.

In conclusion, we applied NGS and linkage analysis for PGT in a case of a complex pedigree. We successfully selected an appropriate embryo that resulted in a healthy live birth, and the clinical results proved the effectiveness of our diagnostic strategy.

## Data availability statement

The original contributions presented in the study are publicly available. This data can be found here: https://gosspublic.alicdn.com/oss-browser/1.16.0/oss-browser-win32-x64.zip?spm=a2c4g.11186623.0.0.43179c1d6w6l8u&file=oss-browser-win32-x64.zip.

## Ethics statement

The studies involving human participants were reviewed and approved by the Ethics Committee of the Woman Hospital School of Medicine Zhejiang University. Written informed consent to participate in this study was provided by the participants' legal guardian/next of kin.

Written informed consent was obtained from the individual(s), and minor(s)' legal guardian/next of kin, for the publication of any potentially identifiable images or data included in this article.

## Author contributions

BS contributed to the concept of the study and drafting of the manuscripts. YY contributed to the concept of the study, drafting of the manuscript, and provided critical discussions. Both authors approved the final manuscript.

## Funding

This work was supported by the key R&D program of Zhejiang (2021C03G2013079), National key R&D program of China

(2021YFC2700100) and National Natural Science Foundation of China (81974228).

## Acknowledgments

The authors thank Yeqing Qian. for his provision of clinical data and helpful discussions.

## Conflict of interest

The authors declare that the research was conducted in the absence of any commercial or financial relationships that could be construed as a potential conflict of interest.

## Publisher's note

All claims expressed in this article are solely those of the authors and do not necessarily represent those of their affiliated organizations, or those of the publisher, the editors and the reviewers. Any product that may be evaluated in this article, or claim that may be made by its manufacturer, is not guaranteed or endorsed by the publisher.

## Supplementary material

The Supplementary Material for this article can be found online at: https://www.frontiersin.org/articles/10.3389/fgene.2023.1066199/full#supplementary-material

## References

Chen, L., Diao, Z., Xu, Z., Zhou, J., Yan, G., and Sun, H. (2019). The clinical application of single-sperm-based SNP haplotyping for PGD of osteogenesis imperfecta. *Syst. Biol. Reprod. Med.* 65 (1), 75–80. doi:10.1080/19396368.2018.1472315

Chen, C. P., Lin, M. H., Chen, Y. Y., Chern, S. R., Wu, P. S., Chen, S. W., et al. (2021). Prenatal diagnosis of a 15q11.2-q14 deletion of paternal origin associated with increased nuchal translucency, mosaicism for de novo multiple unbalanced translocations involving 15q11-q14, 5qter, 15qter, 17pter and 3qter and Prader-Willi syndrome. *Taiwan J. Obstet. Gynecol.* 60 (2), 335–340. doi:10.1016/j.tjog.2021.01.012

Choi, L., Levy, G., Donlon, T., Sterbis, J., and Pier, B. (2020). Azoospermia secondary to a novel X-autosomal reciprocal translocation: 46,Y, t(X:16)(p22.1:p11.2). *Mil. Med.* 185 (9-10), e1860–e1863. doi:10.1093/milmed/usaa047

De Deken, X., and Miot, F. (2019). DUOX defects and their roles in congenital hypothyroidism. *Methods Mol. Biol.* 1982, 667–693. doi:10.1007/978-1-4939-9424-3_37

De Rycke, M., and Berckmoes, V. (2020). Preimplantation genetic testing for monogenic disorders. *Genes (Basel)* 11 (8), 871. doi:10.3390/genes11080871

ESHRE PGT-SR/PGT-A Working Group, Coonen, E., Rubio, C., Christopikou, D., Dimitriadou, E., Gontar, J., et al. (2020). ESHRE PGT Consortium good practice recommendations for the detection of structural and numerical chromosomal aberrations. *Hum. Reprod. Open* 2020 (3), hoaa017. doi:10.1093/hropen/hoaa017

Fiorentino, F., Spizzichino, L., Bono, S., Biricik, A., Kokkali, G., Rienzi, L., et al. (2011). PGD for reciprocal and Robertsonian translocations using array comparative genomic hybridization. *Hum. Reprod.* 26 (7), 1925–1935. doi:10.1093/humrep/der082

Gardner, D. K., Lane, M., Stevens, J., Schlenker, T., and Schoolcraft, W. B. (2000). Blastocyst score affects implantation and pregnancy outcome: towards a single blastocyst transfer. *Fertil. Steril.* 73 (6), 1155–1158. doi:10.1016/s0015-0282(00)00518-5

Hoste, C., Rigutto, S., Van Vliet, G., Miot, F., and De Deken, X. (2010). Compound heterozygosity for a novel hemizygous missense mutation and a partial deletion affecting the catalytic core of the H2O2-generating enzyme DUOX2 associated with transient congenital hypothyroidism. *Hum. Mutat.* 31 (4), E1304–E1319. doi:10.1002/humu.21227

Kalz-Fuller, B., Sleegers, E., Schwanitz, G., and Schubert, R. (1999). Characterisation, phenotypic manifestations and X-inactivation pattern in 14 patients with X-autosome translocations. *Clin. Genet.* 55 (5), 362–366. doi:10.1034/j.1399-0004.1999.550511.x

Kamath, V., Purna Chacko, M., Kirubakaran, R., Mascarenhas, M., and Kamath, M. S. (2022). Single nucleotide polymorphism array versus karyotype for prenatal diagnosis in fetuses with abnormal ultrasound: A systematic review and meta-analysis. *Eur. J. Obstet. Gynecol. Reprod. Biol.* 271, 235–244. doi:10.1016/j.ejogrb.2022.02.011

Levy, B., and Wapner, R. (2018). Prenatal diagnosis by chromosomal microarray analysis. *Fertil. Steril.* 109 (2), 201–212. doi:10.1016/j.fertnstert.2018.01.005

Ma, S., Yuen, B. H., Penaherrera, M., Koehn, D., Ness, L., and Robinson, W. (2003). ICSI and the transmission of X-autosomal translocation: A three-generation evaluation of X;20 translocation: case report. *Hum. Reprod.* 18 (7), 1377–1382. doi:10.1093/humrep/deg247

Madan, K. (1983). Balanced structural changes involving the human X: effect on sexual phenotype. *Hum. Genet.* 63 (3), 216–221. doi:10.1007/BF00284652

Maruo, Y., Takahashi, H., Soeda, I., Nishikura, N., Matsui, K., Ota, Y., et al. (2008). Transient congenital hypothyroidism caused by biallelic mutations of the dual oxidase 2 gene in Japanese patients detected by a neonatal screening program. *J. Clin. Endocrinol. Metab.* 93 (11), 4261–4267. doi:10.1210/jc.2008-0856

Moreno, J. C., Bikker, H., Kempers, M. J., van Trotsenburg, A. S., Baas, F., de Vijlder, J. J., et al. (2002). Inactivating mutations in the gene for thyroid oxidase 2 (THOX2) and congenital hypothyroidism. *N. Engl. J. Med.* 347 (2), 95–102. doi:10.1056/NEJMoa012752

Morin, S. J., Eccles, J., Iturriaga, A., and Zimmerman, R. S. (2017). Translocations, inversions and other chromosome rearrangements. *Fertil. Steril.* 107 (1), 19–26. doi:10.1016/j.fertnstert.2016.10.013

Muzza, M., and Fugazzola, L. (2017). Disorders of H2O2 generation. *Best. Pract. Res. Clin. Endocrinol. Metab.* 31 (2), 225–240. doi:10.1016/j.beem.2017.04.006

Ohye, H., Fukata, S., Hishinuma, A., Kudo, T., Nishihara, E., Ito, M., et al. (2008). A novel homozygous missense mutation of the dual oxidase 2 (DUOX2) gene in an adult patient with large goiter. *Thyroid* 18 (5), 561–566. doi:10.1089/thy.2007.0258

Perrin, A., Douet-Guilbert, N., Le Bris, M. J., Keromnes, G., Langlois, M. L., Barriere, P., et al. (2008). Segregation of chromosomes in sperm of a t(X;18)(q11;p11.1) carrier inherited from his mother: case report. *Hum. Reprod.* 23 (1), 227–230. doi:10.1093/humrep/dem359

Qian, Y. Q., Fu, X. Y., Wang, X. Q., Luo, Y. Q., Chen, M., Yan, K., et al. (2018). A feasible diagnostic approach for the translocation carrier from the indication of products of conception. *Mol. Cytogenet* 11, 12. doi:10.1186/s13039-018-0362-8

Scriven, P. N., Handyside, A. H., and Ogilvie, C. M. (1998). Chromosome translocations: segregation modes and strategies for preimplantation genetic diagnosis. *Prenat. Diagn.* 18 (13), 1437–1449. doi:10.1002/(sici)1097-0223(199812)18:13<1437::aid-pd497>3.0.co;2-p

Sullivan-Pyke, C., and Dokras, A. (2018). Preimplantation genetic screening and preimplantation genetic diagnosis. *Obstet. Gynecol. Clin. North Am.* 45 (1), 113–125. doi:10.1016/j.ogc.2017.10.009

Sun, F., Zhang, J. X., Yang, C. Y., Gao, G. Q., Zhu, W. B., Han, B., et al. (2018). The genetic characteristics of congenital hypothyroidism in China by comprehensive screening of 21 candidate genes. *Eur. J. Endocrinol.* 178 (6), 623–633. doi:10.1530/EJE-17-1017

Veiga, A., Sandalinas, M., Benkhalifa, M., Boada, M., Carrera, M., Santalo, J., et al. (1997). Laser blastocyst biopsy for preimplantation diagnosis in the human. *Zygote* 5 (4), 351–354. doi:10.1017/s0967199400003920

Wang, Y., Zhu, X., Yan, Z., Zhi, X., Guan, S., Kuo, Y., et al. (2020). Novel PGD strategy based on single sperm linkage analysis for carriers of single gene pathogenic variant and chromosome reciprocal translocation. *J. Assist. Reprod. Genet.* 37 (5), 1239–1250. doi:10.1007/s10815-020-01753-2

Weber, G., Rabbiosi, S., Zamproni, I., and Fugazzola, L. (2013). Genetic defects of hydrogen peroxide generation in the thyroid gland. *J. Endocrinol. Invest.* 36 (4), 261–266. doi:10.3275/8847

Ye, Y., Ma, J., Cui, L., Lu, S., and Jin, F. (2021). A rapid NGS-based preimplantation genetic testing for chromosomal abnormalities in day-3 blastomere biopsy allows embryo transfer within the same treatment cycle. *Front. Genet.* 12, 636370. doi:10.3389/fgene.2021.636370

Zegers-Hochschild, F., Adamson, G. D., Dyer, S., Racowsky, C., de Mouzon, J., Sokol, R., et al. (2017). The international glossary on infertility and fertility care, 2017. *Fertil. Steril.* 108 (3), 393–406. doi:10.1016/j.fertnstert.2017.06.005

Zhang, W., Liu, Y., Wang, L., Wang, H., Ma, M., Xu, M., et al. (2016). Clinical application of next-generation sequencing in preimplantation genetic diagnosis cycles for Robertsonian and reciprocal translocations. *J. Assist. Reprod. Genet.* 33 (7), 899–906. doi:10.1007/s10815-016-0724-2

frontiers | Frontiers in Pediatrics

TYPE Case Report
PUBLISHED 24 February 2023
DOI 10.3389/fped.2023.1111771



OPEN ACCESS

EDITED BY
Xiu-An Yang,
Chengde Medical College, China

REVIEWED BY
Emilia Severin,
Carol Davila University of Medicine and Pharmacy, Romania
Magdalena Budisteanu,
Prof. Dr. Alexandru Obregia Psychiatry Hospital, Romania

*CORRESPONDENCE
Xiaoke Zhao
xiaokezhao@njmu.edu.cn
Jian Tang
tangjian2020008@126.com

†These authors have contributed equally to this work

SPECIALTY SECTION
This article was submitted to Genetics of Common and Rare Diseases, a section of the journal Frontiers in Pediatrics

RECEIVED 30 November 2022
ACCEPTED 06 February 2023
PUBLISHED 24 February 2023

CITATION
Lu F, Xu X, Zheng B, Wang C, Zhou W, Tang J and Zhao X (2023) Case report: Expansion of phenotypic and genotypic data in *TENM3*-related syndrome: Report of two cases. Front. Pediatr. 11:1111771. doi: 10.3389/fped.2023.1111771



# Case report: Expansion of phenotypic and genotypic data in *TENM3*-related syndrome: Report of two cases

Fen Lu[1†], Xin Xu[1†], Bixia Zheng[2], Chunli Wang[2], Wei Zhou[2], Jian Tang[1*] and Xiaoke Zhao[1*]

[1]Department of Rehabilitation, Children's Hospital of Nanjing Medical University, Nanjing, China, [2]Nanjing Key Laboratory of Pediatrics, Children's Hospital of Nanjing Medical University, Nanjing, China

Biallelic *TENM3* variants were recently reported to cause non-syndromic microphthalmia with coloboma-9 (MCOPCB9) and microphthalmia and/or coloboma with developmental delay (MCOPS15). To date, only eight syndromic and non-syndromic microphthalmia cases with recessive *TENM3* variants have been reported. Herein, we report two unrelated new cases with biallelic variants in *TENM3*, widening the molecular and clinical spectrum. Regarding patient 1, WES revealed compound heterozygous variants in the *TENM3* gene: c.3847_3855del; p.Leu1283_Ser1285del and c.3698_3699insA; p.Thr1233Thrfs*20 in the index patient, who was presenting with bilateral microphthalmia, congenital cataract, microcephaly, and global developmental delay. Regarding patient 2, compound missense heterozygous variants in the *TENM3* gene were identified: c.941C > T; p.Ala314Val and c.6464T > C; p.Leu2155Pro in the 3-year-old boy, who presented with congenital esotropia, speech delay, and motor developmental delay. The clinical features of these two cases revealed high concordance with the previously reported cases, including microphthalmia and developmental delay. The presence of microcephaly in our patient potentially expands the neurologic phenotype associated with loss of function variants in *TENM3*, as microcephaly has not previously been described. Furthermore, we present evidence that missense variants in *TENM3* are associated with similar, but milder, ocular features.

KEYWORDS
syndromic microphthalmia, *TENM3*, whole exome sequencing, genotype-phenotype, children

## Introduction

Teneurin transmembrane protein 3 (TENM3) encodes a large transmembrane protein involved in neural development by regulating the establishment of proper connectivity within the nervous system (1–3). It has been found to play a role in the development of the human eye by regulating the formation of ipsilateral retinal mapping to both the dorsal lateral geniculate nucleus and the superior colliculus (4–6). The homozygous null variant was first reported in a Saudi Arabian consanguineous family with non-syndromic bilateral colobomatous microphthalmia (7). Subsequently, very few publications have reported patients with *TENM3* variant-related syndromic microphthalmia to date (8–10). Here, we present two patients with recessive variants in *TENM3*, and we describe their clinical presentations, providing further clinical and molecular delineation of the *TENM3* syndrome.

# Materials and methods

## Study participants

Following informed consent, we obtained pedigree information, clinical data, and blood samples from the families. We obtained approval for human subject research from the ethics committee of the Children's Hospital of Nanjing Medical University.

## Whole exome sequencing

Trio-based WES was performed as previously described (11). In brief, genomic DNA was isolated from blood lymphocytes using the DNA isolation kit (Tiangen, China). Genomic DNA was sheared into fragments and then hybridized with the xGen Exome Research Panel v1.0 probe sequence capture array from IDT (Integrated Device Technology, United States) to enrich the exonic region. The enriched libraries were analyzed on an

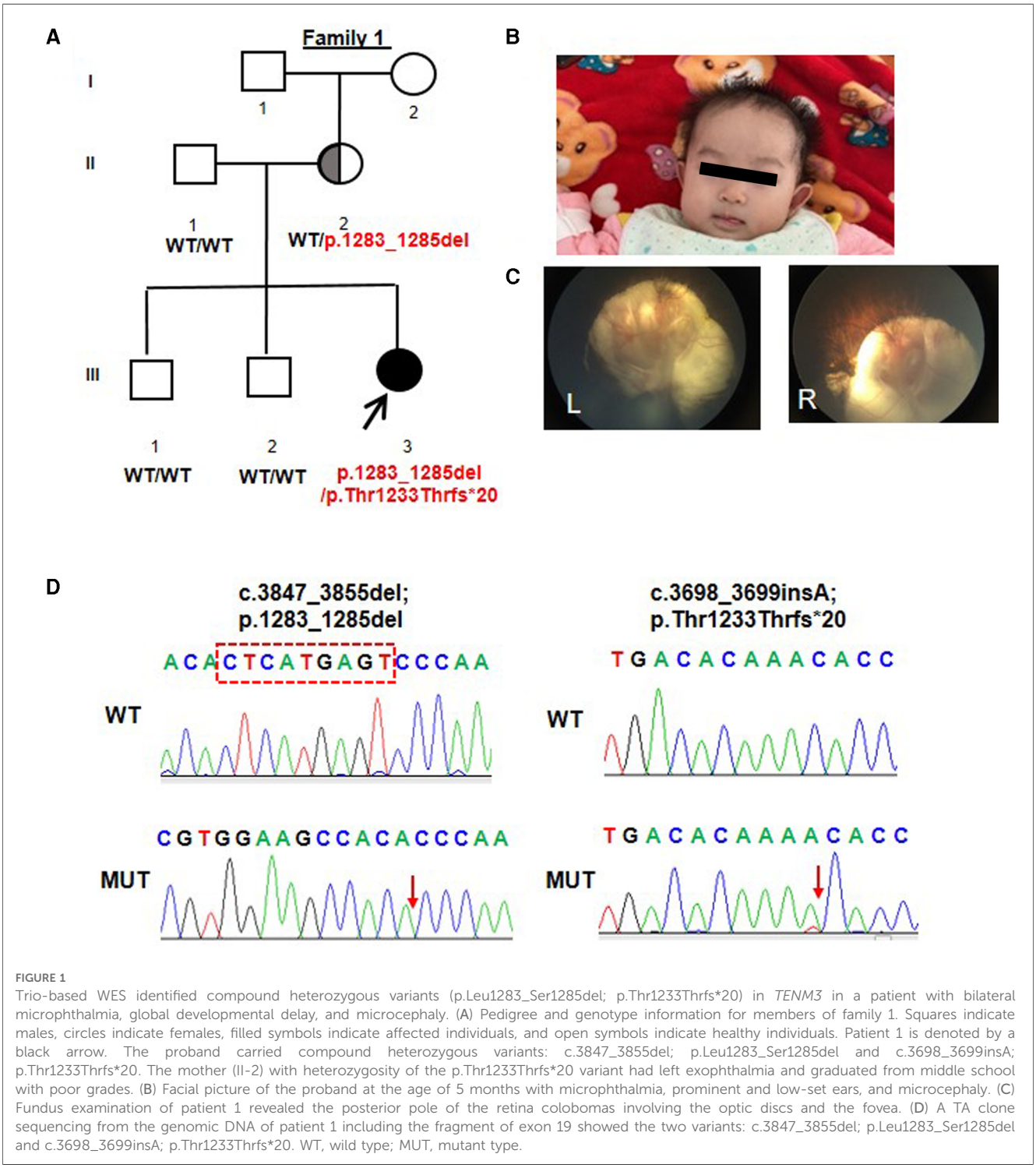


FIGURE 1
Trio-based WES identified compound heterozygous variants (p.Leu1283_Ser1285del; p.Thr1233Thrfs*20) in *TENM3* in a patient with bilateral microphthalmia, global developmental delay, and microcephaly. (**A**) Pedigree and genotype information for members of family 1. Squares indicate males, circles indicate females, filled symbols indicate affected individuals, and open symbols indicate healthy individuals. Patient 1 is denoted by a black arrow. The proband carried compound heterozygous variants: c.3847_3855del; p.Leu1283_Ser1285del and c.3698_3699insA; p.Thr1233Thrfs*20. The mother (II-2) with heterozygosity of the p.Thr1233Thrfs*20 variant had left exophthalmia and graduated from middle school with poor grades. (**B**) Facial picture of the proband at the age of 5 months with microphthalmia, prominent and low-set ears, and microcephaly. (**C**) Fundus examination of patient 1 revealed the posterior pole of the retina colobomas involving the optic discs and the fovea. (**D**) A TA clone sequencing from the genomic DNA of patient 1 including the fragment of exon 19 showed the two variants: c.3847_3855del; p.Leu1283_Ser1285del and c.3698_3699insA; p.Thr1233Thrfs*20. WT, wild type; MUT, mutant type.

10.3389/fped.2023.1111771

Illumina HiSeq XTen (Illumina, United States) platform. Low-quality variations of the quality score <20 (Q20) were filtered out. Sequencing reads were mapped to the GRCh37/Hg19 reference genome *via* Burrows-Wheeler Aligner (BWA) software. Single nucleotide variation (SNV) and inserts and deletions (INDEL) were filtered using GATK software (https://

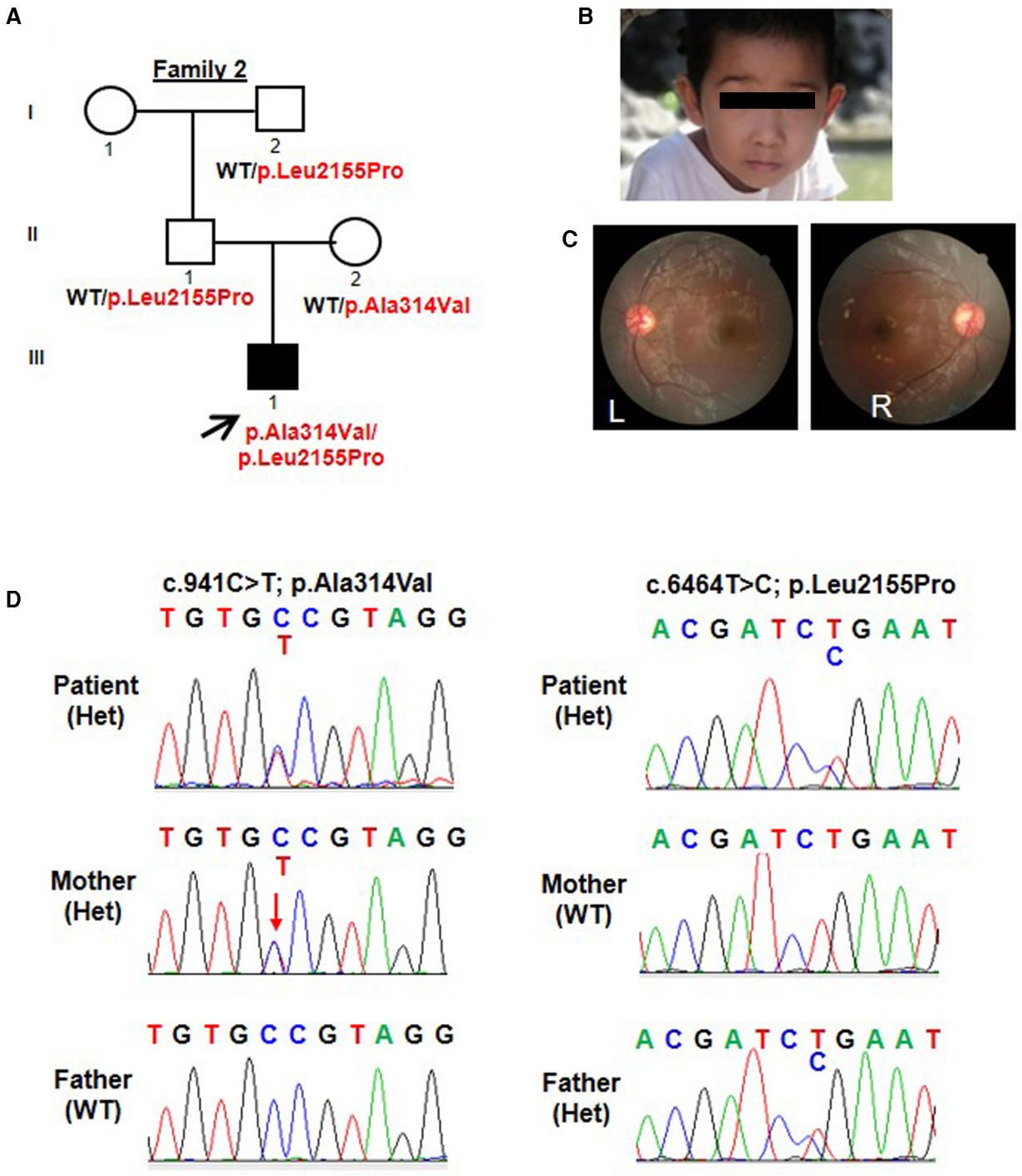


FIGURE 2
Trio-based WES identified compound heterozygous variants (p.Ala314Val; p.Leu2155Pro) in *TENM3* in a patient with speech delay and motor developmental delay. (**A**) Pedigree and genotype information on members of family 2. Squares indicate males, circles indicate females, filled symbols indicate affected individuals, and open symbols indicate healthy individuals. Patient 2 is denoted by a black arrow. The proband carried compound heterozygous variants: c.941C > T; p.Ala314Val and c.6464T > C; p.Leu2155Pro. (**B**) Facial picture of the proband at the age of 3 years old with resolved esotropia. His prominent and big ears were noted. (**C**) Fundus examination of patient 2 showed no structural anomalies. (**D**) Sequencing chromatograms of the compound heterozygous *TENM3* variants (c.941C > T; p.Ala314Val and c.6464T > C; p.Leu2155Pro) in patient 2 and the parents. WT, wild type; Het, heterozygous.

software.broadinstitute.org/gatk/). All identified variants were filtered using the 1000 Genomes Project (Chinese), dbSNP, Genome Aggregation Database (gnomAD), and ExAC database. Variants with a minor allele frequency higher than 5% were filtered out. Finally, the candidate variants were evaluated using the ACMG (American College of Medical Genetics and Genomics) criteria and further validated by direct Sanger sequencing.

## TA cloning of mutant PCR products

The two heterozygous *TENM3* variants in family 1 were both located in exon 19. To obtain a clean Sanger sequence of the two heterozygous variants, we cloned 383 bp-long PCR products of *TENM3* exon19 using the pCR2.1-TOPO plasmid vector system (Invitrogen). PCR products were generated using *TENM3* forward primer 5-ATCCTCAGCGTCAGGCAAGGAA-3 and reverse primer 5-TCCCCTGTCCCTGCGACGAC-3. The TA clone sequencing was conducted as previously described (12).

## Consideration of structural data and evolutionary conservation for variant evaluation

Protein domain structure depictions and evaluation were based on the UniProt (Universal Protein Resource) database. Orthologous proteins used to evaluate evolutionary conservation were obtained from the Ensemble Genome Browser and were aligned using the Clustal Omega multiple sequence alignment tool (EMBL-EBI). And we evaluated the crystal structure of the two missense *TENM3* variants in patient 2 using the online server, UCSF ChimeraX (http://www.cgl.ucsf.edu/chimerax//).

# Results

## Clinical findings

Patient 1 was the 5-month-old daughter of Chinese non-consanguineous parents. She had two older brothers and both are

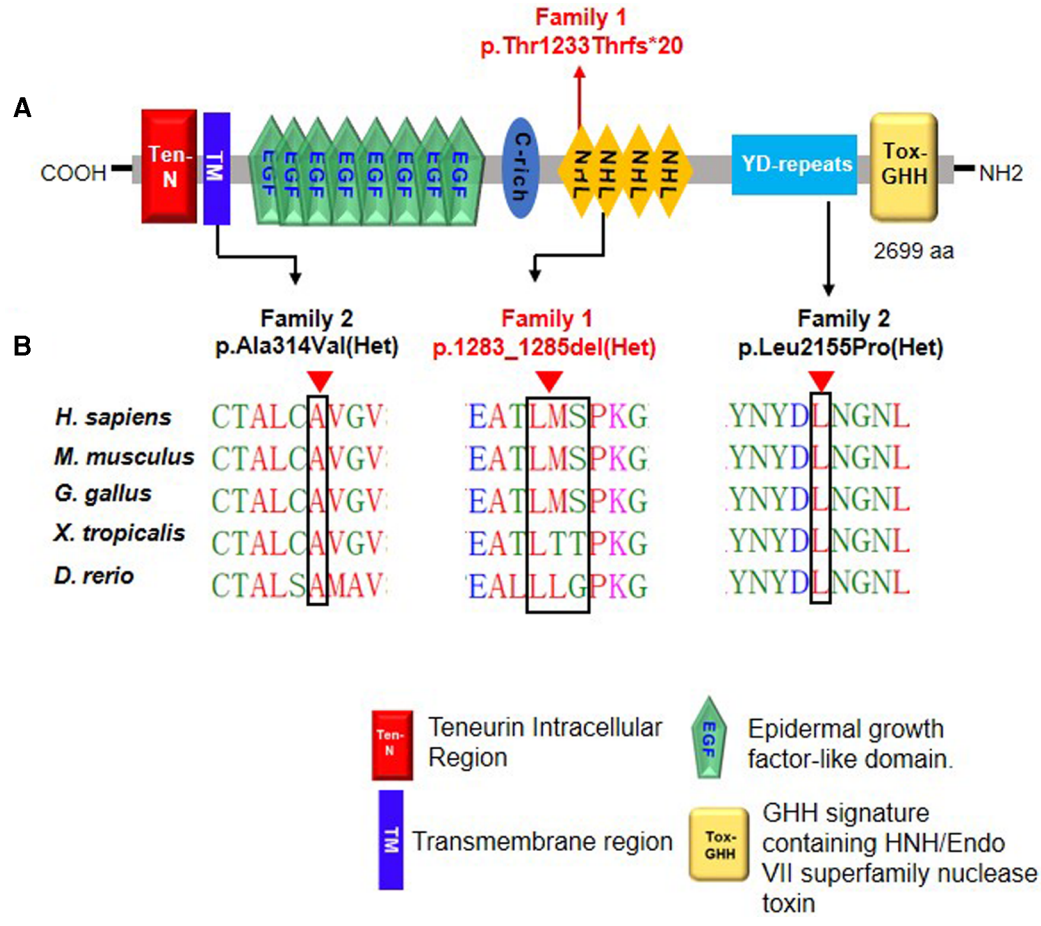


FIGURE 3
Schematic diagram of *TENM3* functional domains and *TENM3* variants identified in this study. (**A**) Depicts the protein domain structure of human TENM3 showing the domain position of the index heterozygous *TENM3* variants. aa, amino acids. (**B**) Evolutionary conservation of amino acid position Ala1283-Ser1285 and Leu2155 in TENM3 protein across evolution.

healthy. She was born at 39 weeks of gestation. Her birth weight was 2.7 kg (−1.46 SD) and her length was 40 cm (−5.89 SD). At birth, she was diagnosed with bilateral microphthalmia and congenital cataract and she appeared to have pendular nystagmus and esotropia (Figure 1B). She first visited our department of rehabilitation at the age of 5 months for developmental delay. Her developmental milestones were delayed. Her head control was unstable and she was unable to turn over and grab the toy on her chest. On careful physical examination, her height, weight, and head circumference were 57 cm (−4.03 SD), 5 kg (−3.75 SD), and 37 cm (−4.28 SD), respectively. Her prominent and low-set ears were noted (Figure 1B). Fundus examination revealed the posterior pole of the retina colobomas involving the optic discs and the fovea (Figure 1C). Her hearing assessment was normal. According to the Gesell Developmental Diagnostic Scale for children, the proband's gross motor skills indicated a developmental age of 8 weeks; the fine motor skills indicated a developmental age of 8 weeks; Her blood counts, liver and renal function tests, thyroid profile, and metabolic screen by mass spectrometry were normal. Brain magnetic resonance imaging (MRI) showed no structure malformations except a widening in the frontotemporal extracerebral space. Her mother had left exotropia and graduated from middle school with poor grades.

Patient 2 was the 3-year-and-5-month-old son of Chinese non-consanguineous parents. His weight was 17 kg (0.8 SD) and his height was 101 cm (0.2 SD). At birth, it was noted that he had bilateral esotropia. At the age of 3 years old, his bilateral esotropia was resolved (Figure 2B). What's more, his anterior segment and fundus examination showed no structural anomalies (Figure 2C). He had astigmatism in both eyes (−1.25 DC). He had mild motor delay. He was able to walk without support at 17 months. He had significant speech delay, not producing any meaningful words at 2 years and 5 months and speaking a few simple words (about 10 words) at 3 years and 5 months. He showed poor eye contact and was not interested in his surroundings, so his social interaction was abnormal. According to the Gesell Developmental Diagnostic Scale for children, the proband's delayed speech indicated a developmental age of only 18 months. He was also evaluated by the Autistic Behavior Checklist (ABC) and Childhood Autism Rating Scale (CARS) (ABC: score 40; CARS: score 32). His blood counts, liver and renal function tests, thyroid profile, and metabolic screen by mass spectrometry were normal. His hearing evaluation was also normal. His prominent and big ears were noted. A brain MRI did not show any intracranial abnormalities. His father had no abnormal eye appearance, but his eyes were myopic (−7.00 DS), and his mother was healthy. His grandfather had a history of fundus abnormality.

## Genetic analysis

Initial genetic testing for patient 1 was carried out *via* WES, revealing two heterozygous variants in the *TENM3* gene (Genbank association number: NM_001080477): c.3847_3855del; p.Leu1283_Ser1285del and c.3698_3699insA; p.Thr1233Thrfs*20 (Figure 1A). Sanger sequencing of the parents confirmed that the variant p.Leu1283_Ser1285del was inherited maternally. The variant p.Thr1233Thrfs*20 was confirmed to be *de novo*. The two variants were both located in exon 19. A TA clone sequencing including the fragment of exon 19 demonstrated that the two variants occurred biallelically (Figure 1D). The two variants were absent from the control database gnomAD. Based on the American College of Medical Genetics and Genomics (ACMG) guidelines, the variant c.3698_3699insA; p.Thr1233Thrfs*20 can be categorized as pathogenic (PVS1 + PM2 + PP4) and the variant c.3847_3855del; p.Leu1283_Ser1285del can be categorized as a variant of likely pathogenic (PM2 + PM3 + PM4).

Similarly, patient 2 had a WES that revealed compound heterozygous variants of the *TENM3* gene, c.941C > T; p.Ala314Val and c.6464T > C; p.Leu2155Pro (Figure 2A). Sanger sequencing confirmed that his mother carried the c.941C > T (p.Ala314Val) mutation and his father carried the c.6464T > C (p.Leu2155Pro)

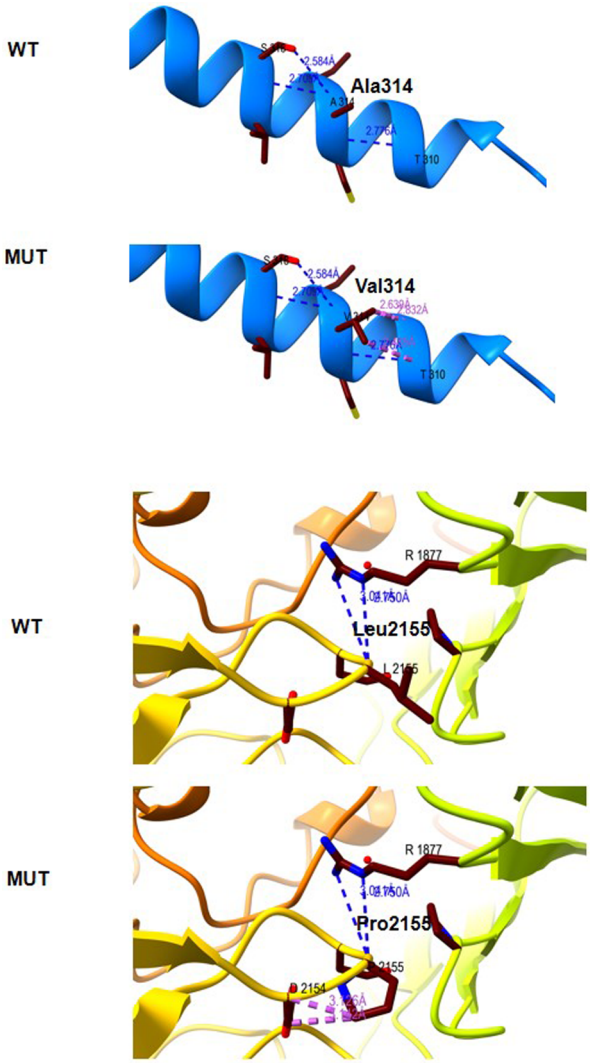


FIGURE 4
Molecular modeling of the wild type (WT) and mutant TENM3 protein (Mut). Three-dimensional structural modeling of the TENM3 protein showed that the mutations did not change the hydrogen bonding in protein (blue), but repulsive force (purple) was generated between the R group of amino acid side chain and other nearby groups.

TABLE 1 Clinical manifestations of patients with variants in *TENM3*.

| Clinical characteristics | Patient 1 | Patient 2 | Patient 3 | Patient 4 | Patient 5 | Patient 6 | Patient 7 | Patient 8 | Patient 9 | Patient 10 |
|---|---|---|---|---|---|---|---|---|---|---|
| Age | 11 | 9 | 9 | 6 | 5y6m | 4y3m | - | 32 | 5m | 3y5m |
| Sex | Male | Female | Male | Male | Female | Female | - | Male | Female | Male |
| Genotype | Homozygous c.2083dup; p.Thr695Asnfs*5 | Homozygous c.2083dup; p.Thr695Asnfs*5 | Homozygous c.2968-2A > T; p. Val990Cysfs*13 | Compound heterozygous c.7687C > T; p. Arg2563Trp and c.4046C > G; p. Ala1349Gly | Homozygous c.1857T > A; p. Cys619* | Homozygous c.1857T > A; p. Cys619* | Homozygous c.1558C > T; p. (Arg520*) | Homozygous c.5069-1G > C; p.1690Asp > Glyfs*2 | Compound heterozygous c.3698_3699insA; p.Thr1233Thrfs*20 and c.3847_3855del CTCATGAGT; p.Leu1283_Ser1285del | Compound heterozygous c.941C > T; p.Ala314Val and c.6464T > C; p.Leu2155Pro |
| Type of mutation | Frameshift | Frameshift | Splice | Missense | Nonsense | Nonsense | Nonsense | Frameshift | Frameshift/In-frame deletion | Missense |
| Motor development | Normal | Normal | Delayed | Delayed | Delayed | Delayed | - | Normal | Delayed | Delayed |
| Cognition | Normal | Normal | Delayed | Delayed | Delayed | Delayed | - | Delayed | Delayed | Delayed |
| Ptosis | No | No | No | No | Unilateral (left) | Bilateral partial ptosis | - | Yes | No | No |
| Microphthalmia | Yes | Yes | Yes | Yes | No | No | Yes | Yes | Yes | No |
| Micro cornea | Yes | Yes | Yes | Yes | Yes | Yes | - | - | Yes | No |
| Iris coloboma | Yes | Yes | Yes | - | Yes | Yes | Yes | - | No | No |
| Retinal coloboma | Yes | Yes | Yes | - | Yes | Yes | Yes | No | Yes | No |
| Visual acuity | 20/50 (R) Hand movement (L) | 20/200 (R) 20/300 (L) | Hand movement both eyes | - | 6/36 both eyes | 6/36 both eyes | - | - | - | Astigmatism in both eyes (−1.25 DC) |
| Facial dysmorphic features | - | - | Mild | - | - | - | - | - | Mild | - |
| References | Aldahmesh and others 2012 | Aldahmesh and others 2012 | Chassaing and others 2016 | Singh and others 2019 | Stephen and others 2018 | Stephen and others 2018 | Farrah Islam and others 2020 | Gholami Yarahmadi and others 2022 | Our present study | Our present study |

*Means termination codon.





10.3389/fped.2023.1111771

mutation (Figure 2D). The p.Ala314Val variant was absent from the gnomAD. The p.Leu2155Pro variant occurred once heterozygously in the gnomAD. Both the missense changes yielded predominantly deleterious prediction scores using five algorithms (Polyphen2_HDIV, MutationTaster, SIFT, Provean, and REVEL); the predicted results can be found in the Supplementary Material.

The Ala314 change was located in the transmembrane domain and was evolutionarily well-conserved from *Homo sapiens* to *zebrafish* (Figures 3A,B). The Leu2155 residue was located in the YD-repeats domain and was well-conserved to zebrafish as well (Figures 3A,B). According to the ACMG guidelines, both variants, c.941C > T; p.Ala314Val and c.6464T > C; p.Leu2155Pro, can be categorized as variants of unknown significance (PM2 + PP2 + PP3). In evaluating the deleteriousness of the two missense variants in patient 2, three-dimensional structural modeling of the TENM3 protein showed that the mutations did not change the hydrogen bonding in the protein (blue), but repulsive force (purple) was generated between the R group of amino acid side chain and other nearby groups, which is unfavorable to the folding of the active protein and results in protein conformational instability (Figure 4).

## Discussion

To date, only eight patients with recessive *TENM3* variants have been described; information on the reported patients is shown in Table 1. The non-syndromic microphthalmia cases with recessive *TENM3* variants only presented with moderate or severe eye abnormalities, including microphthalmia, microcornea, and retinal and iris coloboma, while *TENM3* syndromic cases had additional abnormalities, such as craniofacial, renal, genital, cardiac, brain, and skeletal (9, 13, 14). To expand the *TENM3* gene-related phenotypic spectrum, we describe the clinical features of two Chinese patients with compound heterozygous variants in *TENM3*. The main characteristic feature of this syndrome is eye involvement (15). All previously reported patients presented with moderate or severe eye abnormalities, including colobomatous microphthalmia, ocular coloboma, and cataract (9, 13, 14). The ocular features of patient 1 in our study are highly consistent with previous reports. However, patient 2, who harbored two missense variants (c.941C > T; p.Ala314Val and c.6464T > C; p.Leu2155Pro), did not have a phenotype related to microphthalmia, microcornea, or iris coloboma. At birth, it was noted that he had bilateral esotropia. However, his bilateral esotropia was resolved at the age of 3 years old. Furthermore, his anterior segment and fundus examinations showed normal structure. A literature review revealed that all variants in previously reported cases with microphthalmia and/or coloboma with developmental delay had biallelic truncating variants. The only reported case with compound heterozygote missense likely pathogenic sequence variations in *TENM3* (p.Ala1349Gly and p.Arg2563Trp) showed right eye microphthalmia, sclerocornea of both eyes, anterior segment dysgenesis, and intellectual disability (14). We speculate that the missense mutations in patient 2 may have a mild effect on the structure of the TENM3 protein, which is associated with mild ocular symptoms. However, this must be further verified by *in vitro* experiments or animal experiments.

The mother of patient 1 with heterozygosity of the p.Thr1233Thrfs*20 variant had left exotropia and graduated from middle school with poor grades. The gnomAD constraint metric of TENM3 for loss of function is 1.0, indicating a high intolerance for heterozygous loss of function variants. However, no neurologic or ocular phenotypes were reported in individuals harboring a heterozygous allele in *TENM3*.

The two patients in our study had delayed developmental milestones similar to those observed in patients with recessive *TENM3* variants: these included global developmental delay, speech delay, and motor developmental delay (8). Brain MRIs showed no structural abnormalities. Notably, the presence of microcephaly in patient 1 potentially expands the neurologic phenotype associated with loss of function variants in *TENM3*, as microcephaly has not previously been described. The two patients received rehabilitation training in our department and their motor function and language skills both improved, but there was no improvement in their eye symptoms.

In conclusion, we reported the clinical features of two cases with recessive variants in *TENM3*. While the majority of *TENM3* syndromic or non-syndromic cases are truncating, missense variants have been described much less. It should be noted that biallelic missense variants in *TENM3* seem to have a minor impact on eye involvement.

## Data availability statement

The data presented in the study are included in the article/Supplementary Material, further inquiries can be directed to the corresponding author.

## Ethics statement

The studies involving human participants were reviewed and approved by the ethics committee of Children's Hospital of Nanjing Medical University. Written informed consent to participate in this study was provided by the participants' legal guardian/next of kin. Written informed consent was obtained from the individual(s), and minor(s)' legal guardian/next of kin, for the publication of any potentially identifiable images or data included in this article.

## Author contributions

FL and XX collected the clinical data of the patients. FL, JT, and XZ conceived the project. BZ, CW, and WZ analyzed the result. JT and XZ wrote and revised the manuscript. All authors contributed to the article and approved the submitted version.

## Acknowledgments

We would like to thank the families and study participants for their contributions.

## Conflict of interest

The authors declare that the research was conducted in the absence of any commercial or financial relationships that could be construed as a potential conflict of interest.

## Publisher's note

All claims expressed in this article are solely those of the authors and do not necessarily represent those of their affiliated organizations, or those of the publisher, the editors and the reviewers. Any product that may be evaluated in this article, or claim that may be made by its manufacturer, is not guaranteed or endorsed by the publisher.

## Supplementary material

The Supplementary Material for this article can be found online at: https://www.frontiersin.org/articles/10.3389/fped.2023.1111771/full#supplementary-material.

## References

1. Ben-Zur T, Feige E, Motro B, Wides R. The mammalian odz gene family: homologs of a drosophila pair-rule gene with expression implying distinct yet overlapping developmental roles. *Dev Biol*. (2000) 217(1):107–20. doi: 10.1006/dbio.1999.9532

2. Berns DS, DeNardo LA, Pederick DT, Luo L. Teneurin-3 controls topographic circuit assembly in the hippocampus. *Nature*. (2018) 554(7692):328–33. doi: 10.1038/nature25463

3. Takano I, Takeshita N, Yoshida M, Seki D, Oyanagi T, Kimura S, et al. Ten-m/Odz3 regulates migration and differentiation of chondrogenic ATDC5 cells via RhoA-mediated actin reorganization. *J Cell Physiol*. (2021) 236(4):2906–19. doi: 10.1002/jcp.30058

4. Carr OP, Glendining KA, Leamey CA, Marotte LR. Retinal overexpression of ten-m3 alters ipsilateral retinogeniculate projections in the wallaby (Macropus eugenii). *Neurosci Lett*. (2014) 566:167–71. doi: 10.1016/j.neulet.2014.02.048

5. Glendining KA, Liu SC, Nguyen M, Dharmaratne N, Nagarajah R, Iglesias MA, et al. Downstream mediators of ten-m3 signalling in the developing visual pathway. *BMC Neurosci*. (2017) 18(1):78. doi: 10.1186/s12868-017-0397-5

6. Young TR, Bourke M, Zhou X, Oohashi T, Sawatari A, Fassler R, et al. Ten-m2 is required for the generation of binocular visual circuits. *J Neurosci*. (2013) 33(30):12490–509. doi: 10.1523/JNEUROSCI.4708-12.2013

7. Aldahmesh MA, Mohammed JY, Al-Hazzaa S, Alkuraya FS. Homozygous null mutation in ODZ3 causes microphthalmia in humans. *Genet Med*. (2012) 14(11):900–4. doi: 10.1038/gim.2012.718.

8. Chassaing N, Ragge N, Plaisancie J, Patat O, Genevieve D, Rivier F, et al. Confirmation of TENM3 involvement in autosomal recessive colobomatous microphthalmia. *Am J Med Genet A*. (2016) 170(7):1895–8. doi: 10.1002/ajmg.a.37667

9. Stephen J, Nampoothiri S, Kuppa S, Yesodharan D, Radhakrishnan N, Gahl WA, et al. Novel truncating mutation in TENM3 in siblings with motor developmental delay, ocular coloboma, oval cornea, without microphthalmia. *Am J Med Genet A*. (2018) 176(12):2930–3. doi: 10.1002/ajmg.a.40658

10. Islam F, Htun S, Lai L-W, Krall M, Poranki M, Martin P-M, et al. Exome sequencing in patients with microphthalmia, anophthalmia, and coloboma (MAC) from a consanguineous population. *Clin Genet*. (2020) 98(5):499–506. doi: 10.1111/cge.13830

11. Wang C, Han Y, Zhou J, Zheng B, Zhou W, Bao H, et al. Splicing characterization of CLCNKB variants in four patients with type III bartter syndrome. *Front Genet*. (2020) 11:81. doi: 10.3389/fgene.2020.00081

12. Wang C, Chen Y, Zheng B, Zhu M, Fan J, Wang J, et al. Novel compound heterozygous CLCNKB gene mutations (c.1755A>G/c.848_850delTCT) cause classic bartter syndrome. *Am J Physiol Renal Physiol*. (2018) 315(4):F844–51. doi: 10.1152/ajprenal.00077.2017

13. Yarahmadi SG, Sarlaki F, Morovvati S. Novel mutation in TENM3 gene in an Iranian patient with colobomatous microphthalmia. *Clin Case Rep*. (2022) 10(3):e05532. doi: 10.1002/ccr3.5532

14. Singh B, Srivastava P, Phadke SR. Sequence variations in TENM3 gene causing eye anomalies with intellectual disability: expanding the phenotypic spectrum. *Eur J Med Genet*. (2019) 62(1):61–4. doi: 10.1016/j.ejmg.2018.05.004

15. Williamson KA, FitzPatrick DR. The genetic architecture of microphthalmia, anophthalmia and coloboma. *Eur J Med Genet*. (2014) 57(8):369–80. doi: 10.1016/j.ejmg.2014.05.002

frontiers | Frontiers in Genetics

TYPE Original Research
PUBLISHED 20 March 2023
DOI 10.3389/fgene.2023.1142968



OPEN ACCESS

EDITED BY
Xiu-An Yang,
Chengde Medical College, China

REVIEWED BY
Xiao-Ping Wang,
Shanghai Jiao Tong University School of Medicine, China
Atchariya Chanpong,
University College London, United Kingdom
Carmen Espinós,
Principe Felipe Research Center (CIPF), Spain

*CORRESPONDENCE
Li Li,
lili@etyy.cn
Shufang Xiao,
xiaoshufang@etyy.cn

SPECIALTY SECTION
This article was submitted to Human and Medical Genomics, a section of the journal Frontiers in Genetics

RECEIVED 12 January 2023
ACCEPTED 08 March 2023
PUBLISHED 20 March 2023

CITATION
Wang Y, Fang J, Li B, Li C, Liu S, He J, Tao L, Li C, Yang Y, Li L and Xiao S (2023), Clinical and genetic characterization of pediatric patients with Wilson's disease from Yunnan province where ethnic minorities gather.
*Front. Genet.* 14:1142968.
doi: 10.3389/fgene.2023.1142968



# Clinical and genetic characterization of pediatric patients with Wilson's disease from Yunnan province where ethnic minorities gather

Yanjun Wang[1], Jiahui Fang[1], Bin Li[1], Chongyang Li[2], Shan Liu[3], Juan He[1], Lvyan Tao[1], Cuifen Li[1], Ya Yang[1], Li Li[1]* and Shufang Xiao[1]*

[1]Kunming Children's Hospital, Kunming, China, [2]Department of Oncology, The Affiliated Hospital of Yunnan University, Kunming, China, [3]Yunnan Cancer Hospital, Kunming, China

**Background:** Wilson's disease (WD) is an autosomal recessive disease that is caused by mutations in the *ATP7B* (a copper-transporting P-type ATPase) gene. The disease has a low prevalence and is characterized by a copper metabolism disorder. However, various characteristics of the disease are determined by race and geographic region. We aimed to discover novel *ATP7B* mutations in pediatric patients with WD from Yunnan province, where there is a high proportion of ethnic minorities. We also performed a comprehensive analysis of *ATP7B* mutations in the different ethnic groups found in Southwest China.

**Methods:** We recruited 45 patients who had been clinically diagnosed with WD, from 44 unrelated families. Routine clinical examinations and laboratory evaluations were performed and details of age, gender, ethnic group and symptoms at onset were collected. Direct sequencing of the *ATP7B* gene was performed in 39 of the 45 patients and their families.

**Results**: In this study, participants came from seven different ethnic groups in China: Han, Bai, Dai, Zhuang, Yi, Hui and Jingpo. Three out of ten patients from ethnic minorities presented with elevated transaminases, when compared to the majority of the Han patients. Forty distinct mutations (28 missense, six splicing, three non-sense, two frameshift and one mutation of uncertain significance) were identified in the 39 patients with WD. Four of the mutations were novel and the most frequent mutation was c.2333G > T (p.R778L, allelic frequency: 15.38%). Using the phenotype-genotype correlation analysis, patients from ethnic minorities were shown to be more likely to have homozygous mutations ($p$ = 0.035) than Han patients. The patients who carried the c.2310C > G mutation had lower serum ceruloplasmin levels ($p$ = 0.012). In patients with heterozygous mutations, c.3809A > G was significantly associated with ethnic minorities ($p$ = 0.042). The frequency of a protein-truncating variant (PTV) in Han patients was 34.38% (11/32), while we did not find PTV in patients from ethnic minorities.

**Conclusion**: This study revealed genetic defects in 39 pediatric patients with WD from Yunnan province. Four novel mutations were identified and have enriched the WD database. We characterized the genotypes and phenotypes in different minorities, which will enhance the current knowledge on the population genetics of WD in China.

KEYWORDS
Wilson's disease, pediatric patients, ATP7B, genetic characterization, ethnic minorities

## Introduction

Wilson's disease (WD; OMIM 277900) is an inherited, autosomal recessive copper metabolism disorder that is caused by mutations in the *ATP7B* gene (Cai et al., 2022). The age of onset ranges from eightmonths to 74 years (Ohura et al., 1999; Hahn et al., 2002; Ala et al., 2007; Abuduxikuer et al., 2015). The worldwide prevalence of this disease has been estimated to be approximately 1/100,000 to 3/100,000, whilst it is more prevalent in East Asia, where it is estimated to occur at a prevalence of 1/1,500 to 1/3,000 (Sandahl et al., 2020; Wallace and Dooley, 2020; Li et al., 2022). The carrier frequency of WD is 1/90 and heterozygous mutations are found in up to 2.5% of the general population (Czlonkowska et al., 2018; Sanchez-Monteagudo et al., 2021). Due to the accumulation of copper ions in the body (liver, brain and cornea), typical symptoms of WD include liver function injury, extrapyramidal symptoms, mental symptoms and Kayser-Fleischer rings (K-F ring) (Collins et al., 2021; Shribman et al., 2021). Patients with WD usually present with a variety of clinical subtypes that are characterized by hepatic and/or nervous system manifestations. Due to its various clinical manifestations and the fact that it is one of the few treatable neurogenetic disorders, genetic testing is an important diagnostic tool for this disease (Espinos and Ferenci, 2020). The development of irreversible sequelae can be prevented by timely diagnosis and early interventions in patients with WD (Harada, 2014; Espinos and Ferenci, 2020).

In 1993, the gene that encodes a copper-transporter P-type ATPase (*ATP7B*) was defined as the causative gene of WD. It is composed of 1,465 amino acids that contain a phosphatase domain, a phosphorylation domain, a nucleotide-binding domain, six N-terminal metal binding domains and eight transmembrane ion channels (Telianidis et al., 2013). It is located on chromosome 13q14.3 and contains 21 exons and 20 introns (Tanzi et al., 1993). The protein is used to expel copper ions from the cell and it plays an important role in regulating copper ion metabolism (Tanzi et al, 1993). Worldwide, more than 1,000 different mutations have been identified in the *ATP7B* gene, most of which are missense, non-sense or frameshift mutations (Human Gene Mutation Database, HGMD, http://www.hgmd.cf.ac.uk/ac/index.php). When *ATP7B* mutations lead to the abnormal function of the P-type copper transporter ATPase, the ability of ceruloplasmin to bind and transport copper ions is decreased or removed, which results in the various clinical symptoms of WD (Chen et al., 2015; Ferenci et al., 2019).

To date, several studies have reported the spectrum and frequency of mutations in the *ATP7B* gene in the Chinese WD population. However, genetic profiling in different ethnic groups is still lacking, particularly in pediatric patients with WD. Due to the higher prevalence and more complicated correlation between genotype and phenotype in the Chinese population, when compared with Caucasians (Sanchez-Monteagudo et al., 2020; Couchonnal et al., 2021), it is necessary to study the *ATP7B* profiles of different ethnic groups in China. In this study of WD patients from Yunnan province, we conducted a mutation analysis in 39 patients and their family members and identified four novel mutations in the *ATP7B* gene.

## Materials and methods

### Patients and data collection

Forty-five patients with WD, from 44 families, were recruited between January 2017 and October 2022 at the Children's Hospital Affiliated to Kunming Medical University. The age range of pediatric patients was 0–18 years. The medical history, physical examination results, laboratory test data and imaging results were collected as clinical data. Physical examinations included tests for jaundice, hepatomegaly, K-F rings and neurological symptoms. Laboratory tests included routine blood tests, biochemical liver tests, renal function tests, coagulation function tests, virological tests (hepatitis virus, cytomegalovirus and Epstein-Barr virus), ceruloplasmin and 24-hour urinary copper level. Imaging included liver ultrasound and brain magnetic resonance imaging (MRI). The patients were diagnosed in accordance with their clinical symptoms, biochemical parameters and/or genetic analysis (Czlonkowska et al., 2018). All patients were assessed using the Leipzig score and the total score was ≥4 in every patient. There were two groups used for classifying the patients: Group 1 represented the Han ethnicity and ethnic minorities, while Group 2 represented the general group (patients from general departments) and the severely affected group (patients from the pediatric intensive care unit). Direct sequencing of the *ATP7B* gene was performed in 39 of the 45 patients and their family members. Written informed consent was signed by custodians of the child participants. This study adhered to the Declaration of Helsinki and was approved by the Ethics Committee of the Children's Hospital Affiliated to Kunming Medical University, Kunming, Yunnan, China (No.202303034K01).

### Light and electron microscopy analysis

Liver specimens from patient six were fixed in 10% formalin and embedded in paraffin. The thickness of the paraffin sections was 3 μm and they were stained with hematoxylin and eosin and Masson's trichrome stain. The sections were observed under an Olympus BX53 microscope (Olympus, Tokyo, Japan). The sample for transmission electron microscopy was fixed in 2.5% glutaraldehyde for two hours, then fixed in 1% osmotic acid for one to two hours, dehydrated in acetone and embedded in epoxy resin. Ultrathin sections were sliced and stained with 3% uranyl acetate and lead citrate. The sections were observed under a transmission electron microscope (H7700, Hitachi, Tokyo, Japan).

### DNA extraction and genetic analysis

Peripheral blood was collected from each patient (5 mL) and their parents (2 mL). The blood samples were sent to Beijing Kangso

**TABLE 1 Characteristics of 45 patients with Wilson's disease clinical and laboratory data.**

| Patient characteristics | WD (*n* = 45) | Group 1 | | | Group 2 | | |
|---|---|---|---|---|---|---|---|
| | | Ethnic Han (*n* = 35) | Ethnic minorities (*n* = 10) | *p*-value | General (*n* = 38) | Severe (*n* = 7) | *p*-value |
| General Information | | | | | | | |
| Gender (Male/Female) | 28/17 | 22/13 | 6/4 | 0.869 | 25/13 | 3/4 | 0.25 |
| Age (years) | 7.62 ± 3.46 | 7.60 ± 3.27 | 7.68 ± 4.28 | 0.441 | 7.08 ± 3.17 | 12.33 ± 2.09 | 0.004** |
| Clinical subtypes | | | | | | | |
| Hepatic | 35 (77.78%) | 27 (77.14%) | 8 (80%) | 0.893 | 32 (84.21%) | 3 (42.86%) | 0.031* |
| Neurologic | 1 (2.22%) | 1 (2.86%) | 0 | | 1 (2.63%) | 0 | |
| Mixed | 8 (17.78%) | 6 (11.14%) | 2 (20%) | | 4 (10.53%) | 4 (57.14%) | |
| Others | 1 (2.22%) | 1 (2.86%) | 0 | | 1 (2.63%) | 0 | |
| Affected organs | | | | | | | |
| Liver | 43 (95.56%) | 33 (94.29%) | 10 (100%) | 0.439 | 36 (94.74%) | 7 (100%) | 0.535 |
| Brain | 9 (20%) | 7 (20%) | 2 (20%) | 1.000 | 5 (13.16%) | 4 (57.14%) | 0.008* |
| Eye (K-F ring) | 8 (17.78%) | 7 (20%) | 1 (10%) | 0.466 | 7 (18.42%) | 1 (14.29%) | 0.793 |
| Liver function | | | | | | | |
| ALT (0–40IU/L) | 136 (64–351.5) | 139 (77.75–432.5) | 82 (25–234) | 0.098 | 148 (82–423) | 30 (27–33) | 0.002** |
| AST (0–40IU/L) | 100 (70–231.5) | 98 (71–285.75) | 112 (61–182) | 0.841 | 101.5 (74–281) | 60 (50–104.5) | 0.754 |
| TB (1.71-17.1umol/L) | 12.8 (8.7–27.3) | 11.8 (8.7–18.95) | 17.4 (10.4–69.5) | 0.035* | 11.8 (8.7–17.1) | 343.6 (206.55–345.8) | 0.000** |
| Serum total protein (60–80 g/L) | 62.99 ± 6.65 | 63.27 ± 7.06 | 62.1 ± 5.53 | 0.206 | 63.82 ± 6.06 | 55.77 ± 8.58 | 0.013* |
| Albumin (35–50 g/L) | 37.17 ± 6.42 | 37.81 ± 5.44 | 35.17 ± 9.1 | 0.140 | 38.41 ± 5.3 | 26.47 ± 5.93 | 0.000** |
| Copper related index | | | | | | | |
| Serum ceruloplasmin (200–400 mg/L) | 30 (10–55) | 20 (10–60.75) | 30 (10–40) | 0.324 | 20 (10–40) | 60 (45–75) | 0.094 |
| Urine ketone in 24 h (15–60μg/24 h) | 171.2 (99–445.65) | 156.9 (92.13–441.63) | 179.8 (133.19–987.6) | 0.358 | 156.9 (95.9–296.39) | 2,344.5 (2,326.5–3,172.25) | 0.000** |
| Blood Coagulation Profile | | | | | | | |
| PLT (100–300×10⁹/L) | 258.31 ± 141.45 | 258.41 ± 149.3 | 258 ± 123.95 | 0.417 | 274.81 ± 138.88 | 115.33 ± 69.62 | 0.000** |
| PT (11–14.5s) | 40.2 (31.75–46.4) | 12.65 (12.05–15.02) | 13.2 (11.4–24.5) | 0.206 | 12.5 (11.9–14.4) | 25.6 (24.7–27.35) | 0.000** |
| APTT (28–44.5s) | 40.16 ± 95.01 | 39.85 ± 9.21 | 41.16 ± 12.03 | 0.207 | 38.72 ± 9.18 | 52.17 ± 6.0 | 0.000** |
| FIB (2–4 g/L) | 2.08 ± 0.60 | 2.2 ± 0.59 | 1.71 ± 0.52 | 0.203 | 2.16 ± 0.57 | 1.42 ± 0.47 | 0.000** |
| INR (0.8-1.5) | 1 (0.94–1.42) | 1 (0.95–1.18) | 1.01 (0.92–2.14) | 0.137 | 1 (0.93–1.04) | 2.63 (2.39–2.70) | 0.000** |

Note: K-F, Kayser-Fleischer; ALT, alanine aminotransaminase; AST, aspartic transaminase; TB, total bilirubin; PT, prothrombin time; APTT, activated partial thromboplastin time; FIB, fibrinogen; INR, international normalized ratio; PLT, platelets. General: patients from general departments; Severe: patients from pediatric intensive care unit (PICU). *$p < 0.05$, **$p < 0.01$. "Others" indicates that the function of organs other than the liver and brain is impaired.

Medical Inspection for *ATP7B* genetic testing. The Qiagen FlexiGene DNA kit was used to extract genomic DNA from blood samples. The primers were designed using the Primer Z website (http://genepipe.ncgm.sinica.edu.tw/primerz/primerz4.do). The mutation sites were amplified by PCR and then sequenced by first-generation sequencing. The PCR amplification conditions were: 10 min at 95°C; 35 cycles of 30 s at 95°C, 30 s at 60°C and 45 s at 72°C; followed by 5 min at 72°C. The PCR products were analyzed by electrophoresis on a 1% agarose gel and then sequenced using an ABI PRISM 3730XL DNA automated sequencer (Applied Biosystems; Thermo Fisher Scientific, Inc.).

The mutations identified in this study were compared to the list of reported pathogenic mutations in the Human Gene Mutation Database (https://www.hgmd.cf.ac.uk/ac/index.php), the Wilson Disease Mutation Database (http://www.wilsons-disease.org.uk/) and the gnomAD database (http://gnomad-sg.org/). The pathogenicity of the mutations was evaluated in strict accordance with the American College of Medical Genetics and Genomics (ACMG) Standards and Guidelines (Richards et al., 2015), using Sorting Intolerant From Tolerant (SIFT, http://sift-dna.org), PolyPhen-2 (http://genetics.bwh.harvard.edu/pph2/index.shtml) and Mutation Taster (https://www.mutationtaster.org/). Splice Ai (https://spliceailookup.broadinstitute.org/) was used to evaluate splice sites. The Alpha Fold 2 (Alpha Fold Protein Structure Database, https://alphafold.ebi.ac.uk/) and NetGene2-2.42 (https://mybiosoftware.com/netgene2-2-42-intron-splice-sites-human-c-elegans-a-thaliana-dna.html) sites were used for protein analysis.

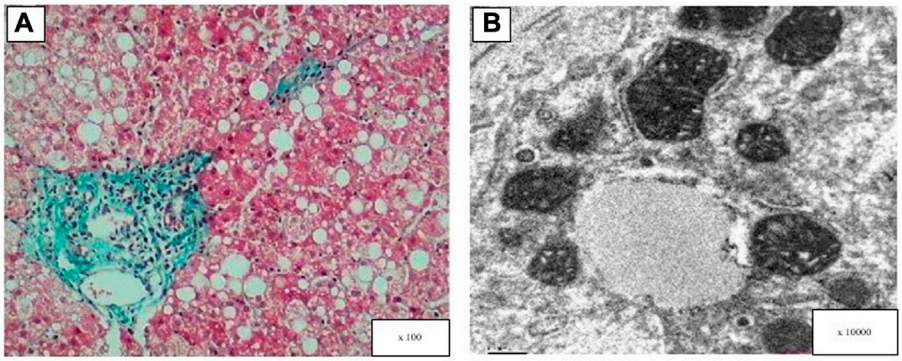


FIGURE 1
Light and electron microscopy analysis of the patient's liver (patient 6). **(A)** Masson's trichrome stain showed hepatic fibrotic lesions, diffuse hepatocellular steatosis (the size of the bubble fat gets mixed, 70%), and a few hepatocytes showed balloon-like. **(B)** Electron microscopy: hepatocyte swelling and variable lipid droplets are seen in diffuse hepatocytes.

## Statistical analysis

Statistical analyses were performed using SPSS version 23. Quantitative data were expressed as the mean ± SD or median and interquartile range (IQR). Categorical variables were given as absolute (number) and relative frequencies (%). To compare quantitative data, the Student's t-test or Mann-Whitney *U* test was used for 2-group comparisons. The $X^2$ test or Fisher's exact test was used to compare categorical variables, as appropriate. The criterion for a significant difference was a *p*-value of less than 0.05.

# Results

## Clinical features and laboratory data for the WD patients

Clinical data and laboratory findings for the WD patients are summarized in Table 1. In this study, we examined 45 pediatric patients with WD, of whom 17 (37.78%) were female and 28 (62.22%) were male. Their mean age of onset was 7.62 ± 3.46 years, with a range of 2.00–13.58 years. Simple elevated transaminases were found in 64.44% (29/45) of patients. The median ceruloplasmin level was 30 mg/L (range: 10–55 mg/L) and the median urine ketone in 24 h level was 171.2 ug (range: 99-445.65 ug). Ten patients, including one each from Bai, Dai, Zhuang, Yi, Hui and Jingpo, were from ethnic minorities, while the majority of patients were Han Chinese. Liver disease was found in 43 (95.56%) individuals and nine (20%) had brain disease. One patient (2.22%) presented with simple neurological symptoms. We found abnormalities in the basal ganglia, thalamus or brainstem in the craniocerebral MRI in seven out of the 45 (15.56%) patients. Eight (17.78%) patients presented with K-F rings. There was no significant difference in age of onset between Han patients and patients from ethnic minorities ($p > 0.05$). Male patients were more prevalent in our overall sample of pediatric patients, regardless of whether they were Han or members of an ethnic minority.

The laboratory data showed that, when compared to Han patients, ethnic minority patients had higher total bilirubin (TB) ($p = 0.035$). We also found that severely affected patients were significantly older at the onset of symptoms than general patients ($p = 0.004$). The severely affected patient group had a higher percentage of individuals with mixed subtype ($p = 0.031$) and symptoms that affected the brain ($p = 0.008$). General patients had increased alanine aminotransaminase (ALT), while severely affected patients had a normal ALT range ($p = 0.002$). Increased TB, prothrombin time (PT), activated partial thromboplastin (APTT), International Normalized Ratio (INR), urine ketone in 24 h and decreased platelets (PLT), serum total protein, albumin and fibrinogen (FIB) were observed in severely affected patients ($p < 0.05$).

Three pediatric patients underwent a liver biopsy during hospitalization. As shown inFigure 1, hepatocyte steatosis, cloudy swelling and ballooning were commonly observed. Glycogenated nuclei were present in hepatocytes and the Masson's trichrome stain showed hepatic fibrotic lesions. Ultrastructural analysis showed pleomorphic dilated mitochondria.

## Characterization of genetic mutations in the *ATP7B* gene

A total of 39 pediatric patients, from 38 unrelated families, were analyzed by direct sequencing. The results are shown in Table 2. Patient 20 and patient 21 were from the same family. Among the 39 patients, 25.64% (10/39) harbored homozygous mutations and 74.36% (29/39) harbored compound heterozygous mutations. Of the patients that harbored compound heterozygous mutations, 75.86% (22/29) had two mutations and 24.14% (7/29) had three mutations (Figure 2A). Interestingly, we observed that the c.2310C > G mutation always accompanied the c.2333G > T mutation (100%), while the c.2333G > T mutation was either a homozygous site or was found with other mutations. In the patients that had three mutations, it was noted that 71.43% (5/7) had the combination of c.2310C > G and c.2333G > T. Phenotype-genotype correlation analysis suggested that, when compared with Han patients, patients from ethnic minorities tended to have homozygous mutations ($p = 0.035$) (Figure 2B).

**TABLE 2 Clinical and genetic data of the 39 patients with WD.**

| Patient | Gender | Ethnic group | Age at presentation(y) | ATP7B genotypes | | |
|---|---|---|---|---|---|---|
| | | | | Patient | Father | Mother |
| 1 | Female | Han | 4.5 | c.1708–5T > G | c.1708–5T > G | c.1708–5T > G |
| 2 | Female | Han | 3.83 | c.2975C > T/ c.1286-1delG | c.2975C > T | **c.1286-1delG** |
| 3 | Male | Han | 3 | c.1708-1G > C/ c.1543+1G > T | c.1708-1G > C | c.1543+1G > T |
| 4 | Male | Han | 5.5 | c.2333G > T/ c.3443T > C | c.3443T > C | c.2333G > T |
| 5 | Male | Han | 12.92 | c.2549C > T/ c.3809A > G | c.3809A > G | c.2549C > T |
| 6 | Male | Han | 3.17 | c.2333G > T/ c.2297C > T/ c.2310C > G | c.2333G > T/c.2310C > G | c.2297C > T |
| 7 | Male | Han | 8.92 | c.2621C > T/ c.3859G > A | c.3859G > A | c.2621C > T |
| 8 | Male | Han | 4.5 | c.2310C > G/ c.2333G > T/ c.2755C > G | c.2755C > G | c.2310C > G/c.2333G > T |
| 9 | Female | Han | 6.58 | c.3443T > C/ c.2310C > G/ c.2333G > T | c.3443T > C | c.2310C > G/c.2333G > T |
| 10 | Male | Han | 7.58 | c.2333G > T/ c.4112T > C | c.2333G > T | c.4112T > C |
| 11 | Female | Han | 7.25 | c.2120A > G | — | c.2120A > G |
| 12 | Male | Han | 8.58 | c.2333G > A/ c.2668G > A | c.2668G > A | c.2333G > A |
| 13 | Male | Han | 7.75 | c.2212_2213del AGinsCA/ c.2333G > T | — | — |
| 14 | Male | Han | 4 | c.2294A > G/ c.3089G > A | — | — |
| 15 | Female | Han | 13.58 | c.3809A > G/ c.3818C > A | — | — |
| 16 | Female | Han | 9 | c.2975C > T/ c.2333G > T | — | c.2333G > T |
| 17 | Male | Han | 3 | c.2621C > T/ c.2570_2572del | c.2621C > T | **c.2570_2572del** |
| 18 | Male | Han | 4 | c.2668G > A/ c.2333G > T/ c.2310C > G | c.2333G > T/c.2310C > G | c.2668G > A |
| 19 | Male | Han | 4.5 | c.2621C > T | c.2621C > T | c.2621C > T |
| 20 | Male | Han | 10.5 | c.3993T > G/ c.2804C > T | c.3993T > G | c.2804C > T |
| 21 | Female | Han | 5.58 | c.3993T > G/ c.2804C > T | c.3993T > G | c.2804C > T |
| 22 | Male | Han | 5 | c.2333G > T/ c.2310C > G | c.2310C > G | c.2333G > T |
| 23 | Male | Han | 11.42 | c.2333G > T | c.2333G > T | c.2333G > T |
| 24 | Female | Han | 5.92 | c.2662A > C | c.2662A > C | c.2662A > C |

(Continued on following page)

**TABLE 2 (*Continued*) Clinical and genetic data of the 39 patients with WD.**

| Patient | Gender | Ethnic group | Age at presentation(y) | ATP7B genotypes | | |
|---|---|---|---|---|---|---|
| | | | | Patient | Father | Mother |
| 25 | Female | Han | 6.17 | c.2975C > T/ c.2332C > T | c.2975C > T | c.2332C > T |
| 26 | Male | Han | 2 | c.3742A > G/ c.2304dupC | c.2304dupC | **c.3742A > G** |
| 27 | Male | Han | 9.92 | c.2145C > A/ c.2299C > T | c.2299C > T | c.2145C > A |
| 28 | Female | Han | 9.92 | c.2621C > T | not found | c.2621C > T |
| 29 | Male | Han | 9 | c.1870–8A > G/ c.2804C > T | c.2804C > T | c.1870–8A > G |
| 30 | Male | Han | 3 | c.3532A > G/ c.1869 + 20A > G/ c.2121+3A > G | **c.1869 + 20A > G** /c.2121+3A > G | c.3532A > G |
| 31 | Female | Han | 8.25 | c.2333G > T/ c.1369C > T/ c.2310C > G | c.2333G > T/c.2310C > G | c.1369C > T |
| 32 | Male | Han | 3.33 | c.2975C > T/ c.2662A > C | c.2662A > C | c.2975C > T |
| 33 | Male | Bai | 3 | c.2785A > G/ c.2906G > A/ c.3809A > G | — | c.2785A > G/c.2906 G > A |
| 34 | Male | Zhuang | 10.17 | c.3079G > C | c.3079G > C | c.3079G > C |
| 35 | Female | Yi | 10.58 | c.2228A > G/ c.3932T > A | c.3932T > A | c.2228A > G |
| 36 | Male | Dai | 13.5 | c.3079G > C | c.3079G > C | c.3079G > C |
| 37 | Female | Dai | 7.33 | c.4112T > C | c.4112T > C | c.4112T > C |
| 38 | Male | Bai | 3.42 | c.3809A > G/ c.2333G > T | c.2333G > T | c.3809A > G |
| 39 | Male | Jingpo | 12 | c.3932T > A | c.3932T > A | — |

Note: Novel mutations are highlighted in bold. Gene reference sequence: GRch38, NM_000053.4; Protein reference sequence:NP_000044.2.

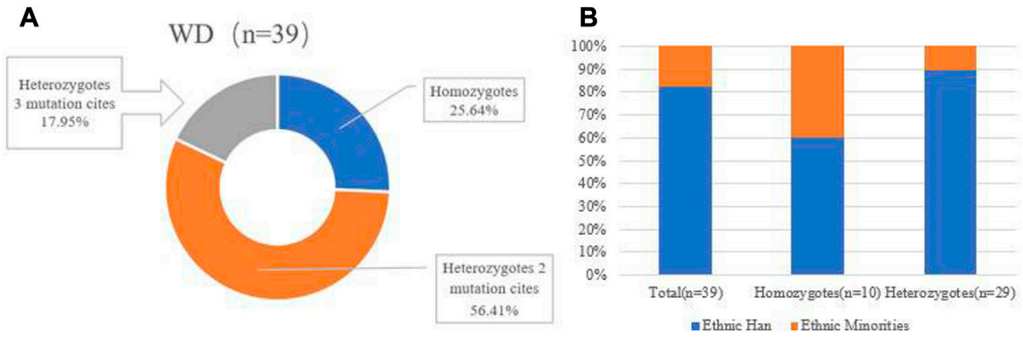


FIGURE 2
**(A)** Distribution of genotype in total patients with WD. **(B)** Distribution of genotype in patients from different ethnic groups ($p$ = 0.035).

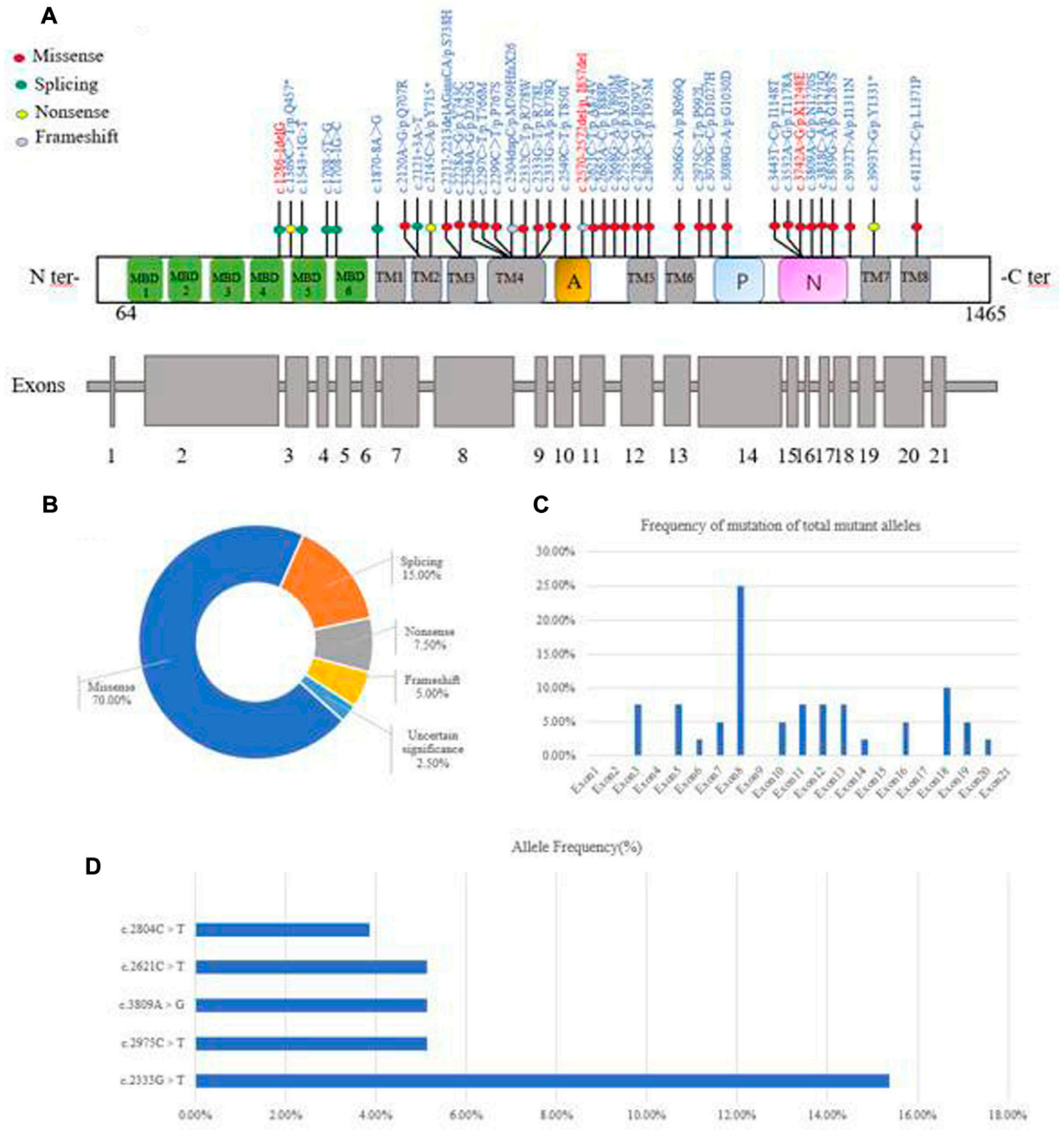


FIGURE 3
Characterization of genetic mutations in the *ATP7B* gene. **(A)** Novel mutations were observed. **(B)** Various mutants identified in this study and their percentage. **(C)** The frequency of mutations found in the 39 WD patients is given per exon as a percentage of the total mutant alleles. **(D)** Allele frequency of common *ATP7B* mutations in Yunnan province. MBDs, metal binding domains; Transmembrane segments are numbered TM1 to TM8; A: actuator domain; *p*: phosphorylation domain; N: nucleotide-binding domain.

In 39 patients with WD, 39 potential pathogenic *ATP7B* mutations, one known polymorphism (c.2310C > G) that does not disrupt gene function and one mutation of uncertain significance (c.1869 + 20A > G) were identified (Figure 3A). Four of the mutations were novel (c.1286-1delG, c.1869 + 20A > G, c.2570_2572del and c.3742A > G). The mutations consisted of 28 (70%) missense mutations, six (15%) splice-site mutations, three (7.5%) non-sense mutations, two (5%) frameshift mutations and one (2.5%) mutation of uncertain significance (Figure 3B). The mutations were distributed in all exons apart from exons 1, 2, 4, 9, 15, 17 and 21. We found that exon 8 (26.83%) had the highest frequency of mutations, followed by exon 18 (9.76%), exon 3 (7.32%), exon 11 (7.32%), exon 12 (7.32%) and exon 13 (7.32%). This suggested that these exons may be more susceptible to mutations that cause WD in Yunnan province (Figure 3C). The most frequent mutation was c.2333G > T (p.R778L, allelic frequency: 15.38%), followed by c.2975C > T (p.P992L, 5.26%), c.2621C > T (p.A874V,

**TABLE 3 The potential pathogenic *ATP7B* mutations.**

| Number | Loci | Nucleotide | rs ID | MAF | Allelic count |
|---|---|---|---|---|---|
| 1 | Exon3 | **c.1286-1delG** | chr13:52544885-52544886delG | — | 1/78 |
| 2 | Exon3 | c.1369C > T | rs1951795080 | 0.0000 | 1/78 |
| 3 | Exon3 | c.1543+1G > T | rs1360279134 | 0.00002 | 1/78 |
| 4 | Exon5 | c.1708–5T > G | rs770829226 | 0.0003 | 1/78 |
| 5 | Exon5 | c.1708-1G > C | rs137853280 | 0.0003 | 1/78 |
| 6 | Exon5 | **c.1869 + 20A > G** | chr13:52538988A>G | — | 1/78 |
| 7 | Exon6 | c.1870–8A > G | chr13:52536057A>G | — | 1/78 |
| 8 | Exon7 | c.2120A > G | chr13:52534285A>G | — | 1/78 |
| 9 | Exon7 | c.2121+3A > T | rs1248002612 | 0.0000 | 1/78 |
| 10 | Exon8 | c.2145C > A | rs751202110 | 0.0000 | 1/78 |
| 11 | Exon8 | c.2212_2213delAGinsCA | chr13:52534293delAGinsCA | — | 1/78 |
| 12 | Exon8 | c.2228A > G | chr13:52532574A>G | — | 1/78 |
| 13 | Exon8 | c.2294A > G | chr13:52523826A>G | — | 1/78 |
| 14 | Exon8 | c.2297C > T | rs121907997 | 0.0006 | 1/78 |
| 15 | Exon8 | c.2299C > T | rs2139531503 | — | 1/78 |
| 16 | Exon8 | c.2304dupC | chr13:52532499dupC | — | 1/78 |
| 17 | Exon8 | c.2332C > T | rs137853284 | 0.0000 | 1/78 |
| 18 | Exon8 | c.2333G > T/A | rs28942074 | 0.0019 | 13/78 |
| 19 | Exon10 | c.2549C > T | rs777629392 | 0.0003 | 1/78 |
| 20 | Exon10 | **c.2570_2572del** | chr13:52524411–52524413 del TCA | — | 1/78 |
| 21 | Exon11 | c.2621C > T | rs121907994 | 0.0000 | 4/78 |
| 22 | Exon11 | c.2662A > C | rs1455758826 | 0.0000 | 2/78 |
| 23 | Exon11 | c.2668G > A | rs786204718 | 0.0000 | 1/78 |
| 24 | Exon12 | c.2755C > G | rs121907993 | 0.0000 | 1/78 |
| 25 | Exon12 | c.2785A > G | rs534960245 | 0.0166 | 1/78 |
| 26 | Exon12 | c.2804C > T | rs750019452 | 0.0003 | 3/78 |
| 27 | Exon13 | c.2906G > A | rs121907996 | 0.0000 | 1/78 |
| 28 | Exon13 | c.2975C > T | rs201038679 | 0.0006 | 4/78 |
| 29 | Exon13 | c.3079G > C | rs1593672840 | — | 2/78 |
| 30 | Exon14 | c.3089G > A | chr13:52520548G>A | — | 1/78 |
| 31 | Exon16 | c.3443T > C | rs60431989 | 0.0000 | 2/78 |
| 32 | Exon16 | c.3532A > G | rs1387431334 | 0.0000 | 1/78 |
| 33 | Exon18 | **c.3742A > G** | chr13:52513301A>G | — | 1/78 |
| 34 | Exon18 | c.3809A > G | rs121907990 | 0.0000 | 4/78 |
| 35 | Exon18 | c.3818C > A | rs758355520 | 0.0000 | 1/78 |
| 36 | Exon18 | c.3859G > A | rs762866453 | 0.0000 | 1/78 |
| 37 | Exon19 | c.3932T > A | chr13:52511501T>A | — | 2/78 |
| 38 | Exon19 | c.3993T > G | chr13:52511440T>G | — | 2/78 |

(Continued on following page)

**TABLE 3 (*Continued*) The potential pathogenic *ATP7B* mutations.**

| Number | Loci | Nucleotide | rs ID | MAF | Allelic count |
|---|---|---|---|---|---|
| 39 | Exon20 | c.4112T > C | rs1444841250 | 0.0000 | 2/78 |

Note: MAF, Minor Allele frequency in genomAD from East Asian. Novel mutations are highlighted in bold.

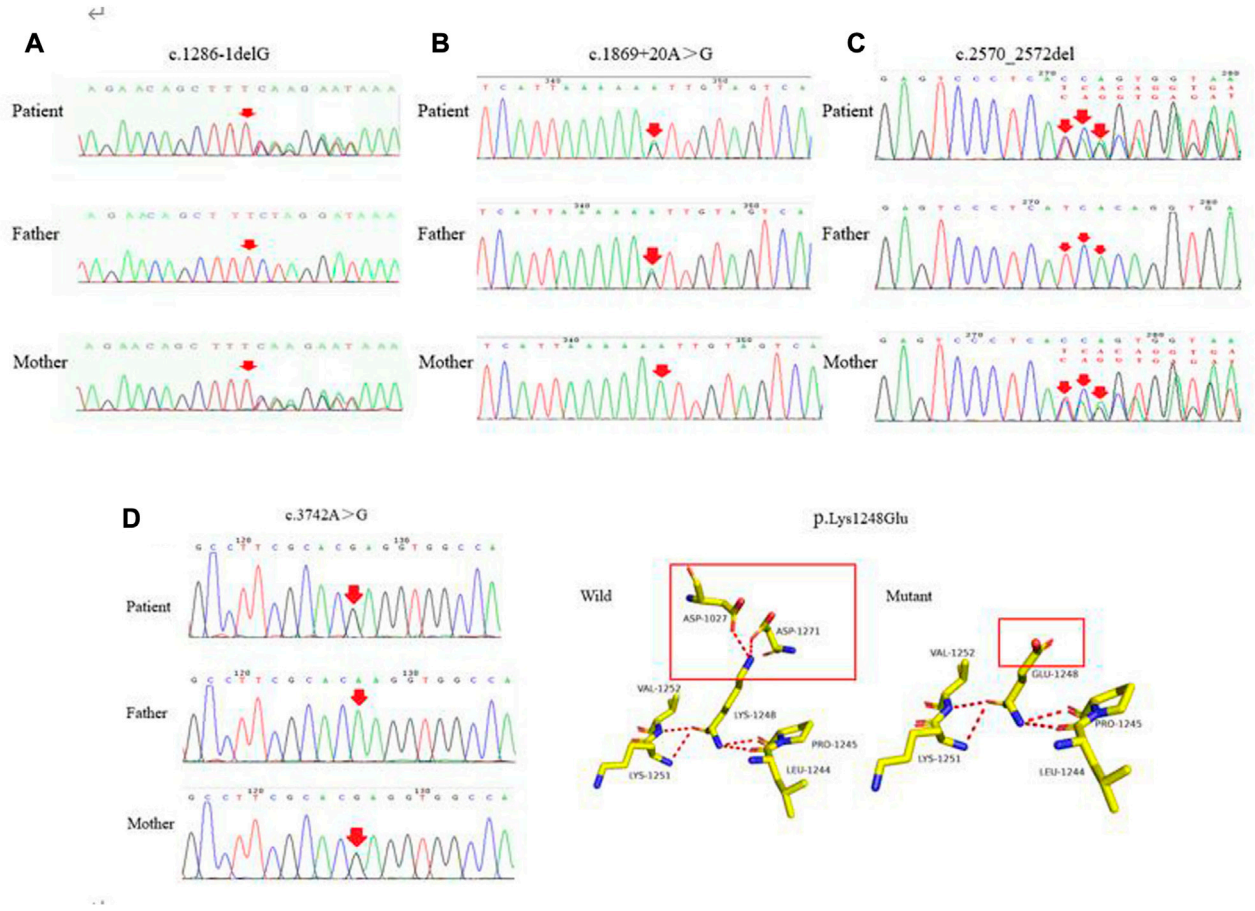


FIGURE 4
**(A–C)** represent the novel mutations (c.1286-1delG, c.1869 + 20A > G, c.2570_2572del), respectively. **(D)** c.3742A > G was detected in the patient and his mother. As shown in the structure of *ATP7B* protein, each color represents different atoms, yellow - C atom, gray - H atoms, blue - N atoms, red - O atoms, orange - S atom, the red dotted line for the hydrogen bond. The red rectangles represent areas of change.

5.13%), c.3809A > G (p.N1270S, 5.13%) and c.2804C > T (p.T935M, 3.85%) (Figure 3D). The allelic frequency of c.2333G > T and c.2975C > T showed the same trend, in terms of the Minor allele frequency in genomAD from East Asian (Minor allele frequency in genomAD from East Asian). The allelic frequency of c.2621C > T and c.3809A > G was 5.13% (4/78), while the MAF was 0.0000. We also found that the allelic frequency c.2785A > G was 1.28% (1/78), which was not consistent with the MAF (0.0166) (Table 3).

## Characterization of novel mutations

The four novel mutations found in the pediatric patients with WD included one splice-site mutation, one missense mutation, one frameshift mutation and one mutation of uncertain significance. As shown in Figure 4A, the novel c.1286-1delG mutation was identified in the *ATP7B* gene of a patient and her mother. Using Splice Ai, we predicted the impact of the mutation on the protein. The NetGene2-2.42 site was used to predict that c.1286-1delG would cause a shift in the splice-site. We also identified the novel c.1869 + 20A > G mutation in a patient and his mother, as shown in Figure 4B. Splice Ai predicted that this mutation would not impact the splice-site. As shown in Figure 4C, the novel c.2570_2572del mutation was detected in a patient and his mother. Figure 4D shows the c.3742A > G mutation that was detected in another patient and his mother. The SIFT, PolyPhen-2 and Mutation Taster programs were used to predict the functional damage to the protein, caused by the mutations. The mutations shown in Figures 4B–D were classed

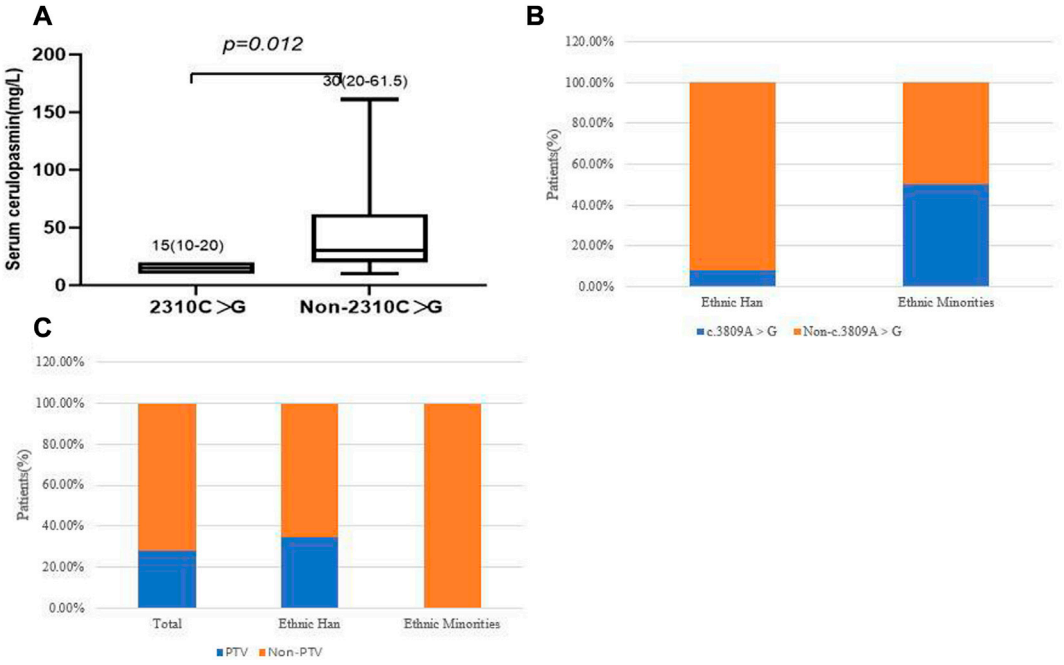


FIGURE 5
**(A)** Correlation of c.2310C > G and serum ceruloplasmin level. **(B)** correlation of c.3809A > G and ethnic groups. **(C)** The frequency of PTV in different ethnic groups.

as "Deleterious," "Probably damaging" and "disease causing," respectively. The structural analysis showed that the c.3742A > G (p.K1248E) mutation leads to the loss of the hydrogen bond between amino acids 1,027 and 1,271, which may affect the protein configuration (Figure 4D)

In conclusion, in accordance with the ACMG Standards and Guidelines, c.1286-1delG was considered to be a "pathogenic variant," c.2570_2572del and c.3742A > G were considered to be "likely pathogenic variants," while c.1869 + 20A > G was classified as a "variant with uncertain significance." Further studies are needed to confirm the changes predicted by the *in silico* tools.

## Correlation between genotype and phenotype

To describe the correlation between the genotype and phenotype, we first studied the association between the exons and clinical subtypes in Yunnan province. The exons that were hotspots were examined in the 39 WD patients. The results showed that exons 8 and 18 harbored the highest percentage of mutations, which was not consistent with previous results that exons 8, 13 and 16 were the hotpot exons in the Chinese population (Li et al., 2021). This result may be due to the differences between Han individuals and ethnic minorities.

We then focused on the correlation between specific mutations and phenotypes. The most prevalent mutations were examined in the 39 WD patients. There was no significant difference, in terms of age of onset, between different clinical subtypes and several common mutations (c.2333G > T, c.2975C > T, c.2621C > T and c.3809A > G), in the different ethnic groups ($p > 0.05$). The results showed that the two most frequent variants were c.2333G > T (p.R778L) and c.2975C > T (p.P992L). We observed that the patients who carried the c.2310C > G mutation had lower serum ceruloplasmin levels than patients with other mutations ($p = 0.012$, Figure 5A). In patients who harbored compound heterozygous mutations, those from ethnic minorities tended to carry c.3809A > G ($p = 0.042$, Figure 5B). We also analyzed the relationship between the phenotypes and PTV (protein-truncated variants, e.g., frameshift, non-sense and splice-sites). The frequency of PTV in patients from Yunnan province was 28.2% (11/39). Interestingly, we found that the frequency of PTV in Han patients was 34.38% (11/32), while we did not find any PTV in patients from ethnic minorities (Figure 5C). Among the patients with PTV, 90.91% (10/11) presented with elevated transaminases and the p.T935M/PTV genotype had a frequency of 27.27% (3/11).

# Discussion

To define the mutation spectrum, clinical characteristics and genotype-phenotype correlations in WD in various ethnic groups, we examined *ATP7B* mutations in 39 pediatric patients from Yunnan province. Patients from seven ethnic groups (Han, Bai, Dai, Zhuang, Yi, Hui and Jingpo) from China were involved in this study. Patients with neurologic

symptoms were not predominant in our cohort, in contrast to previous studies in China (Dong et al., 2021; Zhang et al., 2022). This may be because patients with neurologic symptoms mainly present during adolescence. However, male pediatric patients were predominant in our study, which is consistent with some studies in China and Korea (Cheng et al., 2017; Seo et al., 2018; Zhang et al., 2022). Most Han patients presented with elevated transaminases, while only three out of 10 patients from ethnic minorities presented with elevated transaminases. Three out of the six severely affected patients were from ethnic minorities. Several studies have shown that clinically asymptomatic patients have an earlier age of onset than patients with typical clinical manifestations (Li et al., 2021; Zhang et al., 2022). In our study, most pediatric patients presented with abnormal liver enzymes, without symptoms. We also found that pediatric patients from ethnic minorities had more severe disease.

This study identified homozygous mutations in 10 pedigrees and compound heterozygous mutations in 29 pedigrees. The frequency of homozygous mutations was 25.64% (10/39), which is not consistent with the frequency of 15.67% (204/1,302) that was observed in a previous study (Zhang et al., 2022). Moreover, phenotype-genotype correlation analysis suggested that, when compared with Han patients, patients from ethnic minorities tend to have homozygous mutations. This may indicate the significant genetic characteristics of patients from ethnic minorities from China. Of the patients who had compound heterozygous mutations, seven had three mutations. We observed that the c.2310C > G mutation always accompanied the c.2333G > T mutation, which is consistent with a previous study (AL). The c.2333G > T mutation was found as a homozygous site and also accompanied other mutations. It is possible that the coexistence of c.2333G > T and c.2310C > G may affect the function of the protein in a specific way. Hence, it is necessary to further explore the functional implications of both mutations.

Forty potential pathogenic mutations were identified in this study. Thirty-six of these have already been reported as disease-causing mutations in the Wilson Disease Mutation Database. The other four mutations were novel and evidence indicated that c.1286-1delG is considered to be a "pathogenic variant," c.2570_2572del and c.3742A > G are considered to be "likely pathogenic variants," while c.1869 + 20A > G needs further functional analysis and is classified as a "variant with uncertain significance." In the patients who carried three mutations, it was noted that 71.43% had the c.2310C > G mutation, whilst the accompanying two pathogenic mutations had previously been reported. The novel c.1869 + 20A > G mutation co-occurred with two other reported pathogenic mutations (c.3532A > G and c.2121+3A > G) and its pathogenicity should be explored further.

The top five most common mutations in our study were c.2333G > T (p.R778L), c.2975C > T (p.P992L), c.2621C > T (p.A874V), c.3809A > G (p.N1270S) and c.2804C > T (p.T935M), which is not consistent with other reported studies (p.R778L, p.P992L, p.A874V, p.R919G and p.V1216M) (Li et al., 2021). Mutation hotspots in *ATP7B* vary by geographic region, with a higher prevalence of specific mutations reported in certain populations (Wallace and Dooley, 2020). The predominant mutations in the Chinese population include c.2333G > T (p.R778L), c.2975C > T (p.P992L), c.3443T > C (p.I1148T) and c.2804C > T (p.T935M). In contrast, the most common mutation in European populations is p.H1069Q (Wang et al., 2011; Wei et al., 2014). Chinese populations from different regions also have different mutation types. Although p.R778L was always detected as the most common pathogenic mutation, a study of populations in Northern China found that p.A874V was the second most common pathogenic mutation, whilst p.I1148T was the second most common mutation found in Guangdong province, Southern China (Li et al., 2013; Wei et al., 2014). Another study found that in pediatric patients from Southern China, p.R778L and p.I1148T had the highest frequencies, at approximately 23.0% and 10.7%, respectively. This is not consistent with our study (Zhou et al., 2022). A previous study found that p.T935M was significantly associated with Fujian province, which hints at the possibility of a founder effect (Wei et al., 2014). In our study, p.T935M was found in Yunnan province. The gnomAD database also shows a low frequency of p.T935M in the East Asian population, which does not support the previous hypothesis of a founder effect. Due to the vast diversity of mutations in the *ATP7B* gene, analysis of the regional distribution of mutations can help to develop time-saving approaches and speed up the genetic diagnosis of WD in specific regions (Roy et al., 2020).

The overall genetic diagnosis rate in this study was 97.5% (39/40). Previous studies gave 78.4% in Caucasians, by exon-by-exon sequencing, and 87.9% in Poland, by whole-exome sequencing (Ferenci et al., 2019; Kluska et al., 2019). In China, one study showed that the genetic diagnosis rate was 90.0%, by sequencing of the 5' untranslated region (UTR), 21 exons and their flanking regions (Dong et al., 2016). Another study estimated that the genetic diagnosis rate was 97.1%, by mutational analysis of 68 WD patients from China (AL). The reason that not all patients are genetically diagnosed may be related to a large hemizygous deletion, regulatory region variants and genetic alterations outside of the *ATP7B* gene (Dong et al., 2016; Ferenci et al., 2019).

We did not find a significant difference in terms of age of onset between different clinical subtypes and several common mutations (c.2333G > T, c.2975C > T, c.2621C > T and c.3809A > G) in different ethnic groups ($p > 0.05$). This may have been due to the small sample size. Therefore, the sample size in Yunnan province should be expanded further to study these correlations.

We also analyzed the relationship between phenotypes and PTV. The frequency of PTV in patients from Yunnan province was 28.2% (11/39), which is consistent with the previous finding that the frequency of PTV was 26.5% (345/1,302) in a large cohort of patients with WD (Zhang et al., 2022). Interestingly, we found that the frequency of PTV in Han patients was 34.38% (11/32), while we did not find PTV in patients from ethnic minorities. Among the patients with PTV, 90.91% (10/11) presented with elevated transaminases and a specific genotype (p.T935M/PTV) had a frequency of 27.27% (3/11). Previous studies have found that truncating variants are associated with an early onset of WD (Gromadzka et al., 2005; Merle et al., 2010). Recently, one study found that PTV was more common in patients with a younger age of onset in both the hepatic and neurological groups (Zhang et al., 2022). There has been no research into the role of PTV in different

ethnic groups. However, our findings revealed that PTV are not common in ethnic minority patients.

## Conclusion

In this study, we performed mutation analysis of the *ATP7B* gene in 39 WD patients from Yunnan province. In summary, our study identified four novel mutations that expand the spectrum of pathogenic *ATP7B* mutations. In addition, phenotype-genotype correlation analysis suggested that, when compared with Han patients, patients from ethnic minorities tend to carry homozygous mutations. We observed that the patients who carried the c.2310C > G mutation had lower serum ceruloplasmin levels than patients with other mutations. In patients with heterozygous mutations, the c.3809A > G mutation was significantly associated with ethnic minorities. The frequency of PTV in patients from ethnic minorities was lower than in Han patients. Our research highlights the differences in genotypes of WD pediatric patients from different ethnic groups. This may provide valuable insights into the diagnosis, counseling and treatment of WD pediatric patients in China.

## Data availability statement

The original contributions presented in the study are included in the article/supplementary materials, further inquiries can be directed to the corresponding authors.

## Ethics statement

The studies involving human participants were reviewed and approved by the Ethics Committee of the Children's Hospital Affiliated to Kunming Medical University. Written informed consent to participate in this study was provided by the participants' legal guardian/next of kin.

## Author contributions

YW designed the research study and drafted the manuscript. JF, BL, and CL performed the research and analysis. JH, CL, and YY performed routine examinations and assessments. SL and LT performed the validation. LL, and SX supervised the study and edited the manuscript.

## Funding

The work was supported by the National Natural Science Foundation of China (No. 82160367), the Joint Special Fund for Basic Research from Yunnan Provincial Science and Technology Department and Kunming Medical University (No. 202001AY070001-269), Yunnan Provincial Key specialty (Critical Care Medicine Department) construction project, the Sixth Cycle Key Discipline of Kunming (Critical Care Medicine Department) and Kunming high-level talents Training Special Project- Spring City famous doctor Special project.

## Conflict of interest

The authors declare that the research was conducted in the absence of any commercial or financial relationships that could be construed as a potential conflict of interest.

## Publisher's note



## References

Abuduxikuer, K., Li, L. T., Qiu, Y. L., Wang, N. L., and Wang, J. S. (2015). Wilson disease with hepatic presentation in an eight-month-old boy. *World J. Gastroenterol.* 21, 8981–8984. doi:10.3748/wjg.v21.i29.8981

Ala, A., Walker, A. P., Ashkan, K., Dooley, J. S., and Schilsky, M. L. (2007). Wilson's disease. *Lancet* 369, 397–408. doi:10.1016/S0140-6736(07)60196-2

Cai, H., Cheng, X., and Wang, X. P. (2022). ATP7B gene therapy of autologous reprogrammed hepatocytes alleviates copper accumulation in a mouse model of Wilson's disease. *Hepatology* 76, 1046–1057. doi:10.1002/hep.32484

Cater, M. A., La Fontaine, S., and Mercer, J. F. B. (2007). Copper binding to the N-terminal metal-binding sites or the CPC motif is not essential for copper-induced trafficking of the human Wilson protein (ATP7B). *Biochem. J.* 401, 143–153. doi:10.1042/BJ20061055

Chen, C., Shen, B., Xiao, J.-J., Wu, R., Duff Canning, S. J., and Wang, X. P. (2015). Currently clinical views on genetics of Wilson's disease. *Chin. Med. J.* 128, 1826–1830. doi:10.4103/0366-6999.159361

Cheng, N., Wang, H., Wu, W., Yang, R., Liu, L., Han, Y., et al. (2017). Spectrum of ATP7B mutations and genotype-phenotype correlation in large-scale Chinese patients with Wilson Disease. *Clin. Genet.* 92, 69–79. doi:10.1111/cge.12951

Collins, C. J., Yi, F., Dayuha, R., Duong, P., Horslen, S., Camarata, M., et al. (2021). Direct measurement of ATP7B peptides is highly effective in the diagnosis of Wilson disease. *Gastroenterology* 160, 2367–2382.e1. doi:10.1053/j.gastro.2021.02.052

Couchonnal, E., Lion-Francois, L., Guillaud, O., Habes, D., Debray, D., Lamireau, T., et al. (2021). Pediatric Wilson's disease: Phenotypic, genetic characterization and outcome of 182 children in France. *J. Pediatr. Gastroenterol. Nutr.* 73, e80–e86. doi:10.1097/MPG.0000000000003196

Czlonkowska, A., Litwin, T., Dusek, P., Ferenci, P., Lutsenko, S., Medici, V., et al. (2018). Wilson disease. *Nat. Rev. Dis. Prim.* 4, 21. doi:10.1038/s41572-018-0018-3

Dong, Y., Ni, W., Chen, W. J., Wan, B., Zhao, G. X., Shi, Z. Q., et al. (2016). Spectrum and classification of ATP7B variants in a large cohort of Chinese patients with Wilson's disease guides genetic diagnosis. *Theranostics* 6, 638–649. doi:10.7150/thno.14596

Dong, Y., Wang, R.-M., Yang, G.-M., Yu, H., Xu, W.-Q., Xie, J. J., et al. (2021). Role for biochemical assays and kayser-fleischer rings in diagnosis of Wilson's disease. *Clin. Gastroenterology Hepatology* 19, 590–596. doi:10.1016/j.cgh.2020.05.044

Espinos, C., and Ferenci, P. (2020). Are the new genetic tools for diagnosis of Wilson disease helpful in clinical practice? *JHEP Rep.* 2, 100114. doi:10.1016/j.jhepr.2020.100114

Ferenci, P., Stremmel, W., Czlonkowska, A., Szalay, F., Viveiros, A., Stattermayer, A. F., et al. (2019). Age and sex but not ATP7B genotype effectively influence the clinical phenotype of Wilson disease. *Hepatology* 69, 1464–1476. doi:10.1002/hep.30280

Gromadzka, G., Schmidt, H. H., Genschel, J., Bochow, B., Rodo, M., Tarnacka, B., et al. (2005). Frameshift and nonsense mutations in the gene for ATPase7B are associated with severe impairment of copper metabolism and with an early clinical manifestation of Wilson's disease. *Clin. Genet.* 68, 524–532. doi:10.1111/j.1399-0004.2005.00528.x

Hahn, S. H., Lee, S. Y., Jang, Y.-J., Kim, S. N., Shin, H. C., Park, S. Y., et al. (2002). Pilot study of mass screening for Wilson's disease in Korea. *Mol. Genet. metabolism* 76, 133–136. doi:10.1016/s1096-7192(02)00026-4

Harada, M. (2014). Pathogenesis and management of Wilson disease. *Hepatology Res. official J. Jpn. Soc. Hepatology* 44, 395–402. doi:10.1111/hepr.12301

Kluska, A., Kulecka, M., Litwin, T., Dziezyc, K., Balabas, A., Piatkowska, M., et al. (2019). Whole-exome sequencing identifies novel pathogenic variants across the ATP7B gene and some modifiers of Wilson's disease phenotype. *Liver Int.* 39, 177–186. doi:10.1111/liv.13967

Li, K., Zhang, W. M., Lin, S., Wen, L., Wang, Z. F., Xie, D., et al. (2013). Mutational analysis of ATP7B in north Chinese patients with Wilson disease. *J. Hum. Genet.* 58, 67–72. doi:10.1038/jhg.2012.134

Li, M., Ma, J., Wang, W., Yang, X., and Luo, K. (2021). Mutation analysis of the ATP7B gene and genotype-phenotype correlation in Chinese patients with Wilson disease. *BMC Gastroenterol.* 21, 339. doi:10.1186/s12876-021-01911-5

Li, W. J., Chen, H. L., Wang, B., Yao, L., and Wang, X. P. (2022). Wilson's disease: Food therapy out of trace elements. *Front. Cell Dev. Biol.* 10, 1091580. doi:10.3389/fcell.2022.1091580

Merle, U., Weiss, K. H., Eisenbach, C., Tuma, S., Ferenci, P., and Stremmel, W. (2010). Truncating mutations in the Wilson disease gene ATP7B are associated with very low serum ceruloplasmin oxidase activity and an early onset of Wilson disease. *BMC Gastroenterol.* 10, 8. doi:10.1186/1471-230X-10-8

Ohura, T., Abukawa, D., Shiraishi, H., Yamaguchi, A., Arashima, S., Hiyamuta, S., et al. (1999). Pilot study of screening for Wilson disease using dried blood spots obtained from children seen at outpatient clinics. *J. Inherit. metabolic Dis.* 22, 74–80. doi:10.1023/a:1005455401076

Richards, S., Aziz, N., Bale, S., Bick, D., Das, S., Gastier-Foster, J., et al. (2015). Standards and guidelines for the interpretation of sequence variants: A joint consensus recommendation of the American College of medical genetics and genomics and the association for molecular pathology. *Genet. Med.* 17, 405–424. doi:10.1038/gim.2015.30

Roy, S., McCann, C. J., Ralle, M., Ray, K., Ray, J., Lutsenko, S., et al. (2020). Analysis of Wilson disease mutations revealed that interactions between different ATP7B mutants modify their properties. *Sci. Rep.* 10, 13487. doi:10.1038/s41598-020-70366-7

Rui, H., Fang, H., Yonggeng, J., Yu, P., Xu, Y., Shanshan, P., et al. (2016). Mutational analysis of ATP7B in Chinese Wilson disease patients. *Am. J. Transl. Res.* 8 (6), 2851–2861.

Sanchez-Monteagudo, A., Alvarez-Sauco, M., Sastre, I., Martinez-Torres, I., Lupo, V., Berenguer, M., et al. (2020). Genetics of Wilson disease and Wilson-like phenotype in a clinical series from eastern Spain. *Clin. Genet.* 97, 758–763. doi:10.1111/cge.13719

Sanchez-Monteagudo, A., Ripolles, E., Berenguer, M., and Espinos, C. (2021). Wilson's disease: Facing the challenge of diagnosing a rare disease. *Biomedicines* 9, 1100. doi:10.3390/biomedicines9091100

Sandahl, T. D., Laursen, T. L., Munk, D. E., Vilstrup, H., Weiss, K. H., and Ott, P. (2020). The prevalence of Wilson's disease: An update. *Hepatology* 71, 722–732. doi:10.1002/hep.30911

Seo, G. H., Kim, Y.-M., Oh, S. H., Chung, S. J., Choi, I. H., Kim, G. H., et al. (2018). Biochemical and molecular characterisation of neurological Wilson disease. *J. Med. Genet.* 55, 587–593. doi:10.1136/jmedgenet-2017-105214

Shribman, S., Poujois, A., Bandmann, O., Czlonkowska, A., and Warner, T. T. (2021). Wilson's disease: Update on pathogenesis, biomarkers and treatments. *J. Neurol. Neurosurg. Psychiatry* 92, 1053–1061. doi:10.1136/jnnp-2021-326123

Tanzi, R. E., Petrukhin, K., Chernov, I., Pellequer, J. L., Wasco, W., Ross, B., et al. (1993). The Wilson disease gene is a copper transporting ATPase with homology to the Menkes disease gene. *Nat. Genet.* 5, 344–350. doi:10.1038/ng1293-344

Telianidis, J., Hung, Y. H., Materia, S., and Fontaine, S. L. (2013). Role of the P-Type ATPases, ATP7A and ATP7B in brain copper homeostasis. *Front. Aging Neurosci.* 5, 44. doi:10.3389/fnagi.2013.00044

Wallace, D. F., and Dooley, J. S. (2020). ATP7B variant penetrance explains differences between genetic and clinical prevalence estimates for Wilson disease. *Hum. Genet.* 139, 1065–1075. doi:10.1007/s00439-020-02161-3

Wang, L. H., Huang, Y. Q., Shang, X., Su, Q. X., Xiong, F., Yu, Q. Y., et al. (2011). Mutation analysis of 73 southern Chinese Wilson's disease patients: Identification of 10 novel mutations and its clinical correlation. *J. Hum. Genet.* 56, 660–665. doi:10.1038/jhg.2011.76

Wei, Z., Huang, Y., Liu, A., Diao, S., Yu, Q., Peng, Z., et al. (2014). Mutational characterization of ATP7B gene in 103 Wilson's disease patients from southern China: Identification of three novel mutations. *Neuroreport* 25, 1075–1080. doi:10.1097/WNR.0000000000000216

Zhang, S., Yang, W., Li, X., Pei, P., Dong, T., Yang, Y., et al. (2022). Clinical and genetic characterization of a large cohort of patients with Wilson's disease in China. *Transl. Neurodegener.* 11, 13. doi:10.1186/s40035-022-00287-0

Zhou, J., Zhang, Q., Zhao, Y., Chen, M., Zhou, S., and Cheng, Y. (2022). Early diagnosis of Wilson's disease in children in southern China by using common parameters. *Front. Genet.* 13, 788658. doi:10.3389/fgene.2022.788658

frontiers | Frontiers in Genetics

TYPE Case Report
PUBLISHED 21 March 2023
DOI 10.3389/fgene.2023.1126555



OPEN ACCESS

EDITED BY
Jordi Pérez-Tur,
Institute of Biomedicine of Valencia (CSIC), Spain

REVIEWED BY
Monica Panzaru,
Grigore T. Popa University of Medicine and Pharmacy, Romania
Weibing Qin,
National Health and Family Planning Commission, China

*CORRESPONDENCE
Min Gao,
anhngm@126.com

†These authors have contributed equally to this work and share first authorship

SPECIALTY SECTION
This article was submitted to Genetics of Common and Rare Diseases, a section of the journal Frontiers in Genetics

RECEIVED 18 December 2022
ACCEPTED 07 March 2023
PUBLISHED 21 March 2023

CITATION
Zhong Z, Yang T, Liu S, Wang S, Zhou S, Du S, Zheng L, Wang X, Wang H, Wang Y and Gao M (2023), Case report: Gene mutation analysis and skin imaging of isolated café-au-lait macules. *Front. Genet.* 14:1126555. doi: 10.3389/fgene.2023.1126555



# Case report: Gene mutation analysis and skin imaging of isolated café-au-lait macules

Zhenyu Zhong[1,2,3,4,5†], Tianhui Yang[1,2,3,4,5†], Siqi Liu[1,2,3,4,5], Shan Wang[1,2,3,4,5], Shan Zhou[1,2,3,4,5], Shuli Du[1,2,3,4,5], Liyun Zheng[1,2,3,4,5], Xiuli Wang[1,2,3,4,5], Hui Wang[1,2,3,4,5], Yifan Wang[1,2,3,4,5] and Min Gao[1,2,3,4,5*]

[1]Department of Dermatology, First Affiliated Hospital of Anhui Medical University, Hefei, China, [2]Institute of Dermatology, Anhui Medical University, Hefei, China, [3]Key Laboratory of Dermatology, Ministry of Education, Anhui Medical University, Hefei, China, [4]Anhui Provincial Institute of Translational Medicine, Hefei, China, [5]Inflammation and Immune-Mediated Diseases Laboratory of Anhui Province, Hefei, Anhui, China

**Background:** Café-au-lait macules (CALMs) are common birthmarks associated with several genetic syndromes, such as neurofibromatosis type 1 (NF1). Isolated CALMs are defined as multiple café-au-lait macules in patients without any other sign of NF1. Typical CALMs can have predictive significance for NF1, and non-invasive techniques can provide more accurate results for judging whether café-au-lait spots are typical.

**Objectives:** The study aimed to investigate gene mutations in six Chinese Han pedigrees of isolated CALMs and summarize the characteristics of CALMs under dermoscopy and reflectance confocal microscopy (RCM).

**Methods:** In this study, we used Sanger sequencing to test for genetic mutations in six families and whole exome sequencing (WES) in two families. We used dermoscopy and RCM to describe the imaging characteristics of CALMs.

**Results:** In this study, we tested six families for genetic mutations, and two mutations were identified as novel mutations. The first family identified [NC_000017.11(NM_001042492.2):c.7355G>A]. The second family identified [NC_000017.11(NM_001042492.2):c.2739_2740del]. According to genotype-phenotype correlation analyses, proband with frameshift mutation tended to have a larger number of CALMs and a higher rate of having atypical CALMs. Dermoscopy showed uniform and consistent tan-pigmented network patches with poorly defined margins with a lighter color around the hair follicles. Under RCM, the appearance of NF1 comprised the increased pigment granules in the basal layer and significantly increased refraction.

**Conclusion:** A new heterozygous mutation and a new frameshift mutation of NF1 were reported. This article can assist in summarizing the properties of dermoscopy and RCM with CALMs.

KEYWORDS

**isolated café-au-lait macules(CALMs), NF1, dermoscopy, reflectance confocal microscopy, mutation, genetic testing**

# 1 Introduction

Café-au-lait macules (CALMs), also referred to as café-au-lait spots (CALs), are common birthmarks that can be present at birth and dynamically increase in number and range over time. At least one CALM may occur in as many as 2%–3% of healthy newborns (Alper et al., 1979; Alper and Holmes, 1983) and in about one-third of all school-aged children (Whitehouse, 1966; Burwell et al., 1982; Sigg et al., 1990; McLean and Gallagher, 1995; Rivers et al., 1995).

However, having six or more typical CALMs is less common and strongly suggests the diagnosis of neurofibromatosis type 1 (NF1). Isolated CALMs are defined as multiple café-au-lait macules in patients without any other sign of NF1 (Bernier et al., 2016).

NF1 (OMIM 162200) is an autosomal dominant, multisystem disease with an incidence of 1:2,500–3,000 worldwide (Williams et al., 2009). Since 1000 AD, there have been reports of individuals with neurofibromatosis. In 1881, von Recklinghausen coined the name "neurofibroma." The condition was classified into two types, NF1 and neurofibromatosis type 2(NF2) in the late 1900's. The National Institutes of Health Consensus Development Conference assembled diagnostic criteria for NF1 that remain utilized in 1988 (Wilson et al., 2021). NF1 is caused by inactivating mutations in *NF1* gene, a tumor suppressor gene mapping to 17q11.2 and encoding neurofibromin. The characteristics of NF1 generally include CALMs, skinfold freckling, Lisch nodules, and neurofibromas.

The diagnostic criteria for NF1 are met in an individual who does not have a parent diagnosed with NF1 if two or more of the following are present:1. ≥6 CALMs over 5 mm in prepubertal and over 15 mm in greatest diameter in postpubertal individuals 2. Freckling in the axillary or inguinal regions 3. Two or more neurofibromas of any type or one plexiform neurofibroma 4. Optic pathway glioma 5. ≥2 iris Lisch nodules identified by slit-lamp examination or ≥2 choroidal anomalies defined as bright, patchy nodules imaged by optical coherence tomography (OCT)/near-infrared reflectance (NIR) imaging 6. A distinctive osseous lesion such as sphenoid dysplasia, anterolateral bowing of the tibia, or pseudarthrosis of a long bone 7. A heterozygous pathogenic NF1 variant with a variant allele fraction of 50% in apparently normal tissue such as white blood cells. Besides, a child of a parent who meets the diagnostic criteria specified in A merits a diagnosis of NF1 if one or more of the criteria in A are present (Legius et al., 2021).

To our knowledge, this is the first study to combine dermoscopy and reflectance confocal microscopy (RCM) to describe the features of CALMs. We combined these two tools aimed at highlighting the use of non-invasive techniques to distinguish typical from atypical CALMs to determine whether the patients should be subjected to further genetic testing.

# 2 Materials and methods

In this study, six Chinese patients with CALMs and their families were recruited from the First Affiliated Hospital of Anhui Medical University in 2022. This study was approved by the Ethical Review Committee of Anhui Medical University and was conducted according to the Declaration of Helsinki guidelines.

For clinical and genetic investigation, all participants signed informed consent forms. The clinical pictures were taken by a digital camera, and lesions were captured under dermoscopy. We also performed the RCM examination, which acquires consecutive series of confocal images from the epidermis to the papillary dermis. Correspondingly, all dermoscopy and RCM images were analyzed appropriately to divide CALMs into typical and atypical.

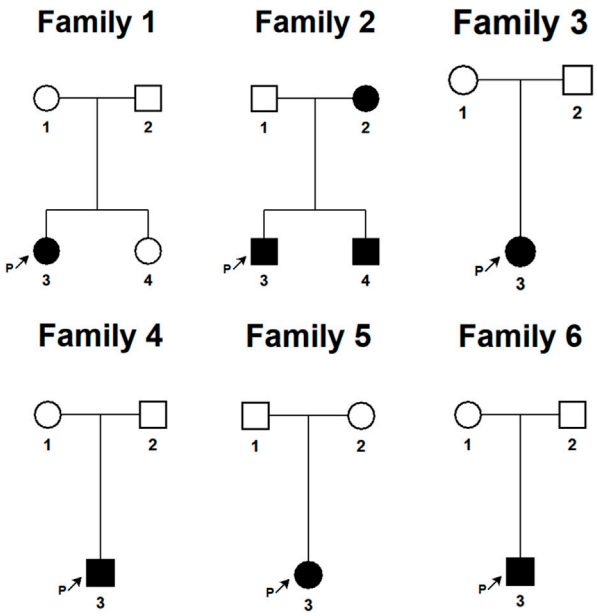


FIGURE 1
The pedigree Gram of six Chinese Han pedigrees of isolated CALMs. The proband was marked with the arrow. Males were indicated by squares; Females were indicated by circles. Blackened symbols represented patients who had CALMs.

Peripheral blood samples were taken from the proband and from their parents. According to the manufacturer's protocol, genomic DNA was extracted from the peripheral blood lymphocytes with kits and stored at −80°C. We used Sanger sequencing to analyze qualified genomic DNA samples. First, we used Primer Premier5.0 to design primers (Supplementary Data Sheet S1) and dilute primers, then we performed PCR amplification. The PCR amplification reaction is completed after the predenaturation stage, amplification stage, and extension phase. The PCR products were purified and recovered after electrophoresis with agarose gels. Finally, we used 3,730 xl sequencer to perform Sanger sequencing and the results were analyzed by DNA sequencing analysis software. We used whole exome sequencing to analyze qualified genomic DNA samples and we got single nucleotide polymorphism (SNP) annotation results. Then, we screened for candidate mutation sites and used SIFT, PolyPhen2, MutationAssessor, MutationTaster and LRT to speculate about the pathogenicity of the mutation sites.

# 3 Results

## 3.1 Basic information about the probands

We have provided the pedigree Gram of the six families (Figure 1). In the first family, the proband, a 7-year-old girl, has several typical CALMs (Figure 2A) and she is the second child of a healthy couple. The

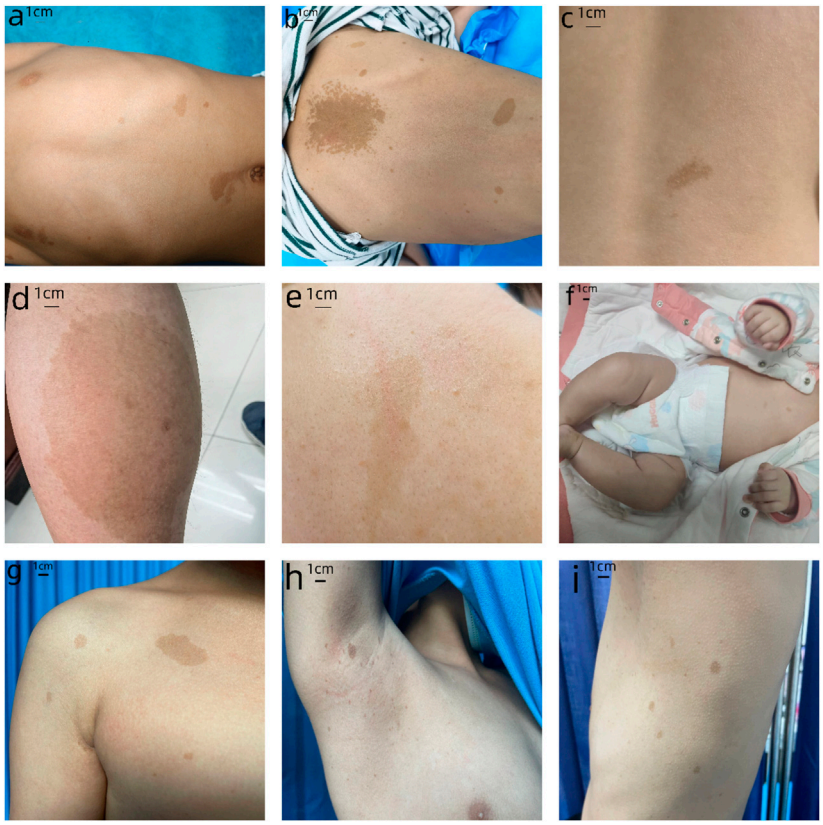


FIGURE 2
Clinical photographs. **(A)** The first proband: sporadic CALMs were observed in the patient's abdomen and back since she was born, which spread slowly to the anterior chest and face. **(B)** The second proband: CALMs were observed in the back and hip of the patient since he was born and then gradually spread to the face and neck. **(C)** The brother of the second proband: a pigmented spot with a size of 2 cm was observed on his back. **(D)** The father of the second proband: a pigmented spot with a size of 10 cm was observed on his left calf. **(E)** The mother of the second proband: several scattered pigmentated spots were observed on the back **(F)**The third proband: CALMs were observed on the patient's chest. **(G)** The fourth proband: CALMs were observed on the patient's armpit and back. **(H)** The fifth proband: CALMs were observed on the patient's thorax, back, and legs. **(I)** The sixth proband: CALMs were observed on the patient's armpit and back.

**TABLE 1 NF1 gene mutations detected in this study.**

| Family | Individuals | Exon | Mutation type | Nucleotide mutation | Protein alteration |
|---|---|---|---|---|---|
| 1 | Family1 (1,3,4) | 50 | Missense | c.7355G>A | p. Arg2452His |
| | Family1 (3) | 18 | SNP | c.2034G>A | p. P678P |
| 2 | Family2 (3) | 21 | Frameshift | c.2739_2740delAC | p. I913Mfs*5 |
| | Family2 (3) | 7 | SNP | c.702G>A | p. L234L |
| 4 | Family4 (3) | 18 | SNP | c.2034G>A | p. P678P |
| 5 | Family5 (3) | 18 | SNP | c.2034G>A | p. P678P |
| 6 | Family6 (3) | 18 | SNP | c.2034G>A | p. P678P |

patient's 9-year-old sister, mother, and father had no symptoms at the time of this study. She was otherwise well and had adequate intellectual and physical development. In the second family, the proband, a 7-year-old male has several typical CALMs (Figure 2B) and he is the first child in the family. He has a 5-year-old brother, and his brother also had a pigmented spot on his back (Figure 2C). His father had a large pigmented spot on the left calf (Figure 2D), and his mother had several scattered pigmentated spots on the back (Figure 2E). In the third family, the proband, a female neonate has several typical CALMs (Figure 2F) and she is the first child in the family. The patient's mother had no symptoms at the time of this study, while her father had CALMs. In the fourth family, the proband, an 8-year-old boy has several typical CALMs (Figure 2G) and he is the only child of his parents. The patient's parents had no symptoms at the time of this study. In the fifth family,

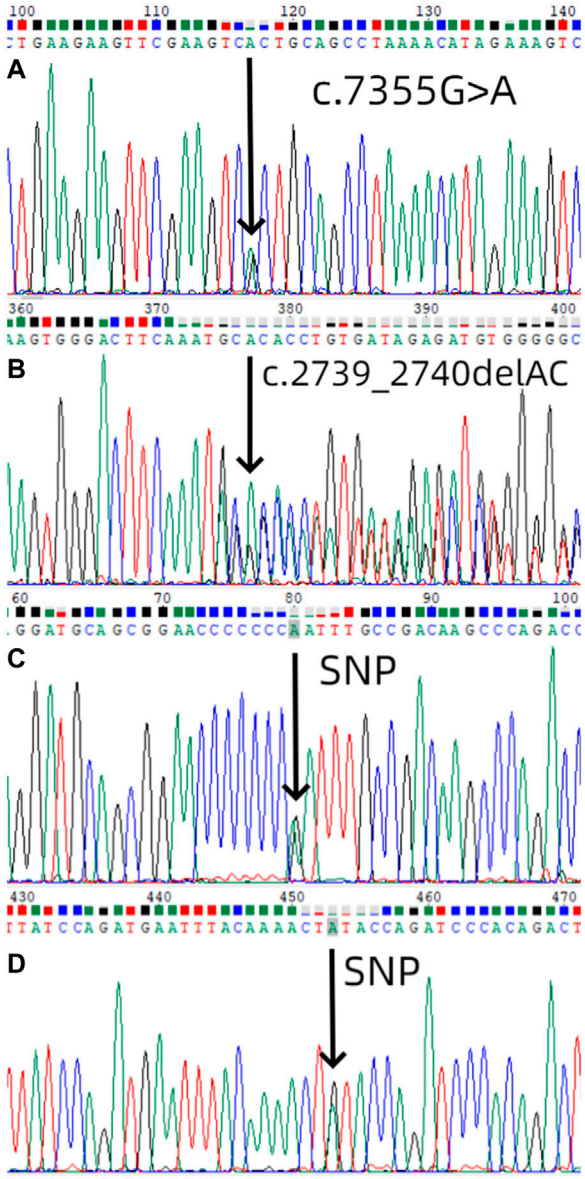


FIGURE 3
Mutation screening. **(A)** Mutational analysis (next-generation sequencing and direct sequencing for proband) of *NF1* in the first family using DNA sequence of exon 50 of *NF1* gene from the proband, with an arrow showing [NC_000017.11(NM_001042492.2): c.7355G>A]. The sister and the mother of the first proband also identified the same mutation. **(B)** Mutational analysis of *NF1* in the second family using DNA sequence of exon 21 of *NF1* gene from the proband, with an arrow showing [NC_000017.11(NM_001042492.2): c.2739_2740del].**(C)** Mutational analysis of NF1 in the first, fourth, fifth, and sixth families using DNA sequence of exon 18 of NF1 gene from the proband, with an arrow showing [NC_000017.11(NM_001042492.2):c.2034G>A].**(D)** Mutational analysis of NF1 in the second family using DNA sequence of exon 7 of NF1 gene from the proband, with an arrow showing [NC_000017.11(NM_001042492.2): c.702G>A].

the proband, a 9-year-old girl has several typical CALMs (Figure 2H) and she is the only child of her parents. The patient's parents had no symptoms at the time of this study as well. In the sixth family, the proband, a 12-year-old boy has several typical CALMs (Figure 2I) and he is the only child of his parents. The patient's parents also had no symptoms at the time of this study.

## 3.2 Gene mutation analysis

We used Sanger sequencing to sequence 9 affected and 11 unaffected members from six families. NF1 gene mutations detected in this study (Table1). In the first family, sequencing of lymphocyte DNA identified [NC_000017.11(NM_001042492.2): c.7355G>A]in the *NF1* gene (Figure 3A). We also performed whole exome sequencing for the first family, and we found the same mutation in the result. All four members in this family received genetic testing and this variant of *NF1* was also identified in her mother and sister but not her father. In the second family, sequencing of lymphocyte DNA identified [NC_000017.11(NM_001042492.2):c.2739_2740del] (Figure 3B). All four members in this family received genetic testing and only the proband identified this mutation. No possible causative mutations in *NF1* were identified in the other four probands and their parents. The proband of the first, fourth, fifth, and sixth families identified [NC_000017.11(NM_001042492.2):c.2034G>A] (Figure 3C). The proband of the second family identified [NC_000017.11(NM_001042492.2): c.702G>A] (Figure 3D).

We performed whole exome sequencing on a total of seven people from the first and third families (four in the first family and three in the third family). High-throughput sequencing of hybrid libraries using BGI's platform yielded an average of 143,344,087 clean reads (14,334,408,742 bps) per sample. Each sample's clean readings were matched to the sequencing of the human reference genome. We used the results of the GATK comparison pair for SNP detection and annotated the results of the SNP. All samples had an average of 122,655 SNPs, of which 99.46% were discovered in the dbSNP database and 93.69% in the 1000 Genomes Project database. There are 660 SNPs that were just found. Base conversion to base switching is compared in a 2.26:1 ratio (Ti/TV). In the coding region, there are typically 10,812 synonymous mutations, 10,164 missense mutations, 27 SNPs that turn the stop codon into a non-stop codon, 95 SNPs that turn the codon into a stop codon, 33 SNPs that invalidate the start codon, and 2,711 SNPs that alter the shear acceptor or splicing donor in the region surrounding the splicing site. The encoder area SNP's Ti/TV is 2.99. We analyzed the results of WES and in the first family [NC_000017.11(NM_001042492.2):c.7355G>A]was identified in the proband, her mother and her sister but not her father. (Supplementary Data Sheet S2)In the third family, no likely pathogenic mutations were identified.

Mutations are classified as pathogenic, likely pathogenic, uncertain significance, likely benign, and benign. In the first family, family members all identified [NC_000017.11(NM_001042492.2):c.7355G>A] except his father. We used a variety of software to analyze, the MutationTaster_score is 1, the MutationTaster_pred is D, the MutationAssessor is M, the LRT is D, SIFT score is 0.003 which is less than 0.05, PolyPhen2 is 0.989 which is greater than 0.909. According to ACMG Standards and Guidelines, the evidence of pathogenicity of this mutation is very strong (PVS1), so this mutation is classified as pathogenic. In

**TABLE 2 The characteristics of CALMs in all affected individuals.**

| | Typical or atypical | Number of calms | Mutations in *NF1* gene |
|---|---|---|---|
| The first proband | Typical | About 15 | Missense mutations in *NF1* gene |
| The second proband | Typical and atypical | >50 | frameshift mutation of *NF1* |
| Brother of the second proband | Typical | 1 | Not found |
| Father of the second proband | typical | 1 | Not found |
| Mother of the second proband | Typical | About 5 | Not found |
| The third proband | Typical | About 10 | Not found |
| The fourth proband | Typical | 5 | Not found |
| The fifth proband | Typical and atypical | About 20 | Not found |
| The sixth proband | Typical | About 10 | Not found |

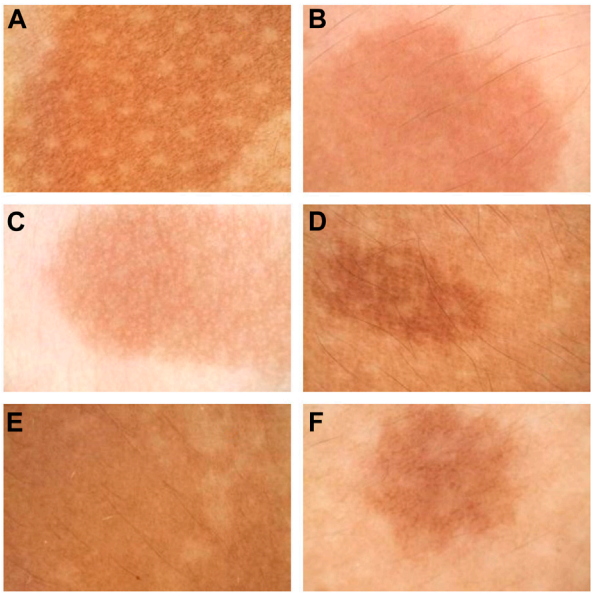


FIGURE 4
Dermoscopy pictures. **(A)** The dermoscopy picture of the first proband. **(B)** The dermoscopy picture of the second proband. **(C)** The dermoscopy picture of the third proband. **(D)** The dermoscopy picture of the fourth proband. **(E)** The dermoscopy pictures of the fifth proband. **(F)** The dermoscopy pictures of the sixth proband.

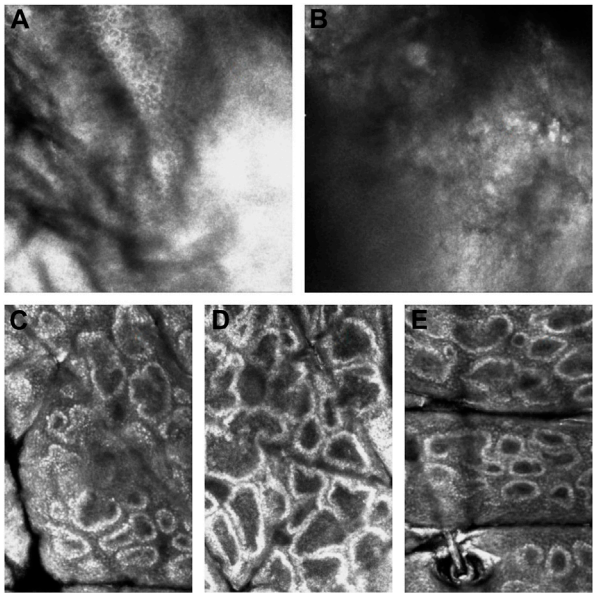


FIGURE 5
RCM pictures. **(A)** The RCM pictures of the first proband. **(B)** The RCM pictures of the second proband. **(C)** The RCM pictures of the fourth proband. **(D)** The RCM pictures of the fifth proband. **(E)** The RCM pictures of the sixth proband. The third proband did not have the RCM images due to the patient's parents refusal.

the second family, only the proband identified [NC_000017.11(NM_001042492.2):c.2739_2740del]. We used the MutationTaster to analyze this mutation and it predicted this mutation as pathogenic and the probability is 1 because this mutation lead to non-sense-mediated mRNA decay (NMD). In the analysis, Phylop is a positive number and PhastCons is 1 which means this mutation occurred in conserved sequences. According to ACMG Standards and Guidelines, the evidence of pathogenicity of this mutation is very strong (PVS1), so this mutation is classified as pathogenic. [NC_000017.11(NM_001042492.2):c.2034G>A]and [NC_000017.11(NM_001042492.2):c.702G>A] were analyzed by SIFT, PolyPhen2 and MutationTaster as Polymorphism (SNP), which were not pathogenic.

According to *NF1* genotype-phenotypic correlation analyses, a higher number of CALMs was observed in patients with truncated mutations compared to patients with missense mutations (Sabbagh et al., 2013). According to our observation, the patient in the second family had more CALMs than the patient in the first family, which complied with the result above. Besides, proband with frameshift mutation tended to have a higher rate of having atypical CALMs.

We summarized the characteristics of CALMs in all affected individuals based on the type of CALMs (typical or atypical), the number of CALMs, and mutations in *NF1* gene (Table 2).

**TABLE 3 Different diseases that cause CALMs.**

| Syndrome | Gene or locus | Location | Protein | Protein function | Clinical features |
|---|---|---|---|---|---|
| RAS/MAPK signaling pathway NF1 | NF1 | 17q11.2 | Neurofibromin | RasGAP | Cafe-au-lait maculae skinfold freckling, Lisch nodules, neurofibromas |
| Legius syndrome | *SPRED1* | 15q14 | SPRED1 | SPROUTY-related, EVH1 domain-containing protein 1 | Multiple CALs with or without intertriginous freckling macrocephaly |
| Noonan Syndro me | *PTPN11* | 12q24.1 | SHP2 | Phosphatase, RasGEF, tyrosine kinases,serine-threoninekinases | Characteristic facial features, lentigines short stature, congenital heart defects |
| | *SOS1* | 2p22.1 | SOS1 | | |
| | *RAF1* | | | | |
| | *KRAS* | | | | |
| | *NRAS* | | | | |
| | *BRAF* | | | | |
| | *SHOC2* | | | | |
| | *CBL* | | | | |
| | *RIT1* | | | | |
| | *MAP2K1* | | | | |
| | *SOS2* | | | | |
| | *LZTR1* | | | | |
| | *A2ML1* | | | | |
| | *RRAS* | | | | |
| | *RASA2* | | | | |
| Noonan syndrome With lentigines | *PTPN11* | 12q24.1 | SHP2 | Phosphatase | Multiple lentigines plus the features of Noonan syndrome |
| Mccune-Albright syndrome (mas) | *GNAS1* | GNAS1 | cAMP pathway-associated G-protein | α-subunit's intrinsic GTPase | CALMs, skeletal abnormalities, endocrine disorders |
| KITLG/KIT signaling pathway Piebaldism | *KIT* | 4q12 | KIT ligand (stem cell factor, steel factor or mast cell growth factor) and its receptor KIT | Ras/mitogen activated protein kinase (MAPK) | Depigmented patches of skin and hair |
| Familial progressive hyperpigmentation (FPH) | *KITLG* | 12q21.32 | KIT ligand (stem cell factor, steel factor or mast cell growth factor) and its receptor KIT | Ras/mitogen activated protein kinase (MAPK) | Diffuse, partly blotchy hyperpigmented lesions intermingled with scattered hypopigmentations, and lentigines |

## 3.3 Skin images

The features of CALMs, as seen under dermoscopy, were visible brown pigment patches with clear borders and different sizes (Figure 4).

The features of CALMs, as seen under RCM, were increased pigment content in the basal layer in the skin lesion area, many highly refractive particles, and no significant changes in the superficial dermis (Figure 5).

# 4 Discussion

CALMs are flat, well-circumscribed light-to-dark brown macules or patches on the skin; however, the lesions can vary in pigmentation. CALMs can be divided into typical and atypical CAL spots based on number, morphology, and pigmentation (Fois et al., 1993; Nunley et al., 2009; Riccardi, 2009; St John et al., 2016; Albaghdadi et al., 2022). Typical CALMs are described as round and smooth with a size of 5 mm–15 cm, and their pigmentation is even and uniform. Atypical CALMs are described as irregular and jagged with a size of <5 mm or >15 cm, and their pigmentation is uneven and non-homogeneous.

CALMs associated with NF-1 are described as typical (Nunley et al., 2009). Previous studies have also shown that typical CALMs have more predictive value for NF-1 than atypical CALMs (Fois et al., 1993; Nunley et al., 2009; Riccardi, 2009). Identifying typical CALMs can serve as a preliminary basis for genetic testing; however, we need further studies with larger samples to verify this.

The pathogenesis of diseases in which CALMs are seen mainly includes the abnormalities in the Ras/MAPK signaling pathway and

KITLG/KIT signaling pathway, which are involved in different diseases that cause CALMs (Table 3) (Zhang et al., 2016).

In our study, the probands all had only CALMs without other manifestations that suggest other diseases; therefore, we only tested them for genetic mutations in *NF1* gene. If other manifestations develop in these probands, then we will test them for mutations in other genes according to their signs and symptoms, followed by a long follow-up.

A novel missense mutation was identified in the proband in the first family, who had about 15 typical CALMs. A novel frameshift mutation was identified in the proband in the second family, who had over 50 typical CALMs and several atypical CALMs. The literature has shown that probands with a frameshift mutation tend to have a higher rate of having atypical CALMs and a larger number of CALMs than probands with a missense mutation, and our research is consistent with this rule.

In the first family, the proband identified [NC_000017.11(NM_001042492.2):c.7355G>A]and this variant of *NF1* was also identified in her mother and sister but not her father. But as far as we observed, the mother and sister of the proband had no symptoms. As we all know, NF1 is an autosomal dominant disorder. According to the medical genetics, heterozygotes with dominant pathogenic genes show disease only after reaching a certain age because the pathogenic genes are not expressed or are not expressed enough to cause obvious clinical manifestations in early lifetime, which is called delayed dominance. What's more, some dominant genes of heterozygotes exhibit the associated dominant qualities, but they can be inconspicuous in others, or they do not express the corresponding traits, which is called irregular dominance. We speculate that the phenomenon in the first family is related to these two conditions. The inheritance of gene mutation traits is influenced by the environment and family background, and therefore appears diverse.

We performed Sanger sequencing on all members of the six families, and whole exome sequencing on all members of the first and third families. Only the first two families found possible causative mutations, possible causative mutations were not identified in the other four families. Whole exome sequencing has been increasingly adopted as the primary genetic diagnostic strategy for the past few years due to its high diagnostic yield and cost-effectiveness (Qiu et al., 2022). But WES cannot provide hitherto complete coverage of the coding region of the genome like whole genome sequencing (WGS). According to the literature, about 10% of the mutations detectable by whole exome sequencing (WES) were missed (Meienberg et al., 2016). The NF1 genome is large and has many hundreds of thousands of bases, using Sanger sequencing cannot completely cover these bases. We speculate that this was one of the reasons why the other four family identified no possible causative mutations. Another reason was that the mutations in these four patients might have been in genes other than *NF1*, resulting in other diseases causing CALMs that we have enumerated above. As a result, it is necessary to broaden the scope of genetic testing and test for more genes, such as *SPRED1* and *NF2*.

Dermoscopy is an important non-invasive technique to diagnose cutaneous pigmented diseases, which can magnify lesions to observe the color from the epidermis to the papillary layer. RCM can be used to image skin to a depth of 250 m (superficial dermis) and has been proven to be a critical non-invasive technique for diagnosing melanocytic lesions. The RCM characteristics of CALMs have been summarized in previous articles, but this article is the first to summarize both dermoscopy and RCM characteristics of CALMs.

Nowadays, as clinicians generally observe the number and shape of CALMs macroscopically, we believe that dermoscopy and RCM can be used as a preliminary basis to examine whether CAL spots are typical and decide whether genetic testing is needed. Thus, we sorted out the characteristics of skin imaging of CALMs to help clinicians make the decision. According to the dermoscopy and RCM results of these six patients with CALMs, we could preliminarily conclude the characteristics of CALMs. Under dermoscopy, CALMs usually manifest as brown pigment spots with a clear rim. Under RCM, CALMs usually demonstrated an increased pigment content in the basal layer of the skin lesion area and no obvious changes in the superficial dermis.

## Data availability statement

The datasets for this article are not publicly available due to concerns regarding participant/patient anonymity. Requests to access the datasets should be directed to the corresponding author.

## Ethics statement

The studies involving human participants were reviewed and approved by the Ethical Review Committee of Anhui Medical University. Written informed consent to participate in this study was provided by the participants' legal guardian/next of kin. Written informed consent was obtained from the individual(s), and minor(s)' legal guardian/next of kin, for the publication of any potentially identifiable images or data included in this article.

## Author contributions

All authors listed have made a substantial, direct, and intellectual contribution to the work and approved it for publication.

## Conflict of interest

The authors declare that the research was conducted in the absence of any commercial or financial relationships that could be construed as a potential conflict of interest.

## Publisher's note



## Supplementary material

The Supplementary Material for this article can be found online at: https://www.frontiersin.org/articles/10.3389/fgene.2023.1126555/full#supplementary-material

# References


Albaghdadi, M., Berseneva, M., Pennal, A., Wan, S., Matviychuk, D., Shugar, A., et al. (2022), Value of a cafe-au-lait macules screening clinic: Experience from the hospital for sick children in toronto. *Pediatr. Dermatol.* 39, 205, 210. doi:10.1111/pde.14947

Alper, J., Holmes, L. B., and Mihm, M. C. (1979). Birthmarks with serious medical significance: Nevocullular nevi, sebaceous nevi, and multiple café au lait spots. *J. Pediatr.* 95 (5), 696–700. doi:10.1016/s0022-3476(79)80713-1

Alper, J. C., and Holmes, L. B. (1983). The incidence and significance of birthmarks in a cohort of 4,641 newborns. *Pediatr. Dermatol.* 1 (1), 58–68. doi:10.1111/j.1525-1470.1983.tb01093.x

Bernier, A., Larbrisseau, A., and Perreault, S. (2016). Cafe-au-lait macules and neurofibromatosis type 1: A review of the literature. *Pediatr. Neurol.* 60, 24–29. doi:10.1016/j.pediatrneurol.2016.03.003

Burwell, R. G., James, N. J., and Johnston, D. I. (1982). CAFE-AU-LAIT spots in school-children. *Archives Dis. Child.* 57 (8), 631–632. doi:10.1136/adc.57.8.631

Fois, A., Calistri, L., Balestri, P., Vivarelli, R., Bartalini, G., Mancini, L., et al. (1993). Relationship between cafe-au-lait spots as the only symptom and peripheral neurofibromatosis (NF1) - a follow-up-study. *Eur. J. Pediatr.* 152 (6), 500–504. doi:10.1007/BF01955059

Legius, E., Messiaen, L., Wolkenstein, P., Pancza, P., Avery, R. A., Berman, Y., et al. (2021). Revised diagnostic criteria for neurofibromatosis type 1 and legius syndrome: An international consensus recommendation. *Genet. Med. Aug* 23(8), 1506–1513. doi:10.1038/s41436-021-01170-5

McLean, D. I., and Gallagher, R. P. (1995). Sunburn freckles, cafe-au-lait macules, and other pigmented lesions of schoolchildren - the vancouver mole study. *J. Am. Acad. Dermatology* 32 (4), 565–570. doi:10.1016/0190-9622(95)90338-0

Meienberg, J., Bruggmann, R., Oexle, K., and Matyas, G. (2016). Clinical sequencing: Is WGS the better WES? *Hum. Genet. Mar.* 135 (3), 359–362. doi:10.1007/s00439-015-1631-9

Nunley, K. S., Gao, F., Albers, A. C., Bayliss, S. J., and Gutmann, D. H. (2009). Predictive Value of Cafe au Lait Macules at Initial Consultation in the Diagnosis of Neurofibromatosis Type 1. *Archives Dermatology* 145 (8), 883–887. doi:10.1001/archdermatol.2009.169

Qiu, Z., Chang, W. T., Chou, Y. C., Wen, K. C., Ziying, Y., Yuen, K., et al. (2022). Prenatal case of RIT1 mutation associated Noonan syndrome by whole exome sequencing (WES) and review of the literature. *Taiwan J. Obstet. Gynecol. May* 61 (3), 535–538. doi:10.1016/j.tjog.2022.03.025

Riccardi, V. M. (2009). Diagnostic and Management Considerations Posed by Multiple Cafe au Lait Spots. *Archives Dermatology* 145 (8), 929–930. doi:10.1001/archdermatol.2009.180

Rivers, J. K., Maclennan, R., Kelly, J. W., Lewis, A. E., Tate, B. J., Harrison, S., et al. (1995). The eastern AUSTRALIAN childhood nevus study - prevalence of atypical nevi, congenital nevus-like nevi, and other pigmented lesions. *J. Am. Acad. Dermatology* 32 (6), 957–963. doi:10.1016/0190-9622(95)91331-9

Sabbagh, A., Pasmant, E., Imbard, A., Luscan, A., Soares, M., Blanche, H., et al. (2013). NF1 molecular characterization and neurofibromatosis type I genotype-phenotype correlation: The French experience. *Hum. Mutat.* 34 (11), 1510–1518. doi:10.1002/humu.22392

Sigg, C., Pelloni, F., and Schnyder, U. W. (1990). Frequency of congenital nevi, nevi-spili and cafe-au-lait spots and their relation to nevus count and SKIN complexion in 939 children. *Dermatologica* 180 (3), 118–123. doi:10.1159/000248009

St John, J., Summe, H., Csikesz, C., Wiss, K., Hay, B., and Belazarian, L. (2016). Multiple Cafe au Lait Spots in a Group of Fair-Skinned Children without Signs or Symptoms of Neurofibromatosis Type 1. *Pediatr. Dermatol.* 33 (5), 526–529. doi:10.1111/pde.12936

Whitehouse, D. (1966). Diagnostic value of the café-au-lait spot in children. *Archives Dis. Child.* 41 (217), 316–319. doi:10.1136/adc.41.217.316

Williams, V. C., Lucas, J., Babcock, M. A., Gutmann, D. H., Korf, B., and Maria, B. L. (2009). Neurofibromatosis type 1 revisited. *Pediatrics* 123 (1), 124–133. doi:10.1542/peds.2007-3204

Wilson, B. N., John, A. M., Handler, M. Z., and Schwartz, R. A. (2021). Neurofibromatosis type 1: New developments in genetics and treatment. *J. Am. Acad. Dermatol. Jun* 84 (6), 1667–1676. doi:10.1016/j.jaad.2020.07.105

Zhang, J., Li, M., and Yao, Z. (2016). Molecular screening strategies for NF1-like syndromes with café-au-lait macules (Review). *Mol. Med. Rep.* 14(5), 4023–4029. doi:10.3892/mmr.2016.5760

frontiers | Frontiers in Genetics

TYPE Original Research
PUBLISHED 23 March 2023
DOI 10.3389/fgene.2023.1108440



OPEN ACCESS

EDITED BY
Hu Hao,
The Sixth Affiliated Hospital of Sun Yat-sen University, China

REVIEWED BY
Nora Urraca,
University of Tennessee Health Science Center (UTHSC), United States
Mingbang Wang,
South China Hospital of Shenzhen University, China

*CORRESPONDENCE
Wei Li,
liwei@bch.com.cn
Yonghua Cui,
cuiyonghua@bch.com.cn
Chanjuan Hao,
hchjhchj@163.com
Xin Ni,
nixin@bch.com.cn

†These authors have contributed equally to this work

SPECIALTY SECTION
This article was submitted to Genetics of Common and Rare Diseases, a section of the journal Frontiers in Genetics

RECEIVED 26 November 2022
ACCEPTED 15 March 2023
PUBLISHED 23 March 2023

CITATION
Zhang Y, Li Y, Guo R, Xu W, Liu X, Zhao C, Guo Q, Xu W, Ni X, Hao C, Cui Y and Li W (2023), Genetic diagnostic yields of 354 Chinese ASD children with rare mutations by a pipeline of genomic tests. *Front. Genet.* 14:1108440. doi: 10.3389/fgene.2023.1108440



# Genetic diagnostic yields of 354 Chinese ASD children with rare mutations by a pipeline of genomic tests

Yue Zhang[1†], Ying Li[2†], Ruolan Guo[1], Wenjian Xu[1], Xuanshi Liu[1], Chunlin Zhao[1], Qi Guo[1], Wenshan Xu[1], Xin Ni[3]*, Chanjuan Hao[1]*, Yonghua Cui[2]* and Wei Li[1]*

[1]Beijing Key Laboratory for Genetics of Birth Defects, Beijing Pediatric Research Institute, MOE Key Laboratory of Major Diseases in Children, Beijing Children's Hospital, Capital Medical University, National Center for Children's Health, Beijing, China, [2]Department of Psychiatry, Beijing Children's Hospital, Capital Medical University, National Center for Children's Health, Beijing, China, [3]National Center for Children's Health, Beijing, China

**Purpose:** To establish an effective genomic diagnosis pipeline for children with autism spectrum disorder (ASD) for its genetic etiology and intervention.

**Methods:** A cohort of 354 autism spectrum disorder patients were obtained from Beijing Children's Hospital, Capital Medical University. Peripheral blood samples of the patients were collected for whole genome sequencing (WGS) and RNA sequencing (RNAseq). Sequencing data analyses were performed for mining the single nucleotide variation (SNV), copy number variation (CNV) and structural variation (SV). Sanger sequencing and quantitative PCR were used to verify the positive results.

**Results:** Among 354 patients, 9 cases with pathogenic/likely pathogenic copy number variation and 10 cases with pathogenic/likely pathogenic single nucleotide variations were detected, with a total positive rate of 5.3%. Among these 9 copy number variation cases, 5 were *de novo* and 4 were inherited. Among the 10 *de novo* single nucleotide variations, 7 were previously unreported. The pathological *de novo* mutations account for 4.2% in our cohort.

**Conclusion:** Rare mutations of copy number variations and single nucleotide variations account for a relatively small proportion of autism spectrum disorder children, which can be easily detected by a genomic testing pipeline of combined whole genome sequencing and RNA sequencing. This is important for early etiological diagnosis and precise management of autism spectrum disorder with rare mutations.

KEYWORDS

**autism spectrum disorder, whole-genome sequencing, RNA sequencing, copy number variation, single nucleotide variation**

## Introduction

Autism spectrum disorder (ASD) is a group of neurodevelopmental disorder with onset at early childhood. According to the Diagnostic and Statistical Manual of Mental Disorders (Fifth Edition, DSM-V), autism, Asperger's syndrome, childhood disintegrating disorder and unclassified pervasive developmental disorder are collectively referred to ASD

(American Psychiatric Association, 2013). The two core symptoms of ASD are 1) impaired social communication and interaction, 2) repetitive and stereotyped behaviors, interests, and activities (Lobar, 2016). The incidence of ASD has been on the rise in recent years. According to the Centers for Disease Control and Prevention (CDC) reports, 1 in 54 children are diagnosed with ASD (Maenner et al., 2020), with a significantly higher proportion of male patients than that of female patients, and the ratio of male to female patients is about 4 : 1 (Rutherford et al., 2016; Loomes et al., 2017; Maenner et al., 2020). Except for the core symptoms, ASD is also accompanied by other comorbidities including but not limited to intellectual disability, epilepsy, facial deformities, neurological imaging abnormalities, movement disorders, attention deficit hyperactivity disorder (ADHD), aggressive behavior, cardiovascular abnormalities, gastrointestinal disorders, sleep disorders, convulsions, oppositional defiant disorder, anxieties, obsessions and compulsions and depression (Simonoff et al., 2008; Popow et al., 2021). Due to the wide spectrum of symptoms, missing diagnosis or misdiagnosis often occurs. Genetic diagnosis is now a routine method for precision diagnosis and intervention of ASD.

The clinical manifestations of ASD are diverse and complex, and its etiology is still largely unknown. ASD shows great heterogeneity in clinical symptoms and genetic alterations (Sandin et al., 2017). More attention has been paid to the genetic factors associated with ASD. Known genetic abnormalities are copy number variants (CNVs), *de novo* single nucleotide variants (SNVs), common genetic variants, mosaicism, non-coding and regulatory pathogenic variations, and inherited recessive variants (Zhang et al., 2021). More than 1,000 genes related to ASD have been described in the SFARI database (https://gene.sfari.org). The reported single gene mutation related to ASD accounts for about 5% (Gaugler et al., 2014), and CNV accounts for 8%–20% of ASD (Sebat et al., 2007). However, to date, at least 70% of the affected individuals have no known genetic etiology (Dias and Walsh, 2020).

The clinical implementation of trio-whole exome/genome sequencing (WES/WGS) has been a significant contribution to the discovery of *de novo* SNVs to autism risk (Neale et al., 2012; Sanders et al., 2012; Iossifov et al., 2014). As these variants usually link to a single gene, it is particularly important in emphasizing the underlying neurobiology of *de novo* SNVs associated with autism. CNVs refer to large deletions or duplications often involving in several genes. The association of phenotype with gene dosage exists, but the confirmation of relationship is often difficult. In 2007, comparative genomic hybridization was used to establish a significant association between *de novo* submicroscopic structural variation (SV) and autism (Sebat et al., 2007). From then on, more CNVs related to autism have been identified. In the genomics era, more genetic architectural changes including SNVs, CNVs and SVs are associated with ASD in different disease cohorts of different populations. Nevertheless, functional experiments are crucial for these validations to better understand the pathogenicity.

Enhanced bioinformatics analyses integrate evolutionary constraints to identify risk genes with a false discovery rate less than or equal to 0.1. In addition to utilizing probability of loss of function (pLI), missense badness, PolyPhen-2 constraint score, researchers are able to identify variants affecting gene functions by predicted impact (Lek et al., 2016). These analyses not only confirm enrichment of *de novo* loss-of-function mutations which affect highly constrained genes, but also identify pathogenic missense mutations. Currently, there are a variety of molecular testing platforms in diagnosing ASD. Trio-WES and CNV sequencing (CNVseq) or chromosomal microarray analysis (CMA) are commonly used first-tier techniques in molecular diagnosis of ASD. In the next-generation sequencing era, with the cost of sequencing declining, WGS is more widely applied to detect SNVs, CNVs and SVs simultaneously to uncover both coding and non-coding variants. RNA sequencing (RNAseq) can increase the diagnostic rate by assessing the gene expression changes. Thus, we here integrate both WGS and RNAseq for the genomic analysis of our ASD cohort to evaluate its efficacy and clinical application in a single-center level, in order to characterize the genetic etiology of the patients for both known ASD genes or new candidate ASD genes by focusing on *de novo* SNVs and CNVs.

# Materials and methods

## General patient information

The patients who met the diagnostic criteria of ASD by DSM-V were all from the Department of Psychiatry, Beijing Children's Hospital. From July 2019 to May 2021, a total of 354 cases from 345 families were enrolled, including 9 families with two affected siblings. The ASD patients aged at 1–12 years, including 279 males and 75 females, with a male-to-female ratio of 3.72 : 1, very close to the ratio of male-to-female of about 4 : 1 (Maenner et al., 2020). The clinical data, imaging reports (if any) and ASD assessment scales of the patients were collected, including the Autism Behavior Checklist (ABC), Clancy Autism Behavior Scale (CABS), Childhood Autism Rating Scale (CARS) and DSM-V Diagnostic Scale (Supplementary Material). The head circumference and eye distance of the children were measured, and the front and side images were captured. The enrollment and diagnosis process are summarized in Figure 1. 5 mL of venous blood from the patient and 2 mL of venous blood from each parent were collected, and genomic DNA and total RNA were extracted. All parents have signed their own written informed consents as well as in representative of their children's guardians. This study has been approved by the Ethics Committee of Beijing Children's Hospital.

## Whole genome sequencing (WGS)

DNA of all collected samples was extracted and purified using DNA Blood Mini Kit (Qiagen, Hilden, Germany). DNA concentration was measured by Qubit DNA Assay Kit in Qubit 2.0 Flurometer (Life Technologies, CA, USA).

### Library preparation

A total amount of 1 μg DNA sample from each proband was used as the input material for DNA library preparation. Sequencing library was generated using CleanNGS DNA Kit (CleanNA, Waddinxveen, Netherlands) following the manufacturer's recommendations and index codes were added to each sample.

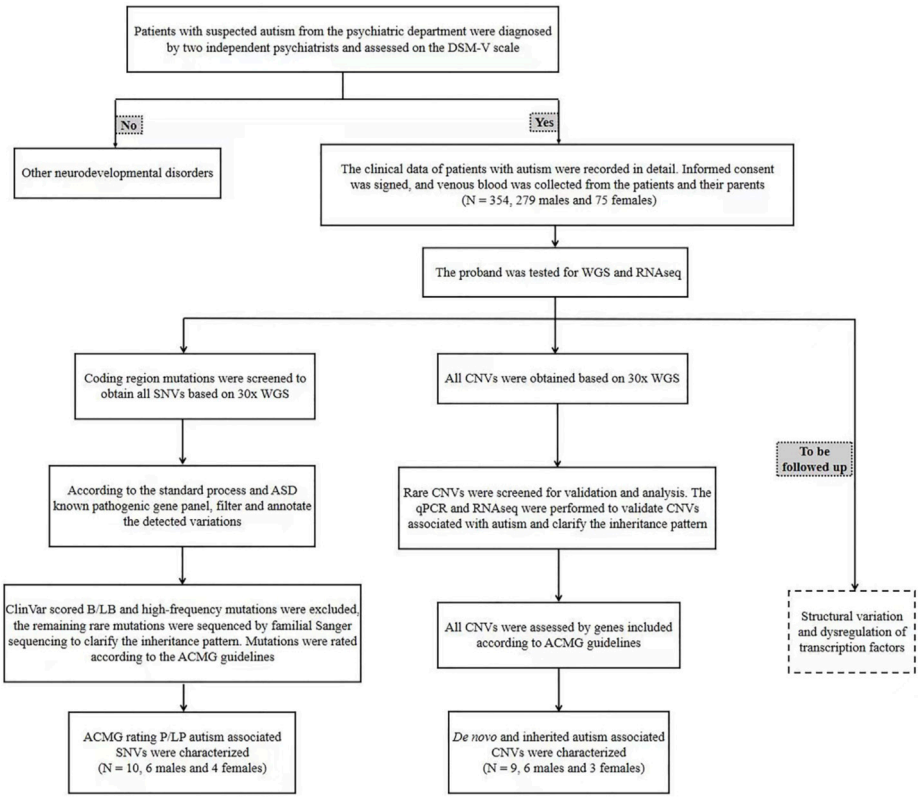


FIGURE 1
The clinical enrollment and diagnosis flowchart of ASD patients. qPCR: quantitative PCR; WGS: whole genome sequencing; SNV: single nucleotide variation; CNV: copy number variation; RNAseq: RNA sequencing.

Briefly, genomic DNA sample was enzymatically digested to fragments of about 350 bp. Then DNA fragments were end-polished, A-tailed, and ligated with the full-length adapter for sequencing, followed by further PCR amplification. After PCR products were purified by AMPure XP System (Beckman Coulter, CA, USA), libraries were analyzed for size distribution by Agilent 2100 Bioanalyzer (Agilent Technologies, CA, USA) and quantified by real-time PCR.

### Clustering and sequencing

The clustering of the index-coded samples was performed on a cBot Cluster Generation System using Novaseq5000/6000 S4 Reagent Kit (Illumina, San Diego, CA, USA) according to the manufacturer's instructions. After cluster generation, the DNA libraries were sequenced on Illumina NovaSeq 6000 platform and 150 bp paired-end reads were generated.

### Quality control

Raw data (raw reads) of fastq format were firstly processed through primary quality control. In this step, clean data (clean reads) were obtained by removing read pairs that contain more than three N or the proportion of base with quality value below 5 is more than 20%, in any end, or adapter sequence was founded. All the downstream analyses were based on the clean data with high quality.

### Reads mapping to reference sequences

Clean reads were compared with reference human genome (UCSC hg19) by using BWA software (http://bio-bwa.sourceforge.net), and the results were converted into bam format and sorted by Samtools software (https://github.com/samtools/samtools/releases). Finally, basic information statistics and map comparison statistics were conducted. The average depth of WGS is about 30×.

## RNA sequencing (RNAseq)

Total RNA of all collected samples was extracted and purified from the fresh venous whole blood using PAXgene Blood RNA Kit (Qiagen). Total RNA concentration was measured by Qubit RNA Assay Kit in Qubit 2.0 Flurometer (Life Technologies).

### RNA quality check

The purity of the sample was determined by NanoPhotometer (Implen, CA, USA), the concentration and integrity of RNA samples were detected by Agilent 2100 RNA Nano 6000 Assay Kit.

### Library preparation

A total amount of 1–3 μg RNA per sample from each proband was used as the input material for RNA sample preparation. Sequencing libraries were generated using VAHTS Universal

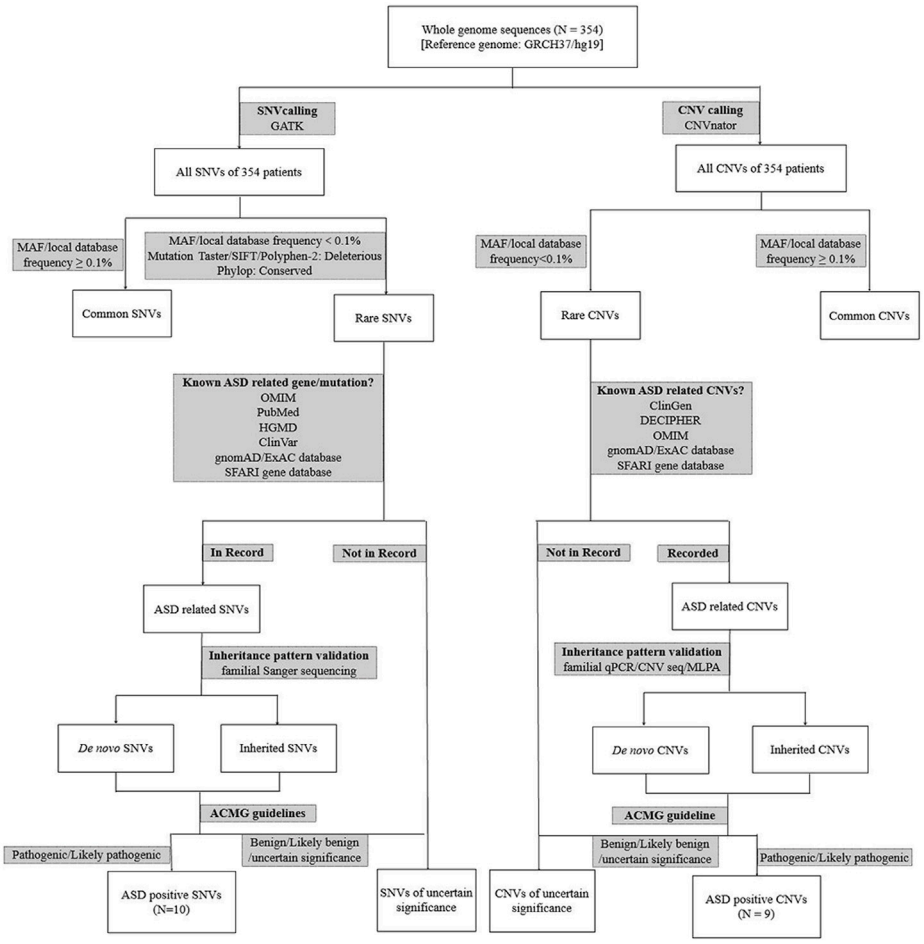


FIGURE 2
The detailed genomics diagnosis pipeline of ASD patients. qPCR: quantitative PCR; WGS: whole genome sequencing; SNV: single nucleotide variation; CNV: copy number variation; CNV seq: CNV sequencing.

V6 RNA-seq Library Prep Kit (Illumina, NR604-01/02) following the manufacturer's recommendations and index codes were added to attribute sequences to each sample. Briefly, mRNA was purified from total RNA using poly-T oligo-attached magnetic beads. Then we added fragmentation buffer to break the mRNA into short fragments. First strand cDNA was synthesized using random hexamer primer and RNase H. Second strand cDNA synthesis was subsequently performed using buffer, dNTPs, DNA polymerase I and RNase H. The double stranded cDNA was purified by AMPure XP beads (Beckman Coulter). The purified double stranded cDNA was repaired at the end, added a tail and connected to the sequencing connector, then the fragment size was selected, and the final cDNA library was constructed by PCR enrichment.

### Library check

RNA concentration of library was measured using Qubit RNA Assay Kit in Qubit 3.0 (Life Technologies) for quantification and then diluted to 1 ng/μL. Insert size was assessed using the Agilent Bioanalyzer 2100 system. After the insert size met the requirement, the CFX 96 fluorescence quantitative PCR instrument (Bio-Rad, CA, USA) was used to quantify the library effective concentration (library effective concentration >10 nm) using Bio-Rad iQ SYBR GRN Kit.

### Library clustering and sequencing

1) HiSeq x ten platform (Illumina). The clustering of the index-coded samples was performed on a cBot cluster generation system using HiSeq PE Cluster Kit v4-cBot-HS according to the manufacturer's instructions. After cluster generation, the libraries were sequenced on an Illumina platform and 150 bp paired-end reads were generated. 2) Novaseq 6000 S4 platform (Illumina). The cluster generation and sequencing were performed on Novaseq 6000 S4 platform, using NovaSeq 6000 S4 Reagent Kit V1.5.

## Sanger sequencing

Amplification primers were designed for the gene variants, and PCR amplification and sequencing verification were performed on the gene products in the family of the indicated patient. ABI 3730XL

**TABLE 1 Clinical features of 19 diagnosed ASD patients.**

| ID | Sex | Age (year) | Featured symptoms |
|---|---|---|---|
| ASD0018 | male | 3 | Intellectual disability, language development delay |
| ASD0027 | male | 3 | Severe intellectual disability, language retardation, wide dental space, abnormal posture |
| ASD0046 | female | 4 | Intellectual disability, language retardation, attention deficit, hyperactivity, feeding difficulties |
| ASD0060 | male | 2 | Intellectual disability, language development delay, sleep disorders, forehead protrusion |
| ASD0061 | male | 5 | Intellectual disability, language development delay, global developmental delay |
| ASD0063 | female | 3 | Intellectual disability, language retardation, movement disorders, epilepsy |
| ASD0134 | male | 3 | Intellectual disability, language retardation, hyperactivity, strabismus, unsteady walking |
| ASD0144 | male | 2 | Intellectual disability, language development delay, learning disabilities, cognitive disorders, attention deficit, feeding difficulties |
| ASD0148 | female | 6 | Intellectual disability, language retardation, motor retardation, increased pain tolerance, spherical nasal tip |
| ASD0162 | male | 2 | Intellectual disability, language deficits, learning disabilities, large head, scoliosis, multiple milky coffee spots |
| ASD0203 | female | 6 | Attention deficit, hyperactivity, global developmental delay |
| ASD0214 | female | 4 | Intellectual disability, language deficits, global developmental delay, cognitive disorders, feeding difficulties |
| ASD0219 | female | 3 | Mild intellectual disability, language development delay, cognitive disorders, hyperactivity, gross/fine motor retardation |
| ASD0221 | male | 3 | Intellectual disability, language absence, motor retardation, instability of gait |
| ASD0222 | female | 3 | Mild intellectual disability, language development delay, motor retardation |
| ASD0294 | male | 5 | Intellectual disability, language development delay, global development delay |
| ASD0326 | male | 4 | Mild intellectual disability, language development delay, global development delay |
| ASD0330 | male | 3 | lost of follow-up |
| ASD0343 | male | 5 | Intellectual disability, language development delay, cognitive disorders, learning disabilities, hyperactivity |

sequencer (Applied Biosystem, CA, USA) was used for Sanger sequencing.

## Quantitative PCR (qPCR)

The CNVs were validated by quantitative PCR (qPCR). qPCR validation was performed using the Roche LightCycler 480 II System (Roche, Basel, Switzerland). One pair of primers was selected from the middle of each CNV. The samples from the family of the indicated patient were analyzed in triplicate in a 10 μL reaction mixture (200 nM each primer, LightCycler 480 SYBR Green Master Mix (2X) and 5 or 10 ng of genomic DNA). The values were evaluated using LightCycler 480 Software (Applied Biosystems). Data analysis was performed using the qBase method (Hellemans et al., 2007). *GAPDH* was used as the reference gene for the minimal coefficient of variation. Data were normalized by setting a normal control to a value of 1.

## Bioinformatic analyses of sequencing data and variants

Verita TreKKer (v1.9.3, Berry Genomics, Beijing, China) was used to identify SNP/InDels. CNVnator(v1.2.2) (Abyzov et al., 2011) and BIC-Seq (v0.7.2) (Xi et al., 2011) were used for CNV detection, while Manta (Chen et al., 2016) was used for SV discovery. EnliVen (v1.9.3, Berry Genomics) was performed to annotate SNP/InDels/CNV/SV. EnliVen and ANNOVAR (Wang et al., 2010) were executed for VCF (variant call format) files. dbSNP (http://www.ncbi.nlm.nih.gov/snp), 1,000 Genomics Project (http://browser.1000genomes.org) and other related existing databases were applied to annotate the variants. By focusing on exonic variants, gene transcript annotation databases, such as Consensus CDS protein set (http://www.ncbi.nlm.nih.gov/CCDS), RefSeq Gene (http://www.ncbi.nlm.nih.gov/RefSeq), Ensembl (https://www.ensembl.org) and UCSC (http://genome.ucsc.edu), were used to determine amino acid changes. Variants were analyzed for pathogenicity according to the American College of Medical Genetics and Genomics (ACMG) grading criteria (Richards et al., 2015).

The clean reads were aligned on genome hg19 along with annotated genes in the Ensembl website using STAR v2.7 aligner (Dobin et al., 2013). Gene expression level was quantified using DROP pipeline with the default parameters (Yépez et al., 2021). Differential gene expression was used to validate the effect of candidate SNVs and CNVs if the gene is stably expressed in blood. Candidate CNV regions cover up to hundreds of in-CNV genes. The average expression level of in-CNV genes were compared to that of equal number of randomly selected out-CNV genes outside the CNV region on the same chromosome. The difference between in-CNV and out-CNV genes was quantified by Z-score and log2-fold change. The duplication/loss CNVs were expected to show greater/smaller Z-score and log2-fold change, respectively.

**TABLE 2 CNV changes in 9 ASD patients.**

| ID | Sex | Chromosome region | CNV site | Type of change | Size (Mb) | Origin | Clinical diagnosis | Affected parents' featured symptoms (if any) |
|---|---|---|---|---|---|---|---|---|
| ASD0018 | male | 22q11.2 | chr22: 18910690-21463171 | duplication | 2.7 | *de novo* | 22q11.2 duplication (proximal, A-D) syndrome | - |
| ASD0027 | male | 7q11.23 | chr7: 72688896-74173668 | duplication | 1.6 | *de novo* | Williams-Beuren syndrome critical region | - |
| ASD0060 | male | 2p16.3 | chr2: 51046035-51696622 | deletion | 0.7 | paternal | 2p16.3 deletion syndrome | Normal |
| ASD0144 | male | 16p13.11 | chr16: 14901699-16492313 | duplication | 1.49 | maternal | 16p13.11 recurrent microduplication syndrome | Normal |
| ASD0203 | female | 15q11q13 | chr15: 23596697-28012138 | duplication | 4.4 | maternal | 15q11q13 recurrent (PWS/AS) region (BP2-BP3, Class 2) | Normal |
| ASD0214 | female | 3q26 | chr3: 176244949-178219435 | deletion | 2 | *de novo* | 3q26 deletion include *TBL1XR1* gene (ASD related gene) | - |
| ASD0222 | female | 3q29 | chr3: 195740002-197962430 | deletion | 1.6 | *de novo* | 3q29 recurrent region (includes *DLG1* gene) | - |
| ASD0330 | male | 15q11q13 | chr15: 23597027-28729564 | duplication | 4.6 | *de novo* | 15q11q13 recurrent (PWS/AS) region (BP2-BP3, Class 2) | - |
| ASD0343 | male | 1q21.1 | chr1: 143691670-148830060 | duplication | 5 | maternal | 1q21.1 recurrent region (BP3-BP4, distal) (includes *GJA5* gene) | Congenital heart disease |

# Results

## Intellectual disability and language delay are the two most common features of ASD

Among 354 patients enrolled, 19 were molecular positive, including 12 males and 7 females, aged from 2 to 6 years. The diagnosis pipeline is summarized in Figure 2. The male-to-female ratio is less than about 4: 1 as these positive cases were mostly having *de novo* mutations. The specific clinical features of 19 patients with positive diagnosis are shown in Table 1. Except for the ASD0330 patient who lost follow-up, 17 of the remaining 18 patients had clinical symptoms of intellectual disability and language delay which are less common in those molecularly unknown ASD patients, suggesting that the co-occurrence of these two symptoms could be suggestive of inborn errors in genetic alterations in ASD patients.

## CNVs detected in this ASD cohort

We applied low-depth WGS CNVseq-algorithm to analyze genomic alterations in 354 ASD patients. The distribution and burden analysis of CNV calls were calculated and summarized in Supplementary Figure S1. Among these CNVs, we found 9 cases were positive for pathological CNVs (Table 2). The resolution of CNVs reached 100 kb (Lord et al., 2018). To verify the CNV results, qPCR was performed on the positive cases, which are all in agreement (Supplementary Figure S2). Among these CNVs, 6 were duplicated CNVs, other 3 were deletional CNVs. Some of these deletions/duplications are known syndromes. Among these 9 CNV cases, 5 were *de novo* and 4 were inherited.

### Duplications

ASD0018 carried a *de novo* duplication of the 22q11.2 proximal (A-D) region, which is associated with a highly variable clinical phenotype, ranging from apparently normal to a broad range of clinical features, including non-specific phenotypes (intellectual disability, learning disability, developmental delays, autism, psychiatric disorder growth delays, hypotonia) as well as phenotypes that overlap clinical findings of DiGeorge syndrome (DGS; OMIM #188400) or velocardiofacial syndrome (VCFS; OMIM #192,430) (ClinGen, 2018). 22q11.2 duplications are frequently inherited and incomplete penetrance has been demonstrated. The 22q11.2 duplication is often found in an apparently normal parent of a proband (Firth, 1993).

ASD0027 carried a *de novo* duplication of the 7q11.23 recurrent region (Williams-Beuren syndrome, OMIM #609757, including the *ELN* gene). Clinical findings in this syndrome may include speech delay, autistic features, motor delay, seizures, hypotonia, brain anomalies, joint laxity, and craniofacial abnormalities. Williams-Beuren region duplication syndrome is considered to be highly penetrant with patients showing variable expressivity. Both inherited and *de novo* cases of 7q11.23 duplications have been reported in the literature. The population frequency of the

**TABLE 3 SNV changes of 10 ASD patients.**

| ID | Sex | Gene | Nucleotide change | Amino acid change | Type of mutation | Origin | Clinical diagnosis |
|---|---|---|---|---|---|---|---|
| ASD0046 | female | *ASH1L* | c.8595delT | p.Gln2866fs | Frameshift | *de novo* | Intellectual developmental disorder, autosomal dominant 52 |
| ASD0061 | male | *EP300* | c.4242T>G | p.Tyr1414* | Non-sense | *de novo* | Menke-Hennekam syndrome 2 |
| ASD0063 | female | *SCN2A* | c.4550_4551del | p.Ala1517fs | Frameshift | *de novo* | Developmental and epileptic encephalopathy 11 |
| ASD0134 | male | *ADNP* | c.2156_2157insA | p.Tyr719* | Non-sense | *de novo* | Helsmoortel-van der Aa syndrome |
| ASD0148 | female | *SHANK3* | c.4728_4740del | p.Leu1577fs | Frameshift | *de novo* | Phelan-McDermid syndrome |
| ASD0162 | male | *NF1* | c.7395-2A>T | - | Splicing | *de novo* | Neurofibromatosis, type 1 |
| ASD0219 | female | *PRKD1* | c.41_71del | p.Leu14fs | Frameshift | *de novo* | Congenital heart defects and ectodermal dysplasia |
| ASD0221 | male | *SCN2A* | c.605 + 1G>A | - | Splicing | *de novo* | Episodic ataxia type 9 |
| ASD0294 | male | *PTEN* | c.546dupA | p.Leu182fs | Frameshift | *de novo* | Macrocephaly/autism syndrome |
| ASD0326 | male | *SCN2A* | c.1570C>T | p.Arg524* | Non-sense | *de novo* | Episodic ataxia type 9 |

chromosome 7q11.23 duplication syndrome was estimated to be 1 in 13,000 to 20,000 (Van der Aa et al., 2009; Levy et al., 2011). This patient presented wide dental space, which has not been reported.

ASD0144 carried a duplication of the 16p13.11 recurrent region (BP2-BP3) (including the *MYH11* gene) inherited from his phenotypically normal father. Duplication of the 16p13.11 region has been associated with a variable clinical presentation including developmental delay, intellectual disability/learning difficulties, behavioral abnormalities (including ASD and ADHD), hypotonia, congenital heart disease (such as tetralogy of Fallot), and variable dysmorphic features. The majority of patients with this duplication are inherited, mostly from an apparently unaffected parent or a parent with abnormal phenotypes similar to the child's phenotype but not that much severe (Khattabi et al., 2020). Penetrance for any clinical phenotype associated with this duplication was estimated to be 7% (Kendall et al., 2019).

ASD0203 and ASD0330 both carried a duplication of 15q11q13 recurrent region (PWS/AS, BP2-BP3, Class 2), which is associated with chromosome 15q11-q13 duplication syndrome (OMIM #608636). Common clinical symptoms of this syndrome are autism, intellectual disability, ataxia, epilepsy, developmental delay and mental and behavioral problems (Bundey et al., 1994; Burnside et al., 2011). Most of the reported cases were familial inherited cases, and few were *de novo* mutations (Christian et al., 2008). The syndrome showed incomplete penetrance, and the clinical manifestations of different patients were highly heterogeneous. ASD0203 inherited the duplication from her phenotypic normal mother, while ASD0330 carried a *de novo* duplication.

ASD0343 carried a duplication of the 1q21.1 recurrent region (BP3-BP4, distal, including the *GJA5* gene) inherited from his mother, who had congenital heart disease. Duplication of the 1q21.1 region has been associated with chromosome 1q21.1 duplication syndrome (OMIM #612475). The clinical phenotypes of the syndrome include varying degrees of intellectual impairment, macrocephaly, hypotonia, congenital heart disease (such as tetralogy of Fallot), and malformation features. Mental and behavioral disorders include ASD, ADHD and others. Most of the reported cases were inherited from unaffected parents with normal or abnormal phenotypes similar to the child but not severe, and the clinical phenotypes of patients are highly variable (Brunetti-Pierri et al., 2008; Bernier et al., 2016).

### Deletions

ASD0060 carried a deletion at 2p16.3 involving exons of a haploinsufficiency gene *NRXN1* inherited from his phenotypic normal father, which is associated with susceptibility to autism, schizophrenia (SCZD17), developmental delay, intellectual disability, and dysmorphic features. The phenotypes are highly variable and show incomplete penetrance (Schaaf et al., 2012; Dabell et al., 2013). Sleeping disorder of ASD0060 has not been reported in previous studies.

ASD0214 carried a *de novo* deletion covering a haploinsufficiency gene *TBL1XR1*, Heterozygous mutation or deletion of this gene is associated with autosomal dominant inherited intellectual disability type 41. The common clinical symptoms of patients include autism, intellectual disability, developmental delay, spasticity and facial deformations. The clinical manifestations of different patients are highly heterogeneous (O'Roak et al., 2012a; O'Roak et al., 2012b; Saitsu et al., 2014).

ASD0222 carried a *de novo* deletion of the 3q29 recurrent region (including the *DLG1* gene). Deletion of this region is associated with chromosome 3q29 deletion syndrome (OMIM #609425). Clinical findings in this syndrome are mild to moderate developmental delay, intellectual disability, ASD, speech delay, walking delay, microcephaly and mild dysmorphic features. Most 3q29 deletions are *de novo* mutations, and a small number of cases are inherited from parents (Ballif et al., 2008; Quintero-Rivera et al., 2010; Città et al., 2013).

## SNVs detected in this ASD cohort

We used the 30× WGS data for analyzing SNVs. Among 354 children with ASD, 10 were found with *de novo* deleterious SNVs (non-sense splicing or frameshift mutation, Table 3). The

TABLE 4 RNAseq results of positive CNVs detected in this ASD cohort.

| ID | Chromosome region | Type of change | gene_in_cnv | RNA_in_cnv | zScore_chr | zScore_cnv | zScore_random1 | zScore_random2 | zScore_random3 | log2fc_chr | log2fc_cnv | log2fc_random1 | log2fc_random2 | log2fc_random3 |
|---|---|---|---|---|---|---|---|---|---|---|---|---|---|---|
| ASD0018 | 22q11.2 | Duplication | 92 | 38 | 0.04 | 0.38 | −0.1 | 0.145 | 0.095 | −0.01 | 0.05 | −0.015 | 0.015 | 0 |
| ASD0027 | 7q11.23 | Duplication | 35 | 16 | 0.095 | 3.745 | 0.345 | 0.245 | −0.155 | 0 | 0.48 | 0.03 | 0.02 | −0.01 |
| ASD0060 | 2p16.3 | deletion | 1 | 0 | - | - | - | - | - | - | - | - | - | - |
| ASD0144 | 16p13.11 | duplication | 42 | 17 | −0.06 | 2.3 | −0.29 | −0.03 | 0.5 | −0.015 | 0.38 | −0.06 | −0.01 | 0.06 |
| ASD0203 | 15q11q13 | duplication | 122 | 3 | 0.06 | 2.56 | 0.8 | −0.09 | −0.85 | 0 | 0.38 | 0.1 | −0.03 | −0.12 |
| ASD0214 | 3q26 | deletion | 15 | 1 | 0.03 | −4.86 | −1.26 | 1.74 | 0.69 | −0.01 | −0.41 | −0.1 | 1.12 | 0.19 |
| ASD0222 | 3q29 | deletion | 59 | 22 | 0.05 | −5.025 | 0.205 | −0.23 | 0.01 | 0 | −0.775 | 0.01 | −0.04 | −0.005 |
| ASD0330 | 15q11q13 | duplication | 130 | 5 | −0.01 | 1.41 | 0.31 | −0.23 | 0.46 | −0.01 | 0.32 | −0.06 | −0.04 | 0.09 |
| ASD0343 | 1q21.1 | duplication | 99 | 18 | 0.07 | 2.075 | 0.205 | 0.12 | −0.065 | 0 | 0.385 | 0.02 | 0.005 | −0.015 |

Gene_in_cnv: gene numbers involved in CNV; RNA_in_cnv: gene numbers expressed in blood of the CNV; zScore_chr: Z-score value of the whole chromosome of the CNV; zScore_cnv: Z-score value of the CNV; zScore_random1/2/3: Z-score value of randomly selected non-mutated locations on the chromosome where the CNV is located; log2fc_chr: log2-fold change value of the whole chromosome of the CNV; log2fc_cnv: log2-fold change value of the CNV; log2fc_random1/2/3: log2-fold change value of randomly selected non-mutated locations on the chromosome where the CNV is located.

mutation sites and parental origins were verified by Sanger sequencing (Supplementary Figure S3). Among these mutational alleles, 7 were previously unreported alleles (PUAs).

ASD0063, ASD0221 and ASD0326 all carried *de novo* mutations of the *SCN2A* gene, which encodes the α-subunit family of voltage-gated sodium channel that is responsible for the action potentials in neurons and muscles. Mutations in *SCN2A* have been linked to epilepsy and ASD (Sanders et al., 2012; Tavassoli et al., 2014). The c. 4550_4551del of the *SCN2A* gene in ASD0063 was a PUA, while the c.605 + 1G>A mutation in ASD0221 and the c.1570C>T mutation in ASD0326 have been previously reported. ASD0063 had developmental and epileptic encephalopathy, seizures, benign familial infantile. ASD0221 and ASD0326 had no seizures, which is consistent with the clinical symptoms of patients with the same mutation reported previously (Kothur et al., 2018; van der Werf et al., 2020).

ASD0046 carried a PUA c. 8595delT of the *ASH1L* gene. The histone methyltransferase encoded by this gene is involved in chromatin epigenetic modifications and is associated with the transcriptional regulation of developmentally important genes. Mutations in the *ASH1L* gene can lead to intellectual developmental disorder, autosomal dominant 52. About 60% of the patients have ASD (Stessman et al., 2017).

ASD0061 carried a PUA c.4242T>G of the *EP300* gene, which encodes p300, a histone acetyltransferase that regulates transcription *via* chromatin remodeling and is important in the processes of cell proliferation and differentiation. Mutations in the *EP300* gene can lead to Menke-Hennekam syndrome-2 (MKHK2), characterized by variable impairment of intellectual development and facial dysmorphisms. Feeding difficulties, autistic behavior, recurrent upper airway infections, and hearing impairment are also frequently seen (Hamilton et al., 2016; Menke et al., 2018).

ASD0134 carried a *de novo* c.2156dupA mutation of the *ADNP* gene, which encodes a zinc finger protein with a homeodomain that has the transcription factor activity and is essential for brain formation. Mutations of the *ADNP* gene can lead to Helsmoortel-van der Aa syndrome, which includes intellectual disability, developmental delay, ASD and facial dysmorphic features (Helsmoortel et al., 2014; Breen et al., 2020). The incidence of this gene mutation in ASD population is 0.17% (Helsmoortel et al., 2014). The c.2156dupA of *ADNP* gene has been reported. Patients with this mutation had neurodevelopmental disorder, ADNP-related multiple congenital anomalies, intellectual disability, and ASD (DDD Study, 2015; Chérot et al., 2018).

ASD0148 carried a PUA c.4728_4740del of the *SHANK3* gene. The scaffold protein encoded by this gene is enriched in the postsynaptic compact of excitatory synapses and is associated with epithelial tubule development and excitatory synaptic transmission in the renal and enteric nervous systems. Mutations in the *SHANK3* gene can lead to Phelan McDermid syndrome (Prasad et al., 2000). Phelan McDermid syndrome is a developmental disorder with a variety of abnormal clinical manifestations, including neonatal hypotonia, global developmental delay, normal to accelerated growth, severe language delay to language loss, autistic behavior, and mild dysmorphic features (Prasad et al., 2000; Durand et al., 2007). Some studies have shown that mutations in the *SHANK3* gene are found in about 0.75% of ASD patients (Moessner et al., 2007). ASD0148 had increased pain tolerance, which has not been previously reported.

**TABLE 5 RNAseq results of positive SNVs detected in this ASD cohort.**

| ID | Gene | Nucleotide change | Type of mutation | Ensemble ID | Express in blood | Patient RNA expression level | Mean RNA expression level |
|---|---|---|---|---|---|---|---|
| ASD0046 | *ASH1L* | c.8595delT | Frameshift | ENSG00000116539 | yes | 1,196.02 | 1,206.834 |
| ASD0061 | *EP300* | c.4242T>G | Non-sense | ENSG00000100393 | yes | 2520.55 | 2718.56 |
| ASD0063 | *SCN2A* | c.4550_4551del | Frameshift | ENSG00000136531 | no | - | - |
| ASD0134 | *ADNP* | c.2156_2157insA | Non-sense | ENSG00000101126 | yes | 1,663.37 | 1791.54 |
| ASD0148 | *SHANK3* | c.4728_4740del | Frameshift | ENSG00000251322 | no | - | - |
| ASD0162 | *NF1* | c.7395-2A>T | Splicing | ENSG00000196712 | yes | 534.96 | 615.19 |
| ASD0219 | *PRKD1* | c.41_71del | Frameshift | ENSG00000184304 | no | - | - |
| ASD0221 | *SCN2A* | c.605 + 1G>A | Splicing | ENSG00000136531 | no | - | - |
| ASD0294 | *PTEN* | c.546dupA | Frameshift | ENSG00000171862 | yes | 3095.66 | 3948.45 |
| ASD0326 | *SCN2A* | c.1570C>T | Non-sense | ENSG00000136531 | no | - | - |

Patient RNA expression level: The RNA expression quantity of indicated gene of the index ASD patient; Mean RNA expression level: The average value of RNA expression quantity of the indicated gene in total 354 ASD patients.

ASD0162 carried a PUA c.7395-2A>T of the *NF1* gene. This gene encodes neurofibrin, which is mainly expressed in neurons, Schwann cells, oligodendrocytes and leukocytes. Mutations in the *NF1* gene can lead to neurofibroma type I, and about 10%–40% of patients with neurofibroma type I have been reported to have ASD (Walsh et al., 2013; Eijk et al., 2018).

ASD0219 carried a PUA c.41_71del of the *PRKD1* gene. The protein encoded by *PRKD1* is a serine/threonine kinase that regulates a variety of cellular functions, including membrane receptor signaling, transport at the Golgi, protection from oxidative stress at the mitochondria, gene transcription, and regulation of cell shape, motility, and adhesion. Mutations in the *PRKD1* gene can lead to congenital heart defects and ectodermal dysplasia (Sifrim et al., 2016). Case-control studies have shown that *de novo* mutations in the *PRKD1* gene occur more frequently in patients with autism than in the general population (Ellaway et al., 2013; Iossifov et al., 2014; Rubeis et al., 2014; DDD Study, 2015).

ASD0294 carried a PUA c.546dupA of the *PTEN* gene. This gene encodes a ubiquitously expressed tumor suppressor dual-specificity phosphatase that antagonizes the PI3K signaling pathway through its lipid phosphatase activity and negatively regulates the MAPK pathway through its protein phosphatase activity. Mutations in the *PTEN* gene lead to macrocephaly/autism syndrome, characterized by increased head circumference, abnormal facial features, and delayed psychomotor development resulting in autistic behavior or intellectual disability (Herman et al., 2007; Page et al., 2009). Some patients may have a primary immunodeficiency disorder with recurrent infections associated with variably abnormal T- and B-cell function (Tsujita et al., 2016).

## RNAseq validation of positive cases in this ASD cohort

RNAseq is often used for candidate disease gene discovery. Hear we use RNAseq to evaluate the expressional changes in the blood samples of the ASD patients with deleterious mutations.

### RNA expression level of detected positive CNVs

For each positive CNV, we first calculate background expression level of all genes located on the same chromosome of the patient. Next, we randomly selected three set of out-CNV genes on the chromosome where the CNV was located as negative controls of the patient. Then we calculated the average expression level of in-CNV and out-CNV genes. Finally, we calculated the value of z-score and log2-fold change of the in-CNV and out-CNV genes. Except that the genes affected in ASD0060 were not expressed in the peripheral blood, the z-score values and log2-fold changes of all other positive CNV cases were consistent with our genomic analysis results (duplication or deletion) (Table 4).

### RNA expression level of detected positive SNVs

We calculated the mutant gene expression level for SNV positive cases and used the average expression level of this gene in all other patients as the control. Several cases (the *SCN2A* gene of ASD0063, ASD0221 and ASD0326, the *SHANK3* gene of ASD0148 and the *PRKD1* gene of ASD0219) were excluded from this validation analysis because these genes were not expressed in peripheral blood. Indeed, the expression of mutant genes in the other five SNV-positive cases decreased compared with the average value of RNA expression level of 354 patients (Table 5).

# Discussion

Large-scale genomic studies have revealed multiple CNVs and SNVs in the pathogenesis of ASD (Ruzzo et al., 2019; Satterstrom et al., 2020). In this study, we found 10 SNVs in 354 ASD children with a positive rate of 2.8%, and 9 CNVs with a positive rate of 2.5%. The total positive rate (5.3%) is relatively lower than previous studies (Sebat et al., 2007; Gaugler et al., 2014). The major reason is that we mostly focused on the known CNVs and *de novo* dominant protein-truncating SNVs. These mutations explain the genetic etiology of ASD with rare mutations. The pathological *de novo* mutations

accounts for 4.2% (15/354) in our cohort. Other types of mutations, such as missense mutation of ASD genes, recessive SNVs, mosaicism, regulatory pathogenic variations or non-coding variants, may explain a large number of ASD in its genetic etiology (Zhang et al., 2021). The diagnostic rate of autism by other Chinese researchers ranges from 4% to 19% (Jiang et al., 2013; Wang et al., 2016; Du et al., 2018; Wu et al., 2018). The variable molecular diagnostic rate may be due to different cohorts of patients, detection methods and mutational types. It is possible in our pipeline that some pathogenic SNVs are missed due to the lower sequencing depth (~30×) compared to regular trio-WES depth (usually > 100×). In addition, we did not exclude the patients with fragile X syndrome or those cases with inborn error of metabolism who present autistic symptoms by biochemical screening. It must be noted that we have uncovered dozens of candidate variants that are characterized as variants of uncertain significance (VUS) to be verified by functional assays as causative variants or genes for ASD.

Three patients with SNVs in our cohort were in the *SCN2A* gene, and two cases with CNVs were in the 15q11q13 recurrent region (PWS/AS, BP2-BP3, Class 2). This data suggests that these ASD genes are more common in Chinese ASD, which agrees with previous findings by other researchers (Wang et al., 2016; Guo et al., 2017).

The combination of WGS and CNVseq can improve the diagnostic rate to a certain extent. However, since the cause of most ASD is unclear, complex SV may be one of the genetic alterations. In subsequent studies, we will explore non-coding region variation and SV in relation to ASD to improve diagnostic rate, as well as to explore new ASD-causative genes in combination with functional assays and animal models.

The RNA sequencing results of peripheral blood of our positive patients were well consistent with expected changes, suggesting that peripheral blood RNAseq can also be used as a means of detection and verification for patients with autism. The gene expression level could be inferred from the expression in peripheral blood detection (Xu et al., 2020). However, some ASD genes are not expressed in peripheral blood, which will have certain limitations for the diagnosis of autism patients.

In our study, autistic patients with comorbidity are more likely to find the genetic etiology, especially those with intellectual disability and language retardation. This also suggests that WGS together with RNAseq is effective in identifying the cause of autism when it is accompanied by other comorbidities, which is important for early diagnosis and precise intervention of ASD.

## Data availability statement

According to national legislation/guidelines, specifically the Administrative Regulations of the People's Republic of China on Human Genetic Resources (http://www.gov.cn/zhengce/content/2019-06/10/content_5398829.htm, http://english.www.gov.cn/policies/latest_releases/2019/06/10/content_281476708945462.htm), no additional raw data is available at this time. The raw sequence data reported in this paper have been deposited in the Genome Sequence Archive (Genomics, Proteomics & Bioinformatics 2021, 19(4):578-583) in National Genomics Data Center, China National Center for Bioinformation/Beijing Institute of Genomics, Chinese Academy of Sciences (GSA-Human: HRA004176/Genetic Diagnostic Yields of 354 Chinese ASD Children with Rare Mutations by a Pipeline of Genomic Tests) that are publicly accessible at https://ngdc.cncb.ac.cn/gsa-human. Data of this project can be accessed after an approval application to the project leader, WL. Please refer to email: liwei@bch.com.cn for detailed application guidance. The accession number HRA004176 should be included in the application.

## Ethics statement

The studies involving human participants were reviewed and approved by The Ethics Committee of Beijing Children's Hospital. Written informed consent to participate in this study was provided by the participants's legal guardian/next of kin.

## Author contributions

WL, YC, CH and XN designed and supervised the study; YZ and WL wrote the manuscript; YZ, RG, and WJX performed the experiments and analyzed the data. YL and YC collected the patient information. XL, CZ, and QG participated in data analysis. WSX collected the samples and prepared DNAs/RNAs.

## Funding

This work was partially supported by the Ministry of Science and Technology of China (2019YFA0802104; 2016YFC1000306); the National Natural Science Foundation of China (31830054); and the Beijing Municipal Health Commission (JingYiYan 2018-5).

## Conflict of interest

The authors declare that the research was conducted in the absence of any commercial or financial relationships that could be construed as a potential conflict of interest.

## Publisher's note



## Supplementary material

The Supplementary Material for this article can be found online at: https://www.frontiersin.org/articles/10.3389/fgene.2023.1108440/full#supplementary-material

# References


Abyzov, A., Urban, A. E., Snyder, M., and Gerstein, M. (2011). CNVnator: An approach to discover, genotype, and characterize typical and atypical CNVs from family and population genome sequencing. *Genome Res.* 21, 974–984. doi:10.1101/gr.114876.110

American Psychiatric Association (2013). *Diagnostic and statistical manual of mental disorders*. 5th ed. Washington, DC: American Psychiatric Publishing. doi:10.1176/appi.books.9780890425596

Ballif, B. C., Theisen, A., Coppinger, J., Gowans, G. C., Hersh, J. H., Madan-Khetarpal, S., et al. (2008). Expanding the clinical phenotype of the 3q29 microdeletion syndrome and characterization of the reciprocal microduplication. *Mol. Cytogenet* 1, 8. doi:10.1186/1755-8166-1-8

Bernier, R., Steinman, K. J., Reilly, B., Wallace, A. S., Sherr, E. H., Pojman, N., et al. (2016). Clinical phenotype of the recurrent 1q21.1 copy-number variant. *Genet. Med.* 18, 341–349. doi:10.1038/gim.2015.78

Breen, M. S., Garg, P., Tang, L., Mendonca, D., Levy, T., Barbosa, M., et al. (2020). Episignatures stratifying Helsmoortel-Van Der Aa Syndrome show modest correlation with phenotype. *Am. J. Hum. Genet.* 107, 555–563. doi:10.1016/j.ajhg.2020.07.003

Brunetti-Pierri, N., Berg, J. S., Scaglia, F., Belmont, J., Bacino, C. A., Sahoo, T., et al. (2008). Recurrent reciprocal 1q21.1 deletions and duplications associated with microcephaly or macrocephaly and developmental and behavioral abnormalities. *Nat. Genet.* 40, 1466–1471. doi:10.1038/ng.279

Bundey, S., Hardy, C., Vickers, S., Kilpatrick, M. W., and Corbett, J. A. (1994). Duplication of the 15q11-13 region in a patient with autism, epilepsy and ataxia. *Dev. Med. Child. Neurol.* 36, 736–742. doi:10.1111/j.1469-8749.1994.tb11916.x

Burnside, R. D., Pasion, R., Mikhail, F. M., Carroll, A. J., Robin, N. H., Youngs, E. L., et al. (2011). Microdeletion/microduplication of proximal 15q11.2 between BP1 and BP2: A susceptibility region for neurological dysfunction including developmental and language delay. *Hum. Genet.* 130, 517–528. doi:10.1007/s00439-011-0970-4

Chen, X., Schulz-Trieglaff, O., Shaw, R., Barnes, B., Schlesinger, F., Källberg, M., et al. (2016). Manta: Rapid detection of structural variants and indels for germline and cancer sequencing applications. *Bioinformatics* 32, 1220–1222. doi:10.1093/bioinformatics/btv710

Chérot, E., Keren, B., Dubourg, C., Carré, W., Fradin, M., Lavillaureix, A., et al. (2018). Using medical exome sequencing to identify the causes of neurodevelopmental disorders: Experience of 2 clinical units and 216 patients. *Clin. Genet.* 93, 567–576. doi:10.1111/cge.13102

Christian, S. L., Brune, C. W., Sudi, J., Kumar, R. A., Liu, S., Karamohamed, S., et al. (2008). Novel submicroscopic chromosomal abnormalities detected in autism spectrum disorder. *Biol. Psychiatry* 63, 1111–1117. doi:10.1016/j.biopsych.2008.01.009

Città, S., Buono, S., Greco, D., Barone, C., Alfei, E., Bulgheroni, S., et al. (2013). 3q29 microdeletion syndrome: Cognitive and behavioral phenotype in four patients. *Am. J. Med. Genet. A* 161A, 3018–3022. doi:10.1002/ajmg.a.36142

ClinGen (2018). *22q11.2 recurrent (DGS/VCFS) region (proximal, A-D) (includes TBX1)*. Available from: https://search.clinicalgenome.org/kb/gene-dosage/region/ISCA-37446.

Dabell, M. P., Rosenfeld, J. A., Bader, P., Escobar, L. F., El-Khechen, D., Vallee, S. E., et al. (2013). Investigation of NRXN1 deletions: Clinical and molecular characterization. *Am. J. Med. Genet. A* 161A, 717–731. doi:10.1002/ajmg.a.35780

DDD Study (2015). Large-scale discovery of novel genetic causes of developmental disorders. *Nature* 519, 223–228. doi:10.1038/nature14135

Dias, C. M., and Walsh, C. A. (2020). Recent advances in understanding the genetic architecture of autism. *Annu. Rev. Genomics Hum. Genet.* 21, 21289–21304. doi:10.1146/annurev-genom-121219-082309

Dobin, A., Davis, C. A., Schlesinger, F., Drenkow, J., Zaleski, C., Jha, S., et al. (2013). STAR: Ultrafast universal RNA-seq aligner. *Bioinformatics* 29, 15–21. doi:10.1093/bioinformatics/bts635

Du, X., Gao, X., Liu, X., Shen, L., Wang, K., Fan, Y., et al. (2018). Genetic diagnostic evaluation of trio-based whole exome sequencing among children with diagnosed or suspected autism spectrum disorder. *Front. Genet.* 9, 594. doi:10.3389/fgene.2018.00594

Durand, C. M., Betancur, C., Boeckers, T. M., Bockmann, J., Chaste, P., Fauchereau, F., et al. (2007). Mutations in the gene encoding the synaptic scaffolding protein SHANK3 are associated with autism spectrum disorders. *Nat. Genet.* 39, 25–27. doi:10.1038/ng1933

Eijk, S., Mous, S. E., Dieleman, G. C., Dierckx, B., Rietman, A. B., de Nijs, P. F. A., et al. (2018). Autism spectrum disorder in an unselected cohort of children with neurofibromatosis type 1 (NF1). *J. Autism Dev. Disord.* 48, 2278–2285. doi:10.1007/s10803-018-3478-0

Ellaway, C. J., Ho, G., Bettella, E., Knapman, A., Collins, F., Hackett, A., et al. (2013). 14q12 microdeletions excluding FOXG1 give rise to a congenital variant Rett syndrome-like phenotype. *Eur. J. Hum. Genet.* 21, 522–527. doi:10.1038/ejhg.2012.208

Firth, H. V. (1993). *22q11.2 Duplication – archived Chapter, for historical reference only*. GeneReviews.

Gaugler, T., Klei, L., Sanders, S. J., Bodea, C. A., Goldberg, A. P., Lee, A. B., et al. (2014). Most genetic risk for autism resides with common variation. *Nat. Genet.* 46, 881–885. doi:10.1038/ng.3039

Guo, H., Peng, Y., Hu, Z., Li, Y., Xun, G., Ou, J., et al. (2017). Genome-wide copy number variation analysis in a Chinese autism spectrum disorder cohort. *Sci. Rep.* 7, 44155. doi:10.1038/srep44155

Hamilton, M. J., Newbury-Ecob, R., Holder-Espinasse, M., Yau, S., Lillis, S., Hurst, J. A., et al. (2016). Rubinstein-taybi syndrome type 2: Report of nine new cases that extend the phenotypic and genotypic spectrum. *Clin. Dysmorphol.* 25, 135–145. doi:10.1097/MCD.0000000000000143

Hellemans, J., Mortier, G., Paepe, A. D., Speleman, F., and Vandesompele, J. (2007). qBase relative quantification framework and software for management and automated analysis of real-time quantitative PCR data. *Genome Biol.* 8, R19. doi:10.1186/gb-2007-8-2-r19

Helsmoortel, C., Vulto-van Silfhout, A. T., Coe, B. P., Vandeweyer, G., Rooms, L., van den Ende, J., et al. (2014). A SWI/SNF-related autism syndrome caused by de novo mutations in ADNP. *Nat. Genet.* 46, 380–384. doi:10.1038/ng.2899

Herman, G. E., Butter, E., Enrile, B., Pastore, M., Prior, T. W., and Sommer, A. (2007). Increasing knowledge of PTEN germline mutations: Two additional patients with autism and macrocephaly. *Am. J. Med. Genet. A* 143A, 589–593. doi:10.1002/ajmg.a.31619

Iossifov, I., O'Roak, B. J., Sanders, S. J., Ronemus, M., Krumm, N., Levy, D., et al. (2014). The contribution of de novo coding mutations to autism spectrum disorder. *Nature* 515, 216–221. doi:10.1038/nature13908

Jiang, Y. H., Yuen, R. K., Jin, X., Wang, M., Chen, N., Wu, X., et al. (2013). Detection of clinically relevant genetic variants in autism spectrum disorder by whole-genome sequencing. *Am. J. Hum. Genet.* 93, 249–263. doi:10.1016/j.ajhg.2013.06.012

Kendall, K. M., Bracher-Smith, M., Fitzpatrick, H., Lynham, A., Rees, E., Escott-Price, V., et al. (2019). Cognitive performance and functional outcomes of carriers of pathogenic copy number variants: Analysis of the UK biobank. *Br. J. Psychiatry* 214, 297–304. doi:10.1192/bjp.2018.301

Khattabi, L. A. E., Heide, S., Caberg, J-H., Andrieux, J., Fenzy, M. D., Vincent-Delorme, C., et al. (2020). 16p13.11 microduplication in 45 new patients: Refined clinical significance and genotype-phenotype correlations. *J. Med. Genet.* 57, 301–307. doi:10.1136/jmedgenet-2018-105389

Kothur, K., Holman, K., Farnsworth, E., Ho, G., Lorentzos, M., Troedson, C., et al. (2018). Diagnostic yield of targeted massively parallel sequencing in children with epileptic encephalopathy. *Seizure* 59, 132–140. doi:10.1016/j.seizure.2018.05.005

Lek, M., Karczewski, K. J., Minikel, E. V., Samocha, K. E., Banks, E., Fennell, T., et al. (2016). Analysis of protein-coding genetic variation in 60,706 humans. *Nature* 536, 285–291. doi:10.1038/nature19057

Levy, D., Ronemus, M., Yamrom, B., Lee, Y-H., Leotta, A., Kendall, J., et al. (2011). Rare de novo and transmitted copy-number variation in autistic spectrum disorders. *Neuron* 70, 886–897. doi:10.1016/j.neuron.2011.05.015

Lobar, S. L. (2016). DSM-V changes for autism spectrum disorder (ASD): Implications for diagnosis, management, and care coordination for children with ASDs. *J. Pediatr. Health Care* 30, 359–365. doi:10.1016/j.pedhc.2015.09.005

Loomes, R., Hull, L., and Mandy, W. P. L. (2017). What is the male-to-female ratio in autism spectrum disorder? A systematic review and meta-analysis. *J. Am. Acad. Child. Adolesc. Psychiatry* 56, 466–474. doi:10.1016/j.jaac.2017.03.013

Lord, C., Elsabbagh, M., Baird, G., and Veenstra-Vanderweele, J. (2018). Autism spectrum disorder. *Lancet* 392, 508–520. doi:10.1016/S0140-6736(18)31129-2

Maenner, M. J., Shaw, K. A., Baio, J., Washington, A., Patrick, M., et al.EdS1 (2020). *Prevalence of autism spectrum disorder Among children aged 8 Years - autism and developmental disabilities monitoring network, 11 sites, United States, 2016. Morbidity and mortality weekly report*, 69. Washington, D.C., 1–12. Surveillance summaries. doi:10.15585/mmwr.ss6904a1

Menke, L. A., Gardeitchik, T., Hammond, P., Heimdal, K. R., Houge, G., et al.DDD study (2018). Further delineation of an entity caused by CREBBP and EP300 mutations but not resembling Rubinstein-Taybi syndrome. *Am. J. Med. Genet. A* 176, 862–876. doi:10.1002/ajmg.a.38626

Moessner, R., Marshall, C. R., Sutcliffe, J. S., Skaug, J., Pinto, D., Vincent, J., et al. (2007). Contribution of SHANK3 mutations to autism spectrum disorder. *Am. J. Hum. Genet.* 81, 1289–1297. doi:10.1086/522590

Neale, B. M., Kou, Y., Liu, L., Ma'ayan, A., Samocha, K. E., Sabo, A., et al. (2012). Patterns and rates of exonic de novo mutations in autism spectrum disorders. *Nature* 485, 242–245. doi:10.1038/nature11011

O'Roak, B. J., Vives, L., Girirajan, S., Karakoc, E., Krumm, N., Coe, B. P., et al. (2012). Sporadic autism exomes reveal a highly interconnected protein network of de novo mutations. *Nature* 485, 246–250. doi:10.1038/nature10989

O'Roak, B. J., Vives, L., Fu, W., Egertson, J. D., Stanaway, I. B., Phelps, I. G., et al. (2012). Multiplex targeted sequencing identifies recurrently mutated genes in autism spectrum disorders. *Science* 338, 1619–1622. doi:10.1126/science.1227764

Page, D. T., Kuti, O. J., Prestia, C., and Sur, M. (2009). Haploinsufficiency for Pten and Serotonin transporter cooperatively influences brain size and social behavior. *Proc. Natl. Acad. Sci. U.S.A.* 106, 1989–1994. doi:10.1073/pnas.0804428106

Popow, C., Ohmann, S., and Plener, P. (2021). Practitioner's review: Medication for children and adolescents with autism spectrum disorder (ASD) and comorbid conditions. *Neuropsych* 35, 113–134. doi:10.1007/s40211-021-00395-9

Prasad, C., Prasad, A. N., Chodirker, B. N., Lee, C., Dawson, A. K., Jocelyn, L. J., et al. (2000). Genetic evaluation of pervasive developmental disorders: The terminal 22q13 deletion syndrome may represent a recognizable phenotype. *Clin. Genet.* 57, 103–109. doi:10.1034/j.1399-0004.2000.570203.x

Quintero-Rivera, F., Sharifi-Hannauer, P., and Martinez-Agosto, J. A. (2010). Autistic and psychiatric findings associated with the 3q29 microdeletion syndrome: Case report and review. *Am. J. Med. Genet. A* 152A, 2459–2467. doi:10.1002/ajmg.a.33573

Richards, S., Aziz, N., Bale, S., Bick, D., Das, S., Gastier-Foster, J., et al. (2015). Standards and guidelines for the interpretation of sequence variants: A joint consensus recommendation of the American College of medical genetics and genomics and the association for molecular pathology. *Genet. Med.* 17, 405–424. doi:10.1038/gim.2015.30

Rubeis, S. D., He, X., Goldberg, A. P., Poultney, C. S., Samocha, K., Cicek, A. E., et al. (2014). Synaptic, transcriptional and chromatin genes disrupted in autism. *Nature* 515, 209–215. doi:10.1038/nature13772

Rutherford, M., McKenzie, K., Johnson, T., Catchpole, C., O'Hare, A., McClure, I., et al. (2016). Gender ratio in a clinical population sample, age of diagnosis and duration of assessment in children and adults with autism spectrum disorder. *Autism* 20, 628–634. doi:10.1177/1362361315617879

Ruzzo, E. K., Pérez-Cano, L., Jung, J-Y., Wang, L-K., Kashef-Haghighi, D., Hartl, C., et al. (2019). Inherited and de novo genetic risk for autism impacts shared networks. *Cell* 178, 850–866.e26. doi:10.1016/j.cell.2019.07.015

Saitsu, H., Tohyama, J., Walsh, T., Kato, M., Kobayashi, Y., Lee, M., et al. (2014). A girl with West syndrome and autistic features harboring a de novo TBL1XR1 mutation. *J. Hum. Genet.* 59, 581–583. doi:10.1038/jhg.2014.71

Sanders, S. J., Murtha, M. T., Gupta, A. R., Murdoch, J. D., Raubeson, M. J., Willsey, A. J., et al. (2012). De novo mutations revealed by whole-exome sequencing are strongly associated with autism. *Nature* 485, 237–241. doi:10.1038/nature10945

Sandin, S., Lichtenstein, P., Kuja-Halkola, R., Hultman, C., Larsson, H., and Reichenberg, A. (2017). The heritability of autism spectrum disorder. *J. Am. Med. Assoc.* 318, 1182–1184. doi:10.1001/jama.2017.12141

Satterstrom, F. K., Kosmicki, J. A., Wang, J., Breen, M. S., Rubeis, S. D., An, J-Y., et al. (2020). Large-scale exome sequencing study implicates both developmental and functional changes in the neurobiology of autism. *Cell* 180, 568–584.e23. doi:10.1016/j.cell.2019.12.036

Schaaf, C. P., Boone, P. M., Sampath, S., Williams, C., Bader, P. I., Mueller, J. M., et al. (2012). Phenotypic spectrum and genotype-phenotype correlations of NRXN1 exon deletions. *Eur. J. Hum. Genet.* 20, 1240–1247. doi:10.1038/ejhg.2012.95

Sebat, J., Lakshmi, B., Malhotra, D., Troge, J., Lese-Martin, C., Walsh, T., et al. (2007). Strong association of de novo copy number mutations with autism. *Science* 316, 445–449. doi:10.1126/science.1138659

Sifrim, A., Hitz, M-P., Wilsdon, A., Breckpot, J., Turki, S., Thienpont, B., et al. (2016). Distinct genetic architectures for syndromic and nonsyndromic congenital heart defects identified by exome sequencing. *Nat. Genet.* 48, 1060–1065. doi:10.1038/ng.3627

Simonoff, E., Pickles, A., Charman, T., Chandler, S., Loucas, T., and Baird, G. (2008). Psychiatric disorders in children with autism spectrum disorders: Prevalence, comorbidity, and associated factors in a population-derived sample. *J. Am. Acad. Child. Adolesc. Psychiatry* 47, 921–929. doi:10.1097/CHI.0b013e318179964f

Stessman, H. A. F., Xiong, B., Coe, B. P., Wang, T., Hoekzema, K., Fenckova, M., et al. (2017). Targeted sequencing identifies 91 neurodevelopmental-disorder risk genes with autism and developmental-disability biases. *Nat. Genet.* 49, 515–526. doi:10.1038/ng.3792

Tavassoli, T., Kolevzon, A., Wang, A. T., Curchack-Lichtin, J., Halpern, D., Schwartz, L., et al. (2014). De novo SCN2A splice site mutation in a boy with Autism spectrum disorder. *BMC Med. Genet.* 15, 35. doi:10.1186/1471-2350-15-35

Tsujita, Y., Mitsui-Sekinaka, K., Imai, K., Yeh, T-W., Mitsuiki, N., Asano, T., et al. (2016). Phosphatase and tensin homolog (PTEN) mutation can cause activated phosphatidylinositol 3-kinase δ syndrome-like immunodeficiency. *J. Allergy Clin. Immunol.* 138, 1672–1680.e10. doi:10.1016/j.jaci.2016.03.055

Van der Aa, N., Rooms, L., Vandeweyer, G., van den Ende, J., Reyniers, E., Fichera, M., et al. (2009). Fourteen new cases contribute to the characterization of the 7q11.23 microduplication syndrome. *Eur. J. Med. Genet.* 52, 94–100. doi:10.1016/j.ejmg.2009.02.006

van der Werf, I. M., Jansen, S., de Vries, P. F., Gerstmans, A., van de Vorst, M., Dijck, A. V., et al. (2020). Overrepresentation of genetic variation in the AnkyrinG interactome is related to a range of neurodevelopmental disorders. *Eur. J. Hum. Genet.* 28, 1726–1733. doi:10.1038/s41431-020-0682-0

Walsh, K. S., Vélez, J. I., Kardel, P. G., Imas, D. M., Muenke, M., Packer, R. J., et al. (2013). Symptomatology of autism spectrum disorder in a population with neurofibromatosis type 1. *Dev. Med. Child. Neurol.* 55, 131–138. doi:10.1111/dmcn.12038

Wang, K., Li, M., and Hakonarson, H. (2010). Annovar: Functional annotation of genetic variants from high-throughput sequencing data. *Nucleic Acids Res.* 38, e164. doi:10.1093/nar/gkq603

Wang, T., Guo, H., Xiong, B., Stessman, H. A. F., Wu, H., Coe, B. P., et al. (2016). De novo genic mutations among a Chinese autism spectrum disorder cohort. *Nat. Commun.* 7, 13316. doi:10.1038/ncomms13316

Wu, J., Yu, P., Jin, X., Xu, X., Li, J., Li, Z., et al. (2018). Genomic landscapes of Chinese sporadic autism spectrum disorders revealed by whole-genome sequencing. *J. Genet. Genomics* 45, 527–538. doi:10.1016/j.jgg.2018.09.002

Xi, R., Hadjipanayis, A. G., Luquette, L. J., Kim, T-M., Lee, E., Zhang, J., et al. (2011). Copy number variation detection in whole-genome sequencing data using the Bayesian information criterion. *Proc. Natl. Acad. Sci. U.S.A.* 108, E1128–E1136. doi:10.1073/pnas.1110574108

Xu, W., Leng, F., Liu, X., and Li, W. (2020). Blood-based multi-tissue gene expression inference with Bayesian ridge regression. *Bioinformatics* 36, 3788–3794. doi:10.1093/bioinformatics/btaa239

Yépez, V. A., Mertes, C., Müller, M. F., Klaproth-Andrade, D., Wachutka, L., Frésard, L., et al. (2021). Detection of aberrant gene expression events in RNA sequencing data. *Nat. Protoc.* 16, 1276–1296. doi:10.1038/s41596-020-00462-5

Zhang, Y., Liu, X. S., Guo, R. L., Xu, W. J., Guo, Q., Hao, C. J., et al. (2021). Biological implications of genetic variations in autism spectrum disorders from genomics studies. *Biosci. Rep.* 41, BSR20210593. doi:10.1042/BSR20210593

frontiers | Frontiers in Genetics

TYPE Original Research
PUBLISHED 24 March 2023
DOI 10.3389/fgene.2023.1135438



OPEN ACCESS

EDITED BY
Xiu-An Yang,
Chengde Medical College, China

REVIEWED BY
Vincent Gache,
INSERM U1217 Institut NeuroMyoGène (INMG), France
Jared C. Roach,
Institute for Systems Biology (ISB), United States
Elisa Di Pasquale,
National Research Council (CNR), Italy
Maria Rosaria D'Apice,
Policlinico Tor Vergata, Italy

*CORRESPONDENCE
Oscar Campuzano,
oscar@brugada.org
Georgia Sarquella-Brugada,
georgia@brugada.org

†These authors have contributed equally to this work and share first authorship

SPECIALTY SECTION
This article was submitted to Human and Medical Genomics, a section of the journal
Frontiers in Genetics

RECEIVED 31 December 2022
ACCEPTED 17 March 2023
PUBLISHED 24 March 2023

CITATION
Cesar S, Coll M, Fiol V, Fernandez-Falgueras A, Cruzalegui J, Iglesias A, Moll I, Perez-Serra A, Martínez-Barrios E, Ferrer-Costa C, Olmo Bd, Puigmulè M, Alcalde M, Lopez L, Pico F, Berrueco R, Brugada J, Zschaeck I, Natera-de Benito D, Carrera-García L, Exposito-Escudero J, Ortez C, Nascimento A, Brugada R, Sarquella-Brugada G and Campuzano O (2023), *LMNA*-related muscular dystrophy: Identification of variants in alternative genes and personalized clinical translation. *Front. Genet.* 14:1135438. doi: 10.3389/fgene.2023.1135438



# *LMNA*-related muscular dystrophy: Identification of variants in alternative genes and personalized clinical translation

Sergi Cesar[1,2,3], Monica Coll[4,5], Victoria Fiol[1,2,3], Anna Fernandez-Falgueras[4,5], Jose Cruzalegui[1,2,3], Anna Iglesias[4,5], Isaac Moll[1,2,3], Alexandra Perez-Serra[4,5], Estefanía Martínez-Barrios[1,2,3], Carles Ferrer-Costa[4,5], Bernat del Olmo[4,5], Marta Puigmulè[4,5,6], Mireia Alcalde[4,5], Laura Lopez[4,5], Ferran Pico[4,5], Rubén Berrueco[7], Josep Brugada[1,2,3,5,8], Irene Zschaeck[1,2,3,9,10], Daniel Natera-de Benito[9,10], Laura Carrera-García[9,10], Jessica Exposito-Escudero[9,10], Carlos Ortez[9,10], Andrés Nascimento[9,10,11], Ramon Brugada[4,5,6,12], Georgia Sarquella-Brugada[1,2,3,6*†] and Oscar Campuzano[4,5,6*†]

[1]Pediatric Arrhythmias, Inherited Cardiac Diseases and Sudden Death Unit, Hospital Sant Joan de Déu, Barcelona, Spain, [2]Arrítmies pediàtriques, Cardiologia Genètica i Mort sobtada, Malalties Cardiovasculars en el Desenvolupament, Institut de Recerca Sant Joan de Déu, Esplugues de Llobregat, Barcelona, Spain, [3]European Reference Network for Rare, Low Prevalence and Complex Diseases of the Heart (ERN GUARD-Heart), Amsterdam, Netherlands, [4]Cardiovascular Genetics Center, University of Girona-IDIBGI, Girona, Spain, [5]Centro de Investigación Biomédica en Red, Enfermedades Cardiovasculares (CIBERCV), Madrid, Spain, [6]Medical Science Department, School of Medicine, Universitat de Girona, Girona, Catalonia, Spain, [7]Pediatric Hematology Service, Hospital Sant Joan de Déu Barcelona, Institut de Recerca Pediàtrica, Hospital Sant Joan de Déu de Barcelona (IRP-HSJD), Universitat de Barcelona, Barcelona, Spain, [8]Arrhythmia Section, Cardiology Service, Hospital Clínic, Barcelona, Spain, [9]Neuromuscular Unit, Department of Neurology, Hospital Sant Joan de Déu, Barcelona, Spain, [10]Investigación Aplicada en Enfermedades Neuromusculares Neurociències Institut de Recerca Sant Joan de Déu, Esplugues de Llobregat, Spain, [11]Instituto Nacional de Investigación Biomédica de Enfermedades Raras (CIBERER), Instituto de Salud Carlos III, Madrid, Spain, [12]Cardiology Department, Hospital Josep Trueta, Girona, Catalonia, Spain

**Background:** Laminopathies are caused by rare alterations in *LMNA*, leading to a wide clinical spectrum. Though muscular dystrophy begins at early ages, disease progression is different in each patient. We investigated variability in laminopathy phenotypes by performing a targeted genetic analysis of patients diagnosed with *LMNA*-related muscular dystrophy to identify rare variants in alternative genes, thereby explaining phenotypic differences.

**Methods:** We analyzed 105 genes associated with muscular diseases by targeted sequencing in 26 pediatric patients of different countries, diagnosed with any *LMNA*-related muscular dystrophy. Family members were also clinically assessed and genetically analyzed.

**Results:** All patients carried a pathogenic rare variant in *LMNA*. Clinical diagnoses included Emery-Dreifuss muscular dystrophy (EDMD, 13 patients), *LMNA*-related congenital muscular dystrophy (L-CMD, 11 patients), and limb-girdle muscular dystrophy 1B (LGMD1B, 2 patients). In 9 patients, 10 additional rare genetic variants

were identified in 8 genes other than *LMNA*. Genotype-phenotype correlation showed additional deleterious rare variants in five of the nine patients (3 L-CMD and 2 EDMD) with severe phenotypes.

**Conclusion:** Analysis f known genes related to muscular diseases in close correlation with personalized clinical assessments may help identify additional rare variants of *LMNA* potentially associated with early onset or most severe disease progression.

KEYWORDS

**sudden cardiac death, laminopathies, muscular dystrophy, genetics, genetic diagnostic**

# 1 Introduction

Muscular dystrophies caused by deleterious variants in the *LMNA* gene are very rare (<1 per 1,000,000; ORPHA:157973). Cervico-axial and scapuloperoneal weakness, joint contractures, and thoracic lordosis associated with a dystrophic muscle biopsy and variably elevated creatine kinase levels are usually associated with these severe entities (Quijano-Roy et al., 2008). Sudden death (SD) also is common in these patients, mainly due to malignant arrhythmias concomitant with heart alterations (Kumar et al., 2016).

Through alternative splicing, *LMNA* encodes proteins lamin A and C, intermediate filaments that are required during development and cell differentiation and are components of the nuclear envelope (Bonne et al., 2003; Paul and Fulka, 2022). More than 500 rare genetic alterations in *LMNA* have been found to be responsible for a group of diseases called laminopathies (Worman and Bonne, 2007; Dittmer and Misteli, 2011). The most common laminopathies are *LMNA*-related congenital muscular dystrophy (L-CMD) (OMIM: 613205), Emery–Dreifuss muscular dystrophy (EDMD) (OMIM: 181350), limb-girdle muscular dystrophy type 1B (LGMD-1B) (OMIM: 159001), and dilated cardiomyopathy with conduction defects (DCM-CD) (OMIM: 115200). A range of phenotypes have been reported in patients carrying deleterious rare *LMNA* variants (Bertrand et al., 2011; Worman, 2012; Carboni et al., 2013a; Carboni et al., 2013b; Ben Yaou et al., 2021). It has been suggested that different phenotypes can be explained by post-transcriptional modifications of the nuclear envelope/lamina proteins (Maraldi et al., 2011; Zheng et al., 2022). Although *LMNA* is accepted as the main cause of disease, the observed phenotype differences remain poorly understood, mainly at early stages of the disease. Genetic background is suggested to be responsible for these phenotypic differences in disease onset and progression, although no studies investigating the role of additional genetic variants have been reported so far. Understanding genetic background variability can facilitate the early diagnosis of *LMNA*-related muscular dystrophy, which is important for prevention of SD, rehabilitation management, and genetic counseling (Charniot et al., 2003; Choi et al., 2019; Murofushi et al., 2022).

In the present study, we performed a targeted genetic analysis and personalized genotype-phenotype interpretation in families diagnosed with *LMNA*-related muscular dystrophies. We identified rare alterations in genes other than *LMNA* that may help explain the differences in disease onset and phenotype progression.

# 2 Materials and methods

## 2.1 Cohort

The study was approved by the Ethics Committee of the Hospital Josep Trueta (Girona, Spain) and Hospital Sant Joan de Déu (Barcelona, Spain), following the Helsinki II declaration. Written informed consent to participate in this study was provided by the participants' legal guardians. Written informed consent was also obtained from all relatives included in the study.

The study enrolled 26 pediatric patients previously diagnosed with any type of *LMNA* muscular dystrophy (2014–2020) and carrying a definite pathogenic rare variant in *LMNA*. We retrospectively collected all available data from each patient's first clinical contact up to their enrollment in our study. Clinical evaluation of index cases included a complete physical examination by a pediatric neurologist, neuromuscular specialist, and pediatric cardiologist. Non-pediatric relatives enrolled in our study also were clinically assessed. Saliva or peripheral blood samples were obtained from each patient as well as all available family members. All individuals were clinically assessed at Hospital Sant Joan de Déu (Barcelona, Catalonia, Spain). The complete pedigree of each family was obtained, including history of neuromuscular and cardiac diseases, syncope, and unexplained deaths.

## 2.2 Genetic analysis

Genomic DNA was analyzed using next-generation sequencing (NGS). A total of 105 genes involved in neuromuscular diseases and risk of malignant cardiac arrhythmias were analyzed (*ACTA1, AGRN, ANO5, B3GALNT2, B4GAT1, BAG3, BIN1, CAPN3, CAV3, CCND3, CFL2, CHAT, CHKB, CHRNA1, CHRNB1, CHRND, CHRNE, CNTN1, COL6A1, COL6A2, COL6A3, COLQ, DAG1, DES, DMD, DNAJB6, DNM2, DOK7, DPAGT1, DPM1, DPM2, DPM3, DSC2, DSG2, DSP, DYSF, EMD, FHL1, FKRP, FKTN, FLNC, FOS, FXN, GAA, GFPT1, GMPPB, GOSR2, HRAS, ISPD, ITGA7, KBTBD13, KCNQ1, KCNH2, LAMA2, LAMP2, LARGE, LDB3, LMNA, MOK2, MTM1, MUSK, MYF6, MYOT, MYH7, MYBPC3, NEB, NESPRIN2, NUP88, PCNA, PLEC, PKCA, PKP2, POMGNT1, POMGNT2, POMK, POMT1, POMT2, RAPSN, RYR1, RYR2, SCN4A, SCN5A, SEPN1, SGCA, SGCB, SGCD, SGCG, SLC25A4, SREBP, TAZ, TCAP, TMEM5, TMEM43, TMPO,*

*TNNT1, TNNI3, TNNT2, TNPO3, TPM2, TPM3, TRIM32,* and *TTN*). All gene isoforms described in Ensembl 75 (www.ensembl.org) that have been linked with either a RefSeq code (www.ncbi.nlm.nih.gov/refseq) or CCDS (www.ncbi.nlm.nih.gov/CCDS) were included. Sequence data coordinates were based on UCSC human genome version hg19 (NCBI GRCh37 built). Biotinylated cRNA probe solution was used as a capture probe (Agilent Technologies, Santa Clara, CA, United States). Probes were designed using eArray (Agilent Technologies).

Non-common genetic variants [minor allele frequency (MAF) < 1%] identified throughout NGS analysis were confirmed using Sanger sequencing. Exons and exon–intron boundaries of each gene were amplified (Verities PCR, Applied Biosystems, Austin, TX, United States), and the resulting PCR products were purified (Exosap-IT, Affymetrix Inc., USB Products, Cleveland, OH, United States) and directly sequenced in both directions (Big Dye Terminator v3.1 and 3130XL Genetic Analyzer, both from Applied Biosystems). The Posterior SeqScape Software v2.5 (Life Technologies, Carlsbad, CA, United States) was used to compare results with the reference sequence from hg19. The identified rare variants were contrasted with the Human Gene Mutation Database (www.hgmd.cf.ac.uk/ac/index.php) and Genome Aggregation Database (gnomAD) (www.gnomad.broadinstitute.org). To detect copy number variation (CNV), we looked for significant differences between expected and obtained normalized coverage for a given sample in a region of interest. Several samples were analyzed to corroborate similar levels of coverage between samples. All CNVs were compared with the CNV Control database (www.gwas.biosciencedbc.jp/cgi-bin/cnvdb/cnv_top.cgi), Database of Genomic Variants (www.dgv.tcag.ca/dgv/app/home), DECIPHER (www.decipher.sanger.ac.uk), and gnomAD (www.gnomad.broadinstitute.org). Rare variants that were potentially deleterious and confirmed in the index case were analyzed using the Sanger method in the relatives.

Each rare variant was classified following current recommendations of the American College of Medical Genetics and Genomics (ACMG) (Richards et al., 2015). A vast majority of pathogenic (P) variants are extremely rare (<0.01%). All available data concerning each rare genetic variant was updated until submission time (June, 2022). Variants classified as Variant of Unknown Significance (VUS) in alternative genes were further sub-classified. Variants identified showed no reported MAF or low MAF. Certain association with any neuromuscular disease were considered as VUS with highly suspicious Likely Pathogenic role (VUS-LP); thus, they were included to clarify their potential role in clinical practice. To avoid bias, five investigators independently investigated genetic data concerning each analyzed variant in our study. Finally, all investigators discussed data included in each item of the ACMG and consensus as well as final classification of all rare variants.

# 3 Results

## 3.1 Cohort

Our study included 26 pediatric patients (mean age 8.2 years at enrollment; IQR, 4–12.5 years; 53.8% males) of 25 families, with a total of 76 individuals (26 index cases and 50 relatives). Two of the index cases enrolled were female monozygotic twins (index cases 23 and 24). Families were originally from Spain (12), United Kingdom (3), United States (3), Australia (2), Canada (1), France (1), Greece (1), Russia (1), and Argentina (1). No consanguinity occurred in any of families. No potential common ancestor was identified after the family interviews. All index cases accomplished with clinical criteria for LMNA-related muscular disease: 11 Patients (42.3%) were L-CMD, 13 (50%) were EDMD, and 2 (7.7%) presented as LGMD1B. Early-onset skeletal muscle impairment before 2 years of age was detected in 23 of the 26 cases (88.4%) (Figure 1). Clinical assessment was performed in all patients included in our cohort, confirming previous diagnosis for each *LMNA*-related muscular disease.

## 3.2 Genetic analysis

Our NGS analysis showed an average call rate of 99.25% achieved at 30x coverage. The median coverage per sample was 892 (749–1286). An average of four failed whole exons occurred in each sample, and all these exons were amplified using Sanger sequencing. All rare variants (MAF < 1%) were confirmed also using Sanger sequencing, discarding false positive signal. No CNV were identified in any of genes analyzed, including *LMNA*. Previous karyotype (performed at time of diagnosis, out of our centre) also discarded any large chromosomic alteration in all patients included in our cohort.

## 3.3 Rare variants in LMNA

All patients included in our study had a previous genetic analysis of the *LMNA* gene. This previous analysis identified rare variants in this gene as potential cause of the disease. Our targeted-gene panel analysis confirmed all previous rare variants in the *LMNA* gene (Figure 2). No additional rare or common variant classified as pathogenic (P) or likely pathogenic (LP) were identified in *LMNA*. As above mentioned, previous genetic analysis identified rare variants in the *LMNA* gene, which were classified according to available data at the moment of genetic analysis was performed. Rare variants in *LMNA* were reclassified following ACMG guidelines and accordingly to current data available (June, 2022). All *LMNA* variants remain classified as P or LP, without any modification in comparison to previous genetic report.

A total of 19 *LMNA* rare variants were identified (17 exonic and 2 intronic). Of exonic rare variants, 4 were delins and 13 missense. All variants were identified in heterozygous state (Figure 2). Eleven rare variants (57.89%) were classified as LP and 7 (36.84%) as definitively P. The most frequent rare variant identified in *LMNA* was p.Arg249Trp (5 patients, 19.23%), as previously reported (Quijano-Roy et al., 2008; Pasqualin et al., 2014; Heller et al., 2017; Ben Yaou et al., 2021; Fan et al., 2021; Jedrzejowska et al., 2021). These 5 patients were diagnosed with L-CMD (4 patients -index case 1, 2, 6, and 26-) and EDMD (1 patient -index case 14-). Other two rare variants were identified two times in different patients each one (p.Asn39Ser, patients 3 and 7; p.Arg453Trp, patients 20 and 21). Both rare variants were also previously

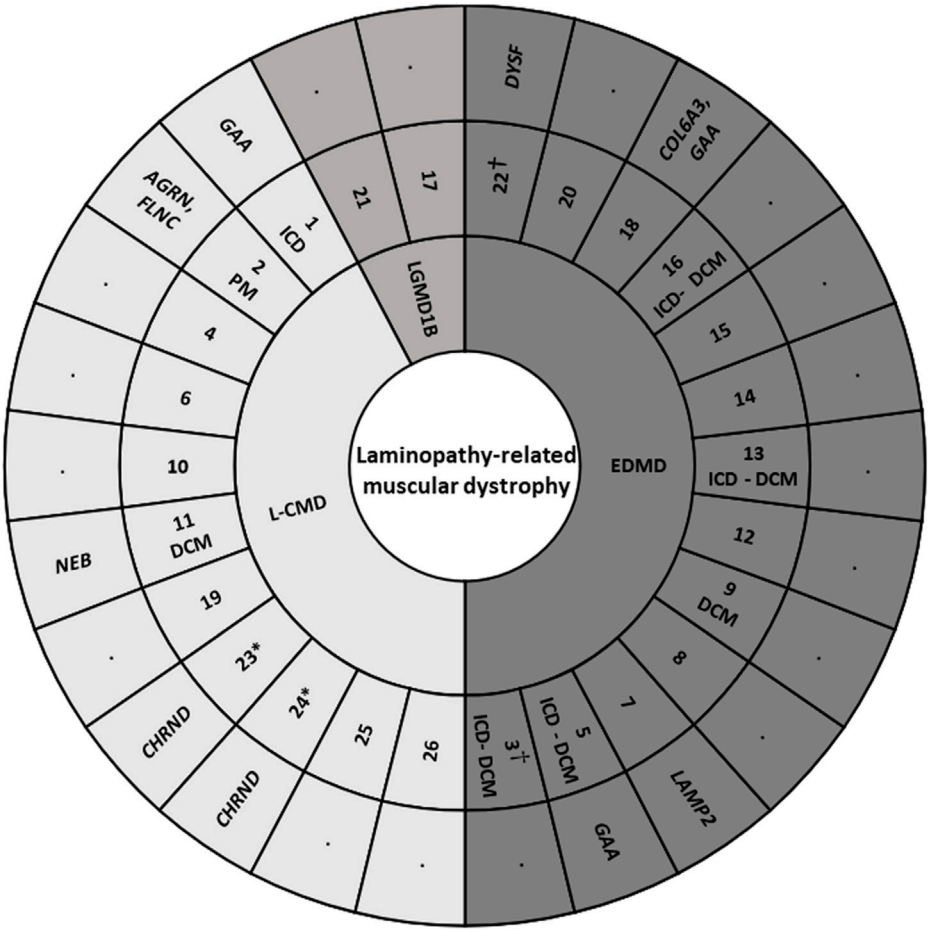


FIGURE 1
Cohort of index cases. DCM, dilated cardiomyopathy. EDMD, Emery-Dreifuss muscular dystrophy. ICD, implantable cardioverter defibrillator. L-CMD, *LMNA*-related congenital muscular dystrophy. LGMD1B, Limb-girdle muscular dystrophy 1B. PM, pacemaker. *, twins. †, sudden death.

reported (Pasqualin et al., 2014; Ben Yaou et al., 2021; Bennett et al., 2021; Fan et al., 2021; Jedrzejowska et al., 2021). A total of 6 cases showed DCM (patient 3, 5, 9, 11, 13, and 16), five of them diagnosed with EDMD and only one with L-CMD (patient 11). Among the patients with ICD (patients 1, 3, 5, 13, and 16), four were diagnosed with EDMD and one with L-CMD (patient 1). Index case number 2, diagnosed with L-CMD and carrying a pacemaker (PM), showed prolonged asystole episodes. Unfortunately, two cases died after inclusion in our study (patient 3 due to rapidly progressive heart failure despite optimal treatment and ICD carrier and 22due to severe respiratory infection) (Tables 1–3) (Figure 1). Finally, focused on intronic *LMNA* rare variant (c.810 + 1G>C) in patient 17, the clinical diagnostic was LGMD1B. The patient was not a carrier of any other rare variant in either the *LMNA* gene or any other gene. In addition, none of relatives showed any clinical symptom (Table 1).

Segregation of genetic variants in families showed that in 24 cases (92.3%), the rare variant in *LMNA* was *de novo* (including intronic variant in case number 17), as widely published (Ben Yaou et al., 2021; Jedrzejowska et al., 2021). Only in two families (index cases 11 and 18), one of parents carried the same deleterious variant in *LMNA*. In both these cases, the parents showed minor muscular impairment (Figure 3).

## 3.4 Additional rare variants

Eleven rare variants were identified in 8 genes (*AGRN, CHRND, COL6A3, DYSF, FLNC, GAA, LAMP2*, and *NEB*) encoding structural proteins. The *AGRN* gene encodes the protein Agrin, associated with Congenital myasthenic syndrome following an autosomal recessive (AR) pattern of inheritance. The *CHRND* gene encodes the Cholinergic receptor nicotinic delta subunit, mainly related to Myasthenic syndrome following autosomal dominant (AD) or AR pattern of inheritance. The *COL6A3* encodes Collagen type VI alpha 3 chain protein and deleterious variants are mainly associated with muscular dystrophy following both AD and AR patterns of inheritance. The *DYSF* gene encodes the protein Dysferlin, mainly associated with muscular dystrophy following an AR pattern of inheritance. The *FLNC* gene encodes the protein Filamin C, mainly associated wit cardiomyopathies following an AD pattern of inheritance. The *GAA* gene encodes Alpha Glucosidase and deleterious variants in this gene are related to Pompe disease following an AR pattern of inheritance. The *LAMP2*

Gene encodes the Lysosomal associated membrane protein 2, related to Danon disease following a X-linked pattern of inheritance. Finally, the *NEB* gene encodes the protein Nebulin, and pathogenic

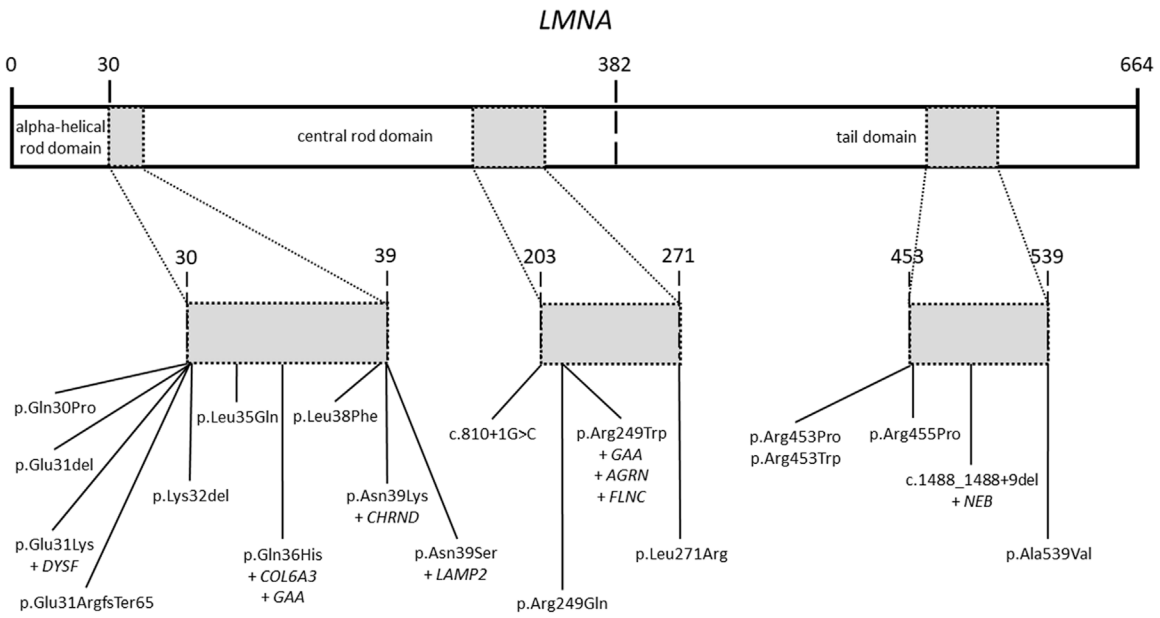


FIGURE 2
Rare variants in the *LMNA* gene. Domains of the *LMNA* gene including rare variants identified in our patients. All rare variants are located in three main zones of the gene.

variants in this gene cause mainly myopathy following an AR pattern of inheritance (Table 2). At this point, it is important to remark that none of these proteins have a close relation to the *LMNA* gene according to consulted protein databases.

These rare variants were identified in 8 families –1, 2, 5, 7, 11, 18, 22, and 23/24- (30.76%). No other rare or common alterations (single variants, delins, or CNV), classified as P, LP, or VUS-LP, were identified in any of additional genes analyzed. All the new 11 rare variants were exonic and in heterozygous state. One variant was non-sense (patient 2), 3 not-in-frame deletions (patients 2, 11, and 18), 2 not-in-frame delins (patients 23/24 -twins-), and 5 missense (patients 1, 5, 7, 18, and 22). All rare variants were classified as LP or VUS-LP following ACMG recommendations. None rare variant was repeated in more than one patient except in twins (patients 23/24) (Tables 1–3) (Figure 1).

Segregation of genetic variants in families showed that none of these rare variants was *de novo*. Curiously, only two variants in *GAA* (p.Arg594His, CM121193-patient 1-and p.Asp645Asn, CM980804-patient 18-) were previously identified and associated with Glycogen Storage Disease (GSD) (Huie et al., 1998; McCready et al., 2007; Liu et al., 2014). None of parents (except families 11 and 18, due to *LMNA*) were previously diagnosed or showed any symptom associated with the genes identified in this study (Figure 3).

## 3.5 Genotype-phenotype correlation

Previous clinical diagnosis and follow-up showed 9 patients with more severe phenotypes (6 EDMD -patients 3, 5, 9, 13, 16 and 22- and 3 L-CMD -patients 1, 2 and 11-). All nine patients carried a rare missense deleterious variant in *LMNA* except two (patient 9-EDMD-and 11-L-CMD-) whose carried deletions (p.Glu31ArgfsTer65 and c.1488_1488+9del, respectively) (Tables 1–3).

Six patients diagnosed with EDMD (patients 3, 5, 9, 13, 16, and 22) showed different phenotypes: DCM (patient 9) or DCM and carried an ICD (patients 3, 5, 13, and 16). Curiously, patient 22 did not show any risk factor but died suddenly. Patient 3 also died suddenly despite carrying an ICD. Only patient 9 carried a rare variant in *LMNA* (c.91delG) while all other patients carried a missense variant in the same gene. Concerning additional rare variants in other genes, only patient 5 carried a rare missense variant (c.1952G>A) in *GAA*, inherited from their unaffected mother (Figure 1).

Three patients diagnosed with L-CMD (patients 1, 2, and 11) also showed different phenotypes: DCM (patient 11) or carried an ICD (patient 1) or a PM (patient 2) but without DCM. Curiously, patients 1 and 2 (no family relationship) carried the same missense rare variant in *LMNA* (p.Arg249Trp) and patient 11 carried an intronic rare variant (c.1488_1488+9del). Additionally, all patients carried at least one rare variant: patient 1 in *GAA* (p.Arg594His) inherited from their mother and without any symptom to date, patient 2 carried two rare variants, one in *AGRN* and other in *FLNC* (p.Arg740Ter and p.Cys644TrpfsTer27, respectively), both rare variants inherited from their healthy mother, and patient 11 carried a rare variant in *NEB* (p.Met5792_Arp5794delinsIle), inherited from their mother who showed a mild neuromuscular affectation but their brother carried the same variant in *NEB* without any symptom diagnosed to date (Tables 1–3) (Figures 1, 2).

# 4 Discussion

A cohort of 26 patients diagnosed with *LMNA*-related muscular diseases were analyzed for the increasing number of additional rare

10.3389/fgene.2023.1135438

**TABLE 1** *LMNA*-related muscular dystrophy patients, major cardiac end points and rare *LMNA* variants.

| Patient | Sex | Age diagnosis | Phenotype | DCM | Device | *LMNA* variants (LP, P) | Other variants |
|---|---|---|---|---|---|---|---|
| 1 | M | 11 | L-CMD | No | ICD | c.745C > T (p.Arg249Trp) | *GAA* |
| 2 | M | 2 | L-CMD | No | PM | c.745C > T (p.Arg249Trp) | *AGRN, FLNC* |
| 3† | F | 16 | EDMD | Yes | ICD | c.116A > G (p.Asn39Ser) | None |
| 4 | F | 9 | L-CMD | No | No | c.91_93delGAG (p.Glu31del) | None |
| 5 | M | 11 | EDMD | Yes | ICD | c.1358G > C (p.Arg453Pro) | *GAA* |
| 6 | M | 9 | L-CMD | No | No | c.745C > T (p.Arg249Trp) | None |
| 7 | M | 3 | EDMD | No | No | c.116A > G (p.Asn39Ser) | *LAMP2* |
| 8 | F | 8 | EDMD | No | No | c.746G > A (p.Arg249Gln) | None |
| 9 | M | 7 | EDMD | Yes | No | c.91delG (p.Glu31ArgfsTer65) | None |
| 10 | F | 2 | L-CMD | No | No | c.89A > C (p.Gln30Pro) | None |
| 11 | F | 3 | L-CMD | Yes | No | c.1488_1488+9del | *NEB* |
| 12 | M | 15 | EDMD | No | No | c.1616C > T (p.Ala539Val) | None |
| 13 | M | 15 | EDMD | Yes | ICD | c.112C > T (p.Leu38Phe) | None |
| 14 | F | 8 | EDMD | No | No | c.745C > T (p.Arg249Trp) | None |
| 15 | M | 13 | EDMD | No | No | c.812T > G (p.Leu271Arg) | None |
| 16 | M | 15 | EDMD | Yes | ICD | c.1364G > C (p.Arg455Pro) | None |
| 17 | F | 11 | LGMD1B | No | No | c.810 + 1G > C | None |
| 18 | F | 3 | EDMD | No | No | c.108G > T (p.Gln36His) | *COL6A3, GAA* |
| 19 | M | 3 | L-CMD | No | No | c.104T > A (p.Leu35Gln) | None |
| 20 | F | 17 | EDMD | No | No | c.1357C > T (p.Arg453Trp) | None |
| 21 | M | 5 | LGMD1B | No | No | c.1357C > T (p.Arg453Trp) | None |
| 22† | F | 18 | EDMD | No | No | c.91G > A (p.Glu31Lys) | *DYSF* |
| 23*,24* | F | 5 | L-CMD | No | No | c.117T > G (p.Asn39Lys) | *CHRND* |
| 25 | M | 4 | L-CMD | No | No | c.94_96delAAG (p.Lys32del) | None |
| 26 | M | 4 | L-CMD | No | No | c.745C > T (p.Arg249Trp) | None |

DCM, dilated cardiomyopathy. EDMD, Emery-Dreifuss muscular dystrophy. F, Female. ICD, implantable cardioverter defibrillator. L-CMD, *LMNA*-related congenital muscular dystrophy. LGMD1B, Limb-girdle muscular dystrophy 1B. LP, Likely Pathogenic. M, Male. P, Pathogenic. PM, pacemaker. *, twins. †, sudden death.

alterations in other genes which may be involved in phenotype differences. We identified that 56% of patients with most severe phenotypes, mainly diagnosed with L-CMD, carried a deleterious rare variant in the *LMNA* gene, but also an additional deleterious rare variant in another gene associated with NMD, and played a potential role in early onset and disease progression.

Only a few cohorts of cases diagnosed with *LMNA*-related muscular diseases have been published to date, all following an autosomal dominant pattern of inheritance, as occurs in our study. In 2007, a cohort including 27 patients (EDMD, 56%; CMD, 15%; LGMD, 30%) (Benedetti et al., 2007). Other cohort was published in 2014, and included 78 cases diagnosed with *LMNA*-related myopathies (EDMD, 21%; L-CMD, 33%; LGMD1B, 46%) (Maggi et al., 2014). In addition, a cohort of 84 patients diagnosed with *LMNA*-related muscular dystrophy were also analyzed (EDMD, 38%; L-CMD, 49%; LGMD1B, 13%) (Fan et al., 2021). Our study shows similar percentages of *LMNA*-related muscular diseases (EDMD, 50%; L-CMD, 42%; LGMD1B, 8%). Recently, the largest cohort including 151 L-CMD patients was also published (Ben Yaou et al., 2021), reinforcing the necessity of anticipatory care of respiratory and cardiac assessment due to rapid progression of symptoms especially in L-CMD. As these are ultra-rare diseases, it is difficult to obtain patients with a definite diagnosis. Various forms of skeletal muscle laminopathies may overlap with each other, creating a phenotypic continuum, as recently reported in a cohort of 15 children with initial symptoms visible during first year of life, included hypotonia, poor head control, or delayed motor development (Jedrzejowska et al., 2021). In addition, involving large number of cases of different ethnic origin, as done in our study for the first time, is crucial to clarify role of genetic background in these ultra-rare diseases in onset as well as progression of disease. Currently, it is widely accepted *LMNA*-related muscular diseases as monogenic entities due to a single P rare variant in the *LMNA* gene. However, due to reported differences in severity of phenotypes,

**TABLE 2 Additional genes identified. AD, Autosomic Dominant; AR, Autosomic Recessive; XLD, X-Linked Dominant.**

| Genes | Location | Protein | Gene ID/ HGNC/MIM | Disease/MIM/Inheritance |
|---|---|---|---|---|
| *GAA* | 17q25.3 | Alpha Glucosidase | 2548/4065/606800 | Pompe/232300/AR |
| *AGRN* | 1p36.33 | Agrin | 375790/329/103320 | Congenital myasthenic syndrome-8/615120/AR |
| *FLNC* | 7q32.1 | Filamin C | 2318/3756/102565 | Cardiomyopathy, familial hypertrophic/617047/AD |
| | | | | Cardiomyopathy, familial restrictive/617047/AD |
| | | | | Myopathy, distal/614065/AD |
| | | | | Myopathy, myofibrillar/609524/AD |
| *LAMP2* | Xq24 | Lysosomal associated membrane protein 2 | 3920/6501/309060 | Danon/300257/XLD |
| *COL6A3* | 2q37.3 | Collagen type VI alpha 3 chain | 1293/2213/120250 | Bethlem myopathy/158810/AD, AR |
| | | | | Dystonia/616411/AR |
| | | | | Ullrich congenital muscular dystrophy/254090/AD, AR |
| *NEB* | 2q23.3 | Nebulin | 4703/7720/161650 | Arthrogryposis multiplex congenita/619334/AR |
| | | | | Nemaline myopathy/256030/AR |
| *DYSF* | 2p13.2 | Dysferlin | 8291/3097/603009 | Miyoshi muscular dystrophy/254130/AR |
| | | | | Muscular dystrophy, limb-girdle/253601/AR |
| | | | | Myopathy, distal, with anterior tibial onset/606768/AR |
| *CHRND* | 2q37.1 | Cholinergic receptor nicotinic delta subunit | 1144/1965/100720 | Myasthenic syndrome, congenital, slow-channel/616321/AD |
| | | | | Myasthenic syndrome, congenital, associated with acetylcholine receptor deficiency/616323/AR |
| | | | | Multiple pterygium syndrome, lethal type/253290/AR |
| | | | | Myasthenic syndrome, congenital, fast-channel/616322/AR |

existence of alternative rare variants as phenotype modifiers is suspected despite not reported to date. Our study aims to solve this gap in *LMNA*-related muscular diseases.

It is widely accepted that early diagnosis of *LMNA*-related muscular diseases is key for appropriate clinical management (Charniot et al., 2003), particularly in L-CMD (Ben Yaou et al., 2021). In addition, clinical familial history and close genotype-phenotype correlation can help clarify the role of genetic variants in onset as well as progression of disease (Cotta et al., 2019; Ben Yaou et al., 2021). Therefore, existence of additional rare genetic modifiers has been suggested as an explanation for clinical phenotype difference observed in families diagnosed with any type of laminopathy (Muntoni et al., 2006; Boudreau et al., 2012; Roncarati et al., 2013) despite no comprehensive genotype-phenotype study. Analysis of variant segregation in families can help unravel the role of the rare variants identified in this study. In summary, we report a targeted genetic analysis and segregation of variants in families, looking for additional rare variants in other genes than *LMNA*, which could explain the phenotypic differences in LMNA-related muscular diseases.

## 4.1 Genotype-phenotype correlation

All *LMNA* variants were deleterious, which was the main cause of the clinically diagnosed disease. However, different onset as well as disease progression seems to be modified by other variants, in concordance to previously suggested but not exhaustively analyzed to date. The variant p.Arg249Trp was identified in 5 patients (4 L-CMD and 1 EMD2). This variant was previously reported in several patients diagnosed with L-CMD (Ben Yaou et al., 2021). The variant was *de novo* in all reported cases and, in addition to early onset of muscular involvement, patients also showed cardiac involvement and malignant arrhythmias (Quijano-Roy et al., 2008; Komaki et al., 2011; Pasqualin et al., 2014; Ben Yaou et al., 2021; Fan et al., 2021; Jedrzejowska et al., 2021). In view of age-dependent penetrance for heart involvement due to deleterious variants in *LMNA*, a regular cardiological supervision should have been offered (Jedrzejowska et al., 2021), particularly in p.Arg249Trp carriers due to clinical severity (Ben Yaou et al., 2021).

Patients 1 and 2, diagnosed with L-CMD showed most severe phenotype and carried additional potentially deleterious rare variants (patient 1 in *GAA* and patient 2 in *AGRN* and *FLNC*). In patient 1, the *GAA*_p.Arg594His (CM121193) was previously reported and associated with GSD following an autosomal recessive pattern of inheritance (Liu et al., 2014). It was inherited from their asymptomatic mother and none showed any symptom of GSD or Pompe disease due to the heterozygous form. In patient 2, both variants were novel, inherited from their mother and classified as deleterious. The variants in *FLNC* are mainly associated with

**TABLE 3** *LMNA* **variants and related features found in our pediatric cohort.**

| Patient | Gene | Nucleotide change | Protein change | dbSNP | gnomAD (MAF%) | HGMD disease | ClinVar disease | ACMG score | Father | Mother | Other relatives |
|---|---|---|---|---|---|---|---|---|---|---|---|
| 1 | *GAA* | c.1781G>A | p.Arg594His | rs775450536 | 2/248732 (0.0008%) | CM121193, GSD | P, GSD | LP | - | + | Sister - |
| | *LMNA* | c.745C>T | p.Arg249Trp | rs121912496 | NA | CM083718, MD | P/LP, MD | LP | - | - | Sister- |
| 2 | *AGRN* | c.2218C>T | p.Arg740Ter | NA | NA | NA | NA | LP | - | + | Sister + |
| | *FLNC* | c.1932delT | p.Cys644TrpfsTer27 | NA | NA | NA | NA | LP | - | + | Sister- |
| | *LMNA* | c.745C>T | p.Arg249Trp | rs121912496 | NA | CM083718, MD | P/LP, MD | LP | - | - | Sister- |
| 3† | *LMNA* | c.116A>G | p.Asn39Ser | rs57983345 | NA | CM083713, MD | P, CMT | P | - | - | NA |
| 4 | *LMNA* | c.91_93delGAG | p.Glu31del | rs864309525 | NA | CD156162, MD | LP, MD | LP | - | - | NA |
| 5 | *GAA* | c.1952G > A | p.Gly651Asp | rs939350425 | NA | NA | VUS | LP | - | + | Siblings - |
| | *LMNA* | c.1358G > C | p.Arg453Pro | rs267607598 | NA | CM083716, MD | NA | LP | - | - | Siblings - |
| 6 | *LMNA* | c.745C > T | p.Arg249Trp | rs121912496 | NA | CM083718, MD | P/LP, MD | LP | - | - | NA |
| 7 | *LAMP2* | c.413A > G | p.Asp138Gly | NA | NA | NA | NA | VUS-LP | - | + | Brother - |
| | *LMNA* | c.116A > G | p.Asn39Ser | rs57983345 | NA | CM083713, MD | P, CMT | P | - | - | Brother - |
| 8 | *LMNA* | c.746G > A | p.Arg249Gln | rs59332535 | NA | CM1617006, MD, ED | P, MD | P | - | - | NA |
| 9 | *LMNA* | c.91delG | p.Glu31ArgfsTer65 | NA | NA | NA | NA | P | - | - | NA |
| 10 | *LMNA* | c.89A > C | p.Gln30Pro | NA | NA | NA | NA | LP | - | - | Brother - |
| 11 | *LMNA* | c.1487_1488 + 9del | | NA | NA | CD1711480, MD | NA | P | - | + | Brother - |
| | *NEB* | c.17376_17381del | p.Met5792_Asp5794delinsIle | rs765184893 | 9/247156 (0.0036%) | NA | NA | VUS-LP | - | + | Brother + |
| 12 | *LMNA* | c.1616C > T | p.Ala539Val | NA | NA | NA | NA | LP | - | - | NA |
| 13 | *LMNA* | c.112C > T | p.Leu38Phe | NA | NA | NA | NA | LP | - | - | NA |
| 14 | *LMNA* | c.745C > T | p.Arg249Trp | rs121912496 | NA | CM083718, MD | P/LP, MD | LP | - | - | NA |
| 15 | *LMNA* | c.812T > G | p.Leu271Arg | NA | NA | NA | NA | LP | - | - | NA |
| 16 | *LMNA* | c.1364G > C | p.Arg455Pro | rs267607597 | NA | CM111722, MD | NA | LP | - | - | NA |
| 17 | *LMNA* | c.810 + 1G > C | | rs267607632 | NA | NA | P, MD | P | - | - | NA |
| 18 | *COL6A3* | c.8883delA | p.Lys2961AsnfsTer40 | NA | NA | NA | NA | LP | + | - | NA |
| | *GAA* | c.1933G>A | p.Asp645Asn | rs368438393 | 2/242414 (0.0008%) | CM980804, GSD | LP, GSD | LP | - | + | NA |
| | *LMNA* | c.108G>T | p.Gln36His | NA | NA | NA | NA | LP | + | - | NA |

(Continued on following page)





10.3389/fgene.2023.1135438

**TABLE 3 (*Continued*) *LMNA* variants and related features found in our pediatric cohort.**

| Patient | Gene | Nucleotide change | Protein change | dbSNP | gnomAD (MAF%) | HGMD disease | ClinVar disease | ACMG score | Father | Mother | Other relatives |
|---|---|---|---|---|---|---|---|---|---|---|---|
| 19 | *LMNA* | c.104T>A | p.Leu35Gln | NA | NA | NA | NA | LP | - | - | NA |
| 20 | *LMNA* | c.1357C>T | p.Arg453Trp | rs58932704 | NA | CM990813, MD | P/LP, MD | LP | - | - | NA |
| 21 | *LMNA* | c.1357C>T | p.Arg453Trp | rs58932704 | NA | CM990813, MD | P/LP, MD | LP | - | - | NA |
| 22† | *DYSF* | c.5546G>A | p.Arg1849Lys | rs786205084 | NA | NA | LP, MD | LP | - | + | Brother + |
| | *LMNA* | c.91G>A | p.Glu31Lys | rs1228406418 | NA | CM123360, MD | P, CMT | LP | - | - | Brother - |
| 23,24 twins | *CHRND* | c.919_920delCCinsAG | p.Pro307Ser | NA | NA | NA | NA | VUS-LP | - | + | Brother +/Twin + |
| | *LMNA* | c.117T>G | p.Asn39Lys | NA | NA | CM156123, MD | NA | LP | - | - | Brother -/Twin + |
| 25 | *LMNA* | c.94_96delAAG | p.Lys32del | rs60872029 | NA | CD033712, MD, ED | P, MD | P | - | - | NA |
| 26 | *LMNA* | c.745C>T | p.Arg249Trp | rs121912496 | NA | CM083718, MD | P/LP, MD | LP | - | - | NA |

dbSNP, single nucleotide polymorphism database. ACMG, score, the American College of Medical Genetics and Genomics score. ClinVar, Clinically relevant Variation database. CMT, Charcot-Marie-Tooth. ED, Emery-Dreifuss. GnomAD (MAF%), Genome Aggregation Database (minor allele frequency %). GSD, Glycogen Storage Disease. HGMD, the Human Gene Mutation Database. LP, Likely Pathogenic. MD, muscular dystrophy. NA, not available. P, Pathogenic. †, sudden death. VUS-LP, variant of unknown significance with highly suspicious likely pathogenic role.





10.3389/fgene.2023.1135438

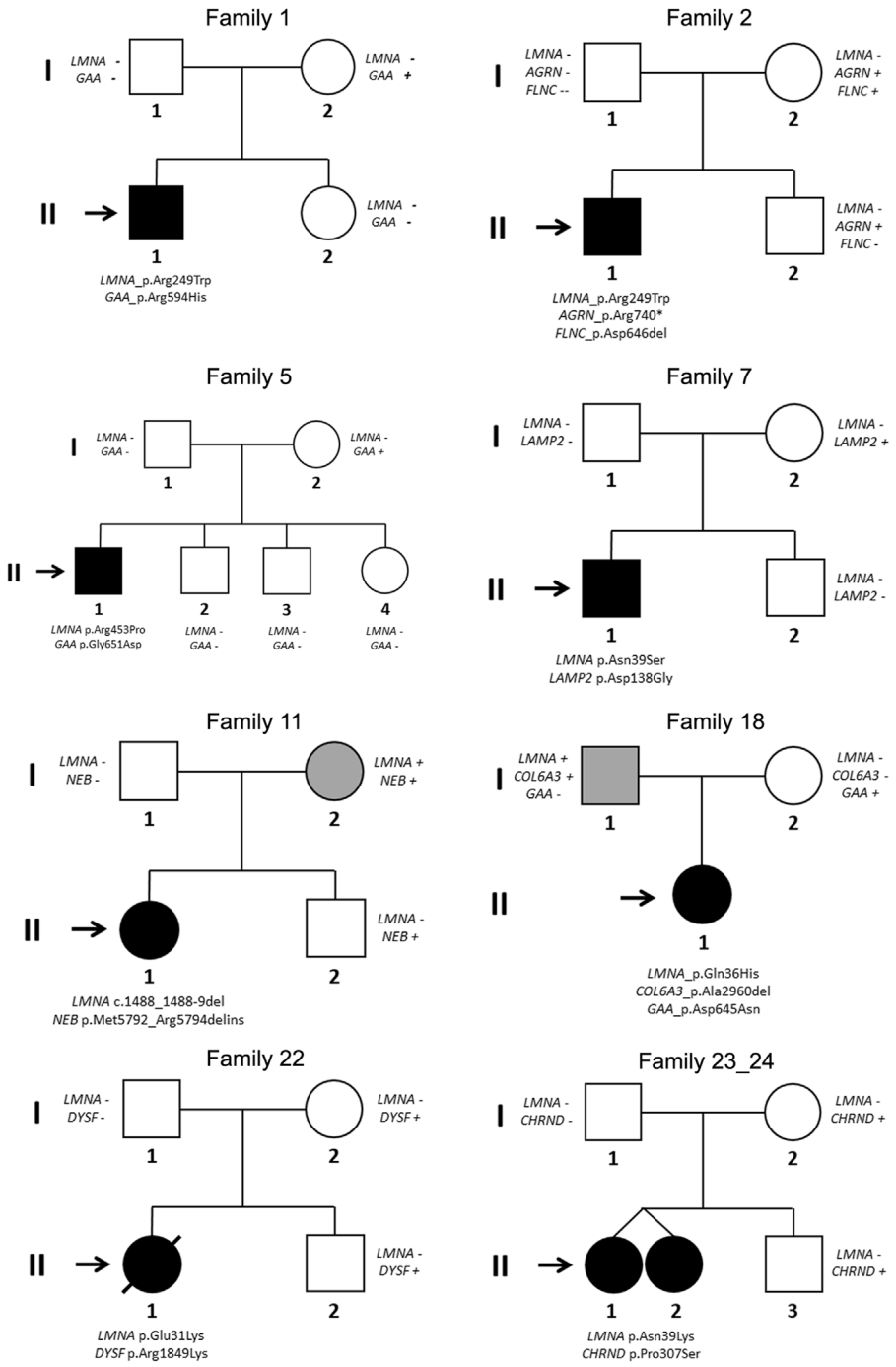


FIGURE 3
Pedigrees of families 1, 2, 5, 7, 11, 18, 22, and 23/24 (twins). Generations are indicated in the left side. Each individual of direct family linage is identified with a number. Clinically affected patients are shows in black, clinically unaffected patients are show in white, and mild phenotype is indicated in grey color. Slash indicates deceased. Index case is indicated with an arrow. Sign plus indicates carrier of the genetic variant. Minus sign indicates not carrier of the genetic variant.

Hypertrophic cardiomyopathy (not observed in patient 2 or the mother) and variants in *AGRN* are mainly associated with congenital myasthenic syndrome following an autosomal recessive pattern of inheritance. Therefore, neither mother or sister showed any symptom of muscular weakness as both are carriers of the same heterozygotic variant. Therefore, the presence of any deleterious rare variant may explain the most severe muscular weakness and malignant arrhythmias observed in patients 1 and 2, in comparison to patients 6 and 26 (both showing same diagnosis and carrying the same *LMNA* variant but without aggressive phenotype). However, further molecular studies should be performed to unravel the pathophysiological mechanism

involved in these potential phenotype modifications. Curiously, patient 14, diagnosed with EDMD and carrying the same variant p.Arg249Trp, showed a different phenotype possibly due to an unidentified alteration, reinforcing the targeted genetic analysis not only limited to the *LMNA* gene in patients diagnosed with *LMNA*-related muscular diseases. In addition, in p.Arg249, other deleterious variants were identified in patient 8, who was diagnosed with EDMD. This variant (p.Arg249Gln) was also previously reported in 3 infants showing slow muscular degeneration and slight arrhythmias (Bonne et al., 2000; Fan et al., 2021; Jedrzejowska et al., 2021), similar to this patient.

Patient 5, who showed a severe phenotype of EDMD, with DCM and implanted ICD due to malignant arrhythmias, carried two rare variants (*LMNA*_p.Arg453Pro and *GAA*_p.Gly651Asp). Both variants were novel. The *GAA* variant was inherited from the asymptomatic mother and no symptoms of GSD/Pompe disease in any carrier were observed due to widely-accepted recessive pattern of inheritance in this gene. Curiously, in the same aminoacid p.Arg453, another deleterious rare variant was previously reported as *de novo* in several cases (p.Arg453Trp) (Bonne et al., 2000; Fan et al., 2021; Jedrzejowska et al., 2021). In these reported cases, the diagnosis was EDMD concomitant with arrhythmias and slow muscular degeneration. Only in one case, the diagnosis was LGMD1B. In our cohort, two cases carried this rare variant *LMNA*_p.Arg453Trp, patient 20 diagnosed with EDMD and patient 21 diagnosed with LGMD1B (both showing slow muscular degeneration, without any arrhythmia or cardiac alteration).

Patient 7, diagnosed with EDMD but without any cardiac alteration, carried the deleterious *LMNA*_p.Asn39Ser variant. She carried an additional rare variant in the *LAMP2* gene, also identified in her mother. Rare variants in this gene are associated with Danon disease, following an X-linked pattern of inheritance. However, the mother did not show any symptom/phenotype related to Danon disease. The rare variant in *LMNA* was previously published in 5 patients, of which 3 were diagnosed with L-CMD and slow muscular weakness progression, and 2 with EDMD and no cardiac affectation (Pasqualin et al., 2014; Fan et al., 2021). In our cohort, patient 3 also carried the same variant but with a clinical diagnosis of EDMD. Despite no additional deleterious variant identified in any of all analyzed genes, DCM and malignant arrhythmias were documented. Unfortunately, this patient died due to rapidly progressive heart failure despite optimal treatment and being an ICD carrier. It suggests the targeted genetic analysis looking for other new genes not currently associated with any muscular diseases. Curiously, in the same aminoacid *LMNA*_p.Asn39, twins included in our cohort (patients 23/24) carried the deleterious variant (p.Asn39Lys) responsible of L-CMD diagnosed. This variant was recently reported in one case of L-CMD with slow muscular weakness progression and no cardiac affectation (Fan et al., 2021) and in two cases showing hypotonia, waddling gait and normal heart (Jedrzejowska et al., 2021), in concordance to our twins.

Patient 11, diagnosed with concomitant L-CMD and DCM, carried a *de novo* and novel deletion *LMNA*_c.1488_1488+9del. This variant was inherited from her mother who showed a minor muscular impairment. No history of any muscular disease was documented in previous generations. Patient 11 also carried an additional deletion in *NEB*, a gene associated with myopathies following an autosomal recessive pattern of inheritance. Both their mother and brother carried this *NEB* variant in heterozygosis form and, as expected, showing no symptom to date. In our cohort, three more *de novo* deletions in *LMNA* were identified in patients 4, 9, and 25, where two were diagnosed with L-CMD (patients 4 and 25) and showed slow muscular weakness progression with no cardiac affectation, while patient 9 was diagnosed with EDMD and DCM. In concordance, both deleterious variants were previously reported in L-CMD patients showing phenotypes similar to our patients (Fan et al., 2021).

Patient 18, diagnosed with EDMD, showed slow muscular weakness progression and no cardiac affectation. The patient carried *LMNA*_p.Gln36His, inherited from the father who showed a minor muscular impairment. No history of any muscular disease was documented in previous generations. This variant was never reported, to the best of our knowledge. This patient also carried the deleterious variant *GAA*_p.Asp645Asn, previously identified and associated with GSD (CM980804) (McCready et al., 2007). This *GAA* variant was inherited during heterozygosis from the healthy mother, not showing any symptom of GSD or Pompe disease. In addition, this patient also carried a deleterious indel in *COL6A3*. This variant has not been reported so far, and the gene is associated with dystonia and muscular dystrophy. The variant was inherited from the father who showed a minor muscular impairment. As mentioned above, no history of any muscular disease was documented in previous generations.

Patient 22, diagnosed with EDMD, showed slow muscular weakness progression and no cardiac affectation. The *LMNA*_p.Glu31Lys variant was *de novo*. Despite no aggressive phenotype, the patient died at 10 years old due to severe respiratory infection. This variant has been recently reported in one patient diagnosed with L-CMD, slow muscular weakness progression, and no cardiac affectation (Fan et al., 2021). This patient also carried a deleterious variant in *DYSF* (p.Arg1849Lys), the gene associated with an autosomal recessive muscular dystrophy. This variant was inherited from the asymptomatic mother, as also observed in the brother who also carried the same *DYSF* variant. No history of any muscular disease was documented in previous generations. Finally, patients 13 and 16, both diagnosed with EDMD, DCM and with an ICD, carried only one deleterious variant in *LMNA* (p.Leu38Phe and p.Arg455Pro, respectively). Both rare variants are novel and *de novo*, after segregation of both variants in relatives.

In conclusion, laminopathies associated with muscular disorders are a group of heterogeneous conditions with different onset and development. We suggest that a targeted genetic diagnosis including *LMNA* as well as other genes related to muscular diseases may help to unravel additional potential rare variants that could be associated with more severe phenotypes. However, translation into clinical practice should be performed with caution due to further studies in large cohorts are necessary to clarify role additional variants.

## 5 Limitations

The study had a few limitations. First was the reduced cohort. Due to the rarity of the disease worldwide, it is difficult get enough number of families to obtained a conclusive result in a genotype-phenotype correlation. Therefore, despite reduced number of patients, our cohort of 26 patients is the largest reported so far, other than the 84 patients reported by Fan et al. (2021). Other limitation is the

potential pathophysiological role of additional genetic alterations located in other genes not included in our NGS custom-panel and that could be implicated in phenotype modification. A potential future approach is to perform whole exome sequencing and/or whole genome sequencing to identify new alteration in any region of the genome. Our study includes a comprehensive genotype-phenotype correlation in relatives, at our point of view the main fact in genetic interpretation and clinical translation of genetic variants identified. However, both *in vivo* and *in vitro* studies should be also performed to clarify the pathophysiological mechanism associated with the progressive disable phenotype associated with the disease. Therefore, classification of rare variants should be done following ACMG recommendations and should be periodically reanalyzed, particularly if classified as having an ambiguous role. A periodic update of previous classification may help to clarify role of rare variants, helping to clinicians to obtain genetic diagnosis and, if appropriate, adopt preventive measures.

## Data availability statement

The raw data supporting the conclusion of this article will be made available by the authors, without undue reservation.

## Ethics statement

The studies involving human participants were reviewed and approved by the ethics committee of Hospital Sant Joan de Déu and followed the World Medical Association Declaration of Helsinki. Written informed consent was obtained both from parents of all patients and from all relatives included in the study. Written informed consent to participate in this study was provided by the participants and legal guardian/next of kin.

## Author contributions

GS-B, SC, OC, and RB developed the concept and prepared the manuscript. VF, MC, AF-F, AI, AP-S, EM-B, IM, JC, CF-C, BO, MP, LL, MA, FP, RB, CO, DA, LC-G, JE-E, IZ, AN, and JB acquired, pre-processed, and analyzed the data. GS-B, SC, OC, JB, and RB supervised the study. All authors contributed to manuscript revision, read and approved the submitted version.

## Funding

This work was also supported by Obra Social. La Caixa Foundation (LCF/PR/GN16/50290001, and LCF/PR/GN19/50320002) and Instituto de Salud Carlos III, Fondo Investigación Sanitaria-FIS-(PI21/00094). Both CIBERCV and CIBERER are an initiative of the ISCIII (Instituto de Salud Carlos III), Spanish Ministry of Economy and Competitiveness.

## Acknowledgments

This long-term work could not have been possible without the unconditional support of Fundación Andrés Marcio–Niños contra la Laminopatía to who we are deeply thankful. Finally, we would like to truly thank all our patients and their families, especially to Carlota who inspired us to become better scientist and doctors.

## Conflict of interest

The authors declare that the research was conducted in the absence of any commercial or financial relationships that could be construed as a potential conflict of interest.

## Publisher's note



## References

Ben Yaou, R., Yun, P., Dabaj, I., Norato, G., Donkervoort, S., Xiong, H., et al. (2021). International retrospective natural history study of LMNA-related congenital muscular dystrophy. *Brain Commun.* 3 (3), fcab075. doi:10.1093/braincomms/fcab075

Benedetti, S., Menditto, I., Degano, M., Rodolico, C., Merlini, L., D'Amico, A., et al. (2007). Phenotypic clustering of lamin A/C mutations in neuromuscular patients. *Neurology* 69 (12), 1285–1292. doi:10.1212/01.wnl.0000261254.87181.80

Bennett, R., Campbell, T., Eslick, A., Pudipeddi, A., Hing, A., Yeates, L., et al. (2021). Ventricular tachycardia in a patient with dilated cardiomyopathy caused by a novel mutation of lamin A/C gene: Insights from features on electroanatomic mapping, catheter ablation and tissue pathology. *Heart Lung Circ.* 30 (2), 310–317. doi:10.1016/j.hlc.2020.08.024

Bertrand, A. T., Chikhaoui, K., Yaou, R. B., and Bonne, G. (2011). Clinical and genetic heterogeneity in laminopathies. *Biochem. Soc. Trans.* 39 (6), 1687–1692. doi:10.1042/BST20110670

Bonne, G., Mercuri, E., Muchir, A., Urtizberea, A., Becane, H. M., Recan, D., et al. (2000). Clinical and molecular genetic spectrum of autosomal dominant Emery-Dreifuss muscular dystrophy due to mutations of the lamin A/C gene. *Ann. Neurol.* 48 (2), 170–180. doi:10.1002/1531-8249(200008)48:2<170::aid-ana6>3.0.co;2-j

Bonne, G., Yaou, R. B., Beroud, C., Boriani, G., Brown, S., de Visser, M., et al. (2003). 108th ENMC international workshop, 3rd workshop of the MYO-CLUSTER project: EUROMEN, 7th international emery-dreifuss muscular dystrophy (EDMD) workshop, 13-15 september 2002, naarden, The Netherlands. *Neuromuscul. Disord.* 13 (6), 508–515. doi:10.1016/s0960-8966(03)00063-4

Boudreau, E., Labib, S., Bertrand, A. T., Decostre, V., Bolongo, P. M., Sylvius, N., et al. (2012). Lamin A/C mutants disturb sumo1 localization and sumoylation *in vitro* and *in vivo*. *PLoS One* 7 (9), e45918. doi:10.1371/journal.pone.0045918

Carboni, N., Mateddu, A., Marrosu, G., Cocco, E., and Marrosu, M. G. (2013a). Genetic and clinical characteristics of skeletal and cardiac muscle in patients with lamin A/C gene mutations. *Muscle Nerve* 48 (2), 161–170. doi:10.1002/mus.23827

Carboni, N., Politano, L., Floris, M., Mateddu, A., Solla, E., Olla, S., et al. (2013b). Overlapping syndromes in laminopathies: A meta-analysis of the reported literature. *Acta Myol.* 32 (1), 7–17.

Charniot, J. C., Pascal, C., Bouchier, C., Sebillon, P., Salama, J., Duboscq-Bidot, L., et al. (2003). Functional consequences of an LMNA mutation associated with a new cardiac and non-cardiac phenotype. *Hum. Mutat.* 21 (5), 473–481. doi:10.1002/humu.10170

Choi, S. A., Cho, A., Kim, S. Y., Kim, W. J., Shim, Y. K., Lee, J. S., et al. (2019). Importance of early diagnosis in LMNA-related muscular dystrophy for cardiac surveillance. *Muscle Nerve* 60 (6), 668–672. doi:10.1002/mus.26700

Cotta, A., Paim, J. F., Carvalho, E., Valicek, J., da Cunha Junior, A. L., Navarro, M. M., et al. (2019). LMNA-related muscular dystrophy with clinical intrafamilial variability. *J. Mol. Neurosci.* 69 (4), 623–627. doi:10.1007/s12031-019-01390-0

Dittmer, T. A., and Misteli, T. (2011). The lamin protein family. *Genome Biol.* 12 (5), 222. doi:10.1186/gb-2011-12-5-222

Fan, Y., Tan, D., Song, D., Zhang, X., Chang, X., Wang, Z., et al. (2021). Clinical spectrum and genetic variations of LMNA-related muscular dystrophies in a large cohort of Chinese patients. *J. Med. Genet.* 58 (5), 326–333. doi:10.1136/jmedgenet-2019-106671

Heller, F., Dabaj, I., Mah, J. K., Bergounioux, J., Essid, A., Bonnemann, C. G., et al. (2017). Cardiac manifestations of congenital LMNA-related muscular dystrophy in children: Three case reports and recommendations for care. *Cardiol. Young* 27 (6), 1076–1082. doi:10.1017/S1047951116002079

Huie, M. L., Tsujino, S., Sklower Brooks, S., Engel, A., Elias, E., Bonthron, D. T., et al. (1998). Glycogen storage disease type II: Identification of four novel missense mutations (D645N, G648S, R672W, R672Q) and two insertions/deletions in the acid alpha-glucosidase locus of patients of differing phenotype. *Biochem. Biophys. Res. Commun.* 244 (3), 921–927. doi:10.1006/bbrc.1998.8255

Jedrzejowska, M., Potulska-Chromik, A., Gos, M., Gambin, T., Debek, E., Rosiak, E., et al. (2021). Floppy infant syndrome as a first manifestation of LMNA-related congenital muscular dystrophy. *Eur. J. Paediatr. Neurol.* 32, 115–121. doi:10.1016/j.ejpn.2021.04.005

Komaki, H., Hayashi, Y. K., Tsuburaya, R., Sugie, K., Kato, M., Nagai, T., et al. (2011). Inflammatory changes in infantile-onset LMNA-associated myopathy. *Neuromuscul. Disord.* 21 (8), 563–568. doi:10.1016/j.nmd.2011.04.010

Kumar, S., Baldinger, S. H., Gandjbakhch, E., Maury, P., Sellal, J. M., Androulakis, A. F., et al. (2016). Long-term arrhythmic and nonarrhythmic outcomes of lamin A/C mutation carriers. *J. Am. Coll. Cardiol.* 68 (21), 2299–2307. doi:10.1016/j.jacc.2016.08.058

Liu, X., Wang, Z., Jin, W., Lv, H., Zhang, W., Que, C., et al. (2014). Clinical and GAA gene mutation analysis in mainland Chinese patients with late-onset Pompe disease: Identifying c.2238G > C as the most common mutation. *BMC Med. Genet.* 15, 141. doi:10.1186/s12881-014-0141-2

Maggi, L., D'Amico, A., Pini, A., Sivo, S., Pane, M., Ricci, G., et al. (2014). LMNA-Associated myopathies: The Italian experience in a large cohort of patients. *Neurology* 83 (18), 1634–1644. doi:10.1212/WNL.0000000000000934

Maraldi, N. M., Capanni, C., Cenni, V., Fini, M., and Lattanzi, G. (2011). Laminopathies and lamin-associated signaling pathways. *J. Cell Biochem.* 112 (4), 979–992. doi:10.1002/jcb.22992

McCready, M. E., Carson, N. L., Chakraborty, P., Clarke, J. T., Callahan, J. W., Skomorowski, M. A., et al. (2007). Development of a clinical assay for detection of GAA mutations and characterization of the GAA mutation spectrum in a Canadian cohort of individuals with glycogen storage disease, type II. *Mol. Genet. Metab.* 92 (4), 325–335. doi:10.1016/j.ymgme.2007.07.006

Muntoni, F., Bonne, G., Goldfarb, L. G., Mercuri, E., Piercy, R. J., Burke, M., et al. (2006). Disease severity in dominant Emery Dreifuss is increased by mutations in both emerin and desmin proteins. *Brain* 129, 1260–1268. doi:10.1093/brain/awl062

Murofushi, Y., Hayakawa, I., Abe, Y., Nakao, H., Ono, H., and Kubota, M. (2022). The most severe form of LMNA-associated congenital muscular dystrophy. *Brain Dev.* 44, 650–654. doi:10.1016/j.braindev.2022.05.006

Pasqualin, L. M., Reed, U. C., Costa, T. V., Quedas, E., Albuquerque, M. A., Resende, M. B., et al. (2014). Congenital muscular dystrophy with dropped head linked to the LMNA gene in a Brazilian cohort. *Pediatr. Neurol.* 50 (4), 400–406. doi:10.1016/j.pediatrneurol.2013.11.010

Paul, J. C., and Fulka, H. (2022). Nuclear lamins: Key proteins for embryonic development. *Biol. (Basel)* 11 (2), 198. doi:10.3390/biology11020198

Quijano-Roy, S., Mbieleu, B., Bonnemann, C. G., Jeannet, P. Y., Colomer, J., Clarke, N. F., et al. (2008). De novo LMNA mutations cause a new form of congenital muscular dystrophy. *Ann. Neurol.* 64 (2), 177–186. doi:10.1002/ana.21417

Richards, S., Aziz, N., Bale, S., Bick, D., Das, S., Gastier-Foster, J., et al. (2015). Standards and guidelines for the interpretation of sequence variants: A joint consensus recommendation of the American College of medical genetics and Genomics and the association for molecular pathology. *Genet. Med.* 17 (5), 405–424. doi:10.1038/gim.2015.30

Roncarati, R., Viviani Anselmi, C., Krawitz, P., Lattanzi, G., von Kodolitsch, Y., Perrot, A., et al. (2013). Doubly heterozygous LMNA and TTN mutations revealed by exome sequencing in a severe form of dilated cardiomyopathy. *Eur. J. Hum. Genet.* 21 (10), 1105–1111. doi:10.1038/ejhg.2013.16

Worman, H. J., and Bonne, G. (2007). Laminopathies": A wide spectrum of human diseases. *Exp. Cell Res.* 313 (10), 2121–2133. doi:10.1016/j.yexcr.2007.03.028

Worman, H. J. (2012). Nuclear lamins and laminopathies. *J. Pathol.* 226 (2), 316–325. doi:10.1002/path.2999

Zheng, M., Jin, G., and Zhou, Z. (2022). Post-translational modification of lamins: Mechanisms and functions. *Front. Cell Dev. Biol.* 10, 864191. doi:10.3389/fcell.2022.864191

frontiers | Frontiers in Genetics

TYPE Original Research
PUBLISHED 06 April 2023
DOI 10.3389/fgene.2023.1125473



OPEN ACCESS

EDITED BY
Hu Hao,
The Sixth Affiliated Hospital of Sun Yat-sen University, China

REVIEWED BY
Nadia Akawi,
United Arab Emirates University, United Arab Emirates
Muhammad Umair,
King Abdullah International Medical Research Center (KAIMRC), Saudi Arabia

*CORRESPONDENCE
Qing Guo,
yfguoqing@163.com
Ying Liang,
ying_liangcn@hotmail.com

†These authors have contributed equally to this work and share first authorship

SPECIALTY SECTION
This article was submitted to Genetics of Common and Rare Diseases, a section of the journal Frontiers in Genetics

RECEIVED 16 December 2022
ACCEPTED 27 March 2023
PUBLISHED 06 April 2023

CITATION
Chen W, Li Y, Zhang J, Yuan Y, Sun D, Yuan J, Yang K, Liang Y and Guo Q (2023), Genetic variations in the *DYNC2H1* gene causing SRTD3 (short-rib thoracic dysplasia 3 with or without polydactyly). *Front. Genet.* 14:1125473.
doi: 10.3389/fgene.2023.1125473



# Genetic variations in the *DYNC2H1* gene causing SRTD3 (short-rib thoracic dysplasia 3 with or without polydactyly)

Wenqi Chen[1†], Yazhou Li[2†], Jing Zhang[1], Yufan Yuan[1], Donglan Sun[1], Jiayu Yuan[2], Kai Yang[3], Ying Liang[4*] and Qing Guo[1*]

[1]Prenatal Diagnosis Center, Shijiazhuang Obstetrics and Gynecology Hospital, Key Laboratory of Maternal and Fetal Medicine of Hebei Province, Shijiazhuang, Hebei, China, [2]Department of Pediatric Orthopaedic, The Third Hospital of Hebei Medical University, Shijiazhuang, Hebei, China, [3]Prenatal Diagnosis Center, Beijing Obstetrics and Gynecology Hospital, Beijing Maternal and Child Healthcare Hospital, Capital Medical University, Beijing, China, [4]Reproductive Medicine Center, Shijiazhuang Obstetrics and Gynecology Hospital, Shijiazhuang, Hebei, China

**Background and aims:** Short-rib thoracic dysplasia 3 with or without polydactyly (SRTD3) represents a type of severe fetal skeletal dysplasia (SD) characterized by shortened limbs, narrow thorax with or without polydactyly, which is caused by the homozygous or compound heterozygous mutations in the *DYNC2H1* gene. SRTD3 is a recessive disorder, identification of the responsible genetic variation would be beneficial to an accurate prenatal diagnosis and well-grounded counseling for the affected families.

**Material and methods:** Two families having experienced recurrent fetal SDs were recruited and submitted to a multiplatform genetic investigation. Whole-exome sequencing (WES) was performed with samples collected from the probands. Sanger sequencing and fluorescent quantitative PCR (qPCR) were conducted as validation assays for suspected variations.

**Results:** WES identified two compound heterozygous variations in the *DYNC*2H1(NM_001080463.2) gene, namely c.2386C>T (p.Arg796Trp) and c.7289T>C (p.Ile2430Thr) for one; and exon (64–83)del and c.8190G>T (p.Leu2730Phe) for the other, respectively. One variant in them, exon (64–83) del, was novelly identified.

**Conclusion:** The study detected two compound heterozygous variation in *DYNC2H1* including one novel deletion: exon (64–83) del. Our findings clarified the cause of fetal skeletal dysplasia in the subject families, provided guidance for their future pregnancies, and highlighted the value of WES in diagnosis of skeletal dysplasia with unclear prenatal indications.

KEYWORDS

***DYNC2H1* gene, short-rib thoracic dysplasia 3 (SRTD3), skeletal dysplasia, whole-exome sequencing, prenatal diagnosis**

## Introduction

Short-rib thoracic dysplasia (SRTD) with or without polydactyly is an umbrella term of a group of genetically heterogeneous skeletal dysplasias consistent with the autosomal recessive (AR) inheritance pattern. SRTDs are characterized by short ribs, short limbs, constricted thoracic cage, a 'trident' appearance of the acetabular roof and anomalies in kidney, heart, liver, pancreas, genitalia and intestine (Chen and Tzen, 2001; Chen et al., 2002; Chen et al., 2003; Chen et al., 2005; Chen et al., 2012a; Chen et al., 2012b). Currently, SRTD are classified into the categories of short-rib thoracic dysplasia with or without polydactyly type 1–21 (SRTD1-21) (Table 1).

The short-rib thoracic dysplasia 3 with or without polydactyly (SRTD3; OMIM #613091) refers to a rare subtype of SRTDs, characterized by the constricted thoracic cage, shortened limbs, and associated visceral abnormalities with or without polydactyly. SRTD3 belongs to the "ciliopathies with major skeletal involvement" conditions according to the revised consensus workshop (Bonafe et al., 2015), and is caused by homozygous or compound heterozygous mutations in the *DYNC2H1* gene (dynein, cytoplasmic 2, heavy chain 1; OMIM #603297), which encodes a component of the cytoplasmic dynein complex (Dagoneau et al., 2009; McInerney-Leo et al., 2015). This complex is associated with the ciliary intraflagellar transport (IFT), an evolutionarily conserved process that is necessary for ciliogenesis and plays an important role in Hedgehog (Hh), Wnt, Platelet-derived growth factor (PDGF), Notch, G-Protein coupled receptor (GPCR), Mammalian target of rapamycin (mTOR), Transforming growth factor beta (TGF-β) and Calcium signaling pathways (Schmidts et al., 2013a; Schmidt et al., 2015).

In general, SRTD3 is lethal in the neonatal period due to respiratory insufficiency secondary to the severely restricted thoracic cage, whereas other SRTD subtypes are compatible with life (Huber and Cormier-Daire, 2012; Schmidts et al., 2013b). Although prenatal ultrasonography could detect the skeletal abnormalities of SRTD3, this condition was often difficult to be precisely diagnosed before birth. Since SRTD3 is a recessive disorder, identification of the responsible genetic variation would be beneficial to an accurate prenatal diagnosis and well-grounded counseling for the affected families.

In the present study, two families with experiences of multiple adverse gestations including recurrent fetal skeletal dysplasias were recruited. Prenatal ultrasonography examination and genetic detection were conducted to identify the causes of these manifestations in affected fetuses.

**TABLE 1 SRTD are classified into the categories of SRTD1-21.**

| Phenotype | Location | PhenotypeMIM number | Gene | Gene MIM number | Inheritance |
|---|---|---|---|---|---|
| SRTD1 | 15q13 | 208500 | SRTD1 | 208500 | AR |
| SRTD2 | 3q25.33 | 611263 | IFT80 | 611177 | AR |
| SRTD3 | 11q22.3 | 613091 | DYNC2H1 | 603297 | AR,DR |
| SRTD4 | 2q24.3 | 613819 | TTC21B | 612014 | AR |
| SRTD5 | 4p14 | 614376 | WDR19 | 608151 | AR |
| SRTD6 | 4q33 | 263520 | NEK1 | 604588 | AR,DR |
| SRTD7 | 2p24.1 | 614091 | WDR35 | 613602 | AR |
| SRTD8 | 7q36.3 | 615503 | WDR60 | 615462 | AR |
| SRTD9 | 16p13.3 | (266920) | IFT140 | 614620 | AR |
| SRTD10 | 2p23.3 | 615630 | IFT172 | 607386 | AR |
| SRTD11 | 9q34.11 | 615633 | WDR34 | 613363 | AR |
| SRTD12 | not mapped | 269860 | SRTD12 | 269860 | AR |
| SRTD13 | 5q23.2 | 616300 | CEP120 | 613446 | AR |
| SRTD14 | 14q23.1 | 616546 | KIAA0586 | 610178 | AR |
| SRTD15 | 2p21 | 617088 | DYNC2LI1 | 617083 | AR |
| SRTD16 | 20q13.12 | 617102 | IFT52 | 617094 | AR |
| SRTD17 | 3q29 | 617405 | TCTEX1D2 | 617353 | AR |
| SRTD18 | 14q24.3 | 617866 | IFT43 | 614068 | AR |
| SRTD19 | 12q24.11 | 617895 | IFT81 | 605489 | AR |
| SRTD20 | 4q28.1 | 617925 | INTU | 610621 | AR |
| SRTD21 | 17p13.1 | 619479 | KIAA0753 | 617112 | AR |

# Materials and methods

## Subjects

Two unrelated cases were recruited between March 2020 and April 2021 at the Prenatal Diagnosis Center, Shijiazhuang Obstetrics and Gynecology Hospital. A comprehensive prenatal ultrasonic examination was conducted on the patients. We carried out a thorough clinical survey. Subsequently, the peripheral blood samples of trio family members in the two pedigrees were collected for the following genetic detection. The studies involving human participants were reviewed and approved by The Ethics Committee of Shijiazhuang Obstetrics and Gynecology Hospital.

## Genomic DNA extraction

Amniocentesis was performed to obtain the fetal cell samples, along with 3 ml of peripheral blood collected from the parents using BD Vacutainer™ tubes (BD Biosciences, New Jersey, United States). Genomic DNA was extracted with the QIAamp DNA Blood Mini-Kit (Qiagen Sciences, New York, United States), and the DNA quality was validated by 1% agarose gels and the Qubit® 2.0 Flurometer (Life Technologies, CA, United States).

## Whole-exome sequencing

WES was performed by MyGenomics, Inc. (Changping, Beijing, China) as described in our previous study (Zhang et al., 2021). Briefly, the enrichment of the exonic region sequences was conducted by the Sure Select Human Exon Sequence Capture Kit (Agilent, United States). The sequencing library was quantified using the Illumina DNA Standards and Primer Premix Kit (Kapa Biosystems, United States), and was massively parallel-sequenced using the Illumina Novaseq6000 platform. After sequencing and filtering out the low-quality reads, the high-quality data (with general quality level Q30 reads >89%) was aligned to the human genome reference sequence [hg19] using Burrows-Wheeler Aligner tool. The third-party software GATK (https://softw are.broad institute.org/gatk/) and the Verita Trekker® Variants Detection system (Berry Genomics, China) were employed for variant calling. Variants with lower quality (read depth<10x, allele fraction<30%) were eliminated. The variations were identified by sequence alignment with the NCBI Reference Sequence (NG_016423.2, NP_001073932.1, NM_001080463.2) using Chromas v2.33. The pathogenicity of the identified variants was then assessed according to the common guidelines issued by the American Association of Medical Genetics and Genomics (ACMG) (Richards et al., 2015) referring to multiple databases (1000g2015aug_eas, https://www.internationalgenome.org/; ExAC_EAS, http://exac.broadinstitute.org; gnomAD_exome_EAS, http://gnomad.broadinstitute.org/; HGMD®: Human Gene Mutation Database Professional v.2021.10) with the Enliven® Variants Annotation Interpretation (Berry Genomics, China) system.

## Validation experiments

The suspected diagnostic variants were validated by Sanger sequencing using ABI 3730 Automated Sequencer (Applied Biosystems, United States) according to the manufacturer's protocol. Fluorescent quantitative PCR (qPCR) was also carried out to verify the suspected deletion variant identified in Case 2.

## Analysis of missense variants

The evolutionary conservatism of amino acid (AA) residues affected by specific missense variants was analyzed using UGENE (http://ugene.net/) with default parameters.

## Structural analysis

Referring to the crystal structure of 6rla. 1. A (Toropova et al., 2019) protein, the DYNC2H1 protein structures at 2241–2520 and 2611–2880 regions were constructed by Swiss-model program. The Swiss-Pdb Viewer program was referred to modeling the wild-type (WT) and DYNC2H1: p. Ile2430Thr and p. Leu2730Phe mutant models of DYNC2H1 protein segments. The molecular dynamics (MD) prediction analysis was generated by GROMACS (version 2020.6) (Rakhshani et al., 2019). We carried out 60 ns MD simulations on the DYNC2H1-WT, DYNC2H1-Ile2430Thr, and DYNC2H1-Leu2730Phe models. The CHARMM36 force field was applied to add hydrogen atoms and N-terminal and C-terminal patches to the models (Soteras Gutiérrez et al., 2016). The wild type or the mutant structure of the protein was immersed in cubic boxes which contains water and placed at least 1.0 nm from the box edge. $Na^+$ and $Cl^-$ ions were used for neutralization. The MD simulations were performed at a temperature of 300K for 60 ns after energy minimization, equilibration. The following GROMACS distribution programs were used in MD trajectories: gmxrms, gmxrmsf, gmx gyrate, gmxsasa, and gmxhbond. These MD analyses generated parameters values for root-mean-square deviation (RMSD), root-mean-square fluctuation (RMSF), radius of gyration, solvent accessible surface area (SASA), and number of h-bonds.

# Results

## Clinical manifestations

**Case 1.** A 32-year-old woman was referred to our center in March 2021 for previous multiple adverse gestations, when she was at the 17th$^+$gestational week. Her husband was 31 years old, with no consanguineous relation to her. Based on the medical record and her personal dictation, we combed through the couple's complete medical history and illustrated the pedigree in a diagram (Figure 1A). They had 3 previous pregnancies: in October 2016 and July 2017, they went through one spontaneous abortion and one stillbirth, respectively; in November 2018, the prenatal sonography revealed a 22-week fetus with short limbs and a narrow chest, which was diagnosed as thanatophoric dwarfism. That pregnancy was subsequently terminated.

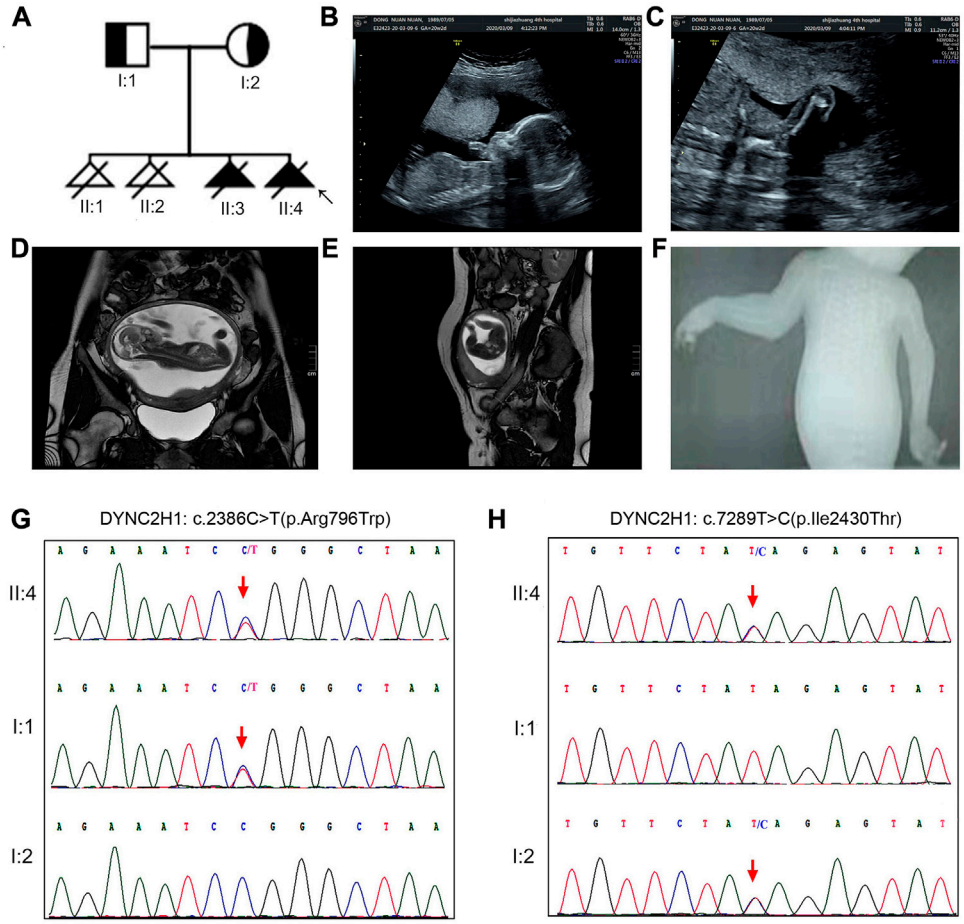


FIGURE 1
The clinical findings and genetic variation in case 1. **(A)** Pedigree diagram of the family with STRD3. **(B–E)** Ultrasonographic and MRI indications of the fetus in case 1: the fetus had extremely short limbs and a small, narrow thorax. **(F)** X-ray indications of the fetus in case 1: the fetus had a narrow thorax and short limbs, but no polydactyly. **(G, H)** The genetic variation identified in this case: proband 1 (II-4 in Case 1) carried two missense variants, namely c.2386C>T (p.Arg796Trp) and c.7289T>C (p.Ile2430Thr). Validation with Sanger sequencing demonstrated that the variants these probands carried were all inherited from their asymptomatic heterozygous carrier parents.

In 2020, they had the 4th gestation, and the serological screening and NIPT (non-invasive prenatal testing) results were normal. At the 17th week, ultrasonic examination and MRI revealed that the fetus had extremely short limbs and small, bell-shaped chest, short ribs, rhizomelic shortening in all extremities (Figures 1B–E). Prenatal ultrasound did not identify abnormalities in the brain, heart, kidneys, or liver. No exposure history to tobacco smoke, alcohol, ir-radiation, or infectious diseases during the pregnancy were admitted. Pregnancy termination was performed at 22 gestational weeks with informed consent. Afterwards, X-ray imaging result demonstrated that the fetus had a narrow thorax and short limbs, but no polydactyly (Figure 1F). And whole-exome sequencing (WES) was introduced afterwards.

**Case 2.** A 31-year-old pregnant woman was referred to our center in April 2021. Her husband and her were non-consanguineous. The pedigree diagram was depicted in Figure 2A: in November 2018, a fetus was diagnosed with constricted thoracic cage, extremely shortened tubular bones and bowing of long bones, and then aborted at 12th week; in April 2021, ultrasonography revealed that their second fetus had extremely short limbs at the 13th week (Figures 2B, C). No brain, heart, kidney, or liver abnormality was found by prenatal ultrasonography. The woman denied to be exposed to tobacco smoke, alcohol, radiation or infectious diseases during pregnancy. After informed consent by the couple, genetic analysis including WES was also performed after induction.

## Genetic variations

Karyotyping by G-bandeding showed that the results of the fetuses in both Case1 and 2 were normal, and array-CGH analysis did not reveal any genomic abnormality associated with known microdeletion or microduplication syndromes, either. On the other hand, according to the WES results, the two fetuses were recognized as positive with compound heterozygous variation in the *DYNC2H1*

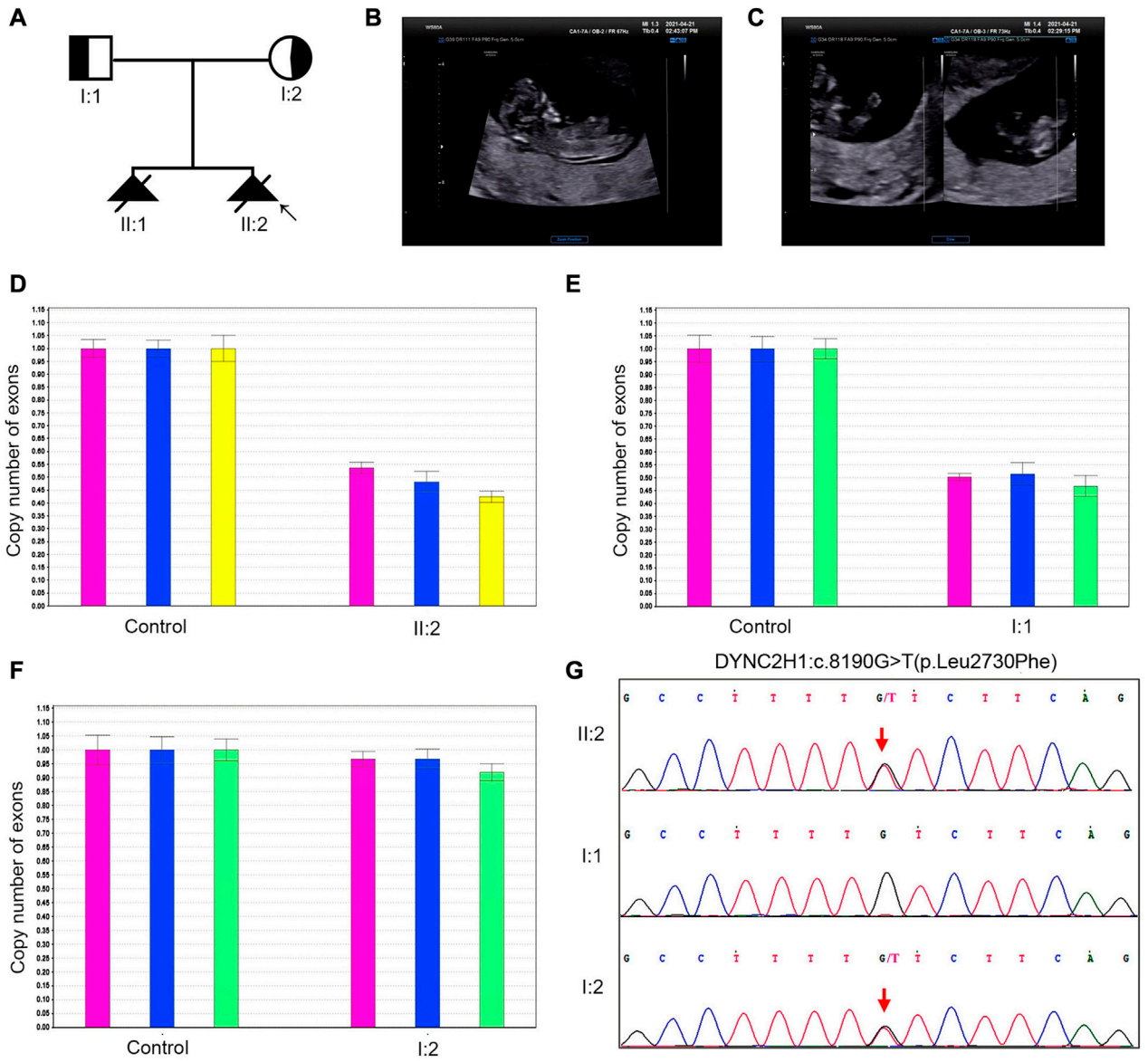


FIGURE 2
The clinical findings and genetic variation in case 2. **(A)** Pedigree diagram of the family with STRD3. **(B, C)** Ultrasonographic indications of the fetus in case 2: the fetus had extremely short limbs and bowing of long bones. **(D–G)** The genetic variation identified in case 2: proband 2 (II-2 in Case 2) carried an exonic deletion and a missense variant: exon (64–83)del and c.8190G>T (p.Leu2730Phe). qPCR validation confirmed one copy loss of the 64-83exons in *DYNC2H1*of proband 2 **(D)**. Validation with Sanger sequencing and qPCR demonstrated that the variants these probands carried were all inherited from their asymptomatic heterozygous carrier parents.

gene. To be specific, Proband 1 (II-4 in Case 1) carried two heterozygous missense variants, namely c.2386C>T (p.Arg796Trp) and c.7289T>C (p.Ile2430Thr) (Figures 1G, H); while Proband 2 (II-2 in Case 2) carried an exonic deletion, exon (64–83)del, and a missense variant, c.8190G>T (p.Leu2730Phe) (Figure 2G). qPCR validation confirmed the one copy loss of 64–83 exons in *DYNC2H1* of Proband 2 (Figure 2D). Validation with Sanger sequencing and qPCR demonstrated that the variants these probands carried were inherited from their asymptomatic heterozygous carrier parents, respectively (Figures 1G, H; Figures 2D–G). The location of each variant was illuminated in the gene and peptide diagrammatic sketches (Figure 3A).

## Conservatism analysis of missense variants

In this study, three missense variants were detected, which were *DYNC2H1*: c.2386C>T (p.Arg796Trp), c.7289T>C (p.Ile2430Thr) and c.8190G>T (p.Leu2730Phe). We analyzed the evolutionary conservatism of AA residues they affected. Results indicated that

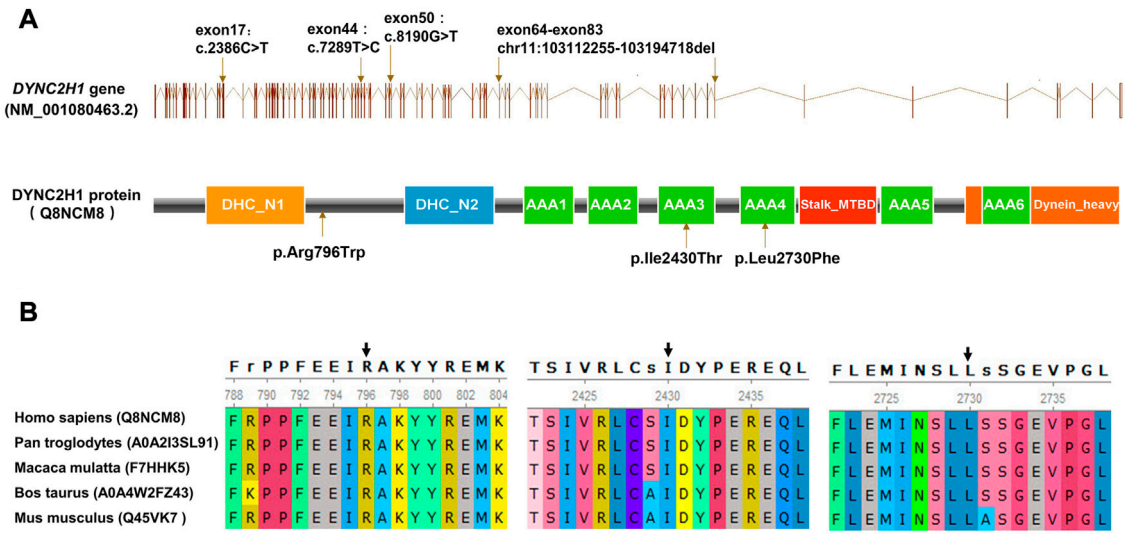


FIGURE 3
**(A)** Schematic diagram of the DYNC2H1 protein and the locations of the variants detected. **(B)** Conservation analysis of DYNC2H1 indicated that the protein at position 796, 2430 and 2730 are highly conserved in various species.

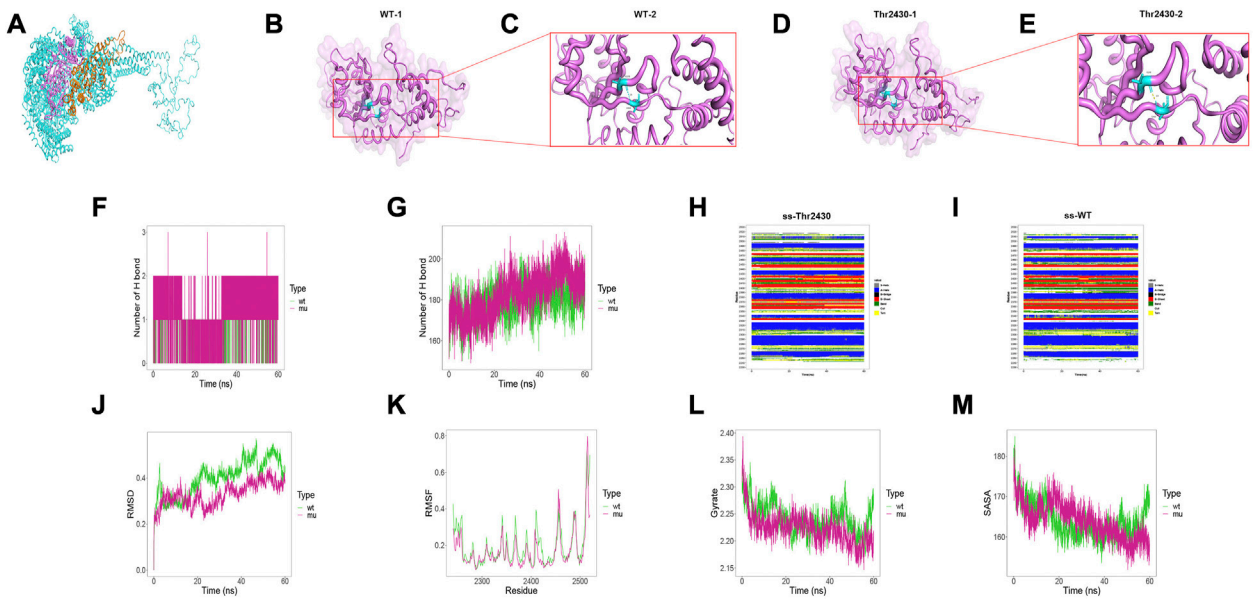


FIGURE 4
Results of structural analysis and molecular dynamics simulation of DYNC2H1: c.7289T>C (p.Ile2430Thr) variation. **(A)** Protein structure of DYNC2H1. **(B, C)** The wild-type structure of DYNC2H1: protein (DYNC2H1), and enlarged image of the segment containing Ile2430 residue. **(D, E)** The mutant structure of DYNC2H1, and segment containing the variant Thr2430 residue. **(F)** The number of hydrogen bonds formed between the target amino acid (meaning Ile2430 or Thr2430) and other residues. **(G)** Total number of hydrogen bonds in the wild-type model and the mutant model, respectively. **(H, I)** Comparison of local secondary structure data between Ile2430Thr mutant and wild-type. **(J)** RMSD: a numerical measurement indicating the difference between two structures. **(K)** RMSF: is a numerical measure similar to RMSD, but instead of indicating differences in position over time between entire structures; it calculates the flexibility of individual residues, or the extent to which a particular residue moves (fluctuates) during a simulation. **(L)** Gyrate: is a measure of the structural displacement of a protein atom with its common center of mass over the course of the simulation and provides comprehensive information about protein tightness over time. **(M)** SASA: measures the exposed surface in a protein structure accessible to solvent molecules.

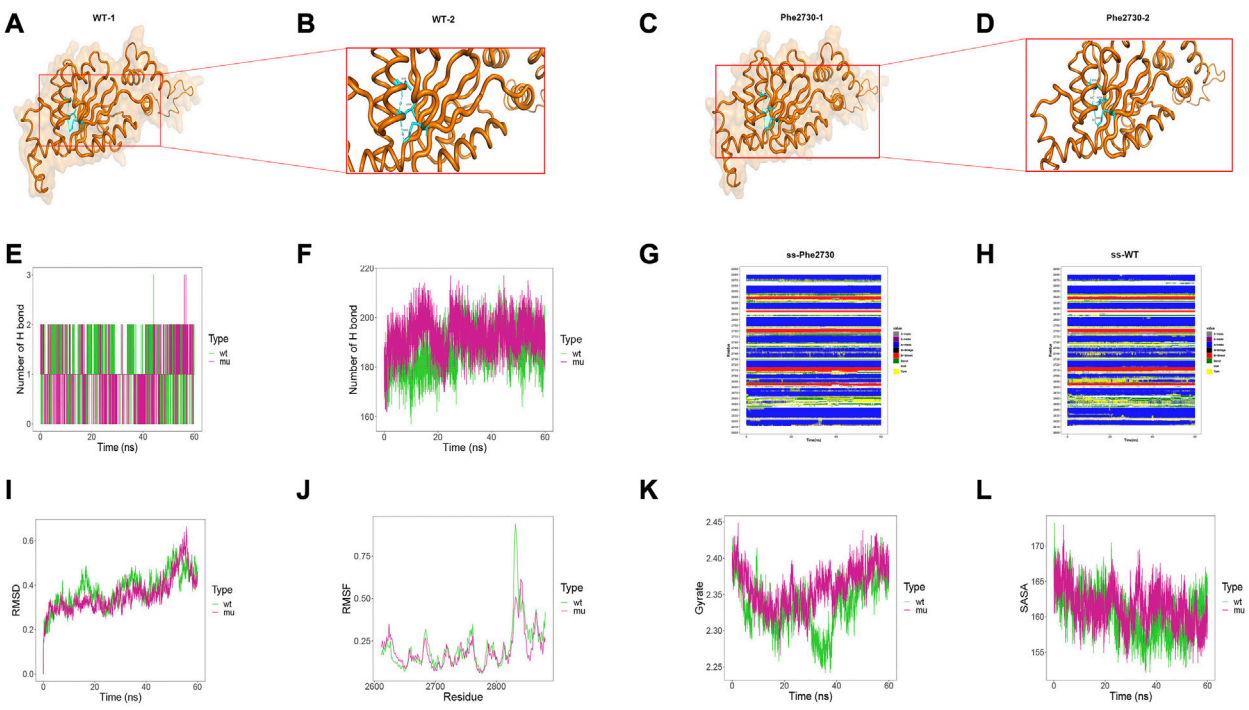


FIGURE 5
Results of structural analysis and molecular dynamics simulation of DYNC2H1: c.8190G>T (p.Leu2730Phe) variation. **(A, B)** The wild-type structure of DYNC2H1: protein (DYNC2H1), and enlarged image of the segment containing Leu2730 residue. **(C, D)** The mutant structure of DYNC2H1, and segment containing the variant Phe2730 residue. **(E)** The number of hydrogen bonds formed between the target amino acid (meaning Leu2730 or Phe2730) and other residues. **(F)** Total number of hydrogen bonds in the wild-type model and the mutant model, respectively. **(G, H)** Comparison of local secondary structure data between Leu2730Phe mutant and wild-type. **(I)** RMSD: a numerical measurement indicating the difference between two structures. **(J)** RMSF: is a numerical measure similar to RMSD, but instead of indicating differences in position over time between entire structures; it calculates the flexibility of individual residues, or the extent to which a particular residue moves (fluctuates) during a simulation. **(K)** Gyrate: is a measure of the structural displacement of a protein atom with its common center of mass over the course of the simulation and provides comprehensive information about protein tightness over time. **(L)** SASA: measures the exposed surface in a protein structure accessible to solvent molecules.

all three AAs maintained highly conserved among species (Figure 3B).

## Structural analysis and molecular dynamics simulation

To investigate the intramolecular effect of these missense variants, we performed structural analysis and MD simulation. Due to the structural inaccuracy of the region where p. Arg796Trp was located, we only analyzed the DYNC2H1 protein structures at 2241–2520 region (violet part in Figure 4A) and 2611–2880 region (orange part in Figure 4A), where p. Ile2430Thr and p. Leu2730Phe were located.

The results demonstrated that the Ile2430Thr variant affected the hydrogen bonding between amino acids inside the protein. Particularly, in the wild-type, Ile2430 formed hydrogen bonds with Val2290 residues, with the hydrogen bond length of 2.9Å; while the Ile2430Thr mutant formed a hydrogen bond with Val2290 with a hydrogen bond length of 1.9Å (Figures 4B–E; 4C and 4E are local amplifications of 4B and 4D, respectively). As for the MD results, first, the Thr2430 mutant formed more hydrogen bonds with other amino acids in the protein than the wild-type residue Ile2430 (Figure 4F); for the total number of hydrogen bonds inside the models within 60ns, the amount of Ile2430Thr mutant was more than that of the wild-type (Figure 4G). Besides, the Ile2430Thr variant resulted in a change in secondary structure around 2350th and 2400th residue (Figures 4H, I). Specifically, in wild-type, the secondary structure at 2350 position was dominated by BEND; yet in the mutant, the secondary structure alternated between BEND and TURN and was dominated by TURN. In wild-type, the secondary structure at 2400 position was dominated by BEND; yet in the mutant, the secondary structure alternated between BEND and TURN and was dominated by TURN. Finally, the Ile2430Thr variant resulted in decreased changes in protein structure (Figure 4J), decreased flexibility of amino acids in protein (Figure 4K), increased protein compactness (Figure 4L), and decreased surface area accessible to protein solvent (Figure 4M).

Structural result demonstrated that Leu2730Phe variant affected the hydrogen bonding between amino acids inside the protein. Particularly, Leu2730 and Phe2730 both formed hydrogen bonds with Ile2726 and Lys2802 residues, yet in the Leu2730Phe mutant the hydrogen bond length is shorter than that in the wild-type (Figures 5A–D; 5B and 5D are local amplifications of 5A and 5C, respectively). As for the MD results, there was no difference between Leu2730 and Phe2730 in the number of hydrogen bonds formed with other amino acids in the protein (Figure 5E); for the number of total hydrogen bonds inside the models within 60ns, the amount of

Leu2730Phe mutant was more than that of the wild-type (Figure 5F). In wild-type, the secondary structure at 2690 position was dominated by H-helix; yet in the mutant, the secondary structure showed a high rate of BEND and TURN (Figures 5G, H). The Leu2730Phe mutation has little influence on RMSD, RMSF, Gyrate, and SASA (Figures 5I–L).

## Discussion

SRTD3 refers to a sort of autosomal recessive skeletal condition characterized by shortened limbs, narrow thorax, with or without polydactyly, non-skeletal involvement can include cleft lip/palate as well as anomalies of major organs such as the brain, eye, heart, kidneys, liver, pancreas, intestines, and genitalia (Chen et al., 2018). The prenatal ultrasound features of SRTD3 are similar to other skeletal diseases, so it is difficult to establish a definite diagnosis, which proposes a challenge in prenatal diagnosis and management on fetuses with similar early manifestations.

In this study, two families with experiences of multiple adverse gestations including recurrent fetal skeletal dysplasia were enrolled. Ultrasonography detection of the two fetuses revealed skeletal abnormalities characteristics of SRTD3, including extreme shortness of the limbs, and narrow thorax. Signs of polydactyly and non-skeletal symptoms were not noted in the two cases. In Case 1, WES detected a compound heterozygous variation in the *DYNC2H1* gene with two variants, c.2386C>T and c.7289T>C. The allele frequencies of c.2386C>T (p.Arg796Trp) and c.7289T>C (p.Ile2430Thr) in gnomAD database were 2.3822e-05 and 9.39391e-06 respectively. In agreement with autosomal-recessive segregation, the parents were heterozygous for these two variants, respectively: the father carried the heterozygous c.2386C>T variant while the mother carried the c.7289T>C variant. The c.2386C>T variant caused a replacement of Arg796 residue by a Trp amino acid, and c.7289T>C caused a substitution of Ile2430 residue by a Thr amino acid. According to the variant interpretation criteria by ACMG, c.2386C>T (p.Arg796Trp), and c.7289T>C (p.Ile2430Thr) variants were classified as VUS, with the evidence of PM2+PP3. The c.2386C>T (p.Arg796Trp) and c.7289T>C (p.Ile2430Thr) variants were predicted to be pathogenic by the SIFT algorithm, Mutation Taster, and PolyPhen-2.

In Case 2, a compound heterozygous variation in *DYNC2H1* gene with 2 variants, exon (64–83) del and c.8190G>T, was identified and confirmed. The former one was a novel variant not indexed in the databases of 1000G (https://www.internationalgenome.org/), gnomAD (http://gnomad.broadinstitute.org/), ExAC_EAS (http://exac.broadinstitute.org) and Berry Genomics inhouse database, which expanded the variation spectrum of *DYNC2H1* gene. The allele frequencies of c.8190G>T (p.Leu2730Phe) in the databases of EXAC and gnomAD were 2.7e-05 and 1.6 e-05 respectively. Consistent with autosomal-recessive segregation, the parents were heterozygous for the identified mutations: the father carried exon (64–83)del, while the mother carried c.8190G>T. According to the variant interpretation criteria by ACMG, the exon (64–83)del variant was classified as pathogenic, with the evidence of PVS1+PM2. According to the variant interpretation criteria by ACMG, the c.8190G>T (p.Leu2730Phe) variant was classified as VUS, with the evidence of PM2+PP3. The c.8190G>T variant caused a replacement of Leu2730 residue by a Phe amino acid, and this variant was predicted to be pathogenic by the SIFT algorithm, Mutation Taster, and PolyPhen-2. The three residues affected by c.2386C>T (p.Arg796Trp), c.7289T>C (p.Ile2430Thr) and c.8190G>T (p.Leu2730Phe) variants maintained conserved across species, which strongly supports the pathogenicity of these variants. The pathogenicity and ACMG classification of all the variants identified in DYNC2H1 were shown in Table 2.

The DYNC2H1 protein consists of an N-terminal tail (DHC_N1), a linker domain (DHC_N2), six identifiable AAA-ATPase domains, a stalk between AAA domains 4 and 5 in the microtubule binding domain (stalk MTBD), and a conserved C-terminal domain arranged on top of the ATPase ring (Carter et al., 2011). DYNC2H1 is essential for ciliogenesis and plays an important role in Hedgehog signaling events which are critical to human skeletal development (Krakow et al., 2000; Pazour et al., 2006). *DYNC2H1* encodes a subunit of cytoplasmic dynein complex, a component of IFTA involved in the retrograde transport from the ciliary tip to the basal body of the ciliary axoneme and plays a role in the generation and maintenance of mammalian cilia (Baujat et al., 2013). Variants in *DYNC2H1* have been associated with a heterogeneous spectrum of conditions related to altered primary cilium function that often involve polydactyly, abnormal skeletogenesis, and polycystic kidneys (Chen et al., 2016). Schmidts et al. (2013a) indicated that *DYNC2H1* missense mutations altered protein function, yet the effects might be "mild" or submorphic. Merrill et al. (2009) hypothesized that homozygosity for two null alleles would lead to early embryonic lethality, but a series of phenotypes with various severity could result from a combination of multiple missense and null mutations. The genotype-phenotype correlation of *DYNC2H1* is pending further elucidation along with larger genetic data.

The c.2386C>T variant affects the highly conserved arginine residues in the stem domain, while the c.7289T>C and the c.8190G>T missense variants are located within the ATP binding and hydrolysis domains (AAA3 and AAA4, respectively). These domains play an important regulatory role for ATP binding (Schmidts et al., 2013a). Blockage of ATP hydrolysis at AAA3 or AAA4 affects the catalytic and mechanical force production activities of dynein (Cho et al., 2008). Modeling the elimination of nucleotide binding at AAA2–4 domains cytoplasmic dynein indicated a severe slowed down in the microtubule sliding activity of the protein, implying dysfunctional motor activity (Zhang et al., 2018). The c.7289T>C and the c.8190G>T were missense changes affecting the ATP binding and hydrolysis domains of the protein (AAA3 and AAA4, respectively), which may disrupt the motor integrity, and interfering with proper retrograde IFT activity. According to the results of structural and MD analysis, the c.7289T>C (p.Ile2430Thr) variant was most likely to significantly affect both local and global hydrogen bond formation to alter protein stability, while also disrupting the desired secondary structure of the protein, thereby disrupting the binding of the protein to ATP. However, the c.8190G>T (p.Leu2730Phe) variant has less influence on the molecular dynamics. Further functional experiments are necessary, not only to clarify the effects of each variant on the protein itself, but also to

**TABLE 2 DYNC2H1 variants (cited from HGMD† database, in order of mutation position).**

| No. | Genomic coordinates | References base(s) | Variant base(s) | HGVS† description | ACMG |
|---|---|---|---|---|---|
| 1 | chr11:102980496–102980496 | A | C | 193A>C | VUS |
| 2 | chr11: 102980498–102980498 | G | T | 195G>T | Likely Pathogenic |
| 3 | chr11: 102984382–102984383 | TA | | 313_314delAT | Likely Pathogenic |
| 4 | chr11:102984397–102984397 | C | G | 327C>G | Pathogenic |
| 5 | chr11:102984407–102984407 | C | T | 337C>T | Likely Pathogenic |
| 6 | chr11: 102985918–102985918 | C | A | 515C>A | VUS |
| 7 | chr11: 102985938–102985938 | T | G | 535T>G | VUS |
| 8 | chr11:102985939–102985939 | G | A | 536G>A | Pathogenic |
| 9 | chr11: 102987300–102987302 | AGT | AAA | 624_625delGTinsAA | Pathogenic |
| 10 | chr11: 102987302–102987302 | T | A | 625T>A | Pathogenic |
| 11 | chr11:102987417–102987417 | G | A | 740G>A | VUS |
| 12 | chr11:102988358–102988358 | A | G | 767-2A>G | Pathogenic |
| 13 | chr11:102988465–102988465 | G | T | 872G>T | VUS |
| 14 | chr11:102988533–102988533 | T | C | 940T>C | VUS |
| 15 | chr11:102988581–102988581 | C | T | 988C>T | Likely Pathogenic |
| 16 | chr11:102991188–102991188 | A | G | 1012A>G | VUS |
| 17 | chr11:102991254–102991254 | C | T | 1078C>T | Pathogenic |
| 18 | chr11:102991434–102991434 | C | T | 1151C>T | Likely Pathogenic |
| 19 | chr11:102991693–102991693 | C | T | 1288C>T | VUS |
| 20 | chr11:102991694–102991694 | G | A | 1289G>A | VUS |
| 21 | chr11:102991711–102991711 | G | T | 1306G>T | Pathogenic |
| 22 | chr11:102991767–102991767 | T | | 1360+2delT | Pathogenic |
| 23 | chr11:102992161–102992161 | T | G | 1421T>G | VUS |
| 24 | chr11:102992166–102992166 | G | | 1427delG | Likely Pathogenic |
| 25 | chr11:102992224–102992224 | A | G | 1484A>G | VUS |
| 26 | chr11:102993672–102993672 | T | C | 1604T>C | VUS |
| 27 | chr11:102993723–102993726 | GTTT | | 1657_1660delTTGT | Pathogenic |
| 28 | chr11:102995926–102995926 | C | T | 1759C>T | Likely Pathogenic |
| 29 | chr11:102996011–102996016 | TTATTC | | 1847_1852delTTCTTA | Likely Pathogenic |
| 30 | chr11:102996022–102996022 | C | T | 1855C>T | Pathogenic |
| 31 | chr11:102999730–102999730 | T | A | 1949T>A | Likely Pathogenic |
| 32 | chr11:102999734–102999734 | G | A | 1953G>A | Likely Pathogenic |
| 33 | chr11:103004369–103004369 | | T | 2040dupT | Pathogenic |
| 34 | chr11:103004417–103004417 | A | C | 2087A>C | VUS |
| 35 | chr11:103005113–103005113 | G | A | 2170G>A | VUS |
| 36 | chr11:103006243–103006243 | T | G | 2225T>G | Likely Pathogenic |
| 37 | chr11:103006359–103006359 | T | G | 2341T>G | Likely Pathogenic |
| 38 | chr11:103006444–103006444 | T | G | 2346-5T>G | Likely Pathogenic |

(Continued on following page)

**TABLE 2 (*Continued*) DYNC2H1 variants (cited from HGMD† database, in order of mutation position).**

| No. | Genomic coordinates | References base(s) | Variant base(s) | HGVS† description | ACMG |
|---|---|---|---|---|---|
| 39 | chr11:103006488–103006488 | C | | 2386delC | Pathogenic |
| 40 | chr11:103006488–103006488 | G | A | 2386C>T | VUS |
| 41 | chr11:103006497–103006497 | A | G | 2394A>G | VUS |
| 42 | chr11:103006498–103006500 | TAT | | 2398_2400delTAT | VUS |
| 43 | chr11:103006546–103006546 | G | C | 2443G>C | VUS |
| 44 | chr11:103006652–103006652 | T | A | 2549T>A | Likely Pathogenic |
| 45 | chr11:103006678–103006678 | G | A | 2574 + 1G>A | Pathogenic |
| 46 | chr11:103013996–103013996 | G | A | 2575-1G>A | Likely Pathogenic |
| 47 | chr11:103014034–103014034 | T | C | 2612T>C | VUS |
| 48 | chr11:103018547–103018549 | ACT | AG | 2750_2751delCTinsG | Likely Pathogenic |
| 49 | chr11:103018617–103018617 | G | C | 2818 + 1G>C | Pathogenic |
| 50 | chr11:103019205–103019205 | A | G | 2819-14A>G | VUS |
| 51 | chr11:103022910–103022910 | C | T | 2992C>T | Likely Pathogenic |
| 52 | chr11:103022977–103022977 | T | G | 3059T>G | Pathogenic |
| 53 | chr11:103023013–103023013 | A | | 3095delA | Pathogenic |
| 54 | chr11:103024028–103024028 | A | G | 3097-4A>G | Benign |
| 55 | chr11:103024068–103024068 | C | T | 3133C>T | Likely Pathogenic |
| 56 | chr11:103024187–103024187 | A | C | 3252A>C | VUS |
| 57 | chr11:103024190–103024190 | | A | 3262dupA | Pathogenic |
| 58 | chr11:103025179–103025179 | G | A | 3303-1G>A | Likely Pathogenic |
| 59 | chr11:103025208–103025208 | G | A | 3331G>A | VUS |
| 60 | chr11:103025230–103025230 | G | | 3353delG | Pathogenic |
| 61 | chr11:103025335–103025335 | G | A | 3458G>A | VUS |
| 62 | chr11:103025423–103025423 | G | A | 3459-1G>A | Pathogenic |
| 63 | chr11:103026124–103026124 | T | G | 3638T>G | VUS |
| 64 | chr11:103026168–103026168 | C | A | 3682C>A | VUS |
| 65 | chr11:103026180–103026180 | G | A | 3694G>A | VUS |
| 66 | chr11:103026205–103026205 | T | C | 3719T>C | VUS |
| 67 | chr11:103027219–103027219 | G | C | 3847G>C | VUS |
| 68 | chr11:103027444–103027444 | C | T | 4072C>T | VUS |
| 69 | chr11:103027445–103027445 | G | A | 4073G>A | Likely Pathogenic |
| 70 | chr11:103029413–103029413 | A | G | 4135A>G | VUS |
| 71 | chr11:103029438–103029438 | | AGTCACAAC | 4162_4170dupGTCACAACA | Likely Pathogenic |
| 72 | chr11:103029637–103029637 | A | G | 4261-2A>G | Likely Pathogenic |
| 73 | chr11:103029645–103029645 | C | T | 4267C>T | Pathogenic |
| 74 | chr11:103029703–103029703 | G | A | 4325G>A | VUS |
| 75 | chr11:103029729–103029729 | C | T | 4351C>T | Likely Pathogenic |
| 76 | chr11:103031700–103031700 | T | C | 4418T>C | Likely Pathogenic |

(Continued on following page)

**TABLE 2 (*Continued*) DYNC2H1 variants (cited from HGMD† database, in order of mutation position).**

| No. | Genomic coordinates | References base(s) | Variant base(s) | HGVS† description | ACMG |
|---|---|---|---|---|---|
| 77 | chr11:103031737–103031737 | T | | 4458delT | Pathogenic |
| 78 | chr11:103031764–103031768 | TAATG | | 4484_4488delATGTA | Likely Pathogenic |
| 79 | chr11:103033818–103033818 | G | A | 4553G>A | Likely Pathogenic |
| 80 | chr11:103033875–103033875 | A | G | 4610A>G | VUS |
| 81 | chr11:103036640–103036640 | C | T | 4625C>T | Likely Pathogenic |
| 82 | chr11:103036714–103036714 | C | G | 4699C>G | Likely Pathogenic |
| 83 | chr11:103039541–103039541 | T | A | 4820T>A | Likely Pathogenic |
| 84 | chr11:103039630–103039630 | G | T | 4909G>T | VUS |
| 85 | chr11:103039685–103039685 | A | G | 4964A>G | Likely Pathogenic |
| 86 | chr11:103040955–103040955 | C | T | 5087C>T | Likely Pathogenic |
| 87 | chr11:103040997–103040997 | T | A | 5129T>A | Likely Pathogenic |
| 88 | chr11:103041020–103041020 | G | T | 5151 + 1G>T | Likely Pathogenic |
| 89 | chr11:103041639–103041639 | C | T | 5176C>T | Pathogenic |
| 90 | chr11:103041680–103041680 | T | | 5220delT | Likely Pathogenic |
| 91 | chr11:103043839–103043839 | T | G | 5363T>G | VUS |
| 92 | chr11:103043994–103043994 | | TA | 5520_5521dupAT | Likely Pathogenic |
| 93 | chr11:103044036–103044036 | T | C | 5558 + 2T>C | Pathogenic |
| 94 | chr11:103044837–103044837 | C | | 5612delC | Pathogenic |
| 95 | chr11:103046970–103046971 | AA | | 5682_5683delAA | Pathogenic |
| 96 | chr11:103047080–103047080 | T | A | 5791T>A | VUS |
| 97 | chr11:103047082–103047082 | G | C | 5793G>C | VUS |
| 98 | chr11:103048286–103048286 | T | A | 5876T>A | Likely Pathogenic |
| 99 | chr11:103048330–103048330 | G | T | 5920G>T | Pathogenic |
| 100 | chr11:103048334–103048334 | T | | 5925delT | Pathogenic |
| 101 | chr11:103048369–103048369 | A | G | 5959A>G | Likely Pathogenic |
| 102 | chr11:103048381–103048381 | A | T | 5971A>T | Pathogenic |
| 103 | chr11:103048382–103048382 | T | A | 5972T>A | Likely Pathogenic |
| 104 | chr11:103048393–103048393 | G | A | 5983G>A | Pathogenic |
| 105 | chr11:103048394–103048394 | C | T | 5984C>T | Likely Pathogenic |
| 106 | chr11:103048445–103048445 | C | T | 6035C>T | VUS |
| 107 | chr11:103048453–103048453 | C | T | 6043C>T | Likely Pathogenic |
| 108 | chr11:103048454–103048454 | G | A | 6044G>A | VUS |
| 109 | chr11:103048457–103048457 | A | G | 6047A>G | Likely Pathogenic |
| 110 | chr11:103048526–103048526 | G | A | 6116G>A | Likely Pathogenic |
| 111 | chr11:103049776–103049776 | G | C | 6161G>C | Likely Pathogenic |
| 112 | chr11:103049821–103049821 | T | C | 6206T>C | VUS |
| 113 | chr11:103049880–103049880 | A | G | 6265A>G | Likely Pathogenic |
| 114 | chr11:103049886–103049886 | A | G | 6271A>G | VUS |

(Continued on following page)

**TABLE 2 (*Continued*) DYNC2H1 variants (cited from HGMD† database, in order of mutation position).**

| No. | Genomic coordinates | References base(s) | Variant base(s) | HGVS† description | ACMG |
|---|---|---|---|---|---|
| 115 | chr11:103049959–103049959 | T | A | 6344T>A | VUS |
| 116 | chr11:103052525–103052525 | G | T | 6387G>T | VUS |
| 117 | chr11:103055609–103055609 | G | A | 6478-16G>A | VUS |
| 118 | chr11:103055627–103055627 | T | A | 6480T>A | Likely Pathogenic |
| 119 | chr11:103055692–103055692 | G | A | 6545G>A | Likely Pathogenic |
| 120 | chr11:103055698–103055698 | A | T | 6551A>T | Likely Benign |
| 121 | chr11:103055709–103055709 | T | C | 6562T>C | Likely Pathogenic |
| 122 | chr11:103055721–103055721 | C | T | 6574C>T | Likely Pathogenic |
| 123 | chr11:103055735–103055737 | TGG | | 6591_6593delTGG | VUS |
| 124 | chr11:103055761–103055761 | G | A | 6614G>A | Pathogenic |
| 125 | chr11:103055779–103055779 | A | T | 6632A>T | VUS |
| 126 | chr11:103056969–103056969 | A | G | 6634-2A>G | Pathogenic |
| 127 | chr11:103057016–103057016 | A | G | 6679A>G | VUS |
| 128 | chr11:103057146–103057146 | G | A | 6809G>A | VUS |
| 129 | chr11:103057171–103057171 | G | T | 6834G>T | VUS |
| 130 | chr11:103057194–103057194 | C | T | 6857C>T | VUS |
| 131 | chr11:103057203–103057203 | T | C | 6866T>C | Likely Pathogenic |
| 132 | chr11:103057220–103057220 | T | C | 6883T>C | Likely Pathogenic |
| 133 | chr11:103058085–103058085 | G | A | 6910G>A | Likely Pathogenic |
| 134 | chr11:103058253–103058253 | G | T | 7078G>T | VUS |
| 135 | chr11:103058260–103058260 | A | G | 7085A>G | Likely Pathogenic |
| 136 | chr11:103058287–103058287 | C | T | 7112C>T | Likely Pathogenic |
| 137 | chr11:103058304–103058304 | T | G | 7129T>G | VUS |
| 138 | chr11:103059233–103059233 | C | T | 7148C>T | VUS |
| 139 | chr11:103059353–103059353 | C | A | 7268C>A | Likely Pathogenic |
| 140 | chr11:103059361–103059361 | C | T | 7276C>T | VUS |
| 141 | chr11:103059362–103059362 | G | T | 7277G>T | Likely Pathogenic |
| 142 | chr11:103059374–103059374 | A | G | 7289T>C | VUS |
| 143 | chr11:103060490–103060490 | G | T | 7382G>T | VUS |
| 144 | chr11:103060517–103060517 | C | G | 7409C>G | Likely Pathogenic |
| 145 | chr11:103060548–103060548 | A | G | 7437 + 3A>G | VUS |
| 146 | chr11:103062244–103062244 | A | G | 7438-2A>G | Pathogenic |
| 147 | chr11:1103062249–103062249 | C | T | 7441C>T | Pathogenic |
| 148 | chr11:103062250–103062250 | G | A | 7442G>A | VUS |
| 149 | chr11:103062294–103062294 | C | T | 7486C>T | VUS |
| 150 | chr11:103062333–103062333 | T | C | 7525T>C | Likely Pathogenic |
| 151 | chr11:103062347–103062347 | A | T | 7539A>T | VUS |
| 152 | chr11:103062846–103062846 | G | C | 7561G>C | VUS |

(Continued on following page)

**TABLE 2 (*Continued*) DYNC2H1 variants (cited from HGMD† database, in order of mutation position).**

| No. | Genomic coordinates | References base(s) | Variant base(s) | HGVS† description | ACMG |
|---|---|---|---|---|---|
| 153 | chr11:103062862–103062862 | T | G | 7577T>G | Likely Pathogenic |
| 154 | chr11:103062879–103062879 | C | T | 7594C>T | Likely Pathogenic |
| 155 | chr11:103062928–103062928 | T | C | 7643T>C | Likely Pathogenic |
| 156 | chr11:103062948–103062948 | G | A | 7663G>A | Likely Pathogenic |
| 157 | chr11:103068671–103068671 | A | G | 7718A>G | VUS |
| 158 | chr11:103068724–103068732 | CCATTACCT | | 7774_7782delTTACCTCCA | Likely Pathogenic |
| 159 | chr11:103068737–103068737 | A | G | 7784A>G | Likely Benign |
| 160 | chr11:103070000–103070000 | T | C | 7883T>C | VUS |
| 161 | chr11:103070036–103070036 | T | C | 7919T>C | VUS |
| 162 | chr11:103070042–103070042 | G | C | 7925G>C | VUS |
| 163 | chr11:103070062–103070062 | G | T | 7945G>T | Likely Pathogenic |
| 164 | chr11:103070083–103070083 | C | T | 7966C>T | Likely Pathogenic |
| 165 | chr11:103070084–103070084 | G | A | 7967G>A | VUS |
| 166 | chr11:103070084–103070084 | G | T | 7967G>T | Likely Pathogenic |
| 167 | chr11:103070098–103070098 | C | T | 7981C>T | VUS |
| 168 | chr11:103070101–103070101 | C | T | 7984C>T | Pathogenic |
| 169 | chr11:103070102–103070102 | G | A | 7985G>A | Likely Pathogenic |
| 170 | chr11:103070104–103070104 | A | C | 7987A>C | VUS |
| 171 | chr11:103070129–103070129 | T | C | 8012T>C | Likely Pathogenic |
| 172 | chr11:103070167–103070167 | G | T | 8050G>T | Pathogenic |
| 173 | chr11:103070179–103070179 | A | | 8063delA | Likely Pathogenic |
| 174 | chr11:103070187–103070187 | C | G | 8070C>G | Likely Pathogenic |
| 175 | chr11:103070194–103070194 | G | T | 8077G>T | VUS |
| 176 | chr11:103070831–103070831 | C | A | 8145C>A | Pathogenic |
| 177 | chr11:103070876–103070876- | C | A | 8190G>T | VUS |
| 178 | chr11:103070883–103070883 | G | T | 8197G>T | Likely Pathogenic |
| 179 | chr11:103074471–103074471 | T | | 8283delT | Pathogenic |
| 180 | chr11:103074506–103074506 | G | A | 8311 + 1G>A | Pathogenic |
| 181 | chr11:103075552–103075552 | A | T | 8313A>T | VUS |
| 182 | chr11:103075578–103075578 | T | C | 8339T>C | VUS |
| 183 | chr11:103075628–103075636 | CCAGCTTTG | | 8390_8398delCAGCTTTGC | VUS |
| 184 | chr11:103075673–103075673 | T | | 8434delT | Pathogenic |
| 185 | chr11:103080607–103080607 | A | G | 8457A>G | VUS |
| 186 | chr11:103080662–103080662 | C | T | 8512C>T | Pathogenic |
| 187 | chr11:103080677–103080677 | A | | 8534delA | Pathogenic |
| 188 | chr11:103082568–103082568 | G | | 8590delG | Pathogenic |
| 189 | chr11:103082595–103082595 | A | G | 8617A>G | VUS |
| 190 | chr11:103082669–103082669 | G | A | 8691G>A | VUS |

(Continued on following page)

**TABLE 2 (*Continued*) DYNC2H1 variants (cited from HGMD† database, in order of mutation position).**

| No. | Genomic coordinates | References base(s) | Variant base(s) | HGVS† description | ACMG |
|---|---|---|---|---|---|
| 191 | chr11:103086484–103086484 | T | C | 8729T>C | Likely Pathogenic |
| 192 | chr11:103086520–103086521 | GT | | 8769_8770delGT | Pathogenic |
| 193 | chr11:103091415–103091415 | C | T | 9010C>T | VUS |
| 194 | chr11:103091449–103091449 | A | G | 9044A>G | Likely Pathogenic |
| 195 | chr11:103091450–103091450 | T | G | 9045T>G | Likely Pathogenic |
| 196 | chr11:103093704–103093704 | G | A | 9242G>A | VUS |
| 197 | chr11:103093816–103093816 | G | A | 9353 + 1G>A | Pathogenic |
| 198 | chr11:103104887–103104887 | C | T | 9565C>T | Pathogenic |
| 199 | chr11:103106471–103106471 | A | G | 9638A>G | VUS |
| 200 | chr11:103106494–103106494 | C | T | 9661C>T | VUS |
| 201 | chr11:103107157–103107157 | A | G | 9710-2A>G | Pathogenic |
| 202 | chr11:103107208–103107212 | GAAAA | | 9760_9764delAAAAG | Pathogenic |
| 203 | chr11:103107263–103107263 | T | A | 9814T>A | Likely Benign |
| 204 | chr11:103107266–103107266 | C | T | 9817C>T | Pathogenic |
| 205 | chr11:103112255–103194718 | | | EX64-EX83 Del | Likely Pathogenic |
| 206 | chr11:103112272–103112272 | C | G | 9836C>G | Pathogenic |
| 207 | chr11:103114423–103114423 | G | A | 9842G>A | VUS |
| 208 | chr11:103114425–103114425 | C | T | 9844C>T | Pathogenic |
| 209 | chr11:103114446–103114446 | G | A | 9865G>A | Likely Pathogenic |
| 210 | chr11:103114510–103114510 | T | C | 9929T>C | VUS |
| 211 | chr11:103116017–103116017 | G | | 9977delG | Likely Pathogenic |
| 212 | chr11:103116062–103116062 | C | G | 10022C>G | VUS |
| 213 | chr11:103116085–103116085 | C | T | 10045C>T | Pathogenic |
| 214 | chr11:103116103–103116103 | G | T | 10063G>T | Pathogenic |
| 215 | chr11:103116105–103116105 | T | G | 10063 + 2T>G | Pathogenic |
| 216 | chr11:103124070–103124070 | C | T | 10120C>T | Likely Pathogenic |
| 217 | chr11:103124071–103124071 | G | A | 10121G>A | Likely Pathogenic |
| 218 | chr11:103124076–103124076 | T | C | 10126T>C | Likely Pathogenic |
| 219 | chr11:103124076–103124076 | T | | 10130delT | Pathogenic |
| 220 | chr11:103124113–103124113 | C | T | 10163C>T | Likely Pathogenic |
| 221 | chr11:103124169–103124169 | C | T | 10219C>T | Pathogenic |
| 222 | chr11:103126224–103126224 | G | A | 10308G>A | VUS |
| 223 | chr11:103126259–103126259 | T | C | 10343T>C | Pathogenic |
| 224 | chr11:103128446–103128446 | T | C | 10592T>C | VUS |
| 225 | chr11:103128448–103128448 | C | T | 10594C>T | Pathogenic |
| 226 | chr11:103128460–103128460 | C | T | 10606C>T | Pathogenic |
| 227 | chr11:103128464–103128464 | C | T | 10610C>T | VUS |
| 228 | chr11:103128478–103128478 | C | T | 10624C>T | Pathogenic |

(Continued on following page)

**TABLE 2 (*Continued*) DYNC2H1 variants (cited from HGMD† database, in order of mutation position).**

| No. | Genomic coordinates | References base(s) | Variant base(s) | HGVS† description | ACMG |
|---|---|---|---|---|---|
| 229 | chr11:103130659–103130659 | T | C | 10669T>C | VUS |
| 230 | chr11:103130699–103130702 | TATT | | 10711_10714delTTTA | Likely Pathogenic |
| 231 | chr11:103151092–103151092 | T | A | 10732T>A | VUS |
| 232 | chr11:103153788–103153788 | C | T | 10885C>T | Likely Pathogenic |
| 233 | chr11:103153789–103153789 | G | C | 10886G>C | VUS |
| 234 | chr11:103156993–103156993 | C | T | 10921C>T | Likely Pathogenic |
| 235 | chr11:103157009–103157009 | C | | 10939delC | Pathogenic |
| 236 | chr11:103173926–103173926 | T | C | 11221T>C | VUS |
| 237 | chr11:103173935–103173935 | C | T | 11230C>T | VUS |
| 238 | chr11:103173983–103173983 | G | A | 11277 + 1G>A | Likely Pathogenic |
| 239 | chr11:103175330–103175330 | A | G | 11284A>G | VUS |
| 240 | chr11:103175337–103175337 | A | G | 11291A>G | Likely Pathogenic |
| 241 | chr11:103175379–103175379 | C | T | 11333C>T | Likely Pathogenic |
| 242 | chr11:103178483–103178483 | C | T | 11437C>T | VUS |
| 243 | chr11:103178484–103178484 | G | A | 11438G>A | VUS |
| 244 | chr11:103178533–103178534 | AC | | 11488_11489delCA | Likely Pathogenic |
| 245 | chr11:103178538–103178538 | C | A | 11492C>A | Likely Pathogenic |
| 246 | chr11:103182652–103182652 | T | G | 11560T>G | VUS |
| 247 | chr11:103182710–103182710- | G | | 11618delG | Pathogenic |
| 248 | chr11:103187334–103187337 | GACA | | 11734_11737delAGAC | Pathogenic |
| 249 | chr11:103187341–103187342 | TT | | 11741_11742delTT | Likely Pathogenic |
| 250 | chr11103191758-103191758 | G | A | 11747G>A | VUS |
| 251 | chr11:103191861–103191861 | C | G | 11850C>G | Pathogenic |
| 252 | chr11:103270549–103270549 | T | G | 12336T>G | VUS |
| 253 | chr11:103306683–103306683 | T | C | 12400T>C | VUS |
| 254 | chr11:103306714–103306714 | C | G | 12431C>G | Likely Pathogenic |
| 255 | chr11:103306743–103306743 | C | T | 12460C>T | Likely Pathogenic |
| 256 | chr11:103325912–103325912 | A | G | 12478-2A>G | Likely Pathogenic |
| 257 | chr11:103325921–103325924 | TAGA | | 12487_12490delGATA | Pathogenic |
| 258 | chr11:103325942–103325942 | C | G | 12506C>G | VUS |
| 259 | chr11:103325974–103325974 | C | | 12538delC | Likely Pathogenic |
| 260 | chr11:103326007–103326007 | C | A | 12571C>A | VUS |
| 261 | chr11:103326024–103326024 | G | T | 12587 + 1G>T | Likely Pathogenic |
| 262 | chr11:103327017–103327017 | | TG | 12605_12606dupTG | Pathogenic |
| 263 | chr11:103327078–103327078 | | T | 12663_12664insT | Pathogenic |
| 264 | chr11:103339363–103339363 | T | G | 12716T>G | VUS |
| 265 | chr11:103339395–103339395 | T | A | 12748T>A | VUS |
| 266 | chr11:103349863–103349863 | T | C | 12827T>C | Likely Pathogenic |

(Continued on following page)

**TABLE 2 (*Continued*) DYNC2H1 variants (cited from HGMD† database, in order of mutation position).**

| No. | Genomic coordinates | References base(s) | Variant base(s) | HGVS† description | ACMG |
|---|---|---|---|---|---|
| 267 | chr11:103349886–103349886 | A | G | 12850A>G | Pathogenic |
| 268 | chr11:103349893–103349893 | G | C | 12857G>C | VUS |
| 269 | chr11:103349953–103349953 | G | A | 12917G>A | VUS |

†HGMD, The Human Gene Mutation Database (http://www.hgmd.cf.ac.uk/ac/index.php); HGVS, Human Genome Variation Society (http://www.hgvs.org/).

understand the mechanistically contributes to the pathology seen in the skeletal ciliopathies.

For any future pregnancy of the couples in this study, the recurrent risk of SRTD3 condition would be 25%. Given such circumstances, the couples were informed of reproductive options such as prenatal testing and preimplantation genetic diagnosis (PGD). Proper genetic counseling for the affected family is essential in the case of rare genetic diseases. Furthermore, parenteral genetic screening/diagnosis is the best strategy for managing this disease, which currently has no therapy (Alyafee et al., 2021a; Alyafee et al., 2021b; Alyafee et al., 2022). Reporting additional cases associated with this gene would help identify genotype–phenotype correlations and lead to clinical trials in the future (Alfadhel et al., 2019).

In summary, this study detected two compound heterozygous variation in *DYNC2H1* including one novel deletion: exon (64–83) del. Our findings clarified the cause of fetal skeletal dysplasias in the subject families, provided guidance for their future pregnancies, and highlighted the value of WES in diagnosis of skeletal dysplasia with unclear prenatal indications.

## Data availability statement

The datasets presented in this study can be found in online repositories. The sequencing results have been deposited to the Figshare repository and can be accessed via the following links: https://doi.org/10.6084/m9.figshare.21738650.v3 and https://doi.org/10.6084/m9.figshare.21738068.v4.

## Ethics statement

The studies involving human participants were reviewed and approved by Shijiazhuang Obstetrics and Gynecology Hospital. The patients/participants provided their written informed consent to participate in this study.

## Author contributions

WC wrote the first draft of the manuscript. YzL and JZ organized the database. DS and JY performed the data curation and visualization. KY wrote sections of the manuscript. YiL and QG contributed to conception and design of the study. All authors contributed to manuscript revision, read, and approved the submitted version.

## Funding

The present study was funded by Medical scientific research project of Health Commission of Hebei Province (No. 20231661) and Medical scientific research project of Health Commission of Hebei Province (No. 20231649).

## Acknowledgments

We thank the patients and their families for their participation in this study.

## Conflict of interest

The authors declare that the research was conducted in the absence of any commercial or financial relationships that could be construed as a potential conflict of interest.

## Publisher's note



## References

Alfadhel, M., Umair, M., Almuzzaini, B., Alsaif, S., AlMohaimeed, S. A., Almashary, M. A., et al. (2019). Targeted SLC19A3 gene sequencing of 3000 Saudi newborn: A pilot study toward newborn screening. *Ann. Clin. Transl. neurology* 6 (10), 2097–2103. doi:10.1002/acn3.50898

Alyafee, Y., Al Tuwaijri, A., Alam, Q., Umair, M., Haddad, S., Alharbi, M., et al. (2021). Next generation sequencing based non-invasive prenatal testing (NIPT): First report from Saudi Arabia. *Front. Genet.* 12, 630787. doi:10.3389/fgene.2021.630787

Alyafee, Y., Al Tuwaijri, A., Umair, M., Alharbi, M., Haddad, S., Ballow, M., et al. (2022). Non-invasive prenatal testing for autosomal recessive disorders: A new promising approach. *Front. Genet.* 13, 1047474. doi:10.3389/fgene.2022.1047474

Alyafee, Y., Alam, Q., Tuwaijri, A. A., Umair, M., Haddad, S., Alharbi, M., et al. (2021). Next-generation sequencing-based pre-implantation genetic testing for aneuploidy (PGT-A): First report from Saudi Arabia. *Genes* 12 (4), 461. doi:10.3390/genes12040461

Baujat, G., Huber, C., El Hokayem, J., Caumes, R., Do Ngoc Thanh, C., David, A., et al. (2013). Asphyxiating thoracic dysplasia: Clinical and molecular review of 39 families. *J. Med. Genet.* 50 (2), 91–98. doi:10.1136/jmedgenet-2012-101282

Bonafe, L., Cormier-Daire, V., Hall, C., Lachman, R., Mortier, G., Mundlos, S., et al. (2015). Nosology and classification of genetic skeletal disorders: 2015 revision. *Am. J. Med. Genet. Part A* 167a (12), 2869–2892. doi:10.1002/ajmg.a.37365

Carter, A. P., Cho, C., Jin, L., and Vale, R. D. (2011). Crystal structure of the dynein motor domain. *Sci. (New York, NY)* 331 (6021), 1159–1165. doi:10.1126/science.1202393

Chen, C. P., Chang, T. Y., Chen, C. Y., Wang, T. Y., Tsai, F. J., Wu, P. C., et al. (2012). Short rib-polydactyly syndrome type II (majewski): Prenatal diagnosis, perinatal imaging findings and molecular analysis of the NEK1 gene. *Taiwan. J. obstetrics Gynecol.* 51 (1), 100–105. doi:10.1016/j.tjog.2012.01.020

Chen, C. P., Chang, T. Y., Tzen, C. Y., Lin, C. J., and Wang, W. (2002). Sonographic detection of situs inversus, ventricular septal defect, and short-rib polydactyly syndrome type III (Verma-Naumoff) in a second-trimester fetus not known to be at risk. *Ultrasound obstetrics Gynecol.* 19, 629. doi:10.1046/j.1469-0705.2002.00731_4.x

Chen, C. P., Chang, T. Y., Tzen, C. Y., and Wang, W. (2003). Second-trimester sonographic detection of short rib-polydactyly syndrome type II (Majewski) following an abnormal maternal serum biochemical screening result. *Prenat. Diagn.* 23, 353. doi:10.1002/pd.574

Chen, C. P., Chern, S. R., Chang, T. Y., Su, Y. N., Chen, Y. Y., Su, J. W., et al. (2012). Prenatal diagnosis and molecular genetic analysis of short rib-polydactyly syndrome type III (Verma-Naumoff) in a second-trimester fetus with a homozygous splice site mutation in intron 4 in the NEK1 gene. *Taiwan. J. obstetrics Gynecol.* 51 (2), 266–270. doi:10.1016/j.tjog.2012.04.018

Chen, C. P., Ko, T. M., Chang, T. Y., Chern, S. R., Chen, S. W., Lai, S. T., et al. (2018). Prenatal diagnosis of short-rib polydactyly syndrome type III or short-rib thoracic dysplasia 3 with or without polydactyly (SRTD3) associated with compound heterozygous mutations in DYNC2H1 in a fetus. *Taiwan. J. obstetrics Gynecol.* 57 (1), 123–127. doi:10.1016/j.tjog.2017.12.021

Chen, C. P., Shih, J. C., Tzen, C. Y., Lin, Y. H., and Wang, W. (2005). Recurrent short-rib polydactyly syndrome: Prenatal three-dimensional ultrasound findings and associations with congenital high airway obstruction and pyelectasia. *Prenat. Diagn.* 25 (5), 417–418. doi:10.1002/pd.976

Chen, C. P., and Tzen, C. Y. (2001). Short-rib polydactyly syndrome type III (Verma-Naumoff) in a third-trimester fetus with unusual associations of epiglottic hypoplasia, renal cystic dysplasia, pyelectasia and oligohydramnios. *Prenat. Diagn.* 21, 1101. doi:10.1002/pd.182

Chen, L. S., Shi, S. J., Zou, P. S., Ma, M., Chen, X. H., and Cao, D. H. (2016). Identification of novel DYNC2H1 mutations associated with short rib-polydactyly syndrome type III using next-generation panel sequencing. *Genet. Mol. Res. GMR* 15 (2). doi:10.4238/gmr.15028134

Cho, C., Reck-Peterson, S. L., and Vale, R. D. (2008). Regulatory ATPase sites of cytoplasmic dynein affect processivity and force generation. *J. Biol. Chem.* 283 (38), 25839–25845. doi:10.1074/jbc.M802951200

Dagoneau, N., Goulet, M., Geneviève, D., Sznajer, Y., Martinovic, J., Smithson, S., et al. (2009). DYNC2H1 mutations cause asphyxiating thoracic dystrophy and short rib-polydactyly syndrome, type III. *Am. J. Hum. Genet.* 84 (5), 706–711. doi:10.1016/j.ajhg.2009.04.016

Huber, C., and Cormier-Daire, V. (2012). Ciliary disorder of the skeleton. *Am. J. Med. Genet. Part C, Seminars Med. Genet.* 160c (3), 165–174. doi:10.1002/ajmg.c.31336

Krakow, D., Salazar, D., Wilcox, W. R., Rimoin, D. L., and Cohn, D. H. (2000). Exclusion of the Ellis-van Creveld region on chromosome 4p16 in some families with asphyxiating thoracic dystrophy and short-rib polydactyly syndromes. *Eur. J. Hum. Genet. EJHG* 8 (8), 645–648. doi:10.1038/sj.ejhg.5200507

McInerney-Leo, A. M., Harris, J. E., Leo, P. J., Marshall, M. S., Gardiner, B., Kinning, E., et al. (2015). Whole exome sequencing is an efficient, sensitive and specific method for determining the genetic cause of short-rib thoracic dystrophies. *Clin. Genet.* 88 (6), 550–557. doi:10.1111/cge.12550

Merrill, A. E., Merriman, B., Farrington-Rock, C., Camacho, N., Sebald, E. T., Funari, V. A., et al. (2009). Ciliary abnormalities due to defects in the retrograde transport protein DYNC2H1 in short-rib polydactyly syndrome. *Am. J. Hum. Genet.* 84 (4), 542–549. doi:10.1016/j.ajhg.2009.03.015

Pazour, G. J., Agrin, N., Walker, B. L., and Witman, G. B. (2006). Identification of predicted human outer dynein arm genes: Candidates for primary ciliary dyskinesia genes. *J. Med. Genet.* 43 (1), 62–73. doi:10.1136/jmg.2005.033001

Rakhshani, H., Dehghanian, E., and Rahati, A. (2019). Enhanced GROMACS: Toward a better numerical simulation framework. *J. Mol. Model.* 25 (12), 355. doi:10.1007/s00894-019-4232-z

Richards, S., Aziz, N., Bale, S., Bick, D., Das, S., Gastier-Foster, J., et al. (2015). Standards and guidelines for the interpretation of sequence variants: A joint consensus recommendation of the American college of medical genetics and genomics and the association for molecular pathology. *Genet. Med.* 17 (5), 405–424. doi:10.1038/gim.2015.30

Schmidt, H., Zalyte, R., Urnavicius, L., and Carter, A. P. (2015). Structure of human cytoplasmic dynein-2 primed for its power stroke. *Nature* 518 (7539), 435–438. doi:10.1038/nature14023

Schmidts, M., Arts, H. H., Bongers, E. M., Yap, Z., Oud, M. M., Antony, D., et al. (2013). Exome sequencing identifies DYNC2H1 mutations as a common cause of asphyxiating thoracic dystrophy (Jeune syndrome) without major polydactyly, renal or retinal involvement. *J. Med. Genet.* 50 (5), 309–323. doi:10.1136/jmedgenet-2012-101284

Schmidts, M., Vodopiutz, J., Christou-Savina, S., Cortés, C. R., McInerney-Leo, A. M., Emes, R. D., et al. (2013). Mutations in the gene encoding IFT dynein complex component WDR34 cause Jeune asphyxiating thoracic dystrophy. *Am. J. Hum. Genet.* 93 (5), 932–944. doi:10.1016/j.ajhg.2013.10.003

Soteras Gutiérrez, I., Lin, F. Y., Vanommeslaeghe, K., Lemkul, J. A., Armacost, K. A., Brooks, C. L., 3rd, et al. (2016). Parametrization of halogen bonds in the CHARMM general force field: Improved treatment of ligand-protein interactions. *Bioorg. Med. Chem.* 24 (20), 4812–4825. doi:10.1016/j.bmc.2016.06.034

Toropova, K., Zalyte, R., Mukhopadhyay, A. G., Mladenov, M., Carter, A. P., and Roberts, A. J. (2019). Structure of the dynein-2 complex and its assembly with intraflagellar transport trains. *Nat. Struct. Mol. Biol.* 26 (9), 823–829. doi:10.1038/s41594-019-0286-y

Zhang, J., Hu, H., Mu, W., Yu, M., Chen, W., Mi, D., et al. (2021). Case report: Exome sequencing identified a novel compound heterozygous variation in PLOD2 causing bruck syndrome type 2. *Front. Genet.* 12, 619948. doi:10.3389/fgene.2021.619948

Zhang, W., Taylor, S. P., Ennis, H. A., Forlenza, K. N., Duran, I., Li, B., et al. (2018). Expanding the genetic architecture and phenotypic spectrum in the skeletal ciliopathies. *Hum. Mutat.* 39 (1), 152–166. doi:10.1002/humu.23362

frontiers | Frontiers in Genetics

TYPE Case Report
PUBLISHED 06 June 2023
DOI 10.3389/fgene.2023.1108852



OPEN ACCESS

EDITED BY
Xiu-An Yang,
Chengde Medical University, China

REVIEWED BY
Simona Coppola,
National Institute of Health (ISS), Italy
Claudia Santoro,
University of Campania Luigi Vanvitelli, Italy

*CORRESPONDENCE
Aleksandra Szczawińska-Popłonyk,
aszczawinska@ump.edu.pl

RECEIVED 26 November 2022
ACCEPTED 23 May 2023
PUBLISHED 06 June 2023

CITATION
Szczawińska-Popłonyk A, Popłonyk N, Badura-Stronka M, Juengling J, Huhn K, Biskup S, Bancerz B and Walkowiak J (2023), The clinical phenotype with gastrostomy and abdominal wall infection in a pediatric patient with Takenouchi-Kosaki syndrome due to a heterozygous c.191A > G (p.Tyr64Cys) variant in *CDC42*: a case report. *Front. Genet.* 14:1108852. doi: 10.3389/fgene.2023.1108852



# The clinical phenotype with gastrostomy and abdominal wall infection in a pediatric patient with Takenouchi-Kosaki syndrome due to a heterozygous c.191A > G (p.Tyr64Cys) variant in *CDC42*: a case report

Aleksandra Szczawińska-Popłonyk[1]*, Natalia Popłonyk[2], Magdalena Badura-Stronka[3,4], Jerome Juengling[5], Kerstin Huhn[5], Saskia Biskup[5,6], Bartłomiej Bancerz[7] and Jarosław Walkowiak[7]

[1]Department of Pediatric Pneumonology, Allergy and Clinical Immunology, Institute of Pediatrics, Karol Jonscher University Hospital, Poznań University of Medical Sciences, Poznań, Poland, [2]Student Scientific Society, Poznań University of Medical Sciences, Poznań, Poland, [3]Centers for Medical Genetics Genesis, Poznań, Poland, [4]Chair and Department of Medical Genetics, Poznań University of Medical Sciences, Poznań, Poland, [5]Zentrum Fur Humangenetik Tübingen, Tübingen, Germany, [6]CeGaT GmbH, Tübingen, Germany, [7]Department of Pediatric Gastroenterology and Metabolic Diseases, Institute of Pediatrics, Karol Jonscher University Hospital, Poznań University of Medical Sciences, Poznań, Poland

The *CDC42* (cell division cycle homolog 42) gene product, Cdc42 belongs to the Rho GTPase family which plays a pivotal role in the regulation of multiple cellular functions, including cell cycle progression, motility, migration, proliferation, transcription activation, and reactive oxygen species production. The Cdc42 molecule controls various tissue-specific functional pathways underpinning organogenesis as well as developmental integration of the hematopoietic and immune systems. Heterozygous c.191A>G (p.Tyr64Cys) pathogenic variants in *CDC42* cause Takenouchi-Kosaki syndrome characterized by a spectrum of phenotypic features comprising psychomotor developmental delay, sensorineural hearing loss, growth retardation, facial dysmorphism, cardiovascular and urinary tract malformations, camptodactyly, accompanied by thrombocytopenia and immunodeficiency of variable degree. Herein, we report a pediatric patient with the Takenouchi-Kosaki syndrome due to a heterozygous p.Tyr64Cys variant in *CDC42* manifesting as a congenital malformation complex accompanied by macrothrombocytopenia, poor specific antibody response, B and T cell immunodeficiency, and low serum immunoglobulin A level. We also suggst that feeding disorders, malnutrition, and a gastrointestinal infection could be a part of the phenotypic characteristics of Takenouchi-Kosaki syndrome supporting the hypothesis of immune dysregulation and systemic inflammation occurring in the p.Tyr64Cys variant in *CDC42*.

KEYWORDS

**Takenouchi-Kosaki syndrome, Cdc42, c.191A>G variant, antibody deficiency, macrothrombocytopenia, neurodevelopmental delay**

## Introduction

The *Cell Division Cycle 42* (*CDC42*) gene encodes a Cdc42 molecule which is a member of the family of Rho GTPases belonging to the Ras superfamily of small GTPases. The Rho-family GTPases are characterized by a multiplicity of physiological functions influencing crucial developmental signals in cell cycle regulation. These biological processes include the establishing and controlling of the cell actin cytoskeleton, vesicle trafficking, cell polarity, proliferation, motility and migration, transcription activation, reactive oxygen species production, and malignant transformation (Ueyama, 2019; Lauri et al., 2021). The Cdc42 protein plays a fundamental role in cell biology and is implicated in a wide array of physiologically pivotal, tissue-specific activities. Cdc42-dependent cytoskeletal reorganization and cell polarity are essential for cardiac organogenesis, tubulogenesis of the pancreas, kidney, lung, and salivary and mammary glands, and differentiation of keratinocytes in the skin and hair follicles (Melendez et al., 2011; Liu et al., 2013). In the central nervous system (CNS), Cdc42 is a positive regulator of its development through neurite initiation, axon growth, branching, myelination and specification, neuronal migration as well as neuronal polarity (Melendez et al., 2011; Liu et al., 2013). Cdc42 coordinates actin turnover and maintenance of actin structures stability in inner ear hair cells and the polarization of the sensory organ of the cochlea which determines the hearing function. The processes of cell polarization and actin microtubule dynamics also play a role in eye morphogenesis and photoreceptor differentiation (Ueyama et al., 2014).

Cdc42 participates in a wide spectrum of immune functions related to hematopoiesis and immune homeostasis as well as effector mechanisms of the innate and adaptive immune responses. In the bone marrow, Cdc42 regulates the multilineage development of blood progenitors and their egress from the bone marrow to the periphery. While Cdc42 is involved in the transcriptional program, it plays an important role in the differentiation of stem and progenitor cells, thus influencing the tight balance between myelopoiesis and erythropoiesis (Mulloy et al., 2010; Nayak et al., 2013), and thereby contributing to the immune system regulation and activation. In neutrophil granulocytes, the Cdc42 molecule, through the cytoskeleton rearrangement, controls migration, activation, degranulation, and reactive oxygen species formation thus influencing pathogen killing efficiency (Tackenberg et al., 2020). The migratory function of dendritic cells upon antigen stimulation and homing to the draining lymph nodes is also Cdc42 activity-depending, reflecting the Cdc42 substantial contribution to the initiation of the adaptive response of T $CD4^+$ helper and $CD8^+$ cytotoxic/suppressor lymphocytes (Luckashenak et al., 2013). The Cdc42 GTPase is an essential coordinator of B lymph cell development, adhesion, motility, antigen and mitogen-driven B cell receptor activation, cognate interaction with T lymph cells, and differentiation into antibody-producing plasma cells (Song et al., 2014; Burbage et al., 2015; Gerasimcik et al., 2015). It has also been shown that Cdc42 plays an important role in T cell thymopoiesis, proliferation, and survival (Smits et al., 2010).

Referring to the multiplicity of key regulatory functions of the Cdc42 GTPase in human biology, governing morphogenesis and functional homeostasis, the growing spectrum of clinical syndromes and pathogenic variants in *CDC42* underpinning the diverse phenotypes have been reported. The patients with a germlin heterozygous missense c.191A>G (p.Tyr64Cys) variant demonstrated a range of congenital phenotypic features termed as Takenouchi-Kosaki syndrome (TKS). The syndrome is characterized by facial dysmorphism, developmental delay, sensorineural hearing loss accompanied by macrothrombocytopenia which compose a universal clinical phenotype observable in all eight hitherto described TKS patients (Takenouchi et al., 2015; Takenouchi et al., 2016; Martinelli et al., 2018; Motokawa et al., 2018; Uehara et al., 2019; Bucciol et al., 2020; Ishikawa et al., 2021; Santoro et al., 2021). Short stature (Takenouchi et al., 2015; Takenouchi et al., 2016; Martinelli et al., 2018; Bucciol et al., 2020; Ishikawa et al., 2021; Santoro et al., 2021), failure to thrive (Takenouchi et al., 2015; Takenouchi et al., 2015; Motokawa et al., 2018; Bucciol et al., 2020; Ishikawa et al., 2021; Santoro et al., 2021) with camptodactyly (Takenouchi et al., 2015; Takenouchi et al., 2016; Martinelli et al., 2018; Motokawa et al., 2018; Bucciol et al., 2020; Ishikawa et al., 2021; Santoro et al., 2021), structural abnormalities of the brain (Takenouchi et al., 2015; Takenouchi et al., 2016; Martinelli et al., 2018; Motokawa et al., 2018; Uehara et al., 2019; Bucciol et al., 2020; Santoro et al., 2021), and antibody deficiency (Martinelli et al., 2018; Motokawa et al., 2018; Bucciol et al., 2020; Ishikawa et al., 2021) represent not constant but frequent findings belonging to the symptomatology in TKS. Herein, we report an another patient presenting with distinctive symptoms of TKS (OMIM #616737) due to the heterozygousp.Tyr64Cys variant in *CDC42* and the clinical phenotype with congenital malformations, immunodeficiency, and gastrointestinal disorders.

## Case report

### The patient

The male patient was born to a non-consanguineous couple from the first pregnancy complicated by premature uterine contracions and spontaneous vaginal delivery at the 38th week of gestational age (WGA), with an Apgar score of 8 points. His anthropometric parameters at birth were the following: weight 3.52 kg [+0.60 standard deviation score (SDS)], length 54 cm (+2.00 SDS), and head circumference 37 cm (+1.25 SDS). The perinatal period was complicated by respiratory distress syndrome due to congenital pneumonia resulting from ascending intrauterine infection and he required non-invasive ventilation support (nCPAP) and antibiotic therapy with ampicillin and gentamycin for 10 days; subsequently, intermittent low-flow supplemental oxygen therapy was needed by the 33rd day of life. He presented features suggesting an underlying genetic syndrome consisting of facial dysmorphism, low-set ears, axial hypotonia with peripheral spasticity, camptodactyly, and cutaneous syndactyly of toes. The abdominal ultrasound examination demonstrated a duplex pelvicalyceal system of the right kidney and in echocardiography, an atrial septal defect (ASD) was found. In the cerebral magnetic resonance imaging (MRI), widening of the supratentorial ventricular system, in particular in the region of occipital and temporal horns of lateral ventricles caused by narrowing of the periventricular white matter as well as hypoplastic cerebellar vermis

were found. Due to the poor sucking reflex in a newborn, making the initiation of breastfeeding and bottle-feeding unsuccessful despite the oral motor stimulation and frenotomy, feeding by a nasogastric tube to secure the nutrition was recommended. However, feeding intolerance and inappropriate weight gain velocity were observable. The infant's diet was modified and he received an amino acid-based formula with nutritional, caloric, and thickening supplementation yet failure to thrive was disturbing the patient's growth and weight gain, and achieving developmental milestones. At the age of 3 months, the patient's weight was 5.15 kg (−0.80 SDS), length 60 cm (+2.30 SDS), and head circumference 37.5 cm (−1.50 SDS). At that time, the patient was admitted to the department of pediatric gastroenterology and metabolic diseases of our tertiary care university hospital to provide enteral feeding, a balloon-assisted endoscopic percutaneous gastrostomy (PEG) feeding tube was inserted using a push method. The procedure was complicated by an infection of the skin, abdominal wall, and intraperitoneal connective tissue of the anterior gastric wall, from which *Staphylococcus aureus* and *Enterococcus faecalis* were cultured, and hence, intensive intravenous antibiotic therapy with meropenem and replacement of PEG were necessary.

At the age of 9 months, the patient was admitted to our university pediatric immunology unit for immunodiagnostics. He presented with proportionate growth retardation, his body mass stood at 6.9 kg (−1.25 SDS), length 70 cm (−1.50 SDS), head circumference 42,5 cm (SDS −1.62), and the weight-for-length ratio below the third percentile (−2.25 SDS), bilateral profound sensorineural hypoacusis, axial hypotonia with peripheral spasticity, sloping forehead and low hairline, facial dysmorphism with an oblique setting of palpebral fissures, nasal tip pointed upwards, downturned corners of the lips, arched palate, low-set ears, camptodactyly and cutaneous syndactyly of toes, micropenis, and cryptorchidism. Developmental psychomotor delay was observable as the boy showed poor facial expression, did not make any sounds, get to a sitting position by himself nor sit without support. The clinical evaluation, biochemical laboratory tests, and ultrasound imaging assessment did not show features of lymphoproliferation, hemophagocytic lymphohistiocytosis (HLH), or bleeding disorders. The immunodiagnostic workup revealed macrothrombocytopenia, lymphopenia, low serum immunoglobulin A level, poor specific antibody response, and impairment of humoral and cellular immunity. An in-depth flow cytometric immunophenotyping showed abnormalities within the B and T lymph cell compartment primarily disrupted T cell development with low T $CD4^+$ helper cell, recent thymic emigrant numbers, and naïve T CD45RA + cell to memory T CD45RO + cell ratio. These were accompanied by low numbers of B cells and a decline in B cell memory development. The immunological diagnostics performed on the patient studied is displayed in Table 1 (Part A). Due to the patient's history pointing to recurrent infections, microbiology studies were performed. The infectious workup targeted at airway and blood-borne viral and bacterial pathogens, proved negative as shown in Table 1 (part B).

The genetic analysis using exome technique on trio was performed. In the patient, it revealed the c.191A>G (p.Tyr64Cys) (NM_001791.4) variant in the *CDC42* gene. The presence of the variant was confirmed in the proband by Sanger sequencing and excluded in both parents, indicating that the variant occurred *de novo* in a heterozygous state (Figure 1). The p.Tyr64Cys variant in conjunction with the patient's clinical phenotype is causative for TKS (Takenouchi et al., 2015; Takenouchi et al., 2016; Martinelli et al., 2018; Motokawa et al., 2018; Uehara et al., 2019; Bucciol et al., 2020; Ishikawa et al., 2021; Santoro et al., 2021). The summary of the clinical phenotypic features, course of the disease including gastroenterological problems, diagnostic procedures uncovering congenital anomalies and immunodeficiency, as well as implemented multidisciplinary care are displayed in Timeline (Figure 2).

# Methods

## The molecular genetic analysis

Trio whole exome sequencing (WES) analysis was performed on the proband and his parents.

Starting from EDTA blood, genomic DNA was isolated according to the manufacturers' instructions using QIAamp DNA Blood Maxi Kit on a QiaSymphony instrument (Qiagen, Hilden, Germany). DNA quantity and quality are determined using Qubit®uFluorometer and NanoDrop ND-8000 (Thermo Fisher Scientific, Dreieich, Germany). Sequencing libraries were prepared for each sample from 50 ng DNA using the Twist enrichment workflow (Twist Bioscience, San Francisco, CA, United States) and a custom-design enrichment probe set (CeGaT ExomeXtra V2). Library preparation and capture was performed according to the manufacturer's instructions and paired-end sequencing was performed on a NovaSeq6000 instrument (Illumina, San Diego, CA, United States) with 2 × 100 base pairs (bp) read length. Sequence data were processed with Illumina bcl2fastq2. Adapter sequences were removed with Skewer and the sequences obtained, were aligned to the human reference genome (hg19) with the Burrows Wheeler aligner (BWA mem). Sequences that could not be clearly assigned to a genomic position were removed, as were sequence duplicates that were probably due to amplification (internal software). Copy number variations (CNV) were computed on uniquely mapping, non-duplicate, high quality reads using an internally developed method based on sequencing coverage depth. Briefly, we used reference samples to create a model of the expected coverage that represents wet-lab biases as well as intersample variation. CNV calling was performed by computing the sample's normalized coverage profile and its deviation from the expected coverage. Genomic regions were called as variant if they deviate significantly from the expected coverage. Sequence variants (single nucleotide exchanges and short insertions/deletions) were determined from the remaining high-quality sequences (CeGaT StrataCall). Resulting variants were annotated with population frequencies from gnomAD (2.1/3.1) and an internal database (CeGaT), factoring in external databases (e.g., HGMD, ClinVar), and with transcript information from Ensembl, RefSeq, Gencode, and CCDS. All variants were manually assessed before inclusion in the final report, and classified and reported based on ACMG/ACGS-2020v4.01 guidelines (Richards et al., 2015).

**TABLE 1 The immunological workup with antibody-mediated response and peripheral blood flow cytometric immunophenotyping (Part A) and the infectious workup (Part B) in the patient with p.Tyr64Cys variant in *CDC42*.**

| A. Immunological workup | | |
|---|---|---|
| Antibody response | Results | Reference values |
| Immunoglobulins | | |
| IgG | 474 mg/dL | 350–1180 mg/dL |
| IgA | 13 mg/dL | 36–165 mg/dL |
| IgM | 30 mg/dL | 30–104 mg/dL |
| IgE | <2 kU/L | >2 kU/L |
| IgG subclasses | | |
| IgG1 | 296 mg/dL | 194–842 mg/dL |
| IgG2 | 34 mg/dL | 22–300 mg/dL |
| IgG3 | 92 mg/dL | 19–85 mg/dL |
| IgG4 | 18 mg/dL | 5-78 mg/dL |
| Antigen-specific antibodies | | |
| Anti-Diphtheria toxoid IgG | 0.11 IU/mL | >1.0 IU/mL |
| Anti-Tetanus toxoid IgG | 0.66 IU/mL | >1.0 IU/mL |
| PB lymphocyte immunophenotyping | | |
| Full PB count | | |
| WBC | 4,160cc | 4,000–20,000cc |
| Lymphocytes CD45+/SSC low | 58.0%, 2,400cc | 57.0-83.6%, 4000–8,600cc |
| B cell compartment | | |
| B CD19+ | 16.0%, 400cc | 15.7–34.1%, 700–2,800cc |
| Transitional B CD19+CD38+IgM++ | 47.2%, 189cc | 7.2–19.7%, 100–300cc |
| Mature naïve B CD19+CD27-IgD+ | 89,3%, 357cc | 85.5–93.4%, 600–2,590cc |
| Non-switched memory B (MZL) CD19+CD27+IgD+ | 1.9%, 8cc | 2.8–7.4%, 30–120cc |
| Switched memory B CD19+CD27+IgD- | 2.3%, 9cc | 1.6–7.0%, 20–140cc |
| Immature B CD19+CD21lo | 34.2%, 137cc | 6.2–20.3%, 70–290cc |
| Immature activated B CD19+CD38loCD21lo | 3.4%, 14cc | 0.4–3.3%, 0–50cc |
| Plasmablasts CD19+CD38++IgM- | 0.8%, 3cc | 0.2–4.0%, 0–60cc |
| T cell compartment | | |
| T CD3+ | 51.0%, 1254cc | 49.0–95.0%, 1,400–11,500cc |
| T helper CD3+CD4+ | 24.0%, 593cc | 27.0–81.0%, 1,000–7,200cc |
| T suppressor/cytotoxic CD3+CD8+ | 23.0%, 561cc | 10.0–35.0%, 200–5,400cc |
| CD4+/CD8+ | 1.1 | 1.5–2.5 |
| CD45RA+/CD45RO+ | 1.0 | >1.0 |
| Recent thymic emigrants CD3+CD4+CD45RA+CD31+ | 48.1%, 285cc | 65.0–90.0%, 800–6,200cc |
| Naïve T helper CD3+CD4+CD45RA+CD27+ | 48.1%, 285cc | 77.0–97.0%, 800–7,600cc |
| Central memory T helper CD3+CD4+CD45RA-CD27+ | 46.1%, 274cc | 2.0–59.0%, 100–1,300cc |
| Effector memory T helper CD3+CD4+CD45RA-CD27- | 4.8%, 28cc | 0.1–1.0%, 1–72cc |
| Terminally differentiated memory T helper CD3+CD4+CD45RA+CD27- | 1.0%, 6cc | 0.0–7.3%, 0–400cc |
| Follicular CXCR5+ T helper CD3+CD4+CD45RO+CD185+ | 19.7%, 56cc | 9.0–47.0%, 15–110cc |

(Continued on following page)

**TABLE 1 (*Continued*) The immunological workup with antibody-mediated response and peripheral blood flow cytometric immunophenotyping (Part A) and the infectious workup (Part B) in the patient with p.Tyr64Cys variant in *CDC42*.**

| A. Immunological workup | | |
|---|---|---|
| Antibody response | Results | Reference values |
| Regulatory T helper CD3+CD4+CD25++CD127- | 2.6%, 15cc | 4.0–18.0%, 60–740cc |
| Naïve T suppressor/cytotoxic CD3+CD8+CD27+CD197+ | 26.0%, 146cc | 31.0–100%, 150–3200cc |
| Central memory T suppressor/cytotoxic CD3+CD8+CD45RA-CD27+CD197+ | 5.4%, 30cc | 0.1–13.0%, 2–150cc |
| Effector memory T suppressor/cytotoxic CD3+CD8+CD45RA-CD27-CD197- | 33.8%, 180cc | 1.0–100%, 8–1,400cc |
| Terminally differentiated T suppressor/cytotoxic CD3+CD8+CD45RA+CD27-CD197- | 11.8%, 66cc | 5.0–78.0%, 17–2,800cc |
| NK cells | | |
| NK CD3-CD45+CD16+CD56+ | 25.0%, 628cc | 2.0–36.0%, 61–510cc |
| Lymphocyte stimulation tests | | |
| PHA | 3,7261 cpm | >160,000 cpm |
| PHA stimulation index | 142.2 | >65.0 |
| Anti-CD3 | 6,6818 cpm | >15,000 cpm |
| Anti-CD3 stimulation index | 255.0 | >60.0 |
| Pansorbin cells | 4,399 cpm | >2,000 cpm |
| Pansorbin cells stimulation index | 16.8 | >5.0 |
| Complement | | |
| C3 | 148 mg/dL | 90–180 mg/dL |
| C4 | 34 mg/dL | 10–40 mg/dL |
| CH50 | 156 EqU/mL | 70–187 EqU/mL |
| B. Infectious workup | | |
| Blood | | Results |
| Viral panel Cytomegalovirus-DNA, Epstein-Barr virus-DNA, Adenovirus-DNA, Herpes simplex virus 1 and 2-DNA, Human Herpes virus 6 and 7-DNA, Enterovirus-RNA, Human Parechovirus-RNA, Varicella zoster virus-DNA, Human Parvovirus B19-DNA, Hepatitis B-DNA, Hepatitis C-DNA | | All (-) |
| Bacterial panel Streptococcus pneumoniae-DNA, Neisseria meningitidis-DNA, Haemophilus influenzae-DNA | | All (-) |
| Airways | | |
| Airway aspirate Influenza virus A, A H1N1, B-RNA, Rhinovirus-RNA, Coronavirus NL63, 229E, OC43, HKU1-RNA, panel Parainfluenza virus 1,2,3,4-RNA, Human metapneumovirus A, B-RNA, Respiratory syncytial virus A, B-RNA, Enterovirus-RNA, Parechovirus-RNA, Bocavirus-DNA, Mycoplasma pneumoniae-DNA, Chlamydophila pneumoniae-DNA, Staphylococcus aureus-DNA, Streptococcus pneumoniae-DNA, Haemophilus influenzae-DNA | | All (-) |

## Flow cytometric peripheral blood (PB) lymph cell immunophenotyping

Cells were labeled with the following murine fluorochrome-stained monoclonal antibodies: anti-CD45 FITC (fluorescein isothiocyanate), anti-CD14 PE (phycoerythrin), anti-CD19 PE, anti-CD19 PerCP (peridinin chlorophyll protein), anti-IgM FITC, anti-IgD FITC, anti-CD38 APC (allophycocyanin), anti-CD27 PE, anti-CD21 FITC, as well as anti-CD3 FITC, anti-CD4 FITC, CD45RA FITC, CD127 FITC, CD185 FITC, anti-CD8 PE, anti-CD16$^+$CD56 PE, CD25 PE, CD31 PE, CD45RO PE, anti-CD3 PerCP, CD197 PerCP, anti-CD4 APC and anti-CD8 APC (all Beckton-Dickinson Biosciences, United States). The acquisition of cells and analysis was carried out with the use of the flow cytometer FACSCanto and FACSDiva software (Beckton-Dickinson, United States). With sequential gating on biparametric scattering CD45$^+$CD14-lymphocytes, the following lymphocyte subpopulations were identified:

- CD19$^+$ B cells, immature CD19$^+$CD21lo, immature activated CD19$^+$CD38loCD21lo, transitional CD19$^+$CD38hisIgMhi, non-switched memory CD19$^+$CD27+sIgD+, switched memory CD19$^+$CD27+IgD- B cells, and CD19$^+$CD38hisIgM-plasmablasts
- CD3$^+$ T cells, CD3$^+$CD4$^+$ T helper cells, CD3$^+$CD4$^+$CD31$^+$ CD45RA + recent thymic emigrants, naïve CD3$^+$CD4$^+$CD27$^+$

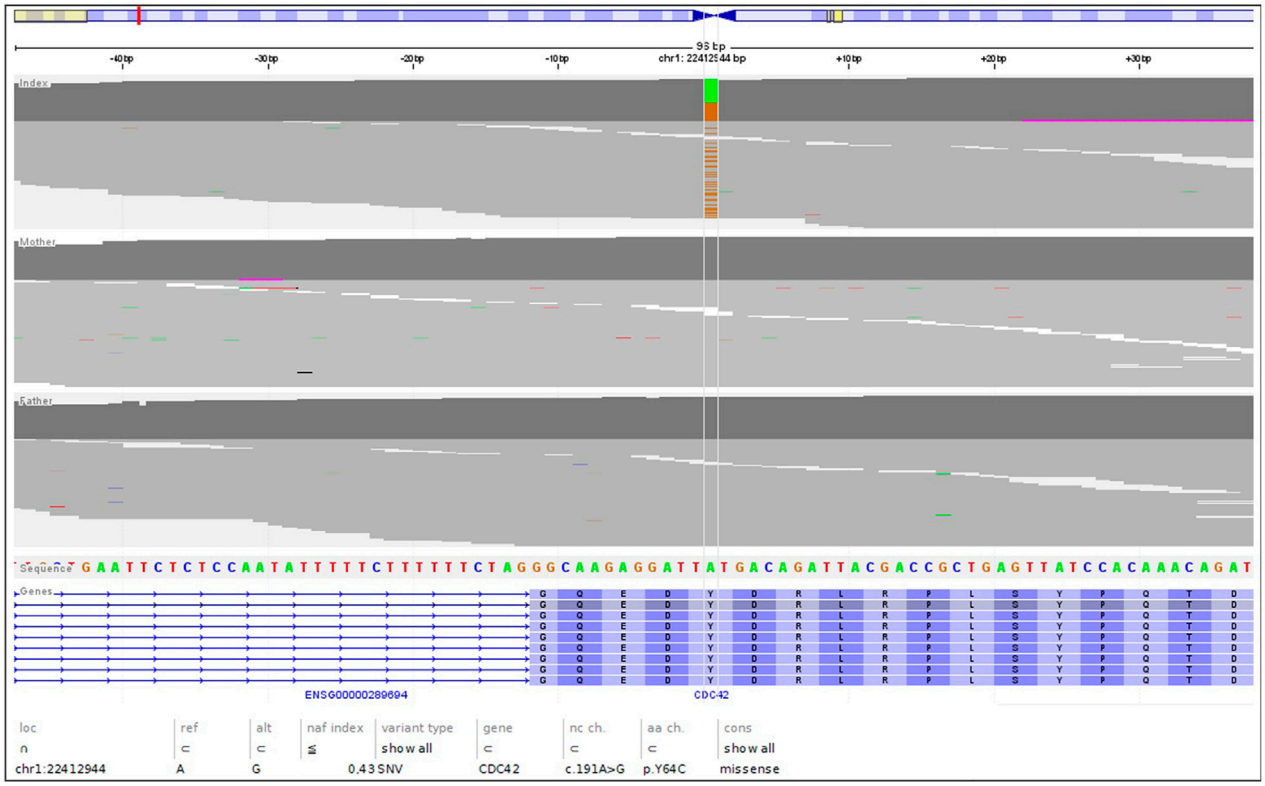


FIGURE 1
The NGS reads of the trio, highlighting the *de novo* nature of the c.191A>G; pTyr64Cys variant.

CD45RA+, regulatory $CD3^+CD4^+CD25{+}{+}CD27^-$, central memory $CD3^+CD4^+CD27^+CD45RO+$, effector memory $CD3^+CD4^+CD27^-CD45RO+$, terminally differentiated $CD3^+CD4^+CD27^-CD45RA+$, follicular $CD3^+CD4^+CD185+CD45RO+$, and regulatory $CD3^+CD4^+CD45RO+CD127\text{-}CD25{+}{+}$ T helper cells. Among $CD3^+CD8^+$ cytotoxic T cells, the following subsets were distinguished: naïve $CD3^+CD8^+CD197+CD27^+CD45RA+$, central memory $CD3^+CD8^+CD197+CD27^+CD45RO+$, effector memory $CD3^+CD8^+CD197\text{-}CD27^-CD45RO+$, and terminally differentiated $CD3^+CD8^+CD197\text{-}CD27^-CD45RA$ + cells.

- $CD3^-CD16^+CD56^+$ NK cells.

The relative values of PB lymphocytes, the B, T, and NK cells of the total lymphocyte population as well as B and T cell subsets were calculated. The absolute counts of all cell subsets were calculated from the PB leukocyte counts. A comparative analysis was done with the reference cut-off values of B and T cell subsets for pediatric populations of different age groups (Piątosa et al., 2010; Schatorje et al., 2012).

## Discussion

Referring to the heterogeneity of clinical manifestations and the complexity of mutual phenotype-genotype interrelations in hitherto reported alterations in *CDC42*, it must be highlighted that establishing the definitive diagnosis of a *CDC42*- related syndrome, including TKS, is challenging for clinicians. The phenotypic features of TKS related to the p.Tyr64Cys variant in *CDC42* comprise psychomotor developmental delay, intellectual disability, dysmorphism, sensorineural hearing loss, cardiac and genitourinary malformations, and macrothrombocytopenia (Takenouchi et al., 2015; Takenouchi et al., 2016; Martinelli et al., 2018; Motokawa et al., 2018; Uehara et al., 2019; Bucciol et al., 2020; Ishikawa et al., 2021; Santoro et al., 2021), consistent also with the herein reported patient. The summary of phenotypic features of patients with TKS due to the c.191A>G; p.Tyr64Cys variant in *CDC42* are summarized in Table 2. Noteworthy, in a single patient with the same p.Tyr64Cys variant, localized in the switch II domain of the *CDC42* gene, affecting Cdc42 binding to multiple effectors and regulators, and causing TKS (Martinelli et al., 2018), immune dysregulation with autoinflammation was observable. It was characterized by interleukin (IL)-6, IL-18, IL-18 binding protein (BPa), and CXCL9 chemokine hypercytokinemia accompanied by myelofibrosis (Bucciol et al., 2020). This phenomenon reflects the clinical intersubject variability within the p.Tyr64Cys variant group and possible overlap with C-terminal variants in the *CDC42* gene and highlights that the p.Tyr64Cys variant does support the hypothesis that the gene is associated with distinct diseases. The clinical phenotypes related to C-terminal variants are characterized by severe neonatal-onset dyshematopoiesis and immune dysregulation including autoinflammation, rash, and HLH (NOCARH syndrome) (Gernez et al., 2019; Lam et al., 2019; He et al., 2020; Coppola et al., 2022) with a chronic excess of the inflammatory cytokine, IL-18 as a hallmark of these disorders (Miyazawa and Wada, 2022;

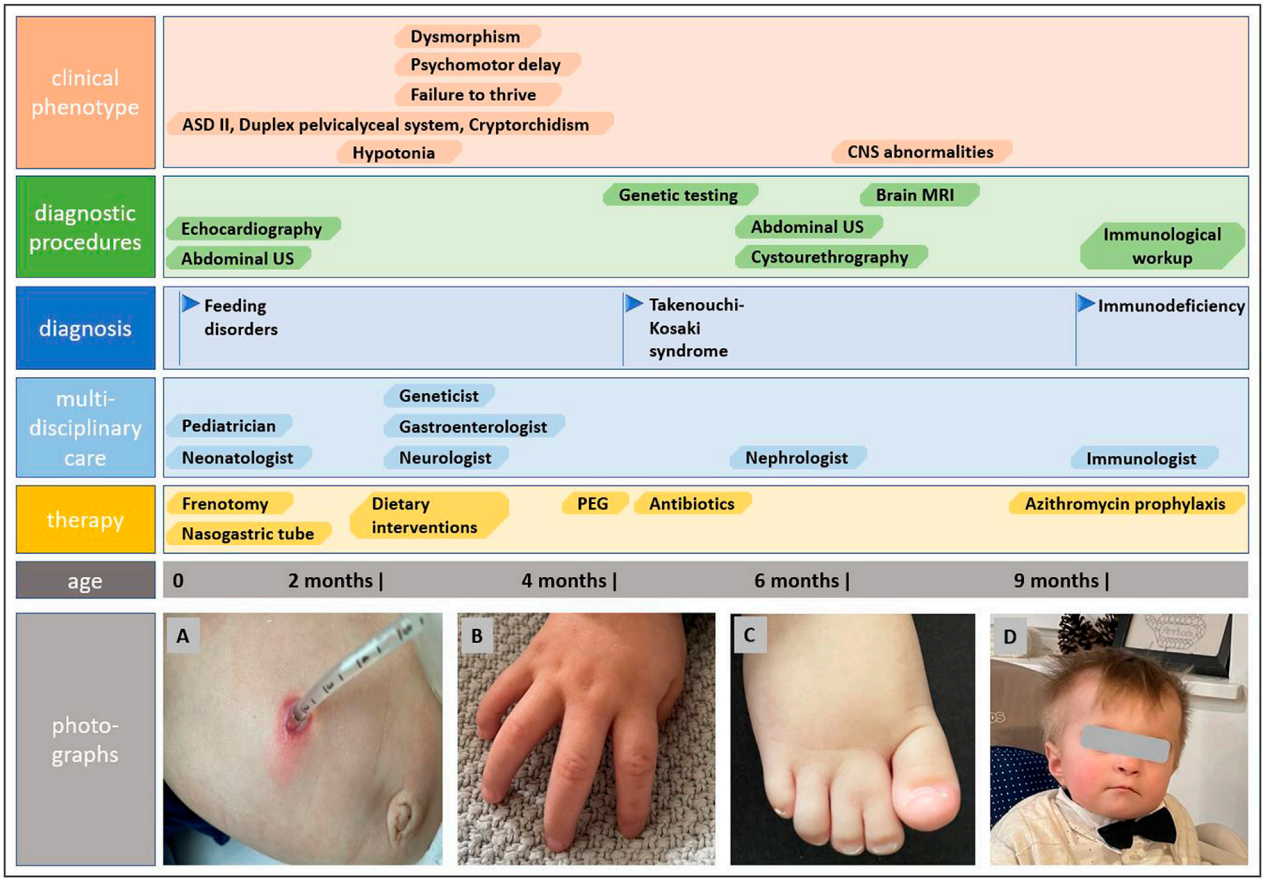


FIGURE 2
Timeline showcasing the course of the disease, establishing the diagnosis of Takenouchi-Kosaki syndrome and the multidisciplinary approach. Photographs show gastrostomy and abdominal wall infection **(A)**, camptodactyly **(B)**, syndactyly of toes **(C)**, and distictive facial gestalt **(D)**.

Shimizu et al., 2022). A similar phenotype distinguished by the hyperinflammatory state, full-blown HLH, and hitherto not reported, development of non-Hodgkin lymphoma has also been described by our group in the patient with a novel p.Cys81Tyr variant (Szczawińska-Popłonyk et al., 2020).

The ever-increasing use of the next-generation sequencing (NGS) approach enabling uncovering molecular genetic diagnosis underpinning the clinical symptomatology has led to better recognition of variable *CDC42* gene alterations and the spectrum of clinical immunophenotypes. A variable degree of immunodeficiency has been primarily linked to the variants affecting the switch II domain in the *CDC42* gene (Takenouchi et al., 2015; Takenouchi et al., 2016; Martinelli et al., 2018; Motokawa et al., 2018; Uehara et al., 2019; Bucciol et al., 2020; Asiri et al., 2021; Ishikawa et al., 2021; Kashani et al., 2021; Santoro et al., 2021). In the reported patients, the antibody immune response ranged from normal referenced serum immunoglobulin levels to panhypogammaglobulinemia affecting the production of all immunoglobulin isotypes with low specific antibody response to diphtheria, tetanus, and mumps vaccine antigens. Antibody deficiency is a consequence of disrupted Cdc42 activity affecting actin cytoskeleton mobility, cellular trafficking, regulation of transcription, and proliferation which occur in multiple cell lineages in *CDC42* mutants, including the B and T cell compartments. Furthermore, in the actin cytoskeleton remodeling and cell polarity regulation, the Cdc42 GTPase activating interaction is required with the GTPase-binding domain of the Cdc42 effector, the Wiskott-Aldrich protein (WASP) that is essential for B and T cell differentiation (Tangye et al., 2019). The presently described patient has normal for age IgG, and IgM, decreased IgA levels, normal distribution of IgG subclasses, low antigen-specific anti-tetanus and anti-diphtheria antibodies, accompanied by lymphopenia and aberrant B and T lymph cell, primarily T helper cell development that might be underpinning the proneness to infections and immune dysregulation. Referring to the clinical reports, in 2022, disorders of the actin cytoskeleton affecting immunity have been included by the International Union of Immunological Societies Expert Committee in the updated classification of human inborn errors of immunity (Tangye et al., 2022).

In this report, we add feeding disorders as well as gastric and abdominal walls infection to the clinical symptomatology of the p.Tyr64Cys variant-related syndrome. Noteworthy, the aberrant immune response in our patient may be an important factor contributing to the chronic inflammation and malfunctioning of the gastrointestinal tract leading to a vicious circle of immunodeficiency with immune dysregulation and malnutrition

**TABLE 2** The summary of clinical symptomatology presented by patients with the same p.Tyr64Cys variant in *CDC42*.

| Clinical workup of takenouchi-kosaki syndrome | | | | | | | | | | |
|---|---|---|---|---|---|---|---|---|---|---|
| Author (references) | Takenouchi et al. (2015) | Takenouchi et al. (2016) | Motokawa et al. (2018) | Ishikawa et al. (2021) | Uehara et al. (2019) | Martinelli et al. (2018) | Bucciol et al. (2020) | Santoro et al. (2021) | Current report | Total |
| Age at diagnosis | 18 years | 22 years | 12 years | 15 years | 4 years | 15 years | 25 years | 7 years | 9 months | |
| Pregnancy | normal | normal | Fetal hydrops<br>Pleural effusion | normal | normal | normal | normal | Abortion threats at first trimester | Premature uterine contractions | 3 (33%) |
| **Feeding disorders** | | | | | | | | | | |
| Feeding intolerance | no | yes, intestinal lymphangiectasia | no | no | no | no | yes | yes, poor sucking and swallowing | yes, poor sucking reflex, oral feeding disability | 3 (33%) |
| Failure to thrive | yes | yes | yes | yes | no | no | yes | yes | yes | 7 (78%) |
| **Infections** | | | | | | | | | | |
| Respiratory | no | yes | yes | no | no | yes | yes, bronchiectasis, fatal pneumonia | no | Congenital pneumonia | 5 (56%) |
| Gastrointestinal | no | no | no | no | no | no | no | no | Anterior gastric wall and intraperitoneal connective tissue | 1 (11%) |
| Genitourinary | no | no | no | no | no | no | no | yes, Hydronephrosis | no | 1 (11%) |
| **Congenital anomalies** | | | | | | | | | | |
| Abnormal development of the internal organs | Persistent ductus arteriosus; Inguinal hernia | Retinal dysplasia with congenital detachment | no | no | no | Cardiac anomaly (unspecified) | no | Persistent ductus arteriosus; Ventricular septal defect | Atrial septal defect; Duplex pelvicalceal system of the right kidney; Small penis, scrotal hypoplasia; cryptorchidism | 5 (56%) |
| Microcephaly | yes | yes | no | no | no data | no | yes | yes | no | 4 (44%) |
| Short stature | yes | yes | no | yes | no data | yes | yes | yes | yes | 7 (78%) |
| Camptodactyly | yes | yes | yes | yes | no | yes | yes | yes | yes | 8 (89%) |
| Syndactyly | no | no | no | no | no | no | no | Cutaneous syndactyly of 2–3 toes bilaterally | Cutaneous syndactyly of 2–4 toes of the left and 2–3 toes of the right foot | 2 (22%) |
| **Facial features** | | | | | | | | | | |
| Arched eyebrows | yes | yes | no data | no | no data | yes | no | yes | yes | 5 (56%) |

(Continued on following page)





10.3389/fgene.2023.1108852

**TABLE 2 (*Continued*) The summary of clinical symptomatology presented by patients with the same p.Tyr64Cys variant in *CDC42*.**

| Clinical workup of takenouchi-kosaki syndrome | | | | | | | | | | |
|---|---|---|---|---|---|---|---|---|---|---|
| Author (references) | Takenouchi et al. (2015) | Takenouchi et al. (2016) | Motokawa et al. (2018) | Ishikawa et al. (2021) | Uehara et al. (2019) | Martinelli et al. (2018) | Bucciol et al. (2020) | Santoro et al. (2021) | Current report | Total |
| Ptosis | yes | yes | yes | no | no data | no | no | no | yes | 4 (44%) |
| Eversion of the lower eyelid | yes | yes | no data | no | no data | yes | yes | yes | no | 5 (56%) |
| Synophrys | yes | yes | yes | yes | no data | no | no | yes | yes | 6 (67%) |
| Exotropia | yes | yes | yes | no | no data | no | yes | yes | no | 5 (56%) |
| Midface hypoplasia | yes | yes | yes | yes | no data | yes | no data | no | yes | 6 (67%) |
| Short philtrum | yes | yes | no | yes | no data | smooth | no data | yes | no | 4 (44%) |
| Thin upper lip | yes | yes | yes | no | no data | yes | no data | yes | yes | 6 (67%) |
| Malocclusion | yes | yes | no data | no | no data | yes | yes | yes | no | 5 (56%) |
| Psychomotor disability | | | | | | | | | | |
| Speech | simple words | no | simple words | no data | no data | no data | no data | no data | Absent (not yet) | 2 (22%) |
| Sensorineural hearing loss | yes | yes | yes | yes | yes | yes | yes | yes | yes | 9 (100%) |
| Walking independency | 4 years | 3 years | 3 years | no data | no data | no data | no data | no data | Absent (not yet) | 3 (33%) |
| Neurological symptoms | tremor; ataxic gait | Nystagmus, agitation, sleep impairment | no | no | no | Seizures | no | no | Poor sucking reflex; axial hypotonia, peripheral spasticity | 4 (44%) |
| MR imaging of the CNS | | | | | | | | | | |
| Cerebellar atrophy | yes | no | no | no | yes | yes | yes, Dandy-Walker variant | no | Hypoplastic cerebellar vermis | 5 (56%) |
| Corpus callosum hypoplasia | no | no | yes | no | no | no | no | no | no | 1 (11%) |
| Ventriculomegaly | yes | yes | yes | no | yes | yes | yes | yes | yes | 8 (89%) |
| Laboratory findings | | | | | | | | | | |
| Macrothrombocytopenia | yes | yes | yes | yes | yes | yes | yes | intermittent | yes | 9 (100%) |
| Antibody deficiency | no data | no data | yes | yes | no data | yes | yes | no data | yes | 5 (56%) |





10.3389/fgene.2023.1108852

with poor weight gaining, which, in turn, may exacerbate dysfunction of the immune system. This hypothesis may be supported by the master regulatory role of Cdc42 GTPase in maintaining the integration and immune homeostasis of the intestinal mucosa, and as a key player in the actin cytoskeleton dynamics, it controls mechanisms of inflammation, autoimmunity, and cancerogenesis. Intestinal cell proliferation, epithelial integrity, and cellular turnover as well as enterocyte extrusion and shedding are tightly controlled processes regulated by Cdc42-dependent actin cytoskeletal contractility and reorganization (Pradham et al., 2021; Ngo et al., 2022).

## The patient's perspective

The patient's perspective is largely dependent on the detection of the causative variant and establishing a definitive genetic diagnosis which primarily means an explanation for the multifaceted disease. Both for the family and leading physicians, it paves the way for future diagnostic and therapeutic interventions, shedding light on the expanded phenotype with immunodeficiency and gastrointestinal disorders. Prophylaxis against infections with azithromycin is legitimate as the first-line protective measure against respiratory tract infections. Administration of inactive vaccines needs to be recommended as an attempt to trigger the mounting of the immune memory yet the antigen-specific response in the patient may not be adequate (Szczawińska-Popłonyk et al., 2015). Regular monitoring is required by a multidisciplinary team including specialists in neurology, hematology, otorhinolaryngology, gastroenterology, cardiology, and nephrology, under the pediatric immunologist's supervision. Further clinical observation is needed as other phenotypic features may appear and novel treatment modalities may be proposed according to the course of the disease. It is worth noting that the Rho GTPase Cdc42 lies downstream of the master regulator Ras, crucial for cell malignant transformation. The crosstalk between the Cdc42 molecule and the network of effectors in the immune system is increasingly recognized, and new therapeutic targets based on new regulator partners are expected, and their translation into the treatment strategies for cancer creating a future therapeutic perspective (El Masri and Delon, 2021).

Importantly, the everyday struggle with the child's intellectual and motor disabilities, failure to thrive and feeding disorders, recurrent infections, increased risk of tumorigenesis, and frequent medical consultations is a disease burden for the patient's relatives. To cope with the multisystemic syndrome of TKS, medical and social support is needed for the family to enhance undertaking positive health-promoting stimulating activities. Therefore, the *de novo* nature of the pathogenic *CDC42* variant has an important informative role for the family.

The ever-increasing progress in molecular genetic studies contributes to better definition and delineation of the Takenouchi-Kosaki syndrome. It is a multifaceted disease with complex phenotypic features and a broad dysmorphology, neurological, hematological, hormonal, respiratory as well as immunological symptomatology. In this report, we add gastrointestinal and feeding disorders to the spectrum of syndromic manifestations. Uncovering the causative pathogenic variant in the *CDC42* gene is of utmost importance for understanding the complex mutual genetic and phenotypic relationships and disease pathophysiology as well as for the informativeness of the patient's family and the leading physician, contributing to diagnostic and therapeutic management and anticipating the prognosis.

## Data availability statement

The datasets for this article are not publicly available due to concerns regarding participant/patient anonymity. Requests to access the datasets should be directed to the corresponding author.

## Ethics statement

Ethical review and approval was not required for the study on human participants in accordance with the local legislation and institutional requirements. Written informed consent to participate in this study was provided by the participants' legal guardian/next of kin. Written informed consent was obtained from the participants' legal guardian/next of kin for the publication of this case report.

## Author contributions

AS-P was responsible for the intellectual conception of the study, data acquisition and interpretation, and drafted the manuscript. NP and BB were responsible for acquisition of data, their analysis, and participated in drafting the manuscript. MB-S was responsible for genetic molecular analysis, participated in acquisition of data and their interpretation, and in drafting the manuscript. JJ, KH, and SB were responsible for the molecular genetic analysis, interpretation of data, and participated in drafting the manuscript. JW critically revised the work for its intellectual content. All authors contributed to the article and approved the submitted version.

## Conflict of interest

The authors declare that the research was conducted in the absence of any commercial or financial relationships that could be construed as a potential conflict of interest.

## Publisher's note

# References


Asiri, A., Alwadaani, D., Umair, M., Alhamoudi, K. M., Almuhanna, M. H., Nasir, A., et al. (2021). Pancytopenia, recurrent infections, poor wound healing, heterotopia of the brain probably associated with a candidate novel de novo *CDC42* gene defect: Expanding the molecular and phenotypic spectrum. *Genes* 12, 294. doi:10.3390/genes12020294

Bucciol, G., Pillay, B., Casas-Martin, J., Delafontaine, S., Proesmans, M., Lorent, N., et al. (2020). Systemic inflammation and myelofibrosis in a patient with Takenouchi-Kosaki syndrome due to *CDC42* Tyr64Cys mutation. *J. Clin. Immunol.* 40 (4), 567–570. doi:10.1007/s10875-020-00742-5

Burbage, M., Keppler, S. J., Gasparrini, F., Martinez-Martin, F., Gaya, M., Feest, C., et al. (2015). Cdc42 is a key regulator of B cell differentiation and is required for antiviral humoral immunity. *J. Exp. Med.* 212 (1), 53–72. doi:10.1084/jem.20141143

Coppola, S., Insalaco, A., Zara, E., Di Rocco, M., Pires Marafon, D., Spadaro, F., et al. (2022). Mutations at the C-terminus of CDC42 cause distinct hematopoietic and autoinflammatory disorders. *J. Allergy Clin. Immunol.* 150 (1), 223–228. doi:10.1016/j.jaci.2022.01.024

El Masri, R., and Delon, J. (2021). RHO GTPases: From new partners to complex immune syndromes. *Nat. Rev. Immunol.* 21 (8), 499–513. doi:10.1038/s41577-021-00500-7

Gerasimcik, N., Dahlberg, C. I. M., Baptista, M. A. P., Massaad, M. J., Geha, R. S., Westerberg, L. S., et al. (2015). The Rho GTPase Cdc42 is essential for the activation and function of mature B cells. *J. Immunol.* 194 (10), 4750–4758. doi:10.4049/jimmunol.1401634

Gernez, Y., de Jesus, A. A., Alsaleem, H., Macaubas, C., Roy, A., Lovell, D., et al. (2019). Severe autoinflammation in 4 patients with C-terminal variants in cel division control protein 42 homolog (*CDC42*) successfully treated with IL-1β inhibition. *J. Allergy Clin. Immunol.* 11 (4), 1122–1125. doi:10.1016/j.jaci.2019.06.017

He, T., Huang, Y., Ling, J., and Yang, J. (2020). A new patient with NOCARH syndrome due to CDC42 defect. *J. Clin. Immunol.* 40 (4), 571–575. doi:10.1007/s10875-020-00786-7

Ishikawa, K., Uchiyama, T., Kaname, T., Kawai, T., and Ishiguro, A. (2021). Autoimmune hemolytic anemia associated with Takenouchi-Kosaki syndrome. *Pediatr. Int.* 63 (12), 1528–1530. doi:10.1111/ped.14651

Kashani, P., Marwaha, A., Feanny, S., Kim, V. H. D., Atkinson, A. R., Leon-Ponte, M., et al. (2021). Progressive decline of T and B cell numbers and function in a patient with CDC42 deficiency. *Immunol. Res.* 69 (1), 53–58. doi:10.1007/s12026-020-09168-y

Lam, M. T., Coppola, S., Krumbach, O. H. F., Prencipe, G., Insalaco, A., Cifaldi, C., et al. (2019). A novel disorder involving dyshematopoiesis, inflammation, and HLH due to aberrant CDC42 function. *J. Exp. Med.* 216 (12), 2778–2799. doi:10.1084/jem.20190147

Lauri, A., Fasano, G., Venditti, M., Dallapicola, B., and Tartaglia, M. (2021). *In vivo* functional genomics for undiagnosed patients: The impact of small GTPases signaling dysregulation at pan-embryo developmental scale. *Front. Cell Dev. Biol.* 9, 642235. doi:10.3389/fcell.2021.642235

Liu, Y., Jin, Y., Li, J., Seto, E., Kuo, E., Yu, W., et al. (2013). Inactivation of Cdc42 in neural crest cells causes craniofacial and cardiovascular morphogenesis defects. *Dev. Biol.* 383 (2), 239–252. doi:10.1016/j.ydbio.2013.09.013

Luckashenak, N., Wahe, A., Breit, K., Brakebusch, C., and Brocker, T. (2013). Rho-family GTPase Cdc42 controls migration of Langerhans cells *in vivo*. *J. Immunol.* 190 (1), 27–35. doi:10.4049/jimmunol.1201082

Martinelli, S., Krumbach, O. H. F., Pantaleoni, F., Coppola, S., Amin, E., Pannone, L., et al. (2018). Functional dysregulation of CDC42 causes diverse developmental phenotypes. *Am. J. Hum. Genet.* 102 (2), 309–320. doi:10.1016/j.ajhg.2017.12.015

Melendez, J., Grogg, M., and Zheng, Y. (2011). Signaling role of Cdc42 in regulating mammalian physiology. *J. Biol. Chem.* 286 (4), 2375–2381. doi:10.1074/jbc.R110.200329

Miyazawa, H., and Wada, T. (2022). Immune-mediated inflammatory diseases with chronic excess of serum interleukin-18. *Front. Immunol.* 13, 930141. doi:10.3389/fimmu.2022.930141

Motokawa, M., Watanabe, S., Nakatomi, A., Kondoh, T., Matsumoto, T., Morifuji, K., et al. (2018). A hot-spot mutation in *CDC42* (p.Tyr64Cys) and novel phenotypes in the third patient with Takenouchi-Kosaki syndrome. *J. Hum. Genet.* 63 (3), 387–390. doi:10.1038/s10038-017-0396-5

Mulloy, J. C., Cancelas, J. A., Filippi, M. D., Kalfa, T. A., Guo, F., and Zheng, Y. (2010). Rho GTPases in hematopoiesis and hemopathies. *Blood* 115 (5), 936–947. doi:10.1182/blood-2009-09-198127

Nayak, R. C., Chang, K. H., Vaitinadin, N. S., and Cancelas, J. A. (2013). Rho GTPases control specific cytoskeleton-dependent functions of hematopoietic stem cells. *Immunol. Rev.* 256 (1), 255–268. doi:10.1111/imr.12119

Ngo, P. A., Neurath, M. F., and Lopez-Posadas, R. (2022). Impact of epithelial cell shedding on intestinal homeostasis. *Int. J. Mol. Sci.* 23 (8), 4160. doi:10.3390/ijms23084160

Piątosa, B., Wolska-Kuśnierz, B., Pac, M., Siewiera, K., Gałkowska, E., and Bernatowska, E. (2010). B cell subsets in healthy children: Reference values for evaluation of B cell maturation process in peripheral blood. *Cytom. B Clin. Cytom.* 78 (6), 372–381. doi:10.1002/cyto.b.20536

Pradham, R., Ngo, P. A., Martinez-Sanchez, L. C., Neurath, M. F., and Lopez-Posadas, R. (2021). Rho GTPases as key molecular players within intestinal mucosa and GI diseases. *Cells* 10 (1), 66. doi:10.3390/cells10010066

Richards, S., Aziz, N., Bale, S., Bick, D., Das, S., Gastier-Foster, J., et al. (2015). Standards and guidelines for the interpretation of sequence variants: A joint consensus recommendation of the American college of medical genetics and genomics and the association for molecular pathology. *Genet. Med.* 17 (5), 405–424. doi:10.1038/gim.2015.30

Santoro, C., Gaudino, G., Torella, A., Piluso, G., Perrotta, S., Miraglia del Giudice, E., et al. (2021). Intermittent macrothrombocytopenia in a novel patient with Takenouchi-Kosaki syndrome and review of literature. *Eur. J. Med. Genet.* 64 (12), 104358. doi:10.1016/j.ejmg.2021.104358

Schatorje, E. J. H., Gemen, E. F. A., Driessen, G. J. A., Leuvenink, J., van Hout, R. W. N. M., and de Vries, E. (2012). Paediatric reference values for the peripheral T cell compartment. *Scand. J. Immunol.* 75 (4), 436–444. doi:10.1111/j.1365-3083.2012.02671.x

Shimizu, M., Takei, S., Mori, M., and Yachie, A. (2022). Pathogenic roles and diagnostic utility of interleukin-18 in autoinflammatory diseases. *Front. Immunol.* 13, 951535. doi:10.3389/fimmu.2022.951535

Smits, K., Iannucci, V., Sove, V., Van Hauve, P., Naessens, E., Meuwissen, M. J., et al. (2010). Rho GTPase Cdc42 is essential for human T cell development. *Haematologica* 95 (3), 367–375. doi:10.3324/haematol.2009.006890

Song, W., Liu, C., and Upadhyaya, A. (2014). The pivotal position of the actin cytoskeleton in the initiation and regulation of B cell receptor activation. *Biochim. Biophys. Acta* 1838 (2), 569–578. doi:10.1016/j.bbamem.2013.07.016

Szczawińska-Popłonyk, A., Bręborowicz, A., Samara, H., Ossowska, L., and Dworacki, G. (2015). Impaired antigen-specific immune response to vaccines in children with antibody production defects. *Clin. Vaccine Immunol.* 22 (8), 875–882. doi:10.1128/CVI.00148-15

Szczawińska-Popłonyk, A., Płoski, R., Bernatowska, E., and Pac, M. (2020). A novel CDC42 mutation in an 11-year old child manifesting as syndromic immunodeficiency, autoinflammation, hemophagocytic lymphohistiocytosis, and malignancy: A case report. *Front. Immunol.* 11, 318. doi:10.3389/fimmu.2020.00318

Tackenberg, H., Moller, S., Filippi, M. D., and Laskay, T. (2020). The small GTPase Cdc42 is a major regulator of neutrophil effector functions. *Front. Immunol.* 11, 1197. doi:10.3389/fimmu.2020.01197

Takenouchi, T., Kosaki, R., Niizuma, T., Hata, K., and Kosaki, K. (2015). Macrothrombocytopenia and developmental delay with a de novo CDC42 mutation: Yet another locus for thrombocytopenia and developmental delay. *Am. J. Med. Genet. A* 167A (11), 2822–2825. doi:10.1002/ajmg.a.37275

Takenouchi, T., Okamoto, N., Ida, S., Uehara, T., and Kosaki, K. (2016). Further evidence of a mutation in CDC42 as a cause of a recognizable syndromic form of thrombocytopenia. *Am. J. Med. Genet. A* 170A (4), 852–855. doi:10.1002/ajmg.a.37526

Tangye, S. G., Al-Herz, W., Bousfiha, A., Cunningham-Rundles, C., Franco, J. L., Holland, S. M., et al. (2022). Human inborn errors of immunity: 2022 update on the classification from the international union of immunological Societies Expert committee. *J. Clin. Immunol.* 42, 1473–1507. doi:10.1007/s10875-022-01289-3

Tangye, S. G., Bucciol, G., Casas-Martin, J., Pillay, B., Ma, C. S., Moens, L., et al. (2019). Human inborn errors of the actin cytoskeleton affecting immunity: Way beyond WAS and WIP. *Immunol. Cell Biol.* 97 (4), 389–402. doi:10.1111/imcb.12243

Uehara, T., Suzuki, H., Okamoto, N., Kondoh, T., Ahmad, A., O'Connor, B. C., et al. (2019). Patheogenetic basis of Takenouchi-Kosaki syndrome: Electron microscopy study using platelets in patients and functional studies in a *Caenorhabditis elegans* model. *Sci. Rep.* 9 (1), 4418. doi:10.1038/s41598-019-40988-7

Ueyama, T. (2019). Rho-family small GTPases: From highly polarized sensory neurons to cancer cells. *Cells* 8 (2), 92. doi:10.3390/cells8020092

Ueyama, T., Sakaguchi, H., Nakamura, T., Goto, A., Morioka, S., Shimizu, A., et al. (2014). Maintenance of stereocilia and apical junctional complexes by Cdc42 in cochlear hair cells. *J. Cell Sci.* 127 (Pt9), 2040–2052. doi:10.1242/jcs.143602

# Frontiers in Genetics

**Highlights genetic and genomic inquiry relating to all domains of life**

The most cited genetics and heredity journal, which advances our understanding of genes from humans to plants and other model organisms. It highlights developments in the function and variability of the genome, and the use of genomic tools.

---

## Discover the latest Research Topics

See more →

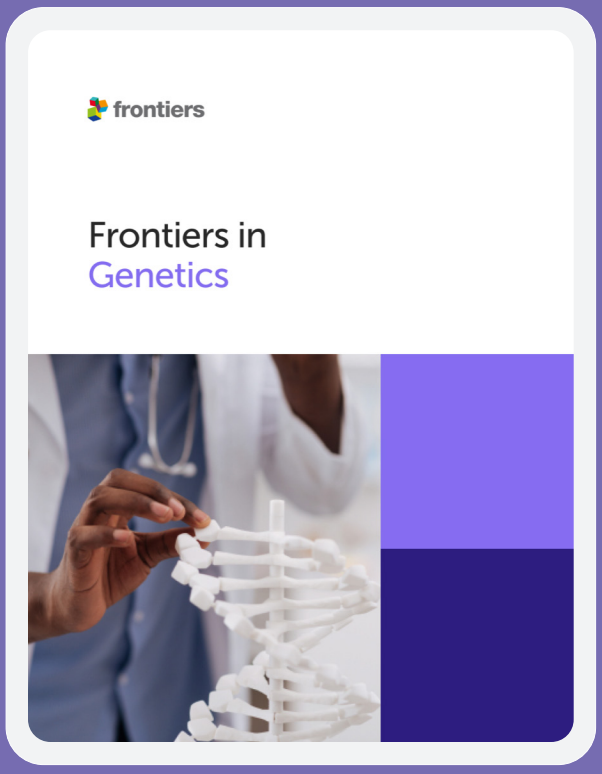


**Frontiers**

Avenue du Tribunal-Fédéral 34
1005 Lausanne, Switzerland
frontiersin.org

**Contact us**

+41 (0)21 510 17 00
frontiersin.org/about/contact